ATDL-79/16
Distribution Category UC-11

Environmental Research Laboratories

Air Resources
Atmospheric Turbulence and Diffusion Laboratory

Oak Ridge, Tennessee

December 1979

1978 ANNUAL REPORT

U. S. Department of Commerce
National Oceanic and Atmospheric Administration

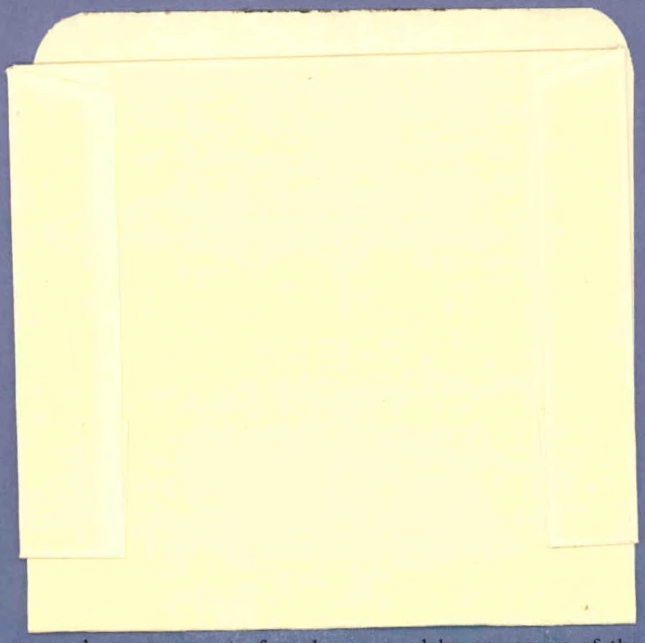

Printed in the United States of America
USDOE Technical Information Center, Oak Ridge, Tennessee

Foreword

The following is a compilation of research contributions from the National Oceanic and Atmospheric Administration Air Resources Atmospheric Turbulence and Diffusion Laboratory for the calendar year 1978. It was prepared by the Technical Information Center, U. S. Department of Energy, Oak Ridge, Tennessee. Subsequent volumes will be issued on an annual basis. The research reported in this document was performed under an agreement between the U. S. Department of Energy and the National Oceanic and Atmospheric Administration.

F. A. Gifford
Director
Atmospheric Turbulence and
Diffusion Laboratory

CONTENTS

Summary of Activities and Plans FY 1979 - 1980

Air Resources
Atmospheric Turbulence and Diffusion Laboratory
National Oceanic and Atmospheric Administration
Oak Ridge, Tennessee
October, 1979

Rayford P. Hosker, Jr.
and
Ruth A. Green

Atmospheric Turbulence
and Diffusion Laboratory

Summary of Activities
and Plans - FY 1979 - 1980

The Atmospheric Turbulence and Diffusion Laboratory (ATDL) in Oak Ridge, Tennessee, is operated for the Department of Energy (DOE) by the National Oceanic and Atmospheric Administration's Air Resources Laboratories. Major funding is from DOE's Office of Health and Environmental Research, Pollutant Characterization and Safety Research Division. ATDL works closely with various divisions of Oak Ridge National Laboratory (ORNL) on environmental projects of joint interest and also functions as a meteorological consultant and advisor to that laboratory.

The Atmospheric Turbulence and Diffusion research program is organized around the following subject areas:

A. Regional-Scale Effects of Energy Generation. There continues to be a great deal of interest in regional-scale environmental impacts of energy generation facilities for reasons ranging from public health to aesthetic concerns. The ATDL program in this area has been devoted to the development of regional assessment models for effluent transport and dispersion, and to the evaluation of potential meteorological effects of the release of very large quantities of heat and moisture from industrial and power production installations. The regional assessment models have been validated with existing field data, some of which was gathered by ATDL during our 1974 Eastern Tennessee Trajectory Experiment (ETTEX). Refinement of these models is continuing, using more recent data sets. Testing of the models using time-averaged meteorological data (supplied largely by the Tennessee Valley Authority) also continues, to establish the sensitivity of the results to the averaging interval.

As the size of power plants and industrial facilities grows, the potential atmospheric effects of the waste heat and moisture released become of increasing concern. Problems ranging from increased cloudiness to possible convective storm initiation or enhancement are possible. ATDL has maintained a strong research program in this area for almost a decade. Models of cooling tower plume rise and cloud growth, and of hypothetical power parks have already been developed. Tests of these against both present and proposed field observations, and improvements and simplification of the techniques will continue.

B. Mesoscale Transport and Diffusion Modeling. Transfer of material between the earth's surface and the atmosphere, dilution of atmospheric pollutants, and dissipation of waste heat are all processes that occur in and are controlled by the planetary boundary layer (PBL). For example, the rate of transport and diffusion of an effluent such as sulfate aerosol is determined by the PBL mean winds, the strength of the turbulence, the depth through which the material is mixed, the rate of physical or chemical transformation of the effluent, and the rate of its transfer to receptors such as foliage, soil, or water.

Our ability to model PBL flows correctly becomes crucial at some point in almost every aspect of energy research, including primary production by photosynthesis, the design and operation of energy production systems of all kinds, and in waste heat and air pollution problems. The ATDL program is organized around the systematic development of a hierarchy of increasingly complete and realistic numerical models of the PBL, including its mean wind fields, turbulence characteristics and statistics, and the effects of complex terrain. ATDL work completed or planned for the next few years includes:

(1) the simulation of strongly buoyant vapor plumes for an accurate representation of anthropogenic sources of heat and moisture, such as power parks;

(2) an investigation of momentum, heat and moisture transfer above and within a forest canopy;

(3) numerical simulation and parameterization of cloud-topped convective mixed layers, and of nocturnal boundary layers;

(4) simulation of the Martian PBL, which is a simpler analog of the earth's PBL;

(5) flows over two-dimensional mountains and valleys;

(6) steady-state three-dimensional flows over complex terrain;

(7) the numerical simulation of flows physically modeled in the ATDL wind tunnel and water channel;

(8) an investigation of the mesoscale and temporal variability of mixing depth over complex terrain.

Studies of flow over complex terrain will include the systematic development of potential-flow numerical models using both finite difference and finite element techniques. A physical modeling program to complement the numerical work is under way. Some initial experiments have already been completed, including estimates of air parcel trajectories near a two-dimensional escarpment at TVA's Widow's Creek power plant in northern Alabama, and a two-week field study of nocturnal drainage winds and valley circulation in the Anderson Creek Valley of the Geysers site. Model development and validation using these data sets are planned. It seems likely, however, that a more complete data base will be required for regional scale model validation in complex terrain; a second ETTEX would probably be suitable. Before an ambitious interlaboratory study of this scale is initiated, however, considerable effort must be devoted to exact data requirements, optimum measurement techniques, instrumentation siting, and manpower and budget requirements. Work on this is planned for the early 1980's.

C. Effluent Plume Behavior. Five different research programs fall under this general heading. Virtually all are concerned with estimating the potential for adverse environmental effects of effluents released to the atmosphere during energy production processes. Following is a brief summary of each of the programs:

1. Plume dispersion parameters. Presently practical techniques for atmospheric dispersion estimates (for instance, those recommended by the NRC Safety Guides and the EPA regulations) depend largely on the numerous diffusion experiments conducted during the 1950's and early 1960's. However, current theories and turbulence experiments are forcing a reconsideration of these results for certain cases, especially for strongly convective daytime conditions, and for stable nocturnal conditions. Recent theoretical and observational advances in understanding of the atmospheric boundary layer are being exploited to provide needed revisions to earlier diffusion estimation techniques.

2. Plume rise. Most routine pollutant sources, and many radioactivity sources, especially accidents of various types at nuclear facilities, involve emission of buoyant clouds and plumes. ATDL took the lead a number of years ago in studying plume rise, and many regulations governing nuclear facilities and conventional air pollution refer to and use our methodology. Current research efforts are concerned with effluent plumes which possess significant initial momentum and/or buoyancy, analyses of data for neutral and unstable conditions in relation to theoretical models, and wind-tunnel studies on the lift-off of a buoyant plume in a building wake.

3. Dispersion of dense gases. In recent years the shipment, storage, and use of flammable, radioactive, toxic, or otherwise hazardous gases, often maintained in liquid form, has become commonplace both in general industry and in energy production. Examples include LNG, UF_6, and the various halogens. Such use is anticipated to increase in the next few years, particularly with regard to LNG. The potential for spills with disastrous consequences is evident. Despite this, little predictive ability presently exists for the transport and dispersion of dense cold gases in the atmosphere.

   Preliminary studies of the various important flow regimes, which enter into the spread and diffusion of a dense gas, have been carried out at the ATDL. Further work is required to test these calculations against experimental data. Little seems to be known of the details of the turbulent mixing process at the gas-atmosphere interface, while the dispersion models which have been employed in various environmental impact analyses have frequently been inappropriate to the problem. Additional work, including a series of controlled experiments, is clearly needed. The goal is an easily applied model which, given the emission and atmospheric conditions, can predict the spread of a hazardous dense gas with time, identifying important

regions such as zones of toxic concentration and/or flammability limit lines. A literature search has been completed and a survey and summary of the available information is planned. Present personnel and funding limitations will defer this until FY 1981, however.

4. Flow and diffusion near obstacles. Aside from questions of structural integrity and microclimate, it is well known that near-building flow fields have significant effects on the dispersion of building effluents, including stack and cooling tower plumes. The path of an effluent plume is determined in any particular instance by the exact configuration of the building and its intake and exhaust system, by their orientation with respect to the wind and to neighboring buildings or other flow obstructions, and by the atmospheric and plume discharge conditions during the time of release. The ATDL has conducted a survey of flow and dispersion near obstacles, to be published as a chapter in Atmospheric Sciences and Power Production. One of the significant findings that emerged during this survey was the presence of major gaps in the available data; in particular, data that are sufficiently detailed to use in developing or verifying theoretical models are largely unavailable. ATDL is carrying out a systematic study of this problem in its Applied Fluid Dynamics Laboratory, utilizing the wind tunnel and water channel. Studies of wake cavity extent behind block buildings and initial studies of flow near an idealized two-dimensional escarpment of variable step incline have begun. A report summarizing the currently available building wake flow and dispersion data was prepared for the Nuclear Regulatory Commission. Guidelines for practical estimation of the extent and rate of spread of near and far wakes and for calculating effluent concentrations downwind of simple block buildings are also being written for NRC.

5. Cooling tower plumes. One of the major consequences of the operation of power generation facilities, be they fossil-fuel or nuclear, is the release of significant quantities of heat and moisture to the atmosphere. Increasingly this "waste" heat is rejected to the atmosphere in concentrated form from large cooling towers. Extensive numerical modeling efforts are under way at ATDL and elsewhere to try to elucidate the effects of such releases on local and, ultimately, on global climate. Personnel and funding limitations have precluded an immediate investigation of aerodynamic influences on cooling tower plumes, although the presence of downwash and recirculation is known to be significant for both plume rise and tower thermodynamic performance. Research aimed at establishing the likelihood of such phenomena and parameterizing their effects for model use is now planned for FY 1980-1981.

D. Forest Meteorology. Effects of forest vegetation upon local, regional, and larger scale climates are exerted through three highly inter-related sets of phenomena. Energy partitioning by forests is a function of radiation balances and of turbulent exchanges of sensible and latent heat across the forest-atmosphere interface. Transport and ultimate fates of materials transported in the atmosphere depend on these turbulent exchanges as well. If biologically active materials are considered, e.g., H_2O or CO_2, then the interactions of forest physiology with radiation balances and turbulent exchanges becomes important. The consequences of the interaction among radiation balances, turbulent exchanges and physiological processes of forests impact energy production and utilization technologies in many ways.

For example, the balance of energy inputs and outputs of a forest plays an important role in the definition of local and regional climates in terms of temperature, humidity, and atmospheric stability. Large expanses of forest cover may also affect regional precipitation, since extensive deforestation in certain tropical areas has coincided with significant reductions in precipitation. These climatic effects further combine to control regional water balances. Consequently, the controversy of the early 20th century over the effects of forests on water balances is being renewed, and because of the rapidly increasing competition for water among domestic, agricultural, and industrial uses in developed, developing, and underdeveloped nations alike, this controversy will soon rage world-wide. These factors are of obvious importance to energy technology.

The transport and fate of materials transported in the atmosphere are also governed, to a high degree, by the interactions among forest radiation balances, forest physiology, and atmospheric stability through their effects upon turbulence. In particular, deposition and uptake of effluents from large power plants, whether fossil or nuclear fueled, are affected by these interactions.

With the growing awareness of potential climatic changes that could result from continued anthropogenic production of CO_2 during fossil fuel combustion, the role of the terrestrial biota in buffering the global CO_2 balance is coming under increased scrutiny. In recent months, a consensus seems to be developing that more is known about deep ocean sink strengths for CO_2 than was previously thought, but that the CO_2 balances of vegetation are much more poorly understood than previously believed, especially for non-agricultural vegetation. Thus, as the problems of pollution, resource limitation, climatic change, and societal demands for ever-growing economies have converged to create current energy crises, micrometeorological research in general, and forest micrometeorology in particular, is needed increasingly to provide information immediately applicable to current problems. The ATDL forest meteorology research program is attempting to provide some of these needed answers. In particular, assessments of forest structure and radiation balance in a deciduous forest are well under way, and instrumentation for direct flux measurement is being procured. Higher-order-closure numerical models of the mean and turbulent wind fields is planned, with validation from the field program.

Accomplishments - FY 1979

A. Regional Scale Effects of Energy Generation

1. Modeling of regional scale transport and diffusion. During FY 1979 the regional models were refined by using wind patterns and diffusion observed during recent regional diffusion experiments to derive parameters necessary for operation of the model. Work continued on using average data in the equation of motion.

2. Energy effects on the atmosphere. The one-dimensional plume and cloud growth model was further tested using recent observations of cooling tower plumes at Keystone, Pennsylvania, and Chalk Point, Maryland. This model and the ATDL drift deposition model were used in the evaluation of field studies undertaken during FY 1978 by DOE's METER (Meteorological Effects of Thermal Energy Releases) project. The two-dimensional second-order-closure model of shallow moist convection was modified to use conservative variable formulations, and tested using cooling pond measurements obtained by Argonne National Laboratory. The model currently assumes that the energy source is a broad area source of heat and moisture at the surface. A one-dimensional radiation model of the lower atmosphere was applied to the problem of estimating the depletion of solar energy by cooling tower plumes and power park clouds.

B. Mesoscale Transport and Diffusion Modeling

1. Planetary boundary layer (PBL) modeling. The IPBL model was used to study geophysical flows of the well-mixed PBL over two-dimensional ridges and three-dimensional hills. The nocturnal boundary layer model was modified to include moisture, radiative, and sloping terrain effects as well as the surface energy budget. Computer programs were developed for both diurnally varying PBL models.

2. Transport modeling. Over mesoscale distances, plume transport is important in determining local air quality. The IPBL model was linked with the ATDL transport and diffusion model to study time-dependent atmospheric transport over complex terrain.

3. Lagrangian turbulence statistics. Data from the 1978 Boulder experiment were studied using spectral analysis to determine the Lagrangian time scale of turbulence, which was then compared with the Eulerian time scale measured by the tower and airplane. During a second Lagrangian turbulence experiment dual-doppler radars gave continuous velocity records of the tetroons and neutral density pilot balloons, while Eulerian data were taken on the Wave Propagation Laboratory tower at Boulder, Colorado.

4. Statistical diffusion model. The model was extended to account for wind fields where correlations between u' and w' exist; e.g., boundary layers or other shear zones.

E. Climatological Studies. Traditionally, ATDL has measured climatological parameters and supplied them to the Department of Energy facilities in Oak Ridge. These measurements are continuing. The historical data include one of the nation's longest solar radiation records.

In FY 1977 the climatological measurement program was upgraded to provide additional needed information. Spectral and radiation balance measurements together with the segregation of direct and diffuse components were added to the traditional global radiation measurement. These measurements, together with wind shear and temperature gradients above the forest and within-canopy profile data, are taken at the experimental site on Walker Branch and are available to scientists in DOE and elsewhere on a routine basis. This upgraded station is classified as a cooperating station in the solar monitoring network established by the National Weather Service through DOE funding, and the data are archived with the data from the entire network.

5. Flow over rough terrain. Additional air parcel trajectory experiments were carried out at the TVA's Widow's Creek steam plant; it was found that the crosswind dispersion parameter σ_y is satisfactorily predicted from the usual relation $\sigma_y = \sigma_\theta x f(x)$. An ATDL-EPA cooperative wind tunnel modeling study of flow and diffusion over a terrain step was begun. ATDL will analyze in detail data from the 15° step, which corresponds to the step slope at Widow's Creek. ATDL participated in a two-week field study of nocturnal drainage winds and valley circulation conducted in the Anderson Creek Valley of the Geysers site as part of the ASCOT program. The SRI data from the Geysers were analyzed to determine the frequency of nocturnal flow patterns.

C. Effluent Plume Behavior

1. Plume dispersion parameters. An analysis of the "Project Prarie Grass" data was made for horizontal dispersion related to various boundary layer parameters. The estimation of diffusion parameters from long-term averages of meteorological data continued, with TVA cooperation.

2. Plume rise. Further wind tunnel studies on the lift-off of a buoyant plume in a building wake were carried out. Analyses of data for neutral and unstable conditions in relation to theoretical models were made, and a paper on the results of the modeling experiments on rise in a calm, stable ambient was written. The sets of temperature and humidity cross sections obtained in the Chalk Point cooling tower plume were used to test our concepts of the dynamic behavior of buoyant plumes.

3. Flow and dispersion near obstacles. The wind tunnel data system was received, tested, and placed in use. Studies of wake cavity extent were performed behind block buildings of particular length and width to height ratios, to fill gaps in the previously available data base. Initial studies of flow near an idealized two-dimensional escarpment of variable step incline were begun in the ATDL wind tunnel. The ATDL water channel was completed. The device will be used primarily for visualization (using multi-colored dyes) of flows near buildings and over relatively small stretches of rough terrain, such as the Walker Branch Watershed field site.

D. Forest Meteorology

1. Instrumentation and field data. The space and time distributions of solar, photosynthetically active, all wave, and long wave radiative fluxes in and above the forest were determined and related to the structure and phenological state of the forest at the Walker Banch site. Assessment of the vertical distribution of woody biomass in this forest was completed. Installation of instruments and data loggers at the field and forest pine plantation sites was completed.

2. Modeling. A topographic model of the Walker Branch site was constructed for the ATDL water flow channel, for visualization of flows from various "wind" directions across the site.

E. Climatological Studies.

Routine data collection and analysis of solar radiation continued. Collection, analysis, and computer storage of basic climatological data continue to be recorded and archived for the Oak Ridge area.

Plans FY 1980

A. Regional Scale Effects of Energy Generation

1. Energy effects on the atmosphere. Work will continue on the second-order model of moist convection and on the introduction of heat and moisture effects into the stream function/vorticity model. An attempt will be made to at least qualitatively validate these models using data from the "Meteotron" experiment (France), a cooling pond (Dresden, IL), and a petrochemical complex (Los Angeles). Plume observations from the French "Meteotron" work will be analyzed and compared to current plume models to gain additional insight into the dynamics associated with large scale energy releases.

B. Mesoscale Transport and Diffusion Modeling

1. Planetary boundary layer modeling. The IPBL model will be used to study time dependent flows over the complex terrains of the Southern Appalachian Mountains and the Geysers site. Model validation will be made using the ETTEX and TVA data. The diurnally varying PBL models will be further improved. Simulation of additional data sets, predictions of mean and turbulence structure of the PBL, tests of parameterizations, and diffusion calculations are planned.

2. Transport and diffusion modeling. The IPBL transport and diffusion model will be used to test the suitability of diffusion simulation schemes for application to complex terrain cases. Schemes to be tested are segmented plumes, puffs, and conditioned particle diffusion theory. After evaluation, the model will be used to study terrain effects on diffusion over the complex terrains of east Tennessee and the Geysers.

3. Lagrangian Eulerian turbulence statistics. Analysis of the data from the Boulder experiments will continue, especially regarding the relations between Eulerian and Lagrangian turbulence.

4. Statistical diffusion model. Application of the diffusion model to the University of Virginia mesoscale wind patterns will continue. A search will be made for real sets of wind and concentration fields for tests of the model.

5. Flow over rough terrain. Data from the ATDL and EPA wind tunnel simulations of the Widow's Creek escarpment will be analyzed, and recommendations made regarding changes to existing diffusion models to account for the effects of a terrain step. Data obtained by ATDL during the Phase I experiment of the ASCOT program will be reduced and analyzed. Some preliminary experiments for the second Eastern Tennessee Trajectory Experiment (ETTEX II) will be performed over the complex terrain of the Cumberland and the Great Smoky Mountains. Models developed through the research at the Geysers site will be applied to the results of these experiments.

C. Effluent Plume Behavior

1. Plume dispersion parameters. Analyses of both vertical and horizontal dispersion in relation to various boundary layer parameters will be completed using the "Green Glow," NRTS, Hanford, Jülich, and Cabauw data sets, as well as data collected by ATDL during the ETTEX experiment. Analysis of the data and models for the variation of σ_y and σ_z with source height will be completed, and recommendations made for use in preparing environmental assessments. A preliminary climatology of diffusion parameters at two or three TVA stations in the Oak Ridge area will be published.

2. Plume rise. A paper describing the results of the fluid modeling experiments on rise in a stable crosswind will be written. TVA data on maximum ground concentration of SO_2 will be analyzed to infer the effective plume rise in neutral and unstable conditions. Modeling experiments on partial penetration of elevated stable layers will be planned and initiated.

3. Flow and dispersion near obstacles. Guidelines for estimating wake behavior and effluent concentrations behind buildings oriented at an angle to the wind will be prepared for the Nuclear Regulatory Commission. The effects of "clustering" of buildings on these wake characteristics will be considered in some detail.

Highly detailed studies of flow adjacent to simple structures will be carried out to illuminate the dominant mechanisms and paths for effluent transfer to and from the wake cavity region. Such insights are essential to developing reasonable mathematical models of the process, which in turn are required for concentration calculations. Studies of plume downwash and reingestion at cooling towers will be initiated. This work should be useful in establishing likely downwash conditions and parameterizing their consequences in numerical models of plume behavior, needed for environmental assessments.

D. Forest Meteorology

1. Field data. Preliminary data on deciduous forest turbulence structure will be collected and analyzed. Studies of the vertical turbulent transfer of momentum, sensible heat, and water vapor will be initiated. Radiation flux and balance data will be analyzed and related to forest structure and forest phenological condition. Using these analyses, models of radiation distributions in agricultural crops will be tested and modified as necessary to simulate deciduous forest conditions.

2. Modeling. A dye injector will be constructed for the water channel, and used in testing a topographic model of the Walker Branch Watershed site. Primary features of interest will be terrain-influenced zones of flow deflection, convergence, and divergence. The model results will be compared to field observations obtained at our meteorological site. Initial development of a mathematical forest canopy flow model will begin, using second-order closure. Data from field work will eventually be used to validate this model.

E. Climatological Studies

Data collection, analysis, summary reports and datasets for archiving both solar radiation and climatological data will continue. A study of low wind statistics will begin because of their great importance to the problem of the prediction of high air pollution concentrations. A sensitive anemometer will be operated continuously at a level within the mixed layer at Oak Ridge, and a climatology of low wind frequency distributions will be developed. If the dat warrant it, additional anemometers will be set up at other sites, so that a variety of terrain and surface characteristics can be studied.

Laboratory Staff

During FY 1979 the ATDL staff totaled approximately 21. Of this number, 11 were professional scientists and five were technical and administrative personnel. Several part-time workers, mostly students, account for the remainder. No overall increase in staff is planned for FY 1980, but it is expected that one professional position will be filled that was delayed during FY 1979. The staff is frequently augmented by visiting scientists from abroad. Several have come via International Atomic Energy Agency-National Research Council Fellowships, to work on problems of nuclear meteorology. Others have been assigned here to work on basic problems of atmospheric diffusion through various programs, such as Oak Ridge Associated Universities (ORAU) faculty research fellowships. Also, much use of university students at various levels is made, including part-time undergraduate workers, summer fellowship students, "co-op" students, and part-time graduate students. University students in these various capacities supplied approximately three person-years in FY 1979, a substantial fraction (~ 15%) of the ATDL total.

Publications and Reports FY-1979

Briggs, Gary A., 1977: Some Theoretical Notes on "Sigma" Curves and Stability Classification. In-house publication.

Briggs, Gary A., 1979: Plume Rise and Buoyancy Effects. Chapter for book - Atmospheric Science and Power Production.

Culkowski, Walter M., 1979: Power Law Variations of Wind Speed Profiles at Three Sites in the Oak Ridge Area. Presented at the 22nd APCA Annual Meeting, Cincinnati, Ohio, June 24-28, 1979.

Culkowski, Walter M., 1979: A Comparison of Temperature and Wind Speed Functions in the Lowest Thirty-Two Meters During Unstable Conditions. In-house publication.

Elliott, David B. and Lee Nipper, 1979: SPIF: A Preprocessor for Structured Programming in FORTRAN. In-house publication.

Gifford, F. A., 1979: Estimating Ground-Level Concentration Patterns from Isolated Air-Pollution Sources: A Brief Summary. Presented at the Second Workshop on Health Surveillance around Point Sources of Pollution, Albuquerque, N. M., January 22-24, 1979.

Gifford, F. A., 1979: Smoke as a Quantitative Atmosheric Diffusion Tracer. Presented at a Workshop on Atmospheric Tracers and Tracer Applications, Los Alamos Scientific Laboratory, May 23-24, 1979.

Gifford, F. A., 1979: Recent Studies of Diffusion Parameters for Air Pollution Applications. In house publication.

Hanna, Steven R., 1979: Measured σ_y and σ_θ in Complex Terrain Near the TVA Widows Creek, AL, Steam Plant. Accepted for publication in Atmospheric Environment.

Hanna, Steven R., 1979: Lagrangian Turbulence Observations using Balloons. Chapter for ERL Report.

Hosker, R. P., Jr., 1979: Chapter 7: Flow and Dispersion Near Obstacles. Chapter for book - Atmospheric Science and Power Production.

Hutchison, Boyd A., 1979: Forest Meteorology, Research Needs for an Energy and Resource Limited Future Workshop Summary. BAMS 60, 4, pp. 31.

Hutchison, B. A., D. R. Matt and R. T. McMillen, 1978: Diffuse Radiation in a Deciduous Forest Varies with Sky Brightness Distribution. Presented as a poster paper at the Forest Meteorology Workshop, Ottawa, Canada, August 21-25, 1978.

Hutchison, Boyd A., 1979: Forest Meteorology--Research for an Energy and Resource Limited Future. Proceedings of a Workshop held in Ottawa, Canada, August 28-31, 1978.

Hutchison, Boyd A., 1979: Instrument Guidelines for Measurement of Meteorological Characteristics of Long-Term Ecological Research Sites. In-house publication.

Matt, D. R., R. T. McMillen and B. A. Hutchison, 1978: Spectral Radiation Balances Above an Oak-Hickory Stand During the Spring Leafing Season. Presented as a poster paper at the Forest Meteorology Workshop, Ottawa, Canada, August 21-25, 1978.

Nappo, Carmen J. and Linda J. Gabbard, 1979: Horizontal Variability of Precipitation over the Eastern Tennessee River Valley. Submitted to Monthly Weather Review.

Rao, K. S., 1979: On Modeling the Nocturnal Drainage Flows. (A Literature Survey.) In-house publication.

Rao, K.S., 1979: Drainage Flow Modeling. Part of an ASCOT report by Marvin Dickerson.

78-40.3

An Exercise in Estimating Vertical Diffusion Coefficients from Averaged Data

Walter M. Culkowski
Searle D. Swisher

National Oceanic and Atmospheric Administration
Oak Ridge, Tennessee

For Presentation at the 71st Annual Meeting of the Air Pollution Control Association

Houston, Texas **June 25-30, 1978**

ATDL Contribution File No. 78/1

Introduction

While constructing a numerical model for estimating diffusion and deposition [1], it became apparent that the most time consuming, subjective, and non-standardized task was assigning the proper stability category to each period of calculation (hour, week, month, or season). Pendergast[2] has outlined the difficulties in detail and Culkowski[3] has provided a scattergram showing the poor agreement between the vertical standard deviation of wind direction (σ_ϕ) with temperature-gradient data (ΔT). Fortunately, many applications of dispersion modeling deal with long term (monthly, seasonal, and yearly) effects, which tend to smooth the more erratic effects resulting from hourly estimates of stability. The present paper tries to determine whether averaging hourly data over an extended period of time can yield vertical diffusion estimates similar to those currently employed. Various parameters are compared to determine if they agree with standard theoretical formulation, and a simple objective technique for determing the stability is developed.

The Data and the Site

The Tennessee Valley Authority (TVA) has three well-equipped and maintained meteorological towers within 50 km of Oak Ridge, Tennessee. These towers support the air quality programs of TVA, monitoring the Kingston and Bull Run coal fired steam plants. The Atmospheric Turbulence and Diffusion Laboratory (ATDL) obtained several data sets of meteorological information from TVA. Of the data sets, the Kingston valley site was selected because of the height of the tower (110 m) and the instrumentation for vertical diffusion estimates that will be described below.

The tower has its highest sensors at 370 m MSL, about 140 m from the surface of an embankment area. The base is some 15 m below the crest of a hill. The crest is southwest of the tower, subjecting the tower to a slight downslope flow from the prevailing southwest winds. The tower is well instrumented; temperature is measured at the 1.2, 10.0 and 110.0 meters levels. Wind speed (u), direction, and standard deviation of horizontal wind direction (σ_θ), are available at the 110 and 10 m levels. Standard deviation of vertical wind direction (σ_ϕ), solar, and total radiation are available at the 110 m level. Barometric pressure and rainfall are also monitored. The entire area is wooded, and located in a northeast-southwest series of valleys and hills between the Cumberland Mountains to the west and the Great Smoky Mountains to the east. The data tape we received covered the period April 14 - September 30, 1975.

The data in Table I are simply the hourly data averaged over the entire period; the potential temperatures (θ's) have been computed from the averaged dry bulb temperatures by adding 1°C per 100 m of height, to permit the lapse rate to be computed in potential, rather than dry-bulb, temperature.

Analysis

The following discussion relies heavily on correlation coefficients (r) to examine the relative behavior of two parameters. Since the sample size is necessarily small (24 hourly values) in each trial, the authors have attempted to restrict the discussion to parameters generally having correlations of $r = \pm.95$ or better, and never less than $r = \pm.90$.

Solar Radiation

Two closely linked observations from Table I are σ_ϕ and solar radiation (SOLAR). Between the hours of 0600 and 2000, the correlation coefficient was r = +.97. The physical explanation for the high correlation is, of course, obvious; the heating of the earth by the sun's rays creates convection currents, a component of σ_ϕ. From these tabulations one may write, by the method of least squares,

$$\sigma_\phi = 9.54 \text{ SOLAR} + 5.56^o$$
$$r(\sigma_\phi, \text{ SOLAR}) = .97 \qquad (1)$$

which gives some estimate of the relative contributions of surface heating and mechanical turbulence to σ_ϕ at 110 m.

Wind and Temperature Profiles

Using the nomenclature of Pasquill (1974),

$$dS/dz = K_s \rho / F_s \qquad (2)$$

$$K_s = k u_* z / \phi_s \qquad (3)$$

where S = specific property of the atmosphere (wind, temperature, water vapor) z = height (meters), ρ = density of the atmosphere (gm/m^3), K_s = eddy diffusivity (m^2/sec), k = von Karman's coefficient (0.4), F_s = flux of S (momentum, heat, water vapor) (grams/(S) sec), ϕ_s = dimensionless flux. For the convenience, we may write the basic Monin-Obukhov profile formulation for a property S as:

$$dS/dz = S_*(z^{-1} + A) \qquad (4)$$

$$S = S_*(\ell n\ z/z_o + Az) \qquad (5)$$

The inverse length A in (4) and (5) is a multiple of the well known Monin-Obukhov length L. Assuming similarity,

$$\text{when } u = S, \quad u_*/k = S_* \qquad (6)$$

$$\text{when } \theta = S \quad \theta = S_* \qquad (7)$$

From Table I, the three constants θ_*, z_o and A can be obtained using equations (5) and (7). Unfortunately, use of the Monin-Obukhov profiles with these temperature data lead to unrealistic profiles during daytime conditions and has been abandoned. The wind data could not be directly applied to equation (5) since only two heights are reported, while three are necessary to solve the equation; therefore z_o is assumed to equal one meter.

The expressions

$$du/dz = (u_*/kz)\ \exp(Az) \qquad (8)$$

$$u = (u_*/k)(\ell n\ z + Az + (Az)^2/4 + \ldots), \qquad (9)$$

are similar to (4) and (5), but have been used to provide more realistic profiles above 30 meters. Table II lists the associated u_*'s, A's, K_{z10}'s and K_{z110}'s for each hour. K_z's were computed from (8) and (3), with $F_s = \tau$, $u_*^2 = \tau/\rho$, $K_z = K_s$

$$K_z = u_* kz/\exp(Az) \tag{10}$$

Table II shows the afternoon K_z's to be too high by an estimated factor of about 2, but the nighttime diffusivities appear reasonable.

Several additional variations of the logarithmic profile were tested without noticeable improvement. On applying a power law profile, however, results improved considerably. Strictly speaking, the power law may be expanded into a logarithmic form as shown by Deacon [4] but is seldom, if ever, considered in other than its basic form, which is written,

$$du/dz = (1-n)u_*/kz^n \tag{11}$$

$$u = (u_*/k)(z/z_1)^{1-n} \tag{12}$$

$$K_z = u_* kz_1(z/z_1)^n/(1-n) \; ; \tag{13}$$

the exponent n is to be calculated from Table 1 data, with $z_1 = 1$ meter. Columns 2 thru 4 of Table III give the diffusion parameters obtained from equations (11) thru (13). Note that K_z-values now appear reasonable throughout the day; moreover the n-values in the table are comparable to those listed by Frost[5] for a 400 ft tower.

The above values of K_z are derived quantities, and there is no absolute measure of their validity. However, some assurance may be obtained by comparing K_z with σ_ϕ. From Pasquill[6] one may obtain

$$\sigma_\phi(z) \propto K_z^{1/2}/u_z \tag{14}$$

Using the data in Tables I and III it is found that

$$\sigma_\phi = 3.01\, K_z^{1/2}/u + 3.64 \tag{15}$$

with a correlation coefficient $r(\sigma_\phi, K_z^{1/2}/u)$ equal to .985.

The equations of motion require that wind and temperature fields must be interdependent. Data from Table I clearly show the basic dependence of wind and temperatures; the method of least squares yields

$$u_{110} = .267\, \theta_{110} + 2.82 \tag{16}$$

$$r(u_{110}, A_{110}) = .952$$

$$u_{10} = .218\, \theta_{10} + 2.93 \tag{17}$$

$$r(u_{10}, \theta_{10}) = .943$$

Nevertheless, the correlation between temperature gradient and wind shear is low (r = .67). Diurnal temperature curves at the 110 and 10 m levels (Table I) are substantially in phase; the wind speed curves, however, show substantial phase difference, particularly in the morning hours. An explanation for the wind speed variation was given by Taylor[7] who showed that the variation in K_z's and departure of surface directions from the geostrophic direction produces a variation of wind speed with height. Note the weak secondary maximum in wind speed at the 110 m level at 0700 hours, followed two hours later by the overall minimum for the day. No such secondary is found at the 10 m level, consistent with Taylor's development.

Table I (with a slight correction given below) shows that, on the average, the temperature gradient even during the most unstable hours (1000-1400) is only slightly greater than adiabatic. We may infer from Dyer and Hicks[8] that, with less than a 30% error, the eddy viscosity K_m equals the eddy diffusivities of heat K_H, and K_z, so that

$$K_z \simeq K_m \simeq K_H \tag{18}$$

From similarity arguments based on dimensional analysis,

$$\theta_* = (u_*/k)(\Delta\theta/\Delta u) \tag{19}$$

$$\theta_* = -(ku_*)^{-1}(H/\rho c_p) \tag{20}$$

$$H/\rho c_p = u_*^2(\Delta\theta/\Delta u) \tag{21}$$

Over the period in question, (April-September) one might anticipate that the daily average of $H/\rho c_p$ equals zero.

The quantity $H/\rho c_p$, calculated using the values of θ_{110} and θ_{10} of Table I, differs from zero. By adjusting each hourly gradient $(\theta_{110}-\theta_{10})$ by $-0.2^{o}C$, a near zero sum of the heat flux term is achieved. This is the procedure used in calculating θ_* and $H/\rho c_p$ in Table III. The values are in good agreement with Smith's[9] estimate of the behavior of H as a function of solar radiation. The final column in Table III, net radiation, was calculated by subtracting the black body radiation derived from surface temperature from the value of the incoming solar radiation, summing the twenty-four values, and adjusting the values to achieve a zero sum.

The classic heat conduction equation

$$\partial\theta/\partial t = \partial/\partial z(K_z\ \partial\theta/\partial z) \tag{22}$$

can be combined with the vertical gradient term of the thermal wind equation,

$$du/dz = (u/\theta)(d\theta/dz) \tag{23}$$

and equations (12) and (13) to provide

$$d\theta/dt \propto (du/dz), \quad \text{when } z = z_1 \ . \tag{24}$$

Equation (24) suggests that change in surface temperature should be reflected in vertical wind gradient. Calculating from tables it is found that

$$\Delta u/\Delta z = 1.42-0.45(\Delta\theta/\Delta t) \qquad (25)$$

$$r(\Delta u/\Delta z,\ \Delta\theta/\Delta t) = -.963$$

As an exercise, the value of $K_z^{1/2}/u_{110}$ was also calculated from equations (25), (12), and (13) using only the hourly surface temperatures and hourly wind speeds at 110 m. The correlation between the resulting value and σ_ϕ was r = .90, indicating increased scatter, but the least squares line was very close to equation (15),

$$\sigma_\phi = 2.91\ (K'_z)^{1/2}/u_{110} + 3.58, \qquad (26)$$

where K'_z is the vertical thermal diffusivity calculated from hourly surface temperatures and 110 m wind speeds.

Applications

Table II provides an insight into the relative differences of the average hourly vertical eddy diffusivities. One may proceed a step further and employ the solution to the vertical diffusion equation given by Sutton[10].

$$\chi = (Qr/u/\Gamma(s))(u_1/r^2K_1x)^s \exp(-u_1z^r/r^2K_1x) \qquad (27)$$

where r = 3-2n > 0, s = (2-n)/(3-2n), and K_1 is K_z at one meter. The similarity of the equation to the Fickian or Gaussian diffusion equation is apparent. Using equations (12), (13), and (27), we may approximate the standard deviation of material in the vertical plane, σ_z, in the point source case, by

$$\sigma_z = (3-n)(k)(.5)[z_1x/(1-n)]^{0.5} \quad . \qquad (28)$$

Equations (26) and (27) apply only after very long periods of time. Thus many published experimental results would not apply directly, since their associated autocorrelation coefficients would not be zero-valued as required by the assumptions of equation (27). The values of n and K_1 were obtained from $(u_{110}-u_{10})$ which filters out the frequencies below the period of one hour. The non-dimensional wind energy spectra of Panofsky and McCormick[11] and and Gurvic[12] indicate that approximately one-fourth of the energy spectrum lies below a frequency of one hour, for the conditions given in Table I. Therefore, we may infer that equations (27) and (28) may be adjusted to the entire spectrum by multiplying by a factor of 4. Thus, we may now write

$$\sigma_z = (3-n)(k)[x/(1-n)]^{1/2} \quad . \qquad (29)$$

The σ_z's obtained from (29) can be compared to F. B. Smith's 1972 curves as summarized by Hosker[13]. It is found for example, that at 1,000 meters downwind, a n-value at 2200 hours of .624 (σ_z = 155 m), represents an E (stable) condition, and an n-value at 1100 hours of .867 (σ_z = 234 m), represents a D condition. The common assumption for average daylight conditions is usually a C condition (σ_z = 300 m), indicating that the K_z's and their derived σ_z's are close (20%) to their commonly ascribed values.

Summary

Tall tower, wind and temperature data averaged over several months are formed to follow theoretical expectations quite well. In this averaging, a relatively simplified structure of turbulence and its parameters emerges. Some residual turbulence is evident in the early morning hours as σ_ϕ remains near 5.5° as a low limit. The expected linear relationship between solar heating and the vertical component of turbulence also emerges. The Monin-Obukhov formulation, known to apply in the surface layer, does not fit the tower data as well as do the older "power law" formulations. Extending the data base in time and space to include more seasons and more sites may suggest a transition from power to M-O formulations without involving too many arbitrary constants; or it may be that these tower levels are simply too high for such an application.

Finally, the stability of these long-term average turbulence statistics is most encouraging. One may average the value over an entire season and estimate a parameter (e.g. σ_ϕ) which is descriptive of short-period turbulence fluctuations. A respectable estimate of hourly turbulence may thereby be obtained simply by incorporating the difference in hourly surface temperatures with the wind speed at one hundred meters or so, a procedure requiring a minimum investment in meteorological equipment.

Acknowledgements

This work would not have been possible without the cooperation of the Tennessee Valley Authority (TVA) in permitting access to their data. Staff of Oak Ridge National Laboratory (ORNL) were also helpful in securing and maintaining the data files. The authors are particularly grateful to Dr. T. L. Montgomery of TVA and Dr. R. J. Raridon of ORNL for their generous granting of time, data, and facilities, and to Dr. K. S. Rao of the ATDL for his help with the manuscript.

This work was performed under an agreement between the National Oceanic and Atmospheric Administration (NOAA) and the U. S. Department of Energy (DOE).

References

1. Culkowski, Walter M., and Malcolm R. Patterson. "A Comprehensive Atmospheric Transport and Diffusion Model." Rept. No. ORNL/EATC-17, 117 pp plus 2 pp Errata sheet, April 1976.

2. Pendergast, M. M., "Estimating Diffusion Coefficients from Meteorological Data." Rept. No. DP-MS-76-24. Proposed for publication in JAM.

3. Culkowski, Walter M., "An Investigation of Various Atmospheric Stability Criteria at the One-Hundred Meter Level in East Tennessee." Rept. No. 77-58.4 - 70th Annual Mtg. of APCA, Toronto, Ontario, Canada, June 1977.

4. Deacon, E. L., "Vertical Profiles of Mean Wind in the Surface Layers of the Atmosphere." Geophysical Memo., No. 91, London: Air Ministry, Meteorol. Office, 1953.

5. Frost, R., "Atmospheric Turbulence." Meteorol. Mag., 76, 14 (1947), pp. 316-338.

6. Pasquill, F., Atmospheric Diffusion - A Study of the Dispersion of Windborne Material from Industrial and Other Sources, Second Edition. John Wiley & Sons, 429 pp, 1974.

7. Taylor, G. I. "Phenomena Connected with Turbulence in the Lower Atmosphere." Proc. of the Royal Society, A., Vol. XCIV, pp. 137-55, 1917. The Scientific Papers of Sir Geoffrey Ingram Taylor, Vol. II - Meteorology, Oceanography & Turbulent Flow, G. K. Batchelor, Editor, pp. 79-95, (1960) University Press.

8. Dyer, A. J., and Hicks, B. B. "Flux-gradient Relationships in the Constant Flux Layer. "Quart. Journal Royal Met. Society, 96, 715-721.

9. Smith, F. A. "A Scheme for Estimating the Vertical Dispersion of a Plume from a Source Near Ground Level," Ch. XVII, Proc. of the Third Meeting of the Expert Panel on Air Pollution Modeling, N.A.T.O. Committee on the Challenges of Modern Society, Paris, France, Oct. 2-3, 1972. (Proceedings no. 14, Air Poll. Tech. Info. Center, U.S. E.P.A., Research Triangle Park, North Carolina, 1973).

10. Sutton, O. G. Micrometeorology - A Study of Physical Processes in the Lowest Layers of the Earth's Atmosphere. McGraw-Hill Book Company, Inc. 1953.

11. Panofsky, H. A., and McCormick, R. A. "The Spectrum of Vertical Velocity Near the Surface," Quart. Journal Royal Met. Society, 86 495. 1960.

12. Gurvic, A. A. "An Experimental Investigation of the Frequency Spectra of the Vertical Component of the Wind Velocity in the Bottom Layer of the Atmosphere," Akad. Nauk. Doklady, 132,806. 1960.

13. Hosker, Jr., R. P. "Estimates of Dry Deposition and Plume Depletion over Forests and Grassland," Rept. No. IAEA-SM-181/19 IAEA Symp. on the Physical Behavior of Radioactive Contaminants in the Atmosphere, Vienna, Austria, Nov. 1973.

Table I

Average Hourly Values Obtained from the Kingston Valley 110 m Tower April 14 - September 20, 1975

Hr	$\theta_{1.2}$	θ_{10}	θ_{110}	u_{10}	u_{110}	$\sigma_{\phi 110}$	SOLAR
1	18.67	19.23	21.37	1.22	2.94	6.0	--
2	18.27	18.74	20.84	1.14	2.66	6.9	--
3	17.94	18.38	20.42	1.10	2.54	6.3	--
4	17.68	18.06	20.06	1.13	2.58	6.7	--
5	17.42	17.76	19.74	1.13	2.60	6.3	--
6	17.19	17.49	19.36	1.17	2.62	5.9	.0051
7	17.37	17.47	19.12	1.20	2.65	6.2	.0710
8	18.25	18.10	19.19	1.27	2.46	7.4	.2315
9	19.79	19.49	19.89	1.56	2.42	10.9	.4410
10	21.66	21.16	21.26	1.86	2.58	13.6	.6476
11	23.32	22.75	22.60	2.13	2.93	14.4	.8228
12	24.62	23.95	23.82	2.38	3.25	14.6	.9238
13	25.43	24.79	24.69	2.48	3.43	14.1	.9699
14	25.88	25.37	25.34	2.63	3.65	13.8	.9194
15	26.12	25.68	25.73	2.71	3.91	12.2	.7923
16	26.09	25.68	25.73	2.79	4.17	10.9	.6420
17	25.78	25.51	25.70	2.71	4.22	9.5	.4679
18	25.03	25.06	25.38	2.51	4.19	7.8	.2718
19	24.05	24.30	24.99	1.99	3.83	6.3	.1063
20	22.46	23.11	24.36	1.66	3.72	5.5	.0179
21	21.16	21.92	23.67	1.45	3.42	5.9	--
22	20.33	21.02	23.03	1.32	3.24	5.9	--
23	19.67	20.32	22.42	1.32	3.21	6.1	--
24	19.14	19.74	21.80	1.27	3.08	5.9	--
Σ/24	21.39	21.46	22.52	1.75	3.18		

$\theta_{1.2}$ = Potential temperature at 1.2 meters (°C)
θ_{10} = Potential temperature at 10 meters (°C)
θ_{110} = Potential temperature at 100 meters (°C)
u_{10} = Wind speed at 10 meters (m/sec)
u_{110} = Wind speed at 100 meters (m/sec)
$\sigma_{\phi 110}$ = Standard deviation of vertical wind direction at 100 meters (Degrees)
SOLAR = Solar radiation (Gm Cal)/Cm^2 min)

Table II

Hourly Dispersion Parameters
Calculated from Equation 10

HR	u_*	A	K_{z10}	K_{z110}
1	.205	.0075	.762	3.96
2	.193	.0061	.728	4.35
3	.185	.0059	.700	4.27
4	.191	.0055	.723	4.59
5	.192	.0055	.728	4.62
6	.199	.0046	.760	5.28
7	.205	.0038	.790	5.94
8	.222	-.0026	.911	13.00
9	.293	-.0176	1.40	89.35
10	.357	-.0228	1.80	193.12
11	.409	-.0230	2.06	225.71
12	.454	-.0229	2.27	246.61
13	.475	-.0228	2.39	256.57
14	.506	-.0228	2.54	273.17
15	.514	-.0210	2.54	227.84
16	.527	-.0194	2.56	195.77
17	.508	-.0171	2.40	146.16
18	.460	-.0127	2.09	81.82
19	.350	-.0032	1.45	21.89
20	.281	.0047	1.07	7.38
21	.245	.0067	.915	5.15
22	.221	.0083	.813	3.90
23	.221	.0080	.816	4.03
24	.212	.0080	.782	3.87

Table III

Diffusion Parameters Calculated Using Power Law Profiles

HR	u_*	n	K_{z10}	K_{z110}	θ_*(a)	$H/\rho C_p$	Net Rad
1	.210	.633	.98	4.48	.591	-.050	-.330
2	.204	.648	1.03	4.87	.636	-.052	-.327
3	.196	.650	1.00	4.75	.625	-.049	-.324
4	.204	.654	1.01	4.80	.628	-.051	-.323
5	.204	.654	1.07	5.11	.619	-.051	-.321
6	.215	.663	1.18	5.76	.615	-.053	-.315
7	.225	.670	1.28	8.35	.562	-.051	-.250
8	.267	.723	2.04	11.55	.495	-.053	-.097
9	.411	.818	5.94	42.21	.242	-.040	.100
10	.544	.864	11.69	92.80	-.189	.041	.290
11	.628	.867	13.90	111.19	-.687	.173	.453
12	.692	.866	15.18	121.10	-.642	.182	.542
13	.724	.864	15.58	123.67	-.572	.166	.581
14	.769	.864	16.46	130.01	-.434	.133	.526
15	.762	.847	14.01	106.81	-.238	.073	.398
16	.760	.833	12.38	91.29	-.193	.059	.247
17	.709	.815	10.01	70.65	-.012	.003	.077
18	.612	.786	7.00	46.05	.109	-.027	-.112
19	.425	.727	3.32	18.99	.283	-.048	-.271
20	.304	.662	1.65	8.08	.386	-.047	-.344
21	.254	.641	1.24	5.75	.499	-.051	-.351
22	.222	.624	.99	4.43	.511	-.045	-.344
23	.224	.628	1.02	4.60	.559	-.050	-.339
24	.216	.629	.99	4.47	.554	-.048	-.334

(a) after $\theta_{110}-\theta_{10}$ was reduced by 0.2°C each hour

H = heat flux
ρ = density of air
C_p = specific heat of air at constant pressure

Table IV

Correlations and Least Squares Fits Among Several Variables
Obtained by Hourly Averaging

Variables	Correlation Coefficient	Least Squares
σ_ϕ, $K_z^{1/2}/u_{110}$	.985	$\sigma_\phi = 3.01(K_{z110})^{1/2}/u + 3.64$
σ_ϕ, Net Radiation	.983	$\sigma_\phi = 9.53$ Net R + 9.18
σ_ϕ, Solar Radiation	.972	$\sigma_\phi = 9.54$ Solar + 5.56
θ_{110}, u_{110}(1 HR Lag)	.969	$\theta_{110} = 3.82\ u_{110} + 10.35$
$\Delta u/\Delta z$, $\Delta\theta/\Delta t$	-.963	$\Delta u/\Delta z = 1.42-0.45(\Delta\theta/\Delta t)$
θ_*, Net Radiation	-.961	$\theta_* = 0.144 - 1.27$(Net Radiation)
n, Net Radiation	.953	n = 0.269(Net Radiation) + .747
θ_{110}, u_{110}	.952	$\theta_{110} = .375\ u_{110} + 10.58$
θ_{10}, u_{10}	.943	$\theta_{10} = 4.58\ u_{10} + 13.43$
n, σ_ϕ	.942	$n = 0.0275\ \sigma_\phi + 0.495$
u_*, n	.934	$u_* = 2.18\ n - 1.18$
σ_ϕ, $H/\rho C_p$	.933	$\sigma_\phi = 0.379\ H/\rho C_p + 0.86$
u_*, θ_*	-.922	$u_* = -0.460\theta_* + 0.511$
u_*, Net Radiation	.900	$u_* = 0.594$ Net Radiation + 0.45
$K_z(\Delta\theta,\Delta t,U)^{1/2}/u$, σ_ϕ	.902	$\sigma_\phi = 2.91(K_z^{1/2}/u_{110}) + 3.58$
$\Delta u/\Delta z$, $\Delta\theta/\Delta z$	.67	

NOAA Technical Memorandum ERL ARL-72

WORKSHOP ON LONG-RANGE TRAJECTORY-PUFF AND PLUME MODELING OF CONTINUOUS POINT SOURCE EMISSIONS

C. J. Nappo, Jr.

Atmospheric Turbulence and Diffusion Laboratory
Oak Ridge, Tennessee

Air Resources Laboratories
Silver Spring, Maryland
July 1978

ATDL Contribution File No. 78/2

UNITED STATES
DEPARTMENT OF COMMERCE
Juanita M. Kreps, Secretary

NATIONAL OCEANIC AND
ATMOSPHERIC ADMINISTRATION
Richard A. Frank, Administrator

Environmental Research
Laboratories
Wilmot N. Hess, Director

CONTENTS

WORKSHOP ON LONG-RANGE TRAJECTORY-PUFF AND PLUME MODELING OF CONTINUOUS POINT SOURCE EMISSIONS

C. J. Nappo, Jr.

Abstract. Differences in thought exist concerning the computer modeling of long-range transport and diffusion of pollutants from continuous point sources. The differences pertain to the treatment of plumes as continuous or as a series of discrete diffusing puffs. For example, the physics governing the spread of a plume and a puff are different and it is not clear that one can use the mathematics of one process to simulate the physics of the other. Puff modelers argue that the use of puffs expedites the parameterization of removal processes and affords instantaneous realizations of the plume geometry. Furthermore, the use of the integrated plume equation fails to show the meandering of the plume by the large eddies, and since these eddies constitute the primary diffusion mechanism on the regional and synoptic scale, their simulation is quite important. Critics of this approach argue that tracking of many puffs throughout a region is computationally inefficient and unnecessary.

In an attempt to clarify these and other questions, resolve some of the misunderstandings, and provide an opportunity for a free exchange of ideas and opinions, a small workshop was held on 26-27 January 1977 at the Atmospheric Turbulence and Diffusion Laboratory, Oak Ridge, Tennessee. This report summarizes the speaker's presentations and the open discussion periods of the workshop.

1. INTRODUCTION

A workshop on the use of puffs and plumes in modeling long-range transport and diffusion of pollutants from point sources was held at NOAA's Air Resources Atmospheric Turbulence and Diffusion Laboratory, Oak Ridge, Tennessee on 26-27 January 1977. The purpose of the workshop was to identify the problems and resolve some of the misunderstandings surrounding the modeling of emissions from point sources out to mesoscale distances using either continuous plumes or a series of discrete diffusing puffs.

Invited participants[1] included modelers, model users and theoreticians. Government and private research laboratories as well as regulatory agencies were represented. The workshop format consisted of brief presentations followed by open and informal discussions. In this report, summaries of both the speaker's presentations and the discussion periods are presented.

2. SUMMARY OF THE TALK BY G. E. START

Fundamental aspects of the modeling problem that must be addressed by any kind of model used are:

(1) A description of the magnitude of exposure due to the airborne material including ground deposition.

(2) A correct prediction of the area of coverage.

(3) An accurate prediction of where the material goes.

(4) The correct prediction of the duration of exposure.

In making judgments of the accuracy for model prediction, one must consider the air analysis techniques used in obtaining verification data. For example, if the uncertainty in the observations is as great as the variance among model predictions, one should use the cheapest or simplest model. In many cases, one is not interested in predicting the exposure to individual people but rather the impact on a large area or population. These predictions are often in the form of statistical inferences on exposure, i.e., what percent of the population will be exposed to so much radiation which may result in such a percent of cancer tumors. Such predictions do not require high details in the model. Hence, one must keep in mind the details of a model and how it achieves its effects and the problem to be solved which is usually determined by other people besides the modelers.

The types of problems that face modelers extend from the long term or chronic exposure to the very short term or episodic impact of air pollution. The nature of the problem will determine which type of model (plume, puff, windrose) to use. One approach to the long range problem is the use of long term climatological models which have time scales

[1]Attendees were A. Bass, F. A. Gifford, J. L. Heffter, R. A. Kornasiewicz, R. Lange, R. A. Lott, F. J. Ludwig, E. H. Markee Jr., B. D. Murphy, C. J. Nappo Jr., D. W. Pepper, D. C. Powell, C-M Sheih, G. Start, A. D. Taylor, and V. Sharma.

from week to years and distances extending from 25 ~ 50 miles to 500 ~ 1000 miles from the point of release. The premise of these simple models is that random errors or deviations will cancel out as averaging times increase or for long dispersion times. Unfortunately, if the errors are not truly random, then there will be a systematic bias in the answers such as in the case of a preferred wind direction. These considerations have lead to the analysis of windrose models and trajectory-rose models using the MESODIF model (Start & Wendell 1974). In the real world, stability category and dilution rate can change with travel time and if these changes are not allowed in a model, one ends up with a biased result. If initial wind speeds and directions are held constant, as in the simple model, one ends up neglecting the situation where stagnation or curved effluent plumes can occur.

It was felt in the early work that attempting to account for plume dispersion by applying statistical adjustments to a plume axis was not desirable and there was little justification for doing so. Instead, it was decided to break the plume down into a number of chunks or plume segments. When using these plume segments a question concerning time step size must be answered. For example, if a plume segment does not completely pass over a receptor, how does one calculate the dose at the receptor? One way is to apply to the receptor all the dose in the segment. One may, however, wish to partition the dose according to what percent of the segment passed over the receptor. Another way is to eject from the source small pulses of mass as puffs. These puffs would contain the same mass as a plume segment; however, they would be instantly created.

When facing a modeling situation, one must first determine what is going to be calculated and the time scale of the calculation. If the time scales are sufficiently large so that certain effects will cancel out, one can use a simple model. However, if one is faced with a short time scale the simple model cannot be used.

The discussion is concluded by illustrating the difference between a plume axis which is a streak line and the path of a plume element which is the trajectory of the elements center. Streak lines and trajectories are identical only in a steady-state wind field.

3. SUMMARY OF THE TALK BY C-M SHEIH

The central issues concerning the use of puffs for modeling long-range transport and diffusion are:

(1) Why use a puff model?

(2) The theoretical bases for the puff models.

(3) The need for partitioning of diffusion.

(4) Models which might offer some of the solutions.

(1) It is obvious that puff models provide much more flexibility than plume models. For example, a plume model cannot handle the situation where there is a sharp curve or kink in the wind field. In such a case, the use of puffs is more likely to generate the correct concentration distribution. Another reason for using puffs is that they offer the best way of treating plume rise, multiple inversion layers and time dependent mixing heights. Another advantage of using puffs over plumes is the treatment of the calm wind case. In such cases, along-wind diffusion may be greater than advection and the plume formula will be incorrect. The criterion concerning the relative importance of along-wind diffusion is

$$U \frac{\partial C}{\partial X} \leq \frac{\partial}{\partial X} \left(K \frac{\partial C}{\partial X}\right)$$

where U is the wind speed, C is a pollutant concentration, X the along-wind direction, and K is the eddy diffusion coefficient. Now making use of mass continuity and assuming an incompressible flow, the above can be written as

$$\frac{\partial}{\partial X} \left(U - \frac{K}{C} \frac{\partial C}{\partial X}\right) C \leq 0.$$

In this form, $\frac{K}{C} \frac{\partial C}{\partial X}$ is usually defined as a diffusion velocity while U is called the advection velocity. We see that alongwind diffusion must be accounted for whenever the diffusion velocity is greater than the advection velocity.

(2) The theoretical basis for the puff model is that the puff model can be integrated into the plume model. Because plume models have been accepted as correct, one should calibrate a puff model against the plume model. An example of this calibration is found in the case of determining the proper spacing between puffs so as to achieve the most economically smooth distribution of material. By selecting a case with near-uniform and near-steady winds, one runs the puff model with increasing spacings between puffs until a distribution similar to the plume model is achieved.

(3) The motion of a puff center is produced by the action of the measured mean wind field. The growth of the puff size is due to diffusion of the turbulence with scales smaller than the puff. This is usually done in terms of the puff spreading parameters σ_y and σ_z. The

partitioning of the atmospheric kinetic energy into turbulence spreading and puff or plume meandering is justified as a consequence of the spectral gap. However, the correct parameterization of this partitioning must be yet determined for regional scale problems.

(4) For regional-scale long-term problems, the statistical trajectory models may be best (e.g., Sheih, 1977). For the short-term problem, the puff-trajectory model is good (e.g., Start and Wendell, 1974). Note that the puff-trajectory model is to the statistical trajectory model as a signel puff is to a plume, i.e. the statistical trajectory model is obtained from the ensemble averaging of many puff trajections.

4. SUMMARY OF THE TALK BY D. C. POWELL

In using σ_y values in puff models which are measured from plume dispersion experiments, the meandering of the plume is included in the measurements, if the sampling time is long enough. Therefore, if these values are used in conjunction with a puff or plume model which includes the effects of meandering, the effects of meandering may be included twice. If this is the case, the σ_y values now in use may be too large.

As has been mentioned before, meandering and spreading are often viewed as independent processes. An important question regarding this assumption is when does the meandering of the wind, or mesoscale turbulence, dominate over local turbulence diffusion which affects the spreading of a puff? It was shown that predicting concentrations over a sampling grid with a cell size of about (34 km) using 3-dimensional Gaussian puffs with $\sigma_x = \sigma_y$ is equivalent to doing the calculations with a moving element of fixed horizontal spread if enough time is allowed. This is because the transport motions of the puffs have a greater impact on the long time average concentration patterns than the local spreading of each puff. This effect is especially true on a large or regional scale. In this case, use of a segmented plume model with running times of one month or more will distribute material such that errors in σ_y will cancel, if the sampling interval is on the order of an hour. Another statement of the same idea is that the running time should be roughly three orders of magnitude greater than the sampling time if errors in σ_y may be expected to cancel. However, a bias in σ_y would bias the calculated average concentrations of a long time assessment if the probability density function of wind direction in the data is quasi-discontinuous. Such discontinuity will be a true reflection of nature if the wind is channeled into some preferred direction by local terrain features. It will occur in the data without occurring in nature if the wind directions are arbitrarily discretized to certain points on the compass and the location of sampling points is likewise discretized. However, in the basic model we are developing, we are assuming that over most of the northeastern multistate region neither of these effects is important. Rather, we believe it is more pertinent to focus on the

likelihood that the predicted average concentrations may be biased due to over-simplification or inaccurate parameterization in modeling one of the following:

(1) mixed layer depth behavior

(2) transformation rate of SO_2 to sulfate

(3) dry and wet deposition of SO_2 and of sulfate

5. OPEN DISCUSSIONS (MORNING, 26 JANUARY)

In a discussion on chemical reactions, especially $SO_2 \rightarrow SO_4$, F. A. Gifford pointed out the importance of knowing the physical volume or space through which reactions are taking place and the relative speed of reaction and diffusion. What the meteorology should be able to tell is how big is the space within which chemical reactions are taking place. In this regard, the plume approach should be most successful since it gives the volume in a straightforward way.

An observation made by F. A. Gifford is that there appears to be several kinds of models which have their own utility, and which model is to be used depends upon the problem.

G. Start makes the observation that when considering a problem such as chemistry, rainout, etc., always choose the most simple meteorological model that will do the job. One does not want a complicated meteorological model competing for CPU time with the real problem which may be chemistry. One must then choose the simplest model that will do the job needed for the problem.

6. SUMMARY OF TALK BY F. A. GIFFORD

This discussion presents some very elementary aspects of plume modeling. Pasquill shows that there are three ways of predicting the concentrations at a point, K-theory, statistical theory and similarity theory. Excluded in this discussion are second and higher order closure schemes.

Statistical theory tells us that for single particle diffusion

$$\sigma_y \sim \begin{cases} t & t \ll t_\ell \\ t^{\frac{1}{2}} & t \gg \tau_\ell \end{cases}$$

where τ_ℓ is the Lagrangian time scale. These results follow from Taylor's theory for the case of homogeneous turbulence for long sampling times. For relative or two-particle diffusion we have

$$\sigma_y \sim \begin{cases} t \\ t^{3/2} \\ t^{1/2} \end{cases}$$

The asymptotic state for long times is the result that the two particles will have drifted so far apart that they can be considered as individual particles.

In K-theory for very large times, K is constant. By very large times is meant $t \gg \tau_\ell$. When this isn't true, the behavior of K is a very complex function of space and time. In general it is not known how to specify K. K is Eulerian, e.g. it is related to space attached quantities and can be related reasonably to the turbulent structure of the boundary layer.

The problem in statistical theory is to find the dependence of mean concentration distributions on various planetary boundary layer flow parameters when these parameters are set together with the spatial variables and summarized in terms of the Monin-Obukhov length L. In this method, however, one gets more dimensionless ratios then one knows how to deal with. A very precise theory is obtained but it is very inflexible as to the type of sources. As a result, for example, there is no solution from similarity theory for the single point source. Similarity solutions are also very difficult to extend upward into the PBL because specific forces such as Coriolis forces are not explicitly contained in the theory. Such forces enter the theory by way of dimensionless parameters such as the surface Rossby number. Similarity theory can, on the other hand, reproduce the standard type of diffusion observed fairly well out to distances of hundreds of meters.

The question that brought this meeting together is, how does one model diffusion from isolated sources? Frankiel (1957) envisioned air pollution in Los Angeles by modeling using curved trajectories and assumed typical Gaussian puff elements using the argument that along-wind advection outweights along-wind diffusion. These plume elements were generated by assuming a spreading disk or bologna slice model.

In order to handle the distinction between meandering and spreading, the fluctuating plume model was developed. In this model, the plume is deformed in the usual way and the disk elements are allowed to fluctuate. The statistics of the sum of the actions of spreading and meandering were investigated under the assumption of homogeneous turbulence and Gaussian distributions of turbulence statistics. This is a perfectly acceptable way to proceed in this analysis. The net result of this type of spreading and meandering under these conditions can be shown to be equal to precisely the Taylor term for single particle

dispersions. Another fact is that a gap in the spectrum is not necessary to produce a meandering plume type formula. One can still develop a model for the statistical description of meandering plus spreading. What modelers are attempting to do is calculate the meandering of plume elements and supply, through some theory or a combination of theory and observations, a spreading factor. This situation is much more complicated than that involved in the meandering plume formulation. This is because it is difficult to determine what is the mean and instantaneous winds when one only has a single measurement. We only can know the plume path as determined by wind observations to a resolution as fine as that of the wind resolution. Whatever is the physical situation, there are definite limits to the details of the resolution.

Some concerns about the puff models are:

(1) If one is calculating using instantaneous puffs then one must use instantaneous σ's (although this is not a very strong factor).

(2) People are saying that a puff model is necessary because plume paths accelerate and a puff model is necessary to describe this.

(3) If one is going to use a puff model on theoretical considerations one ought to be prepared to deal with the situation in which puffs are not going to look nice and circular but rather quite peculiar. This is especially true when looking at the near field. However, many modelers use puffs because the calculations are quite efficient if one assumes $\sigma_y = \sigma_x$ and this gives symmetrical puffs in which case it is easy to simulate right angle turns in the flow. It appears that this does not have to be assumed and that a segmented plume model will work just as well.

7. SUMMARY OF TALK BY F. L. LUDWIG

When using a puff model, one must generate puffs, move them around, change their dimensions, calculate concentrations and get rid of them. In generating puffs, attention must be paid to the spacing of the puffs so that in the case of uniform winds, the plume equation results. Experimental results show that puffs should be generated on an equal-space rather than on equal-time spacing, with a maximum spacing of $\Delta X \tilde{\sim} 2\sigma_H$ where ΔX is the sampling grid cell size and σ_H is the horizontal standard deviations of the puff.

The use of puffs over plumes is required when considering non-steady conditions. The use of spherical puffs over segmented plumes comes as an expedient. It seems to be the most straightforward approach to the problem at hand. The use of puffs enables one to model any situation whereas the plume formula or segmented plume model requires some special conditions. In short, it's easier to move puffs around rather than segmented plumes.

Regarding the time resolution of the wind field, it is shown that when one has a source oriented problem and has certain specific things to look for, such as areas of maximum concentration, constant winds of 15-minute duration are adequate. These times are related in some way to the box size.

8. SUMMARY OF TALK BY R. LANGE

A review was given of some of the transport modeling being done at L.L.L. as well as a description of the ADPIC model and a few examples of its application. In ADPIC whether a puff or plume formalism is used depends upon the length of the release time. For release times shorter than 1 hour, a puff is assumed, and for longer release times a plume is assumed. The great advantage of the PIC method is that each particle is tagged and has a memory, and deposition, chemistry, etc. become easy to handle.

Because advection rates are hourly in ADPIC, the description of a plume is correct if σ values are taken from the Pasquill-Gifford curves. However, after the hour a new plume axis is defined and it is assumed that this is the proper way to handle the meandering problem.

9. OPEN DISCUSSION (AFTERNOON, 26 JANUARY)

In answer to a question on the justification of breaking down the distribution of continuous particle releases (plume) into discrete puffs or elements of material, it was pointed out by Albion Taylor that in the case of linear partial differential equations, Green's functions can be used to model a continuous distribution by using discrete elements.

Frank Gifford pointed out that many people use puffs and advance these puff models as cases of applications of Taylor's statistical theory. In about all cases of models, it appears that use is made of the statistical predictions for homogeneous turbulence since these are easily used and represent the only judgments that have thus far been made concerning diffusion in the atmosphere. Modelers taking the puff form of this theory and advecting puffs out along streak lines, assume they are generating an equivalent plume. This can be done, but one must be aware that the Gaussian puff model as conceived by Sutton and Frenkiel does not refer to an instantaneous release of marked particles. What it does refer to is the ensemble average of many such releases with respect to some fixed coordinate axis. One can use these statistical treatments in another sense, but one must then justify this use. So far this justification has not appeared, and the Green's function approach does not stand as a justification.

Brian Murphy pointed out that a puff has a σ_y and the puff follows the instantaneous wind vector while a plume follow the mean wind. The whole problem is that part of the atmosphere must be defined as a mean transport wind and part must be defined as turbulence. The problem is how to make these definitions in the proper physical way.

Another problem is deciding how to use the sigmas. For a long range problem, the sigmas, which are defined from observations less than an hour and more like 3 minutes, must be applied to plume or puff diffusion on time scales small when compared to the transport times. This diffusion process can be thought of as a kind of subgrid scale parameterization - subgrid in time.

A problem that Frank Gifford sees is the proper specification of σ_x. It is not obvious that one can assume $\sigma_x = \sigma_y$ and physical observations of σ_x do not appear to have been made. It may be argued that since in the limit of many puffs the true plume is approached, the along-wind diffusion cancels out and hence the specification of σ_x is not important. However, when the limiting number of puffs necessary for this to be true is not reached, i.e. when there are not many puffs - what can be said about the non-importance of σ_x. In these cases, the specification of σ_x may be extremely important.

Frank Gifford asked the question, at what distance can diffusion be neglected and only the trajectory need be considered? It is assumed that when material is uniformly distributed throughout the boundary layer, the material can be identified with an air mass and the path of this air mass is what needs to be determined. Nick Heffter answered this question by describing the results of a single long-range verification experiment. It was found that if one allows a puff (or plume) to continue to expand, eventually everything smears out and one has real problems in growth and over estimations of the concentration. At some point, something goes on and this point is estimated to be around 4 or 5 days. Beyond these times, one gets utter nonsense by letting the material still expand.

Frank Gifford points out that at some distance downwind, the motions of a plume across a receptor as a result of the hourly variation of the wind field will be much stronger than the plume diffusion. C-M Shieh points out that the sampling time at the receptor determines the magnitude of this effect.

Gene Start spoke of a study to compare the results of a MESODIF type model against weekly air samples taken in the area. While the data was not all good, one result was that with say on the order of 168 trajectories or so, it didn't matter too much what kind of day or night conditions these trajectories were initiated under, the single best correlation of the variations of the environmental sampling was "yes" or "no". That is whether or not a trajectory passed over a receptor.

Obviously, if such a distance or travel time existed where and when advection dominates over diffusion, the necessary calculation will be much simpler. The time resolution of the wind field must somehow restrict how the diffusion is used.

These arguments lead again to the question of how one separates diffusion from the transport or meandering. Gene Start discussed the results from a study by Sagendorff (1974) which dealt with diffusion under low windspeed conditions out to about 400 M over flat terrains in Idaho. Under low wind speed inversion conditions, one can imagine the plume would go in any number of directions so that after a time of about 1 hour one would achieve a total integration at a number of samplers set out in an array. About a dozen tests were made. The simplest approach taken was that

$$\sigma^2_{total} = \sigma^2_M + \sigma^2_T$$

where σ^2_M = mean variance based over all end to end 2-minute time periods within that hour time period, and σ^2_T = variance of the 2-minute mean wind distribution. A substantial amount of bivane data was collected and sampled and one of the things looked at was σ_M. The results of this study were that one could probably describe a short term dispersion of the chunk of plume by σ_T spreading and the meandering of the plume by σ_M and if these were close to a Gaussian function one could get a good estimate of the total σ_y. This is the main part of the paper.

Dividing σ_{total} into σ_M and σ_T enables one to describe these in terms of local and mean conditions. For example, σ_T is felt to be due to stability, surface roughness, etc. while σ_M is (or may be) a function of terrain, windspeed or synoptic situation. σ_T controls plume spreading about the plume axis while σ_M controls plume meandering.

10. OPEN DISCUSSION (MORNING, 27 JANUARY)

Art Bass opened the discussion period by bringing up the subject of nonlinear chemistry. An important application is the study of sulfate on inter-state scales. It is not obvious that non-linear chemistry can be done in the context of a puff model where the concentration at a given point is the result of the linear superposition of several puffs. In this case, the concentration is due to the simple sum of the contributions of many puffs. Frank Gifford suggests that the shape or form of a plume element is not important, as regards chemistry, but the volume of the element is important. One must get at the essential physical facts of the problem; one must ask if there is a volume that can be characterized by a state of the turbulence and diffusion length as a function of space and time.

Brian Murphy pointed out that the complicated models are quite difficult to work with when the need for quick answers arises. This is almost always the case in the private sector or for regulatory studies. Perhaps these complicated models should be run and the results parameterized into simpler models.

Frank Gifford pointed out that the thing to remember in all chemistry models is the difference between the time scales governing diffusion and the time scales of the chemical reactions. In these cases, the physical scales of the problem are going to be governed by the time scale. For example if chemical changes are occurring on a time scale of 0.1 sec and one is interested in these reactions, then one must have an extremely small grid in order to keep track of the material and its changes. On the other hand, one can choose to parameterize these fairly rapid reactions. It is hoped that some kind of lumped reaction scheme will turn up and can be parameterized by some kind of fairly slow time scale say characterized by the turbulence diffusion.

Sumnar Barr makes what he calls a minority report. In trying to sum up it seems to him as though the conversation went like, "one can construct plume-like behavior out of sequences of puffs in an asymptotic approximation, but the asymptote seems to be made up of a few puffs so that one can get plume-like behavior from collections of from 6 to 10 puffs." The question that comes to mind is, is there something that puffs do that plumes cannot do? It appears that in the non-steady case, the puff formulation is best in defining the plume. There are times when 180° wind shifts occur on the synoptic scale and one also sees 180° wind shifts in the West on a diurnal cycle. Therefore, these extreme cases are not unusual and cannot be ignored. For example, at Four Corners it is a daily occurrence. These conditions must be able to be accounted for in any application work. So there may be a role when the expense of running a puff or trajectory model is necessary.

11. SUMMARY OF TALK BY J. L. HEFFTER

This discussion is concerned with the use of puffs and plumes in a regional to continental scale trajectory model. In such an effort, many practical problems are present concerning the use of puffs and plumes and limited resolution of the wind field. The regional-continental scale transport and dispersion model under study has been described by Heffter et. al. (1975). Portions of the model were later revised (Heffter and Ferber, 1977) to include:

(1) Vertical temperature profiles along a trajectory to determine a mixing layer in which average transport winds are calculated.

(2) Time interpolation of the winds to provide additional data at the four daily observation times.

(3) A better estimate of long-term average concentrations based on the equation where the effluent plume is represented by a series of diffusing puffs rather than the continuous plume equation.

Effluent transport and dispersion are calculated in the following way.

A trajectory, composed of 3-hour segments, is computed assuming time centered persistence of winds. The winds are averaged in a transport layer determined from vertical temperature profiles. After the trajectories have been determined, diffusion calculations are made. It is assumed that there is one puff for each trajectory and that a puff diffuses as it is transported along the trajectory path.

Concentrations can be calculated over a regional area using either puff or plume concepts. The equations are:

$$C_{puff} = \frac{Q}{2\pi Z_m \sigma_h^2} e^{-R^2/2\sigma_h^2} \qquad (1)$$

$$C_{plume} = \frac{Q'}{(2\pi)^{\frac{1}{2}} Z_m \sigma_y \bar{u}} e^{-y^2/2\sigma_y^2} \qquad (2)$$

C = air concentration in the mixed layer

Q = emission amount per puff

Q' = emission rate

Z_m = height of the mixed layer

σ_h = horizontal standard deviation

σ_y = lateral standard deviation

$\bar{u}$ = mean wind speed

R = distance from puff center

y = lateral distance from trajectory

The plume equation (Eq. 2) is derived from the puff equation (Eq. 1) and is applicable, ideally, in a non-variant wind field (where a representative mean wind $\bar{u}$ exists). In reality, especially over regional scales, representative winds that can be used in the plume equation become difficult to define. It is, therefore, assumed that the better estimate of concentration is made using the puff equation, where $\bar{u}$ does not appear, so an assumption about its value is not required.

Heffter described some initial results of a study to compare the differences in using puff and plume formulations. Average surface air concentrations were calculated over the eastern U.S. for January 1977 with a hypothetical source at the Savannah River Plant, South Carolina. In the plume equation, $\bar{u}$ was determined at the source (for the first 3-hour trajectory segment) and held constant for the remainder of segments that comprise a 5-day trajectory. With $\bar{u}$ so defined, the plume equation gave concentrations 5 to 10 times greater than the puff equation at large distances from the source, i.e. New York and the New England states. If, however, $\bar{u}$ was defined for each 3-hour trajectory segment along the trajectory, the results at large distances were greatly improved relative to the puff equation, but close to the source the plume equation concentrations were about twice as great as the puff equation concentrations. Of course, these results apply to the very limited case presented here. A more extensive climatological study is necessary to make general statements about the choice of $\bar{u}$.

Heffter concludes by pointing out that in his judgment, the puff formula is preferable for the regional scale. On the mesoscale, the choice of equations may not be as clear-cut. The puff equation still should be preferable but the differences between puff and plume concepts are probably more subtle and certainly need further investigation similar to that presented here.

12. REFERENCES

Frenkiel, F. N. (1957): Atmospheric Pollution in Growing Communities, Smithsonian Report for 1956, pp. 269-299.

Heffter, J. L., A. D. Taylor, and G. J. Ferber (1975): A Regional-Continental Scale Transport, Diffusion, and Deposition Model, NOAA Technical Memo. ERL ARL-50, Air Resources Laboratories, Silver Spring, MD, 29 pp.

Heffter, J. L., and G. J. Ferber (1977): Development and Verification of the ARL Regional-Continental Transport and Dispersion Model, Preprint - Joint Conference on Applications of Air Pollution Meteorology, Salt Lake City, Utah, pp. 400-407.

Holzworth, G. C. (1972): Mixing Heights, Wind Speeds, and Potential for Urban Air Pollution Throughout the Contiguous U.S., Environmental Protection Agency, Research Triangle Park, NC, pp. 31-35.

Sagendorff, J. F., and C. R. Dickson (1974): Diffusion under low wind speed inversion conditions. NOAA Tech. Memo. ERL ARL-52, U.S. Dept. of Commerce.

Sheih, C. M. (1977): Application of a statistical trajectory model to the simulation of sulfur pollution over Northeastern United States. Atmos. Environ., 11, pp. 173-178.

Start, G. E., and L. L. Wendell (1974): Regional effluent dispersion calculations considering spatial and temporal meteorological variations. NOAA Tech. Memo. ERL ARL-44, U.S. Dept. of Commerce.

COOLING TOWER

ENVIRONMENT - 1978

Proceedings of a Symposium at the

Center of Adult Education, University of Maryland

May 2-4, 1978

A SIMPLE DRIFT DEPOSITION MODEL APPLIED TO THE CHALK POINT DYE TRACER EXPERIMENT

Steven R. Hanna

Sponsored by

POWER PLANT SITING PROGRAM
MARYLAND DEPARTMENT OF NATURAL RESOURCES

and

WATER RESOURCES RESEARCH CENTER
UNIVERSITY OF MARYLAND

in Cooperation With

THE APPLIED PHYSICS LABORATORY
THE JOHNS HOPKINS UNIVERSITY

ELECTRIC POWER RESEARCH INSTITUTE

U.S. DEPARTMENT OF ENERGY

POTOMAC ELECTRIC POWER COMPANY

U.S. ENVIRONMENTAL PROTECTION AGENCY

U.S. DEPARTMENT OF THE INTERIOR

at

The Center of Adult Education

UNIVERSITY OF MARYLAND
COLLEGE PARK, MARYLAND 20742

Co-Chairmen, Richard S. Nietubicz, Power Plant Siting Program
R. Lamar Green, Water Resources Research Center

Published by the Water Resources Research Center, University of Maryland supported in part by funds under PL88-379 as amended and administered by the Office of Water Research and Technology, U.S. Department of the Interior as a contribution to its mission of information dissemination and technology transfer.

ATDL Contribution File No. 78/3

A SIMPLE DRIFT DEPOSITION MODEL APPLIED TO THE CHALK POINT DYE TRACER EXPERIMENT

Steven R. Hanna
Air Resources
Atmospheric Turbulence and Diffusion Laboratory
National Oceanic and Atmospheric Administration
Oak Ridge, Tennessee

ABSTRACT

The Chalk Point Dye Tracer Experiment, conducted during the night of 16-17 June 1977, provided accurate measurements of Na drift deposition at the ground due to emissions from the cooling tower. Meyer and Stanbro (1977a) measured Na deposition over a 30° arc on the ground at distances of .5 km and 1.0 km from the tower to be 1080 and 330 kg/km^2 mo, respectively. Mass median drop diameters on the two arcs were 340 μm and 260 μm, respectively. The necessary cooling tower and atmospheric parameters that must be used in the application of a drift deposition model were also measured.

Drift drop evaporation can be neglected in a model of drift deposition applied to this experiment, because the ambient relative humidity was 90% or greater from the surface up through plume height. The plume trajectory is calculated by the usual 2/3 law. The fraction of drift in each drop size class which breaks away from the plume in each downwind distance increment Δx is assumed to equal v_d $(\Delta x/u)/2R$, where v_d is the fall velocity of the drops, R is plume radius, and u is wind speed. A straight ballistic trajectory is then used to calculate the point at which the drops in a given class, released from a given Δx interval, strike the ground. Based on the observed wind meandering, an arc width of 30° is chosen for the pie-shaped deposition pattern. The calculated Na deposition rate is 3600 kg/mo km^2 at x = .5 km, and 800 kg/mo km^2 at x = 1 km, or about a factor of three greater than the observed Na deposition rate. Predicted mass median drop diameters on the two arcs are 470 μm and 290 μm, respectively, which are within 50% of the observed values.

1. Introduction

The Chalk Point Dye Tracer Experiment, which took place during the night of 16-17 June 1977, is described in reports by Meyer and Stanbro (1977a and b), Meyer and Jenkins (1977), and Environmental Systems Corporation (1977). The resulting drift deposition data are the best to be obtained by any group so far, and provide a good opportunity for the testing of drift deposition models.

The experiment was conducted in response to the need to know the relative contributions of the cooling tower and the scrubbed stack plume to ground level drift deposition. As Pell (1974) explains, the neighbors of the Chalk Point steam plant are concerned about the effects of brackish water sprayed from the tower and stack onto their agricultural crops. After investigating several possible tracers that could be used to tag the cooling tower water, Meyer and Stanbro (1977a and b) settled on pink Rhodamine dye. The dye's only drawback is that it decomposes in the presence of sunlight, and so the experiment had to take place at night.

The relevant cooling tower source parameters were measured by Environmental Systems Corporation (ESC) (1977) during the experiment, and ambient vertical profiles of temperature, relative humidity, and wind speed and direction were measured by Meyer and Stanbro (1977a). Drift deposition at the ground out to distances of 1 km from the tower was observed by the two groups independently.

2. The Drift Deposition Model.

Because this experiment took place during humid, nighttime conditions, the model can be greatly simplified by assuming that no evaporation takes place. Consequently the complicated formulas for estimating drop evaporation (Hanna, 1974) can be neglected. The drop fall velocities, v_d, for drops of various diameters are listed in Table 1. (from Engelmann, 1968, p 212).

The height of the centerline of the plume, z, above the cooling tower is assumed to increase according to the "two-thirds law" for buoyant plumes (Briggs, 1975):

$$z = 1.6\ F^{1/3}\ x^{2/3}\ /\ u \quad , \qquad (1)$$

where x is downwind distance, u is wind speed, and the initial buoyancy flux F is defined by:

$$F = (g/T_{vp})(T_{vp} - T_{ve})\ w_o\ R_o^2 \quad . \qquad (2)$$

In this formula g is the acceleration of gravity, w_o and R_o are initial plume vertical speed and radius, T_v is virtual temperature, and subscripts p and e refer to intial plume and environment. The virtual temperature

equals the actual temperature times (1 + 0.61 q), where q is the specific humidity. A "top hat" distribution of temperature across the plume is assumed. To assure that the plume radius approaches the initial radius, R_o, as height z and distance x approach zero, the radius is assumed to vary according to the formula

$$R = R_o + 0.5\ z \quad . \tag{3}$$

Thus the lower boundary, $z_{p\ell}$, of the plume is given by

$$z_{p\ell} = z - R = 0.5\ z - R_o \quad . \tag{4}$$

Accurate determination of the lower boundary is important because it provides the height at which the drift drop breaks away from the plume.

Table 1

Fall Velocities v_d for Distilled Water Drops in Stagnant Air at 20°C, 760 mm, and 50% Relative Humidity (Engelmann, 1968)

Drop Diameter (μm)	v_d (m/s)	Drop Diameter (μm)	v_d (m/s)
100	.27	1200	4.64
200	.72	1400	5.17
300	1.17	1600	5.65
400	1.62	1800	6.09
500	2.06	2000	6.49
600	2.47	2200	6.90
700	2.87	2400	7.27
800	3.27	2600	7.57
900	3.67	2800	7.82
1000	4.03	3000	8.06

All the drift drops of a given size class are assumed to fall with speed v_d with respect to the plume axis. Usually the drops are divided into about 10 to 30 drop size classes, each covering a range of tens of μm in the small sizes and hundreds of μm in the large sizes (e.g. one class could be for drops with diameters between 130 μm and 150 μm). Calculations are made for the drop diameter in the middle of the class. Since it is assumed that the drops are initially distributed uniformly across the plume, then some fraction of the drops in each class are going to fall out or break away from the plume as the plume moves downwind. The fraction f of drift in each class which breaks away from the plume in each downwind increment Δx is assumed to equal

$$f = \frac{v_d(\Delta x/u)}{2R} \quad . \qquad (5)$$

The numerator, $v_d(\Delta x/u)$, is the distance that the drop with a diameter in the middle of that class will fall as the plume traverses the distance Δx (equivalent to the time $\Delta x/u$), and the denominator is the plume diameter, averaged over the interval Δx. This concept is illustrated in Figure 1, where the solid line is the main plume boundary and the dashed line is the plume boundary for drift drops of a given class. Note that the distance the drops fall in an increment Δx is constant with x, but the plume diameter continues to grow as the plume drifts downwind.

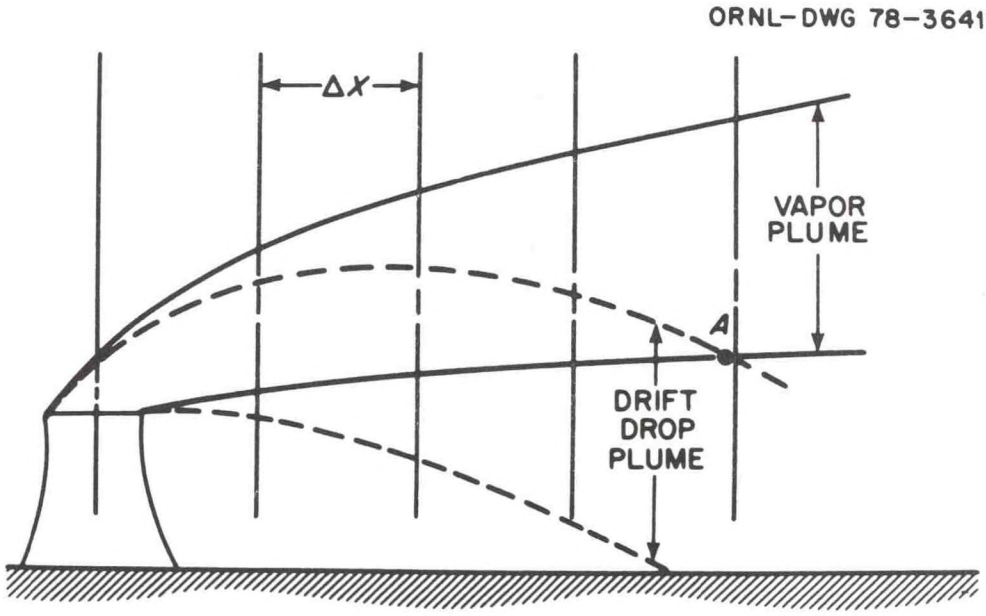

Figure 1: Schematic diagram of the method by which drops break away from the plume. The outline of the drop plume for a given droplet class is shown. The point "A" is where the last drop of this class breaks away from the plume.

Consequently the fraction f is greatest for the increment Δx closest to the tower. At point A on the figure all the drift in that class has dropped out of the plume and the sum of the f's for the Δx increments up to that point will be unity. It is important to set f equal to zero beyond the point A, at which $\Sigma f=1$. A set of f's is calculated for each drop size interval. This technique for removing drops from the plume is similar to a technique developed by Simpson and Wiggert (1969) for drop fallout from precipitating cumulus towers.

In the next step, a ballistic trajectory is calculated for drops with diameters in the middle of each class originating at the lower boundary of the plume, $z_{p\ell}$, at the upwind and downwind boundaries of each Δx interval. In most applications at natural drift cooling towers it is convenient to set Δx equal to 100 m. If the wind speed is constant in the boundary layer, beneath the plume, then the drop strikes the ground a downwind distance $u\, z_{p\ell}/v_d$ from the point it breaks away from the plume. If we know that the mass flux of drift drops is M_j(g/sec) for a certain drop class, that the fraction f_{ij} of this flux breaks away from the plume in an interval x_i to $x_i + \Delta x$ from the tower, and that these drops travel a distance x_{ij1} from position x_i and x_{ij2} from position $x_i + \Delta x$ before striking the ground, then the ground deposition of drift D_{ij} ($g/m^2 s$), in drop class j, at distances from $x_i + x_{ij1}$ to $x_i + \Delta x + x_{ij2}$ from the tower is

$$D_{ij} = M_j f_{ij} / \left\{\theta \left((x_i + \Delta x + x_{ij2})^2 - (x_i + x_{ij1})^2\right)\right\}, \quad (6)$$

where θ is the angular spread (in radians) of the plume over the derived sampling time. This angle can be obtained from measurements of wind direction variability during the experiment, or could be roughly approximated by the ratio 2R/x. It is assumed that deposition is uniform within the angle θ.

Generally we are interested in deposition at a point on the ground located at a given downwind distance x_s from the tower. The contributions D_{ij} from the different drop size classes j and distance increments Δx_i are added only if the location of the sampler x_s is between the distances $x_i + x_{ij1}$ and $x_i + \Delta x + x_{ij2}$. Thus there is at most only one increment Δx_i for each drop size class j that contributes to drift deposition at any given sampling location.

In concluding the discussion of the model, it must be stressed that, if the ambient relative humidity is much less than about 90%, then the effects of droplet evaporation must be included (Hanna, 1974). The basic model framework discussed above will still be applicable.

3. The Chalk Point Dye Tracer Experiment.

During the evening of 16 June 1977, 30 gallons of 20% Rhodamine WT (fluorescent) dye were added to the cooling tower basin water, and makeup and blowdown valves were closed (Meyer and Stanbro, 1977a and b). Consequently the only loss of dye was through drift loss, and the concentration of dye in the water remained nearly constant for the duration

of the test (2200 EST 16 June to 0230 EST 17 June). The plant load remained nearly constant (about 630 Mw) while the experiment was underway.

3.1 Initial Cooling Tower Parameters.

Environmental Systems Corporation (ESC, 1977) monitored conditions at the cooling tower mouth during the experiment. Plume temperature was 308.6°K, implying a virtual temperature, T_{vp}, of 315.3°K. Plume vertical speed was 4.5 m/s. The radius of the tower mouth, R_o, and height of the tower above the ground, h_s, are known to be 27.4 m and 124 m, respectively (Pell, 1974). Since the ambient temperature was 293° K and the ambient air was saturated, the virtual ambient temperature, T_{ve}, was 295.3°K. Consequently the buoyancy flux, F, equals 2100 m^4/s^3 (from eq. (2)).

The total flux of sodium from the tower was measured by ESC to be 1.86 g/s. The fraction of this mass carried by drift drops in various classes is given in Table 2. It is seen from the table that most of the drift mass is carried by the smaller drops. However, the larger drops settle much faster and will be shown to contribute more to drift deposition at distances on the order of one kilometer from the tower.

Table 2

Fraction of Mass Flux Carried by Drops in the Indicated Range (ESC, 1977) During the Chalk Point Dye Tracer Experiment

Diameter Range (μm)	$\frac{\Delta \text{ flux}}{\text{total}}$	Diameter Range (μm)	$\frac{\Delta \text{ flux}}{\text{total}}$
10-30	.138	350-400	.0095
30-50	.288	400-450	.0071
50-70	.134	450-500	.0060
70-90	.089	500-600	.0080
90-110	.062	600-700	.0080
110-130	.042	700-800	.0092
130-150	.034	800-900	.0084
150-180	.038	900-1000	.0071
180-210	.030	1000-1100	.0055
210-240	.023	1100-1200	.0042
240-270	.017	1200-1300	.0013
270-300	.013	1300-1400	.00064
300-350	.014		

3.2 Ambient Meteorological Measurements.

Radiosonde profiles of temperature, relative humidity, and wind speed and direction measured by Johns Hopkins University Applied Physics Laboratory (Meyer and Jenkins, 1977) near the beginning, middle, and end of the experiment are shown in Figures 2 to 5. The lowest 200 m of the profiles is of the most interest to the drift deposition model. In this layer the relative humidity averages about 93%, the temperature profile is nearly isothermal with a mean value of about 20°C, and the wind direction has a mean value of about 180° (excluding the anomalous reading at the surface at 0031 EST), with fluctuations of about 30°. The wind speed profile suggests two layers: above 100 m, the wind speed is nearly constant with height, averaging about 8 m/s; below 100m, the wind speed is nearly linear with height. The mean value in this layer, however, is about 5 m/s. The plume itself will be in the upper layer, while the drift drops must fall through the lower layer before depositing on the ground.

3.3 Drift Deposition Measurements.

Meyer and Stanbro (1977a) placed instruments to measure drift deposition at 5° intervals on 35° arcs at distances of 0.5 and 1.0 km from the cooling tower. The axis of the sampling arcs was oriented along a direction towards 350°, which fortunately corresponded to the direction of the plume axis during the experiment. In addition, Environmental Systems Corporation (1977) measured drift deposition at one station one fourth kilometer upwind of the tower and at four stations ranging from .25 to .70 km downwind of the tower. Since the ESC measurements agreed fairly well with the measurements by Meyer and Stanbro (1977a), only the measurements by Meyer and Stanbro will be plotted here. Furthermore, only the deposition marked by the tracer from the cooling tower will be plotted, since we are not including the contribution from the stack scrubber in our model calculations. At 0.5 km distance, the stack scrubber contributed less than 20% to the total drift on the 35° arc, while at 1.0 km distance, the stack scrubber contributed almost half of the total drift. The contribution of the cooling towers to sodium deposition on the 0.5 and 1.0 km arcs are given in Figures 6 and 7. In order to make comparisons with the results of the drift model, the average deposition over a 35° arc is given as a dashed line. The average sodium deposition on the 0.5 and 1.0 km arcs is 1080 and 360 kg/km^2 mo, respectively.

If the average sodium deposition rate is 10^3 kg/km^2 mo over a pie shaped area with radius 1 km and angular width 30°, then the total deposition over the region of drift measurements is .093 g/s, which is 5% of the total sodium emitted by the tower.

Meyer and Stanbro (1977a) also measured the drift drop sizes at the measurement stations, finding a mass medium drop diameter of 340 and 260 μm on the 0.5 and 1.0 km, arcs, respectively. Most of the drop sizes were between 250 and 450 μm on the 0.5 km arc and 200 and 400 μm on the 1.0 km arc.

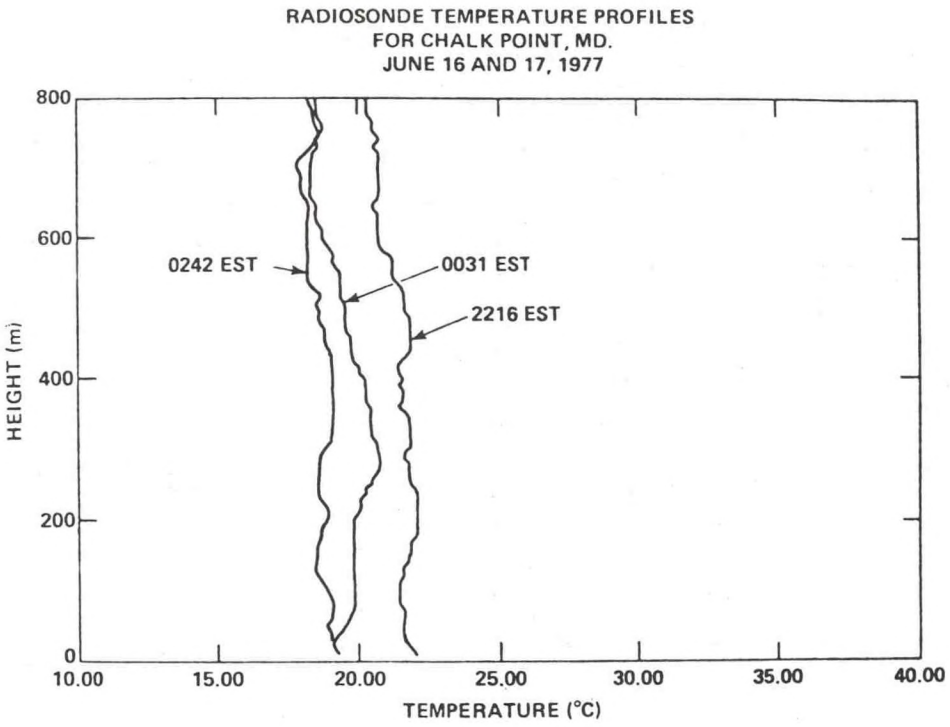

Figure 2: Temperature profile. (from Meyer and Stanbro, 1977a)

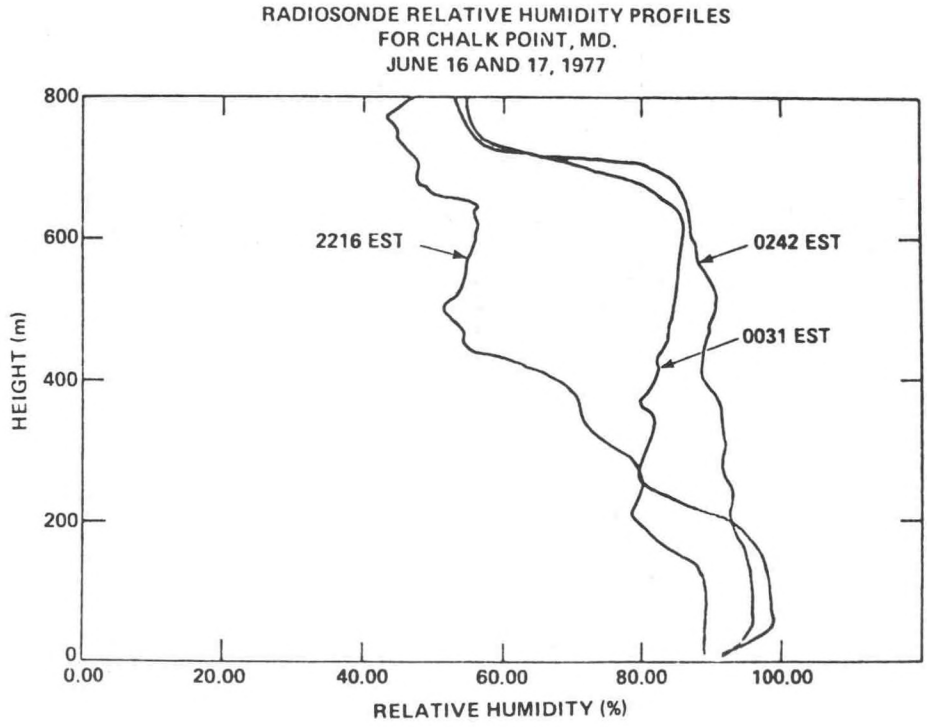

Figure 3: Relative humidity profile (from Meyer and Stanbro, 1977a).

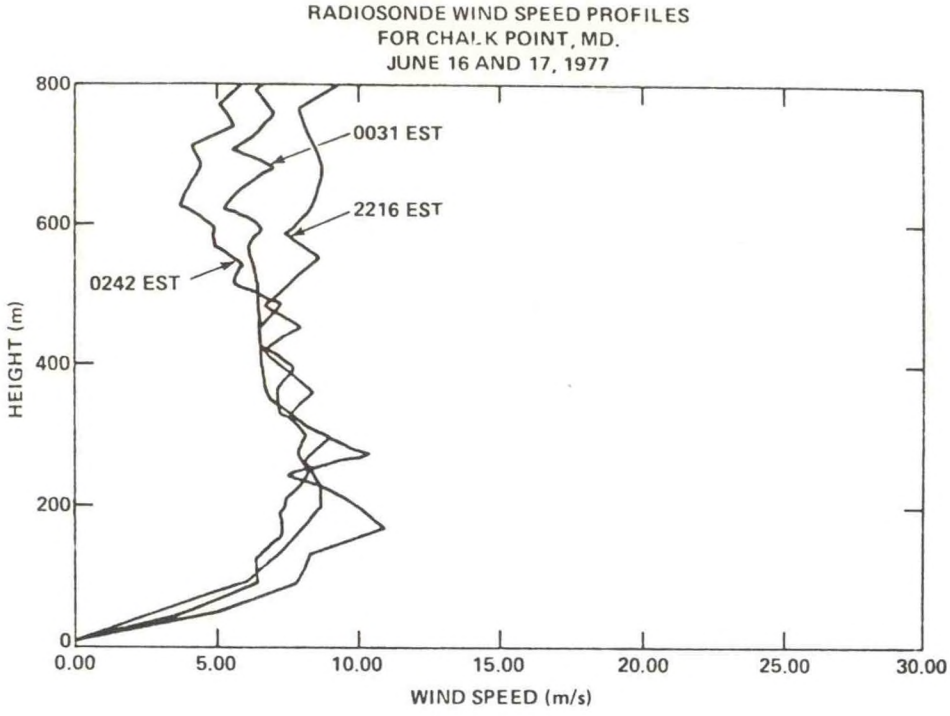

Figure 4: Wind speed profile (from Meyer and Stanbro, 1977a).

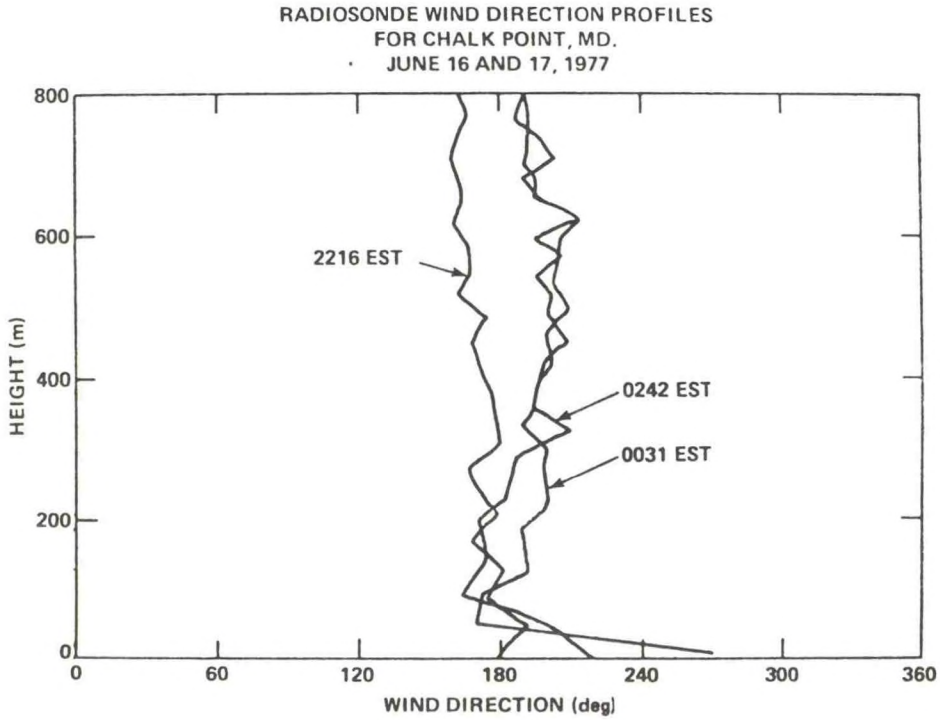

Figure 5: Wind direction profile (from Meyer and Stanbro, 1977a).

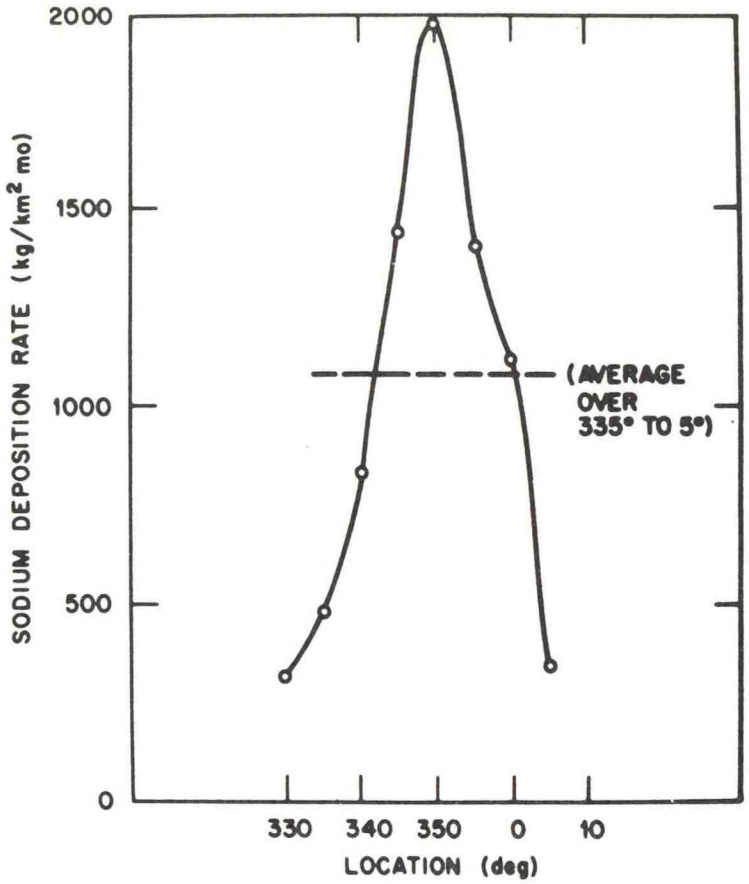

Figure 6: Distribution of observed sodium deposition rate 0.5 km from the Chalk Point Cooling Tower during the Dye Tracer Experiment (from Meyer and Stanbro, 1977a). The average over the arc (dashed line) is 1080 kg/km^2 mo.

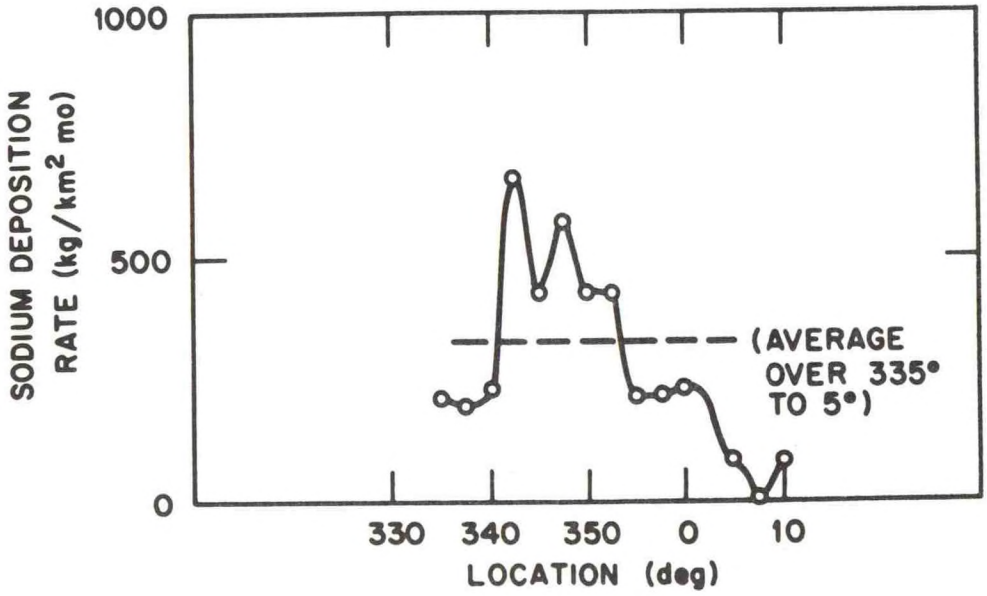

Figure 7: Distribution of observed sodium deposition rate 1.0 km from the Chalk Point Cooling Tower during the Dye Tracer Experiment (from Meyer and Stanbro, 1977a). The average over the arc (dashed line) is 330 kg/km^2 mo.

4. Model Predictions of Drift Deposition.

The plume centerline height predictions made using eq. (1) with buoyancy flux F equal to 2100 m^4/s^3 and wind speed u equal to 8 m/s are within 10 m of the observations by ESC (1977) for the downwind distance range (50 m to 200 m) covered by the observations (see Figure 8). Apparently the error arising from our neglect of the additional rise due to the momentum flux in the plume rise equation is balanced by the error arising from our neglect of a decrease in rise due to downwash.

A quick calculation shows that a 100 μm drop falling from a height of 100 m in a 5 m/s crosswind will travel 2 km before striking the ground, and a 200 μm drop in the same conditions will travel 0.7 km. This height is approximately the lowest limit of the height of the bottom of the plume above the ground. Therefore the drift drops with diameters less than about 150 μm can be neglected when calculating drift deposition at distances 0.5 and 1.0 km from the cooling tower. It is interesting to note from Table 2 that these smaller drops carry about 68% of the drift mass.

For ease in calculations, the drift drop spectra in Table 2 are combined to form 11 drift drop classes for drops with diameters between 150 μm and 1400 μm, as shown in Table 3. The increment of downwind distance Δx used is equal to 100 m. The average wind speed in the layer through which the drops are falling is assumed to be 5 m/s. Using

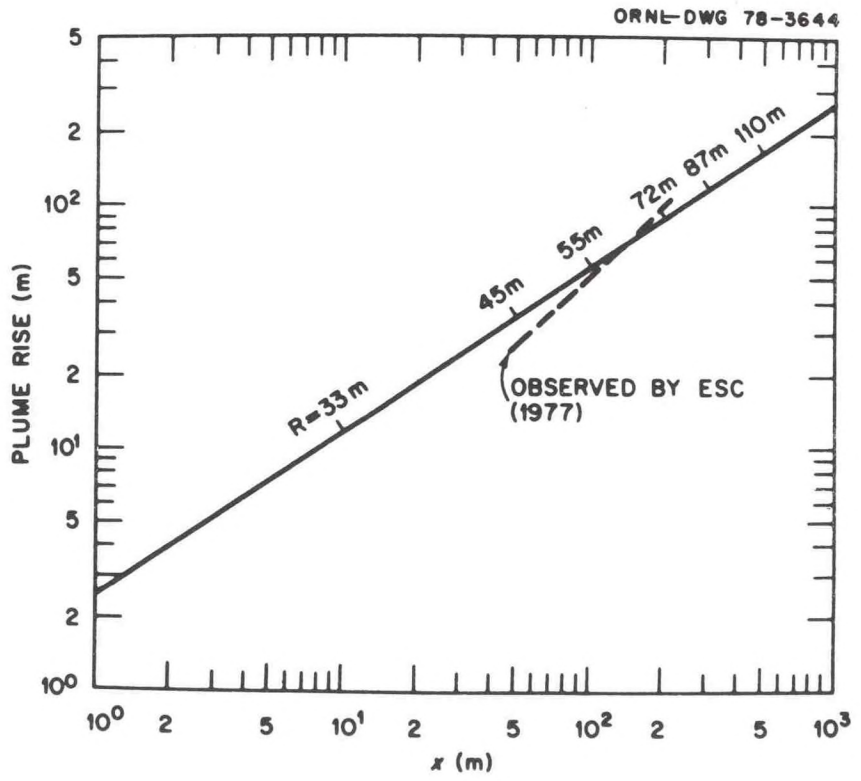

Figure 8: Predicted and observed cooling tower plume centerline trajectory during the Dye Tracer Experiment (Plume Rise = 1.6 $F^{1/3}$ $x^{2/3}/u$, where F = 2100 m^4/s^3 and u = 8 m/s. Values of the predicted plume radius, $R = R_o + 5z$, are indicated along the trajectory.

Table 3

Drift Drop Classes Used in Model Calculations (Adapted from Table 2) and Estimated Breakaway Points

Class j	Drop Diameter Range (μm)	Representative Diameter (μm)	Δ flux / total	All drops Breakaway by Distance A (m)	Breakaway Interval to Strike 0.5 km arc x_{ij1}(m) x_{ij2}(m)	Breakaway Interval to Strike 1.0 km arc x_{ij1}(m) x_{ij2}(m)
1	150 - 240	200	.091	>800	(All drops here strike ground beyond x = 0.5 km)	100 200
2	240 - 350	300	.044	>800		300 400
3	350 - 450	400	.016	800	100 200	400 500
4	450 - 550	500	.012	600	100 200	500 600
5	550 - 650	600	.010	500	200 300	(All drops here strike ground before x = 1.0 km)
6	650 - 750	700	.0095	400	200 300	
7	750 - 850	800	.0089	300	200 300	
8	850 - 950	900	.0079	300	200 300	
9	950 -1050	1000	.0064	200	(All drops here strike ground before x = 0.5 km)	
10	1050 -1300	1200	.0083	200		
11	>1300	1400	.00064	200		

the procedure outlined in detail in section 2, the average drift deposition over a 30° arc at distances of 0.5 and 1.0 km from the tower is calculated to be about 3600 and 1000 kg/km^{2}mo, respectively. These calculations take about one half day using a slide rule. The predicted mass median drift drop diameters are 470 and 290 μm, respectively. Thus this simple untuned model simulates the observed drift deposition within a factor of three and simulates the observed mass median drift drop diameters within 40%. With tuning and adjustments to the assumed parameters, the model could probably be made much more accurate. However, more independent drift experiments are necessary before this can be done.

5. Conclusion

This exercise shows that it is possible to use a simplified drift deposition model during humid conditions to satisfactorily predict drift deposition. The data obtained during the Dye Tracer Experiment are excellent and unique, and it is hoped that further experiments in this series can be made.

Acknowledgement

The cooperation of J. Meyer of the JohnsHopkins University Applied Physics Laboratory in making data available before publication is greatly appreciated. This research is conducted under an agreement between the National Oceanic and Atmospheric Administration (NOAA) and the U.S. Department of Energy (USDOE).

References

Briggs, G. A., 1975: Plume rise predictions, in Lectures on Air Pollution and Environmental Impact Analysis, D. Haugen, ed. American Meteorological Society, 45 Beacon St., Boston, MA 02108, 59-111.

Engelmann, R. J., 1968: The calculation of precipitation scavenging. Meteorology and Atomic Energy - 1968, NTIS, U.S. Dept. of Commerce, Springfield, VA 22151, 208-220

Environmental Systems Corporation, 1977: Cooling Tower Drift Dye Tracer Experiment. PPSP-CPCTP, prepared for Maryland Power Plant Siting Program by ESC, Knoxville, TN, 103 pp.

Hanna, S. R., 1974: Fog and drift deposition from evaporative cooling towers. Nuclear Safety, 15, 190-196.

Meyer, J. H. and W. R. Jenkins, 1977: Cooling Tower Drift Dye Tracer Experiment Surface Weather and Ambient Atmospheric Profile Data June 16 and 17, 1977. PPSP-CPCTP-16, Vol. 3, prepared for Maryland Power Plant Siting Program by The Johns Hopkins Univ. Applied Physics Lab., Laurel, MD 20810, 102 pp.

Meyer, J. H. and W. D. Stanbro, 1977a: Cooling Tower Drift Dye Tracer Experiment June 16 and 17, 1977. PPSP-CPCTP-16, Vol. 2, prepared for Maryland Power Plant Siting Program by the Johns Hopkins Univ. Applied Physics Lab ., Laurel, MD 20810, 102 pp.

Meyer, J. H. and W. D. Stanbro, 1977b: Florescent dye, a novel technique to trace cooling tower drift. Presented at 4th Joint Confer. on Sensing Environ. Pollutants, Nov. 6-11, 1977, New Orleans, available from the Johns Hopkins Univ. Applied Physics Lab., Laurel, MD 20810, 6 pp.

Pell, J., 1974: The Chalk Point Cooling Tower Project, Cooling Tower Environment - 1974 (S. Hanna and J. Pell, eds.). CONF-740302, NTIS, U.S. Dept. of Commerce, Springfield, VA 22161, 88-127.

Simpson, J. and V. Wiggert, 1969: Models of precipitating cumulus towers. Mon. Wea. Rev., 97, 471-479.

NOAA Technical Memorandum ERL ARL-71

THE EASTERN TENNESSEE TRAJECTORY EXPERIMENT (ETTEX): DESCRIPTION AND DATA SUMMARY

C. J. Nappo, Jr.
R. P. Hosker
S. R. Hanna

Atmospheric Turbulence and Diffusion Laboratory
Oak Ridge, Tennessee

Air Resources Laboratories
Silver Spring, Maryland
September 1978

UNITED STATES DEPARTMENT OF COMMERCE
Juanita M. Kreps, Secretary

NATIONAL OCEANIC AND ATMOSPHERIC ADMINISTRATION
Richard A. Frank, Administrator

Environmental Research Laboratories
Wilmot N. Hess, Director

ATDL Contribution File No. 78/4

CONTENTS

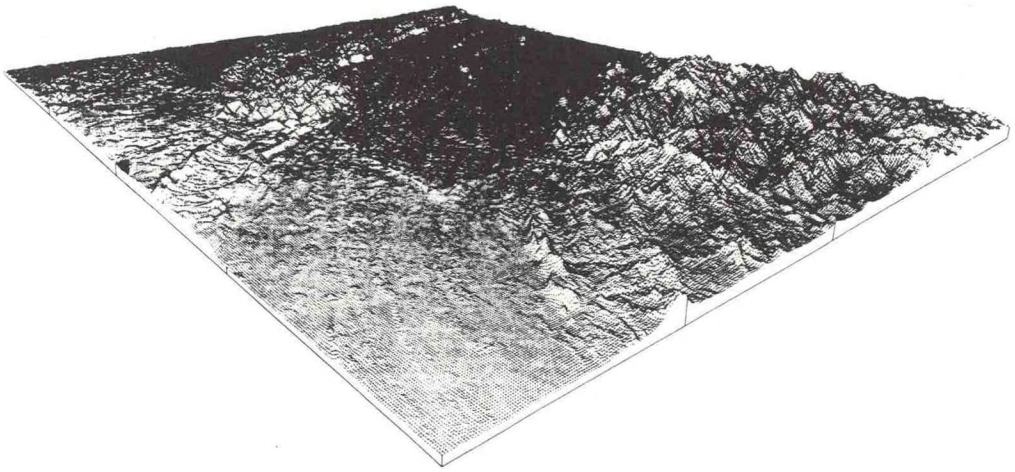

Frontipiece. *Computer-drawn projection of the east Tennessee River valley, site of the ETTEX program. View is from the vicinity of Chattanooga, TN, looking north-east toward the Bristol-Johnson City-Kingsport, TN. region.*

THE EASTERN TENNESSEE TRAJECTORY EXPERIMENT (ETTEX): DESCRIPTION AND DATA SUMMARY

C. J. Nappo, Jr., R. P. Hosker, and S. R. Hanna

Data from the Eastern Tennessee Trajectory Experiment (ETTEX) conducted during July and August, 1974, are presented. These data, taken from several separate experiments, consist of single and double theodolite pilot balloon wind observations, radar-observed trajectories of tetroons released serially or in pairs, time-dependent mesoscale wind field observations, surface and tower meteorological observations, radiosonde observations, and synoptic summaries for the ETTEX region for selected days. Included also is a collection to date of the studies made based on the ETTEX data.

PART I

THE EXPERIMENT

1. INTRODUCTION

Knowledge of atmospheric motions within the planetary boundary layer (PBL) over horizontal scales of 10 to 100 km, especially over complex terrain is quite deficient. This information is essential, however, if atmospheric transport and diffusion processes on these scales are to be understood and their effects accurately parameterized. For example, NOAA's Air Resources Atmospheric Turbulence and Diffusion Laboratory (ATDL) has recently attempted to estimate regional transport and diffusion from nuclear reactors and fossil fuel power plants in the Tennessee River Valley, from lead smelters in Missouri, and from a proposed power park in Louisiana. At present, only rather crude guesses can be made about the probable air motions and diffusion coefficients over such relatively large regions, particularly if the underlying topography is rather complex.

While interest in regional-scale transport and diffusion, especially over complex terrain, continues to grow, the majority of the work recently done is of a theoretical nature supported by limited observational data. These studies, for example those by Mullen, et al. (1977), Kao and Taylor (1977), and Lantz, et al. (1976), consist mostly of adapting existing theoretical models of diffusion over uniform terrain to the complex terrain case. The observational data used in these studies consist mostly of tracer gas and smoke releases with ground sampling and, usually, very sparse meteorological data. Examples of these observational studies are seen in Start, et al. (1974), Roffman, et al. (1976), and Wilson, et al. (1976). While acceptable assumptions can often be made concerning transport and diffusion (or, equivalently, PBL air motions) over uniform terrain, thus reducing the requirement for detailed observations, no such assumptions can be made for the complex terrain case. An observation program becomes essential in this instance.

For adequate verification of transport and diffusion models, one must simultaneously observe the three-dimensional mesoscale wind field and resultant air parcel trajectories. Previous observations of mesoscale wind fields have done one, but not both of these. For example, wind field observations have been made by Bornstein (1968), Ackerman (1973, 1974) and Karl (1976) near urban areas, by Wendell (1970, 1972) over open country, and by Egami, et al. (1974) and Kao, et al. (1974) over fairly rough terrain. These experiments obtained the wind field either from surface stations or from pilot balloon (pibal) ascents; however, air parcel trajectories were not explicitly measured. Over flat terrain it may be possible to construct fairly realistic trajectories from limited measurements of the regional wind field (e.g., Wendell, 1970, 1972), but it has not been demonstrated that this

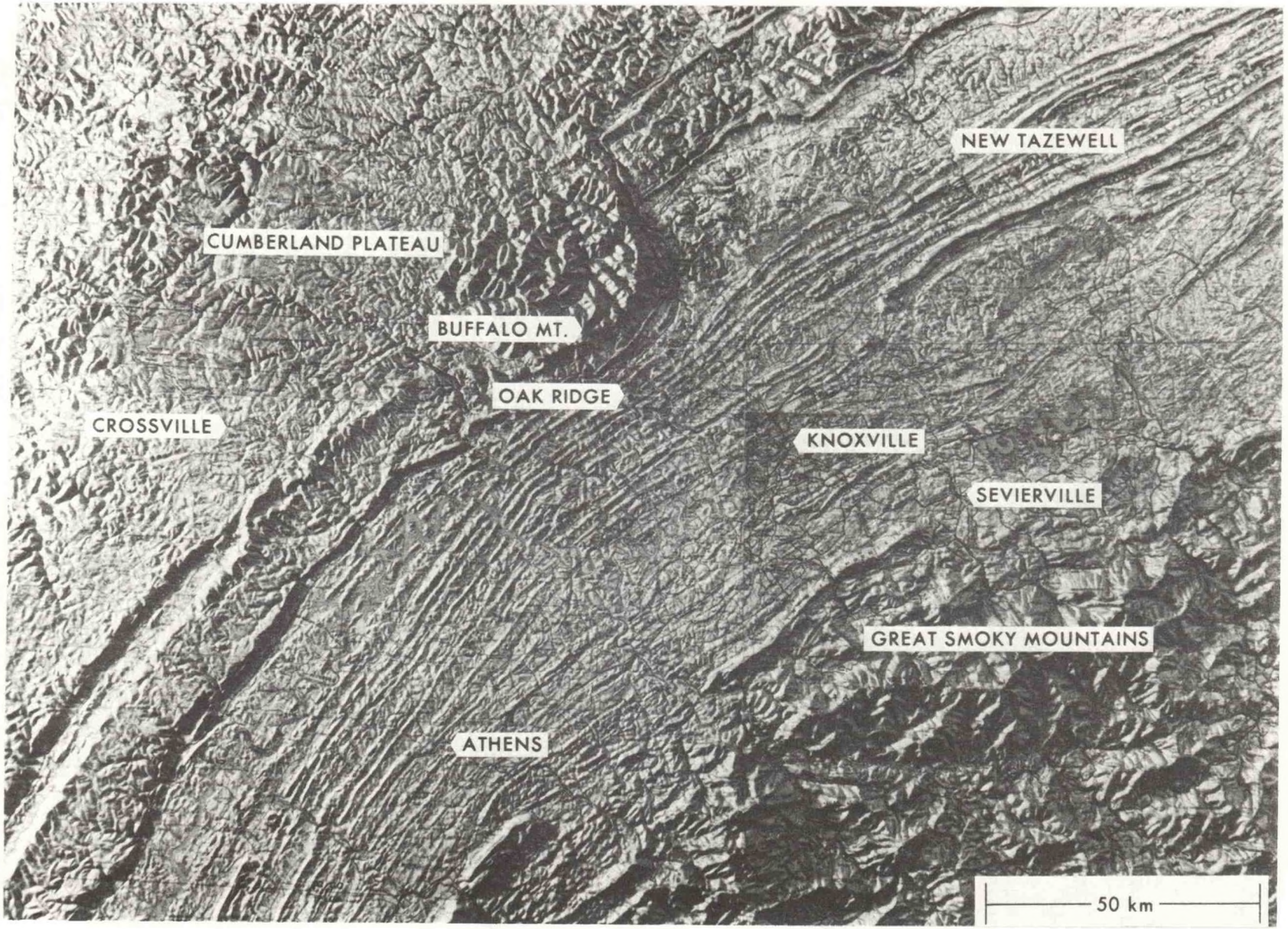

Figure 1. Topography of ETTEX Region.

is feasible over rough terrain. Similarly, observations of the trajectories of "tagged" air parcels have been reported by numerous authors including Angell, et al. (1971, 1973), Hass, et al. (1967), Leahey and Hicklin (1973) and Leahey and Rowe (1974). In almost all cases, the three-dimensional wind field was not determined.

The Eastern Tennessee Trajectory Experiment (ETTEX) represents a first attempt to simultaneously observe the meteorological parameters required to develop techniques for verifying atmospheric transport and diffusion models, as well as studying the dynamics of the PBL, over the fairly rugged terrain of the eastern Tennessee River Valley.

2. THE ETTEX REGION

The ETTEX region is depicted in Figure 1, which as been reproduced from a vertically exaggerated relief map. The valley of the Tennessee River lies generally along a southwest-northeast line which splits the southern Appalachian Range into the Great Smoky Mountains on the southeast and the Cumberland Plateau on the northwest and west. In the Oak Ridge-Knoxville area, which is more or less the center of the ETTEX region, the valley floor has a mean elevation of about 300 m MSL, is about 70 km wide, has relatively steep walls and is corrugated with parallel broken ridges approximately 75 m to 100 m in height. The valley floor descends from the northeast to the southwest. The average height of the Cumberland Mountains immediately north of Oak Ridge is about 1000 m MSL, while that of the Great Smoky Mountains is about 2000 m MSL. Figure 2 shows elevation contours, in meters above sea level, for roughly the same area as shown in Figure 1. Elevations were estimated from topographic maps and represent average values over 10 km square areas.

3. THE EXPERIMENTS

During the period of 15 July - 8 August, 1974, three more or less independent mesoscale experiments were conducted. These were the trajectory, relative diffusion, and convective diffusion experiments.

3.1 The Trajectory Experiment

The trajectory experiment was designed to provide the data necessary to determine the accuracy of air parcel trajectory calculations over complex terrain for different atmospheric stabilities. Such determinations require three-dimensional wind field observations, measured trajectories of "tagged" air parcels, and measurements of the PBL thermal structure.

To provide such data, a network of pibal stations was set up (Figure 3), roughly centered about a radar unit loaned by NOAA's ARL Field Research Laboratory of Idaho Falls, Idaho. Each station's wind profile was envisioned as being, for computational purposes, more or less representative of the winds within a 50 km radius of that station. The station locations were chosen to provide a degree of overlap of these representative regions, while covering fairly completely the area encompassed by the maximum range of the radar (about 100 km). Interpolation to any point within the radar range should thus be feasible. In addition, surface and tower data were obtained from the Tennessee Valley Authority (TVA) sites indicated in Figure 2.

The central pibal station was located in an open field (the so-called "0800" ecology study site) to the southwest of Oak Ridge, about 3.5 km from Oak Ridge National Laboratory (ORNL). The other pibal stations were located at small airports to insure relatively open fetches and ease of access. Each station was equipped with a single optical theodolite, a Thornthwaite low-threshold anemometer for "surface" (i.e., 2m) wind speed, and a standard shelter for temperature and humidity instrumentation (Figure 4). Surface wind direction was obtained from Thornthwaite low-threshold vanes at all stations but Crossville, where the FAA Flight Service Office records surface winds. Observations of the ascent of 30 gm pibals were made at 30 second intervals after launch for a period of 10 minutes. Half-hourly launches were made at each site during the "transition" periods of the day (i.e., sunrise, sunset), with hourly launches at other times.

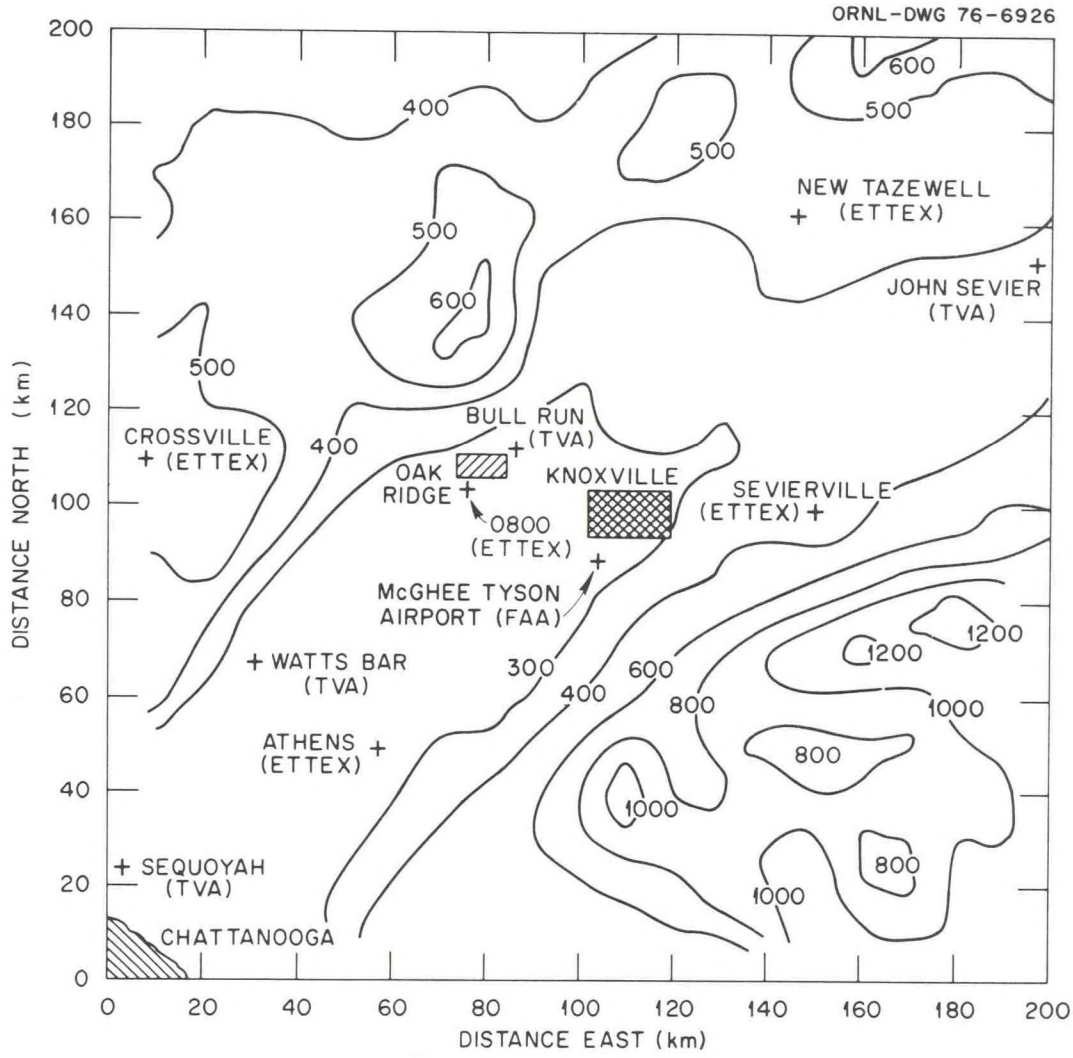

Figure 2. Contour Map of ETTEX Region

The M-33 precision tracking radar (Figure 5) was placed near the summit (1030 m, MSL; about 750 m above the valley floor) of Bullalo Mountain (Figure 1), a peak in the Cumberland range about 15 km northwest of Oak Ridge. A road maintained by the Oliver Springs Mining Company leads to the mountain top.

The tetroons and tracking technique used are similar to those described by Pack (1962). The balloon is a tetrahedron of about 1 m^3 volume, constructed of DuPont Mylar^R (Figure 6). The physical characteristics of this envelope are such that the tetroon volume is virtually constant for superpressurization of less than 70 mb or so. This type of balloon thus floats, in the absence of vertical air motions, along isopycnic surfaces. The inflation and launch procedures required to attain a particular flight altitude have been summarized by Hoecker (1975). A tetroon is tracked by means of a radar-triggered transponder carried beneath the balloon (Figure 6). The radar signal actuates this transponder, which then emits a slightly tuneable 403 MHz signal, indicating that the radar unit's transmitting antenna is pointed more or less toward the transponder. As the broadcast power (and hence the radar beam width) is slowly reduced, the transmitting antenna

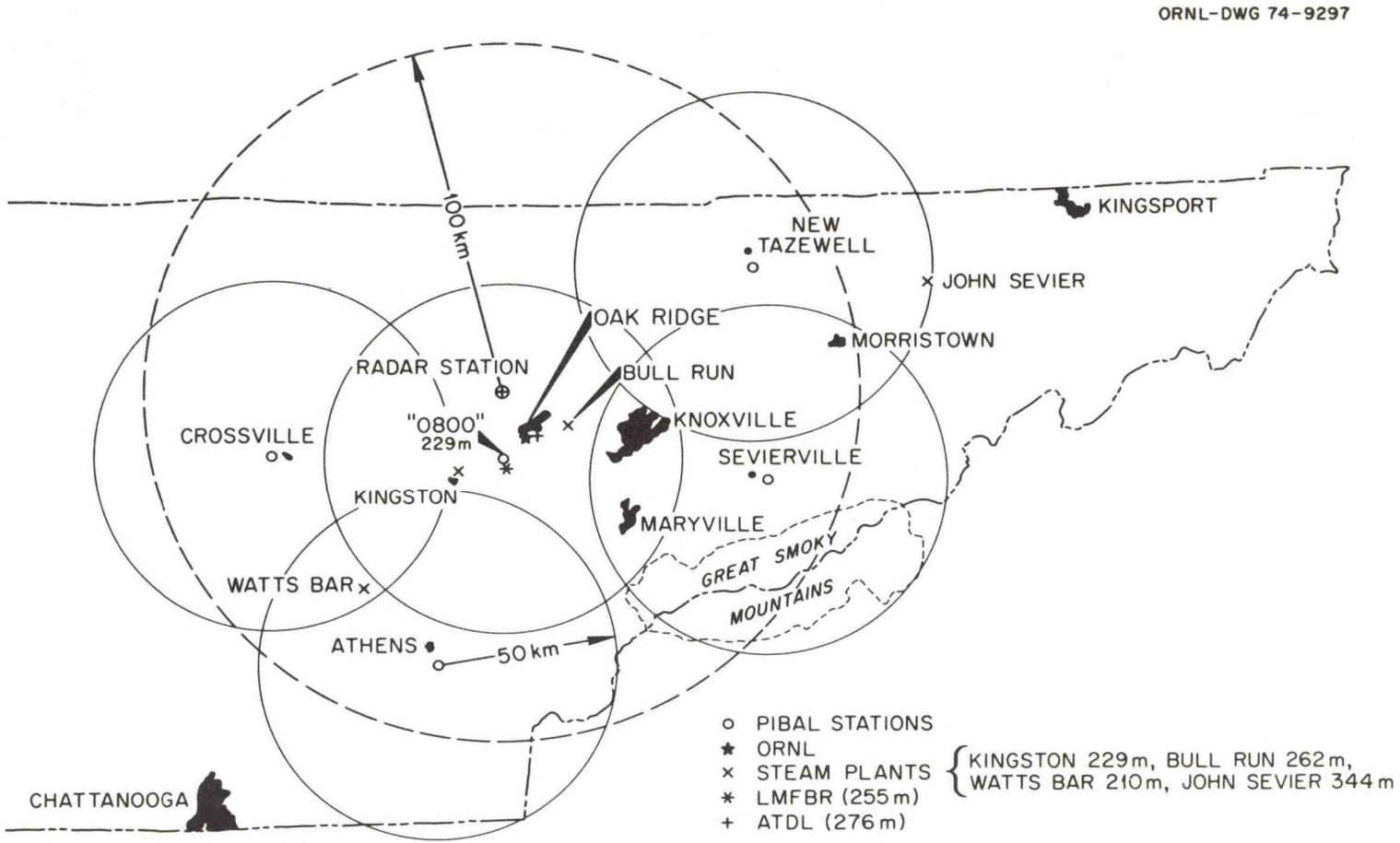

ETTEX Map, Indicating Locations, Elevations (MSL), and Effective Observing Ranges of Radar Unit and Pibal Stations. Tetroon Launch Sites are also Shown.

Figure 3

must be pointed more and more accurately toward the transponder in order to trigger it. It is by this method that the transponder location may be ultimately determined to within about 20 m. A number of other experimenters have developed and used this same radar-tetroon-transponder system (e.g., Moses, et al. 1968; Angell, et al. 1968).

During our experiments, tetroons were launched at various times from the ATDL offices, from our central pibal site near ORNL, from the TVA's Bull Run steam plant, or from the Oak Ridge municipal water treatment plant (on a ridge just above ATDL), depending on the prevailing wind direction and the specific purpose of the individual experiment. Most of these launches were made by W. H Hoecker of NOAA's ARL, Silver Spring, Maryland. Radiosondes to provide the vertical temperature profile required for tetroon inflation and for subsequent meteorological information were launched from the first three of these sites. Because local topography frequently obscured the transponders from the radar signal before launch, it was found advisable to first carry each transponder aloft with a tethered 100 gm pibal, so that transponder operation could be checked just before launching the tetroons. This also permitted adjustment of the transponders to be used in any given experiment to slightly different frequencies, thus allowing the radar to easily distinguish among several balloons.

In our trajectory experiments, three tetroons were released sequentially at 15 minute intervals. Flight altitudes were found to typically range between 300 m and 1000 m above the ground. At the radar, the radio receiver was tuned to the frequency of one of the transponders, and the radar range, elevation angle, and azimuth angle of that transponder were read and manually recorded. The receiver was then tuned to another frequency, and the process repeated. Readings were taken once each minute, so that the interval between successive observations of any given tetroon was typically three minutes.

We had originally planned to follow the tetroons for 12-hour periods covering both night and day. Lack of personnel forced us to cut the experiments to 6 hours in duration, but we were nevertheless able to obtain measurements during most times of the day (sunrise, mid-day, sunset, and mid-night). Most of the tetroons never wandered very far from the center of our observations grid; the light winds experienced during most of these experiments are quite characteristic of eastern Tennessee in summertime (U. S. Weather Bureau, 1953). As expected, most of the tetroons travelled along a SW-NE axis, roughly parallel

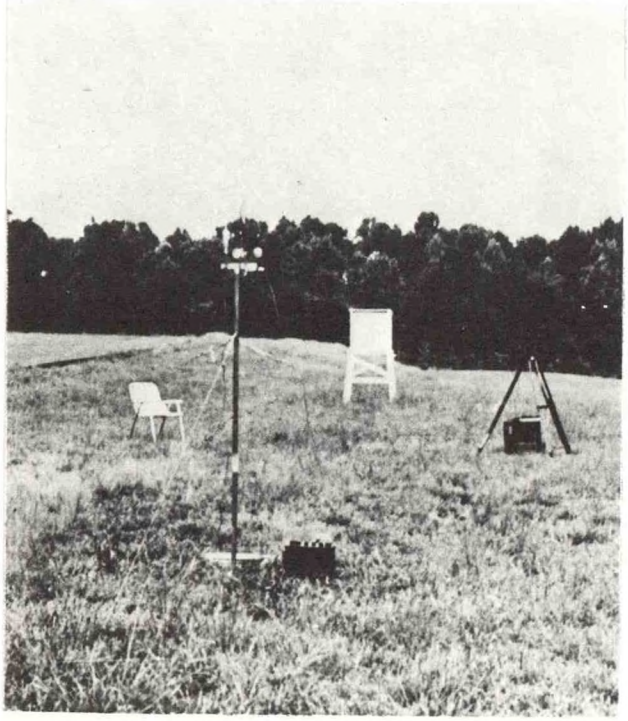

Figure 4. Typical pilot balloon site.

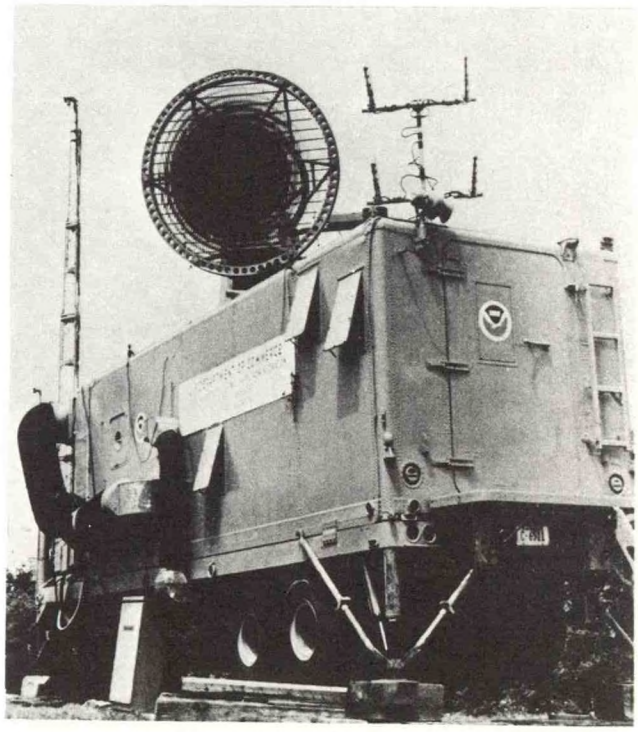

Figure 5. M-33 radar on Buffalo Mountain.

to the local ridge-valley structure described above. A few tetroons were prematurely lost because of transponder malfunctions, topographic interference, and rain. A total of seven trajectory experiments was completed. Interpolated wind fields have been derived and used to estimate air parcel trajectories; these predictions have been compared to the observed tetroon trajectories (Nappo, 1976; included in the Appendix of this report). Analyses of the wind field characteristics have also been carried out (Nappo, 1977; see Appendix).

3.2 Relative Diffusion Experiment

Another aspect of the regional-scale diffusion problem is the need for further study of relative diffusion. Previous observations of relative diffusion (e.g., Kao and Wendell, 1968, and Angell, et al 1971, 1975) were made over relatively uniform terrain and with little supporting meteorological data. During ETTEX, several relative diffusion experiments were conducted using tetroon pairs simultaneously released (Figure 7) and tracked by radar. These flights usually lasted two hours and covered distances up to 40 km from the launch site. The measured relative displacement of each tetroon pair has been compared to theoretical diffusion calculations based on the observed wind and temperature gradients and turbulence in the atmosphere boundary layer (Hanna, 1976; included in the Appendix of this report). These tetroon launches were made from either the ATDL offices or from the Bull Run site. Vertical wind profiles were obtained from either half-hourly double

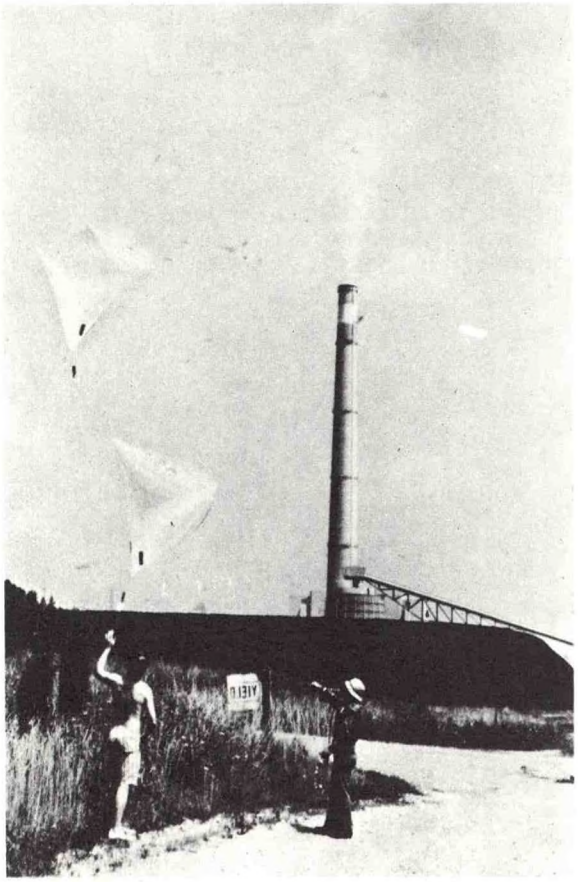

Figure 6. Tetroon & transponder

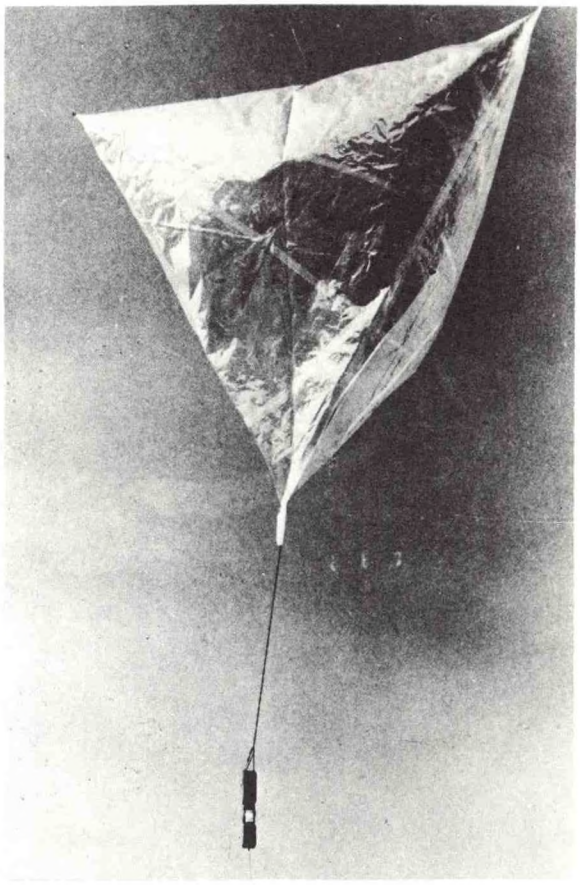

Figure 7. Tetroons near Bull Run

TABLE 1. SUMMARY OF ETTEX EXPERIMENTS, JULY-AUGUST, 1974

Date (1974)	Approx. Time (EDT)	Experiments Conducted*	Tetroons; Launch Site	Pibal Obs.** Launch Sites	Radiosondes; Launch Site	Aircraft Measurements***
7/15	1000-1600	"Rehearsal"	---	ST; All sites	---	---
7/16	1000-1400	TRJ	1;0800	ST; All Sites	---	---
7/17	1000-1600	TRJ	3;ATDL	ST; All Sites	---	T,E
7/18	1600-2100	TRJ	3;ATDL	ST; All Sites	---	---
7/19	1600-2130	TRJ	3;0800	ST; All Sites	---	---
7/22	100-1510	RD	4;ATDL	DT;0800	---	---
7/25	1200-1700	RD;CD	4;Bull Run	DT; Bull Run	5; Bull Run	T,E,SO_2
7/26	1500-1640	RD	2;ATDL	ST;ATDL(rapid)	1; ATDL	---
7/27	1200-1600	RD	4;Bull Run	DT; Bull Run	4; Bull Run	T,E
7/29	1200-1540	RD	4;ATDL	ST; ATDL(rapid)	2; ATDL	---
7/30	1100-1430	RD	4;ATDL	ST; ATDL (rapid)	1; ATDL	---
7/31	1300-1700	RD;CD	4;ATDL	DT; Bull Run	4; ATDL	T,E,SO_2
8/1	1300-1620	RD;CD	4;ATDL	DT; Bull Run	5; ATDL	T,E,SO_2
8/2	1300-1630	RD;CD	4 Bull Run	DT; Bull Run	4; ATDL	T,E,SO_2
8/5	1130-1600	CD	---	DT; Bull Run	4; 0800	T,E,SO_2
8/6	0400-1000	TRJ	3;0800	ST; All Sites but Crossville	6; 0800	---
8/7	0400-1000	TRJ	3;O.R. Water works	ST; All Sites	7; 0800	---
8/8	0400-0830 (rain)	TRJ	3;Water works 2;ATDL	ST; All Sites	5; 0800	---

*TRJ = Trajectory, CD- Convective Diffusion, RD - Relative Diffusion
**ST or DT = Single or Double Theodolite
***T = Temperature Profile, E = Eddy Dissipation Rate, SO_2 = Plume SO_2 Concentration

theodilite or rapid sequence (launches every 15 minutes; readings every 30 seconds for 10 minutes) single-theodolite pibal observations. Radiosonde ascents were completed during all but one of these experiments. In many cases, data such as eddy dissipation rate and vertical temperature profile were also available from airplane measurements associated with the convective diffusion study described below. A total of nine relative diffusion experiments were completed, most of these between noon and 4 p.m. (EDT).

3.3 Convective Diffusion Experiment

It is believed that, on convective summer afternoons, downdrafts may bring effluent from even tall stacks quickly to the ground, with resulting relatively high surface concentrations. To study this phenomenon, concentrations of SO_2 in the plume were measured by helicopter traverses, together with associated meteorological conditions near the TVA's Bull Run coal-fired steam plant. Vertical temperature gradients and eddy dissipation rates were also measured near the plume from a Cessna 172 airplane equipped with an aspirated thermistor and an MRI Universal Indicated Turbulence Meter borrowed from the TVA. Vertical temperature and humidity profiles were determined by radiosondes and vertical wind profiles were obtained from double-theodolite pibal ascents near the Bull Run site.

A total of five experiments, each lasting from roughly 1 p.m. to 4 or 5 p.m. (EDT), was completed. Results of this experiment will be reported separately at a later time.

4. DATA SUMMARY

As indicated above, seven trajectory experiments, nine relative diffusion experiments, and five convective diffusion experiments were completed. Table 1 summarizes the dates and times, experiment types, and meteorological information available for each run. Part II of this report represents these data in tabular form, together with synoptic weather summaries for the days of the experiment. Data analyses completed thus far are included in the Appendix.

5. ACKNOWLEDGEMENTS

The people who assisted this study are legion, and it is unfortunately impossible to thank everyone by name. However, the experiment would have been impossible without the aid of C. R. Dickson of the ARL Field Research Laboratory in Idaho Falls, who provided the M-33 radar unit and the men to set it up and maintain it. G. White and D. Forsythe of Idaho Falls were in charge of the radar's operation. Dickson also loaned us his mobile radiosonde unit, an enormous collection of routine but essential equipment, and assisted us in procuring a long list of expendable items.

The Coal Creek Mining and Manufacturing Corporation and the Oliver Springs Mining Company (specifically, C. H. Smith and C. Owens) were very cooperative in helping us select and travel to and from the radar site on Buffalo Mountain.

We thank the managers of the following airports for allowing us to use their facilities for our pibal observations: Crossville Municipal (E. Donnelly), McMinn County (J. Scruggs), New Tazewell (W. Coffee), and Sevierville (P. Roberts).

The Tennessee Valley Authority permitted us to use their Bull Run and Kingston Steam plants for portions of the study, and provided meteorological data from their surface and tower sites within the ETTEX region. T. L. Montgomery and J. H. Coleman of the TVA's Air Quality Branch loaned several crucial pieces of equipment.

6. REFERENCES

Ackerman, B. (1973): The airflow program in Metromex, in *Summary Report of Metromex Studies*, 1971-1972, ed. by F. A. Huff, Rept. of Invest. 74, State of Illinois, pp 113-124.

Ackerman, B. (1974): Wind profiles and their variability in the planetary boundary layer, in preprints of *AMS Symposium on Atmospheric Diffusion and Air Pollution, Santa Barbara, Cal., Sept. 9-13*, pp 12-22.

Angell, J. K., D. H. Pack, and C. R. Dickson (1968): A Lagrangian study of helical circulations in the planetary boundary layer. *J. Atmospheric Sci. 25* (5), pp 707-717.

Angell, J. K., P. W. Allen, and E. A. Jessup (1971): Mesoscale relative diffusion estimates from tetroon flights. *J. Appl. Meteorol. 10* (1), pp 43-46.

Angell, J. K., W. H. Hoecker, C. R. Dickson, and D. H. Pack (1973): Urban influence on a strong daytime air flow as determined from tetroon flights. *J. Appl. Meteorol. 12* (6), pp 924-936.

Angell, J. K., C. R. Dickson, and W. H. Hoecker, Jr. (1975): Relative diffusion within the Los Angeles basin as estimated from tetroon triads. *J. Appl. Meteorol. 14*, pp 1490-1498.

Bornstein, R. D. (1968): Observations of the urban heat island effect in New York City. *J. Appl. Meteorol. 7*, pp 575-582.

Egami, R. T., V. Sharma, and R. L. Steele (1974): Diffusion study in the vicinity of Mohave Generating Plant, in preprints of *AMS Symposium on Atmospheric Diffusion and Air Pollution, Santa Barbara, Cal., Sept. 9-13*, pp 209-213.

Hass, W. A., W. H. Hoecker, D. H. Pack, and J. K. Angell (1967): Analysis of low-level constant volume balloon (tetroon) flights over New York City. *Quart. J. Roy. Meteorol. Soc. 93*, pp 483-493.

Hanna, S. R. (1976): Relative diffusion of tetroon pairs during convective conditions. *J. Appl. Meteorol. 15*, pp 588-593.

Heffter, J. L. (1973): *Atmospheric Transport and Dispersion of Pollutants and related Meteorological Studies*, Trajectory Programs, July 1971-June 1972, ed. by R. J. List, NOAA Tech. Memo. ERL-ARL-40, pp 21-46.

Hoecker, W. H. (1975): A universal procedure for deploying constant-volume balloons and for deriving vertical air speeds from them. *J. Appl. Meteorol. 14*, pp 1118-1124.

Kao, S. K. and L. L. Wendell (1968): Some characteristics of relative particle dispersion in the atmospheric boundary layer. *Atmospheric Environ. 2*, pp 397-407.

Kao, S. K., H. N. Lee, and K. I. Smidy (1974): A preliminary analysis of the effect of mountain-valley terrains on turbulence and diffusion, in preprints of *AMS Symposium on Atmospheric Diffusion and Air Pollution, Santa Barbara, Cal., Sept. 9-13*, pp 59-63.

Kao, S. K. and G. H. Taylor (1977): Effect of mountain terrain on diffusion in the planetary boundary layer, in preprints of *AMS Joint Conference on Applications of Air Pollution Meteorology, Salt Lake City, Utah, 29 Nov. - 2 Dec.*, pp 119-125.

Karl, T. R. (1976): Summertime surface wind fields in preprints of *AMS Third Symposium on Atmospheric Turbulence Diffusion and Air Quality, Raleigh, N.C., Oct. 19-22*, pp 107-113.

Lantz, R. B., G. F. Hoffnagle, and S. B. Pahwa (1976): Diffusion model comparisons to measured data in complex terrain, in preprints of *AMS Third Symposium on Atmospheric Turbulence Diffusion and Air Quality, Raleigh, N.C., Oct. 19-22*, pp. 476-483.

Leahey, D. M. and H. S. Hicklin (1973): Tetroon studies of diffusion potential in the airshed surrounding the Crowsnest Pass area, *Atmosphere 11* (3), pp 77-87.

Leahey, D. M. and R. D. Rowe (1974): Observational studies of atmospheric diffusion processes over irregular terrain, paper 74-67, 67th Air Pollution Control Assoc. (APCA) Annual Meeting, Denver, Col., June 9-13.

Moses, H., E. Robinson, M. E. Smith, G. C. Gill, E. M. Wilkins, and C. R. Dickson (1968): Meteorological instruments for use in the atomic energy industry, ch. 6-12 of *Meteorology and Atomic Energy*, ed. by D. H. Slade, TID 24190, pp 298-300.

Mullen, J. B., M. W. Chan, I. H. Tombach (1977): Development and validation of a model for diffusion in complex terrain, in preprints of *AMS Joint Conference on Applications of Air Pollution Meteorology, Salt Lake, 29 Nov. - 2 Dec.*, pp 188-191.

Nappo, C. J. (1976): The simulation of atmospheric transport using observed and estimated winds, in preprints of *AMS Third Symposium on Atmospheric Turbulence Diffusion and Quality, Raleigh, N.C., Oct. 19-22*, pp 100-106.

Nappo, C. J. (1977): Mesoscale flow over complex terrain during the Eastern Tennessee Trajectory Experiment (ETTEX), *J. Appl. Meteorol. 16*, pp 1186-1196.

Pack, D. H. (1962): Air trajectories and turbulence statistics from weather radar using tetroons and radar transponders, *Monthly Weather Rev. 90* (12), pp 491-506.

Roffman, A., T. P. Kapsha, P. E. Kueser, G. L. Bethune, and M. P. Sullivan (1976): A field study on the behaviour of a SO_2 plume from a power plant near complex terrain and under stable atmospheric conditions in preprints of *AMS Third Symposium on Atmospheric Turbulence Diffusion and Air Quality, Raleigh, N.C., Oct. 19-22*, pp 421-429.

Start, G. E., N. R. Ricks, and C. R. Dickson (1974): Effluent dilutions over mountainous terrain. NOAA Tech. Memo. ERL-ARL-51.

U. S. Weather Bureau (1953): *A Meteorological Survey of the Oak Ridge Area: Final Report Covering the Period 1948-52*, USAEC Rpt. ORO-99, Oak Ridge, Tenn.

Wendell, L. L. (1970: A preliminary examination of mesoscale wind fields and transport determined from a network of wind towers, NOAA Tech. Memo. ERL-ARL-25.

Wendell, L. L. (1972): Mesoscale wind fields and transport estimates determined from a network of wind towers, *Monthly Weather Rev. 100* (7), pp 565-578.

Wilson, R. B., G. E. Start, C. R. Dickson, and N. R. Ricks (1976): Diffusion under low windspeed conditions near Oak Ridge, Tennessee in preprints of *AMS Third Symposium on Atmospheric Turbulence Diffusion and Air Quality, Raleigh, N.C., Oct. 19-22*, pp 269-276.

PART II

and

APPENDIX

Because of the large number of pages involved, Part II and the Appendix for this NOAA Technical Memorandum are not included in this publication. These sections may be obtained from the Atmospheric Turbulence and Diffusion Laboratory, Post Office Box E, Oak Ridge, Tennessee 37830.

WORLD METEOROLOGICAL ORGANIZATION

PAPERS PRESENTED

AT THE

WMO SYMPOSIUM ON BOUNDARY LAYER PHYSICS APPLIED TO SPECIFIC PROBLEMS OF AIR POLLUTION

Norrköping, 19-23 June 1978

WMO - No. 510

Secretariat of the World Meteorological Organization - Geneva - Switzerland

ATDL Contribution File No. 78/5

A REVIEW OF THE INFLUENCE OF NEW BOUNDARY LAYER RESULTS ON DIFFUSION PREDICTION TECHNIQUES

by

Steven R. Hanna
Air Resources
Atmospheric Turbulence and Diffusion Laboratory
National Oceanic and Atmospheric Administration
Oak Ridge, Tennessee

1. Introduction

Our knowledge of the dynamics of the surface boundary layer and the planetary boundary layer has greatly increased during the past one or two decades, thanks to a series of excellent field experiments in Kansas [2], Minnesota [10], and a laboratory experiment in Colorado [24]. Other experiments in Australia [3] using fixed instruments and in several widely separated portions of the globe [13] using instruments on aircraft have also assisted in the development of these new ideas. A major finding of these experiments is that the depth of the mixed layer, h, is an important scaling parameter during the daytime. Combined with the surface heat flux H, the depth h determines the scaling velocity $w_* = (Hh)^{1/3}$. The structure of the boundary layer is completely determined by external parameters such as h and w_*. For example, at great instabilities, the standard deviations of the horizontal velocity components are proportional to w_*. Similarity relationships in the surface boundary layer among u/u_*, z/z_o, and z/L have been refined so that researchers are very confident of their predictions, at least for steady flow over flat terrain.

In contrast, techniques commonly used to estimate diffusion in the boundary layer remain at nearly the same stage of development they were at over ten years ago. However, a revolution is underway in which the new boundary layer findings are being applied to diffusion calculations. Much of this new work is still underway and is available only in preliminary reports. The purpose of this brief summary is to review these major new developments in diffusion theory.

2. Refinement of Pasquill-Gifford-Turner σ_z Curves

Diffusion specialists have been using the so-called Pasquill-Gifford-Turner (PGT) curves for 17 years to estimate σ_y and σ_z in the Gaussian plume model. It is pointed out in the references [6, 15, 21] that these curves apply to a sampling time of about three minutes, a surface roughness of a few centimeters, latitudes of about 50°, and downwind distances no greater than about one kilometer. Furthermore, these graphs are to be used only if detailed measurements of turbulent wind fluctuations are not available.

F. B. Smith [19, 20] is developing an improved set of σ_z curves for more general conditions by solving the diffusion equation

$$u\partial C/\partial z = \partial(K_z \partial C/\partial z)/\partial z \qquad (1)$$

and then determining σ_z from the resulting distribution of concentration

C. The eddy diffusivity K is estimated from the relationship

$$K_z = .15\sigma_w \lambda_m \qquad (2)$$

postulated by Hanna [7], where σ_w is the standard deviation of the vertical velocity distribution, and λ_m is the wavelength at which peak turbulent energy occurs in the w spectrum. The boundary layer experiments mentioned above, plus some additional experiments at Cardington, England, are used by Smith to relate wind speed u, standard deviation σ_w, and peak wavelength λ_m to easily measured parameters such as surface roughness, solar radiation, surface albedo, state of ground, Coriolis parameter, and geostrophic wind speed. Sets of nomograms are given that permit the graphical solution of complex boundary layer relationships. As an example of the techniques used by this method, the predicted diurnal K profile evolution for a set of fixed external variables is given in Figure 1. Smith's methods are also summarized by Pasquill [16], who presents a graph (Fig. 6.13, p. 374) in which stability class appropriate to the original PGT σ_z curve can be estimated knowing the upward heat flux (daytime) or cloud amount (nighttime) and surface wind speed for z_o = 10 cm.

Pasquill [15], Briggs [1], and Weber, McDonald, and Briggs [23] are using dimensional analysis and similarity theory to revise the PGT σ_z curves. Similarity theories, which operate under the assumption that Eulerian profile measurements apply to Lagrangian diffusion, predict that σ_z is proportional to $z_o^{0.2}$ for releases near the ground during neutral conditions.

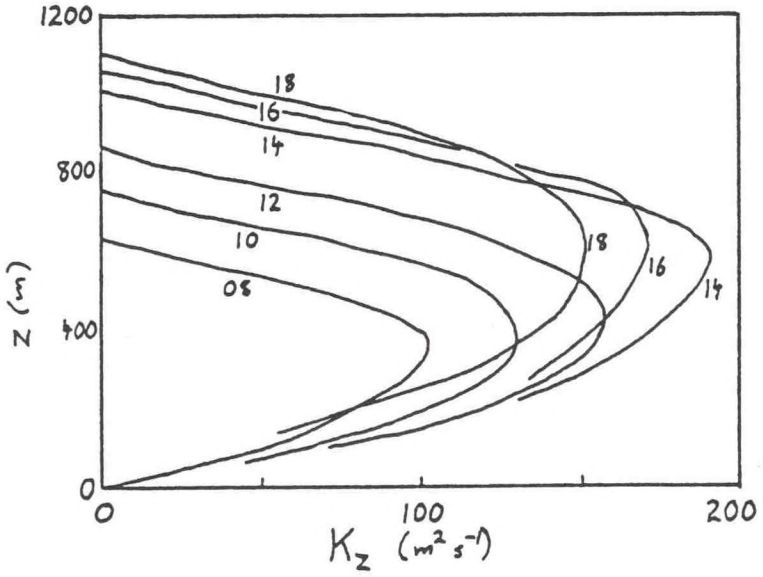

Figure 1: An example of the evolution of K_z with time for a typical spring day over flat farmland, after Smith [20].

Free convection conditions lead to the relation

$$\sigma_z = |L|^{1/2} (u_*/u)^{3/2} x^{3/2} \qquad (3)$$

for $\sigma_z < h/2$ and releases near the ground. The parameters L and u_* are the Monin-Obukhov length and friction velocity, respectively. Thus theory and recent observations substantiate a power p greater than unity in the formula $\sigma_z \propto x^p$ for free convection. The original PGT curves have p greater than unity for category A, a fact which several persons objected to. It appears that their objections may be valid for releases from tall stacks into the upper portion of the boundary layer where h is important, but that the free convection regime does influence ground level releases. There is currently a controversy spurred by Willis and Deardorff's [24] laboratory tank observations of the lifting of the maximum concentration off the tank floor for releases at the tank floor during free convection. The question is whether this lifting occurs when long term averages are made or whether it is just a transient phenomenon associated with a passing thermal.

For the stably stratified boundary layer, σ_z is a function of L at any distance x downwind of a ground level source. Weber, McDonald and Briggs [23] conclude that the relation

$$\sigma_x \propto L^{1/2} x^{1/2} \qquad (4)$$

provides a good fit to stable σ_z observations. During very stable conditions when L is only a few meters, the "mixing layer" may be only a few meters deep, placing an upper limit to possible values of σ_z.

3. Estimates of σ_y.

During the past few years, experiments over the full depth of the convective boundary layer have suggested that σ_v is proportional to the scaling speed w_* and that the wavelength of peak energy in the v spectrum equals about 1.5h [12]. However, unlike the vertical component σ_w, lateral turbulent velocity fluctuations σ_v in the surface boundary layer defy surface layer ($z < 0.1h$) similarity theory. The PGT σ_y curves are considered a default procedure to be used in the absence of good measurements of σ_v or the standard deviation of wind direction fluctuations σ_θ. (For small angles θ, $\sigma_v/U = \sigma_\theta$, where σ_θ is in radians.) A recent workshop on stability classification schemes and sigma curves [9] strongly recommends that σ_y be determined from measurements of σ_v or σ_θ rather than from the PGT curves. The precise relationship to be used is

$$\sigma_y = \sigma_\theta \times f(x/x_L), \qquad (5)$$

where f is a universal function of x/x_L, and x_L is the Lagrangian turbulence length scale, related to the time scale T_L through $x_L = uT_L$. Based on comparisons with many observations Pasquill [17] suggests the following values for f:

x(km)	0	0.1	0.2	0.5	1	2	4	10	10 <
f(x)	1	0.8	0.7	0.65	0.6	0.5	0.4	0.33	$0.33(10/x)^{1/2}$

This table assumes no variation in f(x) with length scale x_L, stability, wind speed, or any other variable. The only stated limitations are that sampling times for the σ_y and σ_θ observations must be matched and that the σ_θ measurement must be at the height at which u is specified.

Doran, Horst, and Nickola [5] derive corrections to the above table which account for varying sampling time, wind speed, and stability. They base their derivation on Taylor's statistical diffusion theory written in spectral form:

$$[\sigma_y^2]_{\tau,t} = [\sigma_v^2]_{\infty,o}\, t^2 \int_o^\infty F_L(n) \left[1 - \frac{\sin^2 \pi n\tau}{(\pi n\tau)^2}\right] \frac{\sin^2 \pi nt}{(\pi nt)^2}\, dn \qquad (6)$$

where n is frequency, $F_L(n)$ is normalized Lagrangian v spectrum, τ is sampling time and t is travel time ($t^L = x/u$). The first and second subscripts indicate sampling and averaging times respectively. The authors show that the function f is theoretically given by

$$S = [\sigma_v]_{\omega,\tau/\beta} / [\sigma_v]_{\infty,o}, \qquad (7)$$

where β is the ratio between the Lagrangian and Eulerian time scales. (Typically equal to about four). Experiments in which the v spectrum and σ_v are both measured are used to derive the effects of sampling time given in the following table:

Values of f for Averaging Time of 5 Seconds. Doran et al.[5]

x(km)	0.1	0.2	0.4	0.8	1.6	3.2	10
f(τ= 1800s)	.95	.85	.76	.70	.64	.58	.52
f(τ= 3600s)	1.04	.98	.92	.85	.77	.67	.54

On the basis of these figures, Doran, Horst and Nickola [5] conclude that Pasquill's table is approximately correct, but that there can be important deviations. They find the low frequency end of the v spectrum is very important because of the dominance of large eddies in the diffusion process as diffusion proceeds. It can be concluded that the best way to estimate σ_v is to obtain good measurements of turbulent wind direction fluctuations, sampled and averaged over times corresponding to the sampling and averaging times of the diffusion.

4. Estimates of K_z.

The vertical eddy diffusivity K_z is thought to relate more strongly to the eddy conductivity K_h than to the eddy viscosity K_m. In the surface layer it is recognized that K_h (or K_z) is given by the formula:

$$K_h = K_z = 0.35 u_* \, z/\phi_h(z/L), \qquad (8)$$

where u_* is the friction speed, L is the Monin-Obukhov length and ϕ_h is a universal function of z/L. Von Karman's constant is taken to be 0.35, in agreement with the results of the 1968 Kansas experiment [2]. The function $\phi_h(z/L)$ suggested by Businger et al.[2] has the form

$$\text{unstable:} \quad \phi_h(z/L) = 0.74(1-9\, z/L)^{-1/2} \qquad (9)$$

$$\text{stable:} \quad \phi_h(z/L) = 0.74 + 4.7\, z/L \qquad (10)$$

These formulas for K_z, coupled with similar formulas for the wind speed u derived from the Kansas data, can be used to obtain solutions to the diffusion equation (eq. 1) for releases in the surface layer.

At elevations above the surface layer, K_z is less well-known. It can be estimated from dimensional analysis (e.g., eq. 2) with some knowledge of the characteristics of the vertical velocity spectrum. Formulas for the wavelength of peak energy λ_m in the w spectrum for convective conditions are suggested by Kaimal et al.[12]. They find that $\lambda_m = 5.9z$ at $z < 0.1h$ and λ_m approaches 1.5h as z approaches h. This behavior is summarized in the formulas

$$\lambda_m \sim \begin{cases} z/(0.55 - 0.38z/L) & 0 < z < |L| \\ 5.9z & |L| < z < 0.1h \\ 1.5h(1 - \exp(-5z/h)) & 0.1h < z < h \end{cases}$$

Wyngaard et al. [25] find that the ratio σ_w^2/w_*^2 for convective days increases from about 0.2 near the surface to 0.4 at $0.1h < z < 0.5h$, and then decreases linearly towards zero at $z = h$. Variation of σ_w with height during nearly neutral or stable conditions is not so well known.

Crane et al. [4] calculate K_z through the depth of the boundary layer during a diffusion experiment in Los Angeles by using the definition

$$K_z = -F/(\partial C/\partial z) \quad , \tag{11}$$

where F is the upward vertical flux of substance C. The flux F is estimated from time-height cross sections of NO_x, methane, or CO by means of the relations:

Highest observing height > h(mixing height)

$$F_z = \int_z^h (dC/dt)dz \tag{12}$$

Highest observing height < h(mixing height)

$$F_z = F_0 - \int_0^z (dC/dt)dz \tag{13}$$

The K_z's calculated by Crane et al. [4] are plotted as a function of height in Figure 2, where K_z is normalized by hw_* and height is normalized by h. The region of large K_z at $0.20 < z/h < 0.55$ occurs where $\partial C/\partial z$ is nearly zero. At lower heights, K_z grows with height at a rate somewhat greater than linear. At the top of the mixed layer, K_z drops down towards zero. Researchers have had a qualitative idea of the behavior of K_z with height in the planetary boundary layer for several years, but the measurements of Crane et al. [4] and Kaimal et al. [12] allow quantitative estimates to be made.

5. Statistical Estimates of Diffusion.

It was stated above that it is best to tie diffusion calculations as closely as possible to turbulence observations. In models by Watson and Barr [22] and Joynt and Blackman [11] diffusion is estimated by following the motions of thousands of individual particles, where the particle velocity at any time is the sum of a mean component obtained from the measured mesoscale wind field, and a turbulent component chosen by a statistical technique. In the model by Joynt and Blackman [11] the time step τ is chosen to be so great that the autocorrelation coefficient $R(\tau)$ is nearly zero and the turbulence component is completely random. In contrast, Watson and Barr [22] choose a time step sufficiently small that $R(\tau)$ is non-zero and then calculate the coefficients B_i so that the turbulent velocity u'_5 at time step 5 is given by

$$u'_5 = B_1u'_1 + B_2u'_2 + B_3u'_3 + B_4u'_4 + u''. \tag{14}$$

where u'' is the random component and u'_1, u'_2, u'_3, and u'_4 are the turbulent velocities at preceding time steps. The coefficients B are functions of the turbulence spectrum, which is required as input to the model.

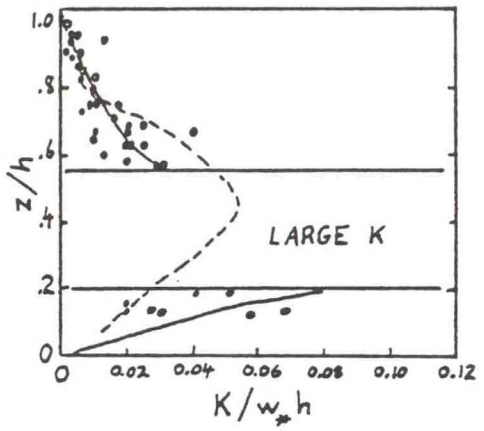

Figure 2: Profile of $K_z/w_* h$ versus z/h derived from concentration profiles in Los Angeles by Crane et al. [4].

Smith [18] suggested that equation (14) could be shortened to:

$$u'(t + \tau) = u'(t)\, R(\tau) + u'' \quad , \tag{15}$$

where $$\sigma_{u''}^2 = \sigma_{u'}^2 \,(1 - R^2(\tau)) \quad . \tag{16}$$

Hanna [8] recently tested equations (15) and (16) using the Eulerian wind measurements from the Minnesota experiment and Lagrangian wind measurements from several tetroon experiments. As Figure 3 shows, the linear relationship between the fluctuation $u'(t + \tau)$ at time $t + \tau$ and the fluctuation $u'(t)$ at time t is verified for the Minnesota data for all except extreme values of $u'(t)$. This simple technique should be very useful in estimating mesoscale diffusion, since all that is needed is a knowledge of the turbulent energy $\sigma^2_{u'}$, the correlation coefficient $R(\tau)$ for time lag or time step τ, and the mesoscale wind field averaged over some suitable period, say 30 minutes.

6. Stability Classification Schemes

The AMS Workshop on Stability Classification Schemes and Sigma Curves [9] dealt with this controversial topic, which centers around whether or not ΔT (the temperature difference across two levels on a tower) is a useful term for classifying stability. Their recommendations, verified by the paper by Weber et al. [23], are that ΔT is practically useless as a stability indicator during unstable conditions, but can be quite useful during stable conditions. By reexamining the 1950's Prairie Grass Diffusion Experiment, the authors find that Ri or z/L correlate best with σ_z in unstable conditions. In stable conditions, Ri, z/L, ΔT, and σ_E (standard deviation of elevation angle) all are comparable in their ability to estimate σ_z. As stated in Section 2, Smith [19, 20] is devising a revision to the PGT stability classification scheme which will more accurately account for the effects of roughness, solar heat flux, and other local effects.

Acknowledgement. This research was performed under an agreement between the U.S. Department of Energy and the National Oceanic and Atmospheric Administration.

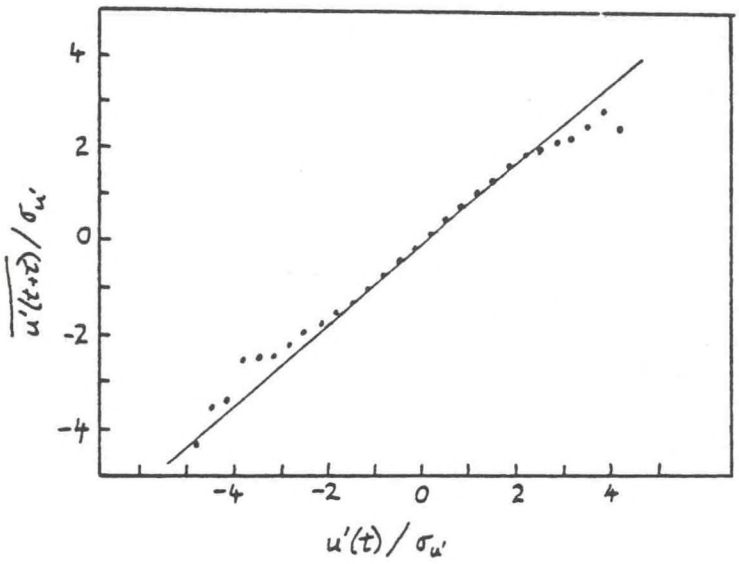

Figure 3: Normalized wind fluctuations at time $t + \tau$ plotted versus normalized wind fluctuations at time t[8]. Summary of unstable Minnesota data for which $R(\tau) > 0.8$.

References

1. Briggs, G. A., 1977: Some theoretical notes on sigma curves and stability classification schemes, presented at AMS Workshop on Stability Classification Schemes and Sigma Curves, Boston, 27-29 June, draft report available from ATDL, P.O. Box E, Oak Ridge, TN 37830, 16 pp.

2. Businger, J. A., J. C. Wyngaard, Y. Izumi and E. F. Bradley, 1971: Flux-profile relationships in the atmospheric surface layer. J. Atmos. Science, 28, 181-189.

3. Clarke, R. H., A. J. Dyer, R. R. Brook, D. G. Raid and A. J. Troup, 1971: The Wangara Experiment: Boundary Layer Data, Div. of Meteor. Phys. Tech. Paper No. 19, Commonwealth Scient. and Ind. Res. Organ., Australia.

4. Crane, G., H. A. Panofsky and O. Zeman, 1977: A model for dispersion from area sources in convective turbulence. Atmos. Environ., 11, 893-900.

5. Doran, J. C., T. W. Horst and P. W. Nickola, 1978: Variations in measured values of lateral diffusion parameters. Submitted to J. Appl. Met., available from Battelle Pac. NW Lab., Richland, Wash., 21 pp.

6. Gifford, F. A., 1961: Use of routine meteorological observations for estimating atmospheric dispersion. Nuc. Safety, 2, 47-51.

7. Hanna, S. R., 1968: A method of estimating vertical eddy transport in the planetary boundary layer using characteristics of the vertical velocity spectrum, J. Atmos. Sci., 25, 1026-1032.

8. Hanna, S. R., 1978: The linear relationship between turbulent wind speeds at constant time lag. Submitted to J. Atmos. Sci., available from ATDL, P.O. Box E, Oak Ridge, TN., 37830, 36 pp.

9. Hanna, S. R., G. A. Briggs, J. Deardorff, B. A. Egan, F. A. Gifford and F. Pasquill, 1977: AMS Workshop on Stability Classification Schemes and Sigma Curves - Summary of Recommendations. Bull. Am. Meteorol. Soc., 58, 1305-1309.

10. Izumi, Y. and J. S. Caughey, 1976: Minnesota 1973 Atmospheric Boundary Layer Experiment Data Report., AFCRL-TR-76-0038, 29 pp.

11. Joynt, R. C. and D. R. Blackman, 1976: A numerical model of pollutant transport. Atmos. Environ., 10, 433-442.

12. Kaimal, J. C., J. C. Wyngaard, D. A. Haugen, O. R. Coté and Y. Izumi, 1976: Turbulence structure in the convective boundary layer. J. Atmos. Sci., 33, 2152-2169.

13. Lenschow, D. H. and E. M. Agee, 1976: Preliminary Results from the Air Mass Transformation Experiment. Bull. Am. Meteorol. Soc., 57, 1346-1355.

14. Panofsky, H. A., H. Tennekes, D. H. Lenschow and J. C. Wyngaard, 1978: The characteristics of turbulent velocity components in the surface layer under convective conditions. Draft report available from Dept. of Meteorol., Penn State Univ., University Park, PA., 16802, 11 pp.

15. Pasquill, F., 1961: The estimation of the dispersion of windborne material. Meteorol. Mag., 90, 33-49.

16. Pasquill, F., 1974: Atmospheric Diffusion, 2nd Ed., Halsted Press, New York, 429 pp.

17. Pasquill, F., 1976: Atmospheric Dispersion Parameters in Gaussian Plume Modeling, Part II. Possible Requirements for Change in the Turner Workbook Values, EPA-600/4-760306, USEPA, Environ. Sci. Res. Lab., Res. Triangle Park, NC. 27711, 44 pp.

18. Smith, F. B., 1968: Conditioned particle motion in a homogeneous turbulent field. Atmos. Environ., 2, 491-508.

19. Smith, F. B., 1972: A scheme for estimating the vertical dispersion of a plume from a source near ground level. Air Pollution: Proceedings of the Third Meeting of the Expert Panel on Air Pollution Modeling. NATO CCMS Committee, Chapter XVII, 14 pp.

20. Smith, F. B., 1977: Application of data from field programs to estimation of K profiles and vertical dispersion, TDN No. 86, Meteorol. Office, Boundary Layer Res. Branch, Bracknell, Berkshire, U.K.

21. Turner, D. B., 1969: Workbook of Atmospheric Dispersion Estimates, U.S. Dept. Health, Ed. & Welfare, Environ. Health Service, Pub. No. 995-AP-26, 84 pp.

22. Watson, C. W. and S. Barr, 1976: Monte Carlo simulation of the turbulent transport of airborne contaminants. UC-41, Los Alamos Scient. Lab., Los Alamos, NM 87545, 28 pp.

23. Weber, A. H., K. R. McDonald and G. A. Briggs, 1977: Turbulence classification schemes for stable and unstable conditions, Proceedings Joint Conf. on Applic. of Air Poll. Meteorol., Am. Meteorol. Soc., 45 Beacon St., Boston, Mass. 02108, 96-102.

24. Willis, G. E. and J. W. Deardorff, 1974: A laboratory model of the unstable planetary boundary layer, J. Atmos. Sci., 31, 1297-1307.

25. Wyngaard, J. C., O.R. Cote and K. S. Rao, 1974: Modeling the atmospheric boundary layer. Advances in Geophysics, Vol. 18A, Academic Press, Inc., New York, 193-211.

Reprinted from JOURNAL OF APPLIED METEOROLOGY, Vol. 18, No. 4, April 1979
American Meteorological Society
Printed in U. S. A.

Some Statistics of Lagrangian and Eulerian Wind Fluctuations

STEVEN R. HANNA

Air Resources Atmospheric Turbulence and Diffusion Laboratory, NOAA, Oak Ridge, TN 37830

(Manuscript received 19 July 1978, in final form 11 December 1978)

ABSTRACT

The linear relationship $u'(t+\tau)=u'(t)R(\tau)+u''(t)$ is shown to be approximately valid for Lagrangian and Eulerian wind speed observations in the planetary boundary layer, where t represents any time and $t+\tau$ is some later time, u' is the turbulent wind speed fluctuation, $R(\tau)$ the autocorrelation coefficient, and u'' a random wind speed component assumed to be independent of u'. Eulerian wind data from the Minnesota boundary layer experiment and Lagrangian wind data from tetroon trajectories near Las Vegas and Idaho Falls are analyzed. At extreme values of $u'(t)$ for the Eulerian data, $u'(t+\tau)$ tends to be slightly less than that predicted by the above relationship. An application of this formula to the calculation of diffusion yields results in agreement with Taylor's theory.

1. Introduction

The main purpose of this research is the study of methods of estimating Lagrangian or Eulerian wind fluctuations at one time based on a knowledge of wind fluctuations at some previous time. Smith (1968), in a study of the conditioned motion of fluid particles, introduced the assumption that the Lagrangian turbulent fluctuation u' of a given fluid parcel at any time $t+\tau$ is linearly related to the turbulent fluctuation at some previous time, t i.e.,

$$u'(t+\tau)=u'(t)R(\tau)+u''(t). \tag{1}$$

The proportionality factor $R(\tau)$ is the autocorrelation coefficient at time lag τ. This assumption is potentially very useful in simulating the time variation of turbulent velocity along an air parcel trajectory. The last term, $u''(t)$, is a random component of the turbulence, assumed to be independent of $u'(t)$. The standard deviation $\sigma_{u''}$ of the random component must be defined by the relation

$$\sigma_{u''}=\sigma_{u'}[1-R^2(\tau)]^{\frac{1}{2}} \tag{2}$$

in order that turbulent energy $\sigma_{u'}^2$ be conserved with time. There are not many Lagrangian turbulence data available to test this assumption. Smith (1968) analyzed a few geostrophic wind trajectories which suggested that $u'(t+\tau)$ was proportional to $u'(t)$, and that $\sigma_{u''}$ was roughly independent of $u'(t)$. By analyzing wind speed data for a single run from an anemometer suspended from a tethered balloon, Smith (1973) also determined that $u'(t+\tau)$ was proportional to $u'(t)$ in all cases except for the extreme 1% at the tails of the wind speed distribution. In the region of extreme turbulence fluctuations, wind speed fluctuations tended to revert toward the mean value to a degree greater than is suggested by Eq. (1).

These concepts will be tested further in this paper using recent Eulerian wind data from the Minnesota boundary layer experiment and Lagrangian wind data from tetroon flights in Las Vegas and Idaho Falls. Lagrangian and Eulerian motions are assumed to be related in a way suggested by several workers, e.g., Gifford (1955) and Hay and Pasquill (1959), i.e., the Lagrangian and Eulerian correlograms and spectra are similar in shape and differ only in their time scales, denoted by T_L and T_E. The ratio T_L/T_E is commonly called β.

2. Analysis of Minnesota Eulerian wind data

During September 1973, the Air Force Cambridge Research Laboratories (AFCRL) and the British Meteorological Office (BMO) cooperated in a series of Eulerian measurements of wind and temperature in the boundary layer over flat farmland in Minnesota. The general experiment is described by Readings *et al.* (1974), a data summary is presented by Izumi and Caughey (1976), and several analyses of the data have appeared in the literature (see, e.g., Kaimal *et al.*, 1976). The wind data used in this analysis are from the BMO instruments, which are cup anemometers located at five levels between about 61 and 1220 m, held aloft by a large captive balloon and its tethering cable. These observations are analyzed together and considered to represent the mid to upper portions of the planetary boundary layer.

The nine runs listed in Table 1 were studied. Monin–Obukhov lengths, friction speeds and other Eulerian turbulence information for the unstable runs are given

TABLE 1. Minnesota runs.

	Unstable					Stable			
Run	3A1	5A1	6A1	6B1	7C1	3	4A	4B	5
Date	9/11/73	9/15/73	9/17/73	9/17/73	9/19/73	9/11/73	9/13/73	9/14/73	9/15/73
Starting time (LT)	1510	1622	1401	1652	1415	2316	2315	0426	2144

by Izumi and Caughey (1976). Each run is 75 min in length, but we used only the first two 15 min segments of a run. The recorded data represent total wind speed. Since the time interval between readings is 0.1 s, each 15 min run contains 9000 individual wind speed records. Wind speeds were moderate, ranging from 4.6 to 11.6 m s^{-1}, and turbulence intensities $\sigma_{u'}/\bar{u}$ were about 0.15 for the unstable runs and about 0.07 for the stable runs.

a. Test of the assumption $u'(t+\tau)=u'(t)R(\tau)+u''(t)$

To test the linearity assumption, initial wind fluctuations $u'(t)$ were grouped into 30 ranges from $-5\sigma_{u'}$ to $+5\sigma_{u'}$, each range or interval covering $\sigma_{u'}/3$. If, for example, $\sigma_{u'}$ were 1 m s^{-1}, then the ranges would be

Range 1: -5.00 m $s^{-1} < u' \leqslant -4.67$ m s^{-1}
Range 2: $-4.67 < u' \leqslant -4.33$
⋮
Range 15: $-0.33 < u' \leqslant 0$
Range 16: $0 < u' \leqslant 0.33$
⋮
Range 29: $4.33 < u' \leqslant 4.67$
Range 30: 4.67 m $s^{-1} < u' \leqslant 5.00$ m s^{-1}

Each wind fluctuation $u'(t)$ is placed into one of the 30 ranges, and the observed $u'(t+\tau)$ is found from the data record, using time lags τ of 1, 5, 10, 30 and 60 s. The $u'(t+\tau)$ values for each range of $u'(t)$ and each time lag τ are then averaged [giving $\overline{u'(t+\tau)|u'(t)}$], and the standard deviation of the random component of turbulence $\sigma_{u''}$ is calculated. The notation $\overline{u'(t+\tau)|u'(t)}$ refers to the average value of $u'(t+\tau)$, given $u'(t)$. For ease in comparing various runs, all fluctuations u' are normalized by the standard deviation of the turbulent fluctuations $\sigma_{u'}$.

In order to more efficiently present the observations used to test the linearity implied by Eq. (1), all runs with correlation coefficients $R(\tau)$ in certain narrow ranges were grouped together. Fig. 1 shows normalized values of $\overline{u'(t+\tau)|u'(t)}$ as a function of $u'(t)/\sigma_{u'}$ for 45 unstable runs with $R(\tau)>0.85$. The average $R(\tau)$ for the 45 runs is 0.89. All correlations $R(\tau)>0.85$ are found at time lag τ equal to 1, 5 or 10 s. Note that in the region $-1.5<u'(t)/\sigma_{u'}<1.5$, which contains ~86% of the data points, the data fall along a straight line with slope exactly equal to $R(\tau)$, as suggested by (1), the basic assumption of this paper. At extreme values of $u'(t)$, where $|u'(t)|/\sigma_{u'}>1.5$, the curve becomes slightly S shaped, as Smith (1973) found with his Eulerian data, and the fluctuations $u'(t+\tau)$ are slightly less than what Eq. (1) would predict. There is much less certainty in the extreme points because comparatively few data records are represented.

Four stable runs were also analyzed, to see if there was any dependence of the linearity relationship on stability. The fluctuation $\overline{(u'(t+\tau)|u'(t))}/\sigma_{u'}$ is plotted as a function of $u'(t)/\sigma_{u'}$ for correlations $R(\tau)$ between 0.8 and 0.9 in Fig. 2. The stable curve is slightly more linear at the extremes than the unstable curve, and the basic linearity assumption [Eq. (1)] is indeed verified by these data over most of the range of $u'(t)$.

Similar plots were made for correlation ranges $0.7<R<0.8$, $0.6<R<0.7$, etc., for both the stable and unstable observations. The curves are linear with

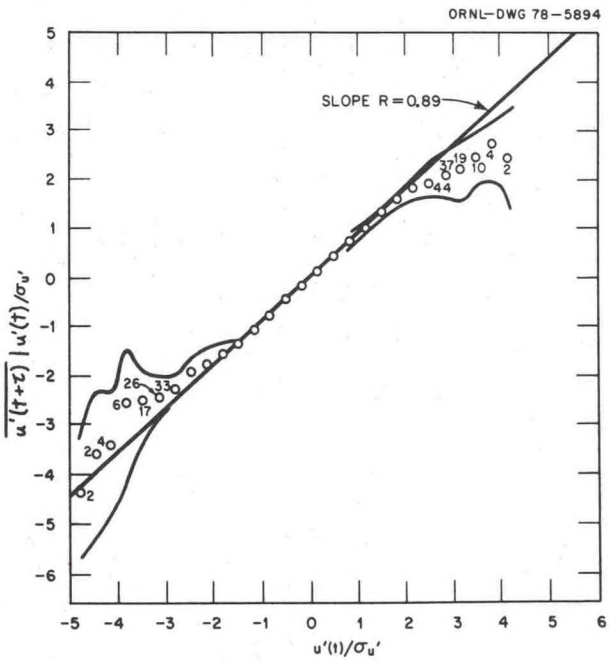

FIG. 1. Normalized average $[\overline{u'(t+\tau)|u'(t)}]/\sigma_{u'}$ of the wind fluctuation at any time $t+\tau$ plotted versus the normalized initial wind fluctuation $u'(t)/\sigma_{u'}$ at time t. 45 unstable Minnesota runs with $R(\tau)>0.85$ are used. $R(\overline{\tau})=0.89$. Where numbers appear beneath the point, they indicate the number of cases represented (if less than 45). The curved line represents $\pm\sigma$ for the 45 cases. The notation $\overline{u'(t+\tau)|u'(t)}$ refers to the average value of $u'(t+\tau)$, given $u'(t)$.

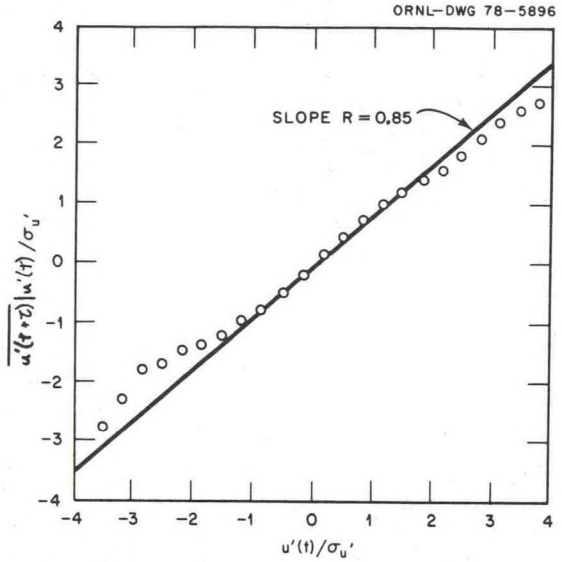

FIG. 2. As in Fig. 1 except that four stable Minnesota runs with $0.8<R(\tau)<0.9$ are used. Time lags of 1, 5 or 10 s are represented.

slope $R(t)$ over the range $1.5\sigma_{u'}<u'(t)<1.5\sigma_{u'}$, in agreement with Figs. 1 and 2, and also have a slight S shape at extreme values of $u'(t)$ outside of this range.

b. Shape of the conditional probability distribution function

The distribution $P[u'(t+\tau)|u'(t)]$, that is, the probability that the wind speed fluctuation at time $t+\tau$ will have a certain value under the condition that the fluctuation at time t is specified, was calculated for various initial values of $u'(t)$. Fig. 3 is a typical example of such a distribution, obtained from run 7, with $u'(t)$ in the range $-1.67\sigma_{u'}$ to $-1.33\sigma_{u'}$. A theoretical Gaussian curve is drawn as a dashed line. The observed frequency of occurrence of $u'(t+\tau)$ is fairly close to the Gaussian curve, and it is expected that agreement would improve if the size of the data sample were increased. All the plotted distributions of this type were roughly Gaussian, exhibiting little evident skewness. The standard deviation of each conditional distribution curve equals $\sigma_{u''}$, which is the previously defined standard deviation of the random component of turbulence.

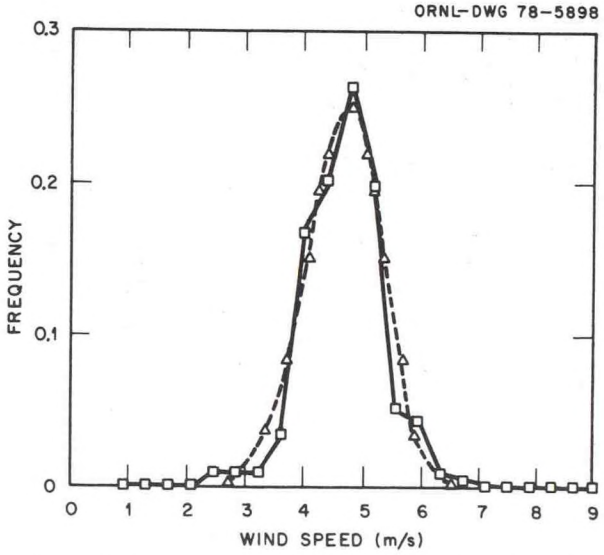

FIG. 3. Observed conditional probability distribution function $P[u'(t+\tau)|u'(t)]$ for $-5/3<u'(t)/\sigma_{u'}<-4/3$, Minnesota run 7, level 1. The squares connected by a solid line are the observed points and the triangles connected by a dashed line are points following a Gaussian or normal distribution. $\bar{u}=5.69$ m s^{-1}, $\sigma_{u''}=0.63$ m s^{-1}, $\tau=1$ s, $R(\tau)=0.89$.

c. Test of the assumption that $\sigma_{u''}$ is independent of $u'(t)$

Smith (1968) presented a few Lagrangian data from barotropic wind trajectories that verified the independence of $\sigma_{u''}$ and u'. In Fig. 4 the normalized ratios $\sigma_{u''}(\text{range})/\overline{\sigma_{u''}}$ are plotted as a function of $u'(t)/\sigma_{u'}$ for unstable Eulerian runs at Minnesota. The primed variable is the turbulent wind speed fluctuation, and the double primed variable is the random component of the total turbulent fluctuation, as defined in Eq. (1). The variable $\overline{\sigma_{u''}}$ is the weighted average standard deviation of 30 ranges in each run. Separate points are plotted for each of the seven correlation (R) groups, and the average curve is drawn as a solid line. In the interval $-2<u'(t)/\sigma_{u'}<2$,

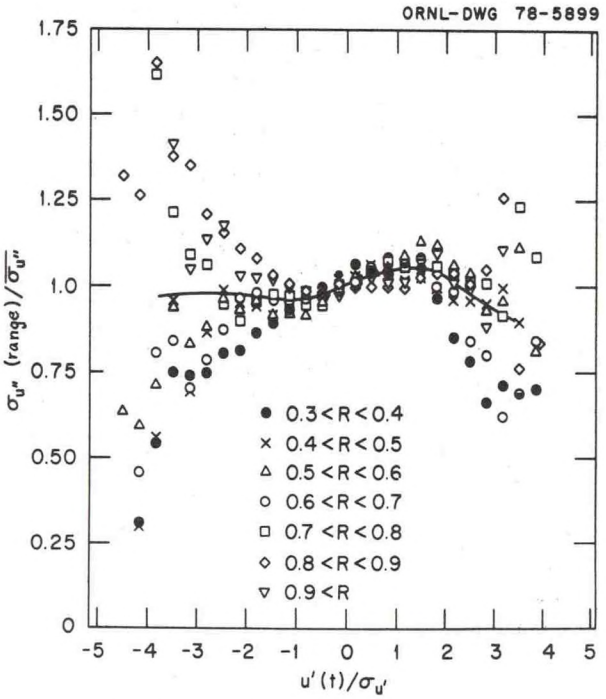

FIG. 4. Variation of the ratio $\sigma_{u''}(\text{range})/\overline{\sigma_{u''}}$ with initial normalized fluctuations $u'(t)/\sigma_{u'}$ for unstable Minnesota runs. Data are separated also into seven groups of $R(\tau)$. The solid line is the best-fit line to the data points.

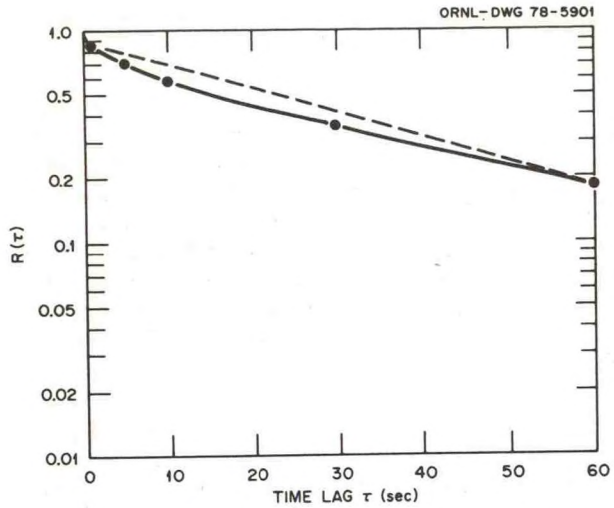

FIG. 5. Autocorrelation coefficient $R(\tau)$ versus time lag τ averaged over all unstable Minnesota runs. A dashed straight line is drawn between the points for τ equal to 1 and 60 s in order to illustrate the departure of the curve from a straight line.

there is a tendency for $\sigma_{u''}$ to be a few percent less than the average for $u'(t)<0$, and a few percent higher than the average for $u'(t)>0$.

On the average, there are slightly reduced values of $\sigma_{u''}$ at the extremes. It is also noticeable that the normalized $\sigma_{u''}$ tends to be larger at the extremes of $u'(t)$ for high correlations $R(\tau)$ than for low correlations. It can be concluded that $\sigma_{u''}$ is nearly independent ($\pm 10\%$) of $u'(t)$ for $-2<u'(t)/\sigma_{u'}<2$, i.e., for 95% of the data.

d. Shape of the correlation function $R(\tau)$

The average correlation $R(\tau)$ for the unstable Minnesota runs is plotted on a logarithmic ordinate in Fig. 5. The observed values curve slightly below a straight line representing the formula $R(\tau)=e^{-\tau/33\text{ s}}$. It can be concluded that the magnitude of $R(\tau)$ can be approximated by an exponential function to within $\sim 20\%$ for the range of time lags studied in this paper.

3. Analysis of Las Vegas Lagrangian wind data

The basic assumptions in this paper were introduced in the framework of Lagrangian flows. Angell *et al.* (1971) published analyses of radar observations of 35 constant volume balloons (tetroons) flown at heights of 400–500 m past the 460 m BREN tower at the Nevada Test Site during the spring of 1968. Turbulent vertical speed fluctuations were estimated from instantaneous tetroon positions observed every $\frac{1}{2}$ min during flights with mean durations of about 1 or 2 h. Since each run contains only 100 or 200 data records, the results of these analyses will not be as statistically significant as the results of the analysis of the Eulerian wind observations at Minnesota where thousands of data records were available for each run. But the tetroon data from Las Vegas and other tetroon data from Idaho Falls to be discussed in the next section are among the only atmospheric Lagrangian wind data currently available. Wind speeds during the Las Vegas runs ranged from 4 to 10 m s^{-1} and $\sigma_{w'}$ ranged from near zero to more than 2 m s^{-1}. The experiments were carried out during the day.

Correlations dropped off to zero at a time lag of ~ 4 min for these data (Fig. 6). The results of two runs with relatively large correlations are given in Fig. 7, where the averaged conditional fluctuation $\overline{w'(t+\frac{1}{2}\text{ min})\,|\,w'(t)}$ is plotted as a function of $w'(t)$. The slope of the curves equals $R(\frac{1}{2}\text{ min})$, as suggested by (1), and there is no S shape to the extreme ends of the curve.

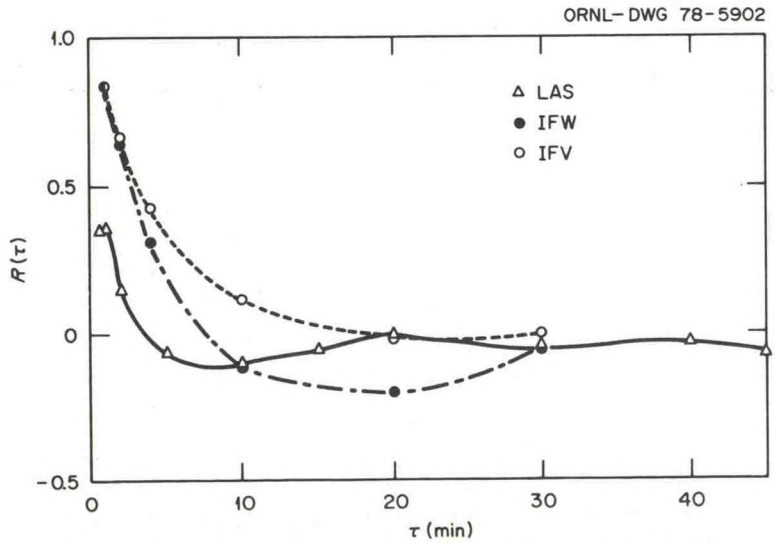

FIG. 6. As in Fig. 5 except averaged over all Las Vegas w' and Idaho Falls w' and v' runs. Lagrangian tetroon data.

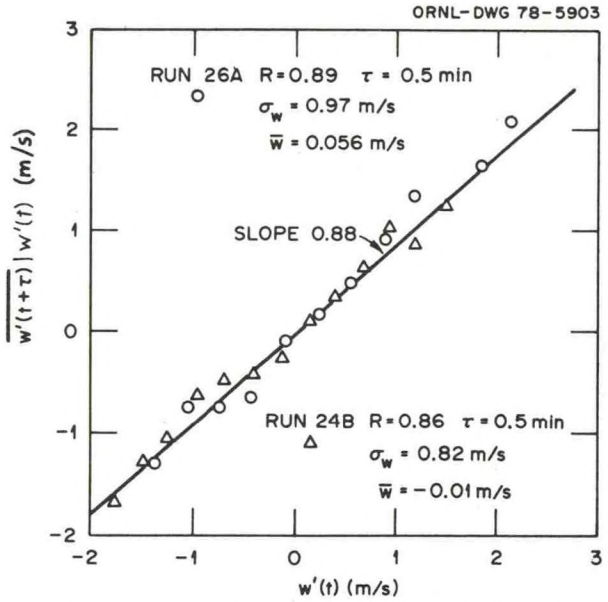

FIG. 7. Average vertical velocity fluctuation $\overline{w'(t+\tau)}\,|w'(t)$ at any time $t+\tau$ plotted versus the fluctuation $w'(t)$ at time t, for two unstable Las Vegas runs. Lagrangian tetroon data.

An indication that $\sigma_{w''}$ is independent of w' is provided by Fig. 8 for these same two runs. There is much scatter, but there seems to be little dependence on w' evidenced by these results.

4. Analysis of Idaho Falls Lagrangian wind data

Nearly 100 tetroon flights were made during July 1966 at Idaho Falls, with the purpose of studying helical circulations in the planetary boundary layer (Angell *et al.*, 1968). Consequently, these data all represent convective daytime situations. Velocity estimates were made from instantaneous tetroon positions

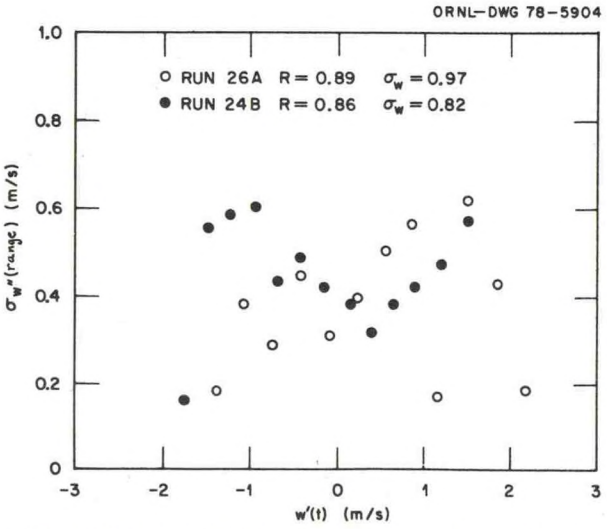

FIG. 8. Random turbulent fluctuation $\sigma_{w''}$ for each range of $w'(t)$ plotted versus $w'(t)$, for two unstable Las Vegas Lagrangian tetroon runs.

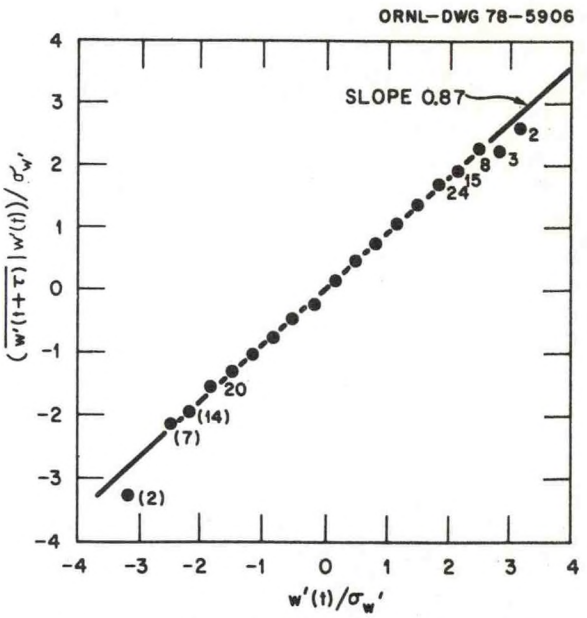

FIG. 9. Normalized average $[\overline{w'(t+\tau)}\,|w'(t)]/\sigma_{w'}$ of the vertical wind fluctuations at any time $t+\tau$ plotted versus the normalized initial fluctuation $w'(t)/\sigma_{w'}$ at time t. 25 Lagrangian tetroon runs from Idaho Falls with $R(\tau)>0.8$ are used. Where numbers appear beneath the point, they indicate the number of runs represented (if less than 25). The straight line has a slope equal to the average correlation $R(\tau)$.

recorded every minute during the runs, which lasted ~2 h. Mean wind speeds ranged from 6.7 to 13.7 m s^{-1} and $\sigma_{u'}$ was about 2.0 m s^{-1}. The data were analyzed

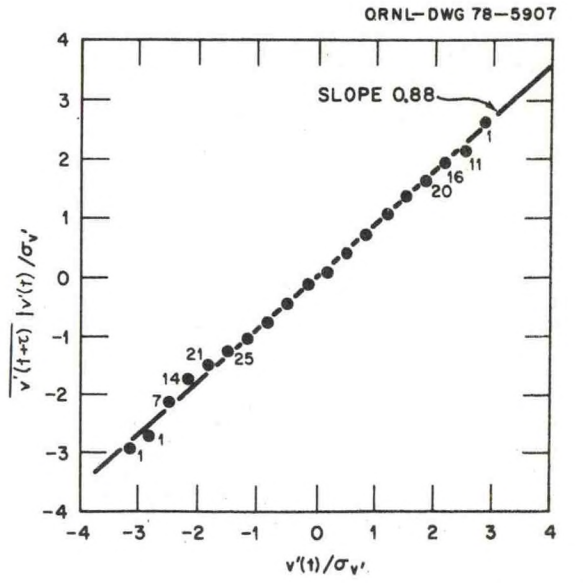

FIG. 10. Normalized average $([\overline{v'(t+\tau)}\,|v'(t)]/\sigma_{v'}$ of the lateral wind fluctuations at any time $t+\tau$ plotted versus the normalized initial fluctuation $v'(t)/\sigma_{v'}$ at time t. 27 Lagrangian tetroon runs from Idaho Falls with $R(\tau)>0.8$ are used. Where numbers appear beneath the point, they indicate the number of runs represented (if less than 27). The straight line has a slope equal to the average correlation $R(\tau)$.

for variations in the lateral and vertical components of the turbulent wind fluctuations, v' and w', respectively. The average correlation curves $R(\tau)$ for the 25 w' runs and the 28 v' runs are compared in Fig. 6 with the Las Vegas correlation curve, showing that the turbulence time scale is two to four times larger in the Idaho Falls experiment. Also, it is seen that $R(\tau)$ is negative for most time lags beyond about 10 min.

a. Test of the assumption $v'(t+\tau)=v'(t)R(\tau)+v''(t)$

Figs. 9 and 10 display values of $\overline{(w'(t+\tau)\,|\,w'(t))}/\sigma_{w'}$ and $\overline{(v'(t+\tau)\,|\,v'(t))}/\sigma_{v'}$ as functions of $w'(t)/\sigma_{w'}$ and $v'(t)/\sigma_{v'}$, respectively, for all runs and time lags such that the correlation coefficient $R(\tau)>0.8$. The observations fall nearly exactly on a straight line with slope equal to the average $R(\tau)$ for both sets of data. There are no systematic departures from the straight line at extreme values of turbulent fluctuations. All the Lagrangian data analyzed are characterized by agreement with the assumption $\overline{v'(t+\tau)\,|\,v'(t)}=v'(t)R(\tau)$ over the entire range of $v'(t)$.

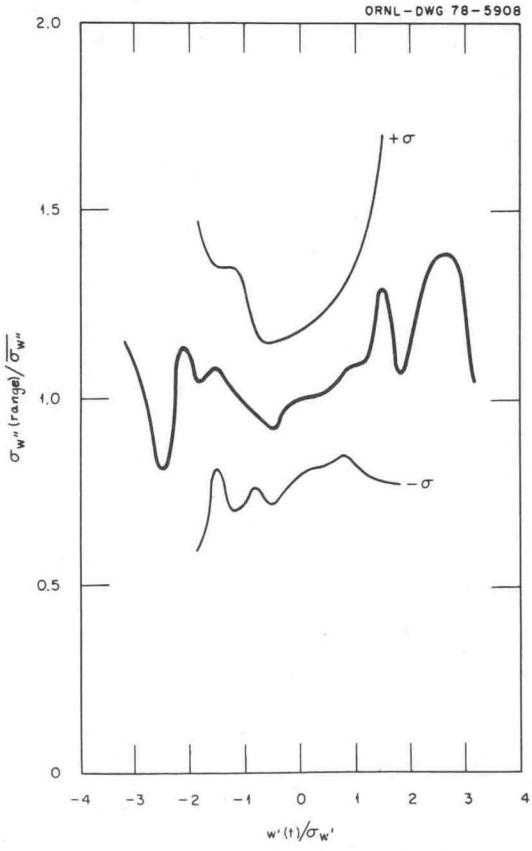

FIG. 11. Variation of the ratio $\sigma_{w''}(\text{range})/\overline{\sigma_{w''}}$ with initial normalized fluctuation $w'(t)/\sigma_{w''}$ for 25 Idaho Falls Lagrangian tetroon runs with $R(\tau)>0.8$. The thin lines represent $\pm\sigma$ for each range or value of $w'(t)/\sigma_{w'}$.

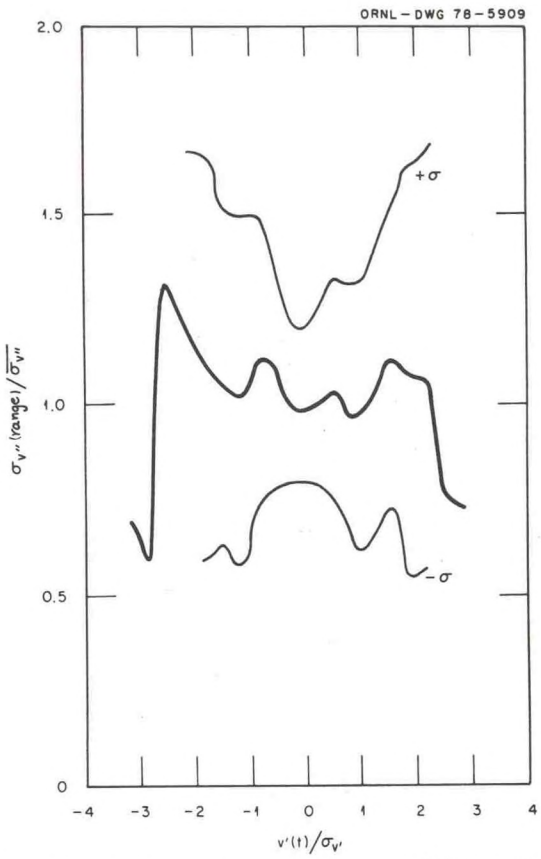

FIG. 12. Variation of the ratio $\sigma_{v''}(\text{range})/\overline{\sigma_{v''}}$ with initial normalized fluctuation $v(t)/\sigma_{v'}$ for 27 Idaho Falls Lagrangian tetroon runs with $R(\tau)>0.8$. The thin lines represent $\pm\sigma$ for each range or value of $v'(t)/\sigma_{v'}$.

b. Test of the assumption that $\sigma_{v''}$ *is independent of* $v'(t)$

The standard deviations $\sigma_{v''}$ and $\sigma_{w''}$ computed for each of the 30 ranges of v' and w' are normalized by the weighted-average $\overline{\sigma_{v''}}$ and $\overline{\sigma_{w''}}$ and plotted versus $v'(t)$ and $w'(t)$ in Figs. 11 and 12, respectively. All runs are used in these figures. There is no clear dependence of the normalized $\sigma_{v''}$ and $\sigma_{w''}$ values as a function of initial turbulent fluctuations.

5. Example of diffusion calculation made using the linearity assumption

To test the applicability of the linearity assumption to diffusion calculations, a simple computer experiment was run in which the trajectories of 1000 particles released from a single point were followed in a uniform wind field. At times up to 1000 min after release, the standard deviation σ of the crosswind position of the 1000 particles was calculated. Eq. (1) $[u'(t+\tau)=u'(t)R(\tau)+u'(t)]$ was used to generate turbulent fluctuations. At the first time step, each u' was chosen randomly from a Gaussian distribution with standard deviation $\sigma_{u'}$. The distribution of the

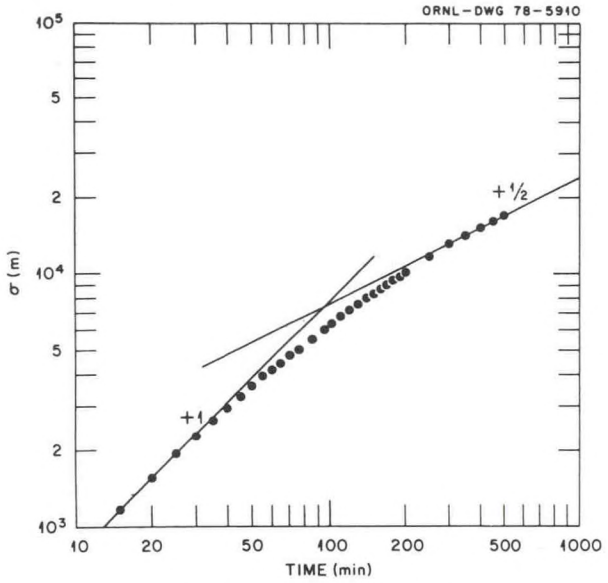

FIG. 13. Dotted line is the standard deviation σ of the spread of 1000 particles from a fixed axis as a function of time after release. The formula $u'(t+\tau)=u'(t)R(\tau)+u''(t)$ is used to generate the particle trajectories, where time step τ is assumed to be 5 minutes and $R(\tau)$ is assumed to be 0.9. The curve is asymptotic to lines representing power laws with slopes 1 and ½, which meet at time $=2\,T$, where T is the time scale in $R(\tau)=e^{-\tau/T}$.

random fluctuation u'' at subsequent times was assumed to be Gaussian with zero mean and variance $\sigma_{u''}^2=\sigma_{u'}^2[1-R^2(\tau)]$. The time step was 5 min and it was assumed that $R(5\text{ min})$ equals 0.9. The resulting variation of the standard deviation σ of particle position with time, plotted in Fig. 13, shows a smooth transition from $\sigma\propto t$ at small times ($t\ll T$) to $\sigma\propto t^{\frac{1}{2}}$ at large times ($t\gg T$). This curve coincides almost exactly with the solution to Taylor's diffusion equation for an exponential correlogram $[R(\tau)=\exp(-\tau/T)]$:

$$\sigma^2=2\sigma_v^2T^2[t/T-1+\exp(-t/T)], \qquad (3)$$

where the time scale T equals 50 min. With this time scale, $R(5\text{ min})=0.9$ as assumed above.

For this simple example, the computer approach is very time-consuming when compared with the analytical solution in Eq. (3). Consequently, the computer application of the linearity assumption will be practical only in situations where standard formulas, such as the Gaussian plume formula or analytical solutions to Taylor's equation do not apply. Examples of complex situations where this approach would be valid are sea breeze flow, flow around rough terrain, or any other situation where mean winds are not uniform. In these cases, an observed or predicted mean wind field plus the application of the linearity assumption will permit calculation of particle trajectories and diffusion.

6. Further discussion

The linearity assumption

$$u'(t+\tau)=u'(t)R(\tau)+u''(t)$$

has been verified using sets of Eulerian and Lagrangian wind data. One feature of this study that is not easily explained is that the $u'(t+\tau)$ versus $u'(t)$ curve is a straight line for the Lagrangian data but tends to be slightly S shaped at the extremes of the Eulerian data. It may be that extreme Eulerian turbulence fluctuations are due to relatively small eddies which are not as persistent as the rest of the turbulence structure. Kaimal (1978) suggests that eddies of different sizes are not translated with equal velocities.

This analysis is being repeated using concurrent Eulerian-Lagrangian measurements from the September 1978 PHOENIX Experiment near Boulder, Colorado. Tower-mounted anemometers will give fixed-point Eulerian readings, an airplane with turbulence instrumentation will give Eulerian-space measurements, and radar tracking of tetroons will give Lagrangian turbulence measurements. These measurements should yield a wealth of information about this hypothesis, as well as other information about the structure of Eulerian and Lagrangian turbulence.

Acknowledgments. The Minnesota data were supplied by Duane Haugen of NOAA's Wave Propagation Laboratory in Boulder, Colorado. Tetroon data were supplied by Walter Hoecker and James Angell of NOAA's Air Resources Laboratory in Silver Spring, Maryland. Discussions with Frank Gifford and Carmen Nappo of this laboratory and F. B. Smith of the British Meteorological Office have helped to clarify questions concerning the structure of turbulence. H. F. Snodgrass of this laboratory carried out most of the computer operations with the data.

This work was performed under an agreement between the National Oceanic and Atmospheric Administration and the Department of Energy.

REFERENCES

Angell, J. K., D. H. Pack and C. R. Dickson, 1968: A Lagrangian study of helical circulations in the planetary boundary layer. *J. Atmos. Sci.*, **25**, 707–717.

——, —— and N. Delver, 1971: Lagrangian-Eulerian time-scale ratios estimated from constant volume balloon flights past a tall tower. *Quart. J. Roy. Meteor. Soc.*, **97**, 87–92.

Gifford, F. A., 1955: A simultaneous Lagrangian-Eulerian turbulence experiment. *Mon. Wea. Rev.*, **83**, 293–301.

Hay, J. S., and F. Pasquill, 1959: Diffusion from a continuous source in relation to the spectrum and scale of turbulence. *Atmospheric Diffusion and Air Pollution*, F. N. Frenkiel and P. A. Shephard, Eds., *Advances in Geophysics*, Vol. 6, Academic Press, 345 pp.

Izumi, Y., and J. S. Caughey, 1976: Minnesota 1973 atmospheric boundary layer experiment data report. AFCRL-TR-76-0038, Air Force Cambridge Res. Lab., Hanscon AFB, MA 01731, 28 pp.

Kaimal, J. C., 1978: Horizontal velocity spectra in an unstable surface layer. *J. Atmos. Sci.*, **35**, 18–24.

——, J. C. Wyngaard, D. A. Haugen, O. R. Coté and Y. Izumi, 1976: Turbulence structure in the convective boundary layer. *J. Atmos. Sci.*, **33**, 2152–2169.

Pasquill, F., 1974: *Atmospheric Diffusion*, 2nd ed. Halsted Press, 429 pp.

Readings, C. J., and H. E. Butler, 1972: The measurement of atmospheric turbulence from a captive balloon. *Meteor. Mag.*, **101**, 286–298.

——, D. A. Haugen and J. C. Kaimal, 1974: The 1973 Minnesota atmospheric boundary layer experiment. *Weather*, **29**, 309–312.

Smith, F. B., 1968: Conditioned particle motion in a homogeneous turbulent field. *Atmos. Environ.*, **2**, 491–508.

——, 1973: The equation of diffusion for a realistic homogeneous atmosphere. TDN No. 39, Meteor. Office, Boundary-Layer Res. Br., Bracknell, UK, 19 pp.

C.E.A. - E.D.F.
CYCLES de CONFERENCES
sur la
"Mécanique de l'atmosphère et l'énergétique industrielle"
Jouy-en-Josas : 16 au 20 octobre 1978

- EFFECTS ON THE ATMOSPHERE OF HEAT REJECTION FROM LARGE WET OR DRY COOLING TOWERS

- Steven R. HANNA

- ATMOSPHERIC TURBULENCE AND DIFFUSION LABORATORY NATIONAL OCEANIC AND ATMOSPHERIC ADMINISTRATION - OAK RIDGE, TN, U.S.A.

- RESUME -

Cooling towers at the largest operating power plants (about 5000 Mw heat rejected) are observed to affect the atmosphere at distances of less than about 50 km. Mediam visible plume lengths are in the range 200 m to 1000 m, and occasionally medium-scale cumulus or stratus clouds are formed. On very few occasions, rain or snow showers fall from these clouds. Serious effects on vegetation due to drift deposition are observed only at distances less than a few hundred meters from wet mechanical draft cooling towers or spray ponds.

As the capacities of power plants increase, the atmospheric effects can also be expected to increase. A primary question is at what level of power production will the increases in cloudiness, precipitation, fog, drift deposition, and winds be unacceptable ? Similarity methods of estimating these effects using current knowledge are described. For example, it is shown that plume merging is minimized if large natural draft cooling towers are separated by distances greater than 1 km. A comparison of the effects of wet and dry mechanical and natural draft cooling towers is made, showing that clouds are more apt to be formed by plumes from dry towers than by plumes from wet towers.

ATDL Contribution File No. 78/7

1. Introduction

Atmospheric effects of heat rejection from cooling towers at the largest operating power plants are minimal and serious environmental damage is observed only within about 200m of the power plant. Limited effects in the form of visible stratus clouds during very humid conditions can be observed as far as 50 km from these power plants. In this paper these observed effects are summarized and an attempt is made to simulate the observations by means of mathematical models. The subjects of visible plumes, cloud formation, precipitation, drift deposition, and chemical interactions are discussed and extensions to possible atmospheric effects of larger power plants are made.

2. Visible Plume

Wet cooling towers nearly always cause a visible or condensed plume to form soon after the warm moist air leaves the tower mouth. A systematic set of observations of visible plume length from three natural draft cooling towers at the 2600 Mw Paradise, Kentucky Steam Plant was made by the Tennessee Valley Authority and reported by Coleman and Crawford (1978). Over a one year period, the mean morning and afternoon visible plume lengths are 620 and 190 m, for an annual mean of 410 m. The maximum observed plume length was 14 km, although several plumes were lost in cloud decks. The annual variation in mean visible plume length was large, from about 150 m during the summer to about 600 m during the winter. These figures are in agreement with less complete observations of visible plume length at many other cooling tower locations

Detailed meteorological measurements made by airplane flights on two days inside a visible cooling tower plume at Chalk Point, Maryland, were listed by Woffinden et al. (1977). On 22 June 1976 numerous aircraft passes through the bent over plume were made at several heights at a distance of 150m downwind of the tower. The excess temperature ΔT cross section in Figure 1 was obtained by averaging the data given by Woffinden et al. (1977). An excess dew point ΔT_d cross section was also constructed, and the plume edges were found to coincide with those in Figure 1. In the cross wind(y) direction the ΔT distribution is fairly close to Gaussian, as shown by the cut through the plume at an elevation of 200m, presented in Figure 2. The observed plume radius

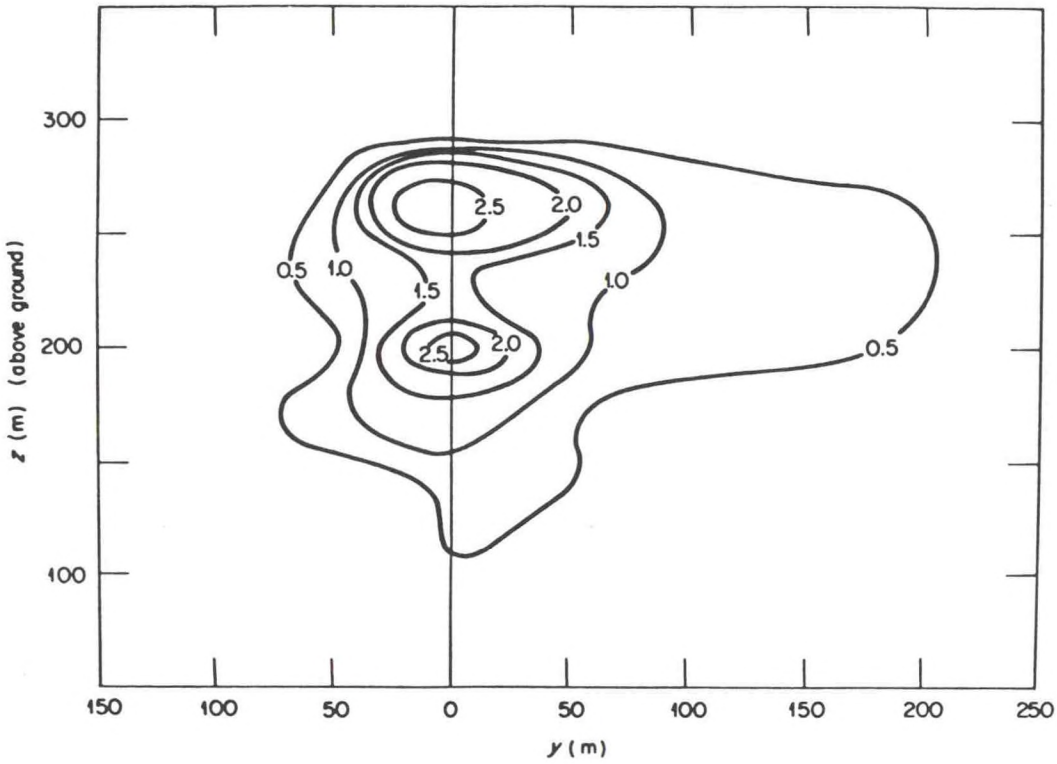

Figure 1: Cross section of temperature excess, ΔT (°C), Chalk Point plume, 22 June 1976, 150 m downwind, traverses 19-27. Bent over plume.

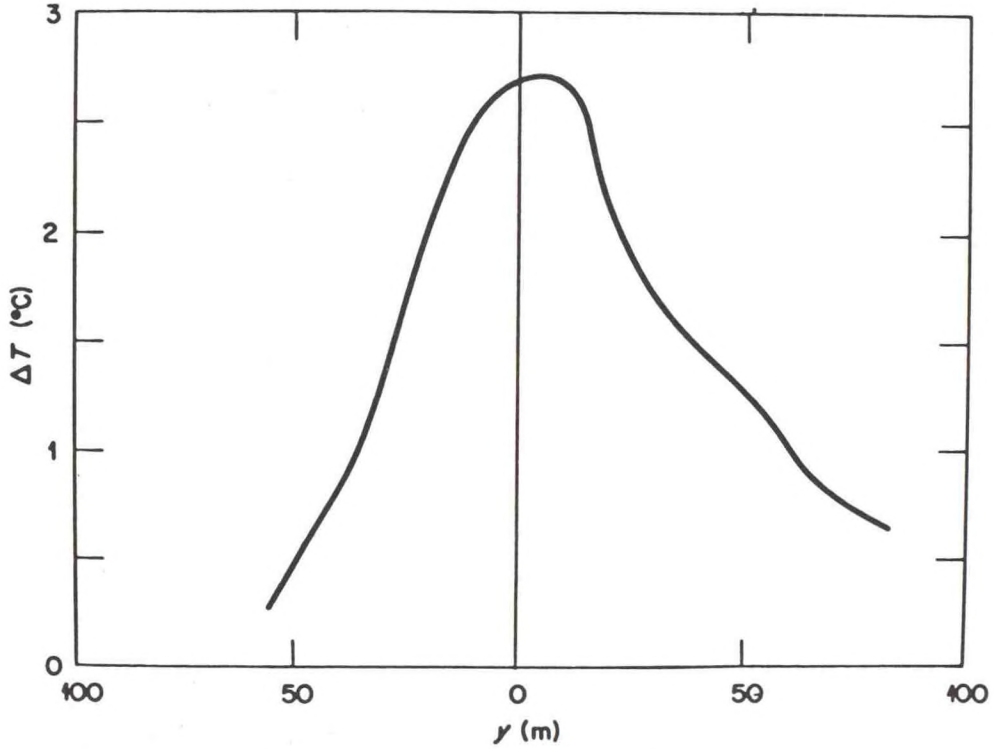

Figure 2: Temperature excess, ΔT, in the Chalk Point plume, at height 200 m, downwind distance 150 m, traverses 19-27 on 22 June 1976

R, 70m, and average ΔT, 1.5C, agree well with Briggs' (1975) entrainment formula for bent over plumes.

$$R = R_o + 0.4z \quad , \tag{1}$$

and Hanna's (1974) formula for ΔT variation in the near-field region of bent over plumes:

$$\Delta T/\Delta T_o = (1 + 0.4(z/R_o)(w_o/u)^{1/2})^{-2} \tag{2}$$

In these formulas subscript o referes to initial values, w is plume vertical speed and u is wind speed. The following initial parameters were measured: w_o = 4.6 m/s, T_{plume} = 36.8C, T_{air} = 24C, u = 4m/s, R_o = 24m.

On 23 June 1976 a vertical or calm plume was observed by the airplane at Chalk Point, yielding the y-z cross section of excess temperature ΔT in Figure 3. The bubble appearance of the plume is only an artifact of the manner of presenting the data, since this is not an instantaneous cross section but is constructed from traverses with turn around times of about two minutes. Again, the cross-plume distribution of ΔT is more Gaussian than top hat (uniform). The simple formula recommended by Hanna (1974) for estimating ΔT (z) in vertical plumes is

$$\Delta T/\Delta T_o = (1 + 0.15z/R_o)^{-2} \tag{3}$$

Predictions of this formula are plotted against height in Figure 4, which shows that the rate of decrease of ΔT with height is well-simulated, but the magnitude of ΔT is consistently overpredicted by a factor of two.

Briggs (1975) suggests that the effective cross-sectional area of the moisture plume is slightly less than that of the temperature plume. This factor accounts for the presence of patches of moist air in the plume. Consequently the ratio of volume flux ($V = uR^2$) at height z to initial volume flux ($V_o = w_o R_o^2$) for the moisture plume is (Hanna, 1978):

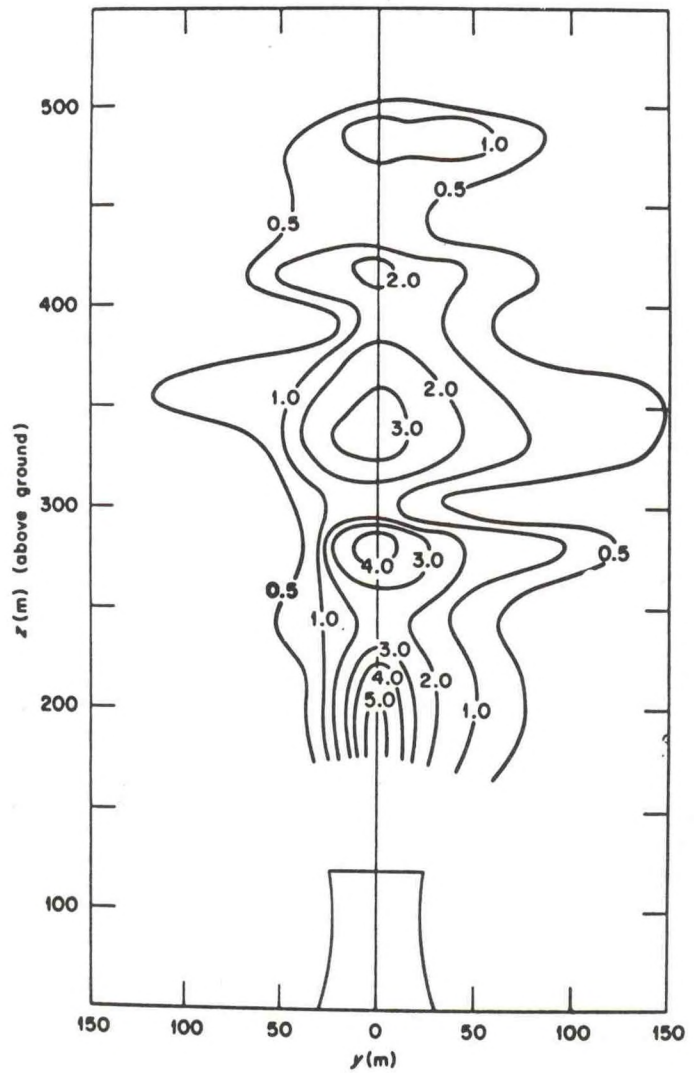

Figure 3: y-z cross section of temperature excess, ΔT (°C), in the Chalk Point plume, 23 June 1976, traverses 1-12. Vertical plume.

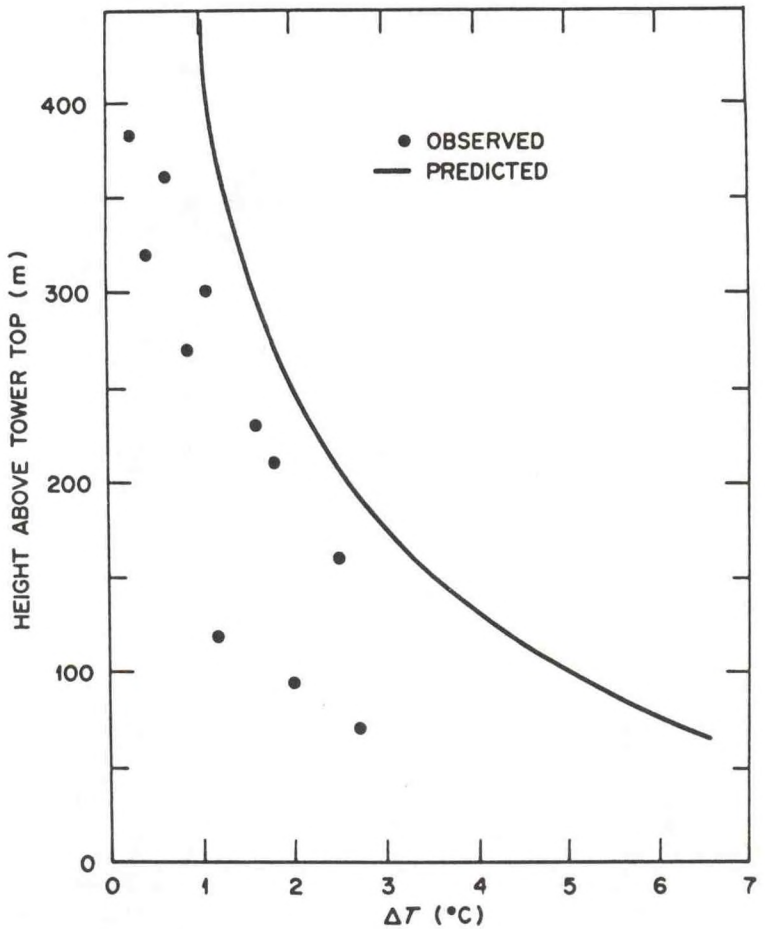

Figure 4: Observed (points) and predicted (line) temperature excess, ΔT in the Chalk Point cooling tower plume on 23 June 1976. Vertical plume.

$$\text{Bent over:}\quad V/V_o = (1 + 0.28(z/R_o)(u/w_o)^{1/2})^2 \tag{4}$$

$$\text{Vertical:}\quad V/V_o = (1 + 0.11\ z/R_o)^2 \tag{5}$$

These ratios can be used to estimate the location of the end of the visible plume, which occurs when the flux of initial water in the plume, $V_o q_o$, just equals the flux of saturation deficit, $V(q_s - q_a)$, where q is specific humidity and subscripts s and a refer to saturated ambient and actual ambient.

$$\text{Visible plume if } V_o q_o \geq V(q_s - q_a) \tag{6}$$

The ambient saturation deficit is the most important variable in determining visible plume length, clearly explaining why the Paradise plumes are four times longer in the winter than in the summer. For bent over plumes, the visible plume length x can be calculated from the height z by means of Briggs' (1975) plume rise formula $z = 1.8\ F^{1/3}\ u^{-1}\ x^{2/3}$, where F is the initial buoyancy flux $(g/T_o)V_o\Delta T$.

3. Cloud Formation

There is always a lifting condensation level in the atmosphere where a parcel of air lifted adiabatically from the surface will condense and form a natural cloud. Cooling tower plumes entrain ambient air so that by the time they are 100 m or more above the tower, they consist mostly of ambient air. Thus the plume acts as a lifting mechanism for ambient air and if the plume rises as high as the lifting condensation level a cloud will form. Such clouds are reported about 10% of the time by Hanna (1974) above the 1000Mw mechanical draft cooling towers at Oak Ridge, Tennessee. You can usually recognize when a "visible plume" changes to a "cloud" because of the increased growth and convection in the condensed plume. On some occasions, the plume is invisible until it reaches the lifting condensation level. By this mechanism it is possible for a small 1000Mw cooling tower plume to "trigger" a large 10^5 Mw cumulonimbus.

A number of numerical cloud models are available which have been applied to cloud formation by cooling tower plumes. Hanna's (1976) one-dimensional plume model is based on Weinstein's (1970) cloud model, and has been applied, for example, to cloud formation over cooling towers at the Wood River, Illinois oil refinery. The

cloud parameters observed by an airplane and predicted by the model are shown in Table 1 for a day on which Auer (1976) reported cloud formation over the refinery. Atmospheric effects of refineries in Los Angeles have been studied by Stinson and Brown (1976), who present numerous photographs of large convective clouds that are apparently the result of heat emissions from the refineries.

Table 1

Comparison of Observations and Predictions for Wood River Refinery

	Observed	Predicted
Cloud base	700m	650m
Cloud top	2050m	2350m

z(m)	Liquid Water Content Observed (g/m^3)	Liquid Water Content Predicted (g/m^3)
930	.046	.56
1270	.10	.75
1860	.44	1.30

z(m)	Observed w(m/s)	Predicted w(m/s)
500	3	2.0
1500	4	2.0
2000	3	2.3

z(m)	Observed $(T_p - T_e)$ (°C)	Predicted $(T_p - T_e)$ °C
500	.2	.1
1500	-.5	.3
2000	-.2	.5

Plume and cloud models are also available that follow the new trend in second order closure turbulence modeling. Yamada (1978) and Rao and Hosker (1978) discuss applications of these models to convection from cooling ponds, and an example of the excess moisture prediction of Rao and Hosker's model is given in Figure 5. It is difficult for grid models to treat clouds from cooling tower plumes, which can increase in scale from 10m to 1000m over their depth.

Differences in convection and cloud formation due to plumes from wet and dry towers were investigated using a cloud model by Koenig, Murray, and Tag (1978). The same amount of total heat was input in each of three special cases: all latent heat, equal parts latent and sensible, and all sensible heat. They conclude that sensible heat is much more likely to initiate convection and clouds than latent heat. The reason is that a plume composed of sensible heat has much more initial buoyancy than a plume composed of latent heat, and is more likely to rise to the lifting condensation level. The latent plume could form a large cloud if it could rise high enough, but in most cases it quickly loses its initial buoyancy and

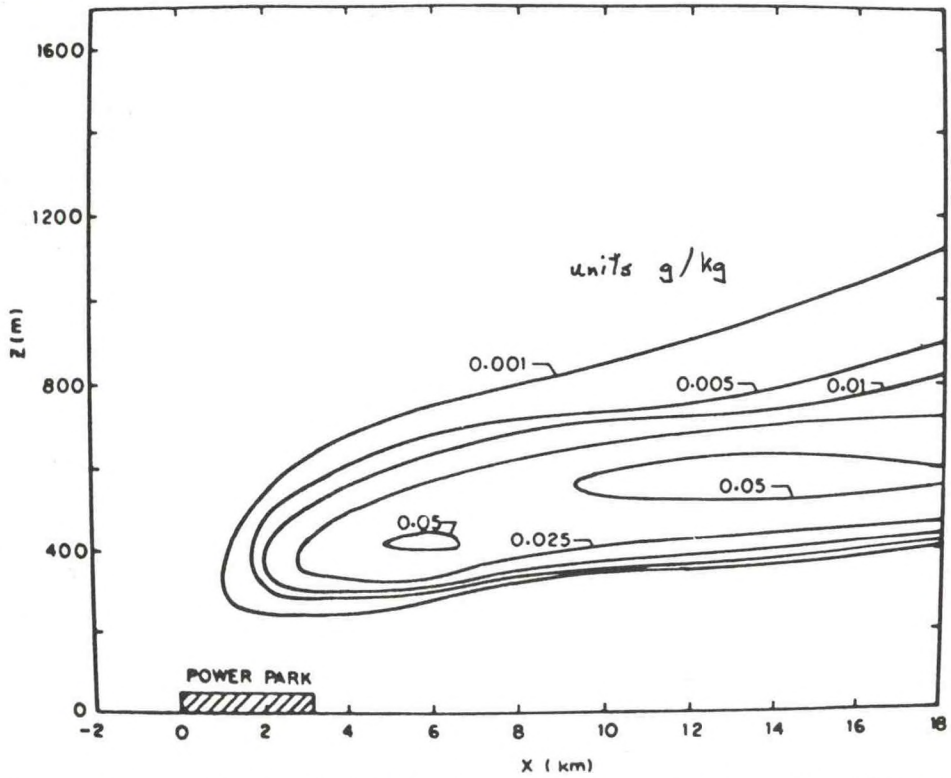

Figure 5: Calculated isopleths of mean specific liquid water content in the convective cumulus clouds spawned by the power park (RH = 90%). (Rao and Hosker, 1978).

stops rising before the lifting condensation level is reached. On the other hand, the dry plume, with no initial excess moisture, entrains ambient air as it rises and thus provides an efficient lifting mechanism for ambient air.

4. Precipitation

While cloud formation can often be seen over cooling towers, precipitation increases have been documented in only a handful of cases. Light snowfalls in plume shaped regions from 10 to 40 km downwind of cooling towers were reported by Culkowski (1961) in Oak Ridge and by Kramer et al. (1976) near Charleston, West Virginia. Otts (1977) describes a heavier snowfall (15 cm) near Charleston downwind of the 2000 Mw John Amos Steam Plant. In all these instances, snow developed from a plume-induced stratocumulus cloud in the mixing layer in very cold air. Because it takes time for the snow to reach a size necessary to fall out of the plume, snow at the ground is not observed until a distance of about 10 km from the cooling tower.

During showery convective conditions on a summer day, the plume may initiate rainfall, but it is difficult to detect in the midst of the natural space and time variation of the showers. Landsberg (1978) suggests that such precipitation increases would be detectable only during special case studies at distances of 1 km or less from the tower. A more significant change in precipitation may occur when the plume is associated with a broad cloud deck which is raining uniformly over a large area. Dana and Wolf (1977) estimated rain enhancement resulting from scavenging of cooling tower drops and found that the increase in rain at the ground should be measurable at downwind distances between 100m and 1000m.

A long term observation program of rainfall within about 25 km of the 3200 Mw Plant Bowen, Georgia, cooling towers is being conducted by Patrinos (1978). The isolines in Figure 6 show the ratio of winter rainfall after the plant went into operation to that before operation. A slight increase is shown downwind from Plant Bowen, but it is uncertain whether this increase is significant. Further study of the natural variability of rainfall in the Bowen area is necessary in order to determine the statistical significance of these results.

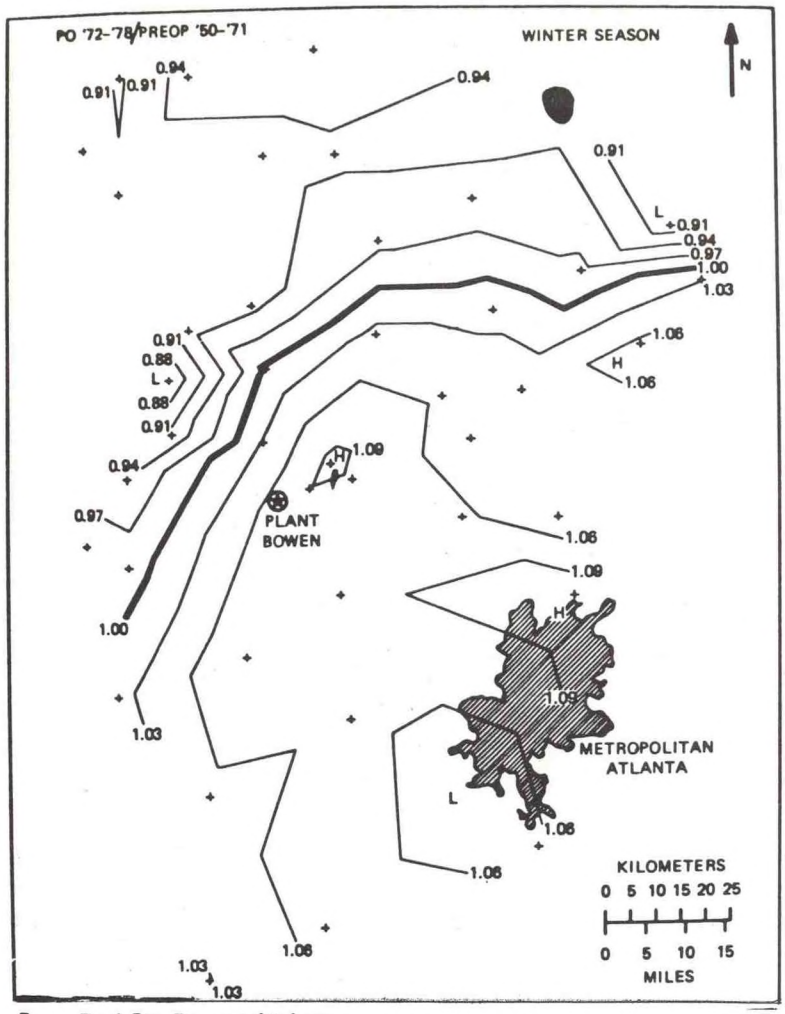

Figure 6:
The lines show the ratios of normalized winter rainfall after the operational period to those before plant operation. A slight high is shown downwind from Plant Bowen.

5. Drift Deposition

Ground deposition of drift drops emitted by wet cooling towers has recently been measured at several locations. The major environmental impact of drift is on structures and vegetation rather than on the atmosphere. Atmospheric variables such as wind speed and saturation deficit determine the magnitude of deposition of drift drops, which may contain salt if the power plant is located near the ocean or chemical additives such as chromate if the power plant is located on fresh water.

Where large natural draft cooling towers are used, effects of drift deposition are seen to be minimal. For example, Lauver et al. and Armbruster et al. (1978) have been monitoring sodium and chloride levels in trees, shrubs, and field crops around the Chalk Point cooling tower for several seasons. They report no accumulations above background levels in the plant species studied. However, Rochow (1978) reports serious damage to trees within 100m of the Palisades mechanical draft cooling towers where downwash often causes the plume to impinge

directly on the adjacent trees. Spray canals cause even more extensive damage because the drift drop source is essentially at ground level. Feder (1978) detected salt injury to trees 6 km downwind of the Brayton Point Power Station, Mass., spray canal, during 1975 with severe damage within a radius of 1 km. As a result of this study, the utility reduced water salinity by dilution with fresh water, and altered the engineering design of the spray units.

There are about ten drift deposition models available, which are compared and reviewed by Chen and Hanna (1978). The results of most of these models are within a factor of two, a difference which cannot be resolved with current accuracy of drift deposition measurements. Most models use ballistic drop trajectories for drops with diameters greater than 200 μm, and use a tilted Gaussian plume for smaller drops. The drift drop plume "tilts" with respect to the gas plume at a rate equal to the gravitational settling speed of the drops. After the drops fall out of the plume into the drier ambient air, they are calculated to evaporate according to basic cloud physics formulas, in which the rate of evaporation is a function of the drop size, the saturation deficit, and the amount of solute in the drop. These formulas are critically reviewed by Policastro et al. (1978).

On June 16, 1977, the Dye Tracer Experiment was conducted at Chalk Point to determine the relative contributions to total drift deposition water from the cooling tower and from the scrubber-equipped stack. Meyer and Stanbro (1977) put uranine dye into the cooling tower water and placed drift samplers on arcs at distances of 0.5 and 1.0 km from the tower. The Environmental Systems Corporation (1977) monitored cooling tower input parameters and ambient parameters. They found that the percentage of total drift deposition due to the cooling tower is 90% and 50% on the 0.5 and 1.0 km arcs, respectively. The cross wind variation of drift deposition has a nearly Gaussian shape, as shown by the plot of drift deposition versus angle on the 0.5 km arc in Figure 7.

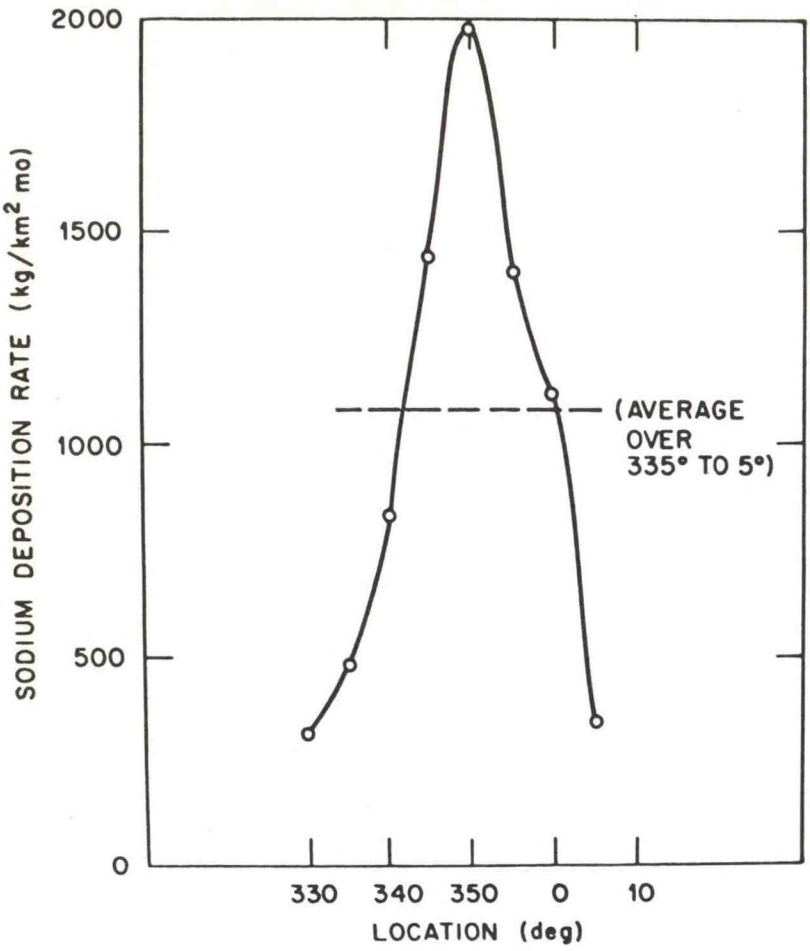

Figure 7:
Distribution of observed sodium deposition rate 0.5 km from the Chalk Point cooling tower during the Dye Tracer Experiment (Meyer and Stanbro, 1977). The average on the arc (dashed line) is 1080 Kg/km^2 mo.

6. Chemical Interactions

At fossil-fired power plants using cooling towers, the possibility exists for chemical interaction of the SO_2 and water vapor plumes. Stockham (1971) and Thomson et al. (1976) sampled plumes from airplanes at the Keystone, PA, power plant, finding that the acidity in the stack plume increased when the plumes merged. Sampling with cascade impactors showed that the smallest drops had the highest acidity.

Another interesting problem occurs at the Geysers thermal area in northern California, where the energy of naturally occuring geysers and hot springs is tapped for power. Mechanical draft cooling towers are used, and the excess H_2S and other gasses and aerosols produced from the wells are discharged into the mouth of the cooling towers. Thus the waste gasses and aerosols are presumably carried upward and away from the ground by the strongly buoyant cooling tower plume. This technique has also been proposed as a means of dispersing radioactive gasses at nuclear power plants. However there are many

difficult problems to be answered regarding the scavenging of the waste gasses and aerosols by drift and fog droplets due to mechanical and chemical processes.

7. Possible Effects of Future Large Power Parks

Future power parks are now being planned which will have many units within a relatively small area, resulting in heat rejection on the order of 10^5 Mw over an area of 10 to 100 km^2. Power parks have many advantages for the utilities, including easier security, construction, maintenance, storage, and transmission. However, the likelihood of atmospheric effects is greatly increased. In the absence of power parks of this size to study, we must rely on models and analogs to predict these effects.

Hanna (1977) used a one dimensional plume and cloud growth model to construct a climatology of visible cooling tower plume lengths and cloud frequencies. Various strengths and configurations of cooling towers were tested, using one year of twice-daily radiosonde observations from Nashville. For multiple plumes, it was assumed that plumes merged when their radii equalled one half of the distance between the towers. Since plume radius is roughly proportional to .5z and typical plume rise from a large cooling tower is 1000m, this assumption leads to the conclusion that plume merging can usually be prevented if cooling towers are separated by a distance greater than 1 km. For example, the frequency of cloud occurrence over the cooling towers in this investigation is given in Table 2. In the first three sources, the heat release is assumed to be from a single cooling tower. In the last 10^5 Mw source, 100 cooling towers are in a square grid 1 km apart. Note that the cloud frequency in this case is about halfway between the frequencies found for single 10^3 and 10^4 Mw cooling towers.

A similar model was applied to a 50,000 Mw power park by Lee (1976). His plume merging assumption is the same as that described above, but his entrainment and cloud microphysics assumptions are slightly different. The model was run using an average July radiosonde sounding for Shreveport, LA, with the result that a cloud formed between heights of 1500 and 4000m. Bhumralkar (1976) has applied a different model, which uses diffusivity or K coefficients, to this problem. However, he

Table 2

Frequency of Cooling Tower Cloud Occurrence Estimated Using Nashville Radiosonde Observations (Hanna, 1977)

Month (all 1974)	Single tower 10^3 Mw	Single tower 10^4 Mw	Single tower 10^5 Mw	100 towers on a 1 km grid 10^5 Mw
Jan.	.41	.70	.97	.59
Apr.	.34	.59	.96	.43
July	.51	.76	.97	.59
Oct.	.31	.54	.89	.39
All runs	.39	.64	.95	.50

initiates the plume in his two dimensional grid by arbitrarily inserting temperature and moisture perturbations at selected grid points in the boundary layer, under the condition that the sum of the perturbations equals the total power plant waste heat output. An example of the resulting visible plume and cloud outlines is given in Figure 8. In this method, the power park is effectively a broad area source of heat.

Comparison with analogous natural and manmade power sources is another way to determine the atmospheric effects of large power parks. A summary of the observed effects of other large energy sources is given in Table 3. It is seen that cumulus clouds commonly occur over such sources and that wind whirlwinds such as dust levels and water spouts are occasionally observed.

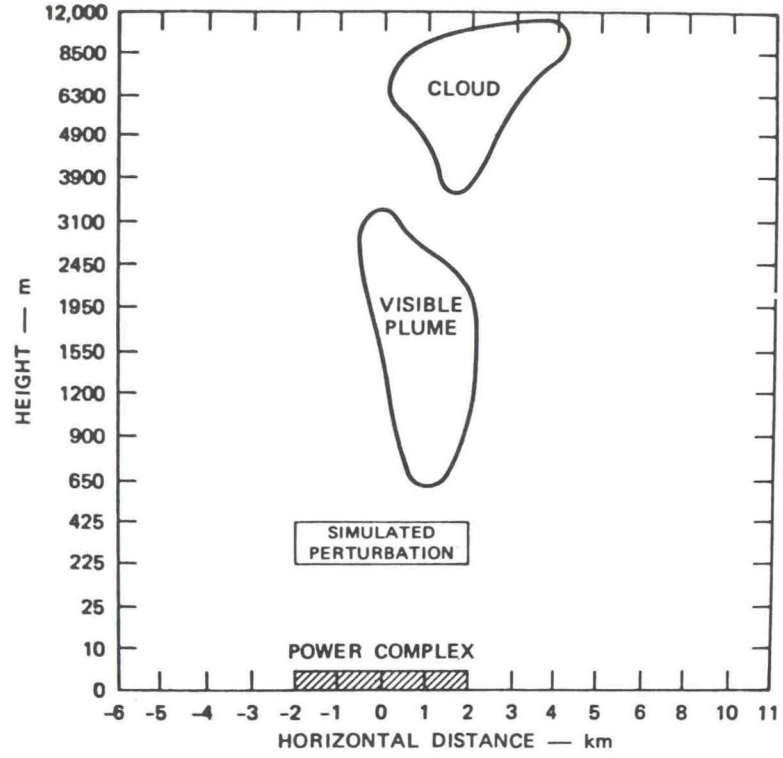

Figure 8: Predicted plume and cloud formation after 15 minutes (Bhumralkar, 1976).

Briggs (1974) suggested a criterion for estimating whether a given buoyant source with characteristic vertical speed V_β would concentrate vorticity (cause whirlwinds) in a fluid with characteristic tangential speed V_∞:

$V_\infty/V_\beta > 0.9$ No concentration of vorticity
The whole flow swirls

$0.15 < V_\infty/V_\beta < 0.9$ Vorticity can be concentrated (7)

$V_\infty/V_\beta < 0.15$ No concentration of vorticity
Buoyancy is dominant.

Table 3

Energy Characteristics of Natural and Man-Made Sources

Source	Area	Time duration	Total power	Observations
Surtsey Volcano (Bourne, 1964)	1 km^2	Several months	100,000 Mw	Continuous cloud Water spouts
Australian Bushfire (Taylor et al., 1973)	50 km^2	Several hours	100,000 Mw	Cumulus cloud Convergence
Booster Rocket Test (Morris, 1968)	300 m^2	150 seconds	148,000 Mw	Cumulus cloud
Oil Burners (Dessens, 1964)	3.2 km^2	Several hours	700 Mw	Cumulus cloud Dust devels
Oil Fires	--	Day	10,000 Mw	Large plume
Large City (Peterson, 1969)	10^3 km^2	Continuous	100,000 Mw	Effects on climate
Thunderstorm (Hanna and Swisher, 1971)	7 km^2	Hour	10,000 Mw	2.5 cm h^{-1} rain
Power Park	5 to 100 km^2	Continuous	100,000 Mw	---

Table 4 summarizes the application of this criterion to several buoyant sources. Observations agree with the predictions for the oil burners (whirlwinds observed), the brushfires (occasional whirlwinds) and the Saturn V firing (no whirlwinds). Strong natural convection occasionally causes dust devels or tornados. On only one occasion was a whirlwind reported at a cooling tower (D. Thomson, private communication). Note that vorticity concentration is predicted by this criterion for power parks, a conclusion which cannot be tested until a power park is constructed.

8. Further Comments

Detailed mathematical derivations of the models referred to in this review can be found in the references. It can be concluded that observations and models agree that atmospheric effects of current operating power plants are minimal, but these same models predict significant atmospheric effects, in the form of large clouds, increased rain, and whirlwinds, if large power parks are built.

Acknowledgements

This research was performed under an agreement between The National Oceanic and Atmospheric Administration and the Department of Energy. Travel funds to present this paper at the conference "Mécanique de l'Atmosphere et Energetique Industrielle" in Jouy-en Josas, France on 18-20 October 1978 were provided by Electricite de France.

Table 4

Calculation of the Vorticity Concentration Parameter V_∞/V_β for Several Sources (from Hanna and Gifford, 1975)

	Source			Environment			
Source	Radius R(m)	Buoyancy Flux $F(m^4/s^3)$	Heat Flux $H\left(\frac{m^2}{s^3}\right)$	Mixing Height z_i(m)	$V_B\left(\frac{m}{s}\right)$	$V_\infty\left(\frac{m}{s}\right)$	V_∞/V_B
Single Cooling Tower Sensible Heat	25	3500	10^{-2}	10^3	5.2	0.32	0.06
Cluster of 20 Cooling Towers	500	70,000	10^{-2}	10^3	5.2	1.7	0.33
Sensible Heat	5000	70,000	10^{-2}	10^3	2.4	1.7	0.71
Strong Natural Convection	500	2500	10^{-2}	10^3	1.7	1.7	1.0
Oil Burners (Dessens, 1964)	125	6000	10^{-2}	10^3	3.6	1.6	0.44
Saturn V (Morris,1968)	10	1,300,000	10^{-2}	10^3	51.	.13	0.0025
Australian Bushfires (Taylor et al, 1973)	10^3	900,000	10^{-2}	10^3	13.8	1.7	0.12

REFERENCES

Armbruster, J. A., C. L. Mulchi, L. W. Douglass and P. C. Wolf. Response of field crops to salt drift from a natural draft cooling tower, Cooling Tower Environment 1978, Proceedings, PPSP-CPCTP-22, WRRC Special Rep. No. 9, sponsored by Power Plant Siting Program, Maryland Dept. of Natural Resources, published by Water Resources Research Center, Univ. Md., College Park, MD, 179-196 (1978).

Auer, A. H., Observations of an Industrial Cumulus, J. Appl. Meteorol., 15: 406-413 (1976).

Bhumralkar, C. M., Weather Modification Caused by Waste Heat Rejected into the Atmosphere from Cooling Towers at Large Power Parks, Proceedings, Third Symp. on Atmospheric Turbulence, Diffusion, and Air Quality, Raleigh, available from Amer. Meteorol. Soc., 45 Beacon St., Boston, MA., 02108: 581-585 (1976).

Bourne, A.G., Birth of an Island, Discovery, 25: (1964).

Briggs, G. A., Plume Rise from Multiple Sources, Cooling Tower Environment-1974, S. Hanna and J. Pell, ed., ERDA Symposium Series, CONF-740302, Nat Tech. Information Service, U.S. Dept. of Commerce, Springfield, VA., 22161, ($13.60), 161-179 (1974).

Briggs, G. A., Plume Rise Predictions, Lectures on Air Pollution and Environmental Impact Analyses, American Meteorological Soc., 45 Beacon St., Boston, MA., 02108: 59-111 (1975).

Chen, N. C. J. and S. R. Hanna, Drift-Modeling and Monitoring Comparisons, Atmos. Environ., in press, (1978).

Coleman, J. A. and T. L. Crawford, Characterization of cooling tower plumes from Paradise Steam Plant, Cooling Tower Environment 1978, Proceedings, PPSP-CPCTP-22, WRRC Special Rep. No. 9, sponsored by Power Plant Siting Program, Maryland Dept. of Natural Resources, published by Water Resources Research Center, Univ. Md., College Park, MD, 1131-1150 (1978)

Culkowski, W. M., An Anomalous Snow at Oak Ridge, Tennessee, Mon. Wea. Rev., 90 (5): 194-196 (1961).

Dana, M. T. and M. A. Wolf, Rainfall Enhancement due to Scavenging of Cooling Tower Condensate, Report BNWL-2295 prepared for U.S.E.R.D.A. by Battelle Pacific Northwest Lab., Richland, WA, 99352, viii + 33 pp. (1977).

Davies, R. W., Large Scale Diffusion from an Oil Fire, In Advances in Geophysics, 6, F. N. Frenkiel and P. A. Sheppard (eds.), New York, Academic Press, Inc.: 413-415 (1959).

Dessens, J., Man Made Thunderstorms, Discovery, 25: 40-44 (1964).

Environmental Systems Corporation, Cooling Tower Drift Dye Tracer Experiment, PPSP-CPCTP-, by Environ. Syst. Corp., Knoxville, TN, 103 pp., (1977).

Feder, W. A., Measurement and Effects of Drift from an Evaporative Cooling System on Surrounding Vegetation, Cooling Tower Environment 1978, Proceedings. PPSP-CPCTP-22, WRRC Special Rep. No. 9, sponsored by Power Plant Siting Program, Maryland Dept. of Natural Resources, published by Water Resources Research Center, Univ. Md., College Park, MD, 1131-1150 (1978).

Hanna, S. R., Meteorological Effects of the Mechanical Draft Cooling Towers of the Oak Ridge Gaseous Diffusion Plant, Cooling Tower Environment-1974, S. Hanna and J. Pell, ed., ERDA Symposium Series, CONF-740302, Nat. Tech. Information Service, U.S. Dept. of Commerce, Springfield, VA., 22161, ($13.60), 291-306 (1974).

Hanna, S. R., Predicted and Observed Cooling Tower Plume Rise and Visible Plume Length at the John E. Amos Power Plant, Atmos. Environ., 10: 1043-1052 (1976).

Hanna, S. R., Predicted Climatology of Cooling Tower Plumes from Energy Centers, J. Appl. Meteorol. 16: 880-887 (1977).

Hanna, S. R., Atmospheric Effects of Energy Generation, to be Chapter 15 in Atmospheric Sciences and Power Production, D. Randerson, ed., ATDL, P.O. Box E, Oak Ridge, TN, 37830, 101pp (1978).

Hanna, S. R., and F. A. Gifford, Meteorological Effects of Energy Dissipation at Large Power Parks, Bull. Am. Meteorol. Soc., 56: 1069-1076 (1975).

Hanna, S. R., and S. D. Swisher, Meteorological Effects of the Heat and Moisture Produced by Man, Nuclear Safety, 12: 114-122 (1971).

Koenig, L. R., F. W. Murray and P. M. Tag, Differences in Atmospheric Convection Caused by Waste Energy Rejected in the Forms of Sensible and Latent Heats, Atmos. Environ., 12, 1013-1020 (1978).

Kramer, M. L., D. E. Seymour, M. E. Smith, R. W. Reeves, and T. T. Frakenberg, Snowfall Observations from Natural Draft Cooling Tower Plumes, Science, 193: 1239-1241 (1976).

Landsberg, H. E., Rainfall Variations around a Thermal Power Station, Atmos. Environ., 11, 565 (1977).

Lauver, T. L., C. R. Curtis G. Patterson and L. W. Douglass, The effects of saline cooling tower drift on seasonal variations of sodium and chloride concentrations in native perennial vegetation, Cooling Tower Environment 1978, Proceedings, PPSP-CPCTP-22, WRRC Special Rep. No. 9, sponsored by Power Plant Siting Program, Maryland Dept. of Natural Resources, published by Water Resources Research Center, Univ. Md., College Park, MD, 149-164 (1978).

Lee, J., A Numerical Simulation of Atmospheric Convection caused by Heat Dissipation at Large Power Centers, Proceedings, Third Symp. on Atmospheric Turbulence, Diffusion, and Air Quality, Raleigh, available from Amer. Meteorol. Soc., 45 Beacon St., Boston, MA, 20108: 563-570 (1976).

Meyer, J. H. and W. D. Stanbro, Fluorescent Dye, a Novel Technique to trace Cooling Tower Drift, presented at 4th Joint Conf. on Sensing Environ. Pollutants, New Orleans, Nov., available from Johns Hopkins Univ., Applied Phys. Lab., Laurel, MD, 20810 6pp. (1977).

Morris, D. G., Initiation of Convective Clouds Due to Static Firing of the Saturn V First Stage, Bull, Amer. Meteorol. Soc., 49: 1054-1058 (1968).

Otts, R. E., Locally Heavy Snow Downwind from Cooling Tower, NOAA Tech. Memo. NWS ER-62, National Wea. Service, Eastern Region, 8 pp. (1976).

Patrinos, A., Is It Raining in Georgia?, Oak Ridge Nat. Lab. Review, 11 (3), 22-29 (1978) (available from ORNL, P.O. Box X, Oak Ridge, TN, 37830).

Peterson, J., The Climate of Cities, A Survey of Recent Literature, U.S. Dept. of Health, Educ., and Welfare, Pub. Health Serv., Raleigh, NC,(1969)

Policastro, A. J., W.E. Dunn, and M. Breig, Evaluation of Theory and Performances of Salt Drift Deposition Models for Natural Draft Cooling Tower, Proceed. of 2nd AIAA/ASME Thermophysics and Heat Transfer Conf., Palo Alto, CA., Available from Environmental Statements Project, Argonne Nat. Lab., Argonne, IL (1978).

Rao, K. S. and R. P. Hosker, A Numerical Study of Meteorological Effects of Waste Heat and Moisture Releases from Hypothetical Power Parks. Proceed. of 2nd AIAA/ASME Thermophysics and Heat Transfer Conf., Palo Alto, CA., available from ATDL, P.O. Box E, Oak Ridge, TN, 37830, 31 pp. (1978).

Rochow, J. J., Compositional structure and chemical changes to forest vegetation from fresh water with cooling tower drift, Cooling Tower Environment 1978, Proceedings, PPSP-CPCTP-22, WRRC Special Rep. No. 9, sponsored by Power Plant Siting Program, Maryland Dept. of Natural Resources, published by Water Resources Research Center, Univ. Md., College Park, MD, 119-138 (1978).

Stinson, J. R. and C. D. Brown, Inadvertant Cloud Formation and Modification by Refineries and Power Plants, Report SRA 76-01, Stinson Res. Assoc., No. 1 Third Place, Suite 603, Long Beach, CA, 90802, 12pp. (1971).

Stockham, J., Cooling Tower Study, Contract no. CPA 22-69-112, IIT Research Institute, Technology Center, Chicago, IL, 60616, for EPA Air Poll. Cont. Office, 411 W. Chapel Hill St., Durham, NC., 27701, 108 pp. (1971).

Taylor, R.J., S.T. Evans, N.K. King, E. T. Stephens, D. R. Packham, and R. G. Vines, Convective Activity above a Large Scale Brushfire, J. Appl. Meteorol., 12: 1144-1150 (1973).

Thomson, D. W., J.M. Norman, and R. L. Miller, Airborne Measurements of Turbulent Temperature and Velocity Fluctuations in Cooling Tower Plumes Proceedings, Third Symp. on Atmos. Turb., Diffusion, and Air Quality, Raleigh, NC, by Amer. Meteorol. Soc., 45 Beacon St., Boston, MA: 576-580 (1976).

Weinstein, A. I., A Numerical Model of Cumulus Dynamics and Microphysics, J. Atmos. Sci., 27: 246-255 (1970).

Woffinden, G. J., J. A. Anderson, and P. R. Harrison, Air-craft Survey, Chalk Point Cooling Tower Plume, Rep. No. 76R-1910 by MRI, Altadena, CA, 91001, for the Md. Power Plant Siting Program, 32 pp. + appendices, (1976).

Yamada, T., A Three Dimensional Second Order Closure Numerical Model of Mesoscale Circulations in the Lower Atmosphere, ANL/RER-78-1, Argonne Nat. Lab., Argonne, IL, 67 pp. (1978).

PROCEEDINGS OF THE NINTH INTERNATIONAL
TECHNICAL MEETING ON AIR POLLUTION
MODELING AND ITS APPLICATION

28 - 31 August 1978

TORONTO, CANADA

PRAIRIE GRASS REVISITED: OPTIMUM INDICATORS OF VERTICAL SPREAD

Gary A. Briggs

Kenneth R. McDonald

June 1978

A Report of the Air Pollution Pilot Study
NATO Committee on the Challenges to Modern Society
1978

ATDL Contribution File No. 78/8

PRAIRIE GRASS REVISITED : OPTIMUM INDICATORS OF VERTICAL SPREAD

Gary A. Briggs
Atmospheric Turbulence and Diffusion Laboratory
National Oceanic and Atmospheric Administration
Oak Ridge, Tennessee 37830

Kenneth R. McDonald
Department of Geosciences, North Carolina State University
Raleigh, North Carolina 27606

Data from the "Prairie Grass" field experiment are used to test various nondimensionalizations of vertical spread from a ground source, $h \equiv Q/\bar{u}\int\chi dy$, versus x. They are also used to test the correlation of h at fixed distances with various measurable parameters. The most general results are empirical formulas fitting the plots of h/L versus $u^*x/\bar{u}L$. Other, simpler nondimensionalizations are found to order the data well, but are harder to apply to other types of sites. Scaling with mixing layer parameters does not work quite as well, but its relative performance improves with distance. At fixed distances, h is best ordered by L. In stable conditions, it is also well ordered by $\bar{u}^2/\Delta\theta$, $\bar{u}^2$, and $\Delta\theta$. In unstable conditions, it is somewhat less well ordered by $\bar{u}^2/\Delta\theta$ and $\bar{u}^2$, but does not correlate with $\Delta\theta$ at all.

Introduction

There have been a number of papers in the literature demonstrating large discrepancies between various schemes for determining the "diffusion category," i.e., the relative rate of spread of passive material released into the atmosphere. It is quite clear that these schemes commonly disagree with each other, but the question remains of which one to use. This can best be answered by making direct comparisons between various stability indicators and diffusion measurements. Besides the indicators in current use, parameterizations suggested by diffusion theory should be directly tested when adequate data exist. While there is a need for well-instrumented diffusion experiments in rough terrains and at larger distances, satisfactory data on short range diffusion over smooth terrains are available from past field experiments.

One recent study compared correlation coefficients between various indicators and vertical diffusion observed in field experiments at O'Neill NB, Richland, WA and Idaho Falls, ID.[1] For unstable conditions, it was concluded that the Monin-Obukhov length, L, and the gradient Richardson number, Ri, correlated best with vertical diffusion. The temperature gradient, ΔT, did not correlate at all. Standard deviations of azimuth and elevation wind angles, σ_a and σ_e, correlated only marginally in these experiments. For stable conditions, L, Ri, ΔT, and σ_e all showed good correlation; ΔT was optimized as an indicator when it was measured through a layer corresponding roughly to the extent of the vertical diffusion. However, these comparisons were limited in

that only linear fits to the parameters were tested.

The present study utilizes logarithmic plots of all tested parameterizations, so that any power law relationship can be fit with a straight line. This study is limited to the data from the "Prairie Grass" experiment of 1956, chosen because of its relative completeness.

The Prairie Grass Experiment

Project "Prairie Grass" was conducted in O Neill, Nebraska, in the summer of 1956 by the Air Force Cambridge Research Center in conjunction with several university research teams.[2,3] The tracer used was SO_2, released for 10 minutes in each run at a height of 46 cm. The samplers consisted of over 500 midget impingers mounted at 1.5 m on arcs 50, 100, 200, 400, and 800 m from the source. In addition, there were 54 samplers mounted on six towers on the 100 m arc. Meteorological measurements near the ground included net radiation, soil temperature profiles, and wind direction, wind speed, vapor pressure, and air temperature profiles to 16 m. Five bivanes measured wind angle fluctuations. In addition, there were both hourly rawinsonde probes of temperature and humidity and aircraft soundings of the same. Altogether, there were about 70 complete runs, equally divided between stable and unstable conditions.

Some Theoretical Considerations

Two lines of approach to parameterization of diffusion are considered here: Monin-Obukov similarity theory and Willis-Deardorff convective scaling. Because most of the data are concentrations measured at near-ground samplers, we use the scale height

$$h = Q/(\bar{u}\int \chi dy) \tag{1}$$

instead of the mean particle height or the vertical standard deviation; Q is the source strength, $\bar{u}$ is the mean wind speed in the cloud layer, and $\int \chi dy$ is the crosswind integral of the ground concentration. This scale height allows us to use the ground sampler data without making any assumption about the shape of the concentration distribution in the vertical. Also, in making long term average concentration estimates, $\bar{u}h$ is exactly the variable we need.

The similarity theory approach can be put quite simply. In the neutral surface layer, the only turbulent scale velocity is the friction velocity, u^*. Therefore we expect that $dh/dt \propto u^*$. In the non-neutral surface layer turbulence quantities become modified by various functions of z/L, where z is height and L is the Monin-Obukhov scaling length.[4] Therefore the rate of vertical diffusion is modified by a function of h/L. Specifically,

$$dh/dt = u^* f(h/L) \tag{2}$$

$$h/L = g(u^* t/L) \tag{3}$$

$$h/L \simeq g(u^* x/\bar{u}L). \tag{4}$$

Equation (3) is obtained by dividing Eq. (2) by Lf(h/L) and integrating. It applies most strictly to a horizontally homogeneous ground release of material at t = 0. However, the diffusion mechanism is very similar for a continuous point source release, except for minor effects due to longitudinal diffusion. In transforming from time to distance coordinates in Eq. (4), $\bar{u}$ must be defined as the mean horizontal transport speed that has been experienced by the particles reaching the distance x. It should be equal to the mean wind speed at some height proportional to h. The ratio of this height to h is lower in unstable conditions than in stable, because dh/dt increases with time in unstable conditions and does the opposite in a stable boundary layer.

In analyzing the Prairie Grass data, we have tried five different approximations to Eq. (4). The first is a direct plot of Eq. (4), except that no attempt is made to properly determine $\bar{u}$; instead, wind speed at a fixed height is used, which is likely to be the case in most practical applications. At small values of $|u^*x/\bar{u}L|$ the choice of $\bar{u}$ has little effect, because g is nearly linear and $\bar{u}$ also appears in the denominator of h; provided that the same $\bar{u}$ is used, it cancels itself. At larger values of $|u^*x/\bar{u}L|$, the resulting plot is more sensitive to the choice of $\bar{u}$, especially in stable conditions.

The second approximation to Eq. (4) simply ignors the effect of wind shear by dropping $\bar{u}/u^*$;h/L is plotted as a function of x/L. However, if this result is applied to a terrain of different roughness, one should expand or contract the x scale by a factor proportional to an average $\bar{u}/u^*$. For neutral conditions, this is proportional to $\ln(\bar{h}/z_o)$, where $\bar{h}$ is a geometric mean expected cloud height and z_o is the terrain roughness. For unstable conditions, $\bar{u}/u^*$ is somewhat more sensitive to z_o, and for stable conditions, somewhat less. The third approximation is very similar, except that $\bar{u}^2\theta_a/g\Delta\theta$ is substituted for L, where θ_a is the average absolute potential temperature, g is gravity, and $\Delta\theta$ is the potential temperature difference between two levels on a tower. This quantity also has dimensions of length, although we have omitted (θ_a/g) since its range is small. This length is far easier to determine than L. However, its relationship to L also involves z_o, and it is more difficult to adapt the result for terrains of different roughness. Use of different heights of measurement further complicates any adaptation attempt.

The fourth approximation to Eq. (4) is simply an inversion of the $\bar{u}^*/\bar{u}$ term; $(\bar{u}/u^*)h/L$ is plotted against x/L. This plot is independent of $\bar{u}$, since it appears in the denominator of h. However, it will not be independent of z_o. This plot's main virtue is utilitarian, since $uh = Q/\int\chi dy$ is the quantity of direct concern in calculating long-term average ground concentrations. The fifth approximation involves a compromise among several asymptotic forms in which $\bar{u}/u^*$ is approximated by powers of $\bar{h}/z_o$ and h/L. This procedure is rather complex, so we omit it here. We are predicting that $hz_o^{0.06}/|L|^{1.06}$ is approximately a function of $xz_o^{0.18}/|L|^{1.18}$ for smooth terrains (the powers in z_o would be larger for rough terrains).

For unstable conditions, it is also appropriate to try Willis-Deardorff convective scaling. On the basis of laboratory and numerical modeling, it appears to be most appropriate when $z > 0.1z_m$ and $z_m/|L| > 10$, where z_m is the height of the convective mixing layer (of the 30 Prairie Grass runs for which z_m could be determined, $z_m/|L| > 10$ for 27 of the runs). Thus, this scaling is likely to produce good ordering of ground source diffusion data only at

relatively large distances, where $h >> 0.1\ z_m$. Vertical lengths, such as h, are scaled by z_m, and convective turbulence velocities are scaled by $w^* = (Hz_m)^{1/3}$, where $H = (g/T)\overline{w'T'}$ at the surface; it is the rate of turbulent kinetic energy production by convection at z = 0, and is proportional to the sensible heat flux. The scale time for material to be carried through the whole mixing layer, the Lagrangian time scale, is z_m/w^*. In the mid-mixing layer, there is very little wind sheer because of vigorous vertical mixing, so there is little approximation involved in the transformation x = ut. Applying convective scaling to ground source diffusion, the prediction is that

$$h/z_m = f(w^*t/z_m) \simeq f(w^*x/\bar{u}z_m).^5 \qquad (5)$$

Determination of Parameters

In order to test the above theoretical forms, u^*, L, z_m, and w^* have to be determined for each run (unstable runs only in the case of z_m and w^*). The friction velocity, u^*, is determined from the tower-measured wind speed profiles using the log-linear assumption:

$$u = (u^*/k)\left|\ln(z/z_o)+az/L\right|. \qquad (6)$$

The dependence on L is eliminated by taking a weighted difference between u at levels z = r and z = 4r:

$$u^* = k(4u_r - u_{4r})/\ln(z_r^3/4z_o^3). \qquad (7)$$

Since the Prairie Grass terrain and surface cover was similar to that of the "Kansas" surface layer turbulence experiment, k = 0.35 is assumed.[6] The roughness length, z_o, was determined to be 0.6 cm.[2] For each run, we carry out the u^* calculation with four different values of the reference height, r = 0.25, 0.5, 1, and 2 m. The median of these four determinations is used.

The Monin-Obukhov length, L, is determined from the tower profiles of wind speed and temperature. For stable conditions, the Dyer and Hicks profiles are used because they lead to the simple result that $\Delta\theta/\Delta u = -\overline{w'T'}/u^{*2}$.[7] The chosen working relationship is

$$L = -u^{*3}/kH = (u^*/k)(T_{2r}/g)(u_{4r}-u_r)/(\theta_{4r}-\theta_r), \qquad (8)$$

with r taking on the same four height values as above. For unstable conditions, the Businger et al. profiles are assumed, and differences between u and θ values are taken from levels chosen so that almost a linear relationship results:[6]

$$L = 0.74(\ln 8)^{-1} f(L)(T_{4r}/g)(u_{4r}-u_r)(u_{8r}-u_r)/(\theta_{8r}-\theta_{2r})$$

$$f(L) \simeq (1 + 20.7r/L + \text{---})/(1 + 19.5r/L + \text{---}). \qquad (9)$$

We set $f(L) \simeq 1$, and make the calculation for four different values of r as above. Quite good consistency is obtained between these determinations of L, except for run 3, which is eliminated. This run involved substantially lower wind speeds than in any other run.

The mixing layer height, z_m, is determined primarily from the aircraft soundings of ambient temperature, T_a, and humidity. A line is drawn through the steepest (largest $\partial T_a/\partial z$) three points of the T_a versus z profile and is intersected with a line representing the average θ of the next lowest three points to determine z_m objectively from the temperature sounding. A similar procedure is applied to the specific humidity profile. Usually, these two z_m determinations agree within 10%, in which case the average value is used. If they disagree, other kinks in the profiles are looked for that might better coincide. In addition, the rawinsonde profiles, which are coarser, are used as a check. With these techniques, z_m is determinable for 30 of the 33 unstable runs with little ambiquity. The other three runs, numbers 31,33 and 34, are omitted from the comparisons involving z_m. First order corrections are made for mean absolute temperature and specific humidity in the mixing layer to convert from pressure altitude to actual height above the surface.

The convective velocity scale, w*, can be calculated from the other three parameters. Using the definitions of w* and L, we have

$$w^* = (Hz_m)^{1/3} = u^* \left|z_m/kL\right|^{1/3}. \tag{10}$$

Finally, h is determined from Eq. (1) using the crosswind integrated concentration from the 1.5 m samplers at the five arc distances. No attempt is made to vary the measurement height for $\bar{u}$ as h increases. Instead, in stable conditions h is determined using both $\bar{u} = u_2$ and $\bar{u} = u_8$, where the subscripts indicate the height of measurement in meters. In unstable conditions, both $\bar{u} = u_8$ and $\bar{u} = u_m$ are used, where u_m is an estimated mean wind speed for the mid-mixing layer based on an unpublished analysis of the "Minnesota" data:[8]

$$u_m = (u^*/k)\ \ln\left[0.2(z_m)^{0.4}|L|^{0.6}/z_o\right]. \tag{11}$$

The parameter h correctly scales the plume thickness only if the samplers are at the height of highest plume concentration. If they only pick up the edge of the plume, a misleadingly high value of h will result. This appears to happen in some of the more stable runs, as anomalously high values of h occur, especially at the inner arcs. This could happen when diffusion is slow, since the release height and sampler heights differed by 1 meter, and the terrain elevation varied nearly this much in some directions. To avoid these cases, we eliminate determinations that give h decreasing with distance. Specifically, h at 50 and 100 m is eliminated for runs 4,13,14,32,35, and 58; also, at 400 m for run 4, 200m for run 13, and all of run 3.

Results

We have tried two kinds of approaches. First, various nondimensionalizations of h are plotted against nondimensionalizations of x, as suggested by the diffusion scaling theories just discussed. Second, h at fixed distances is plotted against various dimensional parameters; here we include more simply measured quantities, such as $\bar{u}^2/\Delta\theta, \bar{u}^2$, and $\Delta\theta$, as well as the more theoretically based quantities L and $z_m u/w^*$. All of these data are plotted and analyzed in log-log form, in hopes that convenient power law relationships will be found, and also so we can more easily compare the ranges of scatter in terms of ratios instead of absolute differences.

Table 1 summarizes the results of least square fits to the nondimensional plots of ln (h) versus ln(x). The first part gives the best-fit slopes for both the "near" and the "far" segments of the abscissa (nondimensionalized x). The second part gives the logarithmic standard deviation of the points relative to the best fit lines. For instance, 0.18 corresponds to a factor of 1.2, 0.34 to a factor of 1.4, and 0.47 to a factor of 1.6. Figure 1 shows four of these graphs, with both stable and unstable runs plotted in each one. The two graphs omitted for space reasons are very similar in appearance to those shown having comparable scatter. For consistency between stable and unstable runs, only the results with $\bar{u} = u_8$ are shown; in this case, $\Delta\theta = \theta_8 - \theta_1$. For the stable runs, the results using $\bar{u} = u_2$ give the same or slightly reduced scatter (by no more than 0.03 in terms of logarithmic standard deviation). For the unstable runs, the results using $\bar{u} = u_m$ give the same or slightly increased scatter.

In the stable plots, we find that the theoretically more basic plot, h/L versus $u^*x/\bar{u}L \equiv X$, and its near relative, $\bar{u}h/u^*L$ versus x/L, give comparatively poor results. Not only is the scatter larger, but the "far" slope is larger than the "near," contrary to expectations. In Figure 1(a) it is seen that this overly large slope is due to a few anomalously high values of h/L, while there is a trend towards a lower slope in the most clustered points. Most of the high values occur at the outer arcs in very stable conditions, with very small values of L (1 to 10 m). The calculated values of h in these cases seem to "explode" at the larger arc distances, which implies that either there was a sudden increase in turbulence or, more likely, that the center of the plume missed the 1.5 m high samplers. The terrain did drop 0.3 to 1 m over most of the 800 m arc. The plots that neglect $\bar{u}/u^*$ tend to compensate for these anomalously large h's by leaving out the large values of u_8/u^* associated with the small L's. Hence, the better performance of the h/L versus x/L and the $h\Delta\theta/\bar{u}^2$ versus $x\Delta\theta/\bar{u}^2$ plots may be an experimental anomaly. The plot in which z_o appears in place of u/u^* also works well. The most versatile relationship in terms of applicability to sites of any roughness is fit by eye to the more clustered points in Figure 1(a), and is given by

$$h/L = X/(1 + X^{1/2}). \qquad (12)$$

Table 1. Least squares fits to ln(h) versus ln(x), $\bar{u} = \bar{u}_8$.

		Stable		Unstable	
		Far	Near	Near	Far
(a) Best-Fit slopes					
h/L	vs. $u^*x/\bar{u}L$	1.01	$.88^{-1*}$	1.02	1.83^{-1*}
h/L	vs. x/L	.68	$.84^{2}$	1.11	$2.00^{2.5}$
$h\Delta\theta/\bar{u}^2$	vs. $x\,\Delta\theta/\bar{u}^2$	.59	$.85^{2}$	1.10	2.01^{2}
uh/u^*L	vs. x/L	1.02	$.90^{2}$	1.05	1.86^{2}
$hz_o^{0.06}/\|L\|^{1.06}$	vs. $x\,z_o^{0.18}/\|L\|^{1.18}$	.62	$.79^{o}$	1.05	1.83^{1}
h/z_m	vs. $w^*x/\bar{u}z_m$	___	___	1.03	1.65^{-3}
(b) Log. standard deviations					
h/L	vs. $u^*x/\bar{u}L$	.49	.21	.16	.44
h/L	vs. x/L	.37	.14	.20	.47
$h\Delta\theta/\bar{u}^2$	vs. $x\Delta\theta/\bar{u}^2$	.34	.14	.27	.55
uh/u^*L	vs. x/L	.48	.19	.16	.45
$hz_o^{0.06}/\|L\|^{1.06}$	vs. $x\,z_o^{0.18}/\|L\|^{1.18}$	.35	.15	.18	.45
h/z_m	vs. $w^*x/\bar{u}z_m$	___	___	.26	.51

*Break point between "near" and "far," in terms of ln of abscissa

In the unstable plots, we find that all of them involving L do about as well as each other; h/L versus x/L shows only slightly more scatter. The omission of u/u^* is less consequential here because it ranges much less than in stable conditions. Willis-Deardorff scaling with z_m results in larger scatter, but not very much larger. Surprisingly, $h\Delta\theta/\bar{u}^2$ versus $x\Delta\theta/\bar{u}^2$ gives relatively poor results, in spite of the fact that $u_8^2/\Delta\theta$ is highly correlated with L (correlation coefficient = 0.98).

More or less definite "kinks" are seen in the unstable log-log plots, with a good straight line (power law) fit to either side of the kinks. At small x, we find essentially that $h \simeq xu^*/\bar{u}$, which is the prediction for neutral stability. At large x, the slopes for the similarity theory plots are greater than that of the "free convective limit" given by $h \propto H^{1/2}(x/\bar{u})^{3/2}$. They more closely approach the limit predicted by theory when it is assumed that $dh^2/dt \propto K_H \propto u^*h/\Phi_H(h/L)$, with $\Phi_H \propto |h/L|^{-1/2}$ in the limit. This gives $|h/L| \propto X^2$. Figure 1(a) is fit by eye with a relationship that satisfies this limit, namely

$$h/L = X\,(1 + 5X^2)^{1/2}. \qquad (13)$$

Figure 1(b), $h/z_m \equiv H_m$ versus $w^*x/\bar{u}z_m \equiv X_m$, agrees with the results of

Willis and Deardorff's convective tank experiment at $X_m = 2$ (solid line), but at larger X_m the Prairie Grass H_m increases more rapidly (we use $\int \chi dy$ at $z = 0$ to define a comparable h_m from the tank experiment).[9] One possible explanation for this difference is that the viscous sublayer attached to the surface is significantly thick in the tank, so it takes a longer time to "sweep out" surface concentrations than it does at sampler height in the atmosphere, which is well into the turbulent layer. The field experiment results suggest that "sweep out" of surface concentrations into thermals occurs rather rapidly near $X_m = 0.4$.

Table 2 summarizes the results of the least squares fits to ln(h) at fixed distances versus the logarithms of various parameters; only the results for x = 100 and 800 m are shown. The first part of the table gives the best-fit slopes, and the second part gives the logarithmic standard deviations from the best-fit lines. Figure 2 shows all of these plotted, with separate plots for stable and unstable runs. Again, for consistency, $u = u_8$ is used throughout. For the stable case, use of u_2 instead of u_8 had little effect on the scatter, except that the logarithmic standard deviations were reduced by about 0.04 for h versus $\bar{u}^{-2}$. For the unstable case, use of u_m instead of u_8 had very little effect.

In the stable plots, we find surprisingly similar correlations between h and $L, u^2/\Delta\theta$, $\Delta\theta$, and $\bar{u}^{-2}$ (especially if $u = u_2$ is used). It appears that any of these would function adequately as a diffusion category indicator. However, the specific relationship would be affected by different terrain types and by different heights of measurement. Most especially, it has been shown that the correlation with $\Delta\theta$ decreases as the layer of $\Delta\theta$ measurement coincides less with the layer occupied by the diffusant.[1]

Table 2. Least squares fits to ln(h) plots at fixed x, $\bar{u} = u_8$.

	Stable		Unstable	
(a) Best-Fit slopes	x=800m	x=100m	x=100m	x=800m
h vs. $\lvert L \rvert$	.33	.20	-.34	-1.07
h vs. $\lvert \bar{u}^{-2}/\Delta\theta \rvert$	.39	.20	-.36	-1.15
h vs. $\bar{u}^{-2}$	.78	.36	-.41	-1.10
h vs. $\lvert \Delta\theta \rvert$	-.65	-.33	-.10	+ .08
h/z_m vs. $z_m \bar{u}/w^*$	___	___	-1.25	-1.78
(b) Log. standard deviations				
h vs. $\lvert L \rvert$	.36	.20	.20	.49
h vs. $\lvert \bar{u}^{-2}\Delta\theta \rvert$	.33	.20	.24	.60
h vs. $\bar{u}^{-2}$	.40	.23	.16	.66
h vs. $\lvert \Delta\theta \rvert$	.35	.20	.38	1.14
h/z_m vs. $z_m \bar{u}/w^*$	___	___	.24	.65

In the unstable plots, we find the best indicator of h is L ; $\bar{u}^{-2}/\Delta\theta, \bar{u}^{-2}$, and scaling with z_m work about as well at x = 100m, but these give 12 to 18% more scatter at x = 800m. In any case, the scatter at 800 m is relatively large. It seems likely that much of it is inherent in the experiment, because the 10 minute release times do not constitute an adequate "ensemble" average; a typical Eulerian time scale for the passing of a convective eddy in this data set is about 3 minutes (based on $1.5z_m/u_m$). However, these data make it quite clear that $\Delta\theta$ or ΔT is no indicator of diffusion in unstable conditions, except to simply distinguish them from stable conditions. The correlation coefficient for $\ln(h)$ and $\ln|\Delta\theta|$ ranges between 0.0 and 0.2.

The Monin-Obukhov length suggested by similarity theory appears to characterize diffusion quite well, at least when x < 1 km. However, L is difficult to measure. In Figure 3 we see how it relates to the more easily measured parameters. For both stable and unstable conditions, the correlation with $\bar{u}^2/\Delta\theta$ is very good, just as theory indicates. L is rather well correlated with $\Delta\theta$ in stable conditions, but is not at all correlated in unstable conditions. There is a quite useable degree of correlation with wind speed alone, especially in stable conditions.

Conclusions

The "Prairie Grass" diffusion data have been looked at in some detail to see how well various physical parameters correlate with vertical diffusion, as inferred from $\int\chi dy$ measured at 5 arc distances.

The best ordering of the data for all stability categories is obtained with nondimensional plots of $hz_o^{0.06}/|L|^{1.06}$ versus $xz_o^{0.18}/|L|^{1.18}$. For stable conditions, good ordering is also obtained with h/L versus x/L and $h\Delta\theta/\bar{u}^2$ versus $x\Delta\theta/\bar{u}^2$ plots. However, the most versatile result in terms of adaptibility to sites of different roughnesses is given by Eq. (12). For unstable conditions, good ordering is also obtained with h/L versus u*x/uL and uh/u*L versus x/L plots. The most versatile result is given by Eq. (13). Beyond x = 1 km, it is suspected that scaling with z_m and w* may work better than scaling with L.

At a fixed distance, the best ordering of the data for all stability categories is obtained with L. More easily measured, $\bar{u}^2/\Delta\theta$ works equally as well in stable conditions and almost as well in unstable; $\bar{u}^2$ alone correlates only slightly less well, and has the advantage of being relatively easy to reliably measure. In combination with an insolation measurement or a cloudiness estimate, it might do even better. In other words, the original Pasquill approach to diffusion categorization appears to be an excellent compromise between performance and practicality.[10] Temperature difference, or $\Delta\theta$, is a good categorizer in stable conditions if it is measured through a relavant layer, but it appears to be worthless in unstable conditions.

It is cautioned that all of the above is based on an analysis of one data set at one site. Other data sets are available, however, and it is hoped to extend this type of analysis to them and also to lateral diffusion measurements. Much of the present work was done while the first author was on assignment to the Fluid Modeling Laboratory of the U.S. Environmental Protection Agency, Research Triangle, NC.

References

1. A. H. Weber, K. R. McDonald, and G.A. Briggs, "Turbulence Classification Schemes for Stable and Unstable Conditions," Joint Conference on Applications of Air Pollution Meteorology, Salt Lake City, Amer. Meteor. Soc. and Air Pollut. Control Assoc., Nov. 1977.
2. M. L. Barad (ed.), Project Prairie Grass, a Field Program in Diffusion, Geophysical Research Papers No. 59, Vols. 1 and 2, GRD, AFCRC, Bedford, Mass., 1958 (AD-152572 and AD-152573).
3. D. A. Haugen, Project Prairie Grass, a Field Program in Diffusion, Geophysical Research Papers No. 59, Vol. 3, GRD, AFCRC, Bedford, Mass., 1959 (AD-217076).
4. F. Pasquill, Atmospheric Diffusion, 2nd Edition, p. 116, John Wiley and Sons, New York, London, Sydney, Toronto, 1974.
5. J. W. Deardorff and G. E. Willis, "A Parameterization of Diffusion into the Mixed Layer, "J. Appl. Meteor. 14, pp. 1451-1458, 1975.
6. J. A. Businger, J. C. Wyngaard, Y. Izumi, and E.F. Bradley, "Flux-Profile Relationships in the Atmospheric Surface Layer." J. Atmos. Sci. 28, pp. 181-189, 1971.
7. A. J. Dyer and B. B. Hicks, "Flux-Gradient Relationships in the Constant Flux Layer," Quart. J. Roy. Meteor. Soc. 96, pp. 715-721, 1970.
8. Y. Izumi and J.S. Caughey, Minnesota 1973 Atmospheric Boundary Layer Report, Environmental Research Papers No. 547, AFCRL, Hanscom AFB, Mass., 1976 (AFCRL-TR-76-0038).
9. G. E. Willis and J. W. Deardorff, "A Laboratory Model of Diffusion into the Convective Planetary Boundary Layer," Quart. J. Roy. Met. Soc. 102, pp. 427-445, 1976.
10. F. Pasquill, "The Estimation of the Dispersion of Windborne Material," Meteor. Mag. 90, pp. 33-49, 1961.

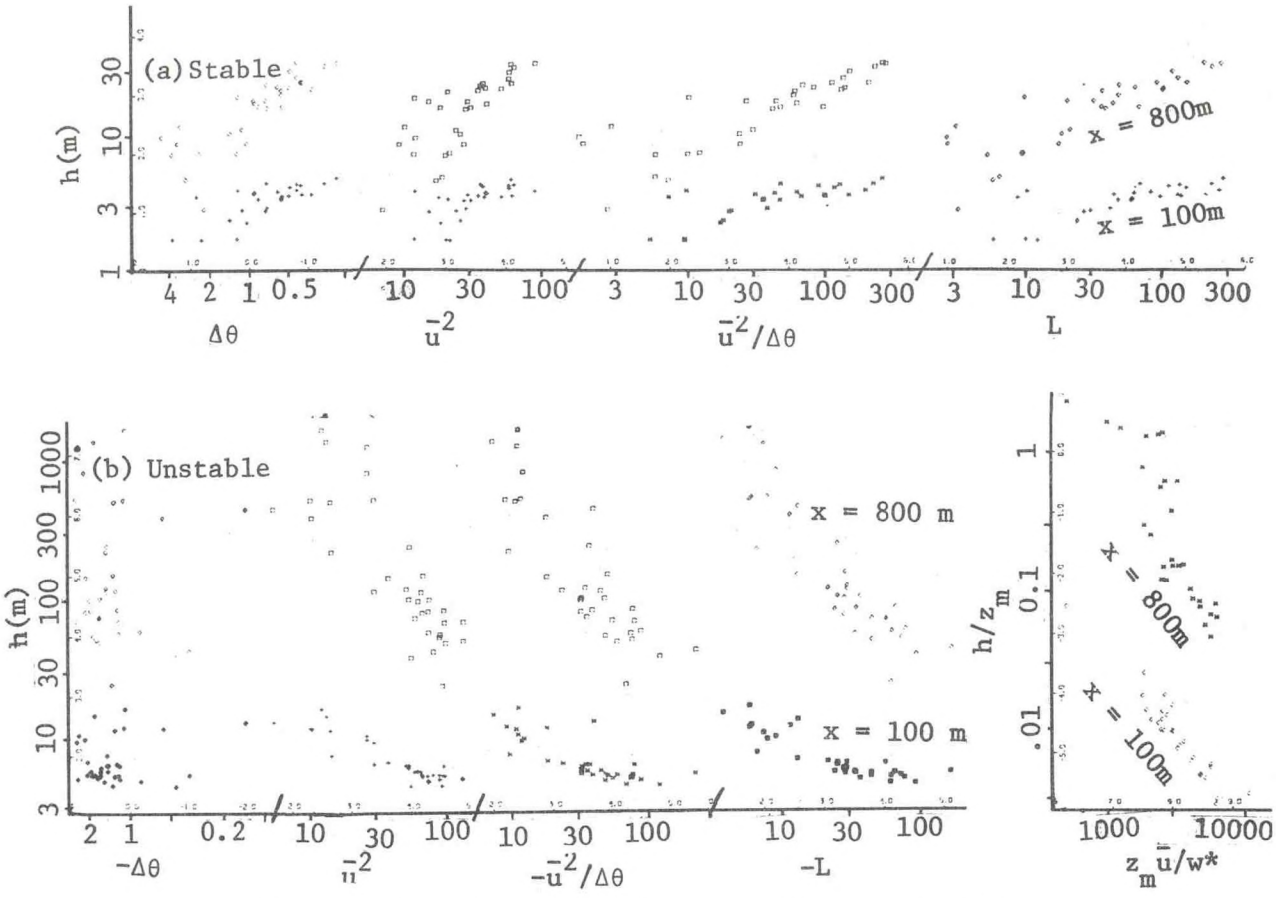

Figures 2. Plots of ln(h) versus ln(parameters).

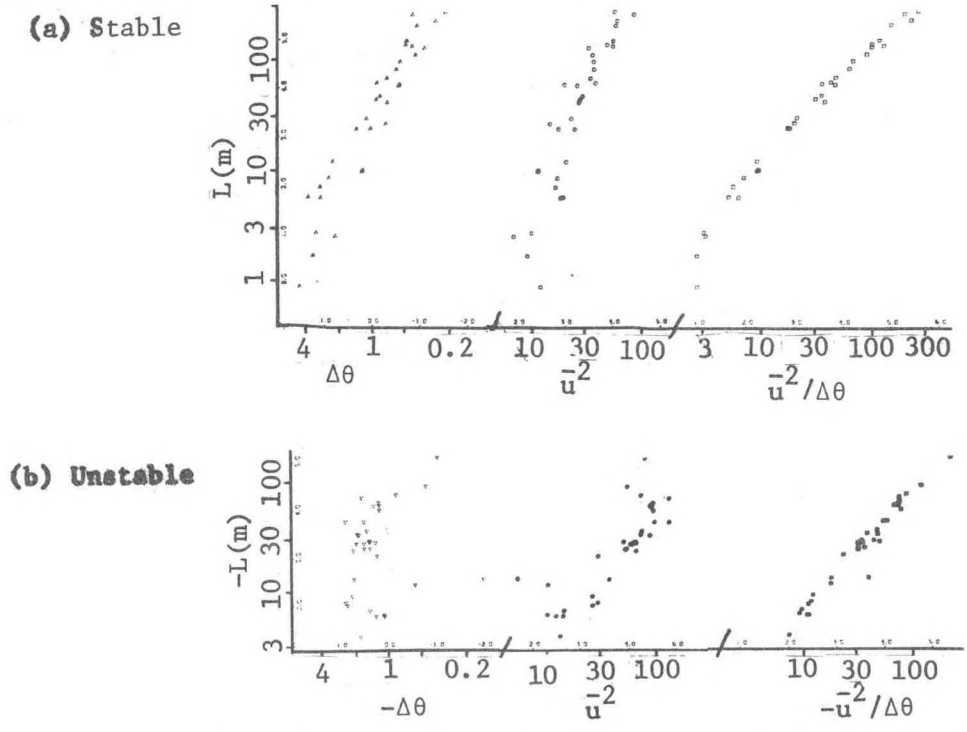

Figures 3. Plots of ln(L) versus ln(parameters).

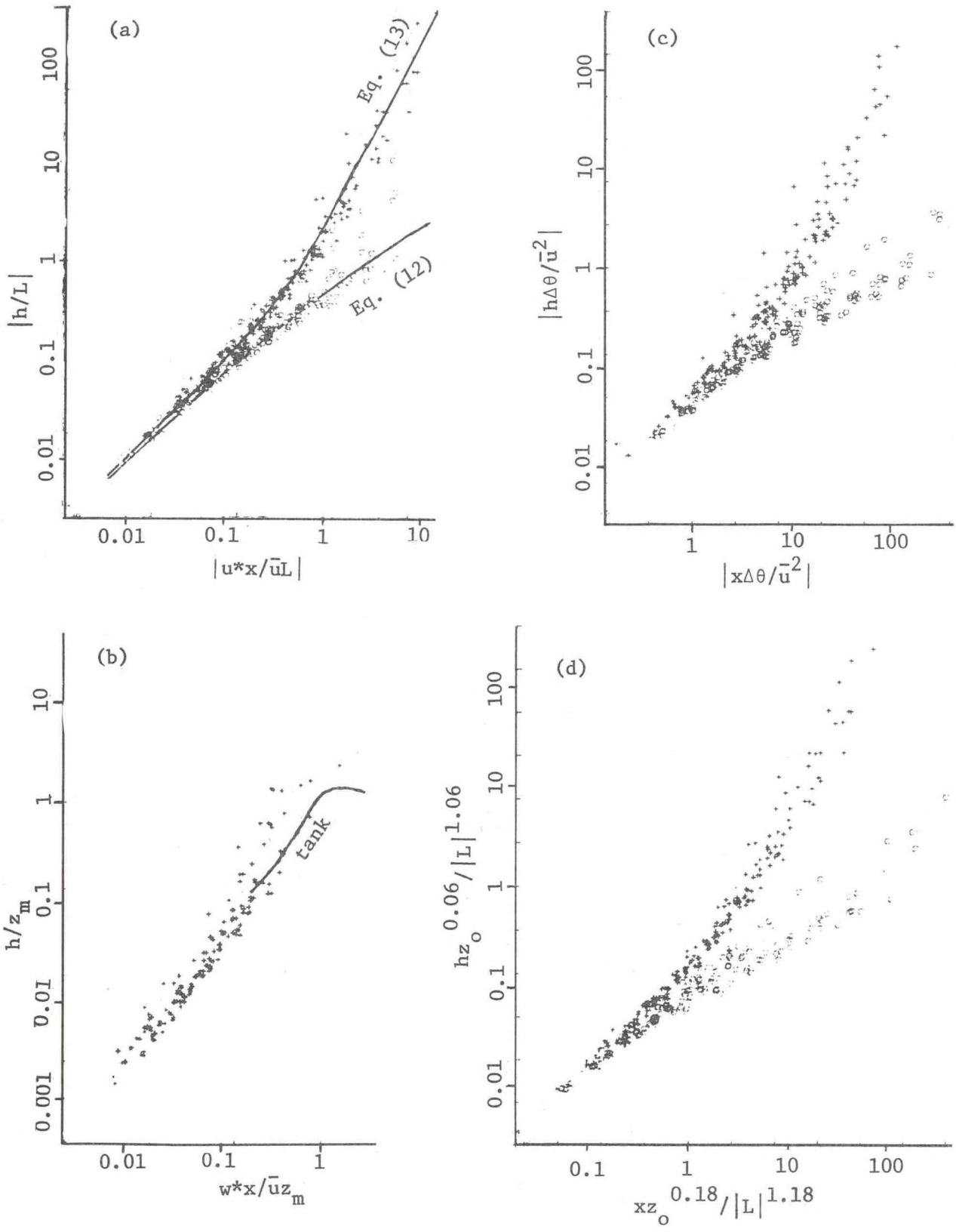

Figure 1. Nondimensional plots of ln(h) versus ln(x). Inner scales are natural logarithms. Stable, o . Unstable, + .

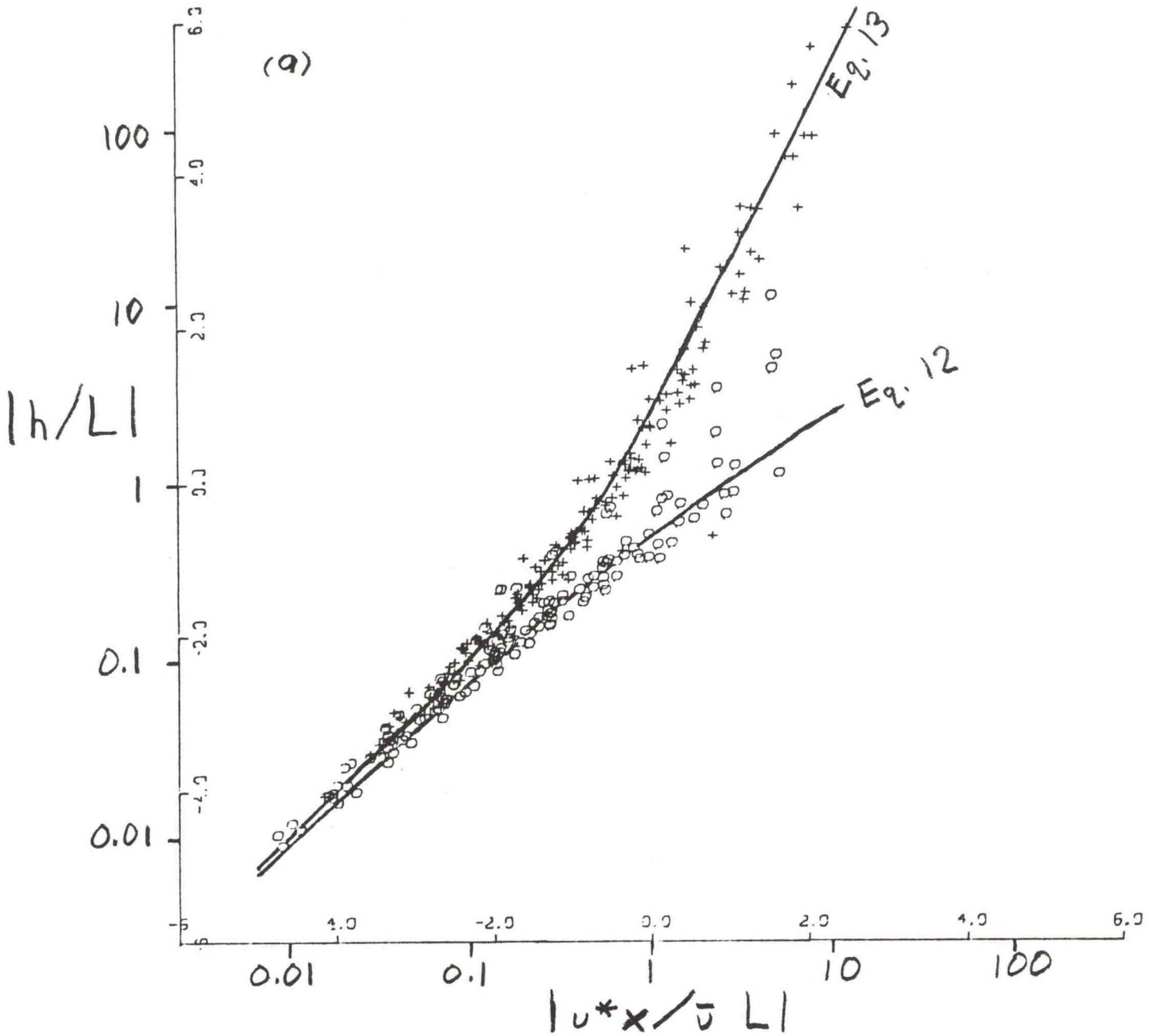
(a)
Eq. 13
Eq. 12
|h/L|
100
10
1
0.1
0.01
6.0
4.0
2.0
0.0
-2.0
-4.0
-6
0.01
0.1
1
10
100
|u*κ/σ L|

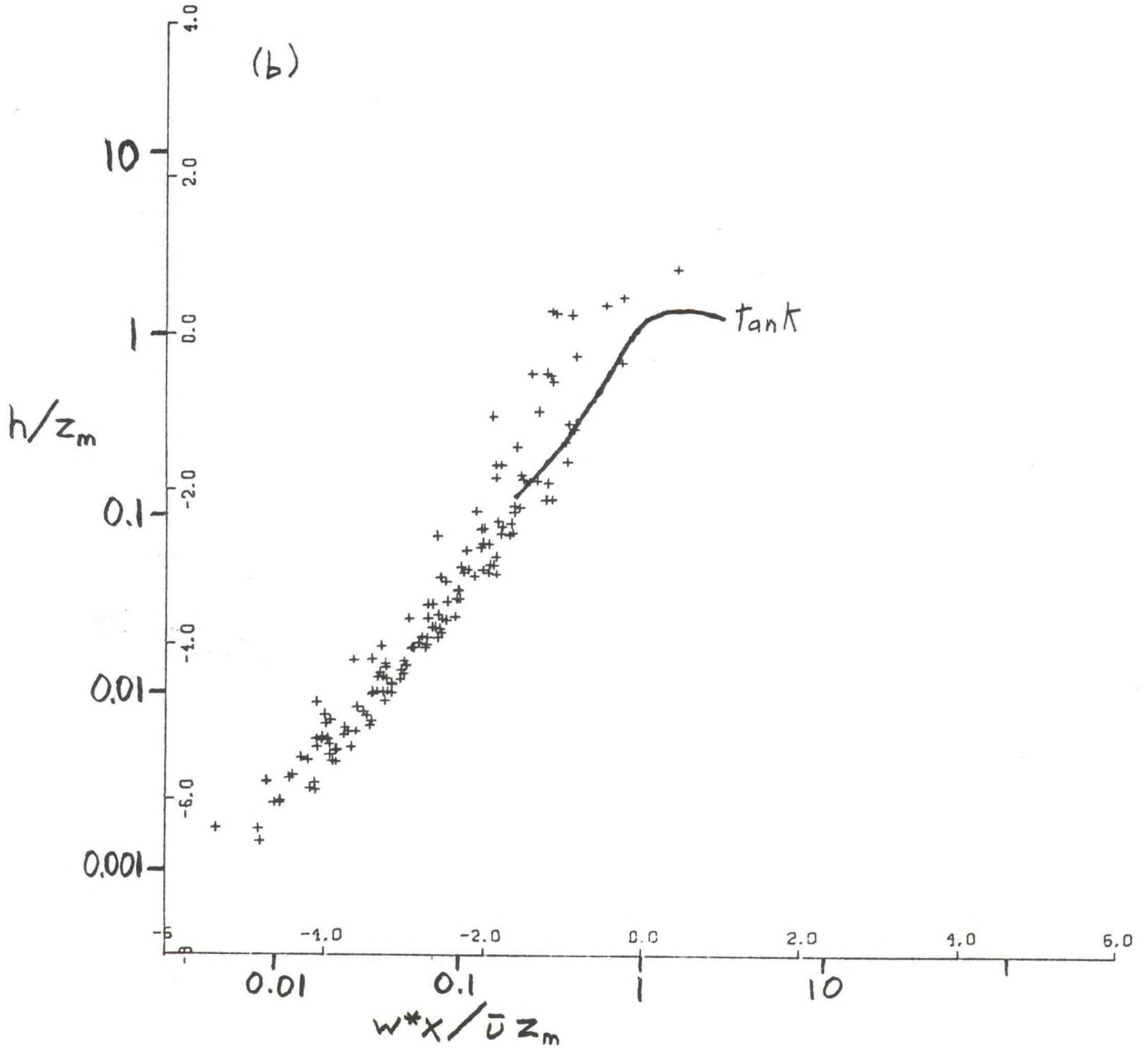
(b)
10
1
0.1
0.01
0.001
h/z_m
4.0
2.0
0.0
-2.0
-4.0
-6.0
-8
-4.0
-2.0
0.0
2.0
4.0
6.0
0.01
0.1
1
10
w*x/ū z_m
tank

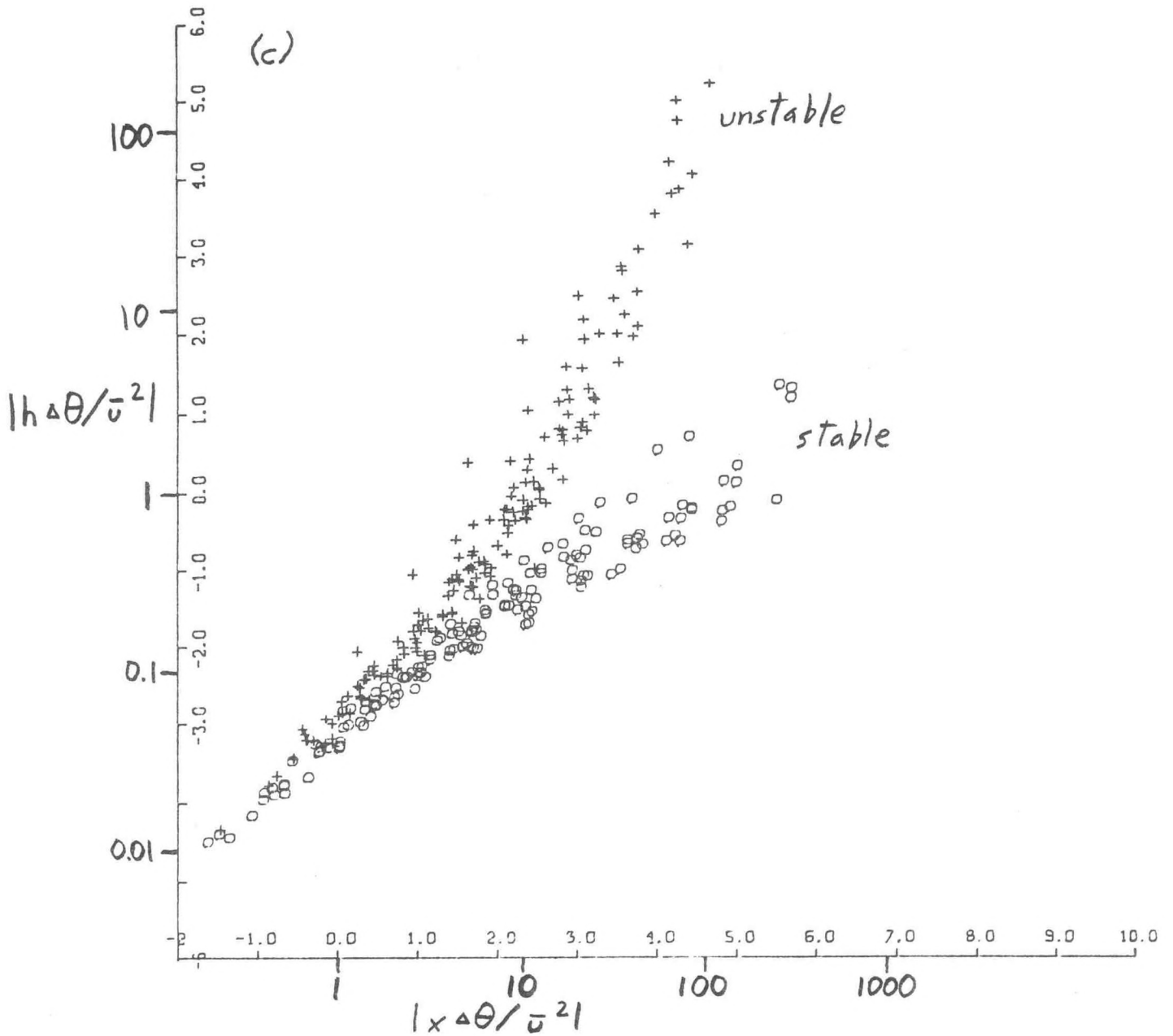
(c)
unstable
stable
100
10
1
0.1
0.01
$|h\Delta\theta/\bar{u}^2|$
6.0
5.0
4.0
3.0
2.0
1.0
0.0
-1.0
-2.0
-3.0
-1.0
0.0
1.0
2.0
3.0
4.0
5.0
6.0
7.0
8.0
9.0
10.0
1
10
100
1000
$|x\Delta\theta/\bar{u}^2|$

(d)
unstable
stable
$h z_o^{0.06}/|L|^{1.06}$
$x z_o^{0.18}/L^{1.18}$
100
10
1
0.1
0.01
0.1
1
10
100
1000

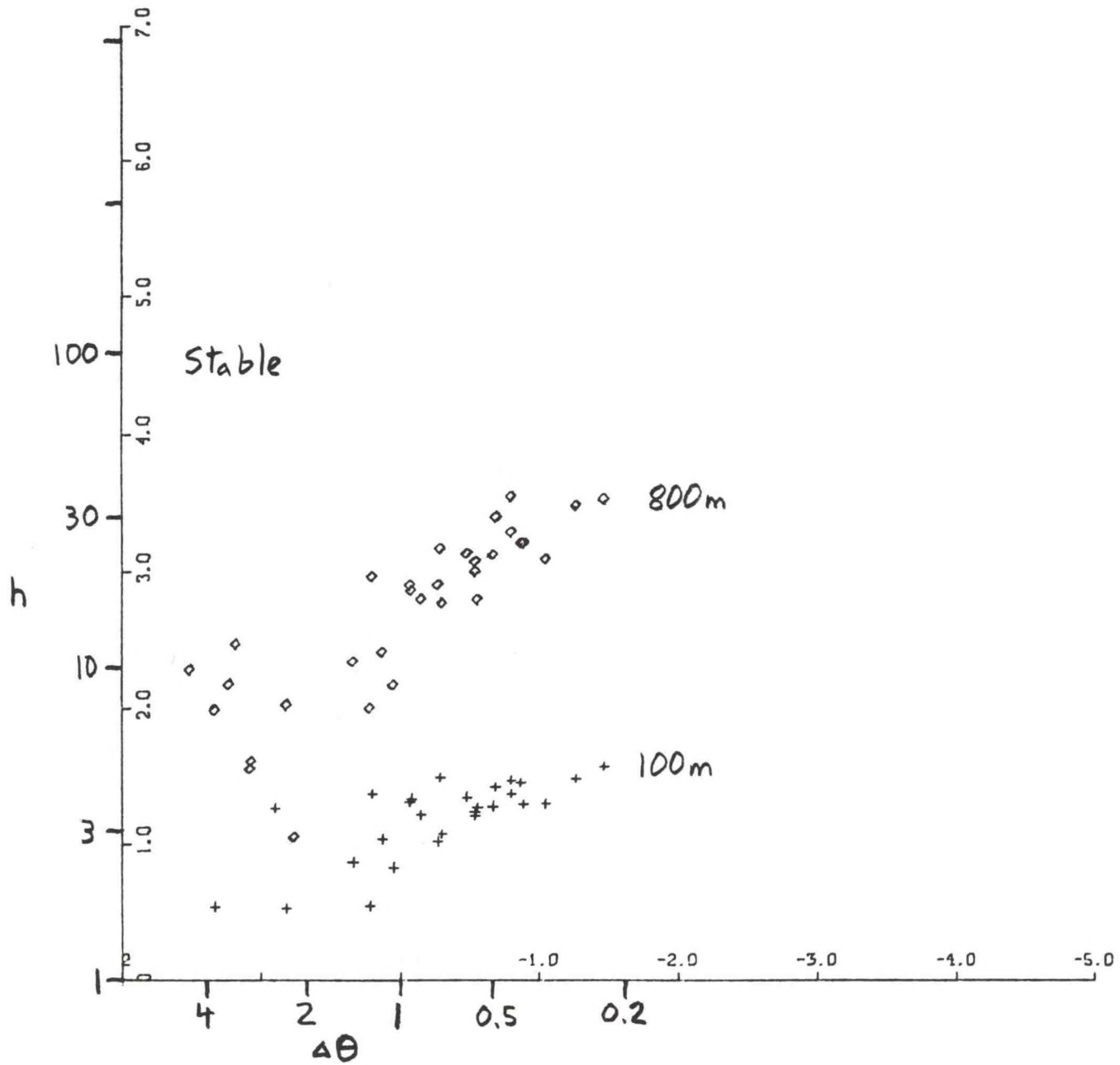
Stable
800m
100m
h
100
30
10
3
1
7.0
6.0
5.0
4.0
3.0
2.0
1.0
0
-1.0
-2.0
-3.0
-4.0
-5.0
4
2
1
0.5
0.2
Δθ

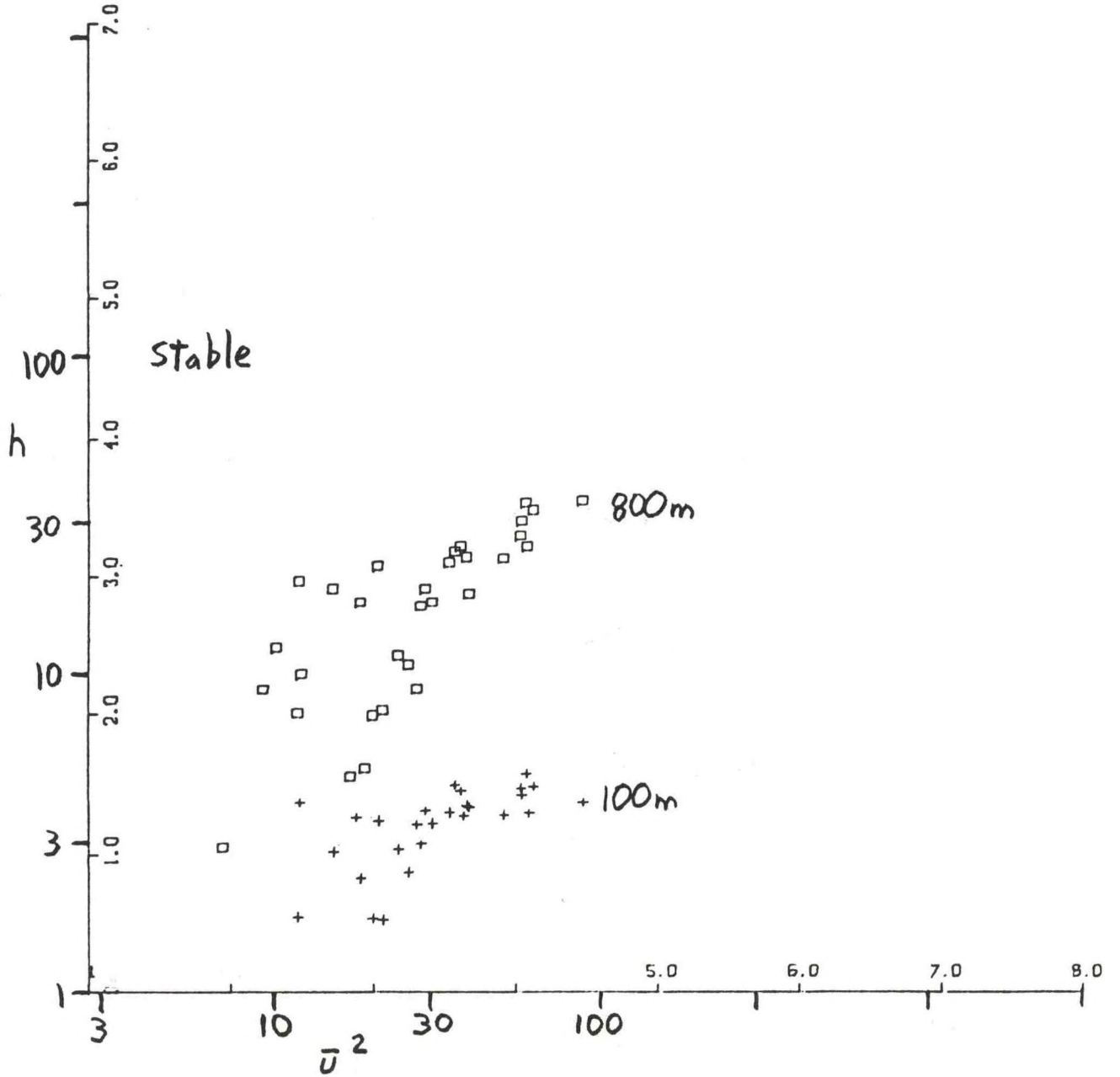
stable
h
100
30
10
3
1
7.0
6.0
5.0
4.0
3.0
2.0
1.0
800m
100m
3
10
30
100
5.0
6.0
7.0
8.0
$\bar{U}^2$

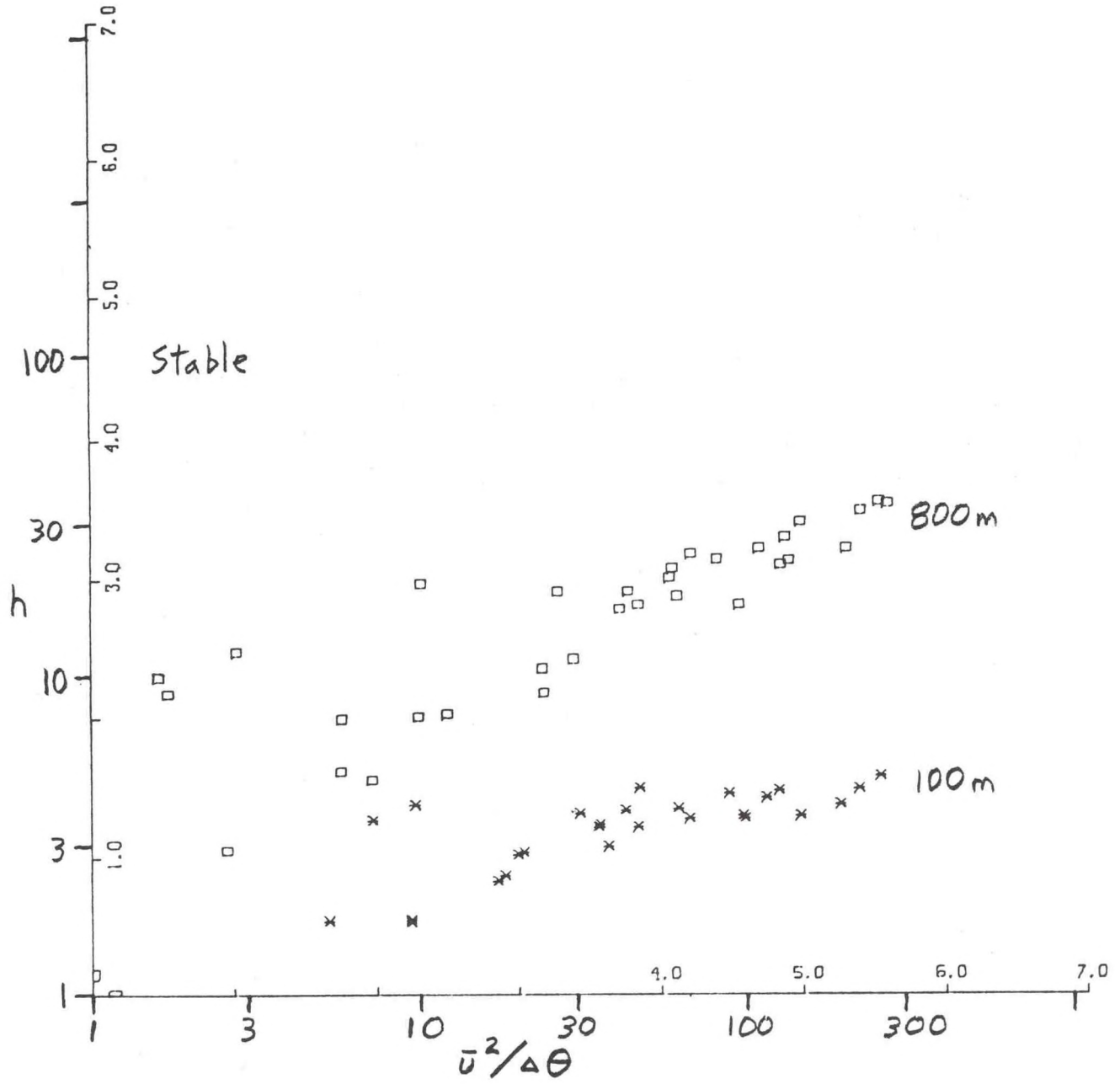
Stable
800 m
100 m
h
$\bar{u}^2/\Delta\theta$
1
3
10
30
100
300
1.0
3.0
4.0
5.0
6.0
7.0

Stable
h
L
100
30
10
3
1
0.0
1
3
10
30
100
1.0
2.0
3.0
4.0
5.0
6.0
7.
1.0
4.0
5.0
6.0

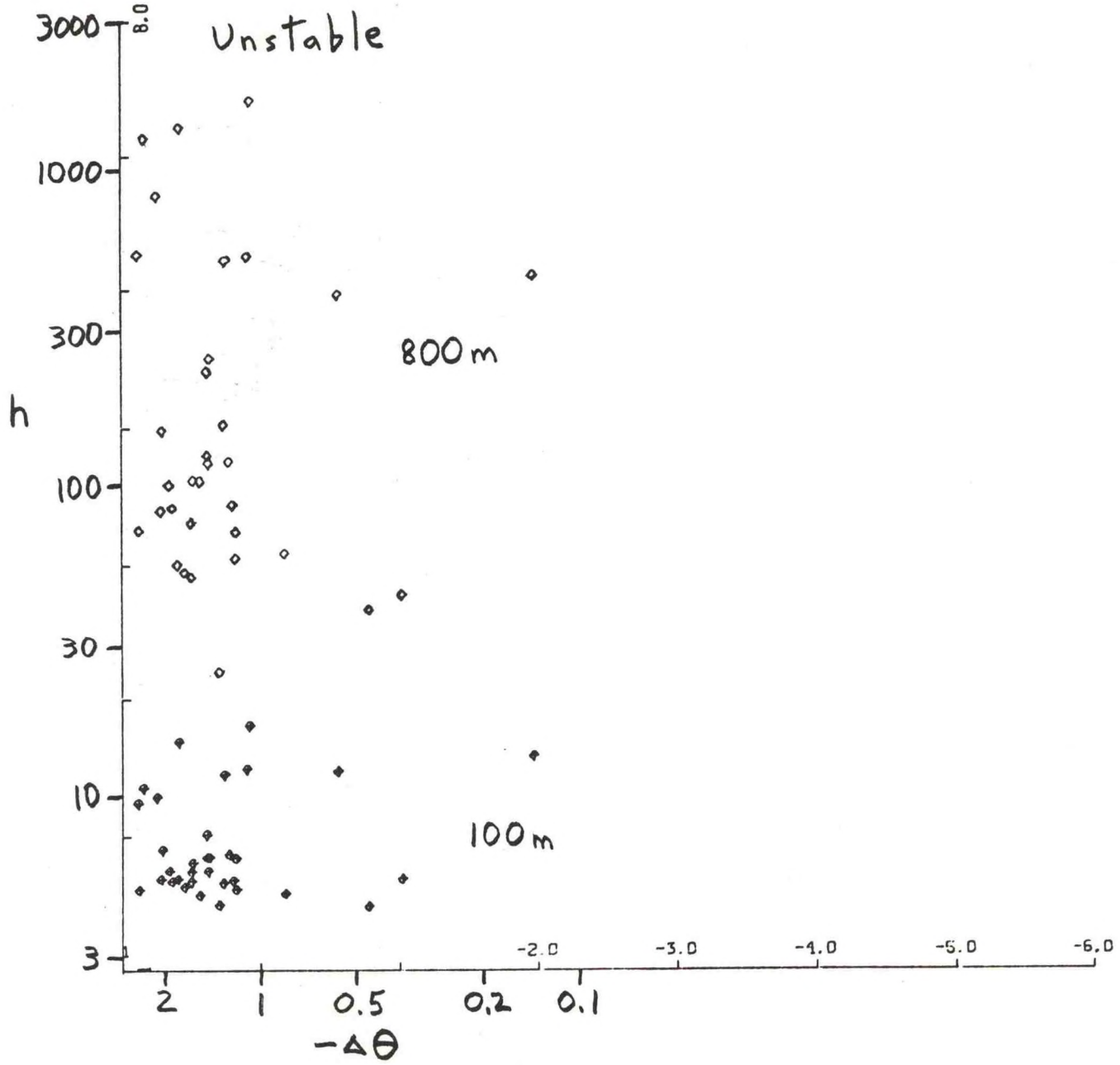
Unstable
3000
1000
300
100
30
10
3
h
800m
100m
8.0
-2.0
-3.0
-4.0
-5.0
-6.0
2
1
0.5
0.2
0.1
-Δθ

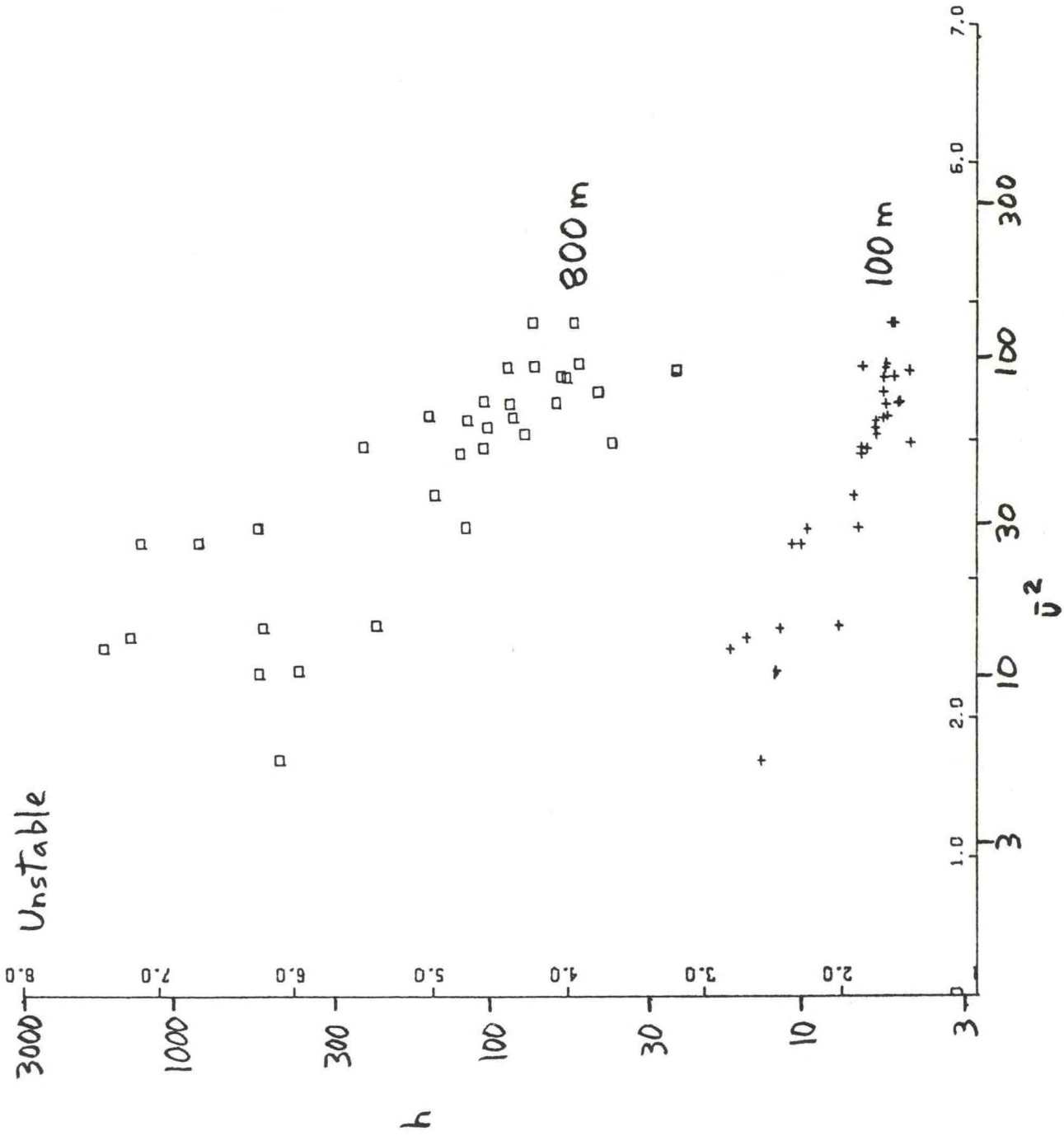
Unstable
800 m
100 m
h
$\bar{v}^2$
3000
1000
300
100
30
10
3
8.0
7.0
6.0
5.0
4.0
3.0
2.0
1.0
3
10
30
100
300
2.0
6.0
7.0

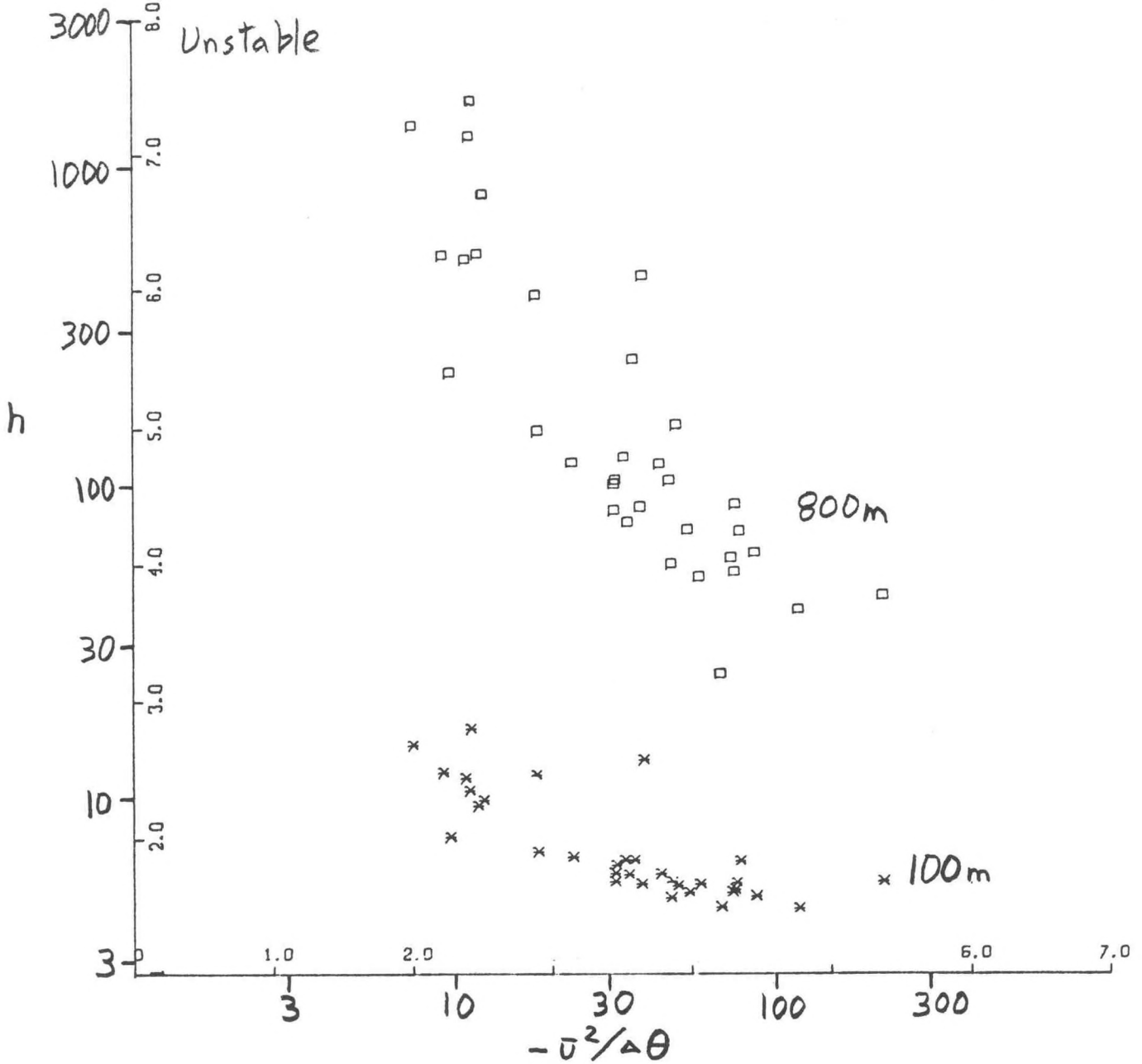
Unstable
3000
1000
300
100
30
10
3
h
8.0
7.0
6.0
5.0
4.0
3.0
2.0
1.0
800m
100m
3
10
30
100
300
6.0
7.0
$-\bar{U}^2/\Delta\theta$

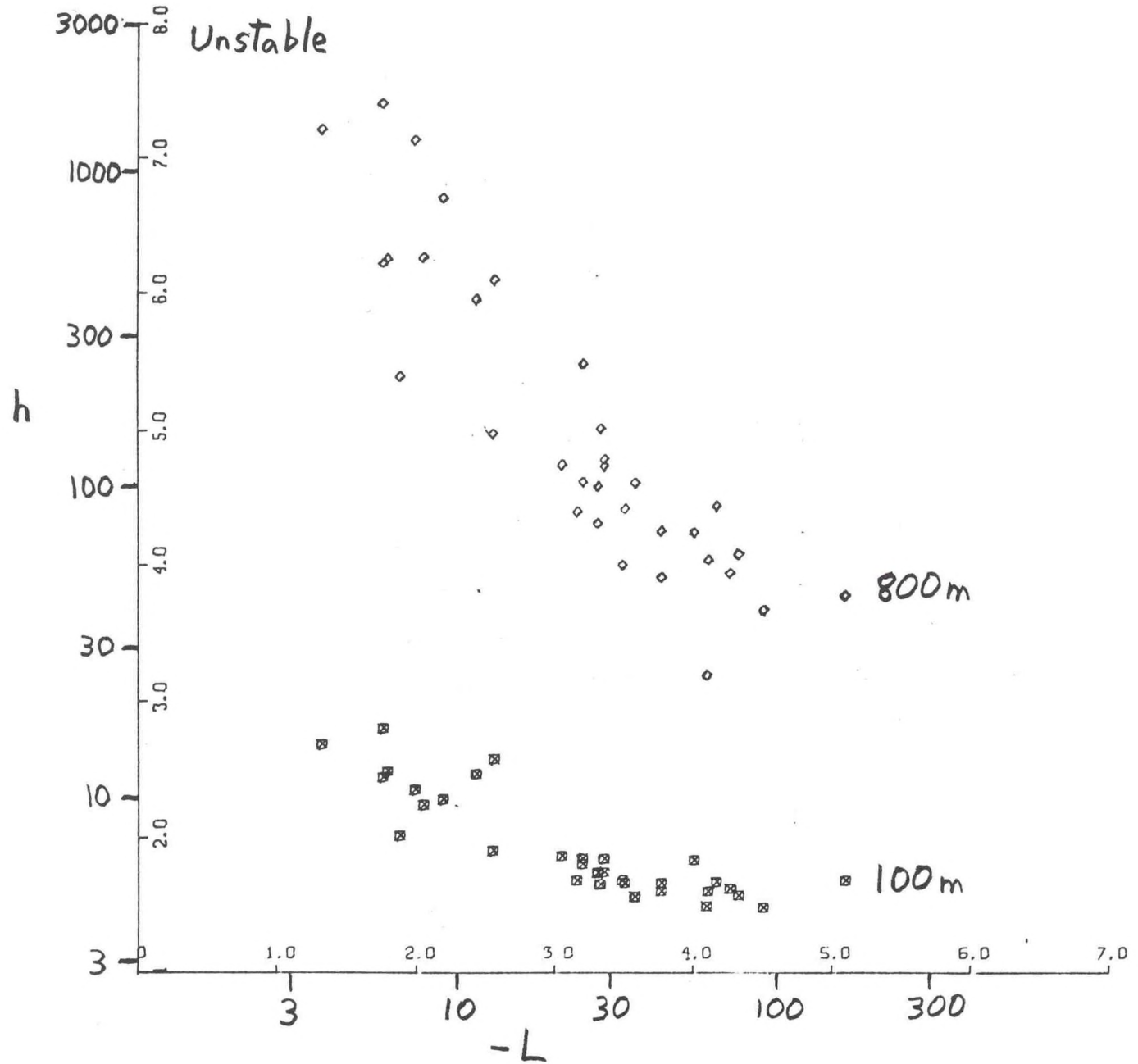
Unstable
3000
1000
300
100
30
10
3
h
8.0
7.0
6.0
5.0
4.0
3.0
2.0
0
1.0
2.0
3.0
4.0
5.0
6.0
7.0
3
10
30
100
300
-L
800m
100m

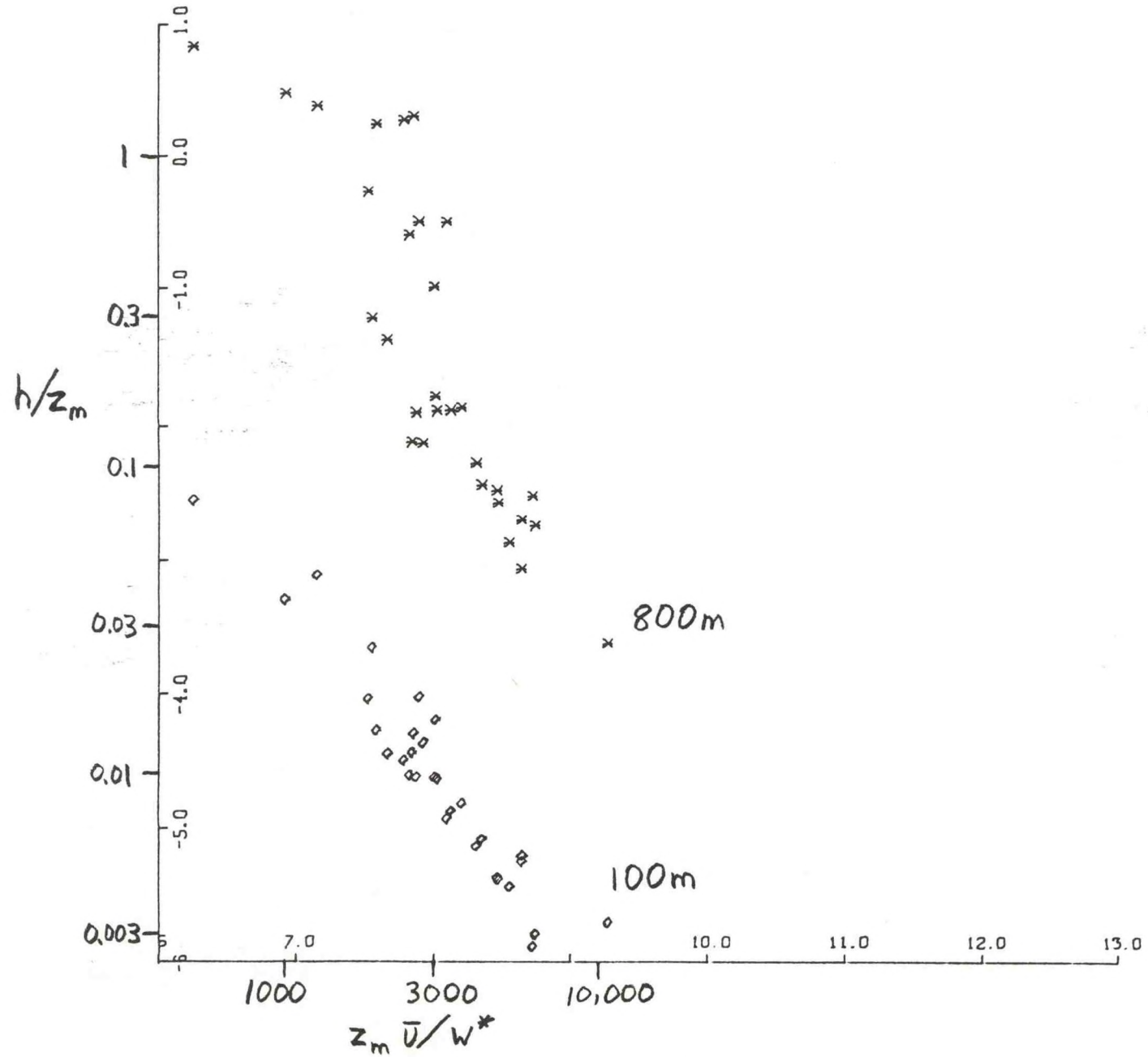
h/z_m
1
0.3
0.1
0.03
0.01
0.003
1.0
0.0
-1.0
-4.0
-5.0
-6
800m
100m
7.0
10.0
11.0
12.0
13.0
1000
3000
10,000
z_m Ū/W*

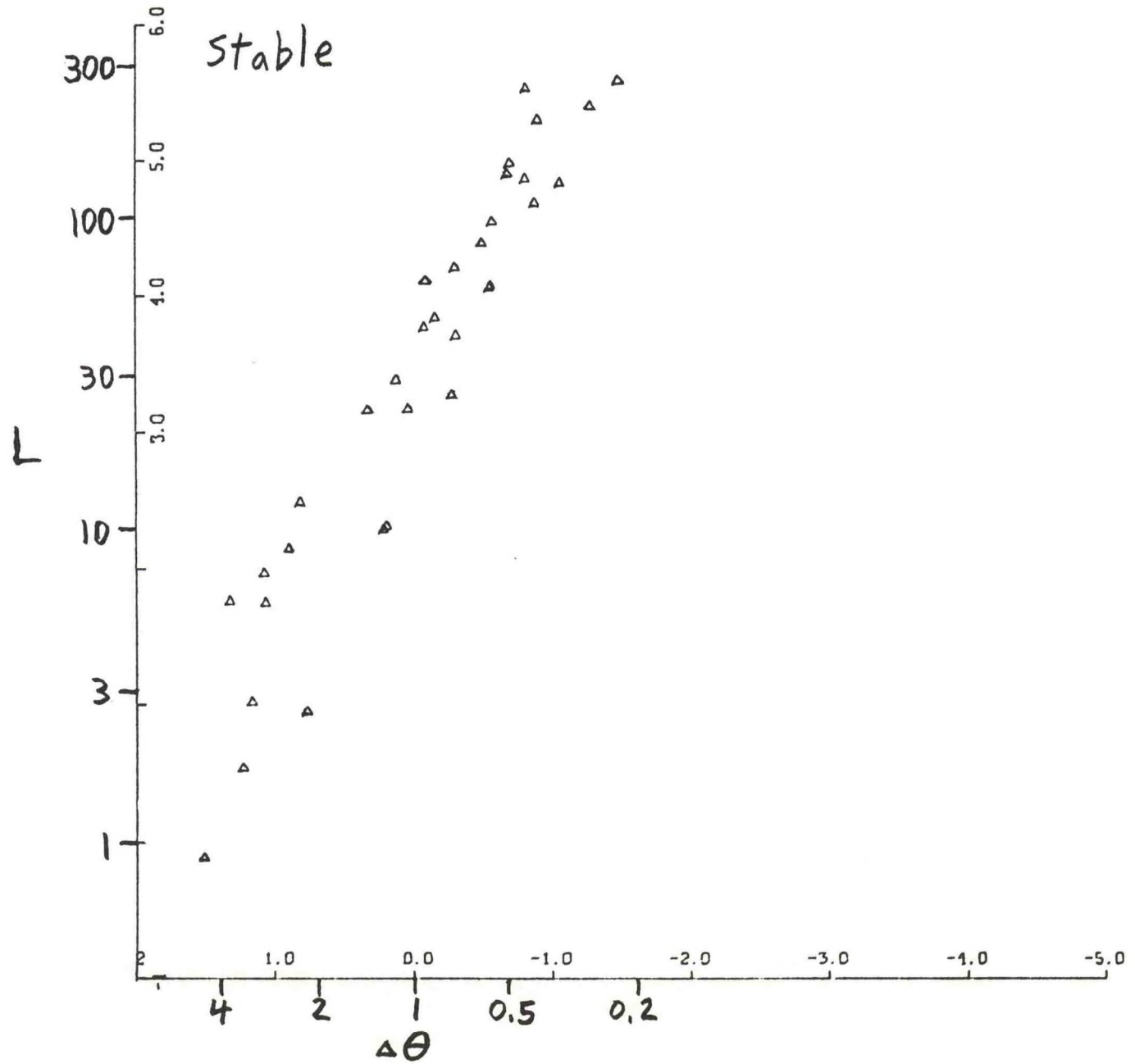
Stable
300
100
30
10
3
1
L
6.0
5.0
4.0
3.0
2
1.0
0.0
-1.0
-2.0
-3.0
-4.0
-5.0
4
2
1
0.5
0.2
Δθ

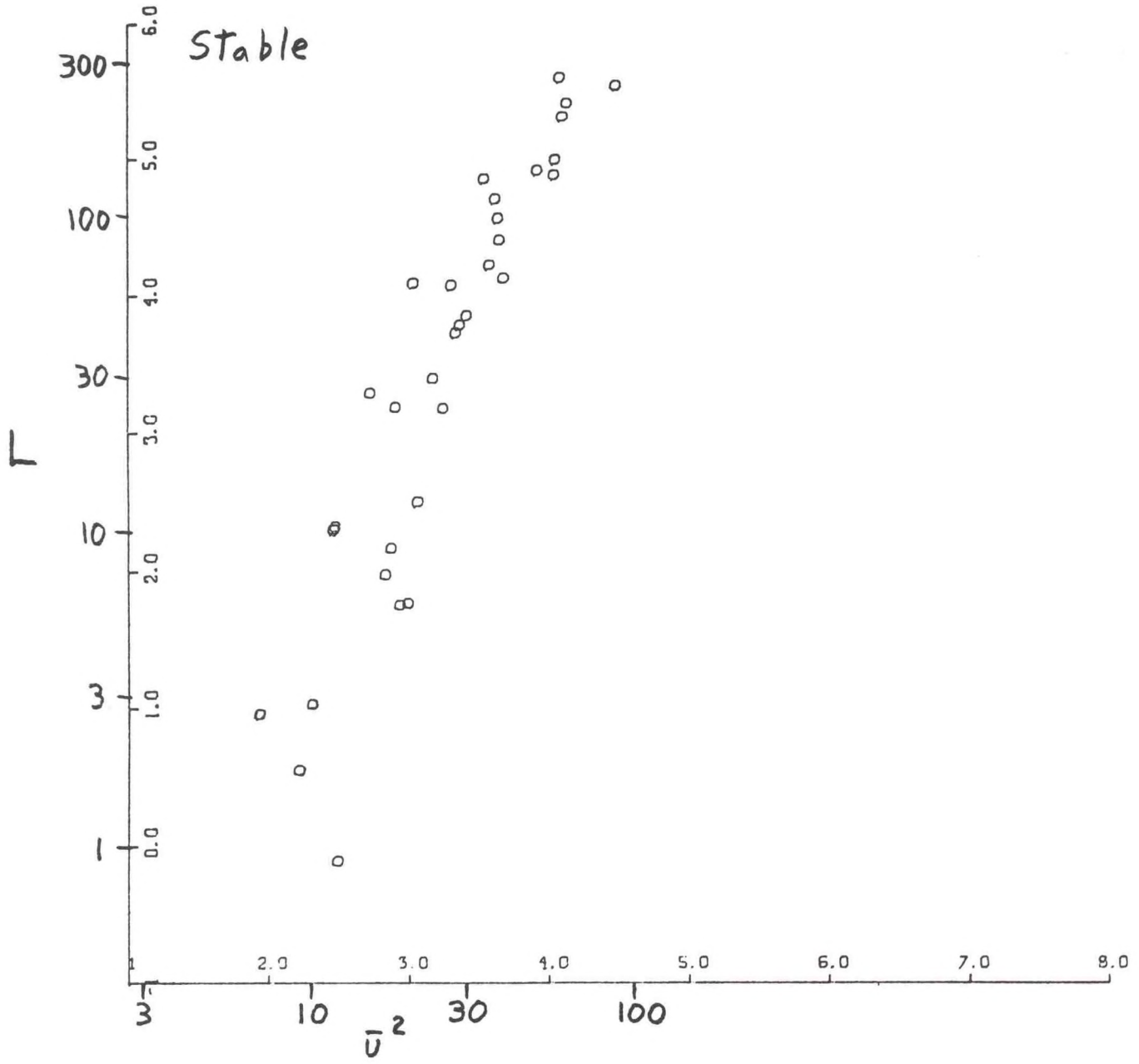
Stable
300
100
30
10
3
1
L
6.0
5.0
4.0
3.0
2.0
1.0
0.0
2.0
3.0
4.0
5.0
6.0
7.0
8.0
3
10
30
100
$\bar{U}^2$

Stable
L
300
100
30
10
3
1
0.0
1.0
2.0
3.0
4.0
5.0
6.0
1
3
10
30
100
300
1.0
2.0
3.0
4.0
5.0
6.0
7.0
$\bar{U}^2/\Delta\theta$

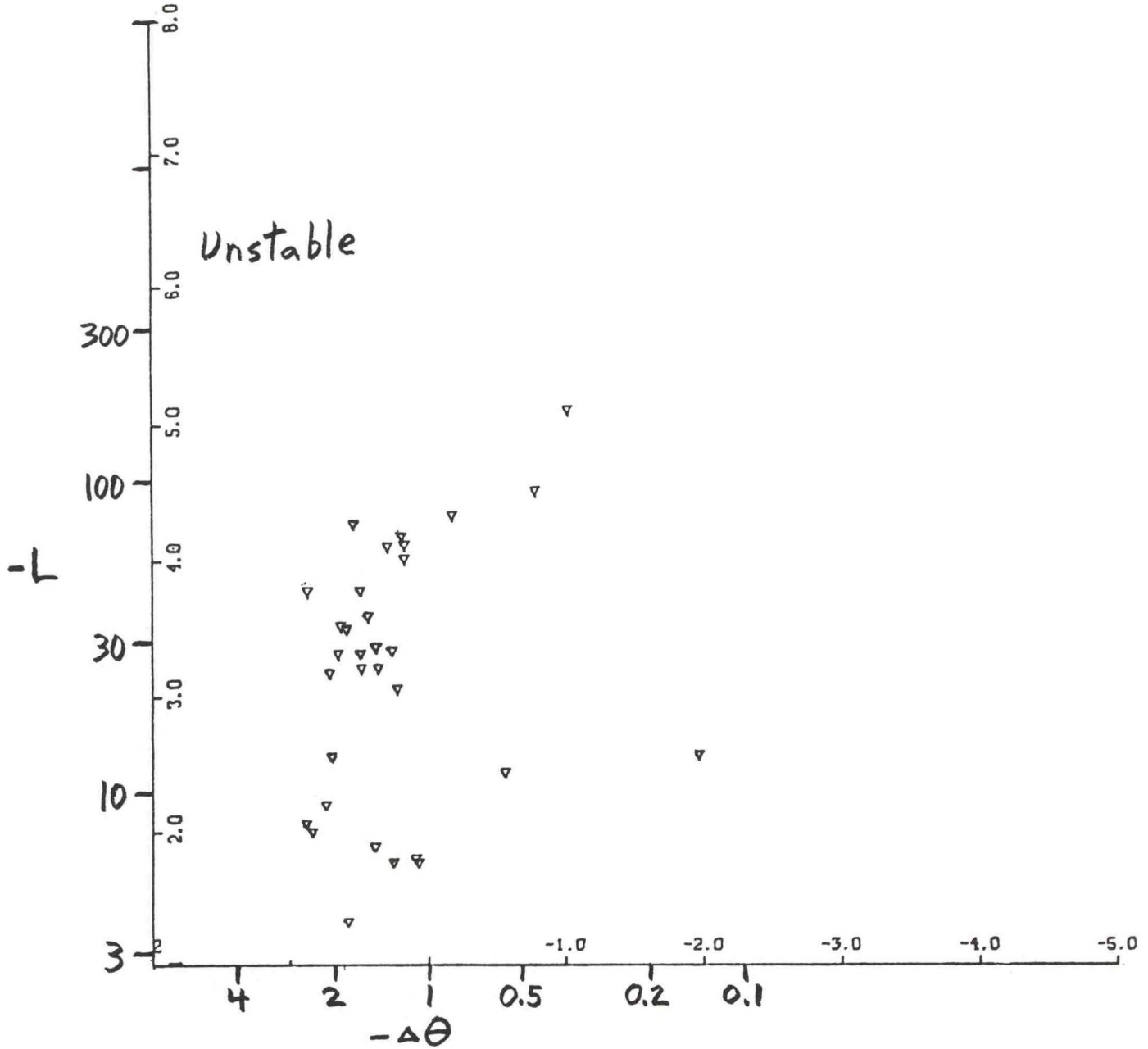
Unstable
-L
300
100
30
10
3
8.0
7.0
6.0
5.0
4.0
3.0
2.0
-1.0
-2.0
-3.0
-4.0
-5.0
4
2
1
0.5
0.2
0.1
-Δθ

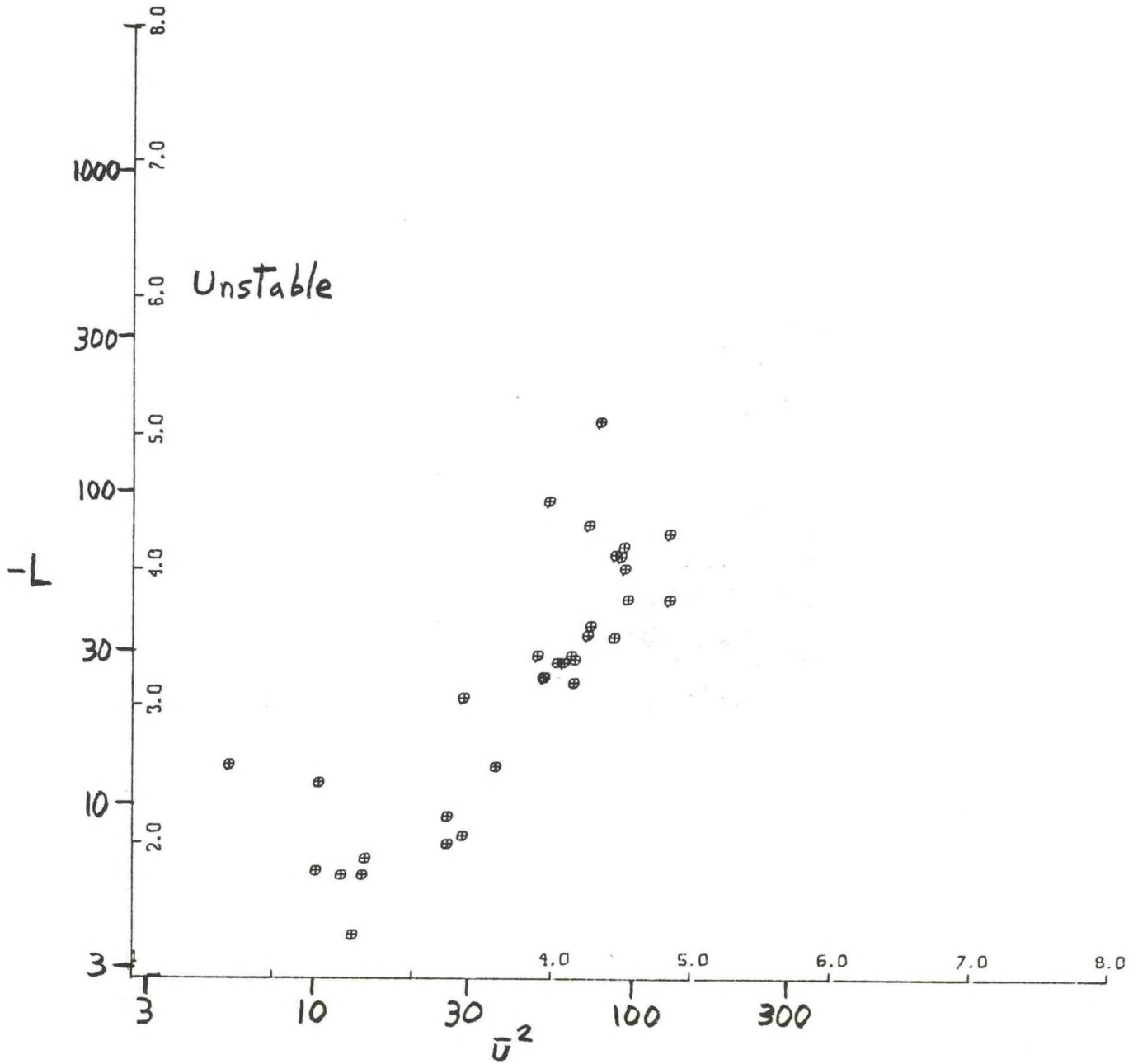
Unstable
-L
1000
300
100
30
10
3
8.0
7.0
6.0
5.0
4.0
3.0
2.0
3
10
30
100
300
$\bar{U}^2$

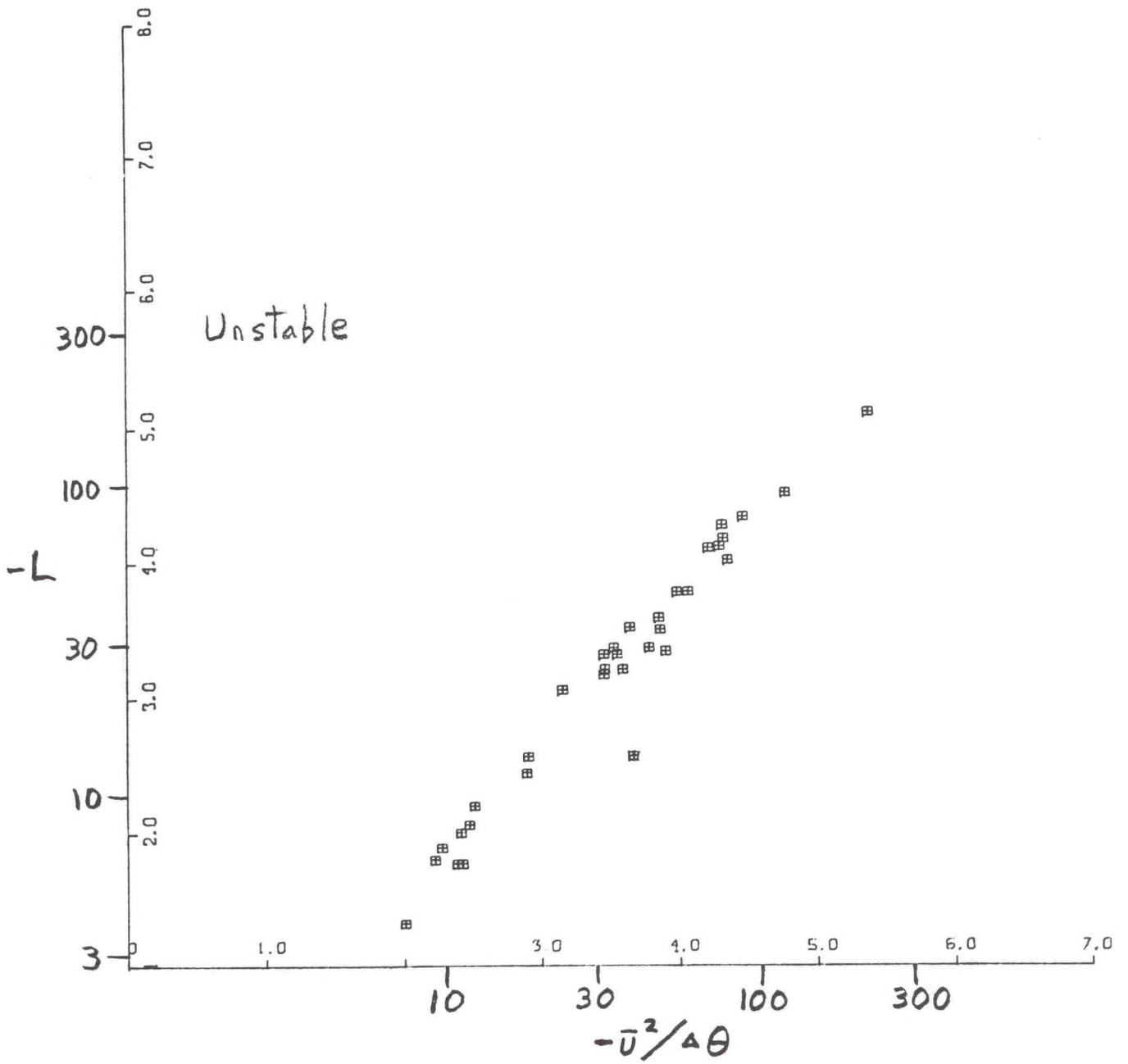
Unstable
-L
300
100
30
10
3
8.0
7.0
6.0
5.0
4.0
3.0
2.0
1.0
0
10
30
100
300
$-\bar{U}^2/\Delta\theta$

THE STRUCTURE OF THE NOCTURNAL PLANETARY BOUNDARY LAYER

K. S. RAO and H. F. SNODGRASS*

Atmospheric Turbulence and Diffusion Laboratory
National Oceanic and Atmospheric Administration
Oak Ridge, Tennessee 37830

ABSTRACT

The evolution and structure of an idealized steady-state nocturnal boundary layer are investigated using a higher-order turbulence-closure model and a constant surface cooling rate. The model predictions are parameterized in the framework of surface-layer and PBL similarity theories and compared with observations and other model results. Several extensions and limitations of the model are discussed.

1. INTRODUCTION

The planetary boundary layer (PBL) is generally stably-stratified over land at night, though persistent daytime inversions also often occur in winter. The nocturnal mechanically-mixed layer is typically much shallower than the daytime convectively-mixed layer. Its depth also varies widely, from a few meters to hundreds of meters, depending on the upper wind, stability, and terrain. This has an important bearing on the dispersion of pollutants in the atmosphere; maximum pollutant-concentration levels are usually associated with strongly stable conditions and low wind speeds, when the diffusive ability of the atmosphere is at a minimum. It is important therefore to study the physical processes of the nocturnal boundary layer and develop models capable of simulating the salient features of its turbulence as well as mean profile structure. The models would enable us to improve diffusion estimates for very stable

*Affiliated with Oak Ridge Associated Universities (ORAU).

ATDL Contribution File No. 78/9

conditions; these estimates are presently based on arbitrary extrapolation of semi-empirical diffusion curves fitted to rather highly-scattered observations.

Several numerical and analytical model studies of the nocturnal PBL have been reported in the literature. Deardorff (1972) simulated the wind and temperature soundings in a nocturnal boundary layer with eddy diffusivities specified as functions of height and stability, and concluded that the boundary layer height determined from the temperature profiles increased with time and could not be described by any steady state similarity theory. Businger and Arya (1974) formulated a steady state model of the stable boundary layer with an implicit expression for the eddy viscosity distribution based on an approximation to the vertical variation of momentum flux. They found that the boundary layer height h, determined from the stress profiles, varied as a function of the stability parameter following Zilitinkevich's (1972) similarity prediction. Delage (1974) used locally-determined eddy diffusivities from the turbulent kinetic energy equation and a specified mixing length. With a time-dependent surface cooling rate, he simulated the evolution of the nocturnal boundary layer and concluded that the magnitude of the geostrophic wind is the dominant factor in determining the inversion depth. He suggested that a steady-state treatment of the nocturnal PBL may not be appropriate since changes in external conditions can generate inertial oscillations with periods comparable to the night itself. Blackadar (1976) simulated the variation of wind and temperature profiles during the night using a simple model of the soil heat budget. His eddy diffusivities, specified in terms of a mixing length and the Richardson number, vanish when the latter exceeds a critical value of 0.25.

Wyngaard (1975) extended a higher-order-closure model (Wyngaard *et al.*, 1974), which contains equations for turbulence covariances as well as the mean field, to the stable case. Specifying a constant cooling rate at 1 m height, he demonstrated that the evolving structure of the nocturnal PBL could reach a steady state within a few hours after transition. He found good agreement between the predicted turbulence structure and the stable surface layer data, and the calculated h varied as predicted by Zilitinkevich (1972). Based partly on Wyngaard's (1975) results, Briggs (1977) developed an analytical "mixing model" for the steady state nocturnal boundary layer in which most parameters were predicted as simple power laws of the initial friction velocity, the cooling rate near the ground, and the Coriolis parameter. Another hypothesis for the nondimensional wind shear variation, together with Zilitinkevich's similarity prediction for h, led to the development of a "wind-profile" model, which allowed determination of steady state parameters from the geostrophic wind. Brost and Wyngaard (1978) used a simplified "diagnostic" version of Wyngaard's (1975) model with a specified turbulent mixing length to study the general characteristics of the stable boundary layer and the influences of several "real-world" features such as sloping terrain, a variable cooling rate through the surface energy budget and different soils, and *in situ* long-wave radiative effects. They found that terrain slope has a strong effect on h depending on the wind direction.

In the present study, we essentially adopt Wyngaard's (1975) higher-order turbulence closure model to investigate the evolution and structure of the steady state nocturnal PBL with a constant cooling rate at the surface. The emphasis is on prediction and parameterization of eddy diffusivities and the stability-dependent universal functions in the geostrophic drag and heat transfer relations. The model predictions are presented and discussed in terms of surface-layer and PBL similarity theories, and compared with observations. The specific objective of this study is to gain a better understanding of the nocturnal PBL structure and to develop a numerical modeling capability within ATDL which could be used to study the relative importance of various parameters or specific cases of interest, and extended to simulate real-world situations. The numerical model results, after testing with atmospheric data, would be useful in developing simpler analytical models and parameterizations, and better prediction techniques for diffusion in the stable boundary layer.

2. THE MODEL

We consider the barotropic PBL over a horizontally homogeneous surface of infinite extent, and choose the x-y plane parallel to the surface such that the x-coordinate is oriented along the mean surface wind

direction and the z coordinate represents the height above the surface. We do not consider moisture and radiative flux divergence in this study. The mean field equations for a time-dependent one-dimensional flow, within the Boussinesq and boundary layer approximations, are

$$\begin{aligned} \partial U/\partial t &= -\partial\overline{uw}/\partial z + f\,(V - V_g) \\ \partial V/\partial t &= -\partial\overline{vw}/\partial z + f\,(U_g - U) \\ \partial \Theta/\partial t &= -\partial\overline{\theta w}/\partial z \end{aligned} \tag{1}$$

Here (U, V, W = 0) are the mean velocity components in (x, y, z) directions, respectively, and Θ is the mean potential temperature. The corresponding fluctuating quantities are given by (u, v, w) and θ; $f = 2\Omega \sin\phi$ is the Coriolis parameter, where Ω is the earth's rotation rate and ϕ is the latitude; the components of the geostrophic wind vector $G = U_g\mathbf{i} + V_g\mathbf{j}$, assumed to be independent of z, are defined by $f\,U_g = -\partial P/\partial y$ and $f\,V_g = \partial P/\partial x$, where P is the mean kinematic pressure.

In order to solve Eq. (1), one needs information on the turbulent fluxes of momentum and heat. We adopt a higher-order-closure model here, and write the transport equations for the fluxes; these second moment equations introduce further unknowns which are of three types: (i) velocity or temperature and pressure-gradient covariances, (ii) third-moment divergence (turbulent transport) terms, and (iii) molecular destruction (dissipation rate) terms. To close the equations, we parameterize these third moments in terms of dimensionally-consistent, physically-plausible, semi-empirical expressions involving the mean quantities, the second moments, and a turbulence relaxation time $\tau = 2E/\bar{\epsilon}$, where $\bar{\epsilon}$ is the mean viscous dissipation rate of the turbulent kinetic energy ($E = \overline{u_i u_i}/2$). The time scale τ is determined by the model itself, not specified *a priori*, since the model also includes a dynamical equation for $\bar{\epsilon}$. These approximations constitute the higher-order-closure technique discussed by Wyngaard (1975), and reference should be made to that paper for details. Here we give only the closed equations for the turbulence covariances.

Kinetic Energy Components:

$$\frac{\partial}{\partial t}\begin{bmatrix}\overline{u^2}\\ \overline{v^2}\\ \overline{w^2}\end{bmatrix} - \mathcal{D}\begin{bmatrix}\overline{u^2}\\ \overline{v^2}\\ \overline{w^2}\end{bmatrix} = 2\begin{bmatrix}(1-c_1)\cdot SP_1\\ (1-c_2)\cdot SP_2\\ (1+c_3)\cdot BP\end{bmatrix} + \frac{2}{3}\begin{bmatrix}c_2\cdot SP - c_3\cdot BP - \bar{\epsilon}\\ c_2\cdot SP - c_3\cdot BP - \bar{\epsilon}\\ c_2\cdot SP - c_3\cdot BP - \bar{\epsilon}\end{bmatrix}$$

$$-\frac{c}{\tau}\begin{bmatrix}\overline{u^2} - 2E/3\\ \overline{v^2} - 2E/3\\ \overline{w^2} - 2E/3\end{bmatrix} + 2f\begin{bmatrix}\overline{uv} - \overline{uw}/\tan\phi\\ -\overline{uv}\\ \overline{uw}/\tan\phi\end{bmatrix} \tag{2}$$

Shear Stress Components:

$$\frac{\partial}{\partial t}\begin{bmatrix}\overline{uw}\\ \overline{vw}\\ \overline{uv}\end{bmatrix} - \mathcal{D}\begin{bmatrix}\overline{uw}\\ \overline{vw}\\ \overline{uv}\end{bmatrix} = -(1-c_2)\begin{bmatrix}\overline{w^2}\,\partial U/\partial z\\ \overline{w^2}\,\partial V/\partial z\\ \overline{uw}\,\partial V/\partial z + \overline{vw}\,\partial U/\partial z\end{bmatrix} + c_1 E\begin{bmatrix}\partial U/\partial z\\ \partial V/\partial z\\ 0\end{bmatrix}$$

$$+(1+c_3)\cdot\frac{g}{T_0}\begin{bmatrix}\overline{u\theta}\\ \overline{v\theta}\\ 0\end{bmatrix} - \frac{c}{\tau}\begin{bmatrix}\overline{uw}\\ \overline{vw}\\ \overline{uv}\end{bmatrix} + f\begin{bmatrix}\overline{vw} + (\overline{u^2} - \overline{v^2})/\tan\phi\\ -\overline{uw} + \overline{uv}/\tan\phi\\ \overline{v^2} - \overline{u^2} - \overline{vw}/\tan\phi\end{bmatrix} \tag{3}$$

Heat Flux Components:

$$\frac{\partial}{\partial t}\begin{bmatrix}\overline{w\theta}\\ \overline{v\theta}\\ \overline{u\theta}\end{bmatrix}-\mathcal{D}\begin{bmatrix}\overline{w\theta}\\ \overline{v\theta}\\ \overline{u\theta}\end{bmatrix}=-\begin{bmatrix}\overline{w^2}\,\partial\Theta/\partial z+(1-d_2)\,g\,\overline{\theta^2}/T_0\\ \overline{vw}\,\partial\Theta/\partial z-(1+d_1)\,\overline{w\theta}\,\partial V/\partial z\\ \overline{uw}\,\partial\Theta/\partial z-(1+d_1)\,\overline{w\theta}\,\partial U/\partial z\end{bmatrix}-\frac{d}{\tau}\begin{bmatrix}\overline{w\theta}\\ \overline{v\theta}\\ \overline{u\theta}\end{bmatrix}+f\begin{bmatrix}\overline{u\theta}/\tan\phi\\ -\overline{u\theta}\\ \overline{v\theta}-\overline{w\theta}/\tan\phi\end{bmatrix} \tag{4}$$

Temperature Variance:

$$\partial\overline{\theta^2}/\partial t-\mathcal{D}(\overline{\theta^2})=-2(\overline{w\theta}\,\partial\Theta/\partial z+d_3\,\overline{\theta^2}/\tau) \tag{5}$$

In the above, $\mathcal{D}(\ )=\frac{\partial}{\partial z}\left[\overline{w^2}\,\tau\,\frac{\partial}{\partial z}(\ )\right]$ is the diffusion operator, $SP=-\overline{u_iu_j}\,\partial U_i/\partial x_j$ is the shear production and $BP=(g/T_0)\cdot\overline{w\theta}$ is the buoyant production of turbulent kinetic energy, $SP_1=-\overline{uw}\,\partial U/\partial z$, $SP_2=-\overline{vw}\,\partial V/\partial z$, g is the acceleration due to gravity, and T_0 is a mean reference temperature. The Coriolis terms in the equations are written such that the components of a unit vector η along the earth's rotation axis are given by $\eta_i=(o,\cos\phi,\sin\phi)$; therefore, the y-axis is taken parallel to the north-south line (see Busch, 1973) such that y is positive to the north and x is positive to the east.

The constants in Eqs. (2) to (5) are specified as

$$c=6.67\,(1-c_2),\ c_1=0.23\,(1-c_2),\ c_2=0.3,\ c_3=-0.5,\ d=9.7,\ d_1=-0.5$$

$$d_2=\begin{cases}0.5, & Ri\leqslant 0\\ 0.5+1.5\,Ri^2-Ri^3, & 0<Ri<1\\ 1.0, & Ri\geqslant 1\end{cases} \tag{6}$$

$$d_3=1.4$$

where $Ri=\frac{g}{T_0}\frac{\partial\Theta}{\partial z}\Big/\left[\left(\frac{\partial U}{\partial z}\right)^2+\left(\frac{\partial V}{\partial z}\right)^2\right]$ is the gradient Richardson number. The relations for c and c_1 and the values for d and d_3 are determined by forcing the model equations to yield an equilibrium surface layer and satisfy observations in the neutral limit. The values for c_2 and c_3 are determined by comparing the model calculations to stable surface layer data. The value of d_1 follows from the work of Launder (1975). It was found that d_2 should be slightly larger than 0.5 in a stable PBL to avoid the spurious generation of heat flux by temperature fluctuations; the Ri-dependent functional form of d_2 was chosen such that it approaches smoothly a buoyancy cut-off value at Ri = 1.

As mentioned above, the time scale $\tau(z,t)$ is determined by the model itself as $\tau=(\overline{u^2}+\overline{v^2}+\overline{w^2})/\overline{\epsilon}$, where $\overline{\epsilon}$ is calculated from the parameterized form of the dissipation-rate equation (see Wyngaard, 1975) at large Reynolds numbers:

$$\frac{\partial\overline{\epsilon}}{\partial t}-a_t\mathcal{D}(\overline{\epsilon})=\frac{\overline{\epsilon}}{\tau}\left[-A+B(SP/\overline{\epsilon})+C(BP/\overline{\epsilon})+D(BP/\overline{\epsilon})^2\right] \tag{7}$$

Here, A = 4, B = 3.5, C = 1, and D = 2 are constants, and the transport constant is $a_t=0.041$, consistent with the neutral surface layer data.

Equations (1) to (7) provide a closed set of 14 partial differential equations for the PBL model. The complexity of this higher-order-closure scheme is justified in that it allows for an adequate prediction of the fluxes, variances, and other much-needed information for understanding the turbulence structure and behavior of the PBL.

3. COMPUTATIONAL TECHNIQUES, BOUNDARY AND INITIAL CONDITIONS

The closed equation set, subject to the given boundary and initial conditions to be described in this section, was numerically integrated in time on a digital computer using a Dufort–Frankel explicit finite-difference scheme. To obtain a fine computational mesh near the ground, a logarithmic transformation of the vertical coordinate was used from the lower boundary, which was set at $z_1 = 1$ m instead of z_0, the surface aerodynamic roughness, in order to reduce computing time, to the upper boundary at H = 1000 m, with a total of 51 grid points.

In an equilibrium surface layer, the wind direction essentially remains constant with height and coincides with the direction of the constant shear stress. In a coordinate system with the positive x-axis taken along the surface wind (or stress) direction, hereafter referred to as coordinate system-1 or CS-1 (Fig. 1a), it is often convenient to regard the surface friction velocity $u_* = (\tau_0/\rho)^{1/2}$ and the surface heat flux $Q_0 = H_0/\rho c_p$ as inputs, and the mean wind speed and temperature at the upper boundary H as outputs. If U_g and V_g are unknown in a barotropic PBL model, it is convenient to use CS-1 and rewrite Eq. (1), by replacing the mean variables with their z-derivatives, as follows:

$$\begin{aligned} \partial(\partial U/\partial z)/\partial t &= -\partial^2 \overline{uw}/\partial z^2 + f\,\partial V/\partial z \\ \partial(\partial V/\partial z)/\partial t &= -\partial^2 \overline{vw}/\partial z^2 - f\,\partial U/\partial z \\ \partial(\partial \Theta/\partial z)/\partial t &= -\partial^2 \overline{\theta w}/\partial z^2 \end{aligned} \tag{8}$$

Integration of the calculated mean-gradient profiles over the vertical grid then yields U_g, V_g and Θ_H at the upper boundary H.

For some problems, it is more appropriate to consider G and Θ_H as inputs, and u_* as an unknown. In the nocturnal PBL, for example, the friction velocity decreases sharply after sunset in response to radiation cooling at the surface, even while the geostrophic wind remains essentially constant. In this case, the mean field equations (1) are carried as written, U_g and V_g are specified as inputs, and u_* and Q_0 are determined from the model. It is convenient here to use a coordinate system with the positive x-axis aligned with the direction of the geostrophic wind vector G, hereafter referred to as coordinate system-2 or CS-2 (Fig. 1b), and adjust the lower boundary conditions to account for the angle α between the surface wind and the geostrophic wind (x-axis). The mean field equations (1) in this case reduce to

$$\begin{aligned} \partial U/\partial t &= -\partial \overline{uw}/\partial z + f\,V \\ \partial V/\partial t &= -\partial \overline{vw}/\partial z + f\,(G - U) \\ \partial \Theta/\partial t &= -\partial \overline{\theta w}/\partial z \end{aligned} \tag{9}$$

The lower boundary conditions at $z = z_1$ are based on the relations derived from the Monin–Obukhov similarity theory, surface layer measurements (Businger *et al.*, 1971; Panofsky *et al.*, 1977), and numerical experiments (Wyngaard *et al.*, 1974; Wyngaard, 1975). In PBL models, irrespective of the thermal stratification and the coordinate system chosen, the lower boundary conditions can be conveniently specified in a most general form as follows.

Mean Field Variables:

$$\begin{aligned} U &= S\cos\alpha, \qquad V = S\sin\alpha \\ S &= (U^2 + V^2)^{1/2} = u_*[\ln(z/z_0) + f_1]/k \\ \Delta\Theta &= \Theta - \Theta_0 = 0.74\,\theta_*\,[\ln(z/z_0) + f_2]/k \end{aligned} \tag{10a}$$

Mean Field Gradients:

$$\partial U/\partial z = (\partial S/\partial z)\cos\alpha, \qquad \partial V/\partial z = (\partial S/\partial z)\sin\alpha$$
$$\partial S/\partial z = u_* \phi_m/kz, \qquad \partial\Theta/\partial z = \theta_* \phi_h/kz \tag{10b}$$

Turbulent Shear Stresses:

$$\overline{uw} = -u_*^2 \cos\alpha, \qquad \overline{vw} = -u_*^2 \sin\alpha$$
$$\overline{uv} = 2.25\, u_*^2 \sin\alpha \cos\alpha, \qquad u_*^2 = \tau_0/\rho \tag{10c}$$

Turbulent Kinetic Energies:

$$\overline{u^2} = (4\cos^2\alpha + 1.75\sin^2\alpha + f_3)\, u_*^2$$
$$\overline{v^2} = (4\sin^2\alpha + 1.75\cos^2\alpha + f_3)\, u_*^2 \tag{10d}$$
$$\overline{w^2} = (1.75 + f_4)\, u_*^2$$

Turbulent Heat Fluxes:

$$\overline{w\theta} = -u_*\theta_* = Q_0 = H_0/\rho c_p$$
$$\overline{u\theta} = (4\phi_m\phi_h\cos\alpha)\, u_*\theta_*, \ \overline{v\theta} = (4\phi_m\phi_h\sin\alpha)\, u_*\theta_* \tag{10e}$$

Temperature Variance:

$$\overline{\theta^2} = 4\, f_5\, \theta_*^2 \tag{10f}$$

Dissipation Rate:

$$\bar{\epsilon} = -(\overline{uw}\,\partial U/\partial z + \overline{vw}\,\partial V/\partial z) + g\,\overline{w\theta}/T_0 \tag{10g}$$

The various nondimensional functions appearing in Eq. (10) are defined below, depending on the thermal stratification.

Function	Unstable	Neutral	Stable
ϕ_m	$(1 - 15\zeta)^{-1/4}$	1	$1 + 4.7\zeta$
ϕ_h	$0.74\,(1 - 9\zeta)^{-1/2}$	0.74	$0.74 + 4.7\zeta$
f_1	$-\left[2\ln\left(\frac{1+\phi_m^{-1}}{2}\right) + \ln\left(\frac{1+\phi_m^{-2}}{2}\right) - 2\tan^{-1}(\phi_m^{-1}) + \pi/2\right]$	0	4.7ζ
f_2	$-2\ln\left[\frac{1+(\phi_h/0.74)^{-1}}{2}\right]$	0	$4.7\zeta/0.74$
f_3	$0.2\,(w_*/u_*)^2$ or $0.2\,(-z_i/kL)^{2/3}$	0	0
f_4	$2\,(-\zeta)^{2/3}$	0	0
f_5	$(1 - 8.3\zeta)^{-2/3}$	1	1

In the above, $\zeta = z/L$, $L = u_*^3 T_0/(kgQ_0)$ is the Monin–Obukhov length, k is the von Kármán constant (taken as 0.35), $w_* = (gQ_0 z_i/T)^{1/3}$ is the bulk convective velocity, z_i is the height of the lowest inversion base in the convective case, and Θ_0 is the potential temperature at the surface.

The lower boundary conditions for coordinate system-1 can be obtained now by setting $\alpha = 0$ in Eq. (10), since the angle between the surface wind and the positive x-axis is zero. For coordinate system-2, the boundary conditions are carried as written and α, u_* and Q_0 are determined at each time t from Eqs. (10c) and (10e) by extrapolating the computed shear stress and heat flux profiles near the surface to the lower boundary. In this study, CS-2 was used for modeling the nocturnal PBL.

At the upper boundary H, a simulated inversion lid, all turbulence quantities and the vertical gradients of the mean variables were set to zero.

In order to study the temporal evolution of the nocturnal PBL structure, it is necessary to initialize the model with typical distributions of variables in a decaying convective PBL around sunset at the instant of transition when $Q_0 \to 0$. To obtain these initial conditions, we simulated a full diurnal cycle using the model outlined above, by starting with an equilibrium neutral PBL at sunrise with $G = 10$ ms^{-1}, $z_0 = 0.01$ m, $\phi = 45°$N, and specifying a sinusoidal variation of surface heat flux over an 11-hour heating period with a peak surface heat flux of 0.027 mK s^{-1}. This generated a moderately convective PBL with $u_* = 0.4$ ms^{-1} and $-z_i/L \simeq 5$ when Q_0 is at its peak value. After transition, following Wyngaard (1975), a constant surface-cooling rate, $\partial\Theta_0/\partial t$, is specified for the nocturnal PBL, and Q_0 is calculated as outlined above.

The computing (CPU) time on an IBM-360/91 digital computer is about 10 min for the simulation of the entire diurnal cycle including the nocturnal case. This time can be substantially reduced by optimizing the vertical grid and the integration time step, and by using improved programming techniques.

4. RESULTS AND DISCUSSION

In a horizontally homogeneous nocturnal PBL, a cooling rate specified at the surface gradually reduces the mean potential temperature in the PBL. If the radiation flux divergence is negligibly small, the PBL cooling rate is balanced entirely by the turbulent flux divergence. For a constant surface-cooling rate, a quasi-steady state may be established when

$$\partial\Theta/\partial t = -\partial\overline{w\theta}/\partial z = Q_0/h = \text{constant}$$

or

$$\frac{\partial}{\partial t}(\partial\Theta/\partial z) = 0 \tag{12}$$

where h is the PBL height. This implies that both Q_0 and h, as well as other key PBL parameters such as u_*, α and L, should approach constant values as the PBL approaches a quasi-steady state.

Following Wyngaard (1975), we have tested here four constant cooling rates, 0.2, 0.5, 1.0, and 2.0 C hr^{-1}, all applied at the surface (z_0) instead of the 1 m level. Each cooling rate leads to a near-constant value for the PBL scaling parameter $\mu = |u_*/fL|$ in the quasi-steady state; μ is the ratio of the dynamic length scale of the neutral boundary layer, $|u_*/f|$, to the Monin-Obukhov stability length L, and it represents the ratio of the Coriolis time scale ($\sim|f^{-1}|$) to the turbulence time scale ($\sim L/u_*$) in the stable case. The steady-state value of μ increases with the surface cooling rate. The results of model calculations are presented and discussed in this section.

PBL Parameters

Figure 2 shows the predicted variation of the surface friction velocity (u_*) as a function of time t after transition and the surface cooling rate, $|\partial\Theta_0/\partial t|$. Similar plots showing the predicted evolutions of the surface heat flux (Q_0), M–O length (L), cross-isobar angle (α), and the nocturnal PBL depth (h) are given in Figs. 3 to 6, respectively. Since turbulent mixing is confined to a layer of thickness h, we have somewhat arbitrarily calculated the latter as the height where the stress decreases to 5% of its surface value. The

results indicate that, after an initial period of rapidly changing values, a quasi-steady nocturnal PBL, characterized by near-constant values for these parameters, is obtained within a few hours after transition; this is contrary to speculation by Businger and Arya (1974) that a steady state stable boundary layer would occur only at very large t, possibly during an arctic polar night. The results indicate that a quasi-steady nocturnal PBL might be established in 4–10 hours after transition, depending on the surface cooling rate. Since we require the latter to be constant in the model, this may be in reality an idealized and perhaps short-lived steady state, but nevertheless useful in understanding the equilibrium structure of the stable PBL.

For the large surface cooling rate of 2 C hr^{-1}, the model predicts that u_* (Fig. 2) falls by a factor of 3 within 2 hours after transition. Fig. 3 shows the surface heat flux ($-Q_0$) increasing initially in response to this cooling. As the stability increases, the turbulent heat transfer in the surface layer is inhibited and $-Q_0$ starts decreasing. This can be explained by a simple scaling argument as follows:

$$-\overline{w\theta} = k_h \, \partial\Theta/\partial z, \quad K_h \propto u_* \ell \tag{13a}$$

where ℓ is a turbulent length scale characteristic of the dominant eddy size. Initially, when the effects of thermal stratification are small,

$$\ell \propto z, \; -\overline{w\theta} \propto u_* z \, \partial\Theta/\partial z \tag{13b}$$

As the positive mean potential temperature gradient (i.e., the stability) increases, the eddy size is limited entirely by the stability and not by distance from the surface. As the surface layer asymptotically approaches this local "z-less" stratification (Wyngaard, 1973), the eddy size is set by L:

$$\ell \propto L \propto u_* N^{-1}, \qquad N = (g/T_0 \cdot \partial\Theta/\partial z)^{1/2} \tag{13c}$$

where N is the Brunt–Väisälä frequency. Then we can write,

$$-\overline{w\theta} \propto u_* L \, \partial\Theta/\partial z \propto (g/T_0)^{-1/2} \, u_*^2 \, (\partial\Theta/\partial z)^{1/2} \tag{13d}$$

Since u_* and L decrease as $\partial\Theta/\partial z$ increases, we conclude from (13d) that the turbulent heat flux in the surface layer decreases as the stability increases. Fig. 3 shows that $-Q_0$ increases again after t = 3 hours in response to an increasing wind speed in the nocturnal jet, to be discussed later.

The stability length L and the PBL depth h (Figs. 4 and 6) decrease dramatically and reach a near-constant value in a few hours after transition, with higher rates of cooling requiring shorter times to reach a steady state. After transition, U near the surface drops rapidly while V increases slowly in magnitude, leading to a sharp decrease in the surface wind S. Since, from Eq. (10) and Fig. 1(b), $\tan\alpha = V/U$ or $\sin\alpha = V/S$, we see that the cross-isobaric angle α increases rapidly (Fig. 5) after transition. The increased cross-isobaric flow towards low pressure near the surface compensates the increase in frictional force (or turbulent stress gradient which is approximately $\sim u_*^2/h$) in the shallow stable layer that forms around sunset.

Mean Wind and Temperature Profiles

Figs. 7(a) and (b) show the predicted vertical profiles of mean wind speed S and potential temperature Θ, for a cooling rate of 1 C hr^{-1}, at t = 0, 6, and 12 hours. Within the deepening nocturnal inversion, the turbulence, maintained by the large wind shear, transfers momentum and heat from the upper layers of the inversion downward to the surface where they are effectively dissipated by friction and radiation cooling, respectively. The rapid momentum loss from the upper layers after transition results in the dramatic reduction of the nocturnal mixed layer depth, while the uncompensated heat loss from the upper layers results in the continuous upward growth of the inversion during the night.

After a shallow stable layer begins to form around sunset, the turbulence aloft becomes essentially decoupled from the surface layer, decays rapidly, and ceases to influence the motion at these levels. Above the top of the inversion, therefore, the momentum equations (9) reduce to

$$\partial U/\partial t = fV$$
$$\partial V/\partial t = f(G - U) \tag{14a}$$

which can be combined to yield

$$\partial S^2/\partial t = 2fVG \tag{14b}$$

Since V does not change rapidly after transition and remains positive, Eq. (14b) predicts increasing wind speeds aloft after transition. A pronounced jet-like velocity profile, usually referred to as the nocturnal jet, develops at the top of the nocturnal inversion, with a sharp supergeostrophic wind speed maximum as shown in Fig. 7(a). The occurrence of the nocturnal jet is associated with extremely large values of wind shear at low levels.

The supergeostrophic wind speeds suggest that an inertial oscillation is induced when the constraint imposed by daytime turbulent mixing is removed by the initiation of inversion at transition. Above the stable layer, the mean momentum equations (1), for a horizontally homogeneous flow with a steady horizontal pressure gradient, can be written as

$$\partial(U - U_g)/\partial t = f(V - V_g)$$
$$\partial(V - V_g)/\partial t = -f(U - U_g) \tag{15a}$$

which indicates that U and V oscillate about U_g and V_g, respectively. Following Blackadar (1957), we introduce the complex function

$$F = (U - U_g) + i(V - V_g) \tag{15b}$$

which reduces Eq. (15a) to

$$\partial F/\partial t = -ifF \tag{15c}$$

The solution is

$$F = -F_0\, e^{-i\omega} \tag{15d}$$

where $\omega = ft$, and $F_0(z) = [(U_0 - U_g)^2 + (V_0 - V_g)^2]^{1/2}$ is the initial deviation from the geostrophic wind at transition. This equation indicates that the wind speed deviation F remains constant in magnitude but rotates clockwise with a time period $t = 2\pi/f$ for one complete revolution. A supergeostrophic maximum in wind speed occurs when $\omega = \pi$ or t = 8.5 hours at a latitude of 45° N.

The horizontal velocity deficits in the PBL may be expressed as $(U - U_g)/u_* = F_u(zf/u_*, \mu)$ and $(V - V_g)/u_* = F_v(zf/u_*, \mu)$. Fig. 8 shows the steady state velocity-defect spiral in the stable Ekman layer for a value of $\mu = 65$. Since the coordinate system (CS-2) is chosen such that $U_g = G$ and $V_g = 0$, the intercept on the negative x-axis represents $-G/u_*$, and the cross-isobar angle α can be obtained as shown in the figure.

Surface Layer Similarity

In a horizontally homogeneous equilibrium surface layer ($z_0 < z < \delta \simeq 0.1h$), where the turbulent fluxes are essentially constant and the Coriolis effects are negligible, the M–O similarity theory postulates

that the turbulence structure is determined entirely by the parameters u_*, Q_0, z and g/T_0. All surface layer quantities appropriately nondimensionalized by these parameters then depend only on the dimensionless height $\zeta = z/L$. The M–O similarity theory has been extensively tested with the 1968–Kansas data. In the following, we compare some of the model predictions in the stable surface layer against the empirical similarity relations from the Kansas data (Businger et al., 1971).

The computed nondimensional mean wind shear, $\phi_m = (kz/u_*) \cdot \partial S/\partial z$, and temperature gradient, $\phi_h = (kz/\theta_*) \cdot \partial \Theta/\partial z$, are shown in Figs. 9 and 10, respectively, where they are compared with the empirical expressions:

$$\phi_m = 1 + 4.7\, z/L, \quad \phi_h = 0.74 + 4.7\, z/L \tag{16}$$

The model predictions of ϕ_h agree well with observations, while the calculated ϕ_m are somewhat larger.

The empirical similarity relations for the gradient and the flux Richardson numbers in the stable surface layer can be expressed as follows:

$$\begin{aligned} Ri &= \frac{g}{T_0}\frac{\partial \Theta}{\partial z}\Big/\left(\frac{\partial S}{\partial z}\right)^2 = \zeta\phi_h/\phi_m^2 = \frac{\zeta(0.74 + 4.7\zeta)}{(1 + 4.7\zeta)^2} \\ R_f &= -BP/SP = \zeta/\phi_m = \zeta/(1 + 4.7\zeta) \end{aligned} \tag{17}$$

These relations are compared in Fig. 11 with the model-calculated Ri and R_f; the agreement is good for the latter, while the predicted Ri are slightly smaller. The ratio of the eddy diffusivities of heat and momentum is given by

$$K_h/K_m = R_f/Ri = \phi_m/\phi_h = (1 + 4.7\zeta)/(0.74 + 4.7\zeta) \tag{18}$$

Near the surface, as $\zeta \to 0$, $K_h/K_m \to 1.35$ or a neutral turbulent Prandtl number of 0.74 is implied. The calculated values of the ratio K_h/K_m are slightly larger than indicated by Eq. (18), though it averages about 1.35 in the surface layer. Away from the surface layer ($z \gg \delta$), this ratio decreases with increasing height to a value less than 1 at $z = h$; it also decreases with increasing stability in the outer layer. These model results agree with laboratory data (Arya, 1972) for a stably stratified boundary layer. As the stability increases, it is apparent from Eq. (17) that Ri approaches a limit. If the heat flux and shear stress approach zero at the same rate, then $L \to 0$, $\zeta \to \infty$, and $Ri \to Ri_{cr} \simeq 0.21$. Therefore the profile behavior in the surface layer predicts an asymptotic approach to the critical Richardson number.

The turbulent kinetic energy equation in an equilibrium surface layer can be written as

$$\bar{\epsilon} = SP + BP \tag{19a}$$

where, from Eq. (10), $SP = u_*^2 \partial S/\partial z$. Multiplying both sides by kz/u_*^3, we obtain

$$(kz/u_*^3) \cdot \bar{\epsilon} = \phi_\epsilon = \phi_m - \zeta \tag{19b}$$

Fig. 12(a) shows the calculated ϕ_ϵ values compared to $\phi_\epsilon = 1 + 3.7\zeta$ from the Kansas data. Keeping in mind that the dimensionless surface layer thickness, δ/L, ranges approximately from 0.13 to 0.28 for the range of $\mu = 19 - 118$ shown, the agreement with data is good. Above the surface layer, the predicted ϕ_ϵ show a systematic deviation depending on the value of μ. This is a consequence of the surface-layer assumption that the fluxes are constant at their surface values; this approximation is valid only over a limited height interval, which rapidly decreases as the stability increases. Though available atmospheric data suggest that the log-linear profile extends well into the height range where the flux variation must be considered, the similarity functions discussed above are generally functions of μ as well as ζ in the outer layer of the PBL.

PBL Turbulence Profiles

Postulating that $\phi_\epsilon = \phi_\epsilon(\zeta, \mu)$, the calculated steady-state $\bar{\epsilon}$-profiles in the nocturnal PBL are adequately represented, see Fig. 12(b), by

$$\phi_\epsilon = (\phi_m - \zeta) \cdot e^{-6.5\eta} \tag{20a}$$

where $\eta = \zeta\mu^{-\frac{1}{2}}$ and the calculated ϕ_m variation is as shown in Fig. 9.

Fig. 13(a) shows the nondimensional vertical profiles of turbulent kinetic energy components in the steady-state nocturnal PBL in CS-2 for a surface cooling rate of 1 C hr^{-1}. The corresponding profiles in CS-1, obtained by converting the computed (CS-2) values through the relations given in Eq. (10), are shown in Fig. 13(b). The nondimensional shear stress profiles in the two coordinate-systems are shown in Figs. 14(a) and (b), and the dimensionless turbulent heat flux profiles are given in Figs. 15(a) and (b).

The vertical distributions of eddy viscosity, K, are of considerable interest since several recent papers on the nocturnal PBL are based on the eddy viscosity models in which the stresses in the mean momentum equation (1) are replaced by

$$\overline{uw} = -K_{xz}\,\partial U/\partial z, \quad \overline{vw} = -K_{yz}\,\partial V/\partial z \tag{20b}$$

The vertical profiles of K_{xz}, plotted nondimensionally in Fig. 16(a) show a strong dependence on the PBL stability parameter μ. As μ increases, the eddy viscosity profiles become flatter; both the maximum eddy viscosity, K_{max}, as well as the height where it occurs, z_{max}, decrease by nearly two orders of magnitude as the PBL changes from neutral ($\mu = 0$) to strongly stable ($\mu = 118$). The calculated variations of K_{max} and z_{max} are shown as functions of μ in Fig. 16(b); for $\mu > 10$, they are given by the best-fit expressions

$$\begin{aligned} K_{max}\, f/u_*^2 &= 0.016\,\mu^{-0.83} \\ z_{max}\, f/u_* &= 0.168\,\mu^{-0.80} \end{aligned} \tag{21}$$

In PBL models, it is often taken that $K_{yz} = K_{xz}$; this assumption is consistent with our results in Fig. 17, which shows identical vertical profiles of K_{xz} and K_{yz} calculated for $\mu = 65$. It will be useful to compare these profiles with the corresponding K-distributions used by others in stable PBL models based on K-theory. Businger and Arya (1974) specified steady-state eddy viscosity distributions by the equation

$$Kf/u_*^2 = \frac{k\, fz/u_*}{(1 + \beta\,\mu\, fz/u_*)} \exp\left(-\left|\frac{V_g}{u_*}\right| fz/u_*\right) \tag{22}$$

where $k = 0.35$, $\beta = 4.7$, and $|V_g| = |G \sin\alpha|$. Delage (1974) used the expression

$$K = \ell\,(0.16E)^{\frac{1}{2}} \tag{23a}$$

where ℓ is a mixing length given as

$$\ell = [1/k\,(z + z_0) + 1/\lambda + \beta/kL]^{-1} \tag{23b}$$

with $k = 0.4$, $\beta = 5$, and $\lambda = 0.0004\,Gf^{-1}$. Using the steady state values of α and E calculated by the present model for $\mu = 65$, Eqs. (22) and (23) are evaluated and compared with the K-profiles in Fig. 17. Both equations predict somewhat larger K values in the upper layer with higher peaks than the present model; however, the general profile shape and behavior are similar in all models.

The K_m-variation shown in Fig. 16 may be parameterized as $K_m/u_*z = F(\zeta, \mu)$. The predicted steady-state K-profiles are represented well (see Fig. 18) by

$$K_m = \frac{ku_*z}{(1+4.7\zeta)} e^{-b\eta} \tag{24}$$

where $k = 0.35$, $b = 9.1$, and $\eta = \zeta\mu^{-1/2}$. Using the relations to be developed later in this section, Businger and Arya's (1974) K-expression, Eq. (22), can also be reduced to this form. The advantage of Eq. (24) is that the steady-state eddy viscosity profile in the nocturnal PBL can be specified entirely from the surface layer parameters, u_* and L. Since the average value of K_h/K_m in the outer layer is near unity according to our calculations, the same equation may be used to predict the thermal eddy diffusivity profile in this layer, to a good approximation.

Nocturnal PBL Depth

The steady-state values of h are plotted in the dimensionless form shown in Fig. 19. The best fit to the variation of h, for $\mu > 10$, is given by

$$h|f|/u_* = a\mu^{-1/2}, \quad \text{or} \quad h/L = a\mu^{1/2} \tag{25}$$

where a is a constant. This relation was first suggested by Zilitinkevich (1972) from similarity considerations and dimensional analysis. From Eqs. (25) and (13c), we can write $h \sim |u_* L/f|^{1/2} \sim u_*|f|^{-1/2}N^{-1/2}$. Thus the steady state nocturnal PBL depth is proportional to the geometric mean of the length scales $u_*/|f|$ and L, and it is uniquely determined by wind shear, earth's rotation, and gravitational stability represented by the Brunt–Väisälä frequency. In the present model, calculating h as the height where the stress decreases to 5% of its surface value, we evaluated $a = 0.27$; other model predictions of this constant are about 0.47 (Businger and Arya, 1974), 0.22 (Wyngaard, 1975), and 0.40 (Brost and Wyngaard, 1978). Thus, its value appears to be strongly dependent on some of the model parameterizations.

From temperature soundings under stable conditions, Blackadar (1957), Izumi and Barad (1963), and Deardorff (1972) found that the nocturnal boundary layer height typically increases with time during the night. Yamada (1976) analyzed the Wangara data (Clarke et al., 1971) representing h as the height of the surface inversion layer as determined from the radiosonde-measured Θ_v profiles, and found that, under strongly stable conditions, $h > 0.3|u_*/f|$, the neutral PBL height. These findings indicate that h determined from the Θ_v profile, unlike in the convective case, usually exceeds the height to which turbulence extends in the nocturnal PBL, probably due to radiative effects. Therefore, though h obtained from the temperature profile provides a conservative estimate, it may not be a good indicator of the turbulent boundary layer height in the stable case.

In the steady state PBL, from Eq. (1),

$$\partial\overline{uw}/\partial z = f(V - V_g), \quad \partial\overline{vw}/\partial z = f(U_g - U) \tag{26}$$

which, upon integration over the PBL depth, yield the constraints:

$$\begin{aligned} \int_{z_0}^{h} (V - V_g)\, dz &= \frac{1}{f}\int_{z_0}^{h} \frac{\partial\overline{uw}}{\partial z} dz = u_*^2/f \\ \int_{z_0}^{h} (U_g - U)\, dz &= \frac{1}{f}\int_{z_0}^{h} \frac{\partial\overline{vw}}{\partial z} dz = 0 \end{aligned} \tag{27}$$

The latter indicates that U must overshoot U_g within the PBL. We can write the first constraint, to a good approximation, as

$$u_*^2/f \propto -\int_{z_0}^{h} V_g dz = h\, G \sin\alpha$$

or

$$h = a_1\, u_*^2/(fG \sin\alpha) \tag{28}$$

which gives another relation for the PBL depth. This can also be expressed as

$$G \sin\alpha/u_* = a_1\, (u_*/fh) \tag{29a}$$

or

$$u_*/G = a_2\, (fh \sin\alpha/G)^{1/2} \tag{29b}$$

where $a_2 = a_1^{-1/2}$. The last relation, shown in Fig. 20, fits the model predictions well with the constants $a_2 = 0.80$ and $a_1 = 1.56$; these values agree with $a_2 = 0.79$ and $a_1 = 1.6$ obtained by Brost and Wyngaard (1978) from a different model.

Geostrophic Drag and Heat Transfer Relations

Asymptotic matching of the similarity profiles of mean velocity and temperature in the inner and outer layers of the stable PBL leads to the well-known geostrophic drag and heat transfer relations:

$$\begin{aligned} G \cos\alpha/u_* &= \frac{1}{k}\,[\ln|u_*/fz_0| - A(\mu)] \\ G \sin\alpha/u_* &= \frac{B(\mu)}{k}\,\text{sign}\,(f) \\ (\Theta_h - \Theta_0)/\theta_* &= \frac{0.74}{k}\,[\ln|u_*/fz_0| - C(\mu)] \end{aligned} \tag{30}$$

where Θ_h is the potential temperature at the top of the boundary layer, and A, B, and C are universal functions of μ to be determined from theory and observations. The first two equations may be combined to give an implicit relation between the geostrophic drag coefficient, $C_g = u_*/G$, and the surface Rossby number, $Ro = |G/fz_0|$, as follows:

$$\ln Ro = A(\mu) - \ln C_g + \left[\frac{k^2}{C_g^2} - B^2(\mu)\right]^{1/2} \tag{31}$$

which implies that $u_*/G = C_g(Ro, \mu)$; for a given Rossby number, C_g should only depend on μ. Fig. 20 shows the variation of the geostrophic drag coefficient with μ in the present model ($Ro \simeq 10^7$).

The functions $A(\mu)$, $B(\mu)$ and $C(\mu)$, calculated from Eq. (30) in the model, are shown in Fig. 21, where they are compared with the best-fit polynomial expressions through the Wangara data given by Arya (1975). There is fair agreement between model predictions and observations. For $\mu > 10$, the present model results can be represented by the best-fit expressions shown in Table 1, where they are compared with the functions given by Arya (1977), Briggs (1977), and Brost and Wyngaard (1978), all obtained from different

models of the stable barotropic PBL. Except for $B(\mu)$, the agreement between various models is good. From Eqs. (29a) and (30), one can write

$$B(\mu) \propto |u_*/fh| \tag{32a}$$

Substituting $h \propto L\mu^{1/2}$ from Eq. (25) gives

$$B(\mu) = b_1 \mu^{1/2} \tag{32b}$$

where the constant $b_1 = 1.71$ from Table 1.

TABLE 1
Comparison of PBL Similarity Functions A, B, and C from Different Models

	$A(\mu)$	$B(\mu)$	$C(\mu)$
Present model	$\ln \mu^{1/2} - 0.98\,\mu^{1/2} + 2.5$	$1.79\,\mu^{1/2} - 0.6$ or $1.71\,\mu^{1/2}$	$\ln \mu^{1/2} - 3\,\mu^{1/2} + 6.5$
Arya (1977)	$\ln \mu^{1/2} - 0.96\,\mu^{1/2} + 2.5$	$1.15\,\mu^{1/2} + 1.1$	$\ln \mu^{1/2} - 3\,\mu^{1/2} + 7.0$
Briggs (1977)	$\ln \mu^{1/2} - 1.0\,\mu^{1/2} + 2.5$	$1.86\,\mu^{1/2}$	——
Brost & Wyngaard (1978)	$\ln \mu^{1/2} - 0.9\,\mu^{1/2} + 2.0$	$1.40\,\mu^{1/2}$	——

Comparison with Observations

There is a paucity of good quality observations in the atmospheric boundary layer under strongly stable conditions. The difficulty in measurements can be attributed to the rapid decrease in wind speed and intensity of turbulence in the surface layer following transition, comparatively large averaging periods required to obtain statistically-stable averages for the nonstationary field data above a few tens of meters height, and the large data scatter, which gets worse with increasing stability, resulting from the uncertainties in the determination of the PBL scaling parameters and baroclinicity.

An attempt has been made to compare some of the model predictions against the atmospheric data from the 1973 Minnesota Experiment (Izumi and Caughey, 1976). The observations within the 32 m-tower layer of an evolving nocturnal PBL on September 10 (Run-2) used in the present study are taken from Wyngaard (1975). The transition ($t = 0$) was set at 1845 local time. Turbulence was nearly extinguished within 3.5 hours after transition and the experiment was terminated. The daytime surface heat flux was assumed to peak at 1315 local time or $t = -5.5$ hours; the convective PBL parameters at this time were given by Izumi and Caughey (1976) as $u_* = 0.45\ ms^{-1}$, $Q_0 = 0.2094\ mKs^{-1}$, $L = -38$ m, $z_i = 1615$ m, and $z_0 = 0.0018$ m. The last was estimated from the surface wind observations. The latitude of the site is $\phi = 48.6°N$. The surface geostrophic wind data for this day were given by Wyngaard (1975). The geostrophic wind was essentially steady in direction, but the speed decreased with time; its variation over $-6 \leqslant t \leqslant 6$ hours was specified by the best-fit relation, $G(t) = 11.714 - 0.239\,t - 0.019\,t^2$, in the model.

Starting with initial profiles of an equilibrium neutral PBL in the morning, the daytime convective PBL was numerically simulated, as described before, such that it yields the midday structure with the parameters given above. A constant surface cooling rate of 2.75 C hr^{-1} was specified after transition to simulate the evolving nocturnal PBL. The model predictions are shown in Figs. 22 to 25, where they are compared with observations.

The predicted surface friction velocity variation (Fig. 22) shows excellent agreement with observations. The heat flux at 4 m height, shown in Fig. 23, increases sharply after transition, followed by a rapid drop characteristic of high stabilities that inhibit turbulent heat transfer. The standard deviations of the vertical velocity (σ_w) and temperature (σ_θ) are shown in Fig. 24. Except near transition, the predicted σ_w agree well with observations; σ_θ results do not agree quite as well. Fig. 25 shows the variation of the PBL depth

h, calculated here as the height where the heat flux goes to zero; the observed h were deduced from profiles drawn through the heat flux measurements at 4 and 32 m on the tower, and at 61 m on the tethering cable of a balloon.

5. CONCLUSIONS AND RECOMMENDATIONS

A time-dependent one-dimensional model, based on a higher-order-turbulence closure theory, was developed to simulate the ensemble-averaged structure of an evolving nocturnal PBL. The results indicate that the latter reaches a quasi-steady state within a few hours after transition. The model predictions of the turbulence structure show good agreement with the atmospheric surface layer observations from Kansas and Minnesota experiments. The variation of the nocturnal PBL depth, and the geostrophic drag and heat transfer relations calculated by the model compare favorably with those given by other models.

It is unlikely that long periods of this steady-state occur in reality in the nocturnal PBL since intermittent episodes of turbulence, initiated in the laminar flow above when the local Richardson number decreases to a value below $Ri_{cr} \simeq 0.25$, eventually reach the ground with a burst of momentum and heat which disrupt the steady state. A new quasi-steady state evolves after some time and the entire sequence of events may repeat itself (see Businger, 1973). Also the constant flux layer becomes quite small or disappears altogether, as the PBL becomes increasingly stable. The effects of internal gravity wave motions, and the associated transport of momentum and intermittent bursts of turbulence on the PBL structure are unknown, and require further experimental and theoretical studies.

A serious limitation of the present model is the assumption of a barotropic flow over a large, non-sloping, horizontally-homogeneous surface. Over a uniformly-sloping terrain, this model is applicable only when the downslope (katabatic) acceleration is much smaller than the synoptic pressure gradient; for a terrain with a small slope angle β, we must therefore satisfy $\beta \ll |fGT_0/g\Delta T|$, where $|\Delta T|$ is the temperature drop in the PBL. With our model values of $G = 10\ ms^{-1}$ and $|\Delta T| \simeq 10°K$, at middle latitudes this gives $\beta \ll 0.003$ radians, which indeed is a very stringent requirement that few real sites can satisfy. However, the model may be applicable over large areas of terrain with a uniform gentle slope, and uniform surface roughness and temperature, if the geostrophic wind G is replaced by an "effective" geostrophic wind, $G_e = |-\overline{\nabla}P + (g/T_0)\ \Delta T\ \beta|/f$, which includes contributions from both the synoptic pressure gradient and the downslope acceleration. Since ΔT varies with z, G_e is height-dependent; this thermal wind, associated with vertical temperature gradient and sloping terrain (Lettau, 1967; Holton, 1967), also occurs in a PBL over an unsloped terrain with a horizontal temperature gradient (Arya and Wyngaard, 1975). The downslope drainage forces can be of the same order as the turbulent frictional forces when the terrain slope is of the order $\beta \sim |u_*^2 T_0/gh\Delta T|$. The model calculations of Brost and Wyngaard (1978) indicate that even a moderate terrain slope has a strong effect on the nocturnal PBL depth depending on the upper-level geostrophic wind direction relative to the slope. Our knowledge of the behavior of the nocturnal PBL over a complex topography is poor, and the present model is inadequate to account for drainage forces in a hilly terrain.

We ignored moisture and long-wave radiation flux divergence in the model. Preliminary calculations by Brost and Wyngaard (1978) for mid-latitude, non-desert conditions, with no liquid water and a uniform humidity profile suggest that radiation effects produce no change in the gross PBL structure since the calculated radiative flux divergence is generally much smaller than the turbulent flux divergence. However, in situations with low geostrophic wind speeds and weak turbulence, the radiative cooling could be comparable with or exceed the turbulent heat transfer. Long-wave radiation depends on several atmospheric parameters including moisture, carbon dioxide, aerosols, surface emissivity and cloud cover, and can be a significant factor when the humidity is high or when fog forms in the nocturnal PBL. In a well developed fog with a uniformly-high liquid water concentration profile, appreciable radiative cooling occurs at the top of the fog, which may drive a PBL into convection even when its surface layer is stable. In this case, the PBL-averaged heat flux, $I = \frac{1}{h}\int_0^h \overline{w\theta_v}\ dz > 0$, is the correct indicator of stability, and the nocturnal PBL is similar in some respects to a daytime mixed layer. This clearly indicates the need for a comprehensive study of radiative effects on the nocturnal PBL structure.

A 1 ms^{-1} change in wind speed or 1°C change in mean temperature over a horizontal distance of 100 km is not uncommon for even an idealized PBL above a homogeneous terrain. With typical values of U = 5 ms^{-1}, $u_* = 0.1\ ms^{-1}$, $Q_0 = -0.01\ mKs^{-1}$, and h = 100 m, we see that the advection terms, omitted in our model, are nearly as large as the turbulence flux divergence terms. Wyngaard (1975) suggests that advection may also influence the evolution of the nocturnal jet in the laminar flow above h. The role of advection in the nocturnal PBL requires further investigation.

Though we assumed that the surface cooling rate remains constant for convenience, it is generally known to decrease during the night. A more realistic alternative to specifying either a cooling rate or a heat flux variation is to use the surface energy budget (Blackadar, 1976). Following this approach, Brost and Wyngaard (1978) found that the surface temperature drops as $t^{1/2}$ for the first few hours and then decreases more slowly. They also report that the nocturnal PBL typically does not reach a steady state due to the large characteristic response time, which is of order $h^2/K_m \sim |f|^{-1}$, of the PBL to adjust to the changing surface conditions. Since this time is comparable with the diurnal variation period, hysteresis in diurnal oscillations of PBL internal parameters could be expected (Monin and Zilitinkevich, 1974).

Finally, the model can be considerably simplified by using the diagnostic turbulence equations which contain only the dominant terms and neglect the tendency, Coriolis and transport terms. The closure models also can be simplified by using a turbulent mixing length ℓ instead of the time scale τ. This allows us to drop the dissipation-rate equation and its poorly-understood closure parameterizations, since $\bar{\epsilon}$ can be modeled now as $\bar{\epsilon} \propto E^{3/2}/\ell$ with the variation of ℓ specified according to Eq. (13). This approach considerably simplifies the calculations and reduces the computing time, and it may be adequate for most practical applications of the model.

ACKNOWLEDGEMENTS

This work was performed under an agreement between the National Oceanic and Atmospheric Administration and the Department of Energy.

REFERENCES

Arya, S. P. S., 1972: The critical condition for the maintenance of turbulence in stratified flows. *Quart. J. Roy. Meteorol. Soc.*, 98, 264-273.

——, 1975: Geostrophic drag and heat transfer relations for the atmospheric boundary layer. *Quart. J. Roy. Meteorol. Soc.*, 101, 147-161.

——, and J. C. Wyngaard, 1975: Effect of baroclimicity on wind profiles and the geostrophic drag law for the convective planetary boundary layer. *J. Atmos. Sci.*, 32, 767-778.

——, 1977: Suggested revisions to certain boundary layer parameterization schemes used in atmospheric circulation models. *Mon. Wea. Rev.*, 105, 215-227.

Blackadar, A. K., 1957: Boundary layer wind maxima and their significance for the growth of nocturnal inversions. *Bull. Amer. Meteorol. Soc.*, 38, 283-290.

——, 1976: Modeling the nocturnal boundary layer. *Third Symposium on Atmospheric Diffusion and Air Quality*, Raleigh (Oct. 1976), pp. 46-49, preprints, Amer. Meteorol. Soc., Boston.

Briggs, G. A., 1977: Predictions of nocturnal mixing layer parameters. *Manuscript*, 40 pp., ATDL, Oak Ridge, Tn.

Brost, R. A., and J. C. Wyngaard, 1978: A model study of the stably stratified planetary boundary layer. *Manuscript*, 61 pp., CIRES, Univ. of Colorado/NOAA, Boulder.

Busch, N. E., 1973: On the mechanics of atmospheric turbulence. *Workshop on Micrometeorology*, D. A. Haugen, Ed., 1973, pp. 1-66, Amer. Meteorol. Soc., Boston.

Businger, J. A., J. C. Wyngaard, Y. Izumi and E. F. Bradley, 1971: Flux-profile relations in the atmospheric surface layer. *J. Atmos. Sci.*, 28, 181-189.

——, 1973: Turbulent transfer in the atmospheric surface layer. *Workshop on Micrometeorology*, D. A. Haugen, Ed., pp. 67-100, Amer. Meteorol. Soc., Boston.

——, and S. P. S. Arya, 1974: The height of the mixed layer in the stably stratified planetary boundary layer. *Adv. in Geophys.*, 18A, Academic Press, New York, 73-92.

Clarke, R. H., A. J. Dyer, R. R. Brook, D. G. Reid and A. J. Troup, 1971: The Wangara experiment: boundary layer data. Tech. Pap. No. 19, CSIRO, Div. Meteor. Phys., Melbourne, Australia, 362 pp.

Deardorff, J. W., 1972: Rate of growth of the nocturnal boundary layer. *Proc. of the Symposium on Air Pollution, Turbulence and Diffusion*, New Mexico (Dec. 1971), H. W. Church and R. E. Luna, Eds., 183-190.

Delage, Y., 1974: A numerical study of the nocturnal atmospheric boundary layer. *Quart. J. Roy. Meteorol. Soc.*, 100, 351-364.

Holton, J. R., 1967: The diurnal boundary layer wind oscillation above sloping terrain. *Tellus*, 19, 119-205.

Izumi, Y., and M. Barad, 1963: Wind and temperature variations during development of a low-level jet. *J. Appl. Meteorol.*, 2, 668-673.

Izumi, Y., and J. R. Caughey, 1973: Minnesota 1973 atmospheric boundary layer experiment data report. Meteorology Laboratory Report No. AFCRL-TR-76-0038, Air Force Cambridge Research Labs., Hanscom AFB, Mass., 28 pp.

Launder, B. E., 1975: On the effects of a gravitational field on the turbulent transport of heat and momentum. *J. Fluid Mech.*, 67, 569-583.

Monin, A. S., and S. S. Zilitinkevich, 1974: Similarity theory and resistance laws for the planetary boundary layer. *Boundary-Layer Meteorol.*, 7, 391-397.

Panofsky, H. A., H. Tennekes, D. H. Lenschow, and J. C. Wyngaard, 1977: The characteristics of turbulent velocity components in the surface layer under convective conditions. *Boundary-Layer Meteorol.*, 11, 355-362.

Wyngaard, J. C., 1973: On surface-layer turbulence. *Workshop on Micrometeorology*, D. A. Haugen, Ed., pp. 101-149, Amer. Meteorol. Soc., Boston.

——, O. R. Coté and K. S. Rao, 1974: Modeling the atmospheric boundary layer. *Adv. in Geophys.*, 18A, Academic Press, New York, 193-211.

——, 1975: Modeling the planetary boundary layer—extension to the stable case. *Boundary-Layer Meteorol.*, 9, 441-460.

Yamada, Y., 1976: On the similarity functions A, B and C of the planetary boundary layer. *J. Atmos. Sci.*, 33, 781-793.

Zilitinkevich, S. S., 1972: On the determination of the height of the Ekman boundary layer. *Boundary-Layer Meteorol.*, 3, 141-145.

ORNL-DWG 78-7354

(a)

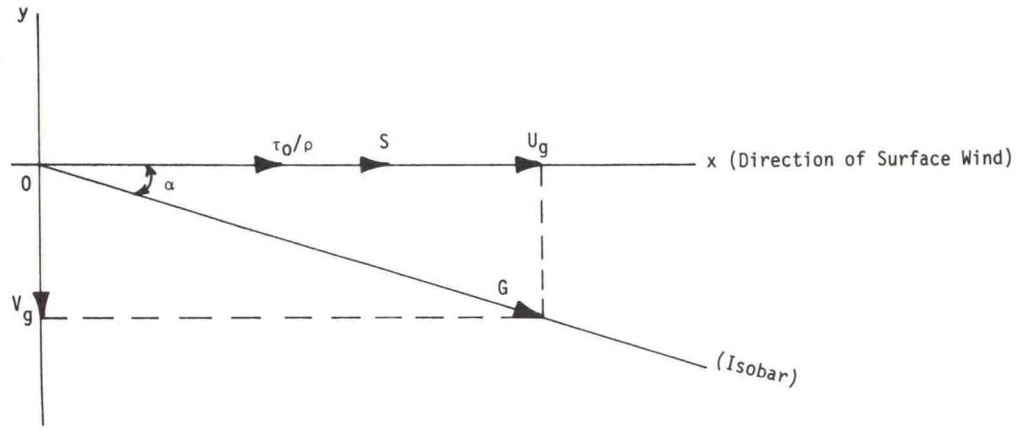

(a) Coordinate System -1.

(b)

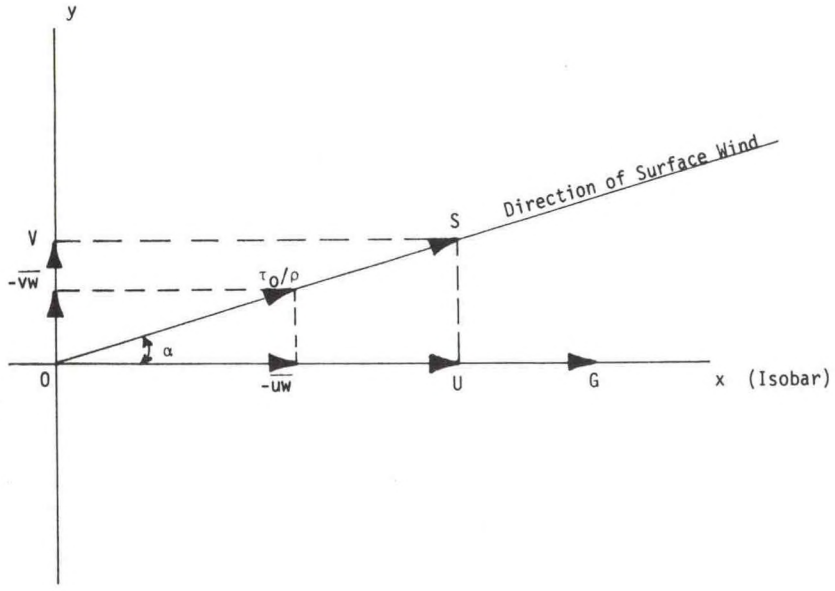

(b) Coordinate System -2.

Fig. 1. Schematic diagrams of the coordinate systems used in PBL modeling.

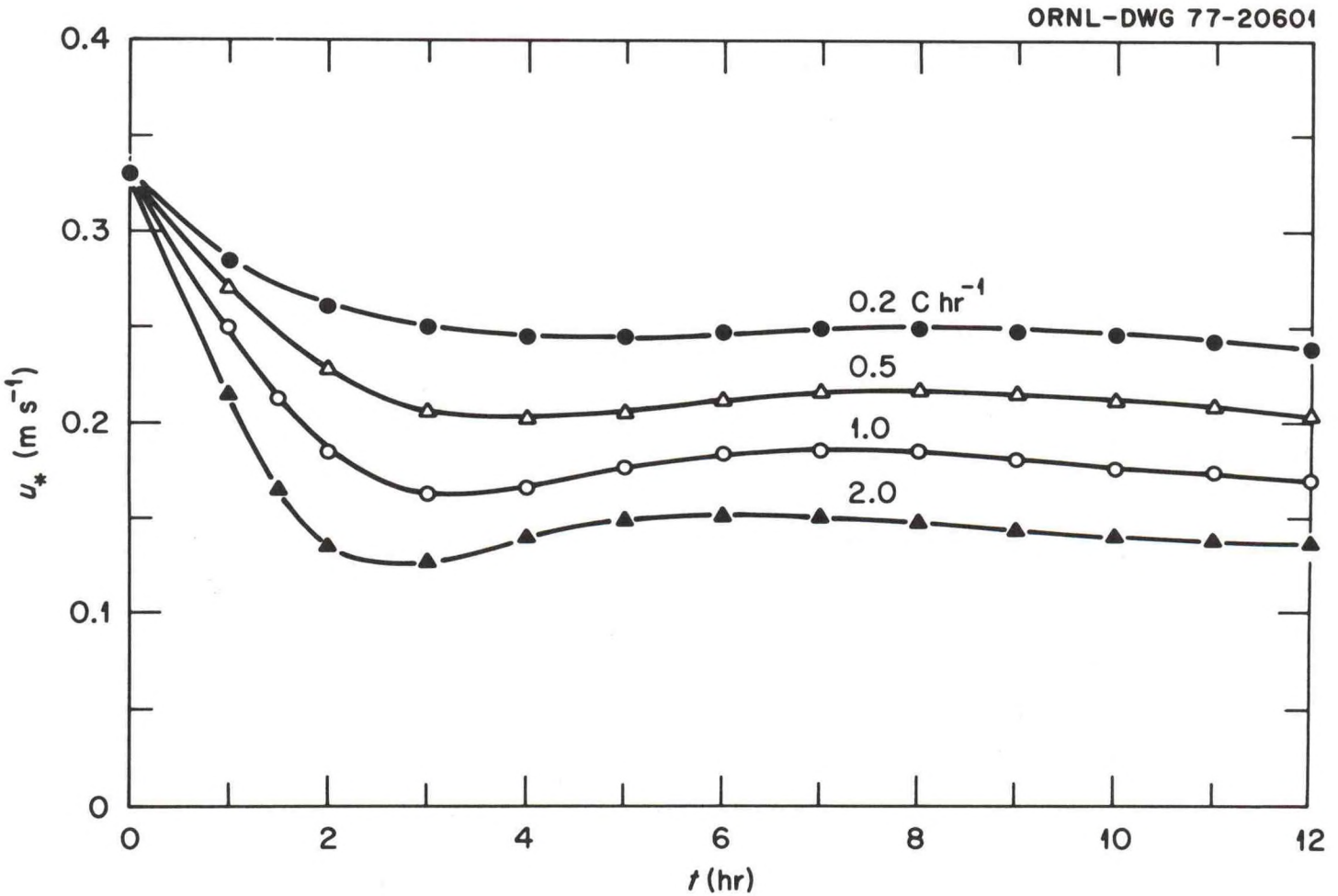

Fig. 2. Predicted evolution of the surface friction velocity as a function of the surface cooling rate.

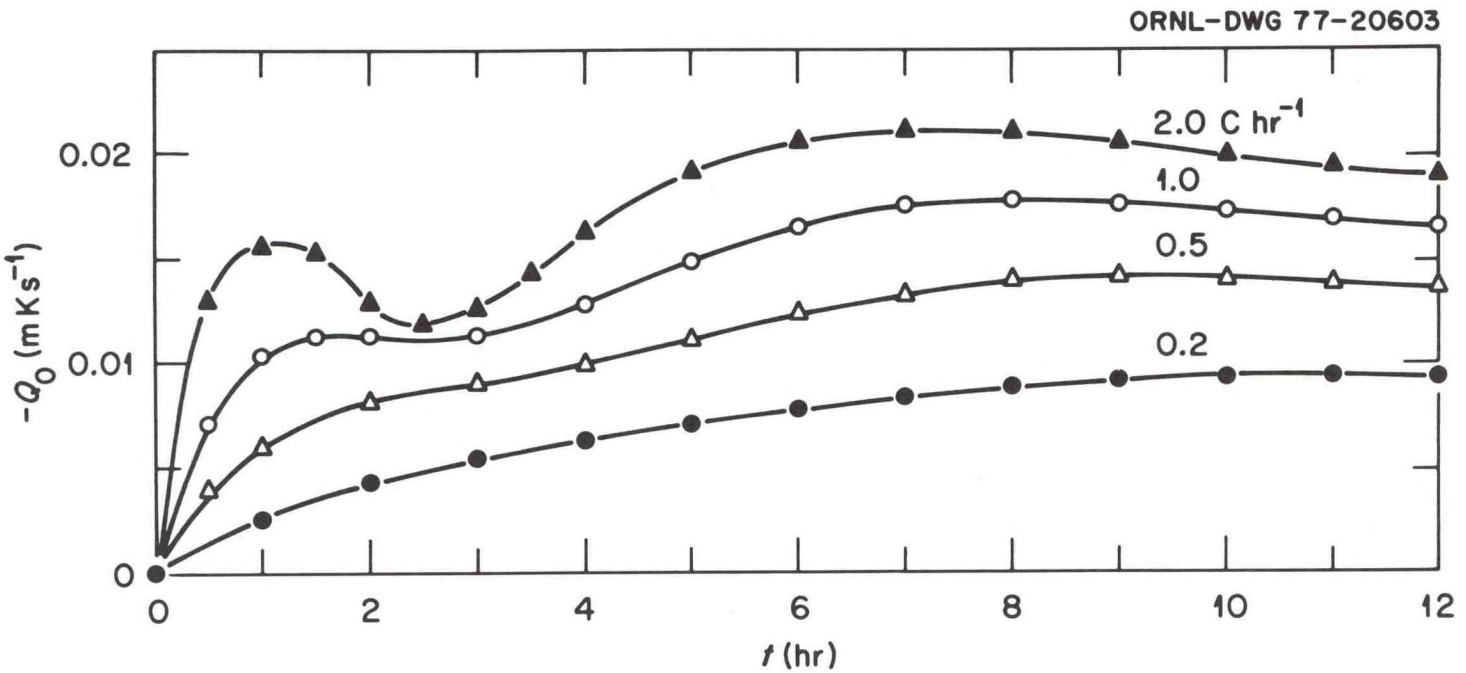

Fig. 3. Predicted evolution of the surface heat flux as a function of the surface cooling rate.

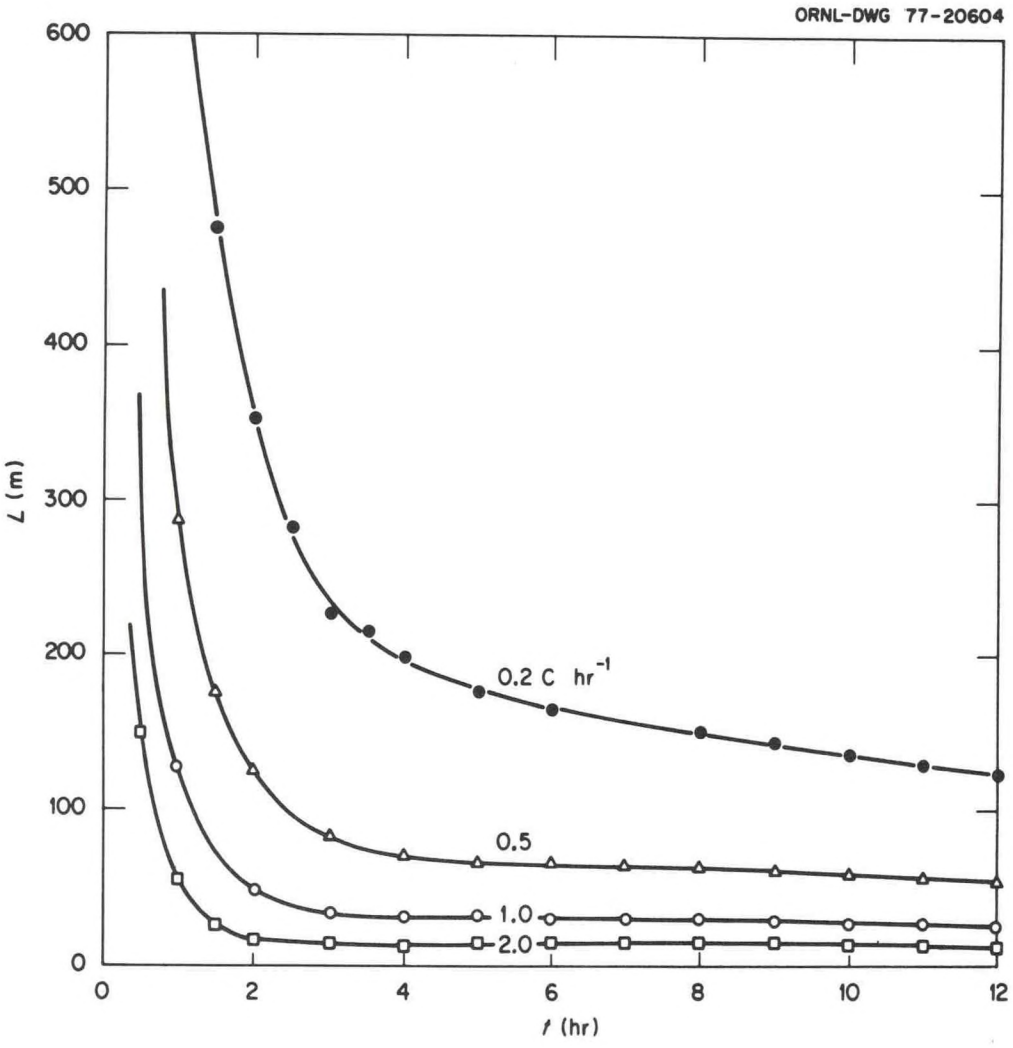

Fig. 4. Predicted evolution of the Monin-Obukhov stability length as a function of the surface cooling rate.

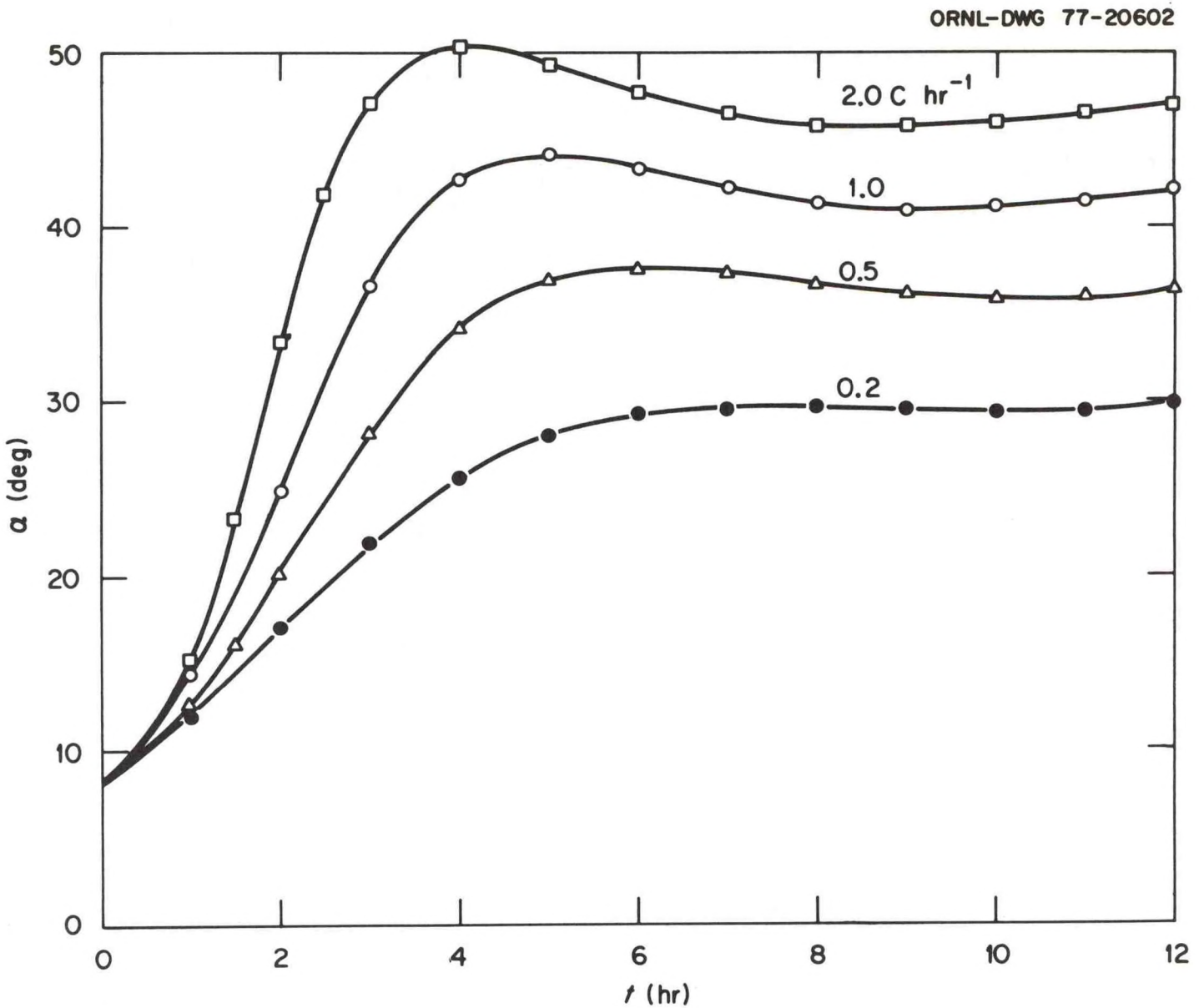

Fig. 5. Predicted evolution of the cross-isobar angle as a function of the surface cooling rate.

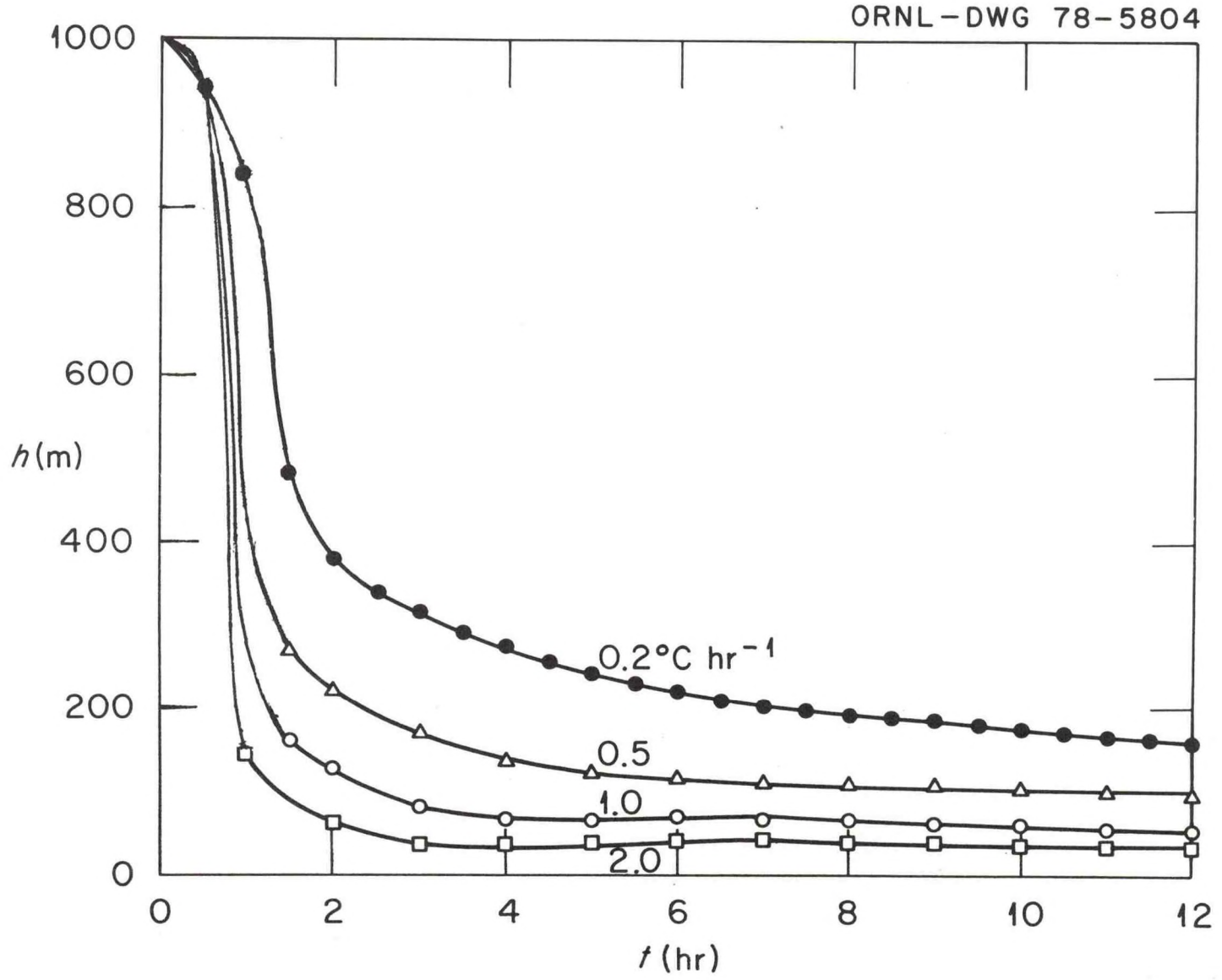

Fig. 6. Predicted evolution of the nocturnal PBL depth as a function of the surface cooling rate.

ORNL-DWG 78-6155

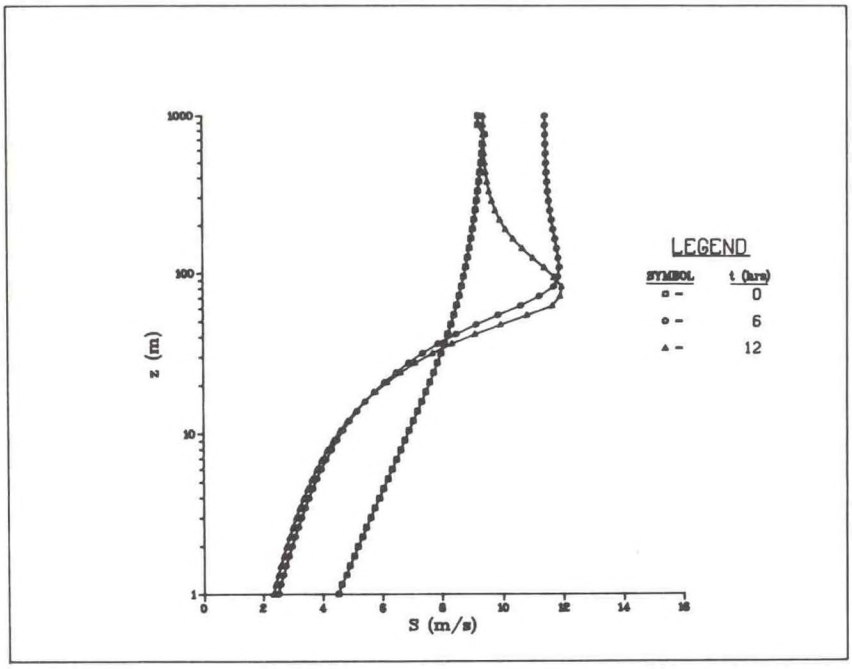

(a) Wind Speed.

ORNL-DWG 78-6156

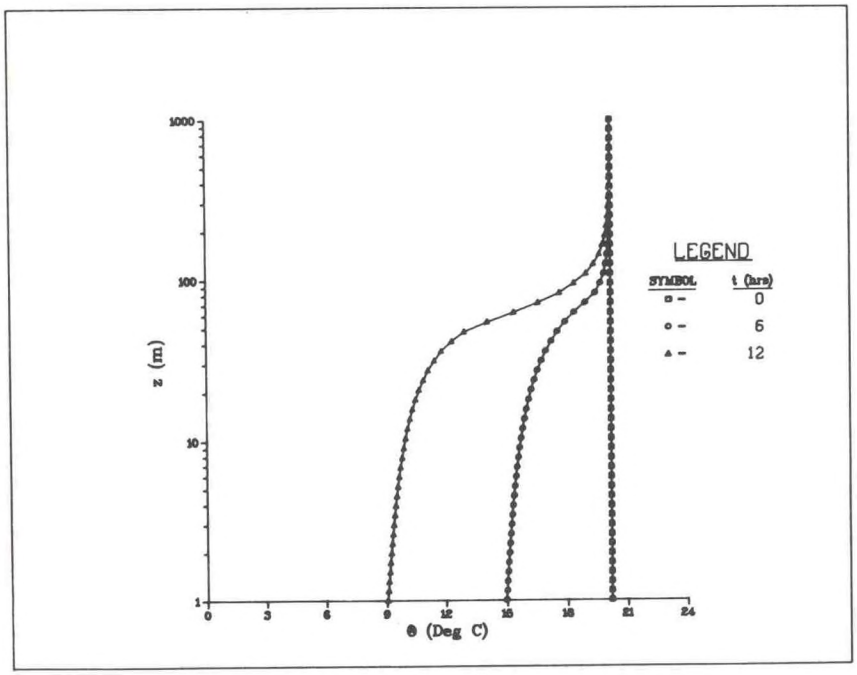

(b) Potential Temperature.

Fig. 7. Predicted vertical profiles of mean wind and temperature.

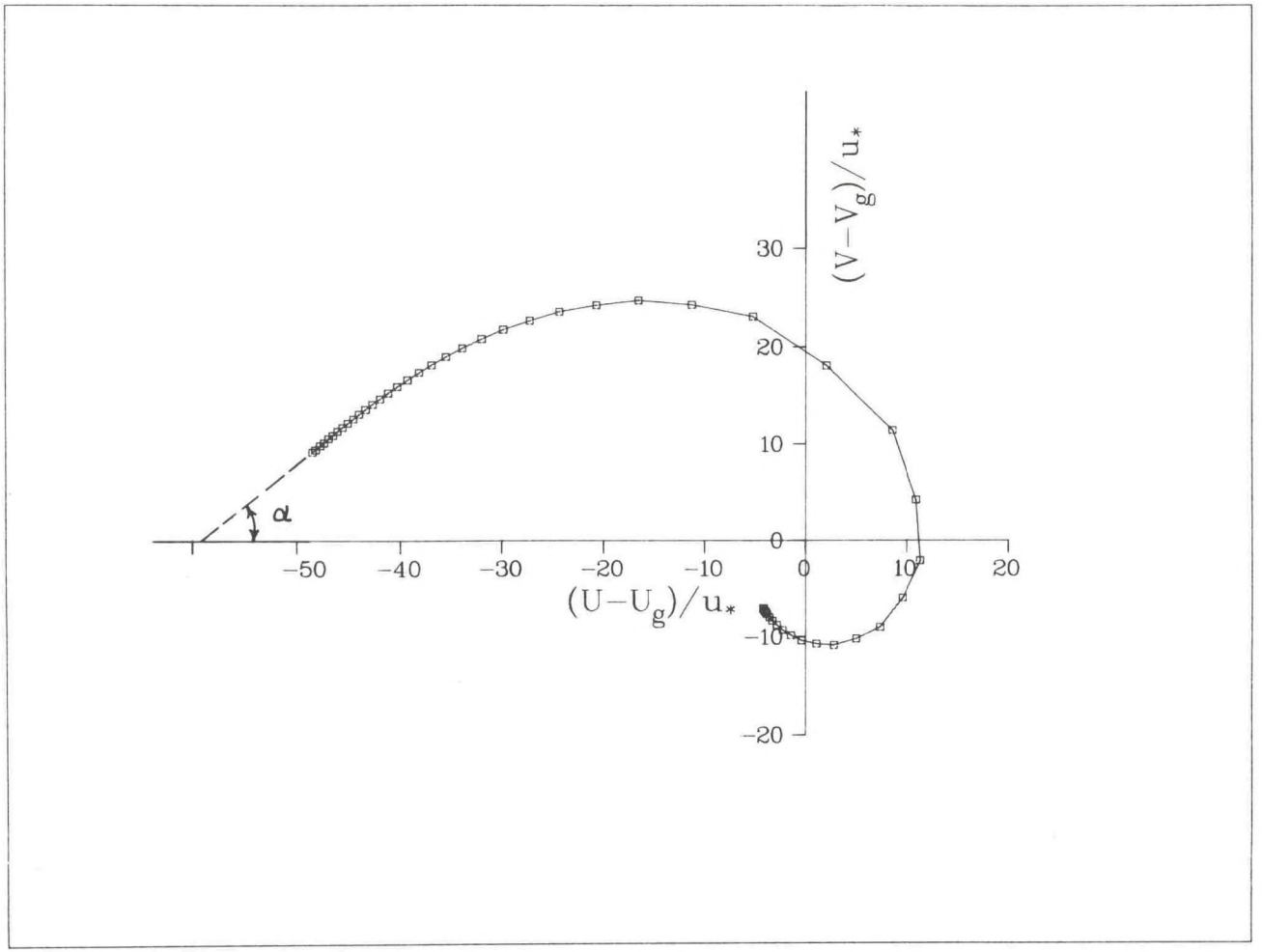

Fig. 8. The velocity-defect spiral in the quasi-steady stable Ekman layer.

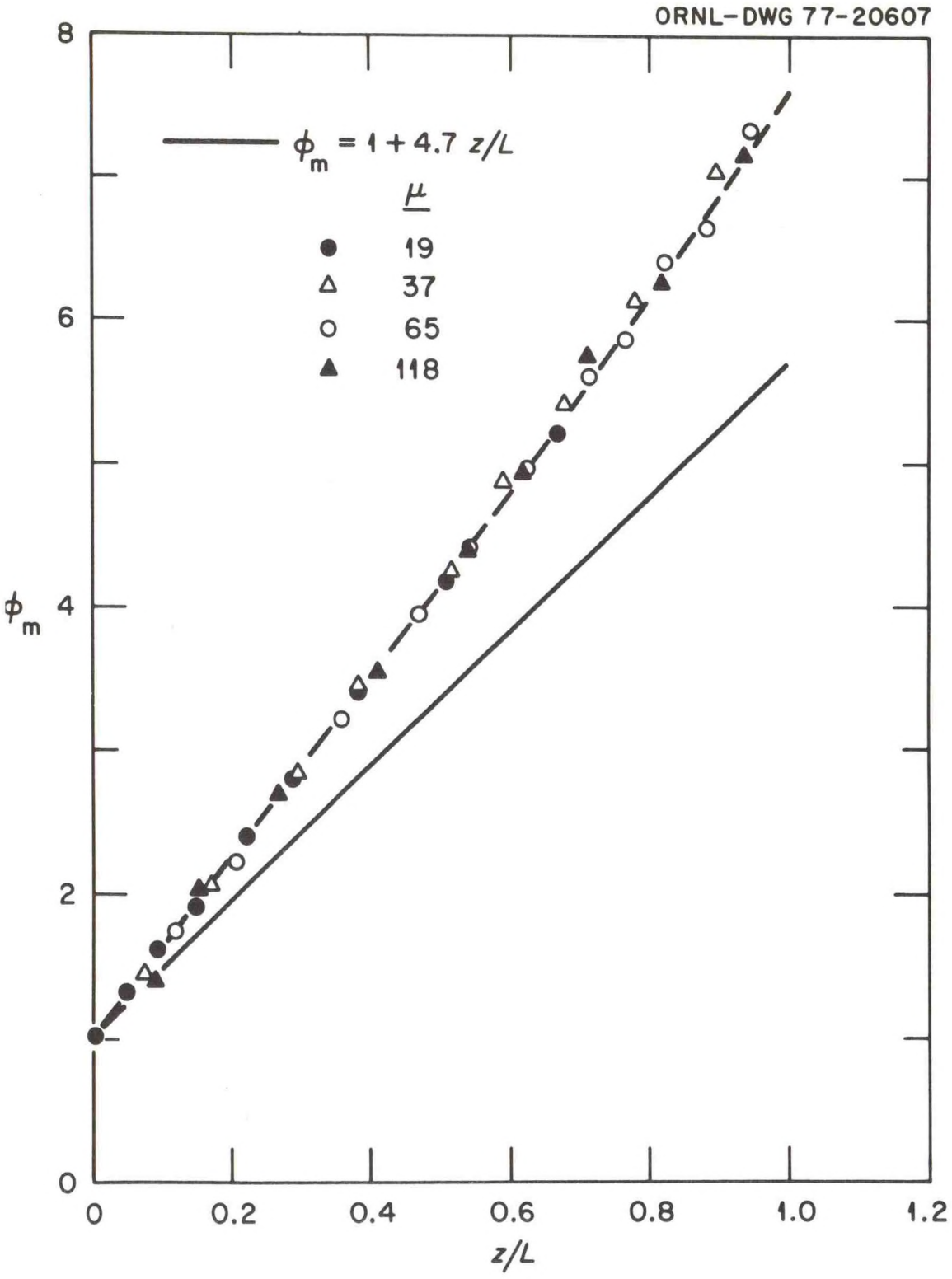

Fig. 9. Comparison of predicted nondimensional mean wind shear with the stable surface layer data (⟷) from Kansas experiment.

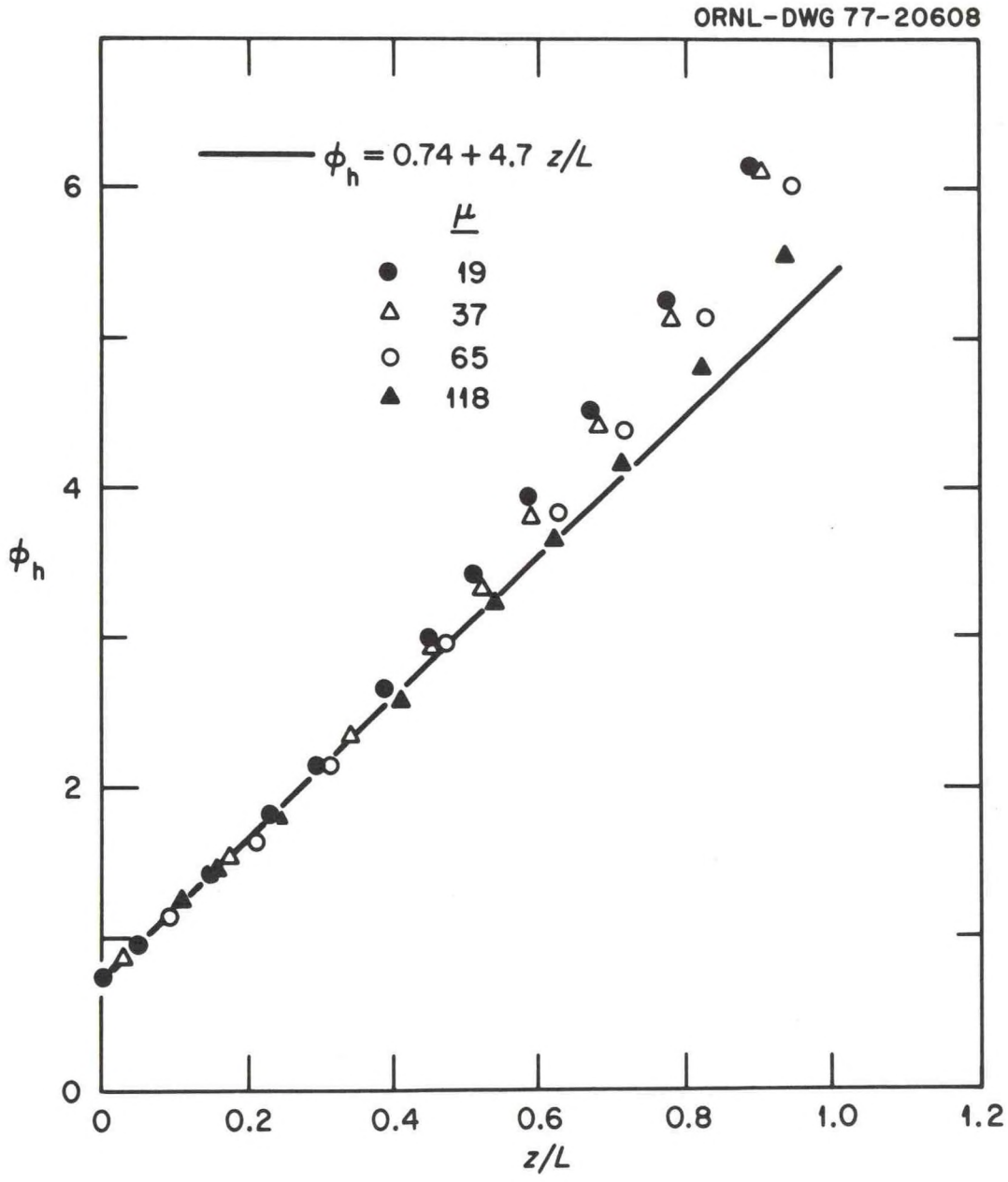

Fig. 10. Same as in Fig. 9, except for the non-dimensional mean temperature gradient.

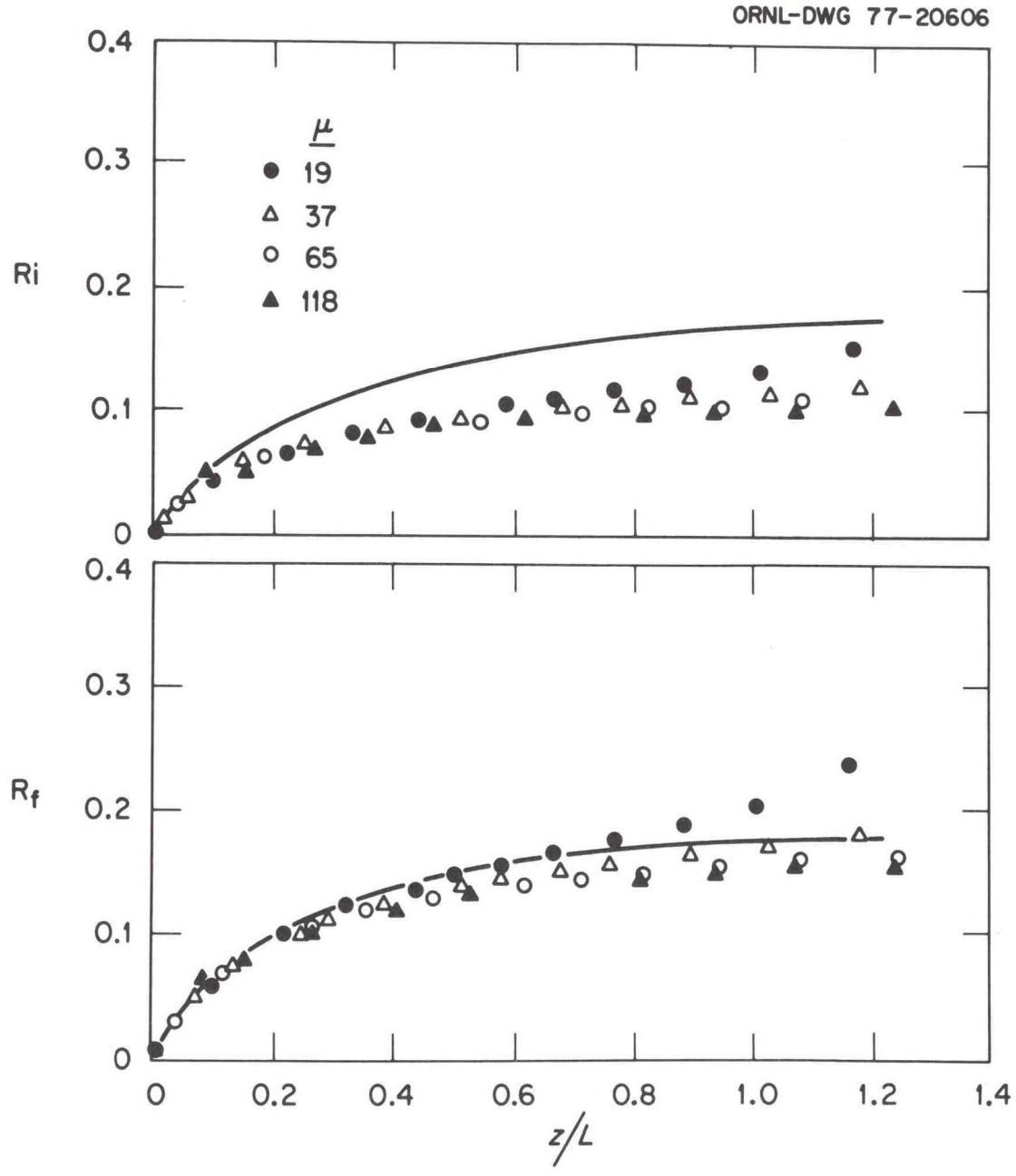

Fig. 11. Predicted variations of gradient and flux Richardson numbers compared to the stable surface layer data (—) from Kansas experiment.

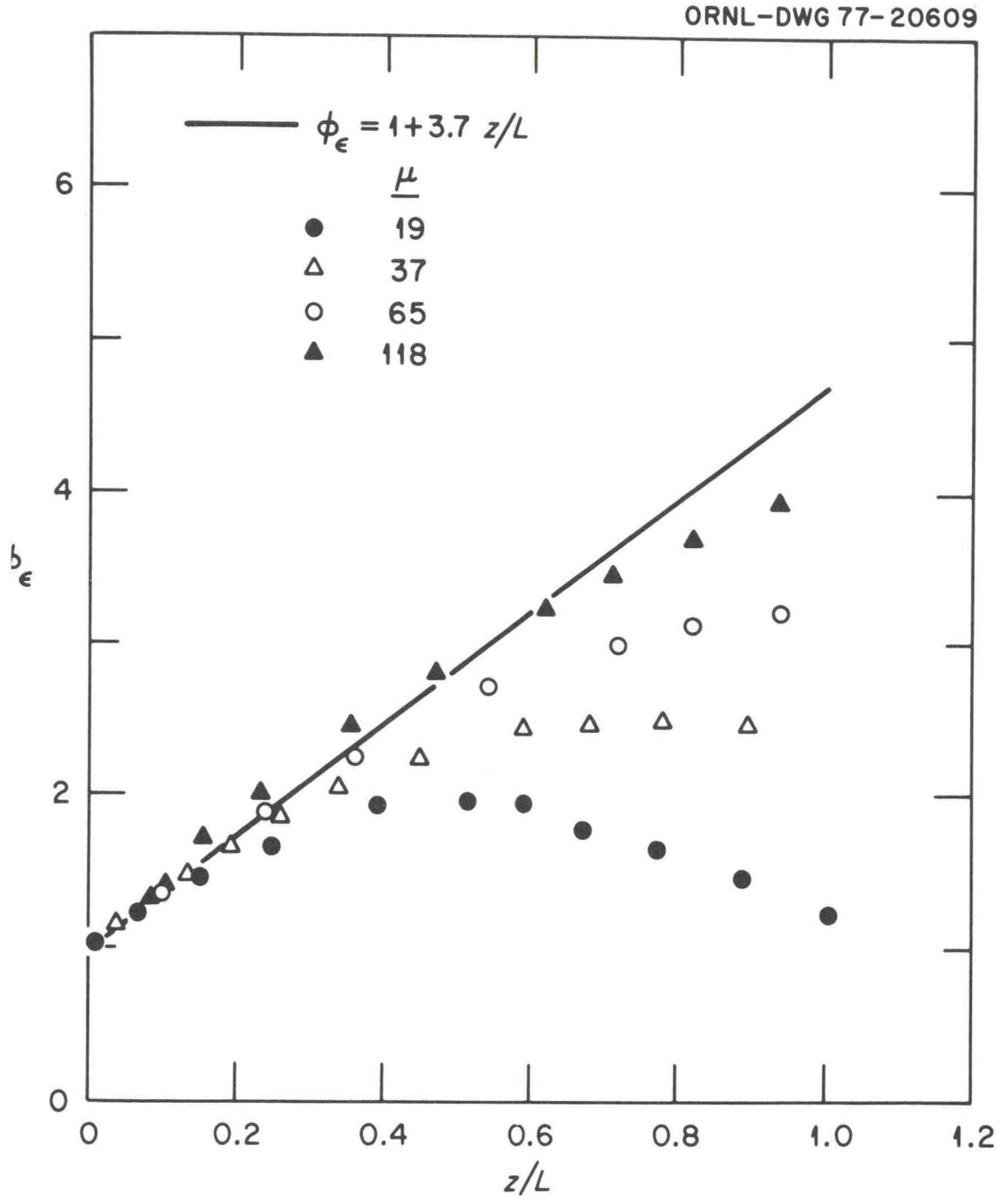

Fig. 12 (a). Calculated variation of dimensionless dissipation-rate compared to the prediction from Kansas surface layer data (—).

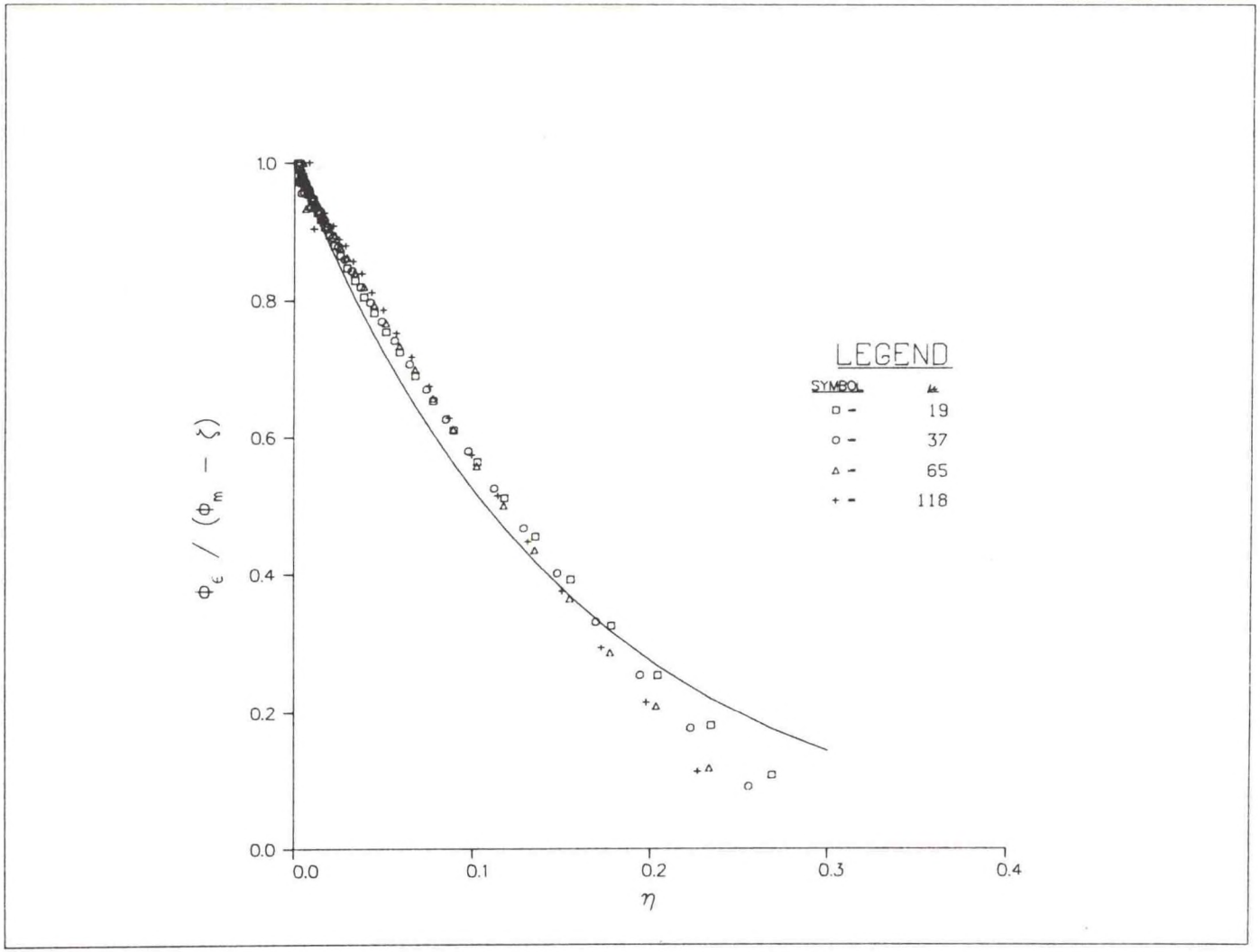

Fig. 12 (b). Similarity representation of the predicted dimensionless dissipation-rate in the quasi-steady stable PBL. The best fit curve is indicated by ——. See text, Eq. (20a).

ORNL-DWG 78-6161

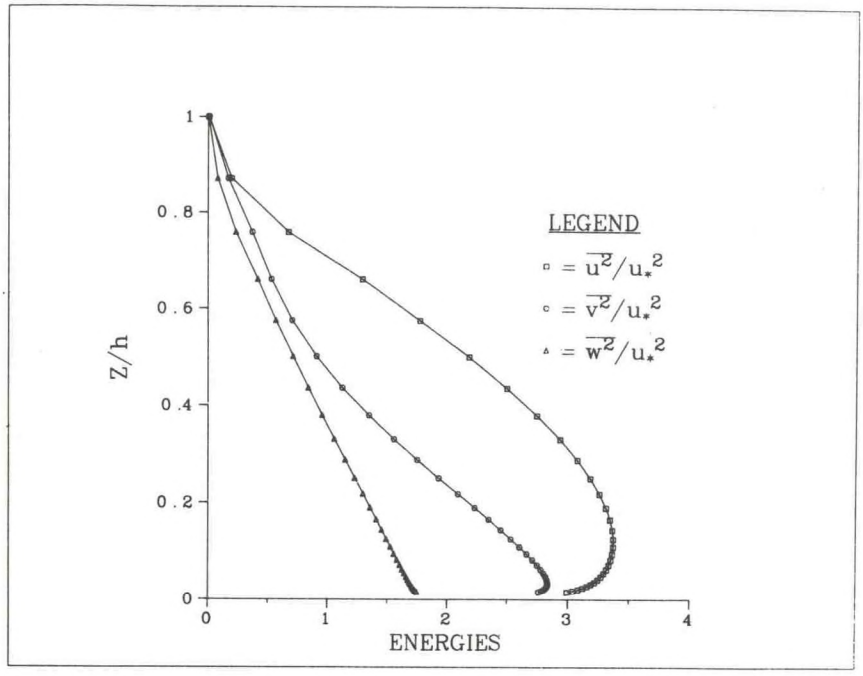

(a) Coordinate System -2.

ORNL-DWG 78-6160

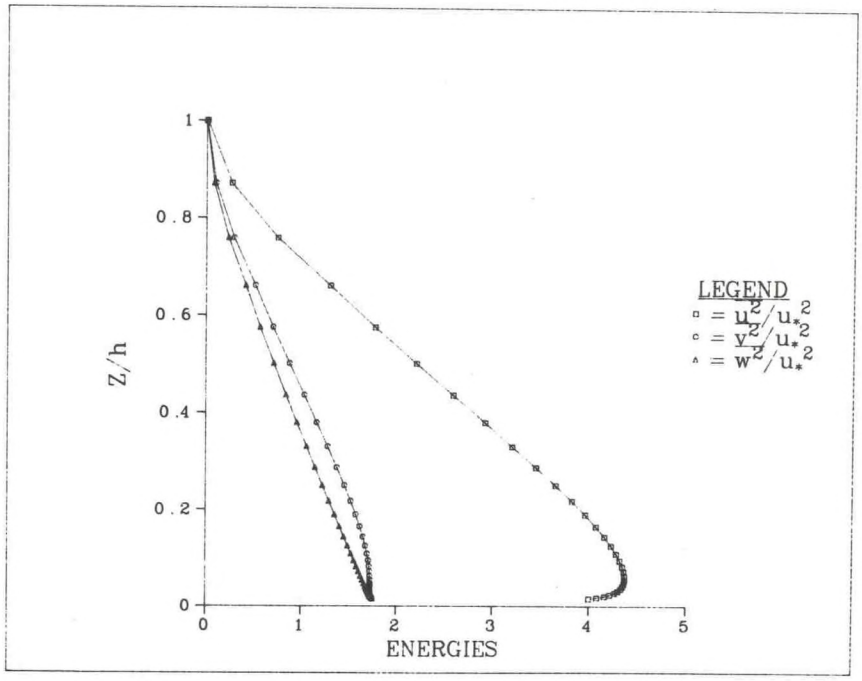

(b) Coordinate System -1.

Fig. 13. Predicted nondimensional vertical profiles of turbulent kinetic energy components in the quasi-steady stable PBL.

ORNL-DWG 78-6157

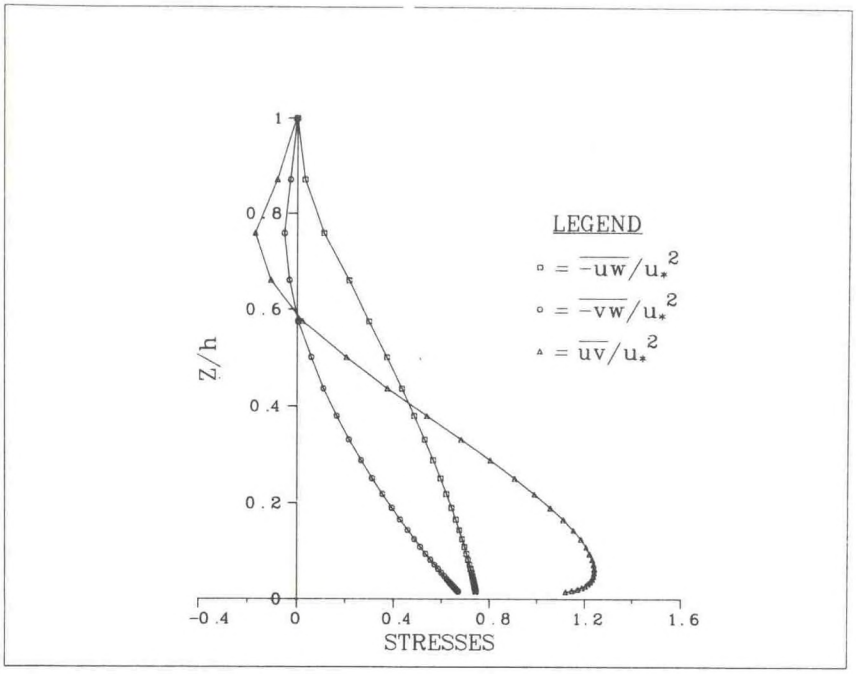

(a) Coordinate System -2.

ORNL-DWG 78-6154

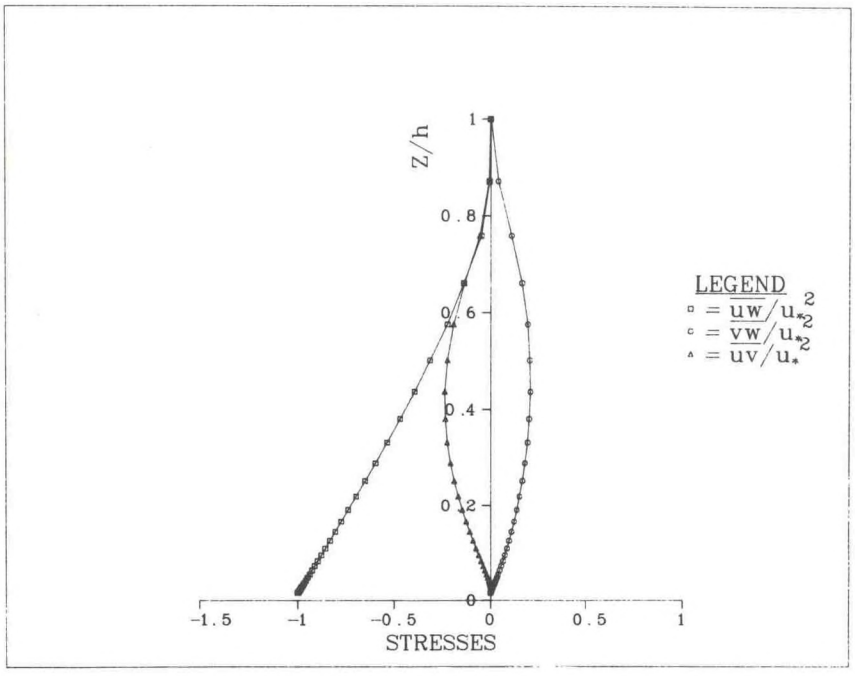

(b) Coordinate System -1.

Fig. 14. Same as Fig. 13, except for the turbulent shear stress components.

ORNL-DWG 78-6159

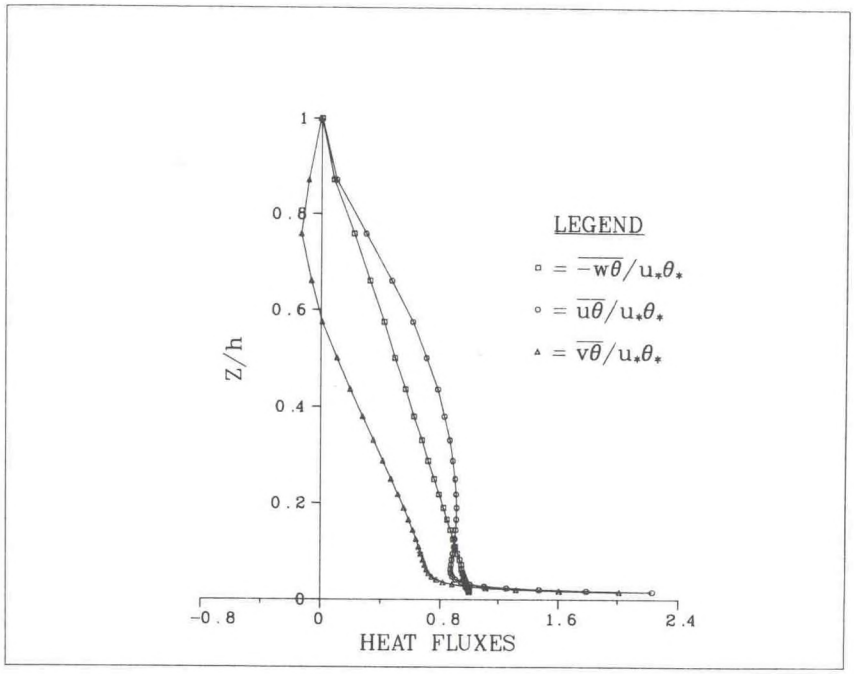

(a) Coordinate System -2.

ORNL-DWG 78-6158

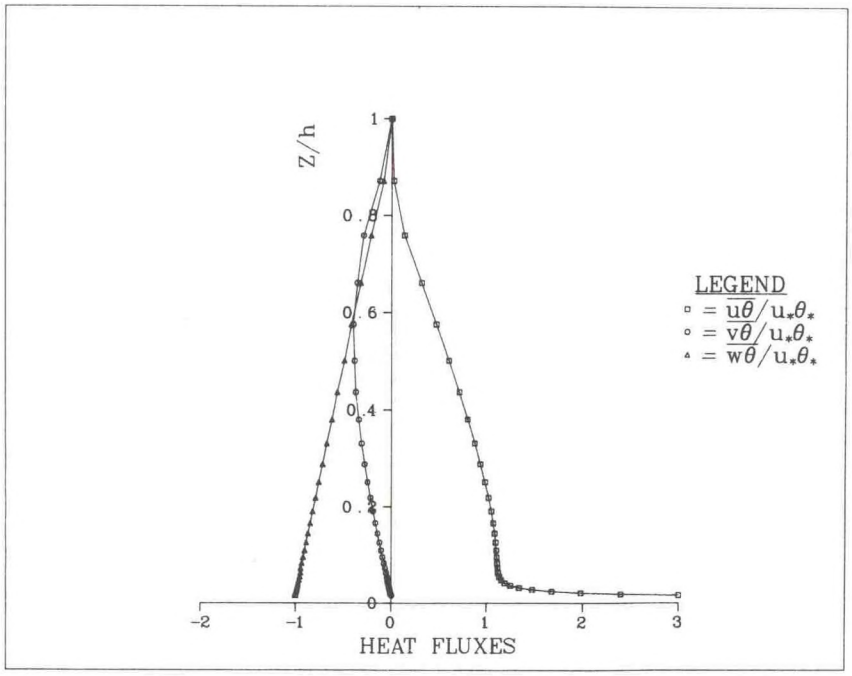

(b) Coordinate System -1.

Fig. 15. Same as Fig. 13, except for the turbulent heat flux components.

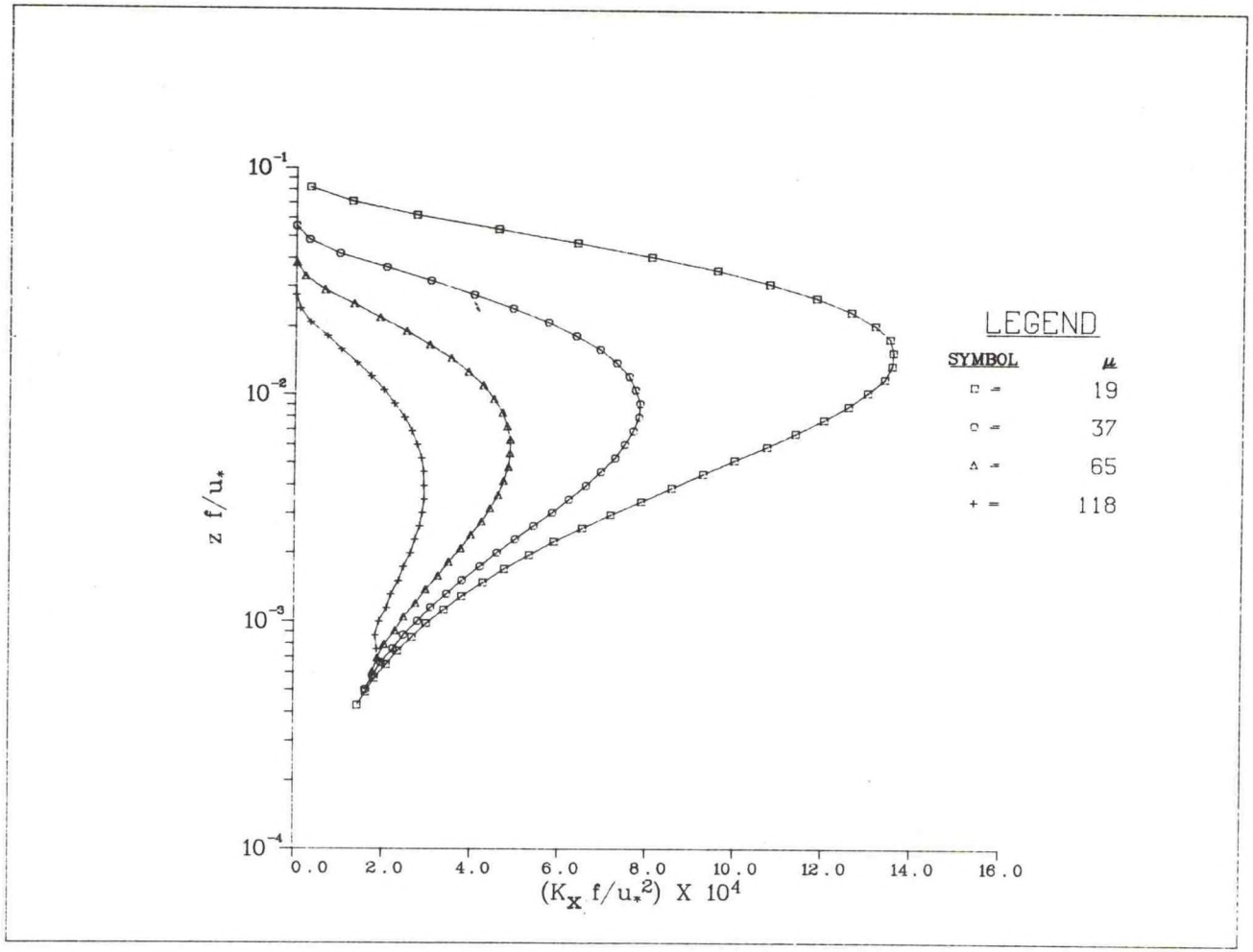

Fig. 16(a). Predicted nondimensional eddy viscosity distributions in the quasi-steady stable PBL for different stabilities.

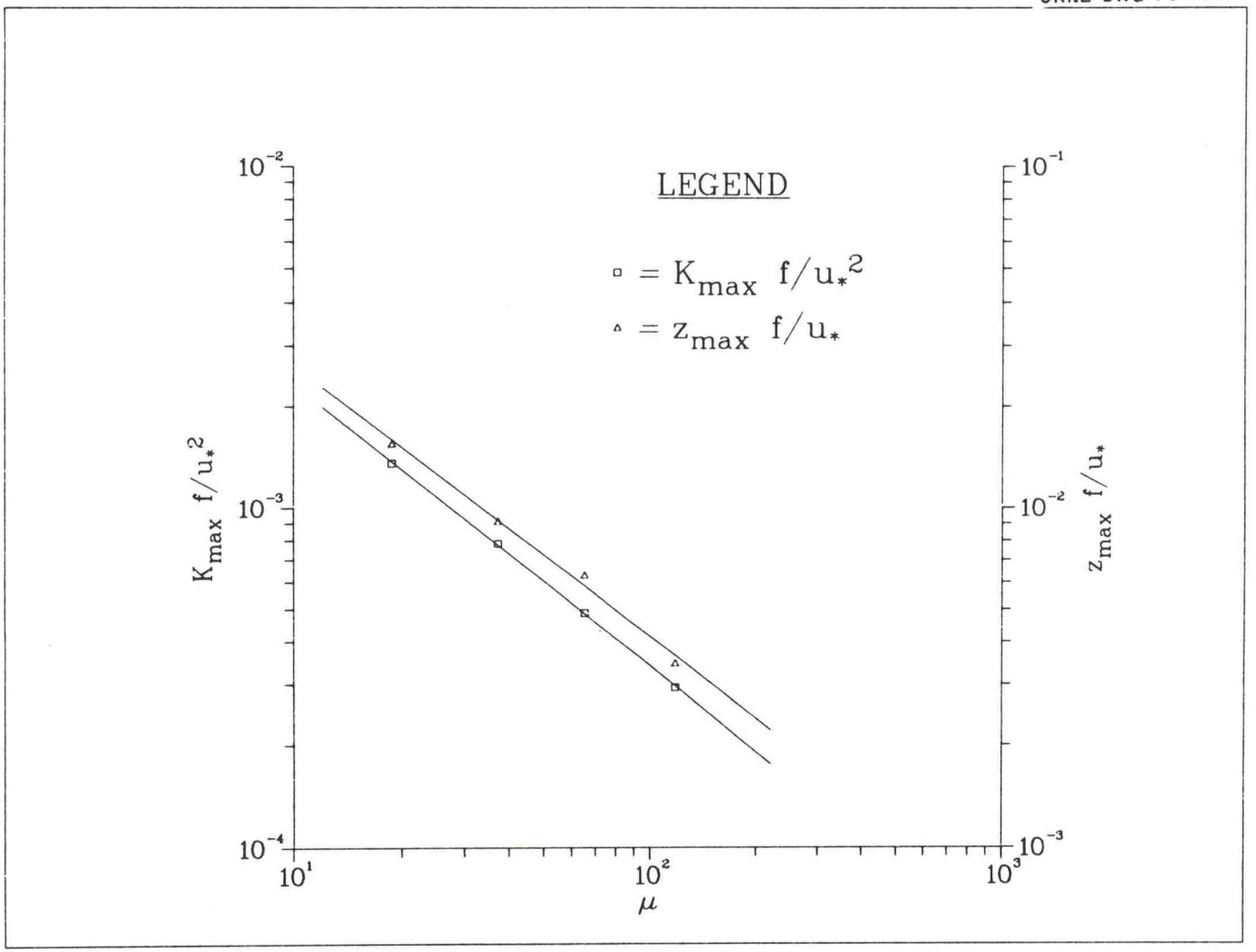

Fig. 16(b). Predicted nondimensional variations of magnitude and height of the maximum eddy viscosity as functions of the stability parameter. See text, Eq. (21).

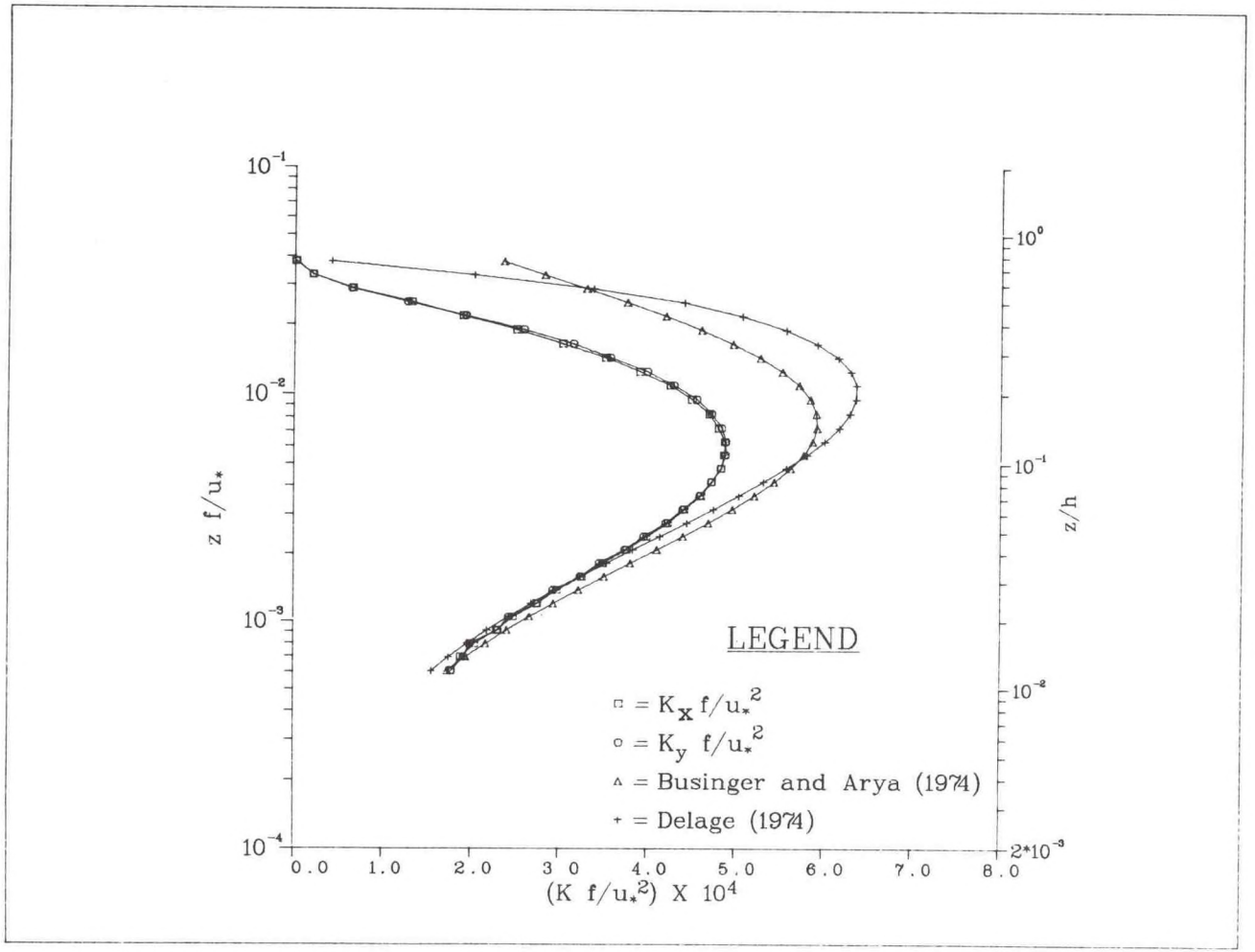

Fig. 17. Comparison of predicted nondimensional eddy viscosity profiles with those used in other stable PBL models. See text for details.

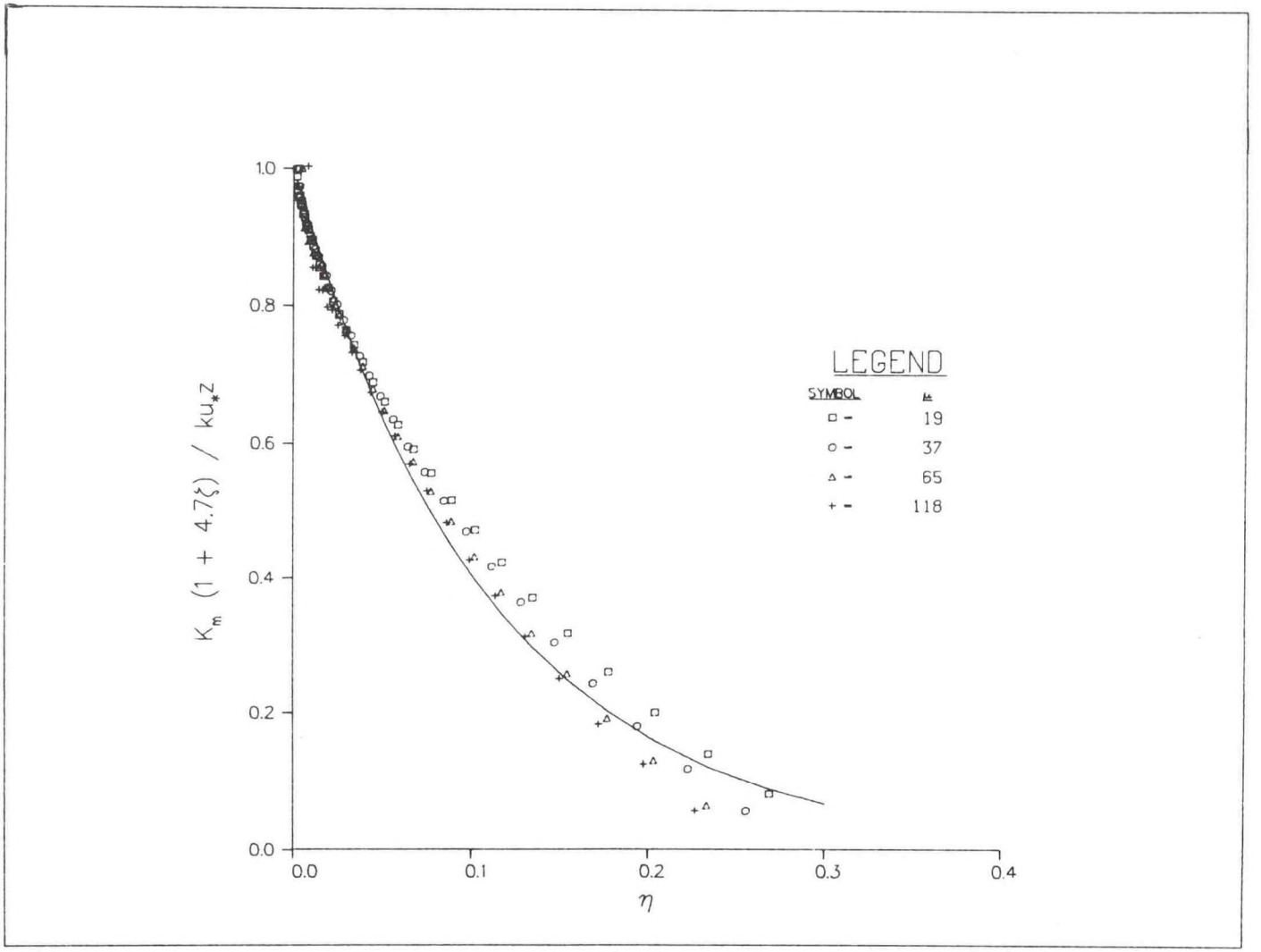

Fig. 18. Similarity representation of the predicted eddy viscosity distribution in the quasi-steady stable PBL. The best fit curve is indicated by ——. See text, Eq. (24).

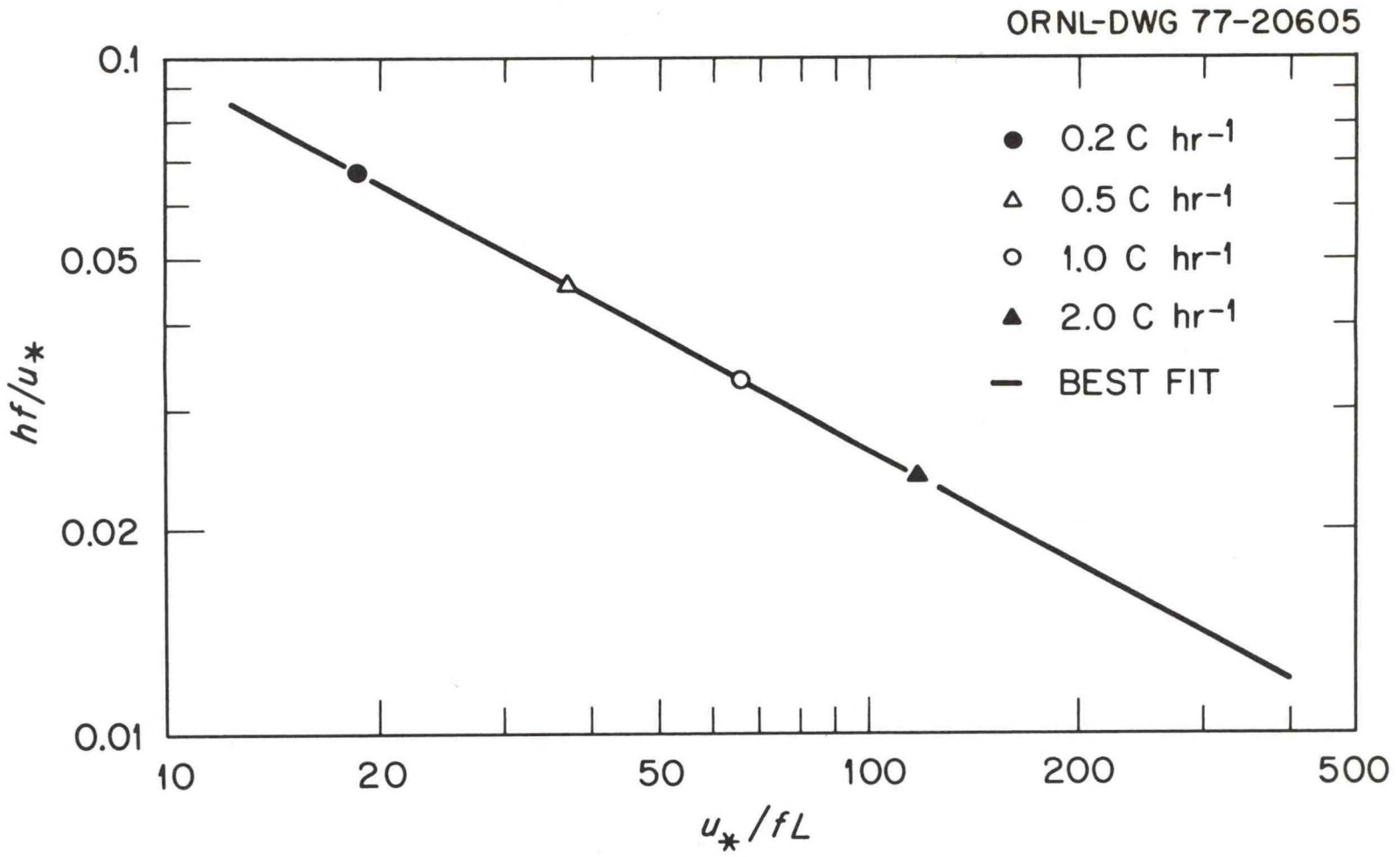

Fig. 19. Predicted variation of the dimensionless stable PBL depth as a function of the stability parameter. See text, Eq.(25).

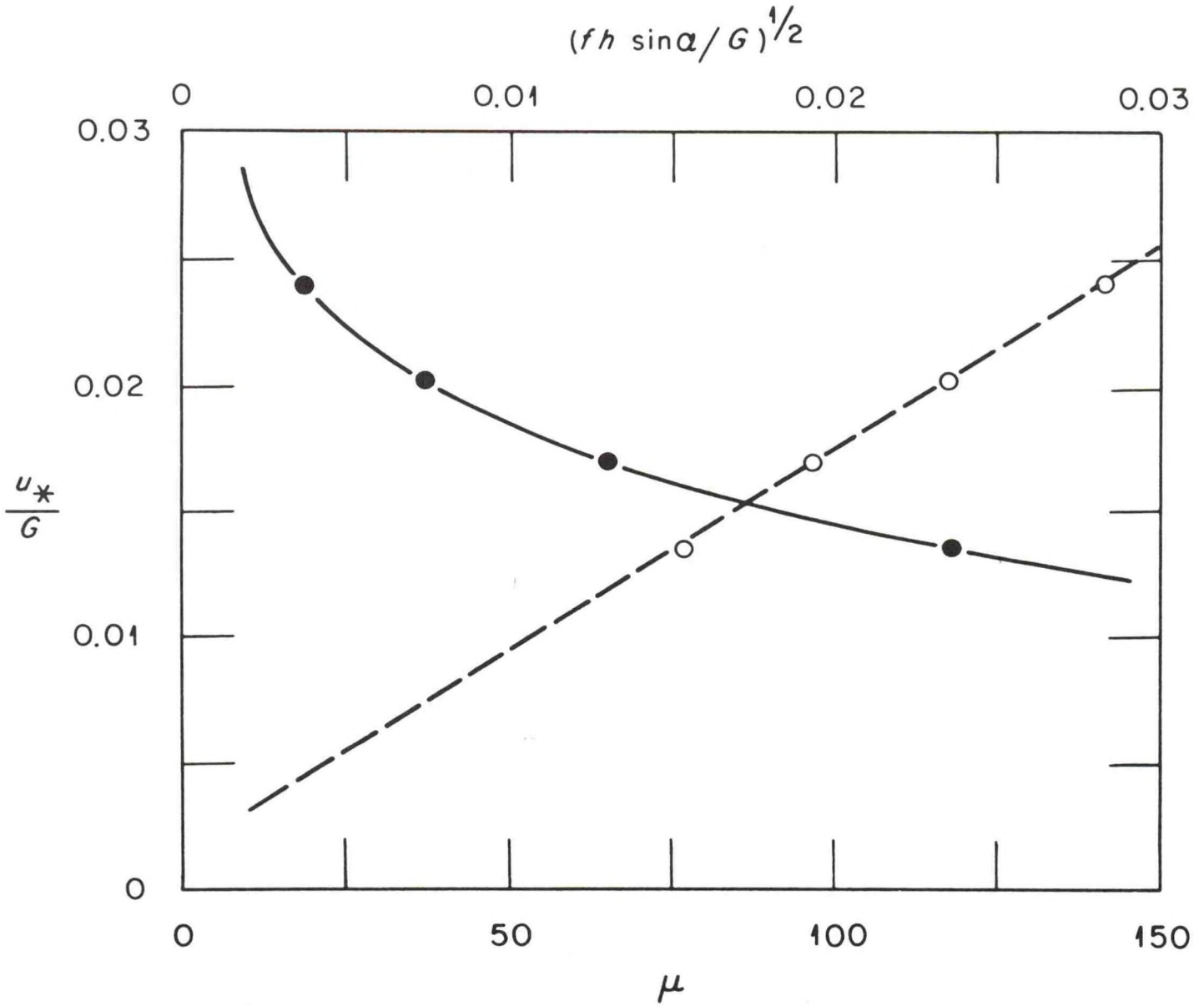

Fig. 20. Predicted variation of the geostrophic drag coefficient in the nocturnal PBL as a function of $(f\ h\ \sin\alpha/G)^{1/2}$, indicated by solid line, and the stability parameter, indicated by broken line. See text, Eqs. (29b) and (31).

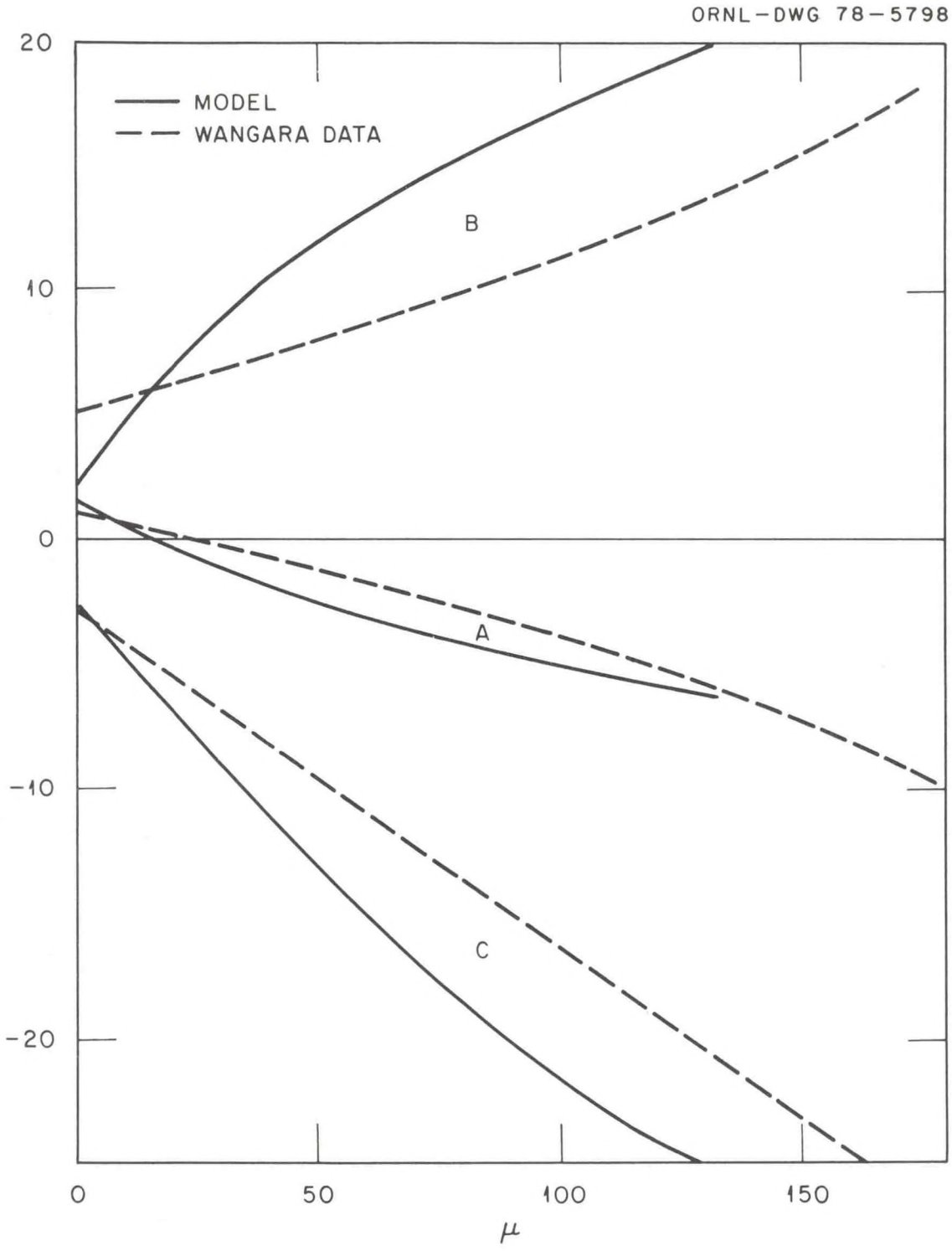

Fig. 21. Comparison of predicted similarity functions A, B, and C in the geostrophic drag and heat transfer relations with the polynomial best-fits to the Wangara stable PBL data. See text for details.

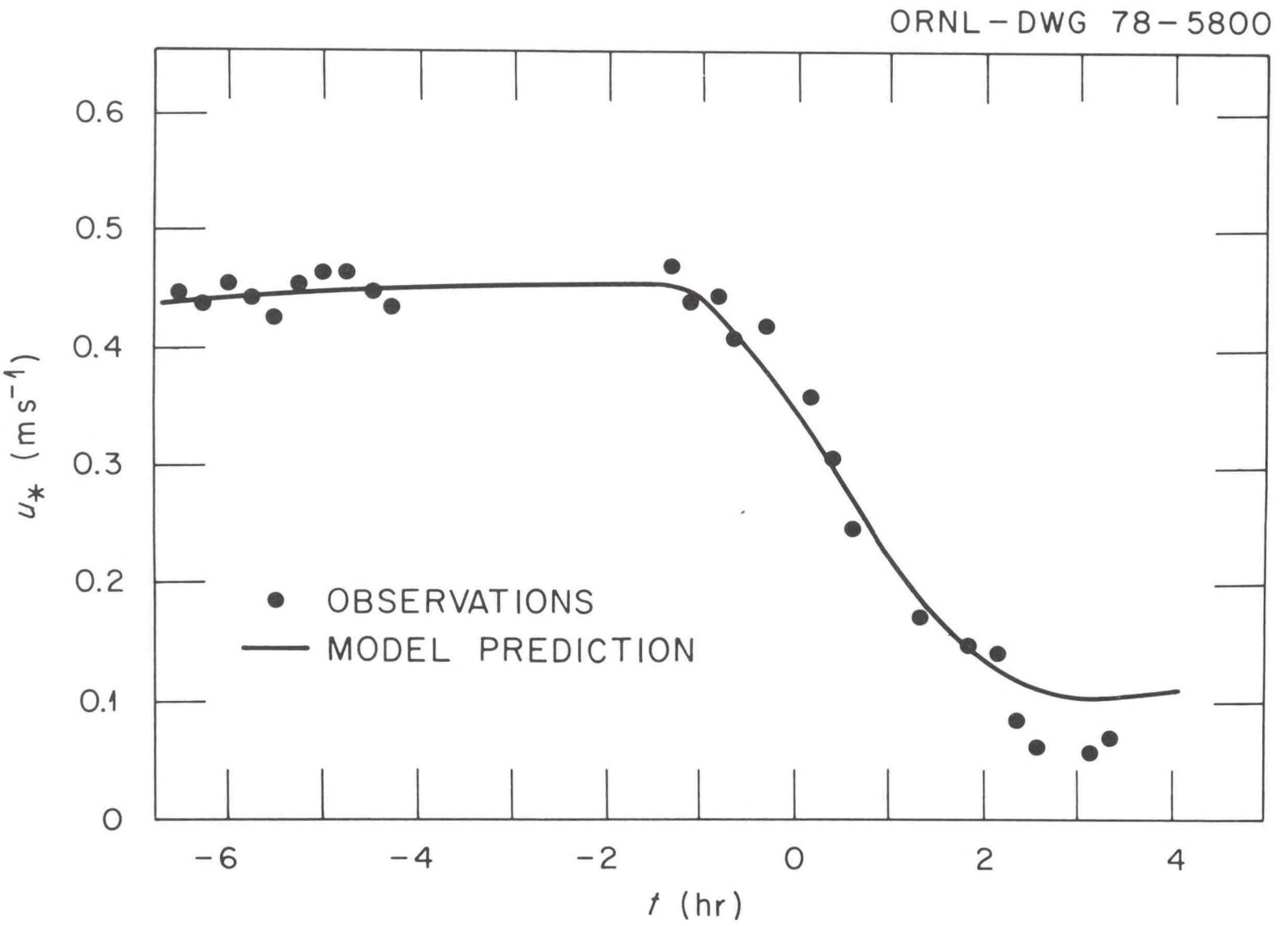

Fig. 22. Predicted variation of surface friction velocity compared with observations from the Minnesota experiment. See text for details.

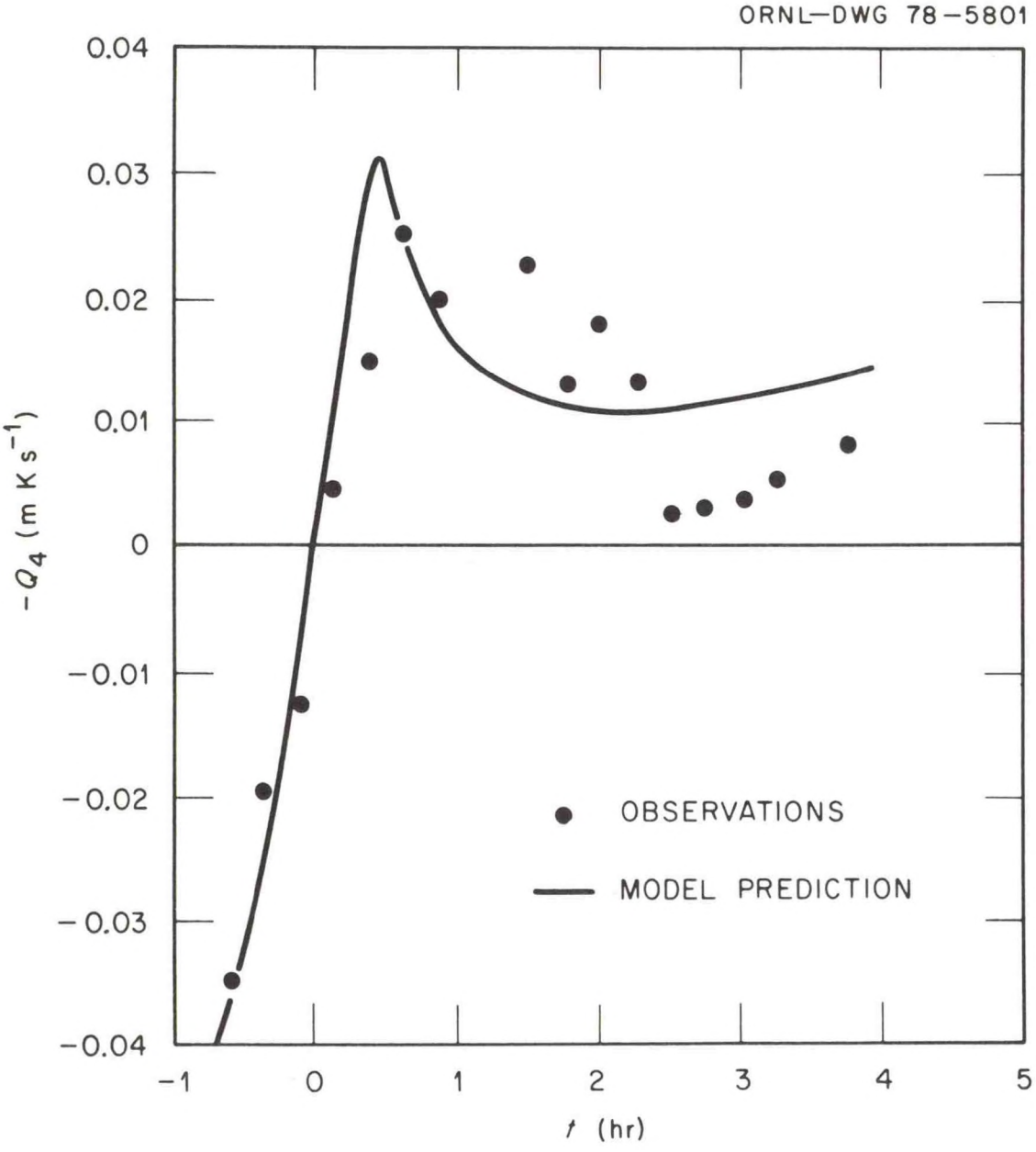

Fig. 23. Same as Fig. 22, except for the heat flux at **z** = 4 m.

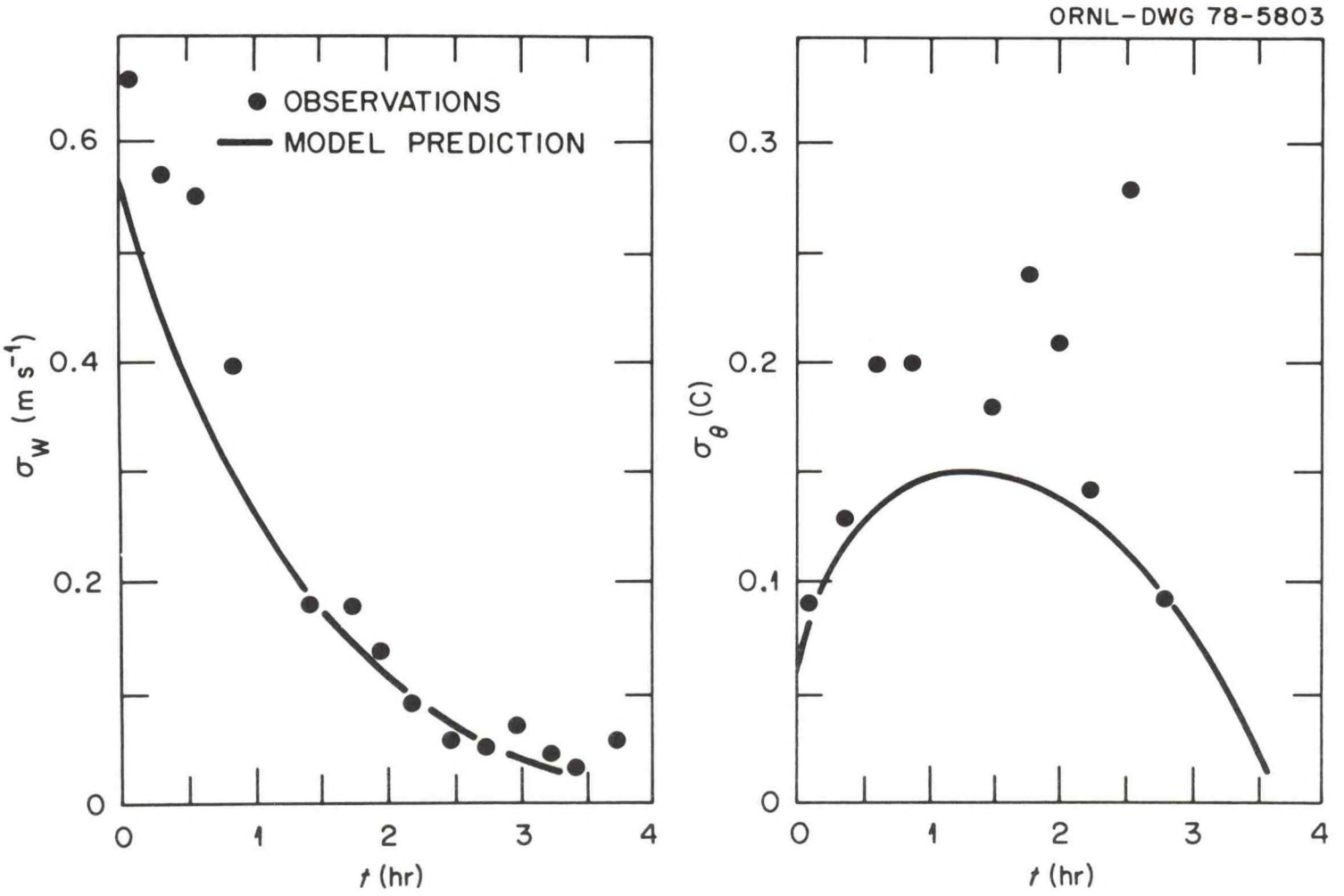

Fig. 24. Predicted standard deviations of vertical velocity (σw) and temperature ($\sigma\theta$) fluctuations, at z= 32 m, compared with observations from the Minnesota experiment.

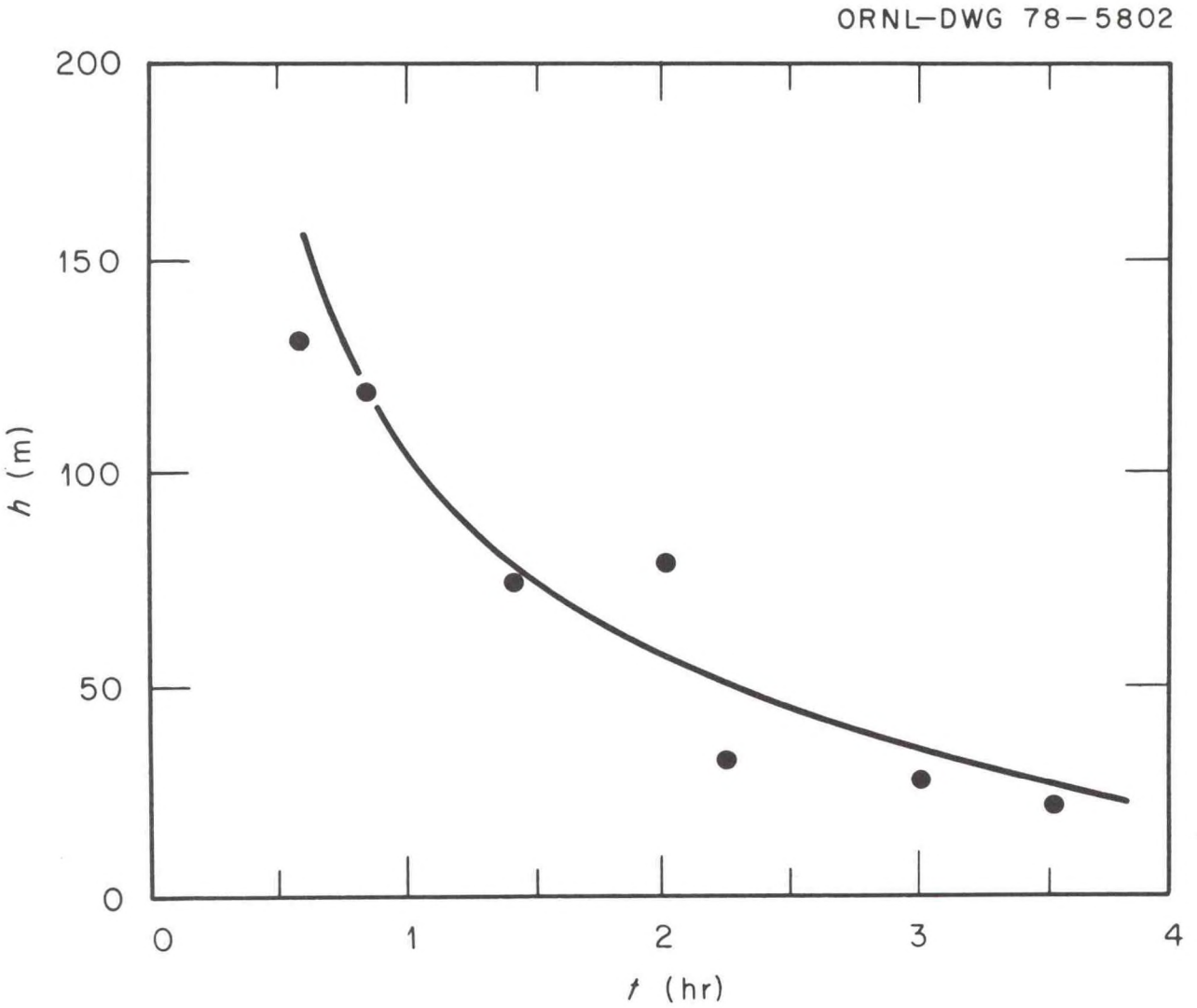

Fig. 25. Predicted variation (——) of PBL depth h compared with observations from the Minnesota experiment.

Chapter 10: Turbulent Diffusion: Chimneys and Cooling Towers*

Steven R. Hanna
Air Resources Atmospheric Turbulence and Diffusion Laboratory
National Oceanic and Atmospheric Administration
Oak Ridge, Tennessee
May 1979

ATDL Contribution File No. 78/10

---

* To be published in the book Industrial Meteorology, E. Plate, ed.

List of Symbols

		First mentioned
a	Similarity parameter $\ln \sigma_z = ax^b$	Eq. 10.16 10.99
A	Parameter in area source model	10.100
	Stability class	Table 1
b	$\ln \sigma_z = ax^b$	10.99
$B(g\ cm^{-3}s^{-1})$	External function	10.22
B, B_1, B_2	Stability classes	Table 1,2
c	Constant in similarity theory	10.15
c'	Constant in relative diffusion	10.20
c_1	Constant in downwash eq.	10.55
$c_p(cal\ g^{-1}{}^oC^{-1})$	Specific heat	10.81
C	Stability class	Table 1
	(g/m^3) Concentration (occurs with various subscripts and primes)	10.21
C_y	Sutton diffusion parameter	10.13
D(cm)	Drop diameter	10.56
D	Stability class	Table 1
$\overline{D^2}(m^2)$	Diffusion due to meandering	10.46
e	Subscript: ambient	
E_m	Ratio of moment. to temp. plume R	p.46
E_N	Enhancement of Δh due to N stacks	10.73
E_w	Ratio of temp. to moist. plume R	p.46
E	Stability class	Table 1
δ	Fraction of latent heat released	p.41
f	Diffusion function	10.36
f_i	Fraction of drift drops removed	10.90
F	Stability class	Table 1
$F_o(m^4s^{-3})$	Buoyancy flux	10.38
$F_{mo}(m^4s^{-2})$	Momentum flux	10.38
Fr_o	Froude number	p.32
$F(n)(m^2s^{-1})$	Variance spectrum	10.7
g	Dimensionless similarity function	10.15
	$(cm\ s^{-2})$ accel. of gravity	10.38
g'	Dimensionless wind profile function	10.16
g_i	Wind frequency	10.97
h(m)	Mixing depth	10.32
$h_A(m)$	Plume elev. after downwash	Fig. 10.10
$h_B(m)$	Building height	Fig. 10.10
$h_d(m)$	Downwash	Fig. 10.10
$h_s(m)$	Stack height	Fig. 10.5

		First mentioned
H(m)	Effective plume height	10.33
$H_o(m^2s^{-2})$	Surface heat flux	p.9
i	Van't Hoff factor	10.92
$k_i(m^3g^{-1}s^{-1})$	Rate constant	10.65
k_t(erg $cm^{-1}{}^oC^{-1}s^{-1}$)	Therm.cond. of air	10.92
$K_i(m^2s^{-1})$	Eddy diffusivity in i direction	10.21
$K_h(m^2s^{-1})$	Eddy conductivity	p.15
K_2	Correction factor	10.85
L(m)	Monin Obukov length	10.15
(cal/g)	Latent heat, water-vapor	10.81
L_i(cal/g)	Latent heat, ice-water	10.81
m	In $u \propto z^m$	10.27
(g)	Drop mass	10.91
m_s(g)	Mass of solute	10.92
M_o(g/mole)	Mol. wt. of water	10.92
M_s(g/mole)	Mol. wt. of solute	10.92
n	Power in Sutton formula	10.11
	In $K \propto z^n$	10.27
N	Number of stacks	10.73

		First mentioned
o subscript : Initial		10.18
$O_m(m^{-1})$	Entrainment parameter for mom. plume	10.39
$O_t(m^{-1})$	Ent. par. for temp. pl.	10.39
$O_w(m^{-1})$	Ent. par. for moist. pl.	10.72
p subscript : Plume		
P/M	Peak to mean conc. ratio	10.47
Pr	Prandtl number	10.92
q_d	Spec. hum. at drop surface	10.92
q_e	Ambient specific humidity	10.77
q_{eo}	Initial ambient spec. hum.	p.41
q_L	Liquid water concentration	p.41
q_{po}	Initial plume spec. hum.	p.41
q_s	Saturation spec. hum.	10.77
$Q(gs^{-1})$	Pollution source strength	10.27
$Q_A(gm^{-2}s^{-1})$	Pollution area source strength	10.98
$Q_L(gm^{-1}s^{-1})$	Pollution line source strength	10.95
Re	Reynolds number	10.91
R_g	8.31×10^7 erg $mole^{-1}{}^o K^{-1}$	10.92
RH	Relative humidity	10.92

		First mentioned
R_m(m)	Radius of momentum plume	10.39
R_o(m)	Initial plume radius	10.38
R_t(m)	Radius of moisture plume	10.39
R_v	Autocorrelation coefficient	10.2
R_w(m)	Radius of moisture plume	10.72
s	Power in Robert's solution	10.27
(s^{-2})	Stability parameter	10.38
S(g/sec)	Internal sources	10.22
	Spacing factor	10.74
Sh	Sherwood number	10.91
t(s)	Time	10.4
T(s)	Integral time scale	10.4
T_p(^oK)	Plume temperature	10.38
T_e(^oK)	Ambient temperature	10.38
T(^oK)	(many varied subscripts) Temperature	
u(ms^{-1})	Windspeed	10.1
$\bar{u}$(ms^{-1})	Average wind speed	10.1
u'(ms^{-1})	Turbulent fluctuation	10.1
u''(ms^{-1})	Random component of turb.	10.14
u_i(ms^{-1})	Wind speed component	10.21
u_*(ms^{-1})	Friction speed	10.15
v_d(ms^{-1})	Deposition speed	10.59
v_g(ms^{-1})	Gravitational settling speed	10.56
v'(ms^{-1})	Crosswind turb. fluct.	10.2
V(m^3s^{-1})	Plume volume flux	10.38
w(ms^{-1})	Plume vertical speed	10.38
w_B(m)	Building side dimension	Fig. 10.10
w_*(ms^{-1})	Scaling speed	p.9
x(m)	Downwind position	10.22
$\bar{x}$(m)	Mean downwind position	10.16
x_ℓ(m)	Visible plume length	10.78
y(m)	Crosswind distance	10.2
Y(m)	Plume width	10.48
$\overline{y^2}$	Plume variance	10.46
z(m)	Vertical distance	10.12
z_ℓ(m)	Visible plume height	10.77
z_o(m)	Roughness length	10.16
β	Ratio of Lagrangian to Eulerian time scales	10.9
Γ	Gamma function	10.27

		First mentioned
δ	Diffusion coef. of water vapor 0.24 cm^2/s	10.91
Δh(m)	Plume rise	Fig.10.5
ΔT(^oC)	Temperature difference on tower	p.2
Δx(m)	Grid spacing	Fig. 10.18
$\Delta\alpha$	Wind shear	p.62
ε($m^2 s^{-3}$)	Eddy dissipation rate	10.20
λ_m(m)	Peak wave length in energy spectrum	10.31
Λ(s^{-1})	Precip. scavenging coef.	10.62
μ(g $cm^{-1} s^{-1}$)	Dynamic viscosity coef.	10.56
ν($cm^2 s^{-1}$)	Kinematic viscosity coef.	10.11
ρ(g/m^3)	Particle density	10.56
σ_y(m)	Crosswind diff. stand dev.	10.2
σ_z(m)	Vertical diff. stand. dev.	p.9
σ_v(m/s)	Crosswind turb. stand.dev.	10.2
σ_w(m/s)	Vertical turb. stand. dev.	10.3
σ_θ	Standard dev. of wind direction fluctuations	10.36
τ(s)	Time lag	10.4
θ_e	Ambient potential temp.	10.38
θ	Plume angle	10.95
ϕ_n	Dimensionless temp. gradient	10.29
ω(g $cm^{-2} s^{-1}$)	Dry deposition rate	10.58
ω_{ps}(g $cm^{-2} s^{-1}$)	Wet deposition rate	10.63

10.1 Introduction

After briefly reviewing the statistical, similarity and K theories of diffusion, this chapter will emphasize practical methods of making diffusion calculations. The Gaussian plume model will be stressed and techniques for accounting for various removal processes (e.g., wet and dry deposition, chemical reactions) will be outlined. The latest methods for estimating the dispersion parameters σ_y and σ_z will be given, accounting for recent research on turbulence in the full depth of the planetary boundary layer. Plume rise formulas for dry and wet plumes will be given. Special topics such as urban diffusion, diffusion in complex terrain, and peak to mean concentration ratios will be discussed.

All scales of atmospheric motions contribute to turbulent diffusion. Wave motions with wavelengths of thousands of kilometers in the westerly winds at mid-latitudes contribute towards the diffusion of radioactive material from a nuclear test. Likewise, small eddies with wavelengths on the order of centimeters contribute towards the diffusion of smoke from a cigarette. In all applied diffusion problems there is a mean field of motion defined either by observations over a certain averaging time or by the output of a wind prediction model. The diffusion at time scales greater than the averaging time for the mean field of motion is accomplished in a transport and diffusion model by time and space variations in the mean field. The

diffusion at time scales less than this averaging time is then defined to be "turbulent" diffusion because it is due to turbulent deviations from the mean wind. The total wind speed u in practical problems is defined by the relation

$$u = \bar{u} + u' \qquad (10.1)$$

where the bar and prime indicate the average and turbulent components, respectively. The wind speed defined by equation (10.1) strictly refers to the Lagrangian speed sensed by a diffusing fluid particle. Most wind measurements are taken by fixed instruments and are therefore Eulerian. A fundamental problem in the research area of atmospheric diffusion is the determination of the relation between Lagrangian and Eulerian turbulence statistics. It is important in any diffusion model to match as closely as possible the appropriate sampling and averaging times of the Lagrangian concentration distribution and the Eulerian turbulence measurements.

Many people using diffusion formulas for the first time are under the impression that they are highly accurate, and that pollutant concentrations can be estimated within $\pm$ 10%. The fact is that this great accuracy can be achieved only under very ideal circumstances, such as a carefully controlled diffusion experiment out to distances of a few hundred meters over uniform terrain, with a continuous ground level point source, and research-grade meteorological instruments

mounted on towers. The American Meteorological Society Committee on Atmospheric Turbulence and Diffusion (1978) prepared a position paper on the accuracy of diffusion models in which it is claimed that factor of two accuracy is all that can be expected from most applications of diffusion formulas to typical real-world situations with minimum instrumentation available (e.g., one or two anemometers and perhaps a Δ T system on a meteorological tower). At locations such as nuclear reactor sites, which may be surrounded by slightly inhomogeneous terrain but which do possess a well-instrumented meteorological tower, accuracy may improve to as good as $\pm$ 20%. Such good results may also be obtained for annual average conditions at a point source or for some urban area source applications, where the effect of long-term averaging is to remove short term errors. On the other hand, in rugged terrain, several studies have shown order of magnitude differences between predicted and observed concentrations. These accuracy figures should be remembered when regulations are being drafted or when models are being compared to each other. The meteorological variability imposes these uncertainties independent of the "goodness" of the diffusion model.

10.2 Review of Diffusion Theories

10.2.1 Statistical Theory

Since turbulence is responsible for diffusion, a diffusion theory which directly uses turbulence measurements is highly desirable.

Taylor (1921) based his statistical theory of diffusion on integrals involving the turbulent energy σ_v^2 and the autocorrelation coefficient $R_v(\tau) = \overline{v'(t)v'(t+\tau)}/\sigma_v^2$. The parameter τ is referred to as the time lag. Let y be the cross-wind deviation from a fixed axis after a time t of a typical particle due to cross-wind eddy velocity v' in a homogeneous field of turbulence, and σ_y^2 be the mean square of a large number of values of y. Then the rate of change of σ_y^2 with respect to time, $d\sigma_y^2/dt$, is given by

$$d\sigma_y^2/dt = \overline{2ydy/dt} = 2\,\overline{yv'} = 2\int_o^t \overline{v'(t)v'(t+\tau)}d\tau, \quad (10.2)$$

where the overbar indicates an average over a large number of realizations of this experiment. Thus this technique refers to cross-wind diffusion from a continuous point source. The following basic diffusion equation is obtained by integration of equation (10.2)

$$\sigma_y^2(t) = 2\sigma_v^2 \int_o^t \int_o^{t_1} R(\tau)\, d\tau\, dt_1 \quad (10.3)$$

The correlation function $R(\tau)$ can have any form as long as $R(0)=1$, $|R| \leq 1$, and $\int_o^\infty R d\tau$ is finite. Asymptotic analytical solutions to equation (10.3) may be obtained by using the fact that atmospheric correlation functions $R(\tau)$ are characterized by finite integrals:

$$\int_o^\infty R(\tau)\, d\tau = T \quad (10.4)$$

where T is known as the integral time scale. For small t, $R \simeq 1$, and equation (10.3) reduces to

$$\sigma_y^2(t) = \sigma_v^2 t^2 \text{ or } \sigma_y \propto t \qquad (10.5)$$

For large t, $\int_0^t R(\tau)d\tau = T$, and equation (10.3) becomes

$$\sigma_y^2(t) = 2\sigma_v^2 Tt \text{ or } \sigma_y \propto t^{1/2} \qquad (10.6)$$

Thus for diffusion from a continuous point source, as travel time t increases, the rate of dispersion decreases. It can be shown that the whole turbulent energy spectrum contributes to diffusion initially, but a low pass filter with cutoff at a frequency of about 1/t is applied to the spectrum as time increases. Eventually only the very large eddies are effective diffusers, with the small eddies ineffectively moving pollutants back and forth deep within the cloud.

It is known that the variance spectrum F(n) of σ_v^2 is obtained from a Fourier transform of the auto correlation $R(\tau)$

$$F(n) = 4\int_0^\infty R(\tau) \cos 2\pi n\tau \, d\tau \qquad (10.7)$$

Taylor's equation 10.3 then becomes

$$\sigma_y^2(t) = \sigma_v^2 t^2 \int_0^\infty F(n)[(\sin^2 \pi nt)/(\pi nt)^2]dn \qquad (10.8)$$

Note that σ_v^2 refers to the Lagrangian wind speed. If the measurements of σ_v^2 are Eulerian (fixed point), this equation can be written

$$\sigma_y^2(t) = (\sigma_v^2)_{t/\beta} t^2, \qquad (10.9)$$

where the subscript t/β indicates averaging over t/β before σ_v^2 is computed. The parameter β is the ratio of the Lagrangian to the Eulerian time scales, and is observed to equal about 4 on the average (Pasquill, 1974). The function in brackets in equation (10.8) is the filter function mentioned above whose physical meaning is clarified by equation (10. 9). Clearly $(\sigma_v^2)_{t/\beta}$ decreases as time increases, since t/β is the averaging time applied to the data before the variance σ_v^2 is calculated. If the characteristics of the turbulence are well known (i.e., if the spectrum F(n) is available) then the dispersion σ_y can be quite easily estimated. A major drawback of this method is that the turbulence field in which the diffusion is taking place is assumed to be steady and homogeneous. Uncertainties introduced by time variations and spatial inhomogeneities, such as occur in the surface boundary layer, have not been sufficiently determined.

A simple analytical solution is obtained to equation (10.3) when the exponential form $R(\tau) = \exp(-\tau/T)$ is assumed. Integration of equation (10.3) yields the solution:

$$\sigma_y^2(t) = 2\sigma_v^2 T^2 \, (t/T - 1 + e^{-t/T}) \, , \qquad (10.10)$$

which is plotted in Figure 10.1. If tangents are drawn to this curve at small and large times, the $\sigma_y \propto t$ line and the $\sigma_y \propto t^{1/2}$ line meet at $t \simeq 2T$.

Another analytical solution to equation (10.3) was given by Sutton (1953) and became the basis of his diffusion prediction technique, which was in wide use until the development in 1961 of the

Pasquill-Gifford-Turner curves. Sutton's formula for $R(\tau)$ is:

$$R(\tau) = \left(\frac{\nu}{\nu + \sigma_v^2 \tau} \right)^n \qquad 0 < n < 1 \qquad (10.11)$$

where ν is kinematic viscosity and n is a stability parameter determined from the power law formula

$$u_1/u_2 = (z_1/z_2)^{n/(2-n)} \qquad (10.12)$$

It develops that

$$\sigma_y^2(t) = 1/2\ C_y^2\ (ut)^{2-n} \qquad (10.13)$$

where C_u is a coefficient and 2-n gives the rate of growth of the σ_y^2 curve with downwind distance. This method was based on Taylor's fundamental equation, but eventually became so encumbered by empirical factors that it was replaced by other methods.

Another type of statistical modeling is the so-called "Monte Carlo" method, where a computer is used to follow the trajectories of thousands of air parcels. The concentration distribution parameters (e.g. σ_z) are calculated from the statistics of these parcels. Velocity fluctuations u' are calculated through formulas such as that suggested by Smith (1968):

$$u'(t+\tau) = u'(t)\ R(\tau) + u'' \qquad (10.14)$$

where u'' is a random (Gaussian) component with variance $\sigma_{u''}^2 = \sigma_{u'}^2(1-R(\tau)^2)$. For simple applications the results of this formula agree with the analytical solution to Taylor's equation.

The statistical technique has been extended to several other applications including the relative diffusion of two or more particles (e.g., Brier 1950; Batchelor, 1952; Smith and Hay, 1967) and to the motion of particles released with the same initial velocity(F. B. Smith, 1968). Monin and Yaglom (1971) give a comprehensive review of this and other statistical theories. It is found that only eddies with sizes roughly equal to σ_y contribute to relative diffusion. The filter function, or window, which is applied to the energy spectrum to indicate which eddies contribute the most to diffusion has its peak at wavelengths equal to σ_y and drops off rapidly at wavelengths larger and smaller than σ_y. Smaller eddies are unimportant for the same reasons given above for single particle diffusion, and larger eddies are unimportant because they merely transport the two or more particles in the same direction. Thus, as diffusion proceeds, $d\sigma_y/dt$ accelerates at first because the filter function is encountering regions of the spectrum with more and more energy. Eventually $d\sigma_y/dt$ decreases and $\sigma_y \propto t^{1/2}$, as for single particle diffusion.

10.2.2 Lagrangian Similarity Theory

10.2.2.1 Continuous sources at ground level.

In Lagrangian similarity theory, the goal is to properly choose and normalize the important variables and governing parameters so that simple dimensionless relations among them can be written. Detailed derivations of this theory are found in Gifford (1968, pp. 88-90), Pasquill (1974, pp. 116-123) and Monin and Yaglom (1971, Chapter 5).

This approach is primarily applied to diffusion in the surface layer, where the turbulence field is inhomogeneous and Taylor's (1921) statistical theory mentioned above may not apply. If a ground level continuous line source is assumed, the growth of the mean height of the plume, $\bar{z}$, with time is given by the relation

$$d\bar{z}/dt = cu_* g(\bar{z}/L) \qquad (10.15)$$

where c is a universal constant found to equal 0.4 by Pasquill (1974, p. 119) and g is a universal function of the stability parameter $\bar{z}/L$. Equation (10.16) can be written in terms of $d\bar{z}/d\bar{x}$ by dividing by the wind speed. The wind speed that is moving the plume is effective at height $a\bar{z}$, where the constant a is found to be about 0.56 :

$$u(a\bar{z}) = d\bar{x}/dt = (u_*/0.4)(g'(a\bar{z}/L)-g'(z_o/L) \qquad (10.16)$$

The functions g' are given in chapter ___, page ___.

Consequently the variation of mean plume height with downwind distance is obtained by substituting equation (10.16) into the $d\bar{z}/d\bar{x}$ form of equation (10.15) and integrating. For neutral conditions it is found that g = 1 and g' = ln (az), and the result is obtained :

$$\bar{x} = (\bar{z}/0.4c)(\ln a\bar{z}/z_o-(z_o/\bar{z})(\ln a-1)-1) \qquad (10.17)$$

The solution to equation (10.17) for c = 0.4 and a = 0.56 is given in Figure 10.2, where $\bar{x}$ and $\bar{z}$ are normalized by z_o.

Chaudhry and Meroney (1973) show that good results are obtained if the function $g(\bar{z}/L)$ in equation (10.15) is assumed to equal $\phi_h^{-1}(\bar{z}/L)$, where ϕ_h is the dimensionless temperature gradient. The predicted influence of stability on vertical diffusion from ground level sources in the O'Niell experiments agrees well with observed values.

Lagrangian similarity theory can also be used as a guide for calculating diffusion through the whole depth of the planetary boundary layer during convective days and diffusion in the shallow mixed layer during the night. For example, in Chapter 6 it is seen that the depth, h, and scaling velocity, $w_* = (H_o h)^{1/3}$, of the convective boundary layer are important scaling parameters, where H_o is the surface heat flux. Consequently $d\sigma_z/dt \propto w_*$ during convective conditions, where σ_z is the standard deviation of the vertical distribution of pollutant. These relations will be discussed more fully in section 10.3, where better methods of estimating σ_z are described.

10.2.2.2 Instantaneous sources : relative diffusion

The relative diffusion of two or more particles can also be estimated using Lagrangian similarity theory. Batchelor (1950) showed that the rate of increase of the standard deviation of the separation of the particles after time t is a function of the initial separation σ_{yo} and the eddy dissipation rate ε for small times, and ε alone for intermediate times :

$$d\sigma_y^2/dt \propto t(\varepsilon\sigma_{yo})^{2/3} \quad \text{small t} \qquad (10.18)$$

$$d\sigma_y^2/dt \propto \varepsilon t^2 \quad \text{intermediate t} \qquad (10.19)$$

Intermediate times are defined to be longer than the time required for the diffusion to be independent of the initial σ_{yo}, and shorter than the time scale associated with the peak of the energy spectrum (i.e., time scales within the inertial subrange of the energy spectrum). For most practical applications the range covered by equation (10.18) is very short, and equation (10.19) is found to have a wide range of applicability. It may be integrated to give

$$\sigma_y^2 = c'\varepsilon t^3 \qquad (10.20)$$

where the constant c' has been found to be of order unity (Monin and Yaglom, 1971). Two particle (or puff) diffusion and instantaneous plume observations can be used to test this relation, as seen in Figure 10.3 (from Gifford, 1977). It is illustrated that the power law $\sigma_y \propto t^{3/2}$ holds over a wide range of travel times.

At times much greater than the turbulence time scale, relative diffusion should slow down just like single particle diffusion, and σ_y^2 should become proportional to t. However, the $\sigma_y^2 \propto t^3$ regime in Figure 10.3 extends to much greater times than would be expected. An interesting consequence of this theory is that σ_y observed in the snapshot of a plume is proportional to $t^{3/2}$, but the average σ_y obtained by averaging several snapshots of the plume taken over a time period of 30 minutes is proportional to t. (Byzova et al., 1970) This is also illustrated by the measurements of instantaneous and averaged plume spreading shown in Figure 10.4, where the photographic data were taken by Nappo (1979), on a sunny morning in Idaho Falls. The source was an oil fog generator at the

ground surface. These data show very clearly the $\sigma_y \propto t^{3/2}$ and $\sigma_y \propto t$ regimes of relative and single particle diffusion.

10.2.3 Gradient Transport (K) Theory

The gradient transport theory is often referred to as "the diffusion theory," since it was conceived in analogy to the exact molecular diffusion theory. The method is a result of Reynolds averaging of the continuity equation for the concentration of substance C, assuming that turbulent fluxes $\overline{u_i'C'}$ are proportional to the mean gradient of C:

$$\overline{-u_i'C'} = K_i \, \partial \overline{C} / \partial x_i \qquad (10.21)$$

The basic diffusion equation can be written:

$$\partial \overline{C}/\partial t = B + S + \partial (K_x \partial \overline{C}/\partial x)/\partial x + \partial (K_y \partial \overline{C}/\partial y)/\partial y + \partial (K_z \partial \overline{C}/\partial z)/\partial z \qquad (10.22)$$

The terms B and S represent external functions and source terms, respectively. Research on this equation has proceeded in two directions. First, it is a challenging equation for mathematicians, who attempt to find analytical solutions for various functional choices of diffusivities and wind speeds. Second, it is a handy equation for finite difference modeling on a high speed computer.

10.2.3.1 Analytical solutions to the diffusion equation

For diffusion in only one direction during calm conditions with constant K, we may write:

$$\partial C/\partial t = K_x \partial^2 C/\partial x^2 \qquad (10.23)$$

Boundary conditions are:

$C \to 0$ as $t \to \infty$, all x

$C \to 0$ as $t \to 0$, $x \neq 0$

$\int_{-\infty}^{\infty} C\,dx = Q$, where Q is the instantaneous source strength.

The solution is

$$C = \frac{Q}{(4\pi K_x t)^{1/2}} e^{-x^2/4K_x t} \qquad (10.24)$$

This equation has Gaussian form with the standard deviation σ_x of the distribution equal to

$$\sigma_x = (2K_x t)^{1/2} \qquad (10.25)$$

The common name for this type of diffusion is Fickian diffusion, and equation (10.25) is sometimes used to estimate K from measurements of σ. The "1/2 power law" is the same as that predicted at large times by statistical theory. The most common application of K theory is to diffusion from an infinite cross-wind continuous line source near the ground:

$$u\,\partial C/\partial x \quad \partial (K_z \partial C/\partial z)/\partial z \qquad (10.26)$$

Satisfactory progress is made when wind speed u and diffusivity K_z are assumed to be power law functions of height:

$$K_z = K_1 (z/z_1)^n \qquad u = u_1 (z/z_1)^m$$

Boundary conditions:

$C \to 0$ as $x, z \to \infty$

$C \to \infty$ as $x = z \to 0$

$K_z \partial C/\partial z \to 0$ as $z \to 0$, $x > 0$

$\int_0^{\infty} u C\,dz = Q \quad x > 0$

where Q is rate of emissions per unit cross wind length per unit time.

The solution given by Roberts (1923) is:

$$C(x,z) = \frac{Q}{u_1 \Gamma(s)} \left[\frac{u_1}{(m-n+2)^2 K_1 x} \right]^{s} \exp \left[- \frac{u_1 z^{m-n+2}}{(m-n+2)^2 K_1 x} \right] \quad (10.27)$$

where $s = (m+1)/(m-n+2)$ and Γ is the Gamma function. This solution is valid for the boundary layer, where u and K_z often have power law variation with height, and generally the conjugate power law m=1-n holds. Similarity and gradient transport theories are found to work best in the boundary layer, where wind shears exist and turbulence is not homogeneous, and the basic assumptions of the statistical theory and the Gaussian plume model are violated. However, analytical solutions rapidly become very complicated or impossible for all but the simplest power law forms for u and K.

10.2.3.2 Numerical solutions to the diffusion equation

Many papers have been published in which the computer is used to solve equation (10.22). It is recognized that the theory is valid only if the size of the cloud being dispersed is much greater than the turbulence length scale, so that all scales of turbulence can take part in the diffusion. Otherwise, as the plume grows, the "effective" K must be changed. Thus, the major computer applications of the theory have been to multiple industrial sources or urban sources, where a large plume is assured. For example, Roth et al. (1974) apply a numerical K model to the Los Angeles basin, and Shir and Sheih (1977) develop a similar model for the St. Louis region.

Once finite difference methods are introduced in order to solve the diffusion equation, problems of numerical instability appear, caused mainly by advection terms of the type $u\partial C/\partial x$. Much effort has gone into devising numerical schemes which reduce the possibilities of numerical instability. These schemes include straightforward higher order approximations, spectral approximations (Prahm et al., 1977) and Particle-in-Cell methods (McCracken et al, 1978). In many cases models use very crude approximations to u and K profiles, but very sophisticated finite difference techniques.

10.2.3.3 Specifying K_z

The most important applications of gradient transport theory involve vertical diffusion and require specification of the vertical variation of K_z in the boundary layer. The eddy diffusivity coefficient K_z can be assumed to be equal to the eddy conductivity coefficient K_h. In the surface layer, which is generally thought of as the lowest 50m of the atmosphere, Businger et al. (1971) suggest the following formula:

$$K_h = K_z = 0.35u_* z/\phi_h(z/L)$$

Von Karman's constant is found to be 0.35 for the Kansas data analyzed by Businger et al. (1971). They suggest the following form for the dimensionless temperature gradient ϕ_h in the surface layer:

$$\text{unstable } \phi_h(z/L) = 0.74(1-9z/L)^{-1/2} \qquad (10.29)$$

$$\text{stable } \phi_h(z/L) = 0.74 + 4.7z/L \qquad (10.30)$$

At heights ranging between about .1h and .7h in the daytime boundary layer, K_z approaches a constant (equal approximately to its value at a height of 100m), then decreases to nearly zero at h (the top of the boundary layer). Crane et al. (1977) observed this behavior in K_z during a 1973 diffusion experiment in Los Angeles. They calculated K_z from equation (10.21), knowing the flux $\overline{w'C'}$ and the mean gradient $\partial C/\partial z$. At $0.2 < z/h < 0.55$, calculations were not possible because $\partial C/\partial z = 0$.

The eddy diffusivity can also be calculated at any site and height using a formula suggested by Hanna (1968):

$$K_z = .15\ \sigma_w\ \lambda_m \qquad (10.31)$$

where λ_m is the wavelength of peak energy in the w spectrum. Kaimal et al. (1976) find from analysis of data from the Minnesota convective boundary layer experiment that λ_m is given by

$$\lambda_m = \begin{cases} z/(0.55-0.38\,|z|L|) & 0<z<|L| \\ 5.9z & |L|<z<0.1\ h \\ 1.5h(1-e^{-5z/h}) & 0.1h<z<h \end{cases} \qquad (10.32)$$

Smith (1973) is using this technique in a numerical model to calculate concentration distributions. He then extracts σ_z from these distributions and is devising a revision to the standard Pasquill-Gifford-Turner σ_z curves.

10.3 Gaussian Plume Model

10.3.1 Development of Model

It was shown that the Gaussian distribution is a solution to the

diffusion equation for constant wind speed u and diffusivity K. The Gaussian model is therefore not rooted very deeply in theory, but is basically an empirical model which has been proven to fit observed data very well. The Gaussian formula for the concentration C resulting from continuous emissions Q (g/sec) at an effective height H above the ground in a cross wind u is

$$C = \frac{Q}{2\pi u \sigma_y \sigma_z} e^{-y^2/2\sigma_y^2} \left(e^{-(z-H)^2/2\sigma_z^2} + e^{-(z+H)^2/2\sigma_z^2}\right) \quad (10.33)$$

where y is horizontal cross wind distance from the plume axis and z is height above ground. Figure 10.5 is a schematic drawing which attempts to explain these definitions. The second exponential term in the parentheses is an image term which accounts for reflection of the plume at the ground surface. The bell-shaped, normal, or Gaussian distribution has been well-validated for elevated plumes. Most people are interested in ground level concentrations, for which equation (10.33) becomes:

$$C = \frac{Q}{\pi u \sigma_y \sigma_z} e^{-y^2/2\sigma_y^2} e^{-H^2/2\sigma_z^2} \quad (10.34)$$

When differentiated with respect to downwind distance x and set equal to zero, this equation yields the maximum ground level concentration C_m:

$$C_m = (\sigma_y/\sigma_z)\, 2Q/(\pi H^2 u e) \quad (10.35)$$

which shows the desirability of tall stacks (large H). At the point of maximum concentration, assuming $\sigma_y = \sigma_z$, it is found that $\sigma_z = H/\sqrt{2}$.

It must be recognized that this model does not account for wind shear, terrain effects, or other possible reasons for plume distortion. The effect of these distortions on ground level concentrations is usually slight.

10.3.2 Specifying σ_y and σ_z Curves

Much effort has gone into devising simple, accurate methods of estimating the plume parameters, σ_y and σ_z. The most popular methods, developed by Pasquill (1961), Gifford (1961), and Turner (1969), are known as the Pasquill-Gifford-Turner (PGT) curves and may be found in Turner's (1969) Workbook, Gifford's (1968) chapter 3 in Meteorology and Atomic Energy - 1968, or Gifford's (1976) recent update of σ curves. These σ_y and σ_z graphs are reproduced in Figs. 10.6 and 10.7. Knowing the cloud cover, time of year and day, and wind speed, anyone can determine the stability class from Table 1 and turn to these graphs to determine σ_y and σ_z for a particular situation. The authors emphasize that these methods are only default methods, to be used in the absence of good turbulence observations.

In order to intelligently apply the PGT curves, it is important to understand the experiments on which they are based, which have been comprehensively summarized by Islitzer and Slade (1968). Limitations due to the sampling grid, nonhomogeneous turbulence, unsatisfactory

sampling and release time, and removal set an error of 10 to 20% on even the best determination of σ_y or σ_z. Most of the experiments that were used to develop the PGT curves took place during the 1950's, and involved non-buoyant continuous releases at the ground or in the lower part of the boundary layer. Very few observations were made at distances greater than one kilometer from the source, and ground surfaces were generally smooth. Often σ_z was not measured directly but was inferred from measurements of the ground level cross-wind distribution. These curves apply specifically to the following conditions: flat terrain with low vegetation; releases at or near the ground; sampling times of about three to ten minutes; steady winds; and downwind distances no greater than about one kilometer.

Problems sometimes occur when these curves are applied to diffusion situations where the above conditions are not satisfied. For example, one would expect significant deviations from the curves for diffusion over rough terrain, for long sampling times, for variable winds, for buoyant releases from tall stacks, and for large downwind distances. Consequently, correction factors have been proposed for some of these conditions, and are summarized by Gifford (1976). For urban surfaces, the experiments of McElroy and Pooler (1971) suggest that the PGT class should be shifted to one higher class than that determined in Table 1.

To account for varying sampling time T, the σ_y or σ_z determined from the figures should be multiplied by $(T/10)^{0.2}$ when T is in minutes. For elevated releases or buoyant plumes, the Brookhaven (Smith and Singer, 1965) or TVA (Carpenter et al., 1971) σ_y and σ_z curves can be used, because they were developed from observations of diffusion from sources at heights above the surface layer. Briggs (1973) has derived the analytical expressions listed in Table 2, which fit the PGT curves at small distances and the Brookhaven and TVA curves at large distances.

10.3.3 Revisions to σ_y and σ_z Curves

Rather than applying many corrections to the original PGT curves, it is desirable to devise a new system by which σ_y and σ_z can be efficiently estimated. Several scientists are currently working on new systems using the results of recent comprehensive planetary boundary layer observations such as those in Minnesota (Caughey et al, 1973; Izumi and Caughey, 1976). As mentioned earlier, these experiments show that the depth h of the mixed layer is an important scaling length for diffusion through the whole depth of the boundary layer and that $w_* = (hH_o)^{1/3}$ is an important scaling speed, where H_o is the surface heat flux. The depth h can be measured using radiosondes, pibals, or acoustic sounders. Laboratory experiments by Willis and Deardorff (1974) confirm these findings and further suggest that diffusion during free convection conditions follows the law $\sigma_z \propto x^{3/2}$

For crosswind horizontal diffusion, Pasquill (1976) recommends that σ_y be determined as a function of the standard deviation of wind direction fluctuations σ_θ and downwind distance x:

$$\sigma_y = \sigma_\theta \times f(x) \qquad (10.36)$$

where f(x) is given by the following table:

x(km)	0	0.1	0.2	0.4	1	2	4	10	>10
f(x)	1.0	0.8	0.7	0.65	0.6	0.5	0.4	0.33	$0.33(10/x)^{1/2}$

As shown by equations (10.13) and (10.14) f is actually a function of travel time, averaging time, and the Lagrangian time scale. Doran et al., (1978) use the spectral approach (equation 10.13) to the statistical theory of diffusion to determine f more exactly. However, their corrected values of f are only 20% different from Pasquill's approximate values in the above table. If detailed turbulence measurements are available from which the energy spectrum can be calculated, then equation (10.13) can be solved directly. For many practical purposes the above table is sufficient.

Smith (1973, 1977) and Briggs and McDonald (1978) are revising the σ_z curves in light of recent boundary layer experiments. For all other conditions the same, the following relation is found to be valid:

$$\sigma_z \propto z_o^{0.2} \qquad (10.37)$$

Smith uses equation (10.31) ($K_z = .15\ \sigma_w \lambda_m$) to define K_z for use in the diffusion equation. Wind speed u, the standard deviation of vertical turbulence fluctuations σ_w, and the peak wavelength λ_m in the w spectrum are parameterized using the results of the Minnesota experiment, and the resulting concentration distributions from the solutions of the diffusion equation are analyzed to determine σ_z. The end result is that on the order of ten graphs or nomograms must be used to estimate σ_z, rather than the one graph used in the PGT scheme. However, a much wider variety of boundary

and meteorological conditions are covered by Smith's scheme. The nomogram reproduced in figure 10.8 is included in this new procedure. Pasquill (1974, p. 374) reproduces another of Smith's figures, in which the stability class is estimated from the wind speed and the incoming solar radiation for a given roughness. Because of the great number of graphs and the tentative nature of the scheme, it is not outlined in detail here.

10.3.4 Stability Classification

In order to estimate σ_y or σ_z using one of the PGT curves it is necessary to first determine the stability class. Because of inconsistencies associated with some of the schemes in use, the American Meteorological Society convened a workshop to study the problem and make recommendations (Hanna et al., 1977). They concluded that the ΔT criterion (e.g.; $T_{60m}-T_{3m}$) is unsatisfactory as an indicator of diffusion class during unstable conditions but satisfactory during stable conditions. The Richardson number Ri or the stability parameter z/L are satisfactory stability criteria at all stabilities as long as a standard height of measurement is specified. The standard deviation σ_θ is a fair indicator of stability class for σ_y. The so-called STAR system recommended by the USEPA is similar to Pasquill's original scheme (Table 1) but in its present form yields a disproportionate share of neutral stabilities. The various stability classification schemes are compared in Table 3.

10.4 Plume Rise

The effective source height H in the Gaussian plume formula equals the stack height h_s plus the plume rise Δh. A maze of formulas exists to predict buoyant plume rise, but Briggs' (1969, 1975) formulas have been shown to be the most accurate. The fundamental parameters used in his formulas are:

Initial volume flux $V_o = w_o R_o^2$

Initial buoyancy flux $F_o = V_o (g/T_{vpo}) (T_{vpo} - T_{veo})$ (10.38)

Initial momentum flux $F_{mo} = w_o V_o$

Ambient stability $s = (g/T_e) \partial\theta_e/\partial z$

where w_o is initial plume vertical speed

R_o is initial plume radius

g is acceleration of gravity

subscript o indicates initial

subscript v indicates virtual temperatures ($T_v = T(1+.61q)$), where q is specific humidity.

subscript p indicates plume

subscript e indicates environment.

Note that the atmospheric density ρ is factored out of these flux definitions. A crucial assumption in the simplified plume rise formulas is that there is a top-hat (uniform) distribution of temperature on any plume cross section. In Briggs' (1975) latest description of methods for estimating plume rise for bent-over plumes, the radius R_m of the effective momentum plume is larger than the radius R_t of the effective thermal plume, as indicated by the entrainment equations:

Vertical plume: $(1/V)\ \partial V/\partial z = O_t = O_m = 0.15$

$$\partial R_m/\partial z = \partial R_t/\partial z = 0.15 - R_t(g/T_p)(T_p - T_e)/2w^2 \qquad (10.39)$$

Bent over plume: $O_t = 0.8\ \ O_m = 1.2$

$$\partial R_t/\partial z = 0.4 - (R_t/2u)\ \partial u/\partial z \qquad (10.40)$$

$$\partial R_m/\partial z = 1.5\ \partial R_t/\partial z$$

The entrainment coefficient O is the fractional growth of the plume volume flux with height.

For a neutral environment or for any plume near the source when the wind speed is greater than about 1 m/s, the following equation for plume rise Δh is valid:

$$\Delta h = 2.3\ F_{mo}^{1/3}\ u^{-2/3}\ x^{1/3}\ (1 + F_o x/2\ F_{mo}\ u)^{1/3} \qquad (10.41)$$

After a distance $x \simeq 2F_{mo}\ u/F_o$, buoyancy dominates and the well-known "2/3 law" results:

$$\Delta h = 1.6\ F_o^{1/3}\ u^{-1}\ x^{2/3} \qquad (10.42)$$

Above the surface boundary layer, the atmosphere is nearly always stable to some degree and the following formulas for the final rise of buoyancy-dominated plumes in a stable environment can be used:

Bent over $\qquad \Delta h = 2.9\ (F_o/us)^{1/3} \qquad (10.43)$

Calm $\qquad \Delta h = 5.0\ F_o^{1/4}\ s^{-3/8} \qquad (10.44)$

where the stability s is defined as $(g/T)(\partial T/\partial z + .01^{\circ}C/m)$.

These methods can also be used to determine whether a plume has enough buoyancy to penetrate an elevated inversion of strength ΔT. Briggs assumed that the top hat plume will penetrate the inversion if the excess temperature in the plume at the height of the inversion exceeds ΔT. Thus the following criteria are set for inversion penetration:

$$\text{Bent over} \quad \Delta T \leq 4(T_p/g)\ (F_o/u(\Delta h)^2)$$

$$\text{Calm} \quad \Delta T \leq 10(T_p/g)\ F_o^{2/3}/\ (\Delta h)^{5/3} \qquad (10.45)$$

10.5 High Ground Level Concentrations from Elevated Point Sources.

Regulatory guidelines are often aimed at preventing short-lived periods of high ground level concentrations. These high concentrations can result from random looping of the plume or from longer-lived fumigation episodes.

10.5.1 Peak to Mean Concentrations Ratios

Plume looping has been treated by Gifford (1960), who proposes to evaluate the "peak-to-mean" concentration ratio through use of a fluctuating plume model. This model assumes that there are two separate scales of diffusion, where, in addition to the diffusion $\overline{\sigma^2}$ of the instantaneous plume due to small scales of turbulence, there is an additional contribution to diffusion D^2 by meandering or looping of the plume:

$$\overline{y^2} \simeq \overline{\sigma^2} + \overline{D^2} \qquad (10.46)$$

Figure 10.9 illustrates the fluctuating plume concept. An observing station near the edge of a looping plume can experience a very high peak to mean ratio. The formula proposed by Gifford (1960) for the peak to mean ratio for a receptor at the ground and a source at height H is:

$$\frac{P}{M} = \frac{C_{peak}}{C_{mean}} = \frac{(\overline{\sigma^2} + \overline{D^2})}{\overline{\sigma^2}} \exp\left[\frac{\sigma^2}{2(\overline{\sigma^2} + \overline{D^2})} + \frac{(z-H)^2}{2(\overline{\sigma^2} + \overline{D^2})}\right] \qquad (10.47)$$

where it is assumed that $\sigma_y = \sigma_z$

Air pollution measurements have been reported by Gifford (1960) which show that values of P/M as great as 50 to 100 may occur at the ground near a moderately tall (50-100m) stack. As downwind distances increase (20 to 50 stack heights downwind), P/M decreases toward unity. Byzova and Garger (1970) report some diffusion experiments in which both diffusion parameters $\overline{\sigma^2}$ and $\overline{D^2}$ were determined. They find that the instantaneous diffusion $\overline{\sigma^2}$ is proportional to t^3 at intermediate times, as predicted by Batchelor's Lagrangian similarity theory (eq. 10.20). The fluctuating or looping component $\overline{D^2}$ is proportional to t^2 for about 200 seconds, then approaches a constant as time increases further. No conclusions about general relationships for $\overline{\sigma^2}(t)$ and $\overline{D^2}(t)$ could be made.

10.5.2 Fumigation

High ground level concentrations due to emissions from elevated sources may occur when the plume is brought to the ground for time periods ranging from one half to several hours during fumigation conditions. The classical case of fumigation occurs in the morning when a plume trapped in a stable layer aloft is suddenly mixed to the ground when the growing adiabatic mixed layer reaches plume level.

This is called "inversion break-up" fumigation. The resulting high concentrations are usually short lived (~1 hr.) as the plume adjusts itself to the new mixed layer. If Y is the plume width before fumigation, H is plume height, and it is assumed that a uniform profile exists in the fumigated plume, then the concentration at the ground is approximated by:

$$C_{IB} = Q / uHY \qquad (10.48)$$

Shoreline fumigation with onshore winds is governed by the same formula, where Y is now the plume width at the point it breaks free from the stable layer that formed over cold water into the mixed layer forming over the warmer land surface. An internal boundary layer separating the two stability regimes occurs for onshore flow and is observed to gradually rise as the air flows inland (Lyons, 1975; also see Chapter 7). Shoreline fumigation can be more persistent than inversion break-up fumigation.

Limited-mixing fumigation occurs when upward diffusion is restricted by an inversion, below which strong mixing is occurring. In Los Angeles, for example, a subsidence inversion at a height of about 800m persists through most of the year. If the plume has a Gaussian distribution in the crosswind direction but mixes uniformly through the mixed layer of depth h, then the ground level concentration on the plume axis is given by

$$C_{LM} = Q / (2\pi)^{1/2} uh \sigma_y \qquad (10.49)$$

During neutral conditions with high winds, relatively low plume rise occurs and high-wind fumigation can be a problem. The situation is made more severe by the tendency of high winds to persist for several hours. It was shown earlier that the maximum ground level concentration is found at a distance such that $H = 2^{1/2}\sigma_z$. The plume rise formula for neutral conditions is $\Delta h = 1.6\ F_o^{1/3}\ x^{2/3}/u$. Since $H = h_s + \Delta h$ we can eliminate u from this equation and equation (10.34) to obtain

$$C_{HW} = \frac{2\ Q\Delta\ h}{1.6\pi(h_s+\Delta h)^2\ e\ F_o^{1/3} x^{2/3}} \qquad (10.50)$$

This expression has a maximum with respect to Δh at $\Delta h = h_s$. Substituting $\Delta h = h_s$ in this equation yields the result:

$$C_{HW} = \frac{Q}{3.2\pi\ h_s\ e\ F_o^{1/3} x^{2/3}} \qquad (10.51)$$

Taking the ratio of equation (10.49) to equation (10.51), the relative importance of high wind and limited mixing fumigation can be assessed:

$$\frac{C_{LM}}{C_{HW}} = \frac{Q}{(2\pi)^{1/2} uh\ \sigma_y}\ \frac{\pi H^2 Ue}{2Q} = 2.4\ \frac{H}{h} \qquad (10.52)$$

where it is assumed that $\sigma_y = \sigma_z$ and $H = 2^{1/2}\ \sigma_z$ at the maximum point. Thus if the effective plume height H times 2.4 is less than the mixing depth h, then high wind fumigation leads to higher ground level concentrations than limited mixing fumigation. TVA experience shows that

limited mixing fumigation occurs more frequently at very tall stacks (h_s > 100m).

10.6 Process Emissions - Small Stacks and Building Effects

There are several chapters in this book which very thoroughly cover the subject of air flow around obstacles such as industrial structures. To minimize ground level concentrations it is necessary for a plume to rise above the cavity and wake zones behind a structure, which are very turbulent and would mix the plume rapidly towards the ground. Briggs (1973) has developed a set of criteria for determining whether a plume from a stack of height h_s adjacent to a building of height h_B and width w_B will escape the cavity. The length ℓ_B is assumed to be the smaller of h_B and w_B. The various parameters involved are illustrated in Figure 10.10.

For most sources, the plume will lower a distance h_d from the stack top when $w_o/u < 1.5$:

$$h_d = 4 R_o (1.5 - w_o/u) , \qquad (10.53)$$

where R_o is stack radius. The adjusted stack height is then $h_A = h_s - h_d$. An old rule of thumb is that if h_A is greater than 2.5 times h_B, the building height, then the plume will escape the building influence. More recent wind tunnel data have led Briggs (1973) to revise this rule in the following way:

If $h_A > h_B + 1.5\ell_B$	No building influence.
If $h_B + 1.5\ell_B > h_A > h_B + .5\ell_B$	Plume in wake
If $h_A < h_B + .5\ell_B$	Plume in cavity.

In the cavity region the plume is assumed to mix uniformly through an area proportional to the cross sectional area of the building:

$$C = 2\ Q/u\ \ell_B^2 \qquad (10.54)$$

After the plume breaks out of the cavity it still feels the effects of the initial dilution:

$$C = Q/(u(c_1\ell_B^2 + \pi\sigma_y\sigma_z)) , \qquad (10.55)$$

where σ_z is reckoned from the point the plume leaves the cavity and the constant c_1 has the range $0.5 < c < 2$ (Gifford, 1976). It is currently being measured in several wind tunnel and atmospheric tests.

For very large, buoyant sources such as cooling towers the criterion for downwash changes. On the basis of experiments in a laboratory water tank, Overcamp and Hoult (1971) suggest that the critical value of w_o/u for the occurrence of downwash h (i.e., if w_o/u is smaller than the critical value, downwash will occur) has the following dependence on initial Froude number Fr_o:

Fr_o	0.01	0.25	1	5
critical w_o/u	0.2	0.5	1.0	1.5

where $Fr_o = w_o^2/\ 2\ R_o(g/T_{po})\ (T_{po} - T_{eo})$

Thus for large buoyant sources (large Fr_o) downwash is less likely to occur than for less buoyant sources.

10.7 Removal

Dry deposition, precipitation scavenging, and chemical reactions are the major agents for removal of plume material.

These topics are the subjects of comprehensive textbooks and symposium proceedings (i.e., Junge, 1961; Engelmann and Sehmel, 1974). A few brief recommendations will be made here for the case of a continuous point source at effective height H.

10.7.1 Dry Deposition

Dry deposition refers to the removal of material from the plume at the ground surface by gravitational settling or by some impaction process. Small particles with diameter D less than 20 μm settle at a speed v_g given by Stokes' law:

$$v_g = D^2 g\rho_p/18\mu \qquad (10.56)$$

where ρ_p is particle density and μ is dynamic viscosity. At sea level the fall speed of larger particles with density $\rho_p = 5$ g/cm^3 is given by the following table:

D(μm)	12	40	80	160	400	800	1600
v_g(cm s^{-1})	0.6	6	24	64	230	410	820

As Van der Hoven (1968) points out, for v_g > 100 cm/sec the particles fall through the turbulence and diffusion is no longer important. The problem is then reduced to the calculation of ballistic trajectories for particles with diameter D greater than about 200 μm. For v_g < 100 cm/s the tilted plume hypothesis proposed by Csanady (1955) is used, where the effective plume height sinks with speed v_g relative to the gaseous plume height H_o:

$$H = H_o - xv_g/u \qquad (10.57)$$

The Gaussian model is used to calculate diffusion, and deposition $\omega(g/m^2 s)$ at the ground is calculated by the formula

$$\omega = v_g C_o \qquad (10.58)$$

Inertialess particles and gasses are also observed to be deposited on surfaces due to chemical absorption and impaction. For these substances a deposition speed v_d takes the place of v_g in equation (10.58). The speed v_d is defined by observations of deposition ω and ground level concentration C_o by dividing equation (10.58) by C_o:

$$v_d = \omega/C_o \qquad (10.59)$$

Measurements of dry deposition speed v_d range from .01 to 10 cm/sec, with higher deposition speeds associated with wet, rough ground surfaces, unstable atmospheres, and chemically reactive substances. A commonly used average value for the deposition speed v_d is 1 cms^{-1}.

If enough material is removed from the plume, it is necessary to account for a reduced flux of material in the Gaussian plume formula. The depletion of the flux per unit distance is given by

$$\partial Q/\partial x = \int_{-\infty}^{\infty} \omega dy = -(2./\pi)^{1/2}(v_d Q/u\sigma_z) e^{-H^2/2\sigma_z^2} \qquad (10.60)$$

Therefore,

$$Q(x)/Q(0) = [\exp \int_o^x (dx/\sigma_z \exp(H^2/2\sigma_z^2))]^{-(2/\pi)^{1/2} v_d/u} \qquad (10.61)$$

Graphical solutions to this equation are given in several references (e.g. Van der Hoven, 1968, p. 205).

10.7.2 Precipitation Scavenging

Slinn (1974) reviews the basic physical principles of precipitation scavenging, which deals with whether or not a given particle, aerosol, or gas molecule will be collected or scavenged by cloud and rain droplets. In general it can be assumed that the concentration decreases due to precipitation scavenging according to an exponential law:

$$C = C_o e^{-\Lambda t} \qquad (10.62)$$

where Λ (sec^{-1}) is the scavenging or washout coefficient. The coefficient Λ is a function of rain rate and particle size, but as a first approximation can be assumed to roughly equal 10^{-4} sec^{-1}.

The ground deposition due to precipitation scavenging ω_{ps} is calculated by vertically integrating the distribution of pollutant as given by the Gaussian plume formula:

$$\omega_{ps} = \Lambda \int_o^\infty C\, dz = (\Lambda Q/u\sigma_y(2\pi)^{1/2}) e^{-y^2/2\sigma_y^2} \qquad (10.63)$$

If significant plume depletion occurs, replace Q by

$$Q(0)e^{-\Lambda x/u} \qquad (10.64)$$

In a heavy rainstorm, most of the pollutant may be removed by precipitation scavenging within an hour after release. Over long time intervals, however, because precipitation scavenging occurs intermittently while dry deposition occurs continuously, it is recognized that removal by dry deposition is just as effective as removal by precipitation scavenging in depleting the cloud.

10.7.3 Chemical Reactions

As a result of chemical reactions, the concentrations of primary pollutants such as SO_2 and NO can decrease, while the concentrations of secondary pollutants such as sulfates and ozone can increase. The half life of SO_2 in a plume has been measured by several investigators and is known to be a function of relative humidity and amounts of catalyst present, but is thought to average about three hours.

Hoffert (1972) reviews the principles of chemical reactions in plumes and explains how the law of mass action may be applied to estimate the rate of change of concentration due to chemical reactions. For example, if the following simple set of chemical equations applies:

$$A + B \xrightarrow{k_1} C \qquad (10.65)$$

$$C + D \xrightarrow{k_2} A \qquad (10.66)$$

where the k's are the rate constants ($m^3\ g^{-1}\ sec^{-1}$) for the reactions, then according to the law of mass action the rates of change of concentration of substances A, B, C, and D are

$$dC_A/dt = -k_1\ C_A\ C_B + k_2\ C_C\ C_D \qquad (10.67)$$

$$dC_B/dt = -k_1\ C_A\ C_B \qquad (10.68)$$

$$dC_C/dt = +k_1\ C_A\ C_B - k_2\ C_C\ C_D \qquad (10.69)$$

$$dC_D/dt = -k_2\ C_C\ C_D \qquad (10.70)$$

The concentrations of radioactive substances also change with time, although the variation is usually a simple exponential function of time. For detailed discussions of radioactive effects the reader is referred to Meteorology and Atomic Energy - 1968 (D. Slade, ed.)

10.8 Plume Diffusion in Special Terrain

The term "special terrain" includes all terrain types which are not flat, homogeneous farmland. Most research studies of diffusion have taken place over flat farmland, but most practical diffusion problems occur over more complicated terrain, with hills or shorelines nearby. There is a trend toward building more new industrial facilities in rough terrain, and the interest of these industries in estimating ground level pollutant concentrations is shown by the large number of research papers on this topic in the Proceedings of the recent AMS-APCA Joint Conference on Air Pollution Meteorology (AMS, 1977) and the AMS Fourth Symposium on Turbulence, Diffusion and Air Pollution (AMS, 1979). No comprehensive study of diffusion in rough terrain

has yet taken place, and researchers must rely on the results of several incomplete observation programs. In addition, wind tunnel studies have been very useful; several of these are described in chapters _____ and 16.

The NOAA model (Van der Hoven, 1972) for diffusion in rugged terrain, developed for use at the Four Corners, N.M. power plant, assumes that plumes are deflected above the terrain by an amount equal to the original effective plume height during neutral and unstable conditions, but are not deflected by hills at all during stable conditions. In this model, when a plume strikes a hillside during stable conditions the concentration on the hillside equals the concentration in the plume calculated as if the hill were not there. Naturally the power plant officials objected to this approach because it predicted very high concentration predictions where plumes strike hillsides. The EPA model currently used for rough terrain (Burt, 1976) is similar, but does not permit the plume centerline to get closer than 10m to the hillside before the plume is deflected around the obstacle. A more plausible model, described in a review by Egan (1975), assumes that during neutral or unstable conditions, the plume rises over the obstacle, with the height of the plume centerline over the obstacle equal to one-half of the height of the obstacle above the original centerline height. If the obstacle height is less than the original effective plume height, the amount

of deflection equals one half the obstacle height. During stable conditions, this deflection is assumed to occur around the side of the hill rather than over it. The Gaussian plume model is then used with this new plume centerline trajectory.

The σ's used in the Gaussian plume model should also be changed from those given by the PGT curves. Based on experiments performed by Start et al. (1975) and other experiments reported in the AMS Conference Proceedings (AMS, 1977 and 1979), it is possible to make the prediction that the PGT σ's should be a factor of five to ten greater if the terrain is very rough, and a factor of two or three greater if the terrain is moderate. Much more work needs to be done to refine these predictions.

At the other extreme of special terrain types is a smooth water surface. Raynor et al. (1975) have been studying diffusion over the ocean near Long Island, N. Y., because of the possibility that power plants may be built on offshore sites. They find that diffusion over water is governed primarily by water and air temperature differences. During stable conditions diffusion proceeds very slowly and observed instantaneous σ_y's are a factor of two to five below the PGT stability F curve. Averaged σ_y's show a great deal of scatter, but appear to be slightly less than the appropriate PGT curves. Due to plume meander the hourly average concentration at

a receptor point beneath the thin dense plume is much less than the instantaneous concentration.

10.9 Cooling Tower Plumes

To conserve water, many utilities and industries are constructing cooling towers. A photograph of two large wet natural draft cooling towers is in Figure 10.11. In these towers, warm water is dripped over baffles and broken up into small drops which provide the largest possible evaporation surface. The towers in Figure 1[redacted] have no fans and operate on the same principle as a chimney, but smaller mechanical draft towers have fans to force air circulation through the towers. Dry cooling towers, which operate on the same principle as an automobile radiator, are in operation at a few locations but are often impractical because of the large size required. Characteristics of the various towers are listed in Table 4 and definitions of parameters are given in Figure 10.12.

TABLE 4

Characteristics of Cooling Towers

	height h_s	radius R_o	w_o	$T_{po}-T_{eo}$	$q_{po}-q_{eo}$
Wet Natural Draft	150m	30 m	5m/s	20°C	30 g/kg
Wet Mechanical Draft	20m	5 m	10m/s	20°C	30 g/kg
Dry	200m	60 m	5m/s	20°C	0

10.9.1 Plume Rise of Moist Plumes

On the average, a wet plume as it leaves the mouth of the cooling tower contains about 80% latent heat and about 20% sensible heat. As the plume rises, only a fraction of the latent heat is released at any time. Figure 10.13 contains a psychrometric chart that may be used to determine the latent and sensible heat fluxes in plumes. For example suppose an initially saturated plume is at point p and ambient conditions are those indicated at point e. The rising plume follows the straight line pe from point p until this line is above the saturation curve, in which case the plume is saturated and the saturation curve is followed. The fraction of initial latent heat, δ, that is released is given by

$$\delta = Vq_L/V_o(q_{po} - q_{eo})$$

where V is the volume flux, q_L is the concentration of liquid or condensed water in the plume and $q_{po} - q_{eo}$ is the difference between the initial plume and ambient specific humidities.

To determine the liquid water concentration from figure 10.13 knowing the volume flux ratio V/V_o first find the point 1 on the straight line pe so that $(T_{po} - T_1)/(T_1 - T_e) = (V-V_o)/V$. If point 1 is above the saturation curve, water must be condensed, warming the mixture to point 1'. The liquid water concentration q_L equals $q_{p1} - q'_{p1}$.

In the example on this figure the fraction δ is always less than 20%, implying that plume rise (proportional to the one-third power of the plume heat flux) increases by no more than six percent due to latent heat release. It can be concluded that latent heat effects do not contribute much to total plume rise, and measurements are not yet sufficiently accurate to detect the difference. For single cooling towers, the formulas for stack plumes in section 10.4 can be used, calculating the flux F_o using virtual temperatures. The dividing line for the use of the bent over or calm plume rise equations is recommended as 1 m/s, for the two formulas yield plume rise estimates that are nearly equivalent at that speed, for fluxes and stabilities typical of cooling towers.

The plume trajectory near the source is given by equation (10.42), which is needed in the calculation of visible plume length or drift deposition. Another important parameter, the plume radius R, is related to the plume trajectory. In section 10.4, equations (10.39) and (10.40), it is seen that the effective radii of the temperature and momentum plumes differ. The effective radius R_w of the moisture plume is still different. Meyer et al. (1974) and Slawson et al. (1974) find that the presence of poorly mixed parcels of air in the plume results in condensation occurring at distances beyond where condensation would be predicted using R_m or R_t. Best agreement is obtained using the following values of the entrainment

rate O_w and radius R_w (Briggs, 1975) for the moisture plume:

$$\begin{aligned} &\text{Vertical plume:} \quad O_w = 0.107 \\ &\qquad\qquad\quad\ \partial R_w/\partial z = \partial R_t/\partial z \\ &\text{Bent over plume:} \quad O_w = 0.57 \\ &\qquad\qquad\quad\ \partial R_w/\partial z = 0.71\ \partial R_t/\partial z \end{aligned} \qquad (10.72)$$

Because cooling towers often appear in groups it is necessary to devise ways of estimating the plume rise from multiple sources. There are no good comprehensive cooling tower plume observations that can be used in the development of such a theory, but Briggs (1974) has derived the following enhancement factor E_N, by means of empirical analysis of some data from TVA smoke stacks:

$$E_N = ((N+S)/(1+S))^{1/3} \qquad (10.73)$$

The plume rise from N equal sources equals the plume rise from one source times E_N. The dimensionless spacing factor S is defined by

$$S = 6.0((N-1)\Delta x/N^{1/3}\ \Delta h)^{3/2} \qquad (10.74)$$

where Δx is the spacing between sources and Δh is the plume rise from one source. For a typical power plant with four natural draft cooling towers:

$$N = 4,\ \Delta x = 200m,\ \Delta h = 500m,\ \text{and}\ E_N = 1.17$$

For a single bank of 50 mechanical draft cells:

$$N = 50,\ \Delta x = 10m,\ \Delta h = 100m,\ \text{and}\ E_N = 1.80$$

The plume rise enhancement is barely noticeable at the natural draft towers, but amounts to an increase of 80% for the mechanical draft towers.

10.9.2 Condensation in the Plume

Visible plume and cloud formation are significant environmental effects of cooling towers. The probability of cloud formation increases as the saturation deficit, defined by $q_s - q_e$ decreases. The symbols q_s and q_e refer to the saturated and actual specific humidities of the ambient air, where the variation of the saturated specific humidity q_s with temperature is given by the psychrometric chart in figure 10.13. For condensation to occur at any height, the initial flux of water from the cooling tower, $V_o(q_{po} + q_{Lo})$, must be greater than or equal to the saturation deficit flux, $V(q_s - q_e)$. The specific humidities are known and the ratio of the volume flux of the effective moisture plume at height z to initial volume flux can be estimated from the entrainment laws given previously:

$$V/V_o = (1 + 0.28\ (z/R_o)\ (u/w_o)^{1/2})^2 \quad \text{windy} \qquad (10.75)$$

$$V/V_o = (1 + 0.11\ z/R_o)^2 \quad \text{calm} \qquad (10.76)$$

The ratio u/w_o is used here so that the initial flux of momentum equals the flux of momentum in the bent over plume as height z approaches zero. We obtain the following equations for the height and length of the visible plume (no downwash assumed)

Windy:

$$\text{height } z_\ell = 3.6R_o\ (w_o/u)^{1/2}\ ((q_o/(q_s-q_e))^{1/2}-1) \qquad (10.77)$$

$$\text{length } x_\ell = 3.4\ (R_o^{3/2}u^{3/4}w_o^{3/4}/F^{1/2})\cdot ((q_o/(q_s-q_e))^{1/2}-1)^{3/2} \qquad (10.78)$$

Calm:

$$\text{Height } z_\ell = 9.R_o((q_o/(q_s-q_e))^{1/2}-1) \qquad (10.79)$$

Because it is assumed that ambient variables are constant with height, this method should not be used for plumes that rise through great depths ($\Delta h \gtrsim 200m$).

As relative humidity rises, the saturation deficit rapidly approaches zero, so that the predictions of these three equations are very sensitive to accurate measurements of ambient humidity. For example, the range of relative humidities from 90 to 99% covers an order of magnitude range of saturation deficits.

The method just described is simplified but still includes the basic physics. For applications to plumes at distances beyond where they level off or to boundary layers in which wind speed u or saturation deficit $(q_s - q_e)$ are not constant, models which use differential equations to follow the plume are preferable. Several differential cooling tower plume models are available, including those by Wigley and Slawson (1971), Hanna (1972, 1976), and Weil (1974). These use the equation of motion, the first law of thermodynamics, and equations for water vapor, cloud water, and hydrometer (rain) water, along with the entrainment relations equations (10.39), (10.40), and (10.72) to close the set of equations. Assuming top hat distributions across the plume, it is possible to derive the following basic equations:

Equation of Motion:

$$\partial(w^2/2)/\partial z = (g/E_m\left[(T_p(1 + 0.61q_p/E_w) - T_e(1 + 0.61q_e))/\right.$$
$$\left.(T_p(1 + 0.61q_p/E_w)) - (q_c + q_h)/E_w)\right] - (O_m w^2/R_m) \qquad (10.80)$$

The liquid water is broken down into cloud water q_c (g/g) and hydrometer (rain) water q_h (g/g). The terms E_m and E_w are the ratios of

the cross-sectional areas of the momentum plume to the temperature plume (found to be approximately equal to 2.25) and the temperature plume to the moisture plume (found to be approximately equal to 2.0), respectively. Steady state conditions are assumed ($\partial w/\partial t = 0$). The terms on the right are the buoyant acceleration, the drag due to liquid water drops, and the drag due to entrainment of environmental air.

Thermodynamic Equation:

$$\partial T_p/\partial z = -\left[(L/E_w c_p)\partial q_{ps}/\partial z\right] - g/c_p - \mathrm{O}(T_p - T_e)/R + \left[(L_i/E_w c_p)(q_h + q_c)/\Delta z\right] - \left[(L/e_w c_p)O_w(q_p - q_e)/R_w\right] \qquad (10.81)$$

The term L is the latent heat of vaporization and the term L_i is the latent heat absorbed in the ice-water transition. The terms in square brackets apply only when the plume is saturated. The expression Δz is the vertical height increment in the integration process. The terms on the right side are the heat gain due to latent heat release, the heat loss due to dry adiabatic expansion, the entrainment rate, the heat gained by a phase change of liquid water to ice, and the heat lost as the plume evaporates water in order to saturate the entrained air.

Equation for variation in specific humidity:

Unsaturated $$\partial q_p/\partial z = -O_w(q_p - q_e)/R_w \qquad (10.82)$$

Saturated $$\partial q_p/\partial z = \partial q_{ps}/\partial z \qquad (10.83)$$

Equation for cloudwater change:

$$\partial q_c/\partial z = -\partial q_{ps}/\partial z - 10^{-3}(q_c - 0.0005)/w - 0.00522 q_c (1000 q_h)^{0.875}/w$$
$$- \sigma_w (q_p + q_c - q_e)/R_w \qquad (10.84)$$

The terms on the right-hand side of this equation are the gain due to condensation, the losses to hydrometeor water due to conversion and coalescence (after Kessler, 1969), and the losses due to entrainment. Cloud water is used before hydrometeor water to saturate the entrained air.

Equation for hydrometeor water change:

$$\partial q_h/\partial z = 10^{-3}(q_c - 0.0005)/w + 0.00522 q_c (1000 q_h)^{0.875}/w$$
$$- 4.5 q_h (1000 q_h)^{0.125} \cos(\arctan(w/U))/wR_w \qquad (10.85)$$
$$- \sigma_w q_h/R_w + K_2/\Delta z.$$

The physical meaning of the terms on the right hand side are the gain from cloud water due to conversion and coalescence, the loss due to rainout, the loss due to entrainment, and a final correction term in the numerical process which is used to saturate the entrained air if all the cloud water has been evaporated.

Any consistent equation for the saturated specific humidity can be used. Best agreement with observations of q_{ps} and T are given by the Goff-Gratch formulas (WMO International Meteorol. Tables, 1966), reproduced below:

Saturation specific humidity:

(a) $T_1 = 273.16K < T < 373\ K$

$$\ln q_{ps} = 2.303(10.79574(1-T_1/T) + 1.50474 \times 10^{-4}\ (1-10^{-8.2969(T/T_1-1)}) + 0.42873 \times 10^{-3}\ (10^{4.76955(1-T_1/T)}-1))-5.028\ \ln T/T_1 - \ln p + 1.355 \quad . \qquad (10.86)$$

(b) $T < T_1 = 273.16\ K$

$$\ln q_{ps} = 2.303(-9.09685(T_1/T-1) + 0.87682(1-T/T_1))-3.56654\ \ln T_1/T - \ln p + 1.335 \quad . \qquad (10.87)$$

Given the necessary input conditions at z = 0 and ambient vertical profiles of temperature, wind velocity, and mixing ratio, these equations can be integrated with height to yield vertical profiles of plume parameters. It can be assumed that the plume is initially saturated and that $q_c = q_h = .0005$ g/g. An example of the output of such a model run for the Rancho Seco, Cal., cooling towers is given in figure 10.14. The input data are given by Wolf (1976).

Koenig et al. (1978) used a similar model to study cloud formation by dry and wet cooling towers, given the same total heat flux from both. They found that the plumes from the dry cooling towers generally rose much higher and that the clouds were much larger. The reason for the difference is that the latent heat from the

wet towers is not available unless all the initial water is condensed.

Clouds from cooling towers have not been observed to cause significant precipitation increases. A few isolated instances have been reported in which snowfalls could be traced to cooling towers (Culkowski, 1961; Ott, 1977). While clouds caused by plumes are observed to extend in a narrow band to the horizon, Landsberg (1977) estimates that significant rainfall increases can be measured only within 1 km of the cooling towers.

10.9.3 Drift Deposition Calculations

Drift refers to drops of the circulating water in the tower which are caught in the rising air stream and carried out of the tower mouth. Since the circulating water usually contains dissolved salts and other substances used as fungicides or as rust inhibitors, the deposition of drift drops on land adjacent to the towers may cause harmful environmental effects. The most serious potential exists near towers that use salt water for cooling. However, because of the development of highly efficient drift eliminators, which are sets of baffles that deflect the air flow in the tower, a very small fraction of the circulating water rate (<0.002%) leaves the tower (Holmsberg, 1974). The few measured drift deposition rates at the ground that are available (e.g. Taylor *et al.*,

1974; Environmental Systems Corporation, 1977) suggest that the drift deposition rate of these salts is less than the natural deposition rate. Effects of drift on trees within 200 m of the mechanical draft cooling towers at the Palisades nuclear plant were reported by Rochow (1978). However, studies of trees and other vegetation in the area surrounding the Chalk Point natural draft cooling tower show no detrimental effects of the salt water drift (Lauver et al., 1978; Armbruster et al., 1978).

Deposition calculations for drift drops are made in nearly the same way as the calculations for particles described in section 10.7.1 The eight or ten drift deposition models that are available are reviewed by Chen and Hanna (1978) and Policastro (1978), whose data indicate that most models are similar and that the data are not sufficiently accurate to warrant choosing any one model over the others. Most of these models are described in the proceedings of the symposia Cooling Tower Environment-1974 and Cooling Tower Environment-1978. The chief difference between drift deposition models and particle deposition models is that the drift drops can evaporate, thus changing the fall speed of the drop. The variation of fall speed v_g(cm/s) with drop diameter D(cm) is given by the equations (after Engelmann, 1968):

$$v_g = 3.2 \times 10^5 D^2 \qquad D < .0093 \text{ cm}$$

$$v_g = 6816. D^{1.177} \qquad .0093 < D < .068 \text{ cm}$$

$$v_g = 2155. D^{.746} \qquad .068 \text{ cm} < D < .26 \text{ cm} \qquad (10.88)$$

$$v_g = 1077. D^{.224} \qquad .26 \text{ cm} < D$$

It is important to know the size spectrum of drift drops emitted by the cooling tower. The spectrum observed at the Chalk Point, MD cooling tower during the Dye Tracer Experiment (Environmental Systems Corporation, 1977) given in Table 5 is typical of modern cooling towers. Mass median drift drop size is between 100 and 200 μm for most towers.

Smaller drops with diameters less than about 200 μm are strongly influenced by turbulent diffusion and can be treated using the tilted Gaussian plume hypothesis described in section 10.7.1. However, experience with making these calculations shows that drops with diameters less than about 200 μm do not come to the ground until a distance of several kilometers from the tower, where the resulting deposition rate per unit area is very small.

Maximum drift deposition usually occurs at distances less than one or two kilometers from the tower, and is due to drops with diameters of several hundred microns. A ballistic trajectory is calculated for these drops. Usually calculations are made separately for each of the 10 or 20 drift drop size classes (e.g., one

class may include all drops with diameters between 250 μm and 300 μm). It is assumed that the drops are initially distributed uniformly over the plume cross section. The centerline of the vapor plume, $z_{centerline}$, is assumed to follow a trajectory given by equation (10.41). The bottom of the vapor plume, z_{bottom}, is given by the relation

$$z_{bottom} = z_{centerline} - R_w \qquad (10.89)$$

where the radius of the vapor plume, R_w, is found from equation (10.72). Drift drops of a given class settle in the plume at a constant speed v_g with respect to the rest of the plume. Consequently there are drops continually "breaking away" from the bottom of the plume. A mechanism for estimating the fraction of drops f_i that break away from the plume in the downwind distance interval Δx is illustrated schematically in Figure 10.15. The fraction f_i is given by the formula

$$f_i = (v_g \Delta x_i/u)/2R , \qquad (10.90)$$

which is the ratio of the distance the drops fall in the downwind interval Δx_i divided by the plume diameter at that point. As downwind distance increases, f_i slowly decreases due to the increase in plume radius, and calculations must be stopped when $\sum_i f_i = 1$.

After the drop leaves the plume, it may lose mass, m, by evaporation according to the formula (Hosler et al., 1972):

$$\frac{dm}{dt} = -\pi\delta(q_d - q_e)D\rho Sh \qquad (10.91)$$

where Sherwood number $Sh = 2 + 0.552\ Re^{1/2}/(\delta/\nu)^{1/3}$

δ = diffusion coefficient of water vapor ~0.24 cm^2/s

q_d = specific humidity at drop surface

ρ = air density, g/cm^3

ν = kinematic viscosity of air ~0.15 $cm^2 s^{-1}$

$Re = Dv_g/\nu$, droplet Reynolds number

The difference in specific humidities $(q_d - q_e)$ can be estimated from a relationship given by Mason (1971):

$$\frac{q_d - q_e}{q_e} = \frac{(1 + i\ (M_o/M_s)(m_s/(m-m_s)))^{-1} - RH}{RH + L^2\delta M\ Sh\rho\ q_e/R_g T^2 k_t Nu} \qquad (10.92)$$

where Nusselt number $Nu = 2 + 0.552\ Re^{1/2}\ Pr^{1/3}$

Pr = Prandtl number

R_g = Universal gas constant, 8.31×10^7 erg $mole^{-1}\ {}^{o}K^{-1}$

RH = relative humidity (on scale of 0 to 1.0)

m_s = mass of solute, g

M_s = molecular weight of solute, g/mole

M_o = molecular weight of water, g/mole

i = Van't Hoff factor (usually equal to about 2.0 for sea salt according to Roffman et al., 1973)

k_t = Thermal conductivity of air = 2.4×10^3 erg/cm ^oK sec at 0^oC, 3.2×10^3 erg/cm ^oK sec at 100^oC.

In these formulas it must be assumed that the drop temperature equals the ambient wet bulb temperature. As the drop evaporates and its settling speed decreases, its ballistic trajectory changes slope. The drops in a given size range leaving the plume in the interval Δx_i strike the ground within the range x_{i1} and x_{i2}. The crosswind extent of the deposition can be estimated from the plume angle $\theta = 2R/x$, from the Pasquill-Gifford-Turner σ_y value from figure 10.6, or from observations of the range of wind direction fluctuations during that time period. Then the drift deposition rate ω_{ij} for the mass M_i of drops in that size range leaving the plume in the interval Δx_i is given by

$$\omega_{ij} = M_j f_i / \theta (x_{i2}^2 - x_{i1}^2) \qquad (10.93)$$

The total drift deposition pattern is given by summing the deposition from the various drop size intervals breaking away from the plume in various distance intervals Δx_i.

If the ambient atmosphere is nearly saturated, drop evaporation can be neglected and the ballistic trajectory can be calculated by assuming a constant fall speed. This procedure was followed in an application of the above technique to calculate drift deposition during the Chalk Point Dye Tracer Experiment (Hanna, 1978). Observed (Meyer and Stanbro, 1977) sodium deposition rate on the

0.5 km sampling arc is plotted in figure 10.16. The drift rate predicted by the model is a factor of three greater than observed, and the predicted and observed mass median drop sizes agree within 40%. It is expected that drift deposition models are limited to accuracies of factors of about two to five.

10.10 Line and Area Sources

The Gaussian plume model can be extended to other types of sources. For example, if emissions Q_L(gm/sec m) from a line source such as a well-travelled highway are steady and uniform, then the ground level concentration C at a distance x from the highway is given by the formula:

$$C = (2/\pi)^{1/2} Q_L/(u \sin\theta\ (\sigma_{zo} + \sigma_z(x))), \quad (10.95)$$

where θ is the angle between the wind direction and the highway. The parameter σ_o accounts for the initial mixing at the source, and can be assumed to equal about 3m for automobiles. Calder (1973) shows that this equation is nearly valid for wind directions $\pm$ 60% from the perpendicular to the highway. When the wind blows parallel to a highway of finite length , then the concentration at distance x along the highway and distance y perpendicular to the highway is given by

$$C = (Q_L/\pi u) \int_o^x e^{-y^2/2\sigma_y^2} dx/((\sigma_{yo} + \sigma_y)(\sigma_{zo} + \sigma_z)) \quad (10.96)$$

The initial crosswind σ_{yo} probably equals about five to ten meters.

These relations are most valid for highways in unobstructed level terrain at the same elevation or grade as the adjacent land. For city streets, Johnson et al. (1974) have developed a model which accounts for wind circulations in the street canyons.

Urban regions consist of multiple point, area, and line sources. On an urban scale, the line sources can usually be combined with area sources. Point sources are treated using methods given in section 10.3, and the resulting concentration patterns are superimposed to give the total concentration. Some persons use the McElroy-Pooler (1971) σ_y and σ_z curves, which were derived from diffusion experiments in the St. Louis region. If average concentration patterns are desired, and the standard 16 point wind rose is available, then long term average ground level concentrations from a point source are given by:

$$C = (g_i Q/\pi u \sigma_y (2\pi x/16)) e^{-H^2/2\sigma_z^2} \qquad (10.97)$$

where g_i is the fraction of the time the wind blows from direction i. If wind speed, source strength, and effective source height are also highly variable, then g_i should become a joint distribution function and the average concentration C would be determined from multiple summation.

Area sources can also be handled easily using an application of the Gaussian plume model. The concentration at a point x = 0, y = 0 is due to area source emissions $Q_A(x,y)$ (units g/m^2 sec) from the entire upwind half plane:

$$C(0,0) = \int_{\infty}^{\infty}\int_{o}^{\infty} (Q_A/\pi\sigma_y\sigma_z u)e^{-y^2/2\sigma_y^2}\,dxdy \qquad (10.98)$$

But since the wind usually blows within about a 20^o segment at any given time, it can be safely assumed that the source pattern is a function only of upwind distance x. It is convenient to use the analytical form $\sigma_x = ax^b$. All area source emissions data that we have seen are given in some sort of grid pattern with grid distance Δx as illustrated by the SO_2 emissions data for Frankfurt in figure 10.18. Consequently $Q_A(x)$ is piecewise and equation (10.98) can be integrated to give

$$C=(2/\pi)^{1/2}((\Delta x/2)^{1-b}/ua(1-b))(Q_{AO}+\sum_{i=1}^{n} Q_{Ai}((2i+1)^{1-b}-(2i-1)^{1-b})) \qquad (10.99)$$

where the receptor is assumed to be in the center of the grid block, as in figure 10.18. The power law parameters suggested by M. E. Smith (1968), with a category added for average annual conditions (Pasquill's D), are used:

	Very Unstable	Unstable	Neutral	Pasquill's "D"	Stable
a	0.40	0.33	0.22	0.15	0.06
b	0.91	0.86	0.80	0.75	0.71

It was discovered (Hanna, 1971) that area source emissions patterns were usually sufficiently smooth that the local emissions Q_{AO} in the receptor grid block were all that was needed to simulate observed concentration patterns:

$$C = A\,Q_{AO}/u \qquad (10.100)$$

The following values for the dimensionless factor A are suggested:

neutral or average conditions	A ~ 200	
stable conditions	A ~ 600	(10.101)
unstable conditions	A ~ 50	

Marsh and Withers (1969) find that the grid size Δx which yields the best correlation between observed concentration, C , and grid averaged emissions, Q_{A0} is about 5 km.

The RAM model of the U. S. Environmental Protection Agency (Turner, 1977) is similar to the model just described, and is widely distributed to users. Other models are based on the K diffusion equation, which required the use of sophisticated numerical techniques to reduce errors arising from the finite difference approximations. Liu et al., (1976) discuss the applications of this type of model. All researchers emphasize the importance of accurate knowledge of time and spatial variation of emissions. Wind speed and stability are the most important meteorological parameters. Mixing depth is important only if it is less than about 500 m; otherwise, most of the urban pollution plume remains far below the mixing depth.

10.11 Regional Diffusion Models

Because of the recent emphasis on long range transport of sulfates and other toxic materials, there is great interest in estimating diffusion on scales greater than 50 km. A few models had been developed earlier (e.g., by Crawford, 1966; and Machta, 1970) in order to estimate the spread of clouds of nuclear debris. Crawford (1966) calculates the spread of puffs in the upper atmosphere using estimates of puff σ_y, and Machta (1970) calculates global diffusion using a set of derived K_y and K_z coefficients, given as a function of latitude belt and height.

Recent long range transport models are based more on boundary layer parameters, since the sources of sulfates and oxidants are near ground level. All such models are severely hampered by the lack of observations at these distances. Wind direction shear contributes greatly to diffusion once plumes fill the boundary layer, since the average shear $\Delta\alpha$, is about 30^{o}. Pasquill (1976) suggests that a term $.03\Delta\alpha^2 x^2$ be added to the basic σ_y^2 value in order to account for this effect. Time and space variability in wind lead to further plume distortions, causing several researchers (e.g. Start et al., (1975), Shieh (1978)) to use puff models. The puff center moves with the observed wind, and diffusion is taken care of by an assumed variation of σ_y and σ_z. However, as pointed out in section 10.2.2.2, puff diffusion is relative diffusion and the σ_y and σ_z curves derived from plume observations do not apply to puffs. Researchers using K models must resort to exotic techniques to minimize computational errors.

None of these regional diffusion models is discussed in detail in this section because they are all tentative and based on many assumptions. Experiments are now underway that may be used to make these models more accurate. For example the MAPPPS program (Multistate Air Pollution from Power Production Study) sponsored by the U.S. Department of Energy is measuring sulfur emissions and concentrations and meteorological parameters across the northeastern U.S. (McCracken, 1978).

Acknowledgements: This work was performed under an agreement between the National Oceanic and Atmospheric Administration and the U.S. Department of Energy.

Table 1: Relation of Turbulence Types to Weather Conditions

A-Extremely unstable conditions
B-Moderately unstable conditions
C-Slightly unstable conditions
D-Neutral conditions*
E-Slightly stable conditions
F-Moderately stable conditions

Surface wind speed, m/sec	Daytime insolation			Nighttime conditions	
	Strong	Moderate	Slight	Thin overcast or ≥ 4/8 cloudiness†	≤ 3/8 cloudiness
<2	A	A-B	B	-	-
2	A-B	B	C	E	F
4	B	B-C	C	D	E
6	C	C-D	D	D	D
<6	C	D	D	D	D

*Applicable to heavy overcast, day or night.
†The degree of cloudiness is defined as that fraction of the sky above the local apparent horizon which is covered by clouds.

Table 2: Formulas Recommended by Briggs (1973) for $\sigma_y(x)$ and $\sigma_z(x)$; $10^2 < x < 10^4$ m, Open-Country Conditions

Pasquill type	σ_y, m	σ_z, m
A-B	$0.32x(1 + 0.0004x)^{-1/2}$	$0.24x(1 + 0.001x)^{1/2}$
C	$0.22x(1 + 0.0004x)^{-1/2}$	$0.20x$
D	$0.16x(1 + 0.0004x)^{-1/2}$	$0.14x(1 + 0.0003x)^{-1/2}$
E-F	$0.11x(1 + 0.0004x)^{-1/2}$	$0.08x(1 + 0.0015x)^{-1/2}$

Table 3: Relations Among Stability Classification Schemes

Description	Pasquill	Turner	Brookhaven	$(\frac{Ri}{2m})$	σ_θ(degrees)
Very unstable	A	1	B_2	-.9	25
Moderately unstable	B	2	B_1	-.5	20
Slightly unstable	C	3	B_1	-.15	15
Neutral	D	4	C	0	10
Moderately stable	E	6		.04	5
Very stable	F	7	D	.08	2.5

Table 5: Drop Size Distribution at Mouth of Chalk Point Tower (ESC, 1977)

Drop diameter range (μm)	Percent of total mass	Drop diameter range (μm)	Percent of total mass
10-30	13.8	350-400	0.9
30-50	28.8	400-450	0.7
50-70	13.4	450-500	0.6
70-90	8.9	500-600	1.0
90-110	6.2	600-700	1.0
110-130	4.2	700-800	0.9
130-150	3.4	800-900	0.8
150-180	3.8	900-1000	0.7
180-210	3.0	1000-1100	0.6
210-240	2.3	1100-1200	0.4
240-270	1.7	1200-1300	0.1
270-300	1.3	1300-1400	0.1
300-350	1.4	-	-

References

American Meteorological Society, 1977: Joint Conference on Applications of Air Pollution Meteorology, Salt Lake City, AMS, 45 Beacon St., Boston, Mass. 02108, 413 pp.

American Meteorol. Soc., 1978: Position paper on the accuracy of diffusion models, Bull. Amer. Meteorol. Soc., 59, 1025-1026.

_____., 1979: Fourth Symposium on Turbulence, Diffusion, and Air Pollution, Reno, AMS, 45 Beacon St., Boston, Mass. 02108. 676 pp.

Angell, J. K., P. W. Allen and E. A. Jessup, 1971: Mesoscale relative diffusion estimates from tetroon flights. J. Appl. Meteor., 10, 43-46.

Armbruster, J. A., C. L. Mulchi, L. W. Douglass and D. C. Wolf, 1978: Response of field crops to salt drift from a natural draft cooling tower, Cooling Tower Environment-1978 (see below), 179-196.

Batchelor, G. K., 1950: Application of the similarity theory of turbulence to atmospheric diffusion. Quart. J. Roy. Meteorol. Soc., 76 (328), 133-146.

Batchelor, G. K., 1952: Diffusion in a Field of Homogeneous Turbulence. II The Relative Motion of Particles. Proc. Cambridge Phil. Soc., 48: 345-362.

Brier, G. W., 1950: The statistical theory of turbulence and the problem of diffusion in the atmosphere. J. Meteorol., 7(4), 283-290.

Briggs, G. A., 1969: Plume Rise, AEC Critical Review Series, USAEC-TIC-24635, available from Springfield, VA., National Technical Info. Service (NTIS): vi + 81 pp.

Briggs, G. A., 1973: Diffusion estimation for small emissions, ATDL Cont. No. 79, ATD, P. O. Box E, Oak Ridge, TN 37830, 59 pp.

Briggs, G. A., 1974: Plume Rise from Multiple Sources, Cooling Tower Environment-1974 , S. Hanna and J. Pell, ed., 1974, ERDA Symposium Series, CONF-740302, Nat. Tech. Information Service, U. S. Dept. of Commerce, Springfield, VA., 22161. ($13.60), pp 161-179.

Briggs, G. A., 1975: Plume Rise Predictions, Lectures on Air Pollution and Environmental Impact Analyses, American Meteorological Soc., 45 Beacon St., Boston, MA. 02108, pp. 59-111.

Briggs, G. A. and K. R. McDonald, 1978: Prairie grass revisited, optimum indication of vertical speed. Proceedings NATO/ CCMS Meeting, Toronto, 31 pp.

Burt, E. W. and H. H. Slater, 1977: Evaluation of the VALLEY model, Preprints, Joint Conf. on Appl. of Air Poll. Meteorol., AMS, 45 Beacon St., Boston, Mass. 02108, pp. 192-195.

Businger, J. A., J. C. Wyngaard, Y. Izumi and E. F. Bradley, 1971: Flux-profile relationships in the atmospheric surface layer. J. Atmos. Science, 28, 181-189.

Byzova, N. L. and E. K. Garger, 1970: Experimental study of diffusion parameters with the aid of smoke plumes. Izv. Atmos. & Ocean. Phys., 6, 996-1006.

Byzova, N. L., Ye. K. Garger and V. N. Ivanov, 1970: Experimental estimation of the Lagrangian time scale of turbulence. Izv. Atmos. Oceanic Phys., 6, 315-320.

Carpenter, S. B. et al., 1971 : Principal plume dispersion models TVA power plants. J. Air Poll. Control. Assoc. 21, 491-495.

Chaudhry, F. H. and R. N. Meroney, 1973: Similarity theory of diffusion and the observed vertical spread in the diabatic surface layer. Bound. Layer Meteorol. 3, 405-415.

Chen, N. C. J. and S. R. Hanna, 1978: Drift-modeling and monitoring comparisons, Atmos. Environ., 12, 1725-1734.

Coleman, J. H. and T. L. Crawford, 1978: Characterization of cooling tower plumes from Paradise Steam Plant, Cooling Tower Environment -1978 (see reference), II31-II50.

Cooling Tower Environment-1974, S. Hanna and J. Pell, Ed., 1974, ERDA Symposium Series, CONF-740302, Nat. Tech. Information Service, U. S. Dept. of Commerce, Springfield, VA., 22161, ($13.60), 638 pp.

Cooling Tower Environment-1978, Proceedings, PPSP-CPCTP-22, WRRC Special Report No. 9, sponsored by Power Plant Siting Program, Maryland Dept. of Natural Resources, published by Water Resources Research Center, Univ. Md., College Park, Md.

Crane, G., H. A. Panofsky and O. Zeman, 1977: A model for dispersion from area sources in convective turbulence. Atmos. Environ., 11, 893-900.

Crawford, T. V., 1966: Computer Program for Calculating the Atmospheric Dispersion of Large Clouds, Lawrence Livermore Lab., Rept UCRL-50179.

Csanady, G. T., 1955: Dispersal of dust particles from elevated sources. Australian J. Phys., 8 (4), 545-550.

Culkowski, W. M., 1961: An Anomalous snow at Oak Ridge, Tennessee, Mon. Wea. Rev., 90 (5), 194-196.

Dabbert, W. F., F. L. Ludwig and W. B. Johnson, 1973: Validation and applications of an urban diffusion model for vehicular pollutants, Atmos. Environ., 7, 603-618.

Davies, R. W., 1959: Large-scale diffusion from an oil fire. Advances in Geophysics, Vol. 6, Academic Press 413-414.

Doran, J. C., T. W. Horst and P. W. Nickola, 1978: Variations in measured values of lateral diffusion parameters. Submitted to J. Appl. Met., available from Battelle Pac. NW Lab., Richland, Wash., 21 pp.

Edinger, J. G., 1952: A technique for measuring the detailed structure of atmospheric flow. Geophys. Res. Pap. No. 19, AFGRD, Cambridge, Mass.

Egan, B. A., 1975: Turbulent diffusion in complex terrain. Lectures on Air Pollution and Environmental Impact Analysis (D. Haugen, ed.), Am. Meteorol. Soc., 45 Beacon St., Boston, Mass., 112-135.

Engelmann, R. J., 1968: The calculation of precipitation scavenging. Meteorology and Atomic Energy-1968 (D. Slade, ed.), TID-24190, Nat. Tech. Info. Service, U. S. Dept. of Commerce, Springfield, VA. 22151, 208-220,

Engelmann, R. J. and G. A. Sehmel, 1974: Atmospheric-Surface Exchange of Particulate and Gaseous Pollutants, CONF-740921, Nat. Tech. Info. Service, U. S. Dept. of Commerce, Springfield, VA. 22161, 988 pp.

Engelmann, R. J. and W. G. N. Slinn, 1970: Precipitation Scavenging 1970, CONF-700601, Nat. Tech. Info. Service, U. S. Dept. of Commerce, Springfield, VA., 22151, 499 pp.

Environmental Systems Corporation, 1977: Cooling Tower Drift Dye Tracer Experiment, PPSP-CPCTP, by Environ. Syst. Corp., Knoxville, TN., 103 pp.

Gifford, F. A., 1960: Peak to average concentration ratios according to a fluctuation plume dispersion model. Intern. J. Air Poll., 3(4), 253-260.

Gifford, F. A., 1961: Use of routine meteorological observations for estimating atmospheric dispersion. Nuc. Safety, 2, 47-51.

Gifford, F. A., 1968: An outline of theories of diffusion in the lower layers of the atmosphere. Meteorology and Atomic Energy-1968, (D. Slade, ed.), TID-24190, Nat. Tech. Info. Service, U.S. Dept. of Commerce, Springfield, VA. 22151, 66-116.

Gifford, F. A., 1976: Turbulent diffusion typing schemes - a review. Nuclear Safety, 17, 68-86.

Gifford, F. A., 1977: Tropospheric relative diffusion observations. J. Appl. Meteorol., 16, 311-313.

Hanna, S. R., 1968: A method of estimating vertical eddy transport in the planetary boundary layer using characteristics of the vertical velocity spectrum. J. Atmos. Sci., 25, 1026.

Hanna, S. R., 1971: A simple method of calculating dispersion from urban area sources. APCA Journal, 21, 774-777.

Hanna, S. R., 1972: Rise and condensation of large cooling tower plumes, J. Appl. Meteorol., 11, 793-799.

Hanna, S. R., 1976: Predicted and observed cooling tower plume rise and visible plume length at the John E. Amos Power Plant, Atmos. Environ., 10, 1043-1052.

Hanna, S. R., 1976: Relative diffusion of tetroons pairs during convective conditions. J. Appl. Meteorol. 15, 588-593.

Hanna, S. R., 1978: Diurnal variation of the stability factor in the simple ATDL urban dispersion model. APCA Journal, 28, 147-150.

Hanna, S. R., 1978: A simple drift deposition model applied to the Chalk Point Dye Tracer Experiment, Cooling Tower Environment-1978 (see reference), III105 - III118.

Hanna, S. R. and F. A. Gifford, 1977: Application of the ATDL simple urban dispersion model to Frankfurt, West Germany, Proceedings of the NATO/CCMS 8th Internat. Tech. Meeting on Air pollution Modeling and its Application, 17 pp.

Hanna, S. R., G. A. Briggs, J. Deardorff, B. A. Egan, F. A. Gifford and F. Pasquill, 1977: Summary of recommendations made by the AMS Workshop on Stability Classification Schemes and Sigma Curves. Bull. Amer. Meteorol. Soc.

Hoffert, M. I., 1972: Atmospheric transport, dispersion and chemical reactions in air pollution: a review, AIAA Paper No. 2282, AIAA 10th Aerospace Sciences Meeting.

Holmberg, J. D., 1974: Drift Management in the Chalk Point Cooling Tower, Cooling Tower Environment-1974, S. Hanna and J. Pell, ed., 1974, ERDA Symposium Series, CONF-740302, Nat. Tech. Info. Services, U. S. Dept. of Commerce, Springfield, VA., 22161, ($13.60).pp 128-146.

Hosler, C. L., J. Pena, and R. Pena, 1972: Determination of salt deposition rates from drift from evaporative cooling towers, Department of Meteorology, The Pennsylvania State University Park, PA., 16802

Islitzer, N. F. and D. H. Slade, 1968: Diffusion and transport experiments. Meteorology and Atomic Energy-1968 (D. Slade, ed.) TID-24190, Nat. Tech. Info. Service. U.S. Dept. of Commerce, Springfield, VA. 22151, 117-188.

Izumi, Y. and J. S. Caughey, 1976: Minnesota 1973 Atmospheric Boundary Layer Experiment Data Report. AFCRL-TR-76-0038, Air Force Cambridge Res. Lab., Hanscom AFB, MA. 01731, 28 pp.

Junge, C. E., 1963: Air Chemistry and Radioactivity, Academic Press.

Kaimal, J. C., J. C. Wyngaard, D. A. Haugen, O. R. Cote and Y. Izumi, 1976: Turbulence sturcture in the convective boundary layer. J. Atmos. Sci., 33, 2152-2169.

Kao, S. K., and L. L. Wendell, 1968: Some characteristics of relative particle dispersion in the atmosphere's boundary layer. Atmos. Environ., 2, 397-407.

Kazanski, A. B. and A. S. Monin, 1957: The form of smoke jets. Izv. Atmos. Oceanic Phys., 8, 1020-1033.

Kessler, E., 1969: On the distribution and continuity of water substance in atmospheric circulations, Meteorol. Monographs, 10, 84 + ix pp, published by the Am. Meteorol. Soc., 45 Beacon Street, Boston, MA.

Koenig, L. R., F. W. Murray and P. M. Tag, 1978: Differences in atmospheric convection caused by waste energy rejected in the forms of sensible and latent heats, Atmos. Environ., in press.

Kramer, M. L., D. E. Seymour, M. E. Smith, R. W. Reeves, and T. T. Frakenberg, 1976: Snowfall observations from natural draft cooling tower plumes, Science, 193, 1239-1241.

Landsberg, H. E., 1977: Rainfall variations around a thermal power station, Atmos. Environ., 11, 565.

Lange, R., 1978: ADPIC - A three dimensional particle-in-cell model for the dispersal of atmospheric pollutants and its comparison to regional tracer studies. J. Appl. Meteorol., 17, 370-329.

Lauver, T. L., C. R. Curtis, G. Patterson and L. W. Douglass, 1978: The effects of saline cooling tower drift on seasonal variations of sodium and chloride concentrations in native perennial vegetation, in Cooling Tower Environment-1978 (see above) I49-I96.

Liu, M. K., D. C. Whitney and P. M. Roth, 1976: Effects of atmospheric parameters on the concentrations of photochemical air pollutants. J. Appl. Meteorol., 15, 829-835.

Lyons, W. A., 1975: Turbulent diffusion and pollutant transport in shoreline environments. Lectures on Air Pollution and Environmental Impact Analysis (D. Haugen, ed.), Am. Meteorol. Soc., 45 Beacon St., Boston, Mass., 136-208.

MacCracken, M. L., 1977: MAP3S: Studying the Transport, Transformation, and Fate of Atmospheric Energy-Related Pollutants. DOE/EV-0008/1 and 2. Nat. Tech. Info. Service, U. S. Dept. of Commerce, Springfield, VA. 22161, 72 pp (Part 1) + 114 pp (Part 2)

McElroy, J. L. and F. Pooler, 1968: St. Louis Dispersion Study, U. S. Public Health Service, Nat. Air Poll. Cont. Admin., Report AP-53.

Marsh, K. J. and V. R. Withers, 1969: An experimental study of the dispersion of the emissions from chimneys in Reading-III The investigation of dispersion calculations. Atmos. Environ., 3, 281.

Mason, B. J., 1971: The Physics of Clouds, Clarendon Press, Oxford, England

Meyer, J. H., T. W. Eagles, L. C. Kohlenstein, J. A. Kagan, and W. D. Stanbro, 1974: Mechanical draft cooling tower visible plume behavior: measurements, models, predictions, Cooling Tower Environment-1974. S. Hanna and J. Pell, eds., 1974, ERDA Symposium Series, CONF-740302, Nat. Tech. Information Service, U. S. Dept. of Commerce, Springfield, VA., 22161. ($13.60), pp 307-352.

Meyer, J. H. and W. D. Stanbro, 1977: Fluorescent dye, a novel technique to trace cooling tower drift, presented at 4th Joint Conf. on Sensing Environ. Pollutants, New Orleans, Nov. available from Johns Hopkins Univ., Applied Phys. Lab., Laurel, Md. 20810, 6 pp.

Moni, A. S. and A. M. Yaglom, 1971 and 1975: Statistical Fluid Mechanics, Mechanics of Turbulence, Vol. I and II. (J. Lumley, ed.), The MIT Press, Cambridge, Mass., 769 pp and 874 pp.

Nappo, C. J., 1979: Relative and single particle diffusion estimates determined from smoke plume photographs. Proceedings Fourth Symp. on Turb., Diff., and Air Pollution, 15-19 Jan., Reno, Am. Meteorol. Soc., 45 Beacon St., Boston, Mass., 46-47.

Otts, R. E., 1976: Locally heavy snow downwind from cooling towers, NOAA Tech. Memo. NWS ER-62, National Wea. Service, Eastern Region, 8 pp.

Pasquill, F., 1961: The estimation of the dispersion of windborne material. Meteorol. Mag., 90, 33.

Pasquill, F., 1974: Atmospheric Diffusion, John Wiley and Sons, New York, 429 pp.

Pasquill, F., 1976: Atmospheric Dispersion Parameters in Gaussian Plume Modeling, Part II. Possible Requirements for Change in Turner Workbook Values, EPA-600/4-760306, USEPA, Environ. Sci. Res. Lab., Res. Triangle Park, NC. 27711, 44 pp.

Peterson, K. R., 1968: Continuous point-source plume behavior out to 160 miles. J. Appl. Meteor. 7, 217-226.

Policastro, A. J., W. E. Dunn and M. Breig, 1978: Evaluation of theory and performances of salt drift depoistion models for natural draft cooling tower. Proceeding of 2nd AIAA/ASME Thermophysics and Heat Transfer Conf., Palo Calto, CA., available from Environment Statements Project, Argonne Nat. Lab., Argonne, IL.

Prahm, L. P. and O. Christensen, 1977: Long range transport of pollutants simulated by a 2D pseudospectral dispersion model. J. Appl. Meteorol., 16, 896-910.

Randerson, D., 1972: Temporal changes in horizontal diffusion parameters of a single nuclear debris cloud. J. Appl. Meteor., 11, 670-673.

Raynor, G. S., P. Michael, R. M. Brown and S. Sethuraman, 1975: Studies of atmospheric diffusion near a nearshore oceanic site. J. Appl. Meteorol., 14, 1080-1094.

Readings, C. J., D. A. Haugen and J. C. Kaimal, 1974: The 1973 Minnesota atmospheric boundary layer experiment. Weather, 29, 309-312.

Roberts, O. F. T., 1923: The theoretical scattering of smoke in a turbulent atmosphere. Proc. Roy. Soc. London, A104, 640-654.

Rochow, J. J., 1978: Compositional structure and chemical changes to forest vegetation with fresh water with cooling tower drift. Cooling Tower Environment-1978 (see above), I19-I38.

Roth, P. M., P. J. Roberts, M. K. Liu, S. D. Reynolds and J. H. Seinfeld, 1974: Mathematical modeling of photochemical air pollution, Pt. 2, A model and inventory of pollutant emissions. Atmos. Environ., 8, 97-130.

Sheih, C. M., 1978: A puff-on-all model for computing pollutant transport and diffusion. J. of Applied Meteorol., 17, 140-147.

Shir, C. C. and L. J. Shieh, 1974: A generalized urban air pollution model and its application to the study of the SO_2 distribution in the St. Louis metropolitan area. J. Appl. Meteorol., 13, 185-204.

Slade, D. H. (ed), 1968: Meteorology and Atomic Energy-1968, TID-24190, Nat. Tech. Info. Service, U. S. Dept. of Commerce, Springfield, VA. 22151, 445 pp.

Slawson, P. R., J. H. Coleman, and J. W. Frey, 1974: Some observations on cooling tower plume behavior at the Paradise Steam Plant, Cooling Tower Environment-1974, S. Hanna and J. Pell, eds., 1974, ERDA Symposium Series, CONF-740302, Nat. Tech. Info. Service, U. S. Dept. of Commerce, Springfield, VA., 22161, ($13.60), pp 147-160.

Slinn, W. G. N., 1974: Precipitation scavenging: some problems, approximat solutions, and suggestions for future research. Precipitation Scavenging (1974), ERDA Symposium Series CONF 741003, Nat. Tech. Info. Service, U. S. Dept. of Commerce, Springfield, VA. 22161, 1-60.

Smith, E. J. and K. J. Hefferman, 1956: The decay of the ice-nucleating properties of silver iodide released from a mountain top. Quart. J. Roy. Meteor. Soc., 82, 301-309.

Smith, F. B., 1968: Conditioned particle motion in a homogeneous turbulent field. Atmos. Environ., 2, 491-508.

Smith, F. B., 1972: A scheme for estimating the vertical dispersion of a plume from a source near ground level. Air Pollution: Proceedings of the Third Meeting of the Expert Panel on Air Pollution Modeling. NATO/CCMS Committee, Chapter XVII, 14 pp.

Smith, F. B., 1977: Application of data from field programs to estimation of K profiles and vertical dispersion, TDN No. 86, Meteorol. Office, Boundary Layer Res. Branch, Bracknell, Berkshire, U.K.

Smith, M. E. (ed.), 1968: Recommended Guide for the Prediction of the Dispersion of Airborn Effluents, Am. Soc. of Mech. Engrs., New York.

Smith, F. B., J. S. Hay, 1961: The expansion of clusters of particles in the atmosphere. Quart. J. Roy. Meteorol. Soc., 87 (371), 82-101.

Smith, M. E. and I. A. Singer, 1966: An improved method of estimating concentrations and related phenomena from a point source emission. J. Applied Meteorol., 5, 631-639.

Start, G. E., C. R. Dickson and L. L. Wendell, 1975: Diffusion in a canyon within rough mountainous terrain. J. Appl. Meteorol., 14 (3), 333-346.

Start, G. E. and L. L. Wendell, 1974: Regional effluent dispersion calculations considering spatial and temporal meteorological variations. NOAA Tech. Memo. ERL-ARL-44.

Sutton, O. G., 1953: Micrometeorology, McGraw-Hill Book Co., Inc., New York

Taylor, F. G., Jr., L. K. Mann, R. C. Dahlman and F. L. Miller, 1974: Environmental effects of chromium and zinc in cooling-water drift, Cooling Tower Environment-1974, S. Hanna and J. Pell, eds., 1974, ERDA Symposium Series, CONF-740302, Nat. Tech. Info. Service, U. S. Dept. of Commerce, Springfield, VA., 22161 ($13.60), pp 408-426.

Taylor, G. I., 1921: Diffusion by continuous movements. Proc. London Math. Soc. (2) 20, 196-202.

Turner, D. B., 1969: Workbook of Atmospheric Dispersion Estimates, U. S. Dept. Health, Ed. & Welfare, Environ. Health Service, Pub. No. 995-AP-26, 84 pp.

Vander Hoven, I., 1968: Deposition of particles and gases. Meteorology and Atomic Energy-1968 (D. Slade, ed.), TID-24190, Nat. Tech. Info. Service, U. S. Dept. of Commerce, Springfield, VA. 22151, 202-207.

Vander Hoven, I., 1972: Southwest energy study, report of the meteorology work group, U. S. Dept. of Interior, March 1972, 113 pp.

Weil, J., 1974: The rise of moist buoyant plumes, J. Appl. Meteor., 13: 435-443.

Wigley, T. M. L. and P. R. Slawson, 1971: On the condensation of Buoyant, moist, bent-over plumes. J. Appl. Meteorol., 10, 259-263.

Willis, G. E. and J. W. Deardorff, 1974: A laboratory model of the unstable planetary boundary layer, J. Atmos. Sci., 31, 1297-1307.

Wolf, M. A., 1976: Natural draft cooling tower plume characteristics determined with airborne instrumentations, Pac. Northwest Lab., Annual Rep. for 1975 to the USERDA DBER. Part 3 Atmospheric Sciences, BNWL-2000 PT3, 281-288.

World Meteorol. Org., 1966: International Meteorological Tables, WMO-188-TP-94, Introd. to tables 4.6 and 4.7.

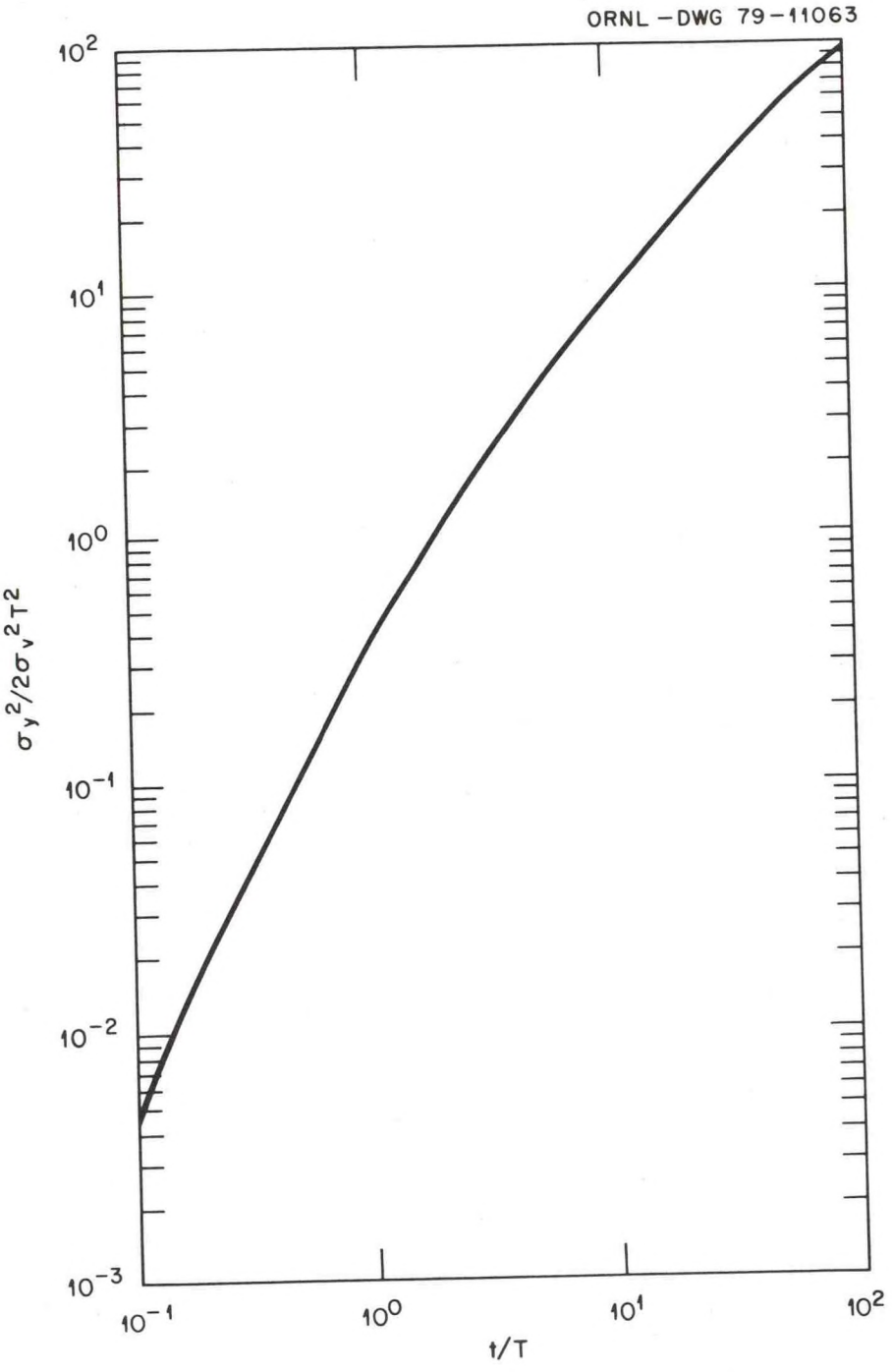

Figure 10.1: Solution to Taylor's statistical diffusion equation for exponential correlation coefficient, $R(\tau) = \exp(-\tau/T)$.

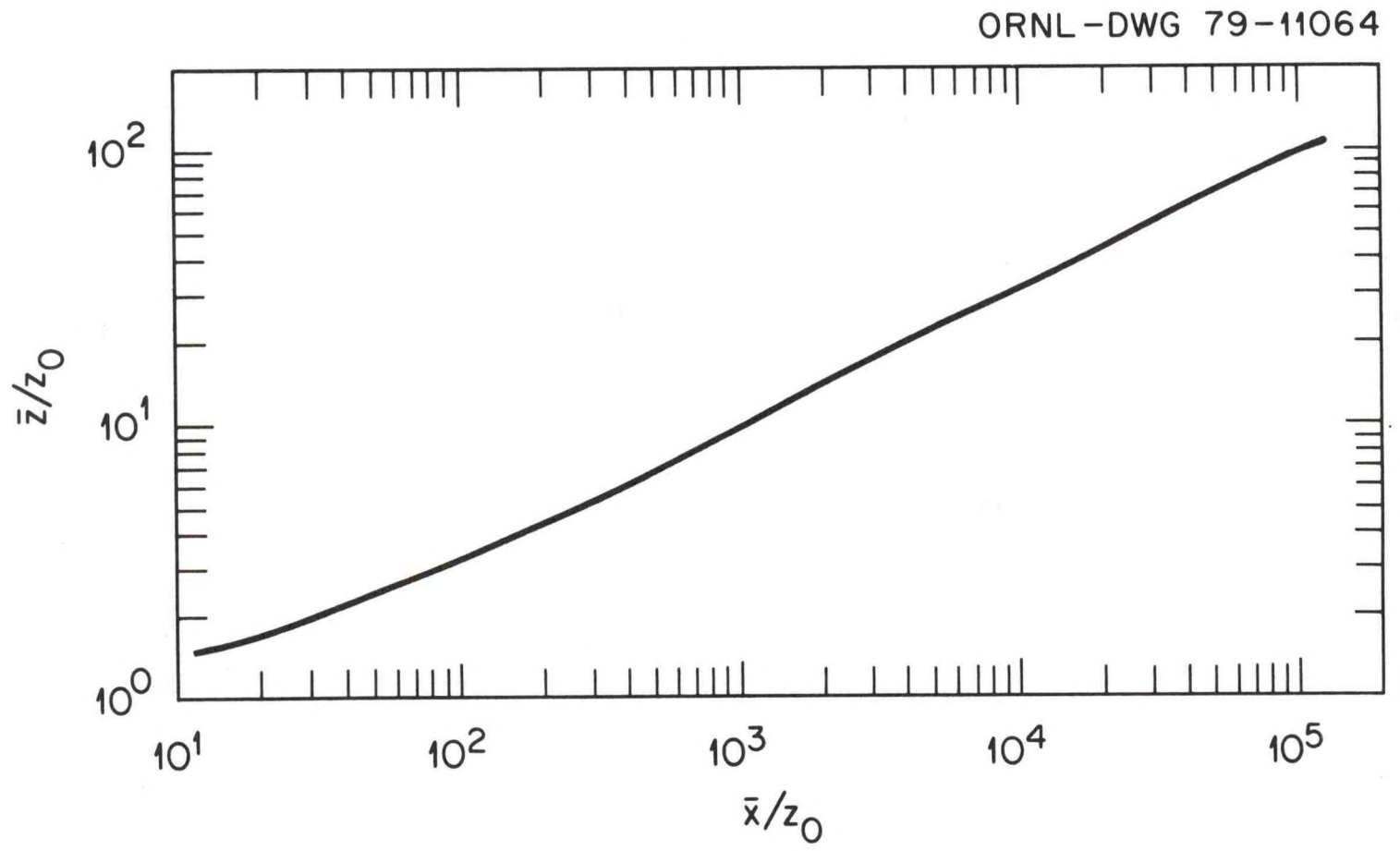

Figure 10.2: Solution to similarity equation (10.17), which gives the variation of mean normalized cloud height with mean normalized downwind distance, for diffusion in the surface boundary layer.

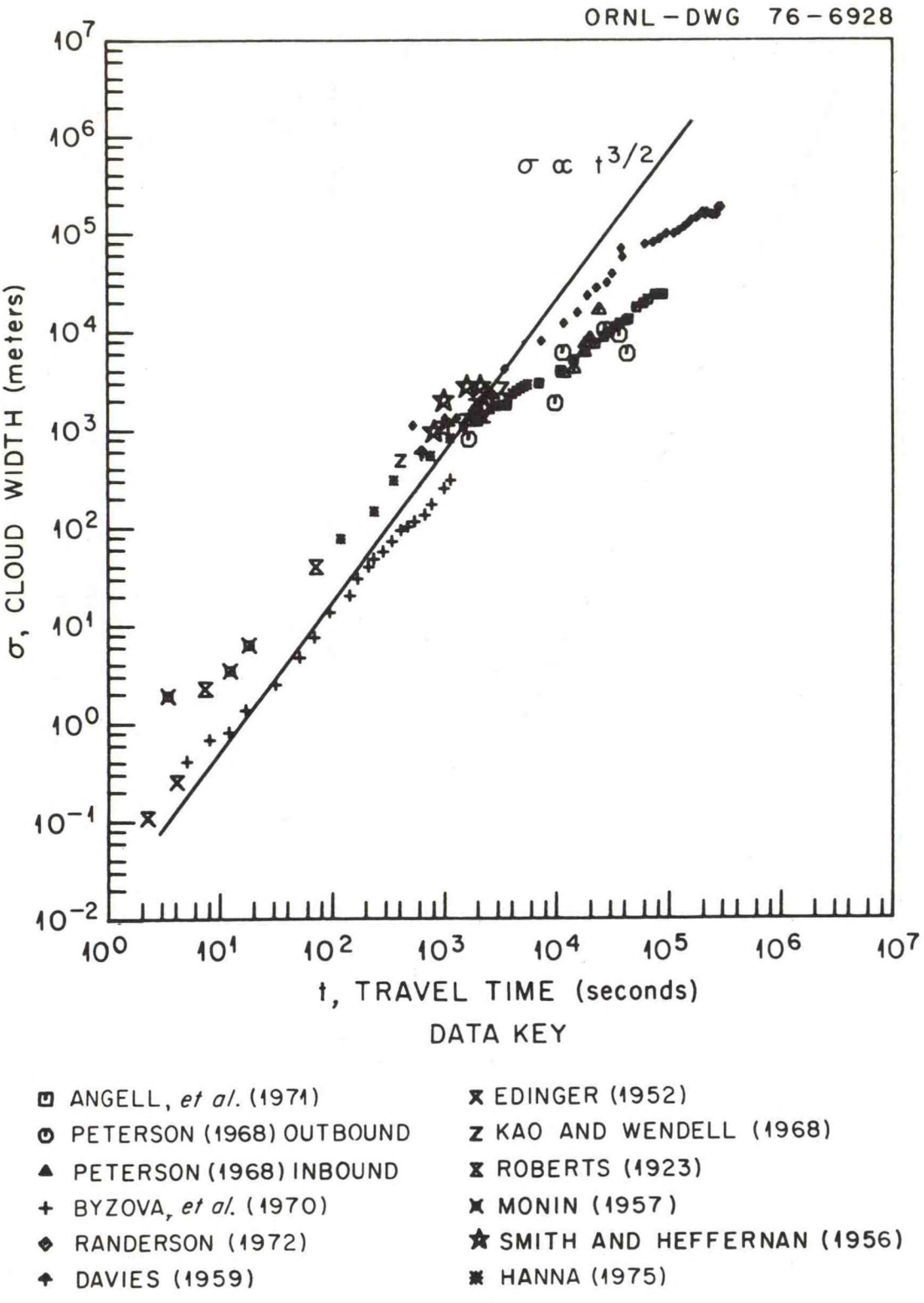

Figure 10.3: Observations of relative diffusion summarized by Gifford (1977).

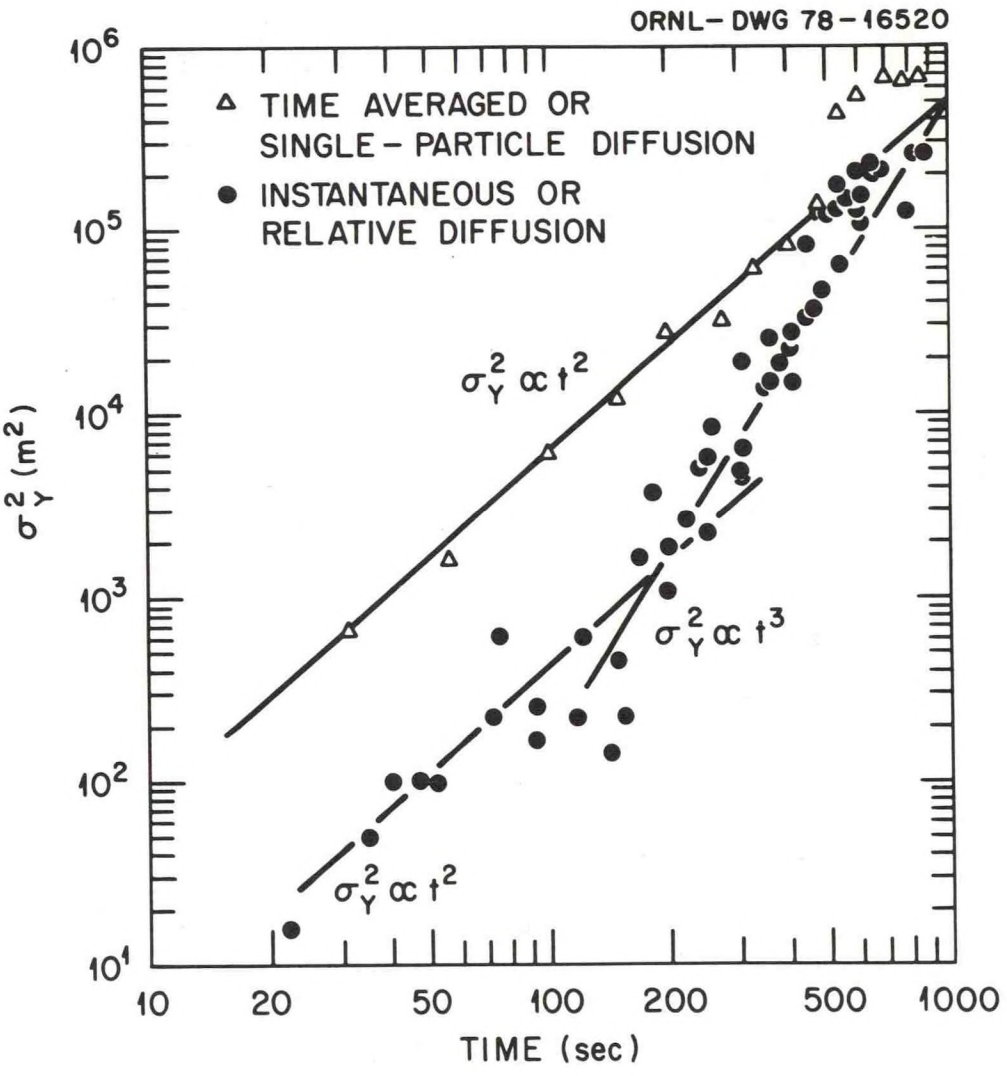

Figure 10.4: Observed $\sigma_y^2(t)$ from photographic studies of diffusion in Idaho Falls (Nappo, 1979). The dots are instantaneous σ_y^2 derived from four individual plume photographs. The triangles are σ_y^2 averaged over the four photographs, referred to an average plume axis. Thus the dots represent relative diffusion ($\sigma_y^2 \propto t^3$ at intermediate times) and the triangles represent continuous source diffusion ($\sigma_y^2 \propto t^2$).

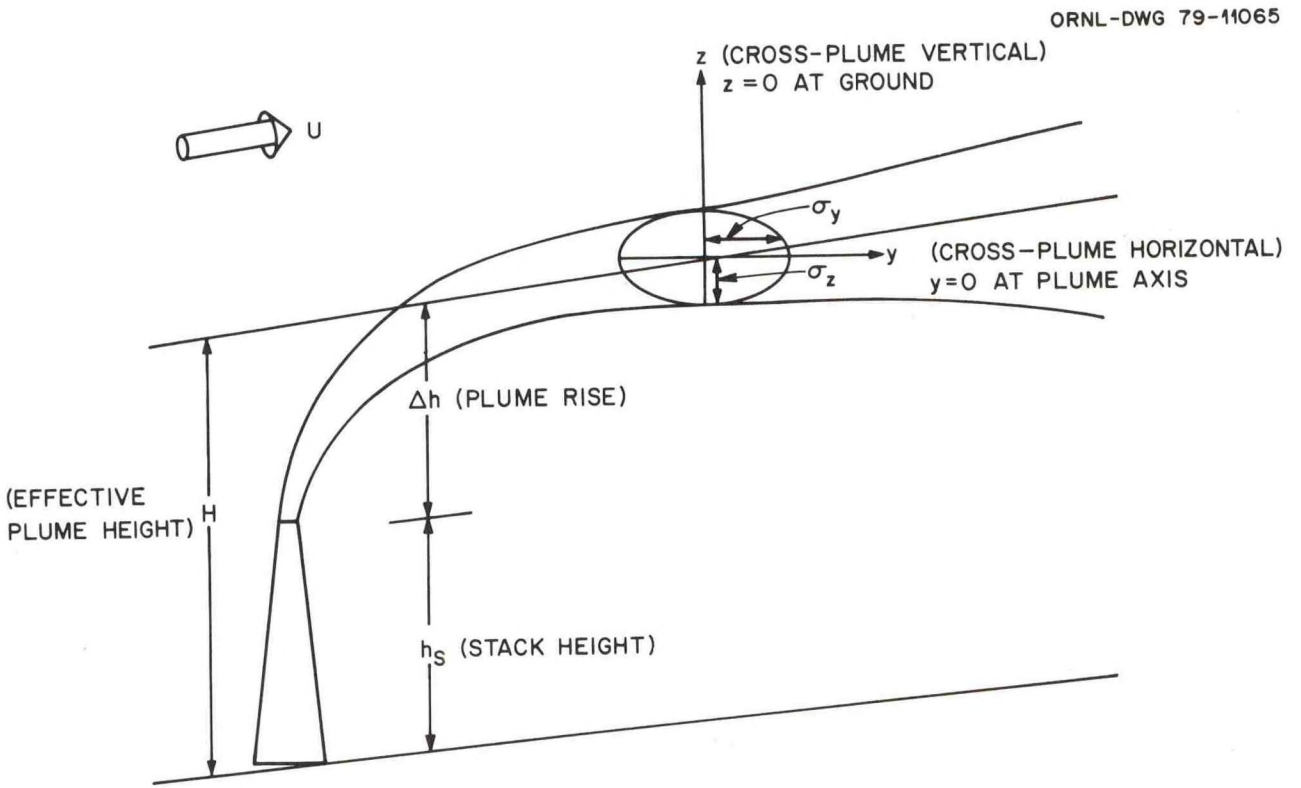

Figure 10.5: Schematic drawing of stack plume illustrating parameters and variables used in the text.

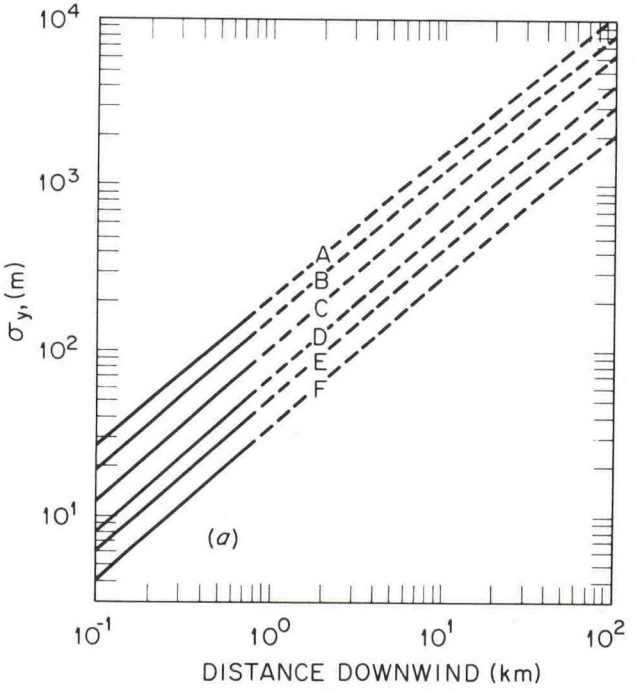

Figure 10.6

Figure 10.6: Lateral diffusion, σ_y, vs. downwind distance from source for Pasquill's turbulence types (Gifford, 1975).

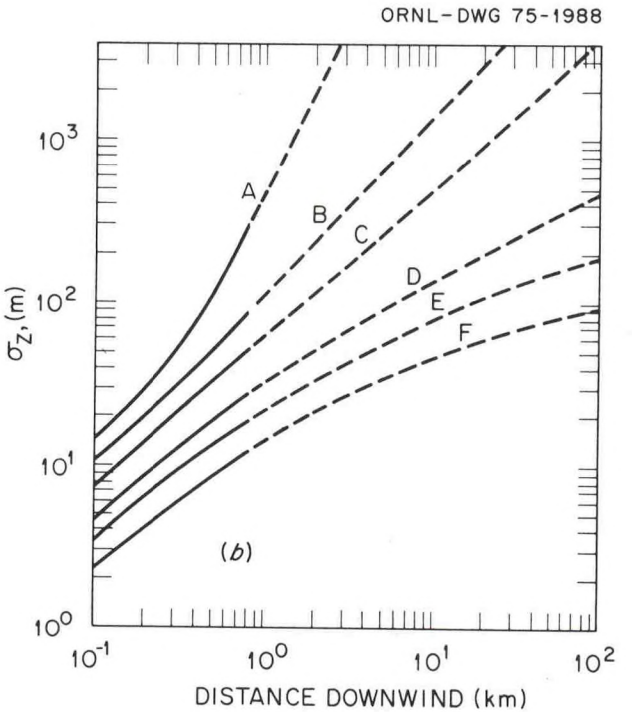

Figure 10.7

Figure 10.7: Vertical diffusion, σ_z, vs. downwind distance from source for Pasquill's turbulence types (Gifford, 1975).

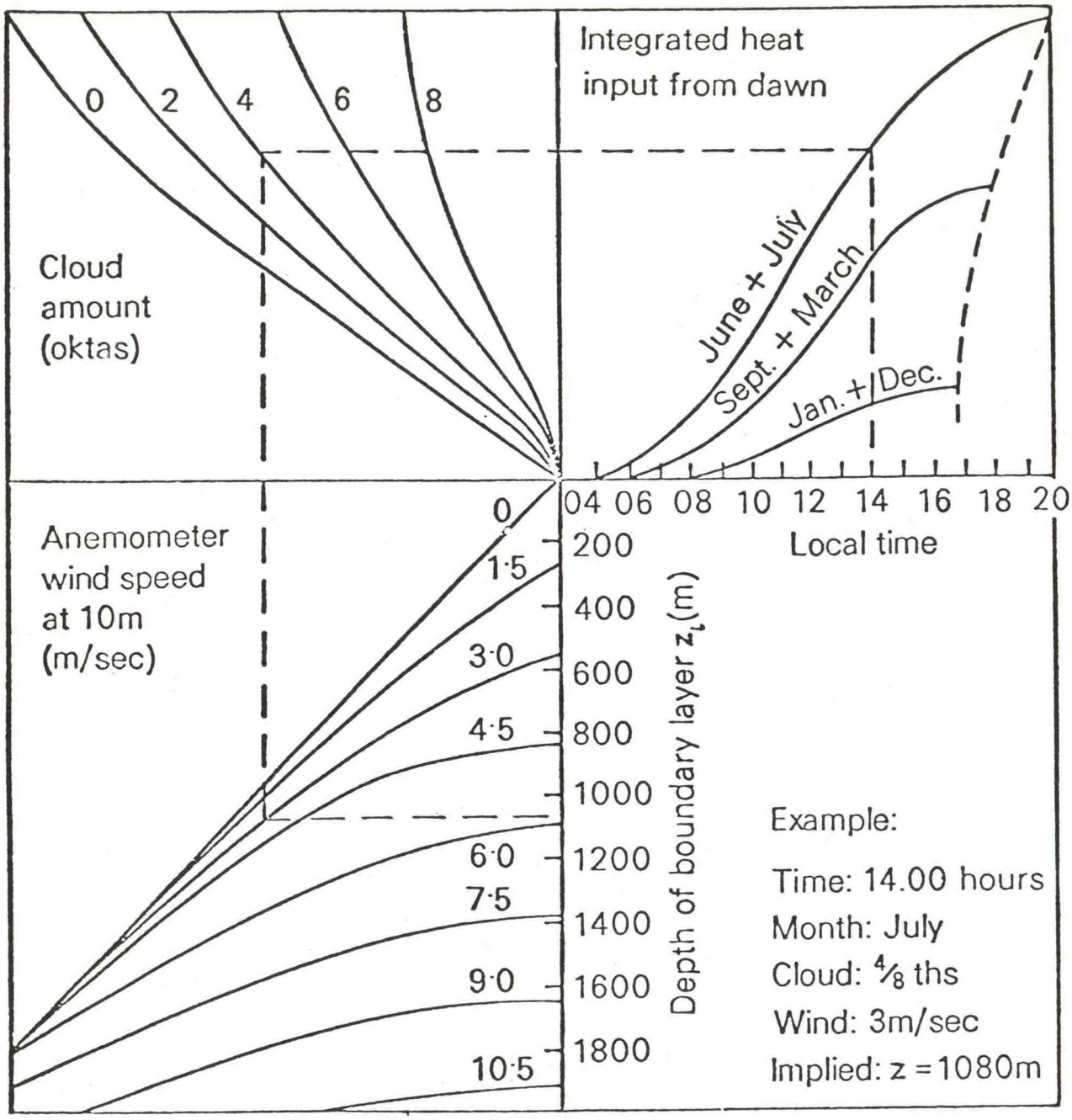

Figure 10.8: A nomogram devised by Smith (1977) for estimating the depth of the boundary layer knowing time of day, month, cloud cover, and wind speed at 10m. This figure is valid in the absence of strong advection or basic changes in weather conditions.

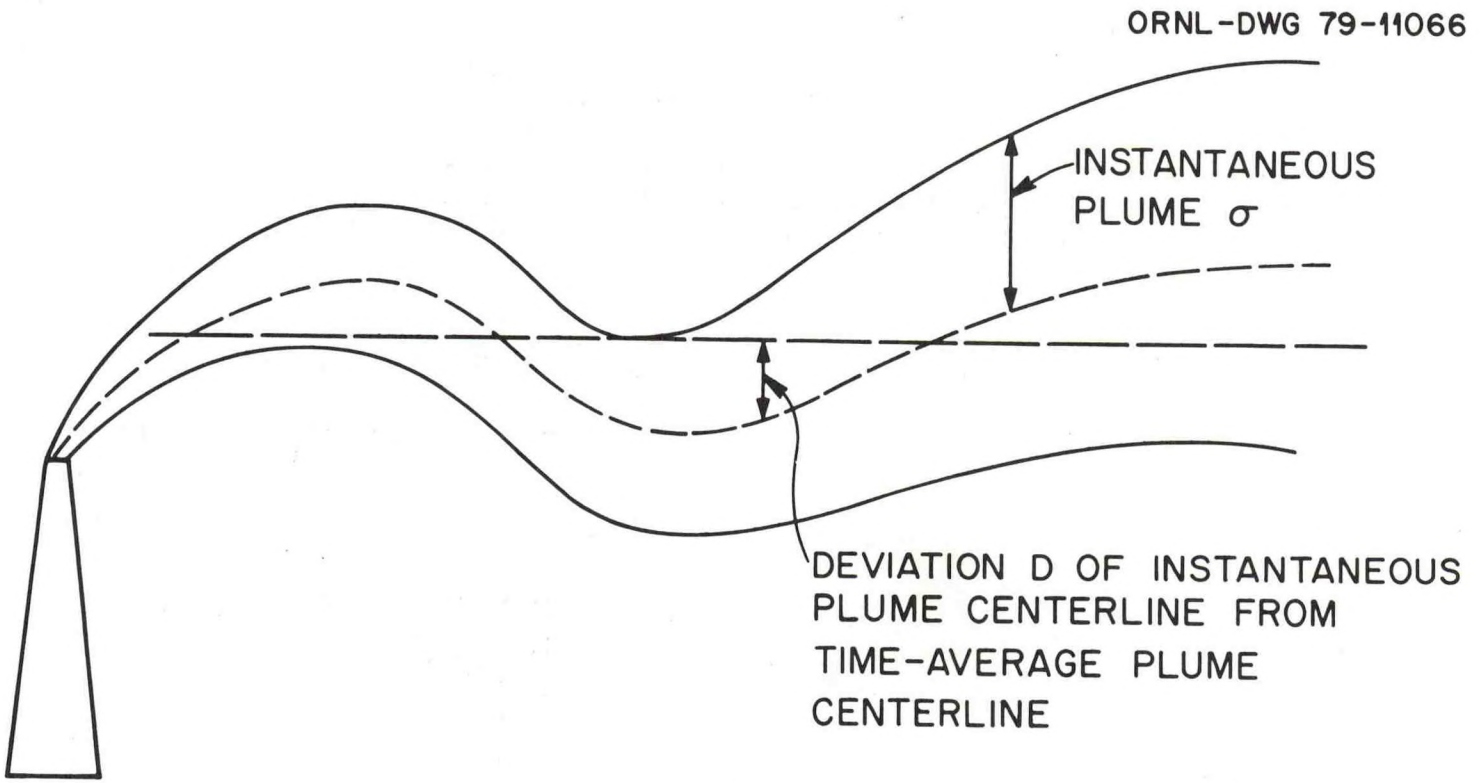

Figure 10.9: Illustration of the instantaneous plume spread (σ) and the deviation of the instantaneous plume centerline (D) from the time-averaged plume centerline (after Gifford, (1960). Total variance of the distribution $\overline{y^2}$ is the sum of σ^2 and $\overline{D^2}$.

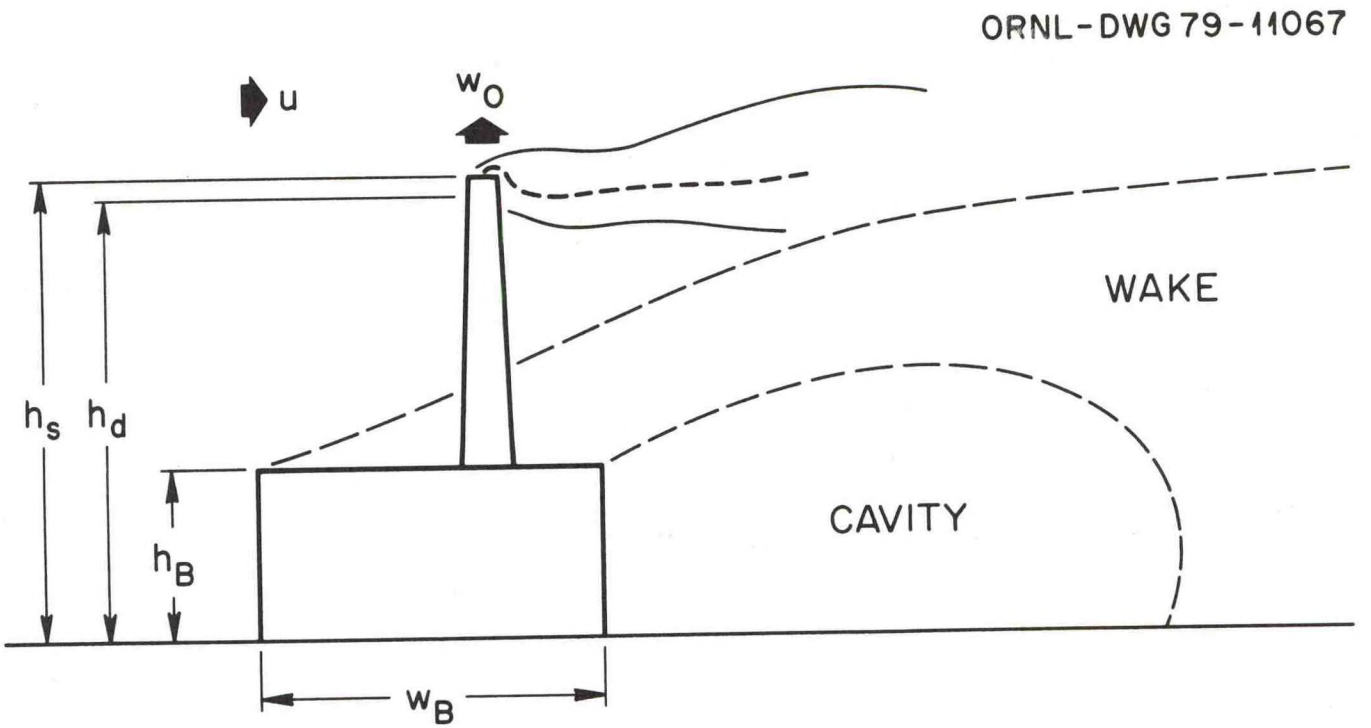

Figure 10.10: Schematic drawing of the parameters affecting diffusion from a stack constructed on or near a building. It is assumed that this building has a square plan with side w_B. Building height is h_B. Stack height and plume centerline height are h_s and h_d. Wind speed and stack effluent speed are u and w_o.

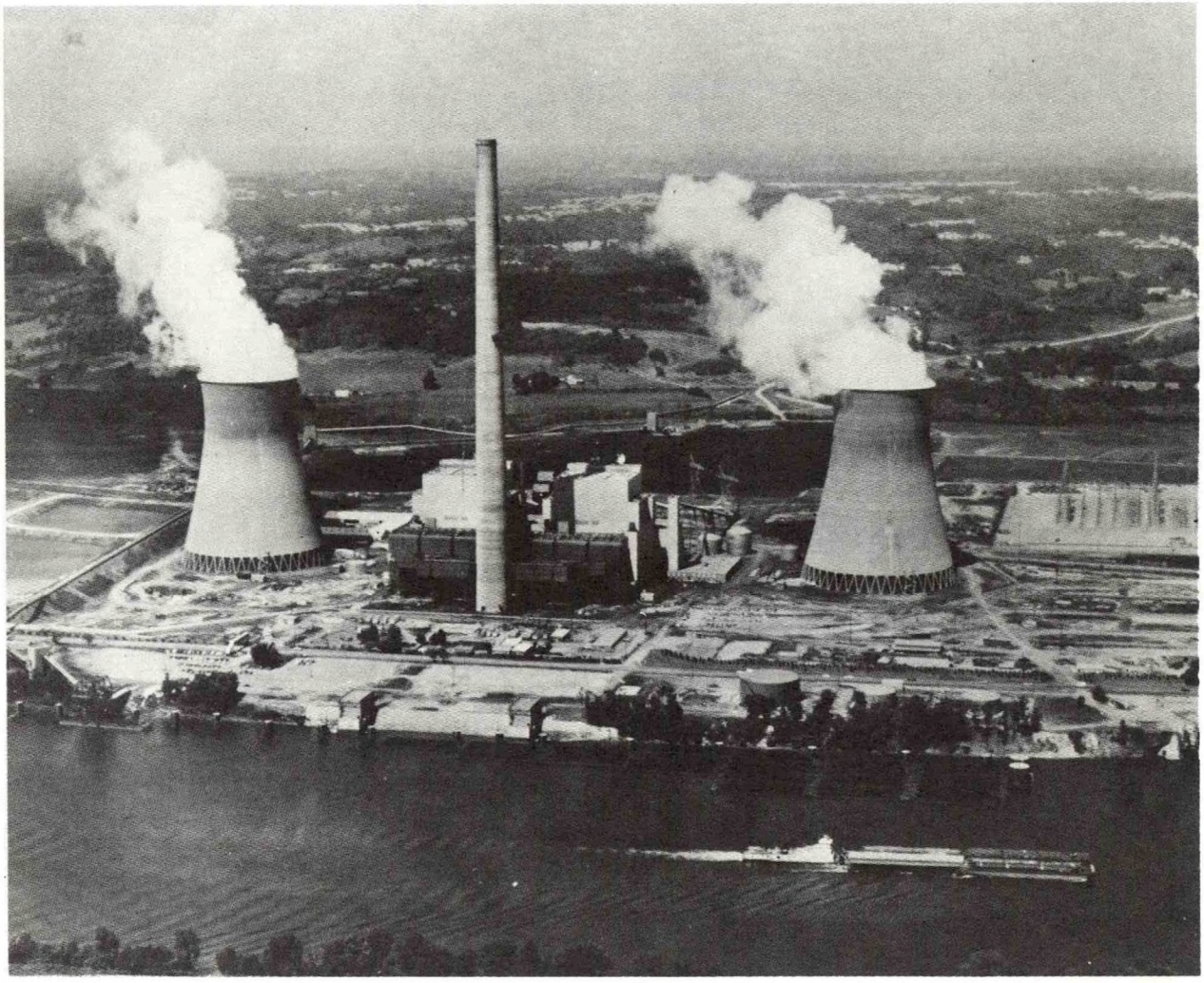

Figure 10.11: Wet natural draft cooling towers (photo courtesy Mark Kramer, Meteorology Evaluation Services, Inc.)

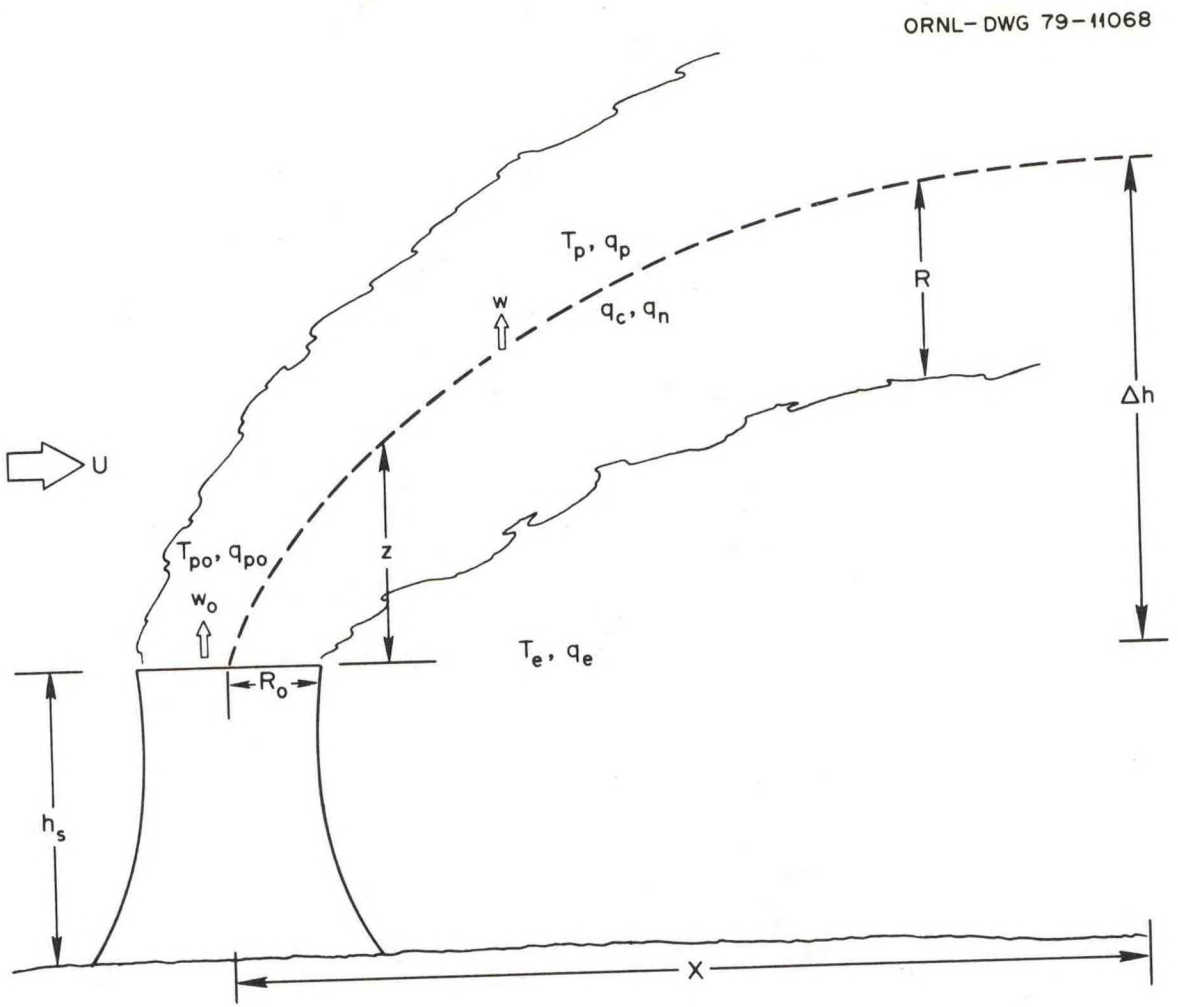

Figure 10.12: Schematic drawing defining parameters important in the analysis of cooling tower plumes.

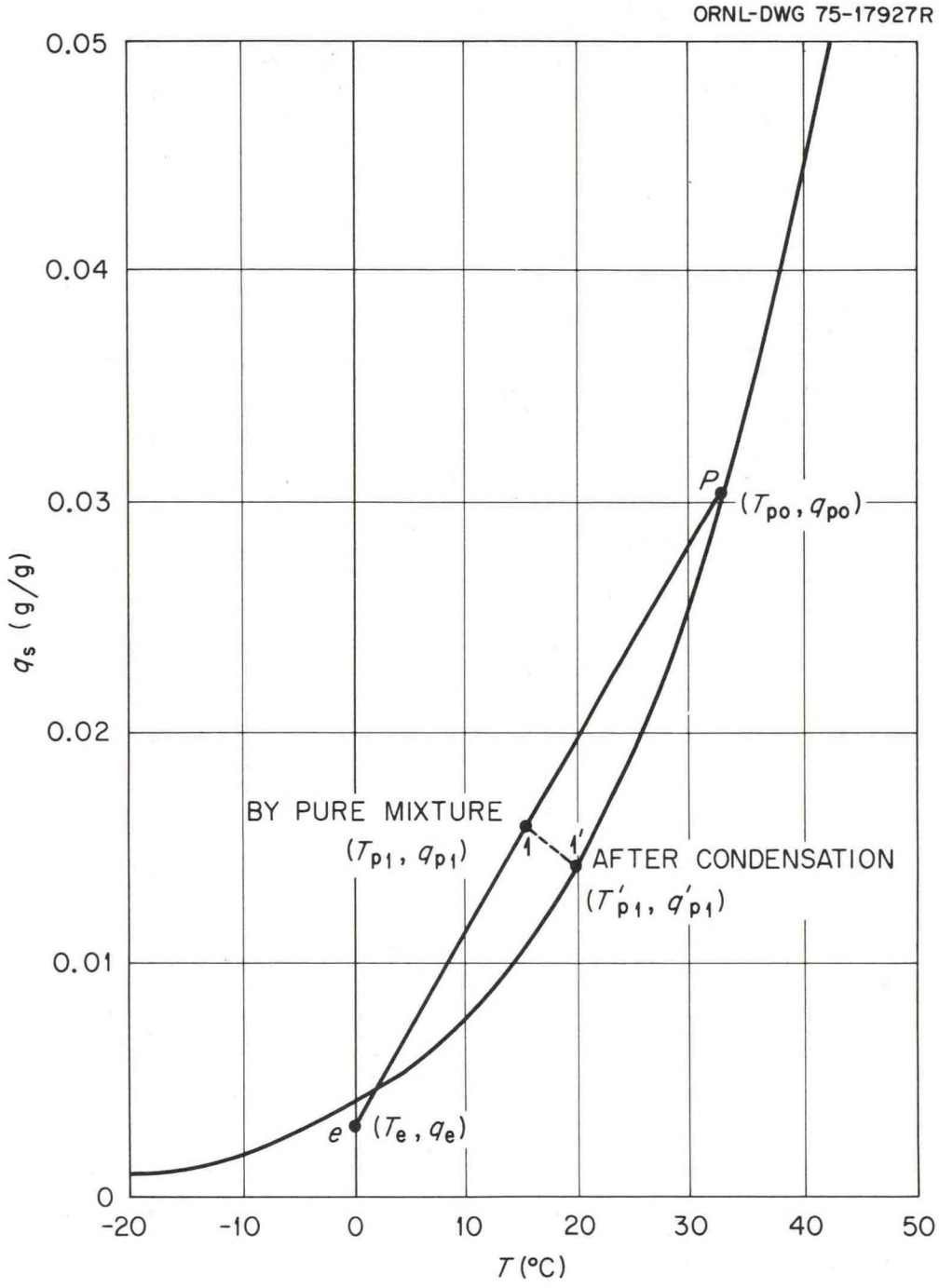

Figure 10.13: Psychrometric chart, in which saturation specific humidity is plotted as a function of temperature. As an illustration, equal parts of plume (subscript o) and environment (subscript e) air are assumed to mix. The mixture arrives at point (T'_{p1}, q'_{p1}) on the curve.

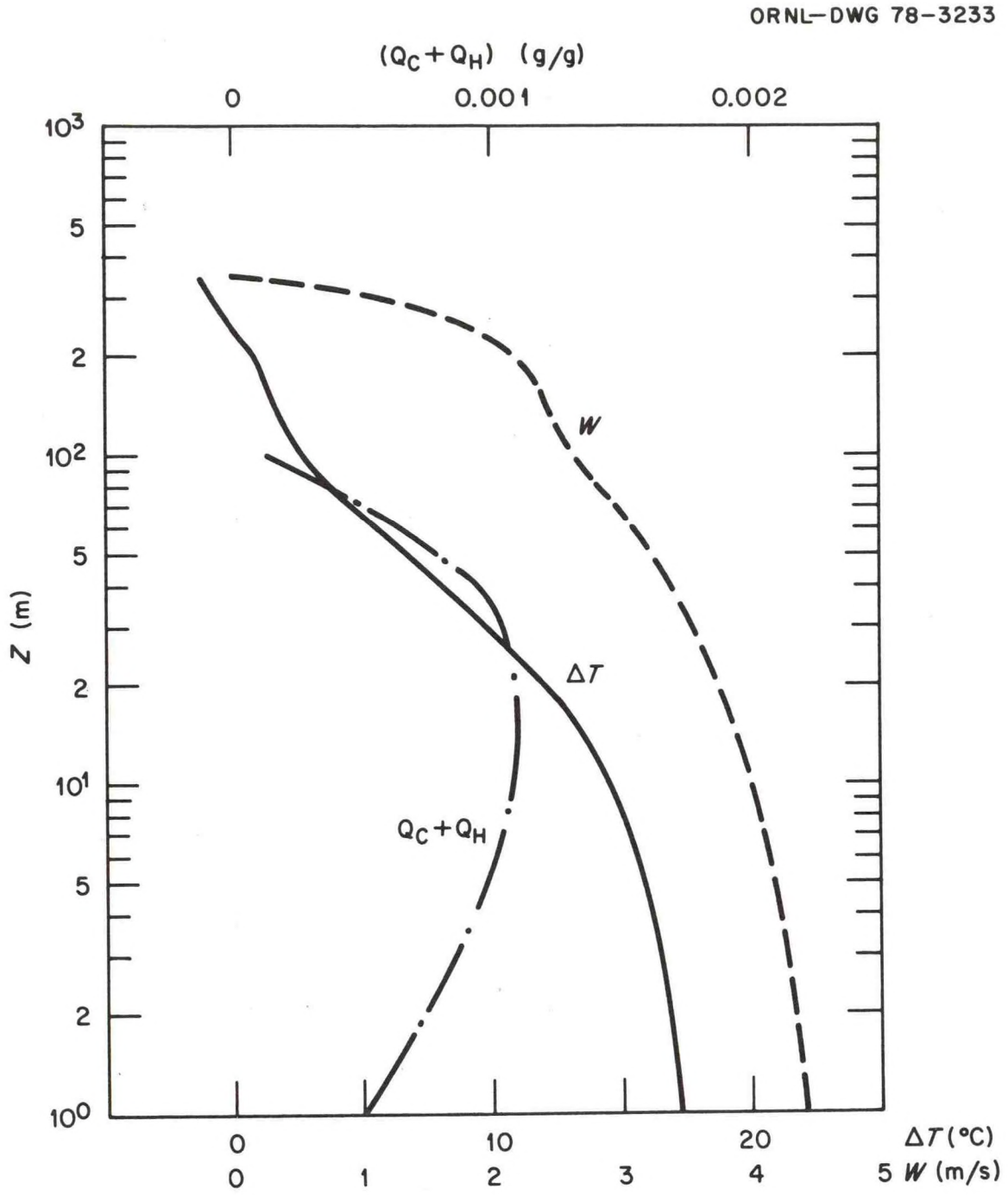

Figure 10.14: Predicted vertical profiles of vertical speed w, temperature excess ΔT, and liquid water content q_L for the Rancho Seco plume, using input data provided by Wolf (1976). Height z is measured above rim of tower, and a top hat distribution of material in the plume is assumed.

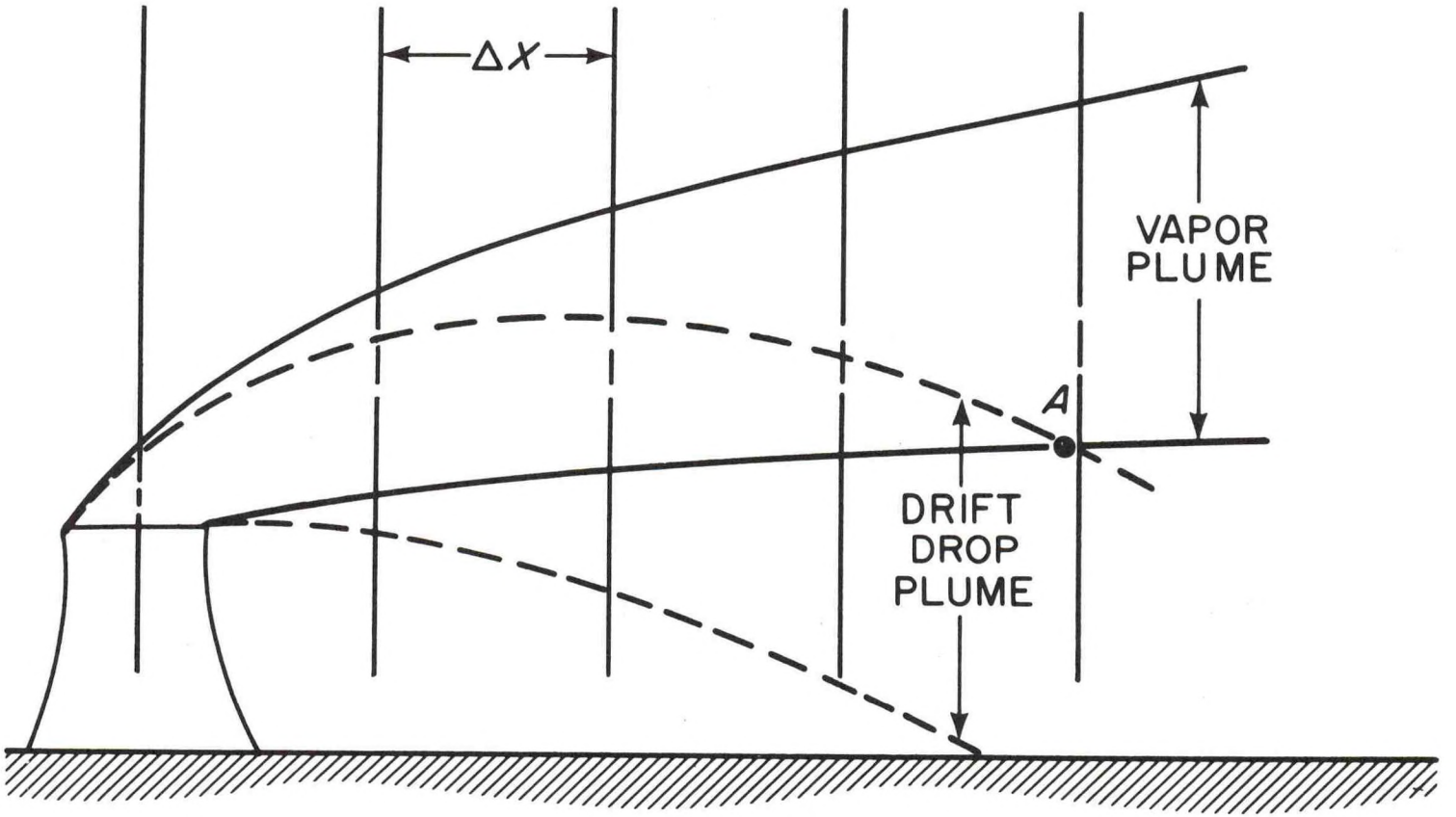

Figure 10.15: Outlines of a cooling tower vapor plume and a drift drop plume (for drops in a narrow size range) are shown, illustrating how the drift drops break away from the humid plume into the drier environment. By point A, all drift drops in this size range have dropped out of the plume. It is assumed that a fraction $(V_g \Delta x/u)/2R$ of the drops break away in the interval Δx.

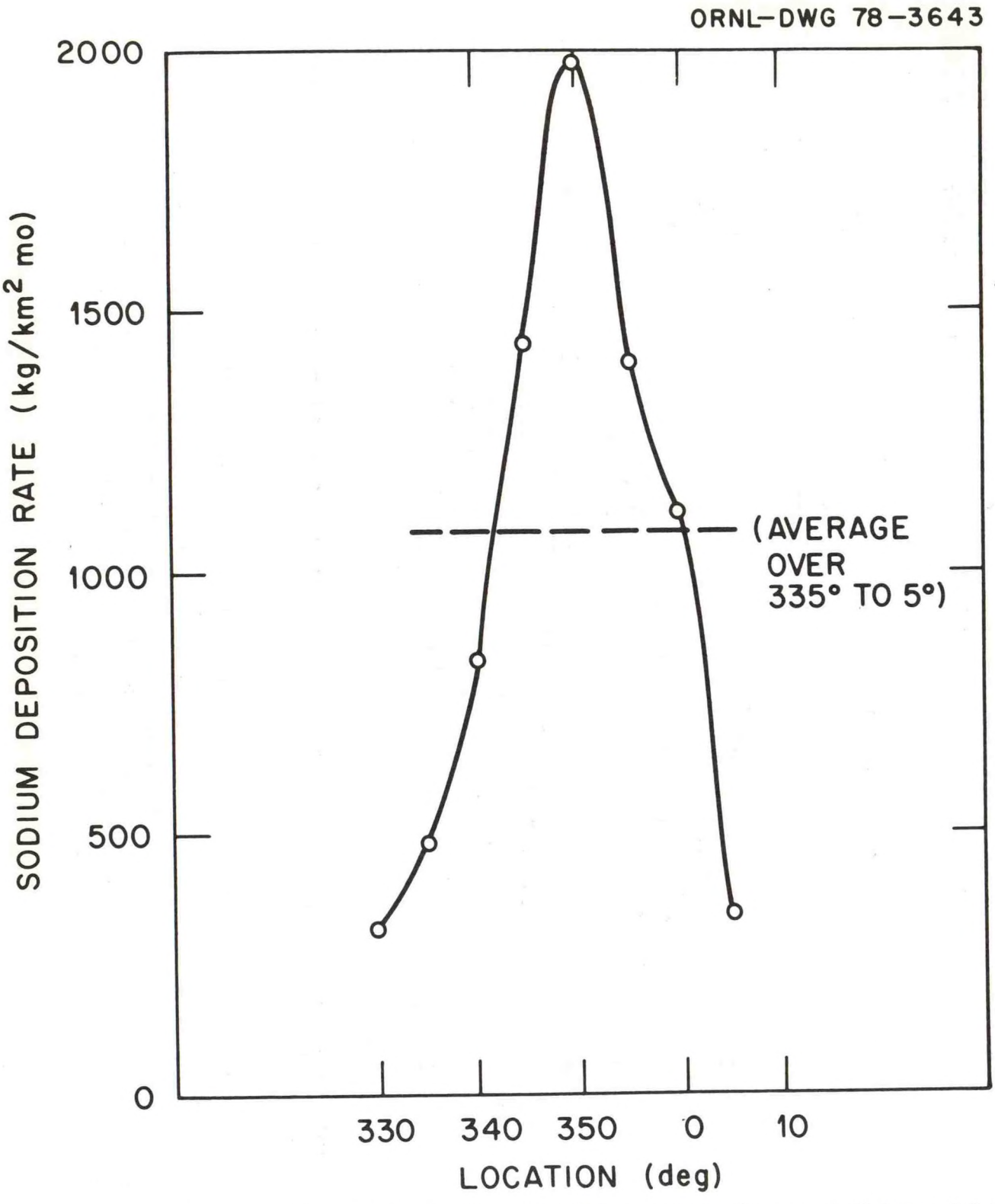

Figure 10.16: Observed sodium deposition rate on the arc at distance 0.5 km from the tower during the Chalk Point Dye Tracer Experiment.

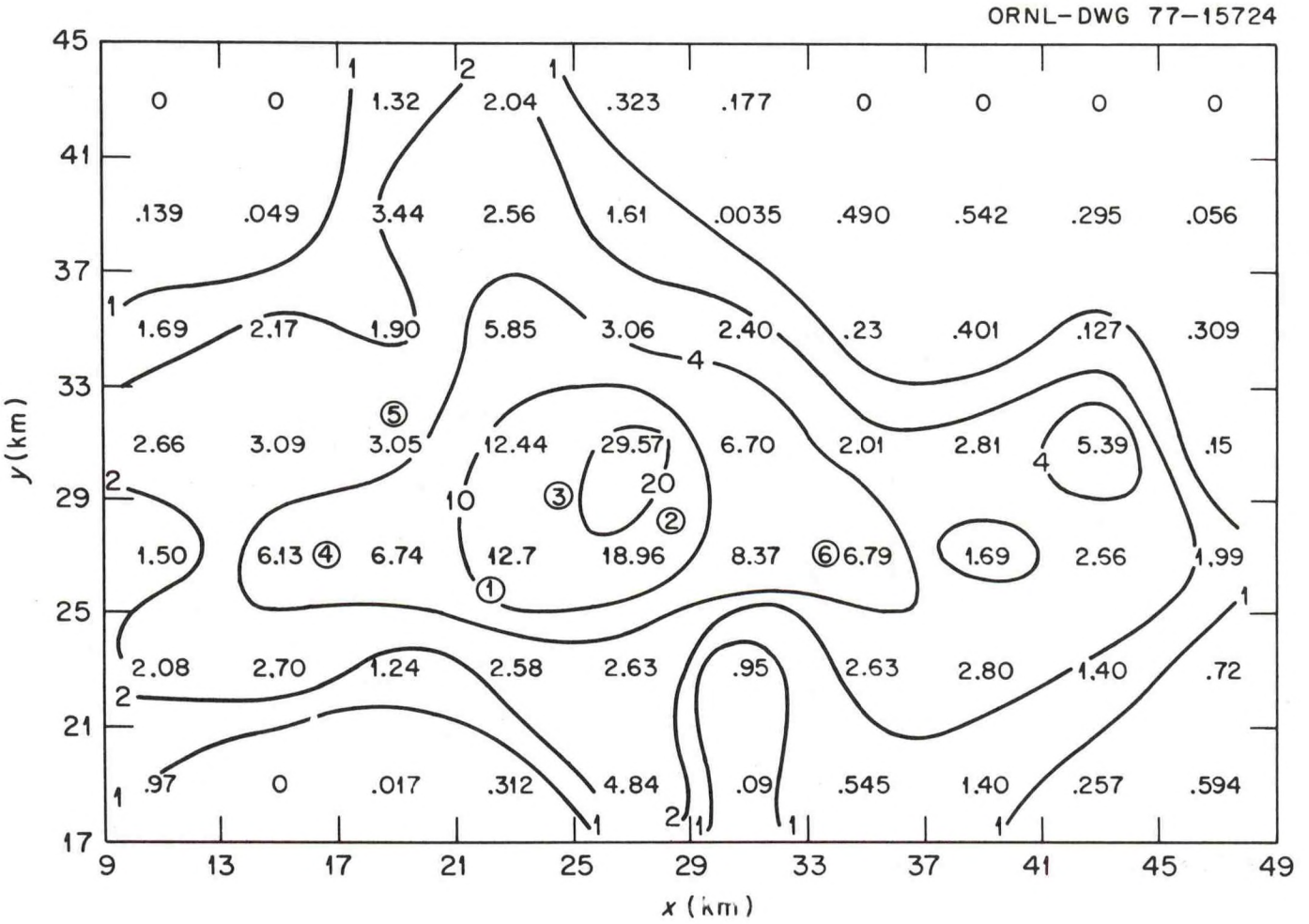

Figure 10.17: SO_2 area source emissions ($\mu g/m^2 sec$) in Frankfurt (Hanna, 1977). The circled numbers indicate locations of sampling stations.

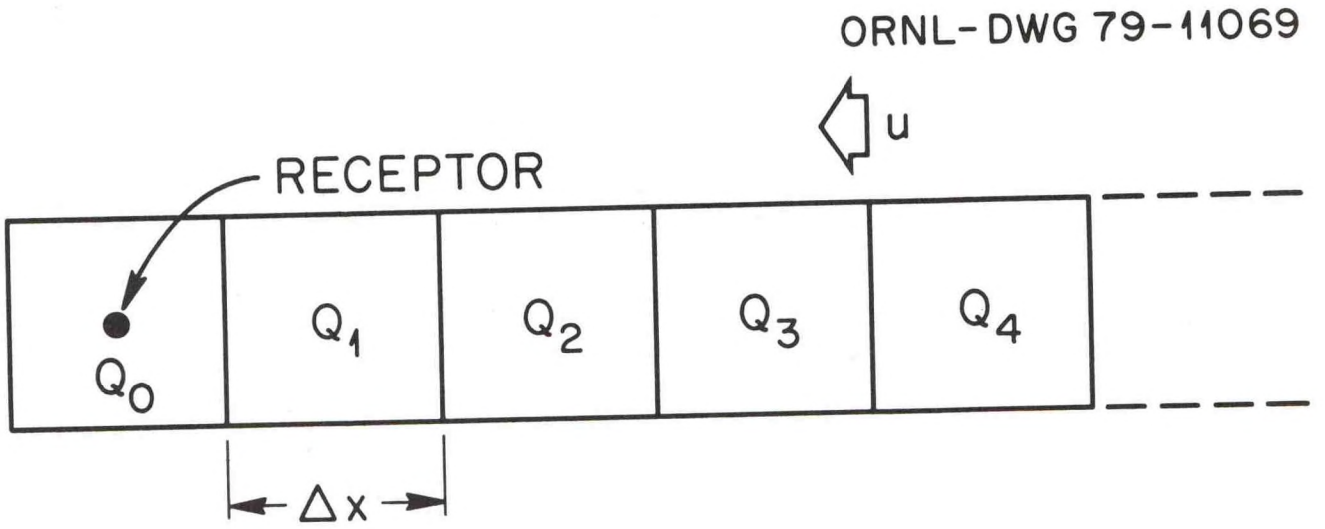

Figure 10.18: Illustration of the square grid pattern and method of assigning subscripts to area source emissions.

PROCEEDINGS OF THE NINTH INTERNATIONAL
TECHNICAL MEETING ON AIR POLLUTION
MODELING AND ITS APPLICATION
28 - 31 August 1978
TORONTO, CANADA

PARAMETERIZING ATMOSPHERIC DIFFUSION

F. A. Gifford

August 1978

A Report of the Air Pollution Pilot Study
NATO Committee on the Challenges to Modern Society
1978

ATDL Contribution File No. 78/11

PARAMETERIZING ATMOSPHERIC DIFFUSION

by

F. A. Gifford
Air Resources
Atmospheric Turbulence and Diffusion Laboratory
National Oceanic and Atmospheric Administration
Oak Ridge, Tennessee USA

Introduction

My assignment, as I understand it, is to summarize the current position of our attempts to parameterize atmospheric diffusion, as a general introduction to the more substantive talks that are to follow in this session. As with all problems that are wholly or mostly controlled by the phenomenon of fluid turbulence, the problem of diffusion of pollutants in the planetary boundary layer has not been solved theoretically despite important recent advances. Consequently all the models, procedures, guidelines, and so on that we use to estimate air concentration patterns necessarily have to rely on a fundamentally empirical understanding of boundary layer diffusion which, however, is continually being reevaluated as new observations and better theory improve our understanding of the structure of boundary layer turbulence.

This understanding has developed and deepened greatly in recent years, as evidenced for instance by results reported in the AMS Workshop on Micrometeorology volume (Haugen, 1973), the definitive book by Lumley and Panofsky (1964), and the emergence of an important new journal, Boundary Layer Meteorology, which is primarily devoted to this subject. As a result boundary layer turbulence structure is now quite well understood from the Eulerian point of view. Diffusion however is a Lagrangian phenomenon. A pollutant cloud is released from some source, which may be elevated or at the surface, fixed or moving, continuous or abrupt, and more or less well-approximated by a point, line, area, or volume. Then this cloud follows some particular space-time path through the boundary layer, during which it grows by diffusion at a rate that depends on the degree of turbulence present in the changing cloud volume along that path. The diffusing and expanding pollutant cloud in effect samples the (Eulerian) field of turbulence in the boundary layer, over a path, and in a growing volume, the exact properties of which must necessarily depend on the particular source location and configuration as well as the prevailing boundary layer turbulence structure.

This situation clearly precludes any such thing as a single, simple, universally applicable diffusion parameterization because for any given (Eulerian) turbulence field, many different samplings are possible, depending on source location and configuration. This unavoidable condition makes the correct parameterization of diffusion a fairly tricky and very source-dependent proposition, a fact that has not always been appreciated in applications.

Diffusion in Idealized Conditions

Diffusion in a steady, horizontally homogeneous boundary layer has been parameterized in various ways, chiefly by specifying either an eddy-diffusivity, K, or the lateral and vertical plume standard deviations σ_y and σ_z. Of these I plan to discuss only the σ's, chiefly because they have been much more widely used in applied studies, but also partly because of problems with the fundamental applicability of K-theory to three-dimensional problems like plume diffusion, as discussed for example by Calder (1965), Monin and Yaglom (1971), and Yaglom (1976). On the other hand K-theory is well known to be a useful description of long-range diffusion from point sources as well as in such essentially one-dimensional applications as vertical heat, mass, and momentum transfer in the boundary layer.

σ_y- and σ_z-Curves

Pasquill (1961) [see also Gifford (1961) and Turner (1969)] summarized existing empirical and theoretical knowledge of boundary layer diffusion from surface-level sources in forms that have subsequently been widely applied in the form of curves of the diffusion lengths $\sigma_y(x)$ and $\sigma_z(x)$, the standard deviations of a diffusing cloud, as a function of atmospheric stability, x being downwind distance. These curves, which are frequently referred to as PG, or PGT curves, were specified to apply to a sampling time of several minutes, to "open country," i.e. a uniform underlying land surface with roughness length equal to several centimeters, to downwind distances up to perhaps a kilometer, and at fairly high latitudes. The PG curves reflected not only the diffusion data base then available but also were consistent with existing theoretical expectations, as Pasquill (1976) has emphasized.

Various alternatives for specifying boundary layer stability conditions, as well as consideration of additional diffusion data, including data for markedly different source height and terrain conditions, have suggested a number of proposals for modifications of, or alternatives to this simple parameterization scheme as workers in the field have confronted increasingly diverse and complex air pollution applications. Gifford (1976) reviewed this considerably body of literature and argued that the real differences to be found among various sets of σ-curves tend generally to reflect differences in source and boundary conditions among the various particular applications involved. Nevertheless, experience has revealed certain problems with applying the original σ-curves, even in the ideal conditions specified. These center around three aspects of the curves; namely, their shape and applicability in conditions of great stability and instability, the question of how to deal with elevated sources, and the problem of specifying the stability condition or "class."

Extension of σ_y-Curve

The PG-$\sigma_y(x)$ curves were presented as a series of parallel straight lines on a log-log plot, having a slope of 0.9. In this respect they strongly reflected the early Porton diffusion data and Sutton's (1932) diffusion theory, which called for a power-law variation of σ_y. This was well supported by the Prairie Grass experiments, which also involved surface-level sources,

and comparatively short travel distances ($x < 800$ m), although the release times were longer (approximately 10 minutes as compared with 3 minutes for the Porton trials). Experimental results for greater downwind distances, as well as expectation based on the asymptotic prediction for long travel time (large x) of Taylor's (1921) diffusion theory, suggest a decrease in the crosswind spreading rate at greater distances. This question has been studied by a number of workers, chiefly Pasquill (1975, 1976), Draxler (1976), Briggs (1974), and Doran, Horst, and Nickola (1978). Pasquill (1976) concludes that both data and theory support use of the relationship $\sigma_y = \sigma_\theta \, xf(x/x_L)$; σ_θ is the standard deviation of the horizontal wind direction fluctuation, x_L is a Lagrangian turbulence length scale, related to the Lagrangian time-scale of turbulence, T_L, by $x_L = U T_L$, and f is a universal function. Values of f based on the available data have been proposed by Pasquill. These values are consistent with PG curves at shorter distances, and agree with the re-examination by Doran, et al., as well as with Briggs' interpolation formulas.

The above-quoted results both extend to greater distances and support the earlier PG-curves of σ_y, placing them in the context of more recent experiments and of developing theoretical understanding of boundary layer turbulence. The main conclusion from the viewpoint of practical applications is to reemphasize the utility of basing estimates of crosswind spread on a representative σ_θ observation, a position Cramer(1957) has long advocated.

The Problem of σ_z

Turning to σ_z we find more, and more difficult problems. The assumption of horizontal turbulence homogeneity over uniform terrain seems to be well justified by experimental results, and this permits various useful theoretical statements, interpolations, and extrapolations to be made about σ_y, within the framework of homogeneous turbulence theory. But vertical spreading from a low-level source in the boundary layer is strongly modulated by two important and related factors; the marked vertical inhomogeneity of the turbulence structure near the ground, and the influence of a definite limit to the depth of the boundary (mixing) layer. Both are crucially influenced by the stability structure of the mixing layer, which is controlled by the prevailing surface-layer heat flux. Again, several investigators are actively studying the resulting problems for the specification of σ_z.

F. B. Smith (1972), see also Pasquill (1974), inferred $\sigma_z(x)$ from numerical solutions to the diffusion equation, primarily in an effort to extend estimates of σ_z to great distances, and presented nomograms by means of which σ_z may be related to the quantities known to govern boundary-layer turbulence, i.e. surface roughness, friction velocity, and heat flux. These curves, as Pasquill (1976) points out, show that the increase in the rate of change of σ_z with x, in unstable conditions, which is quite marked in the PG curve for stability-class A, is maintained only for $x < 100$ m. Various other studies, including the recent Kansas and Minnesota boundary-layer observational results, some results from second-order closure diffusion modeling, and the laboratory and computer modeling studies by Deardorff and Willis (1974) also bear on this problem, and the issues have been discussed in some detail by Pasquill (1976). The problem can not yet be regarded as closed, but some fairly detailed guidance to reliable current practice can be found, in the recommendations

of a recent AMS Workshop on the subject, Hanna, et al. (1977). Their effect is, first, to round off the upward bend of the original σ_z-curve beyond x = 100 m or so, and second to truncate σ_z growth at distances x such that σ_z = 0.8 h, where h is the mixing-layer depth.

Elevated Sources

The considerable differences between σ-curves for surface-level and elevated sources, as judged by comparisons among representative data sets, has been pointed out by a number of workers and discussed for instance by Gifford (1976). Because of the marked variation with height of turbulence in the boundary layer, and the possibility that in some conditions the release height may be above the mixing layer, σ_z-curves for elevated sources typically exhibit marked differences from those from surface releases. Doran, et al. (1978) find that "in neutral and stable conditions σ_z is a generally increasing function of release height" and that differences between surface- and elevated-release σ_z's increased with stability.

The influence of plume buoyancy, summarized in detail by Briggs (1975), is an additional complicating factor, because elevated sources frequently (almost invariably) imply hot, buoyant plumes, the more so the higher the sources is. Buoyancy induces a plume-spreading component (acting both vertically and horizontally), caused by plume-induced turbulence, that is independent of the atmospheric diffusion component, and which to considerable downwind distances is of the same order or exceeds it.

At the moment no particularly neat solution to the impasse created by this situation has been suggested in the form of a simple parameterization. Briggs' interpolation formulas (see Gifford, 1976) try to take the various factors involved into account in such a way as to provide correct estimates of maximum ground level concentration only. They should not be regarded as generally describing the entire concentration distribution of individual plumes. The AMS Workshop (Hanna, et al., 1977) recommends using the σ_z-parameterization that most closely corresponds to the source-type involved, a reasonable if not particularly inspired suggestion, which clearly leaves much room for improvement. On the other hand the various physical effects that are involved appear to be fairly well understood, and so we can reasonably expect that suitably improved parameterization techniques should be forthcoming.

Determining the Stability Class

The prevailing state of turbulence in the boundary layer is usually regarded as varying slowly enough, compared to the sampling times of the diffusion observations upon which σ-curves are based, that the latter can be regarded as determined by a particular, fixed set of boundary layer turbulence parameters, thus defining a turbulence or stability class. Concentration estimates required for longer periods are obtained by averaging over an appropriate number of the basic periods. This approach has proved to be generally satisfactory, at least for downwind distances not too great compared to the time-period over which the turbulence is assumed to be quasi-stationary. But specifying the state of the turbulence, the stability class, in a theoretically satisfactory but practically simple way, has proved to be a problem.

Regulatory agencies naturally prefer a direct, observationally simple method; and a simple $\Delta T/\Delta z$ scheme is currently specified, for instance, in Nuclear Regulatory Guide 1.23, U.S. Nuclear Regulatory Commission (1977). This approach however fails to account correctly for variations in surface heat transfer and roughness conditions among sites and has not generally proved satisfactory. Alternatives that have been suggested emphasize either use of a more fundamental boundary layer turbulence indicator like Richardson's number or the Monin-Obukhov length [Golder (1972), Smith (1972)], or of the horizontal and vertical wind direction fluctuations, σ_θ and σ_ϕ, [Cramer (1957), Pasquill (1976), Draxler (1976), Doran, et al. (1978)]. Briggs (1978) is also attempting to determine optimum methods of specifying the stability class by systematically reanalyzing the classical diffusion data sets in terms of current boundary layer theory. Some preliminary results for the Prairie Grass data have been reported in the study by Weber, McDonald, and Briggs (1977). They conclude from analysis of the Prairie Grass results that, for the usual idealized conditions and a passive (i.e. non-buoyant) tracer, Ri or z/L correlate well with σ_z in unstable conditions, better than σ_ϕ, and much better then $\Delta T/\Delta z$, which "does not correlate at all." In stable conditions, on the other hand, $\Delta T/\Delta z$ relates equally well with the other measures, as long as ΔT is measured in the (possibly extremely shallow) mixed layer.

Exceptional (Non-idealized) Situations

Reviewing the large field of atmospheric diffusion applications, Gifford (1975) identified a number of important problems for which the assumption, which governs all the preceding discussion, is no longer valid that diffusion is driven solely by mechanical and thermal turbulence components in a uniform boundary layer. These include: diffusion over rugged terrain, water, forests, cities, in building and obstacle wakes, and in near-calm stable conditions. In each of these cases the standard, open-terrain diffusion parameters that we have been discussing are considerably influenced by turbulence fluctuations from sources additional to those described by the usual boundary layer thermal and mechanical parameters. Over rugged terrain plume diffusion is enhanced by fluctuations induced by gravity and slope flows, shed vortices, wakes, and flow separations, and as well as by a generally more vigorous, rough-terrain type of mechanical turbulence. In wake flows behind obstacles such as buildings, invariably present near pollutant sources, the decisive question in the first place is usually whether or not the plume is trapped within the wake. Over cities the thermal and mechanical turbulence components are augmented by the large roughness elements and great heat storage capacity, and the latter also markedly modifies the usual, open-country diurnal march of stability conditions. Diffusion in forests is very poorly understood. The scarce data available suggest the possible importance of a kind of turbulence intermittency, in which bursts of turbulence from time to time perturb the usually sluggish forest flow. Diffusion in near-calm, stable conditions, which is very slow on an instantaneous basis, has been observed to be greatly increased by horizontal plume meandering, when averaged over half an hour or so. Over water the interaction between wave development and the boundary-layer structure greatly complicates treatment of the mechanical turbulence component; the waves can only in part be treated as roughness elements. The thermal component is strongly controlled by the air-water temperature difference, and both components are influenced by "fetch" over water. The parameterization of diffusion in all these cases is in its infancy. Gifford's (1976) review and especially the comprehensive survey undertaken by Draxler (1978) summarize the existing data and results. Lack of

suitable diffusion parameterizations in essentially all these cases is a serious obstacle to air pollution modeling because, however exceptional cases may appear compared to the idealized, uniform-terrain situation, for which diffusion parameterizations are best known and most successful, they are all too common in practice, and comprise the bulk of practical applications.

Conclusions

In summary, there is some good news and some bad. Our diffusion parameterizations for ground-level sources in idealized, open-terrain conditions and fairly short travel times rest on a secure and reasonably complete data base, although more observations of vertical plume spread in all conditions, and of the complete plume geometry during conditions of active buoyant convection are necessary. Recent observations of diffusion from elevated sources, and improved understanding of the vertical structure of turbulence, should soon resolve the problem of parameterizing elevated source diffusion, although at the moment, as Weber (1976) remarks, we have no specific way to do this. Empirical diffusion parameterizations are being diligently revised to reflect current improvements in our understanding of boundary layer structure. On the other hand most practical problems involve important, but at present poorly observed and understood departures from the idealized parameters. Extension of parameterizations to great distances is also a difficult question, for which neither theory nor observation is at present providing satisfactory answers. All in all much work remains to be done, and the program for this session should provide useful contributions to many of these important problems.

References

Briggs, G. A., 1974: Diffusion estimates for small emissions, in NOAA-Atmospheric Turbulence and Diffusion Laboratory 1973 Annual Report, U.S.AEC Report ATDL-106, Dec. 1974.

Briggs, G. A., 1975: Plume rise predictions. In Lectures on air pollution and environmental impact analysis, D. Haugen, ed., Am. Meteor. Soc., iii and 295 pp.

Briggs, G. A., 1978: See his paper in this proceedings.

Calder, K. L., 1965: On the equation of atmospheric diffusion, Quart J. Roy. Meteor. Soc., 91, 514-517.

Cramer, H. E., 1957: A practical method for estimating the dispersal of atmospheric contaminants. Proc. First National Conf. on Applied Meteor., pp C-33 to C-55, Am. Meteor. Soc., Hartford, Conn., Oct. '57.

Deardorff, J. W. and G. E. Willis, 1974: Computer and laboratory modeling of the vertical diffusion of non-buoyant particles in the mixed layer, Adv. in Geophys., 18B, 187-200, Academic Press.

Doran, J. C., T. W. Horst and P. W. Nickola, 1978: Variations in measured values of lateral diffusion parameters. Submitted to J. Appl. Met., available from Battelle Pac. NW Lab., Richland, Wash., 21 pp.

Draxler, R., 1976: Determination of atmospheric diffusion parameters, Atmospheric Environment, 10, 99-106.

Draxler, R. R., 1978: Diffusion and transport experiments, MSS, 206 pp. To be published as Ch. 8 in Atmospheric Science and Power Production, U.S.DOE.

Gifford, F. A., 1961: Use of routine meteorological observations for estimating atmospheric dispersion. Nuclear Safety, 2, 47-51.

Gifford, F. A., 1975: Atmospheric dispersion models for environmental pollution applications. In Lectures on air pollution and environmental impact analysis, D. Haugen, ed., Am. Meteor. Soc., iii and 296 pp.

Gifford, F. A., 1976: Turbulent diffusion-typing schemes: a review. Nuclear Safety, 17, 68-86.

Golder, D., 1972: Relations among stability parameters in the surface layer. Boundary Layer Meteor., 3, 47-58.

Hanna, S. R., G. A. Briggs, J. Deardorff, B. A. Egan, F. A. Gifford, and F. Pasquill, 1977: AMS Workshop on stability classification schemes and sigma curves - summary of recommendations. Bull. Amer. Meteor. Soc., 58, 1305-1309.

Haugen, D. A. (Ed.), 1973: Workshop on Micrometeorology, xi and 392 pp, Am. Meteor. Soc., Boston.

Lumley, J. E. and H. A. Panofsky, 1964: The structure of atmospheric turbulence, xi and 239 pp, John Wiley and Sons.

Monin, A. S., and A. M. Yaglom, 1971: Statistical fluid mechanics, xii and 769 pp, MIT Press, Cambridge, Mass. (Vol. I).

Pasquill, F., 1961: The estimation of the dispersion of windborne material. Meteor. Magazine, 90, 33-49.

Pasquill, F., 1975: The dispersion of materials in the atmospheric boundary layer - the basis for generalization. Ch. 1 in Lectures on air pollution and environmental impact analysis, iii and 296 pp, Am. Meteor. Soc., Boston.

Pasquill, F., 976: Atmospheric disperson parameters in Gaussian plume modeling Part II. Possible requirements for change in the Turner Workbook values. U.S. Env. Prot. Agency report EPA-600/4-76-030b, June 1976, 44 pp.

Pasquill, F., and F. B. Smith, 1974: Eddy coefficients for vertical diffusion in the neutral surface layer. Boundary Layer Meteor., 7, 227-228.

Smith, F. B., 1972: A scheme for estimating the vertical dispersion of a plume from a source near ground level. Proc. of the Third Meeting of the Expert Panel on Air Pollution Modeling. NATO-CCHS Report No. 14, Brussels.

Sutton, O. G., 1932: A theory of eddy diffusion in the atmosphere, Proc. Roy. Soc., London, A, 135, 143-165.

Turner, D. B., 1969: Workbook of Atmospheric Dispersion Estimates, vii and 84 pp, USDHEW, PHS Pub. No. 995-AB-26.

U. S. Nuclear Regulatory Commission, 1977: Regulatory guide 1.23, Onsite meteorological programs.

Weber, A. H., 1976: Atmospheric dispersion parameters in Gaussian plume modeling Part I. Review of current systems and possible future developments, x and 59 pp., U. S. Env. Prot. Agency report EPA-600/4-76-030a, July 1976.

Weber, A. H., K. R. McDonald, and G. A. Briggs, 1977: Turbulence classification schemes for stable and unstable conditions. Preprint Volume, Joint Conf. on Applications of Air Pollution Meteorology, Amer. Meteor. Soc., Boston.

Yaglom, A. M., 1976: Semi-empirical equations of turbulent diffusion in boundary layers. Fluid Dynamics Trans. of the Polish Academy of Sciences, 7 Part II, 99-144.

SOME PARAMETERIZATIONS OF THE NOCTURNAL BOUNDARY LAYER

K. S. RAO and H. F. SNODGRASS*

Atmospheric Turbulence and Diffusion Laboratory, National Oceanic and Atmospheric Administration, Oak Ridge, Tennessee, 37830, U.S.A.

(Received 21 December, 1978)

Abstract. The evolution and structure of a steady barotropic nocturnal boundary layer are investigated using a higher-order turbulence closure model which includes equations for the mean quantities, turbulence convariances, and the viscous dissipation rate. The results indicate that a quasi-steady nocturnal PBL might be established in 4–10 hours after transition, depending on surface cooling rate. The latter is assumed to be constant in the model. The emphasis is on prediction of eddy viscosity, nocturnal mixing-layer depth, and the stability-dependent universal functions in the geostrophic drag and heat transfer relations. The model predictions are parameterized in the framework of the PBL similarity theory and compared with observations and results of other models.

1. Introduction

The atmospheric boundary layer is generally stably-stratified over land at night, though persistent daytime inversions also often occur in winter. The nocturnal mechanically-mixed layer is typically much shallower than the daytime convectively-mixed layer. Its depth also varies widely, from a few meters to hundreds of meters, depending on the upper wind, stability, and terrain. This has an important bearing on the dispersion of pollutants in the atmosphere; maximum pollutant-concentration levels are usually associated with strongly stable conditions and low wind speeds, when the diffusive ability of the atmosphere is at a minimum. It is important therefore to study the physical processes of the nocturnal boundary layer and develop models capable of simulating the salient features of its turbulence as well as mean profiles. The models should enable us to improve diffusion estimates for stable conditions.

Several numerical and analytical model studies of the nocturnal boundary layer have been reported in the literature. These include Deardorff (1972), Businger and Arya (1974), Delage (1974), Wyngaard (1975), Blackadar (1976), Briggs (1977), Zeman and Lumley (1978), and Brost and Wyngaard (1978).

In the present study, we use Wyngaard's (1975) higher-order turbulence closure model to investigate the steady-state structure of an idealized nocturnal planetary boundary layer (PBL). The emphasis is on prediction and parameterization of eddy viscosity, dissipation rate of turbulent kinetic energy, mixing-layer depth, and the stability-dependent universal functions in the geostrophic drag and heat transfer relations. The model predictions are parameterized in the framework of the PBL similarity theory and compared with observations and results of other models.

* Affiliated with Oak Ridge Associated Universities (ORAU).

Boundary Layer Meteorology **17** (1979) 15–28. 0006–8314/79/0171–0015$02.10.

ATDL Contribution File No. 78/12

2. The Model

We consider a horizontally homogeneous barotropic PBL over a flat homogeneous surface. Neglecting the moisture effects and radiation flux divergence, the mean flow equations, with x axis in the direction of surface shear stress and z in the vertical, are

$$\begin{aligned} \partial U/\partial t &= -\partial \overline{uw}/\partial z + f(V - V_g) \\ \partial V/\partial t &= -\partial \overline{vw}/\partial z + f(U_g - U) \\ \partial \Theta/\partial t &= -\partial \overline{\theta w}/\partial z. \end{aligned} \tag{1}$$

Here (U, V, $W = 0$) are the mean velocity components in (x, y, z) directions, respectively, and Θ is the mean potential temperature. The corresponding fluctuating quantities are given by (u, v, w) and θ; f is the Coriolis parameter; and the components of the geostrophic wind vector $\mathbf{G} = U_g\mathbf{i} + V_g\mathbf{j}$ are defined by $fU_g = -\partial P/\partial y$ and $fV_g = \partial P/\partial x$, where P is the mean kinematic pressure.

In order to solve Equation (1), we write transport equations for the turbulent fluxes of momentum and heat. These equations are closed approximately by expressing the third moments in terms of dimensionally-consistent, physically-plausible, semi-empirical expressions involving the mean quantities, the second moments, and a turbulence time scale $\tau = 2E/\varepsilon$, where ε is the mean viscous dissipation rate of the turbulent kinetic energy ($E = \overline{u_i u_i}/2$); τ is determined by the model itself, not specified *a priori*, since the model also includes a dynamical equation for ε. These higher-order closure models are discussed by Wyngaard (1975), and reference should be made to that paper for details.

The closed equation set was numerically integrated in time on a digital computer using a Dufort–Frankel explicit finite-difference scheme. A logarithmic transformation of the vertical coordinate was used from the lower boundary, set at $z = 1$ m, to the upper boundary at 1000 m, with a total of 51 grid points. The lower boundary conditions were based on the surface-layer flux–profile relations (Businger *et al.*, 1971) and other data from field measurements and numerical studies. At the upper boundary, a simulated inversion lid, all turbulence quantities and the vertical gradients of mean variables were set to zero.

In order to study the temporal evolution of the nocturnal boundary layer, the model was initialized with equilibrium distributions of variables in a decaying convective PBL around sunset at the instant of transition ($t = 0$) when the vertical surface temperature flux ($Q_0 = H_0/\rho c_p$) goes to zero. To simulate the nocturnal PBL, a constant cooling rate, ranging from 0.2 to 2.0 C hr^{-1}, was specified at the surface (z_0), the geostrophic wind (G) was provided, and the surface friction velocity (u_*), surface heat flux (H_0), Monin–Obukhov stability length (L), and cross-isobar angle (α) were determined from the model at each t. In the calculations, we specified westerly winds, 45 N latitude, a constant $G = 10$ m s^{-1} and a roughness length $z_0 = 0.01$ m. For convenience, we used a coordinate system with the positive x-axis oriented in the direction of the geostrophic wind, and adjusted the lower boundary

conditions to account for the angle $\alpha(t)$ between surface and geostrophic winds. Details of the computational techniques, boundary and initial conditions as well as the model equations can be found in Rao and Snodgrass (1978).

3. Results and Discussion

In a horizontally homogeneous nocturnal PBL with negligibly small radiation flux divergence, the cooling rate is balanced entirely by the turbulent flux divergence. For a constant surface-cooling rate, a quasi-steady state may be established when

$$\frac{\partial \Theta}{\partial t} = \frac{-\partial \overline{w\theta}}{\partial z} = Q_0/h = \text{constant}, \tag{2}$$

or

$$\frac{\partial}{\partial t}(\partial \Theta/\partial z) = \frac{-\partial^2}{\partial z^2}(\overline{w\theta}) = 0\,,$$

where h is the mixing-layer depth. This implies that heat flux decreases linearly with height; both Q_0 and h, as well as other key PBL parameters such as u_*, α and L, should approach constant values as the PBL approaches a quasi-steady state. This leads to a near-constant value for the PBL stability parameter $\mu = |u_*/fL|$, where μ represents the ratio of the rotation time scale, $|f|^{-1}$, to the turbulence time scale, L/u_*, in the stable case. The steady-state value of μ increases with the surface cooling rate.

The results indicate that after an initial period of rapidly changing values, a quasi-steady nocturnal PBL, characterized by near-constant values of u_*, Q_0, L, h and α, might be established in 4–10 h after transition, depending on the surface cooling rate. The model predictions of the mean field and turbulence structure show good agreement with the atmospheric surface-layer observations from Kansas and Minnesota experiments (Wyngaard, 1975; Rao and Snodgrass, 1978). This idealized steady state may be short-lived in reality (see Businger, 1973, p. 86), but nevertheless is useful in understanding the equilibrium structure of the stable PBL.

3.1. Eddy viscosity distribution

The vertical distributions of eddy viscosity, K, are of considerable interest since several recent papers on the nocturnal PBL are based on the eddy viscosity models in which the stresses in the mean momentum equation (1) are replaced by

$$\overline{uw} = -K_{xz}\,\partial U/\partial z, \qquad \overline{vw} = -K_{yz}\,\partial V/\partial z\,. \tag{3}$$

The vertical profiles of K_{xz}, plotted nondimensionally in Figure 1 show a strong dependence on the PBL stability parameter μ. As μ increases, the eddy viscosity profiles become flatter; both the maximum eddy viscosity, K_{max}, as well as the height where it occurs, z_{max}, decrease by nearly two orders of magnitude as the PBL

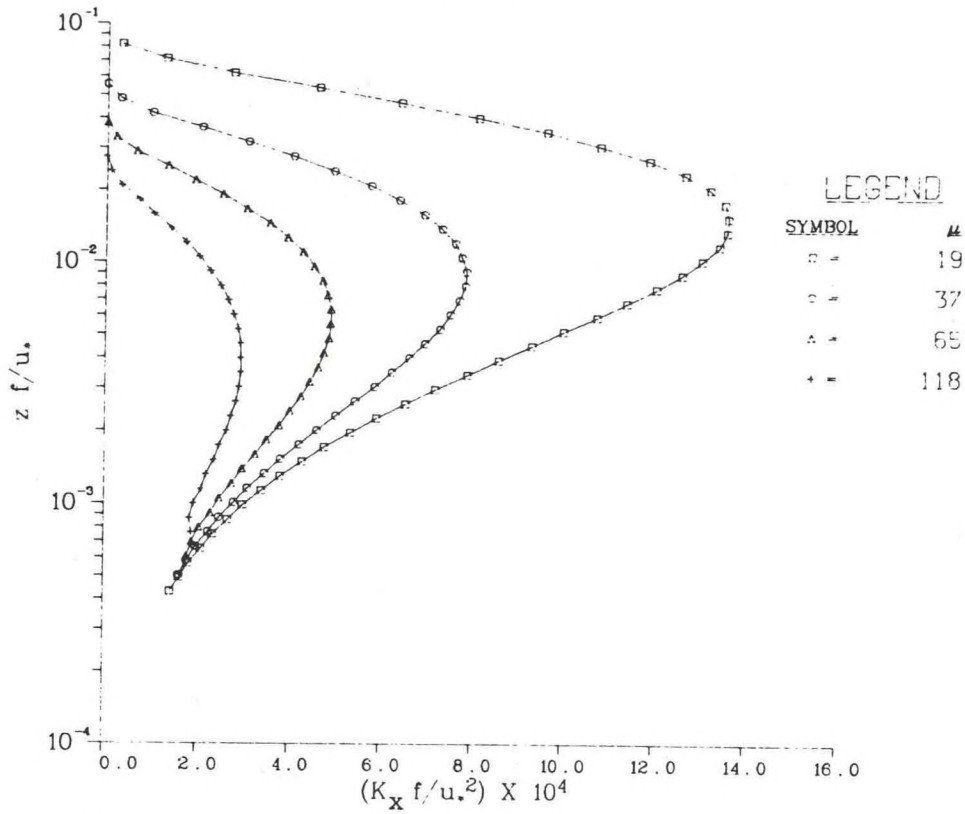

Fig. 1. Nondimensional eddy viscosity distributions in the quasi-steady nocturnal PBL, calculated for different stabilities.

changes from neutral ($\mu \doteq 0$) to moderately stable ($\mu = 118$). The calculated variations of K_{max} and z_{max} are functions of μ; for $\mu > 10$, they are given by the best-fit expressions

$$K_{max} f/u_*^2 = 0.016\mu^{-0.83}$$
$$z_{max} f/u_* = 0.168\,\mu^{-0.80}. \tag{4}$$

In PBL models, it is often taken that $K_{yz} = K_{xz}$ ($= K$, say); this assumption is consistent with our results in Figure 2, which shows identical vertical profiles of K_{xz} and K_{yz} calculated for $\mu = 65$. It will be useful to compare these profiles with the corresponding K-distributions used by other models based on K-theory. Businger and Arya (1974) specified steady-state eddy viscosity distributions by the implicit relation

$$\frac{Kf}{u_*^2} = \frac{k\xi}{(1+\beta\mu\xi)} \exp\left(-\left|\frac{V_g}{u_*}\right|\xi\right), \tag{5}$$

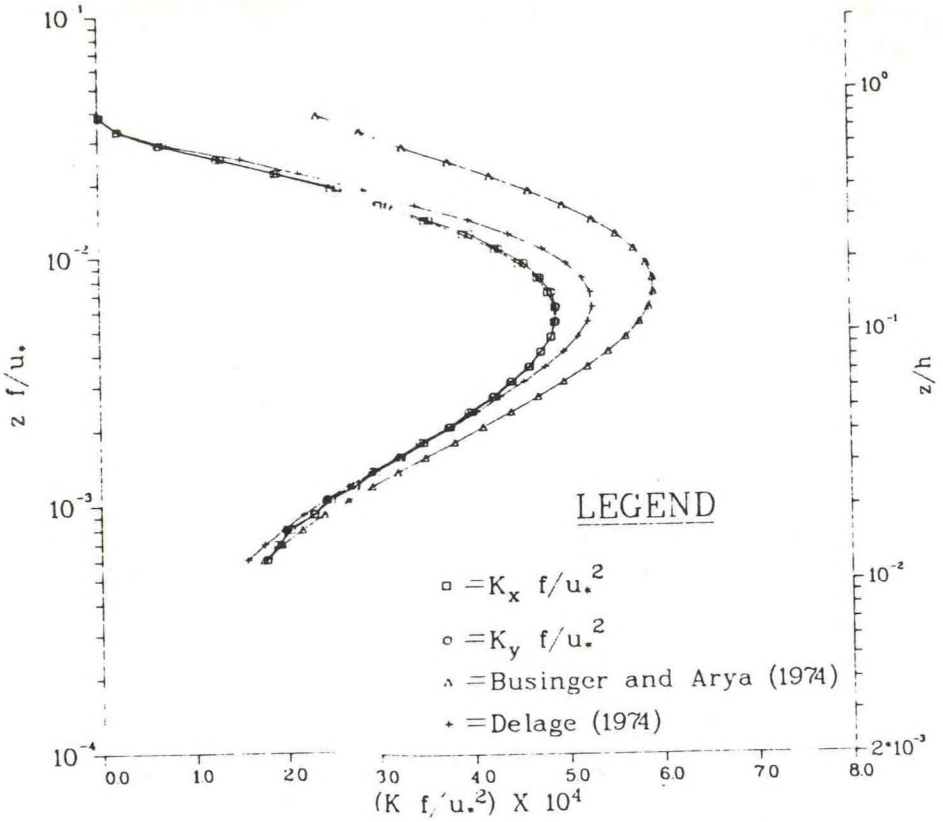

Fig. 2. Comparison of calculated nondimensional eddy viscosity profiles with those used in other nocturnal PBL models.

where $k = 0.35$, $\beta = 4.7$, $\xi = fz/u_*$ and $|V_g| = |G \sin \alpha|$. Delage (1974) used the expression

$$K = l(0.16E)^{1/2}, \tag{6a}$$

where l is a mixing length given as

$$l = \{1/k(z + z_0) + 1/\lambda + \beta/kL'\}^{-1} \tag{6b}$$

with $k = 0.4$, $\beta = 5$, and $\lambda = 0.0004Gf^{-1}$. Here $L'(z)$ is the local value of the Monin–Obukhov stability length. Using the steady-state values of α, E, and L' calculated by the present model for $\mu = 65$, Equations (5) and (6) are evaluated and compared with the K-profiles in Figure 2. Equation (5) gives somewhat larger K values in the outer layer while Equation (6) agrees fairly well with our results. Both equations predict slightly higher peaks than the present model; however, the general profile shape and behaviour are similar in all models.

The K-variation shown in Figure 1 may be parameterized as $K/u_* z = F(\zeta, \mu)$ where $\zeta = z/L$. The predicted steady-state eddy viscosity profiles are represented

well (see Figure 3) by

$$K = \frac{ku_* z}{(1+4.7\zeta)} e^{-b\eta}, \tag{7}$$

where $k = 0.35$, $b = 9.1$, and $\eta = \zeta \mu^{-1/2}$. Using relations given later in this paper, Businger and Arya's (1974) K-expression, Equation (5), can also be reduced to this form. The advantage of Equation (7) is that the steady-state eddy viscosity profile in the nocturnal PBL can be specified explicitly from the surface-layer parameters, u_* and L.

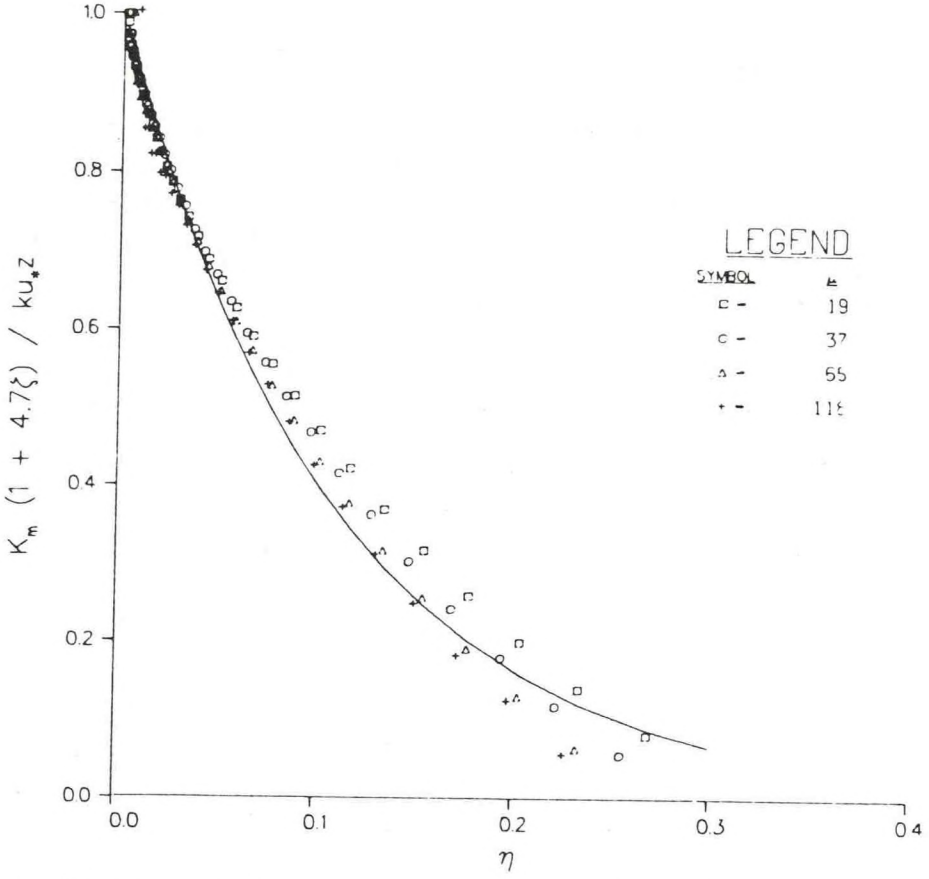

Fig. 3. Similarity representation of calculated eddy viscosity distribution in the quasi-steady nocturnal PBL. The best-fit curve (solid line) is given by Equation (7).

The dissipation rate of turbulent kinetic energy is calculated in the model by a dynamical equation for ε. The steady state ε-profiles in the nocturnal PBL are adequately represented by

$$\phi_\varepsilon = (\phi_m - \zeta)\, e^{-6.5\eta}, \tag{8}$$

where $\phi_\epsilon = (kz/u_*^3)\epsilon$ and $\phi_m = (kz/u_*)\,[(\partial U/\partial z)^2 + (\partial V/\partial z)^2]^{1/2}$ are dimensionless dissipation rate and horizontal mean wind shear, respectively. The decrease of ϵ with height is in qualitative agreement with the recent Minnesota data (Caughey *et al.*, 1978).

3.2. Nocturnal mixing-layer depth

The variation of the nocturnal mixing-layer depth h, calculated somewhat arbitrarily as the height where the shear stress decreases to 5% of its surface value, is plotted in the dimensionless form shown in Figure 4(a). The best fit, for $\mu > 10$, is given by

$$h|f|/u_* = a\mu^{-1/2}, \quad \text{or} \quad h/L = a\mu^{1/2} \tag{9}$$

where a is a constant of order unity. This relation was first suggested by Zilitinkevich (1972, 1975) from similarity considerations and dimensional analysis. From Equation (9), we can write $h \sim |u_* L/f|^{1/2}$; thus the nocturnal mixing-layer depth in the idealized barotropic PBL at middle latitudes is proportional to the geometric mean of the length scales $u_*/|f|$ and L, and it is uniquely determined by the surface stress, Coriolis parameter, and stability. In the present model, calculating h as mentioned above, we evaluated $a = 0.27$ in the steady state; the corresponding values of this constant from other models are 0.55 (Businger and Arya, 1974), 0.22 (Wyngaard, 1975), and 0.40 (Brost and Wyngaard, 1978). Thus, its value appears to be strongly dependent on some of the model parameterizations. The model results in Figure 4(a) show that the value of a also depends on t; at $t = 2$ h, $a = 0.43$ and decreases to 0.27 as the flow approaches steady state.

The nocturnal boundary-layer height, determined from the temperature and wind soundings as the height to which significant surface cooling has extended, typically increases with time during the night (Blackadar, 1957; Izumi and Barad, 1963;

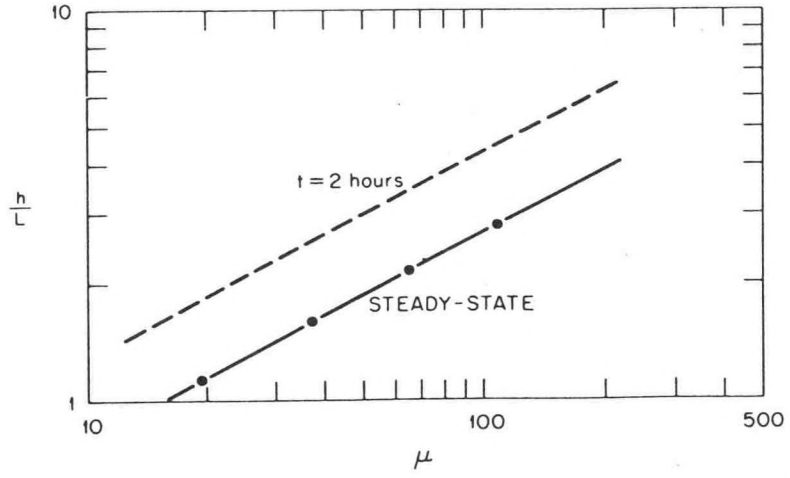

Fig. 4(a). Calculated variation of the dimensionless nocturnal mixing-layer depth as function of the stability parameter μ. See text, Equation (9).

Deardorff, 1972). Yamada (1976) determined h as the height of the surface inversion layer from the radiosonde-measured Θ_v profiles of the Wangara data (Clarke *et al.*, 1971), and found that under strongly stable conditions, $h > 0.3\,|u_*/f|$, the neutral PBL height. These findings indicate that h determined from the Θ_v profile, usually exceeds the height where turbulent shear stress and heat flux become negligible, probably due to radiative and advective effects, and may not be a good indicator of the nocturnal mixing-layer depth. It also appears that, unlike the daytime convective case, the evolution of the nocturnal PBL height cannot be satisfactorily described by a rate equation (Yu, 1978).

It is difficult to verify Equation (9) from available observations. Ideally, one would require turbulence profile measurements in the stable boundary layer under stationary, horizontally-homogeneous conditions. These conditions are rarely satisfied and turbulence data are scarce.

The Kansas surface-layer data (Izumi, 1968), in addition to u_* and L, include 15-min average measurements of $\overline{w\theta}$ at $z = 5.66$, 11.31 and 22.63 m, and the

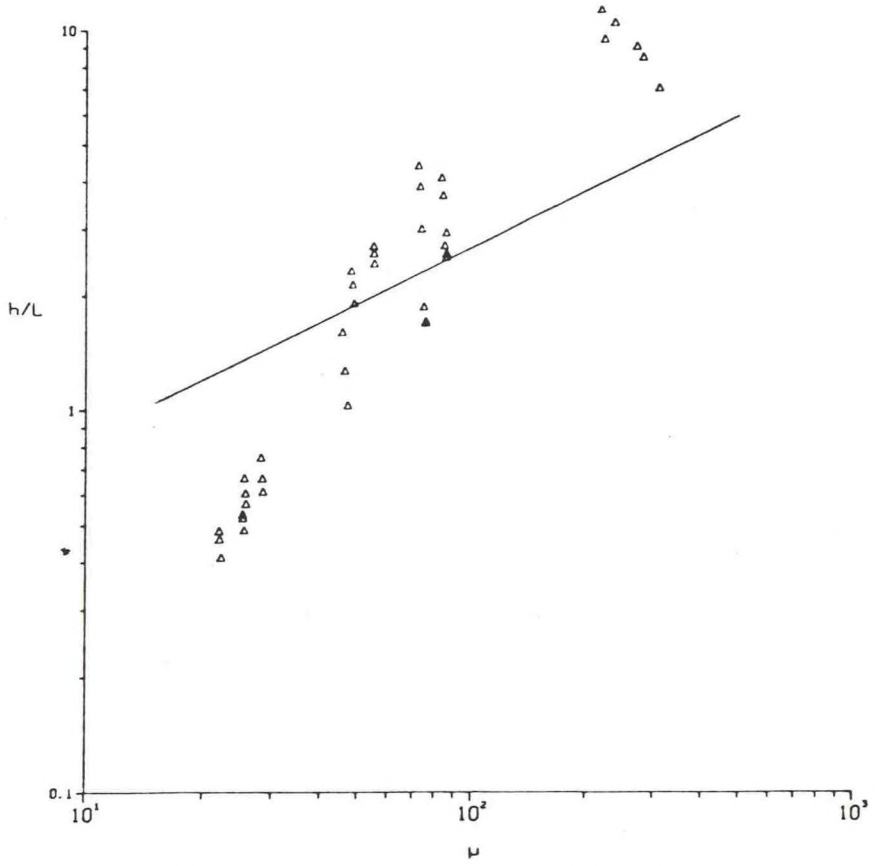

Fig. 4(b). Comparison of model prediction (solid line) with the variation of nocturnal mixing-layer depth deduced from the Kansas data. (See text for details).

corresponding potential temperature profiles which allow the determination of cooling rates at these heights. Assuming a linear decrease of heat flux with height (Wyngaard, 1975; Rao and Snodgrass, 1978) in the nocturnal mixing layer, h is then estimated from Equation (2). The variation of half-hour average estimates of h are plotted in Figure 4(b) along with the present model prediction, $h/L = 0.27\ \mu^{1/2}$, for comparison.

A similar analysis was carried out for the Wangara stable boundary layer data (Clarke *et al.*, 1971) and the results are shown in Figure 4(c). In this case, 1-h average values of the parameters Q_0, L and u_* are based on the calculations of Melgarejo and Deardorff (1975), and the corresponding cooling rates are estimated from screen-level (1.2 m) temperatures. The Wangara results cover a shorter range of μ and show more scatter than the Kansas data, probably due to significant radiation flux divergence, which was not considered in the present model. It should be noted that the preceding analysis for the estimation of h is based on several assumptions, including a continuous turbulence regime in the nocturnal mixing layer and negligible advective effects, which are often not satisfied in the real atmosphere. In a recent

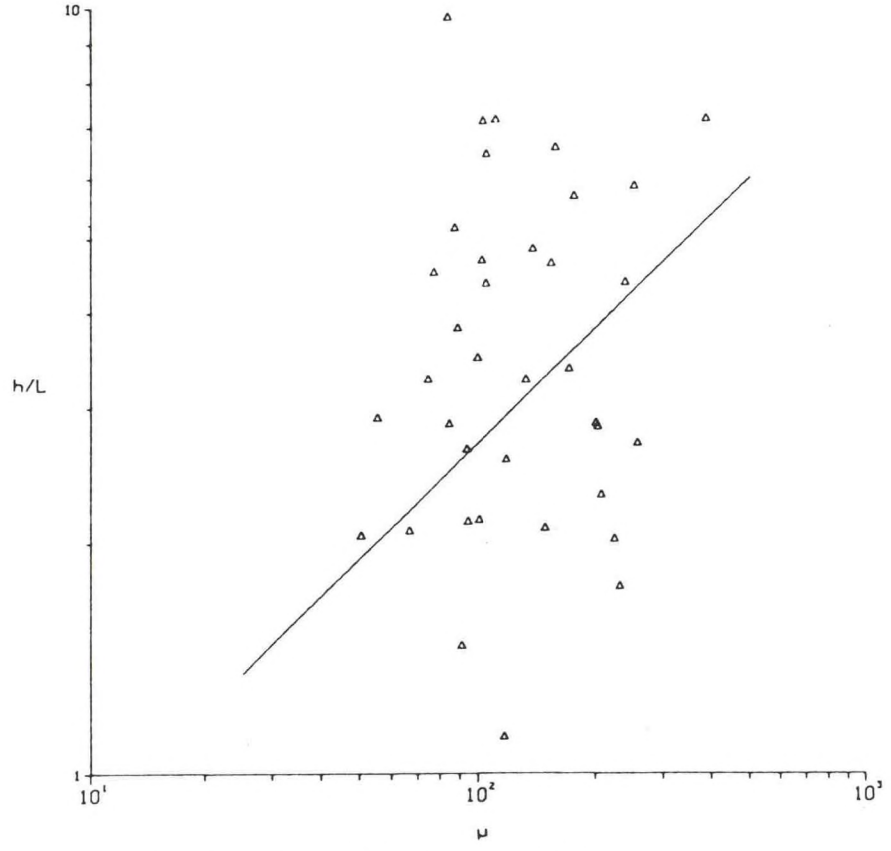

Fig. 4(c). Same as Figure 4(b), but with the Wangara data.

case study of the nocturnal boundary layer, Nieuwstadt and Driedonks (1979) conclude that advection effects are important, especially in the upper part of the boundary layer, and explain the differences between their observed and calculated results in terms of temperature advection.

A more recent analysis of the Minnesota stable data (Caughey *et al.*, 1978) and the accoustic sounder data at the 200 m high meteorological tower at Cabauw in the Netherlands (Nieuwstadt and Driedonks, 1979) tend to support Equation (9), though the value of the constant a still remains unsettled.

Another parameterization for h can be obtained by integrating the equations of motion (1) over the mixing-layer depth in the steady-state limit. This yields the constraints,

$$\int_{z_0}^{h} (V - V_g)\,\mathrm{d}z = \frac{1}{f}\int_{z_0}^{h} \frac{\partial \overline{uw}}{\partial z}\,\mathrm{d}z = u_*^2/f, \tag{10}$$

$$\int_{z_0}^{h} (U_g - U)\,\mathrm{d}z = \frac{1}{f}\int_{z_0}^{h} \frac{\partial \overline{vw}}{\partial z}\,\mathrm{d}z = 0\,. \tag{11}$$

The latter indicates that U must overshoot U_g within the mixing layer. We can write the first constraint, to a good approximation, as

$$u_*^2/f \propto -\int_{z_0}^{h} V_g\,\mathrm{d}z = hG\sin\alpha, \tag{12}$$

or

$$h = a_1 u_*^2/(fG\sin\alpha).$$

This can also be expressed as

$$u_*/G = a_2(fh\sin\alpha/G)^{1/2} \tag{13}$$

where $a_2 = a_1^{-1/2}$. The last relation, shown as the dashed line in Figure 5, fits the model predictions well with the constants $a_2 = 0.80$ and $a_1 = 1.56$; these values agree with $a_2 = 0.79$ and $a_1 = 1.6$ obtained by Brost and Wyngaard (1978) from a different model.

3.3. Geostrophic drag and heat transfer relations

Asymptotic matching of the similarity profiles of mean velocity and temperature in the inner and outer layers of the stable PBL leads to the well-known geostrophic drag

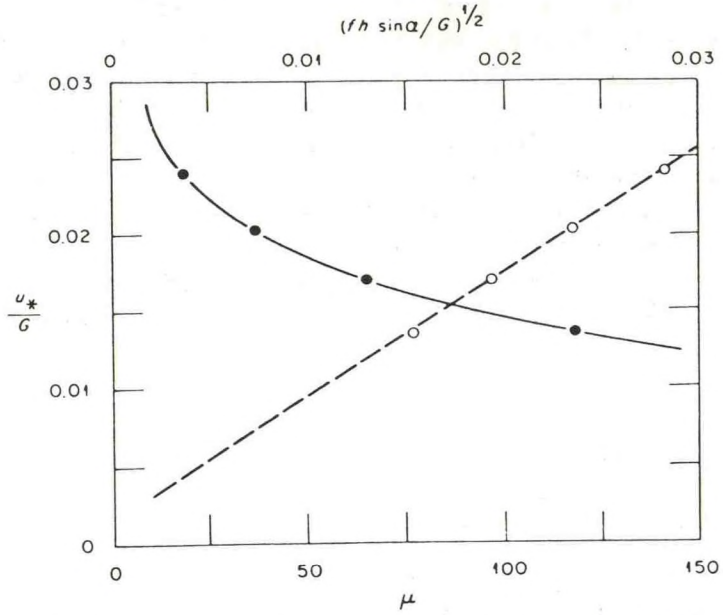

Fig. 5. Calculated variation of the geostrophic drag coefficient in the nocturnal PBL as a function of $(fh \sin\alpha/G)^{1/2}$, indicated by dashed line, and the stability parameter μ, indicated by solid line, for $\mathrm{Ro} = 10^7$.

and heat transfer relations:

$$G\cos\alpha/u_* = \frac{1}{k}\{\ln|u_*/fz_0| - A(\mu)\}$$

$$G\sin\alpha/u_* = \frac{B(\mu)}{k}\,\mathrm{sign}\,(f) \tag{14}$$

$$(\Theta_h - \Theta_0)/\theta_* = \frac{0.74}{k}\{\ln|u_*/fz_0| - C(\mu)\}$$

where Θ_h is the potential temperature at the top of the boundary layer, and A, B, and C are universal functions of μ to be determined from theory and observations. The first two equations may be combined to give an implicit relation between the geostrophic drag coefficient, $C_g = u_*/G$, and the surface Rossby number, $\mathrm{Ro} = |G/fz_0|$, as follows:

$$\ln \mathrm{Ro} = A(\mu) - \ln C_g + \left[\frac{k^2}{C_g^2} - B^2(\mu)\right]^{1/2} \tag{15}$$

which implies that $u_*/G = C_g(\mathrm{Ro}, \mu)$; for a given Rossby number, C_g should only depend on μ. Figure 5 (solid line) shows the variation of the geostrophic drag coefficient with μ in the present model ($\mathrm{Ro} \simeq 10^7$).

The functions $A(\mu)$, $B(\mu)$ and $C(\mu)$, calculated from Equation (14) in the model, are shown in Figure 6 where they are compared with the best-fit polynomial expressions to the Wangara data (Clarke *et al.*, 1971) given by Arya (1975). There is fair agreement between model predictions and observations. From Equations (9), (12), and (14), we can write $B(\mu) = b_1\mu^{1/2}$ where the constant $b_1 = 1.71$. For $\mu > 10$,

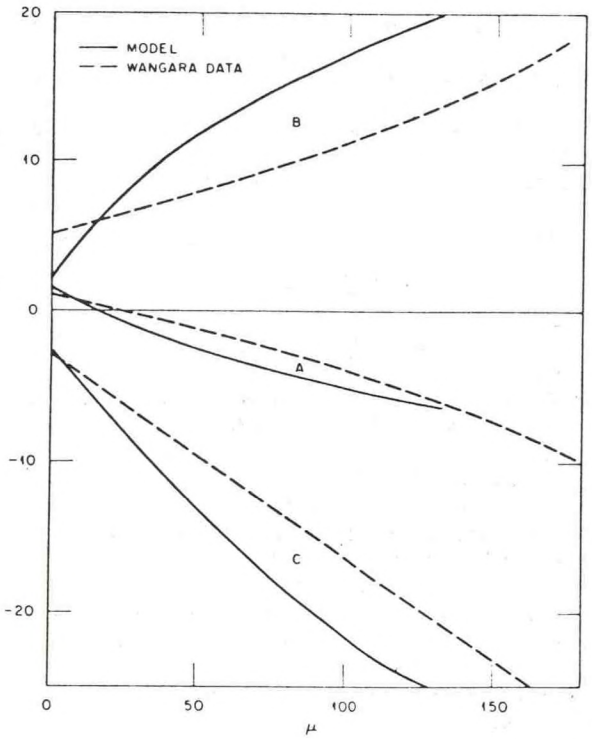

Fig. 6. Comparison of calculated similarity functions A, B, and C in the geostrophic drag and heat transfer relations with the best-fits to the Wangara stable PBL data.

The present model results can be represented by the best-fit expressions shown in Table I, where they are compared with the functions given by Arya (1977), Briggs (1977), and Brost and Wyngaard (1978), all obtained from different models of the stable barotropic PBL. Except for $B(\mu)$, the agreement between various models is good.

TABLE I

Comparison of PBL similarity functions A, B, and C from different models

	$A(\mu)$	$B(\mu)$	$C(\mu)$
Present model	$\ln \mu^{1/2} - 0.98\mu^{1/2} + 2.5$	$1.79\mu^{1/2} - 0.6$ or $1.71\mu^{1/2}$	$\ln \mu^{1/2} - 3\mu^{1/2} + 6.5$
Arya (1977)	$\ln \mu^{1/2} - 0.96\mu^{1/2} + 2.5$	$1.15\mu^{1/2} + 1.1$	$\ln \mu^{1/2} - 3\mu^{1/2} + 7.0$
Briggs (1977)	$\ln \mu^{1/2} - 1.0\mu^{1/2} + 2.5$	$1.86\mu^{1/2}$	–
Brost & Wyngaard (1978)	$\ln \mu^{1/2} - 0.9\mu^{1/2} + 2.0$	$1.40\mu^{1/2}$	–

Acknowledgments

This work was performed under an agreement between the National Oceanic and Atmospheric Administration and the Department of Energy. We gratefully acknowledge several helpful discussions with G. A. Briggs of ATDL.

References

Arya, S. P. S.: 1975, 'Geostropic Drag and Heat Transfer Relations for the Atmospheric Boundary Layer', *Quart. J. Roy. Meteorol. Soc.* **101**, 147–161.

Arya, S. P. S.: 1977, 'Suggested Revisions to Certain Boundary Layer Parameterization Schemes used in Atmospheric Circulation Models', *Mon. Wea. Rev.* **105**, 215–227.

Blackadar, A. K.: 1957, 'Boundary Layer Wind Maxima and their Significance for the Growth of Nocturnal Inversions', *Bull. Amer. Meteorol. Soc.* **38**, 283–290.

Blackadar, A. K.: 1976, 'Modeling the Nocturnal Boundary Layer', *Third Symposium on Atmospheric Diffusion and Air Quality*, Raleigh (Oct. 1976), pp. 46–49, Preprints, Amer. Meteorol. Soc., Boston.

Briggs, G. A.: 1977, 'Predictions of Nocturnal Mixing Layer Parameters', *Manuscript*, 40pp., ATDL, Oak Ridge, Tenn.

Brost, R. A. and Wyngaard, J. C.: 1978, 'A Model Study of the Stably Stratified Planetary Boundary Layer', *J. Atmos. Sci.* **35**, 1427–1440.

Businger, J. A., Wyngaard, J. C., Izumi, Y., and Bradley, E. F.: 1971, 'Flux-Profile Relations in the Atmospheric Surface Layer', *J. Atmos. Sci.* **28**, 181–189.

Businger, J. A.: 1973, 'Turbulent Transfer in the Atmospheric Surface Layer', in D. A. Haugen (ed.), *Workshop on Micrometeorology*, Amer. Meteorol. Soc., Boston, pp. 101–149.

Businger, J. A. and Arya, S. P. S.: 1974, 'The Height of the Mixed Layer in the Stably Stratified Planetary Boundary Layer', *Adv. in Geophys.* **18A**, Academic Press, New York, 73–92.

Caughey, S. J., Wyngaard, J. C., and Kaimal, J. C.: 1978, 'Turbulence in the Evolving Stable Boundary Layer', *Manuscript*, 46 pp., CIRES, Univ. of Colorado / NOAA, Boulder.

Clarke, R. H., Dyer, A. J., Brook, R. R., Reid, D. G., and Troup, A. J.: 1971, 'The Wangara Experiment: Boundary Layer Data', Tech. Pap. No. 19, CSIRO, Div. Meteor. Phys., Melbourne, Australia, 362 pp.

Deardorff, J. W.: 1972, 'Rate of Growth of the Nocturnal Boundary Layer', in H. W. Church and R. E. Luna (eds.) *Proc. of the Symposium on Air Pollution, Turbulence and Diffusion*, New Mexico (Dec. 1971), pp. 183–190.

Delage, Y.: 1974, 'A Numerical Study of the Nocturnal Atmospheric Boundary Layer', *Quart. J. Roy. Meteorol. Soc.* **100**, 351–364.

Izumi, Y.: 1971, 'Kansas 1968 Field Program Data Report', *AFCRL–72–0041*, 79 pp., AFGL, Hanscom Field, Bedford, Mass.

Izumi, Y. and Barad, M.: 1963, 'Wind and Temperature Variations during Development of a Low-Level Jet', *J. Appl. Meteorol.* **2**, 668–673.

Melgarejo, J. W. and Deardorff, J. W.: 1975, 'Revision to "Stability Functions for the Boundary-Layer Resistance Laws Based upon Observed Boundary-Layer Heights"', *J. Atmos. Sci.* **32**, 837–839.

Nieuwstadt, F. T. M. and Driedonks, A. G. M.: 1979, 'The Nocturnal Boundary Layer: a case study compared with model calculations', *Manuscript*, Royal Netherlands Meteorological Institute, De Bilt, 35pp.

Rao, K. S. and Snodgrass, H. F.: 1978, 'The Structure of the Nocturnal Planetary Boundary Layer', *ATDL Contribution File No. 78/9*, NOAA, Oak Ridge, Tenn., 44pp.

Wyngaard, J. C.: 1975, 'Modeling the Planetary Boundary Layer – Extension to the Stable Case', *Boundary-Layer Meteorol.* **9**, 441–460.

Yamada, Y.: 1976, 'On the Similarity Functions A, B, and C of the Planetary Boundary Layer', *J. Atmos. Sci.* **33**, 781–793.

Yu, T. W.: 1978, 'Determining the Height of the Nocturnal Boundary Layer', *J. Appl. Meteorol.* **17**, 28–33.

Zeman, O. and Lumley, J. L.: 1978, 'Buoyancy Effects in Entraining Turbulent Boundary Layers: A Second-order Closure Study', *Proceedings of Symposium on Turbulent Shear Flows*, Springer-Verlag (to appear).

Zilitinkevich, S. S.: 1972, 'On the Determination of the Height of the Ekman Boundary Layer', *Boundary-Layer Meteorol.* **3**, 141–145.

Zilitinkevich, S. S.: 1975, 'Resistance Laws and Prediction Equations for the Depth of the Planetary Boundary Layer,' *J. Atmos. Sci.* **32**, 741–752.

Reprinted from Preprint Volume: Fourth Symposium on Turbulence, Diffusion, and Air Pollution, Jan. 15-18, 1979, Reno, NV. Published by the American Meteorological Society, Boston, Mass.

10.10

EMPIRICAL ESTIMATION OF WAKE CAVITY SIZE BEHIND BLOCK-TYPE STRUCTURES

R. P. Hosker, Jr.

Atmospheric Turbulence and Diffusion Laboratory
National Oceanic and Atmospheric Administration
Oak Ridge, Tennessee 37830

1. INTRODUCTION

The boundary layers which form along the exposed surfaces of a bluff obstacle generally separate from these surfaces at locations determined either by geometry (i.e., at sharp edges) or by aerodynamic effects. The separated layers move out into the surrounding fluid as free shear layers; if the obstacle is sufficiently long, the layers may reattach to the surface at some downwind location, and eventually are shed again at the end of the body. In either case, these separated layers curve inward toward the wake axis, serving to enclose what is usually called a "cavity" or recirculation "bubble" immediately downwind of the body. The cavity zone is characterized by low mean speed, high turbulence intensity, recirculation and relatively large residence times of fluid particles "trapped" within the bubble, and low, nearly constant pressure. As pointed out by Bearman (1972), and Bradshaw and Wong (1972), the steady-state cavity shape and pressure both result from the dynamic balance between fluid withdrawn from the bubble by entrainment into the bounding shear layers, and fluid supplied to the cavity by the reverse flow which originates with the bifurcating shear layers at the point of cavity closure. The flow characteristics of the recirculation zone must therefore depend on the characteristics of the boundary layer shed by the obstacle, and on the details of the turbulent mixing within the resultant free shear layers. Clearly these are not easily predicted, since they depend on the geometry and surface characteristics of individual obstacles, and on the nature of the approach flow.

The boundary-layer wake-flow pattern which has been generally accepted until recently is similar to Figure 1, which shows the cavity as a closed recirculation zone bounded by the separation streamline emanating from the upwind edge of the building roof. Transfer of pollutants into and out of this cavity is accomplished by turbulent transport through the surrounding shear layer.

A picture which has more recently emerged from the work of Morkovin (1972) and his colleagues, Britter, et al. (1976), Woo, et al. (1977), and Hunt et al. (1978) is shown in Figure 2. Here, the streamline "bounding" the cavity is not the separation streamline, and transfer of material into and out of the cavity is not limited to turbulent transport across the interface. Instead, material can be advected into the recirculation zone along the entering streamlines, and can be removed via the rising spiral vortices generated behind the lateral edges of the building. The simple model of Figure 1 may therefore be strictly applicable only to purely two-dimensional problems.

For some purposes, however, the concept of a more or less closed "bubble" may still be adequate. For example, one may need to estimate the extent of a "shelter" zone near a windbreak, or may wish to estimate the boundaries of the recirculation zone where buildup of pollutant concentrations from local emissions is likely. In addition, Vincent (1978) suggests that in a thick turbulent boundary layer flow (like the atmospheric surface layer), the simpler cavity concept may still be adequate since turbulent transfer across the shear layer probably dominates over advective transport.

Regardless of the conceptual details, there is a clear need for estimates of the cavity size as a function of building shape and incident flow parameters. As one example, Bitte and Frost (1976) recently improved the method of Kiya and Arie (1972) for calculating the flow over a two-dimensional building. However, their technique requires prior knowledge of the downwind extent of the recirculation zone. The present paper develops an empirical estimation procedure for cavity length behind two and three-dimensional sharp-edged rectangular buildings.

2. CAVITY SIZE IN UNIFORM FLOW

A thorough study of cavity size behind sharp-edged three-dimensional obstacles was carried out by Evans (1957). He systematically examined the flow behind block-like model buildings of various lengths, widths, and heights, with and without pitched roofs, using smoke in a nearly uniform* incident flow to visualize the extent of the recirculation zone. His observations, a few of which are summarized here, were reported in tabular form and in a lengthy sequence of sketches. For example, he found that an increase in the along-wind building dimension L (relative to the height H) leads to a decrease in the length of the cavity; this continues until $L/H \gtrsim 2$, when the flow (which

*"Nearly uniform" here means that the boundary layer portion of the incident flow is shallow compared to the building height.

ATDL Contribution File No. 78/13

had initially separated at the upwind roof edge) reattaches onto the flat roof. Final separation then takes place at the trailing edge of the roof; the separation streamline leaves the body roughly parallel to the roof, and the cavity length becomes nearly independent of L/H. Evans also found that as the cross-wind dimension W increases (for a given L), both the width and length of the cavity increase. He observed that, at least in a near-uniform incident flow, the flow pattern near the top of the buildings was largely invariant with building height, while the amount of air displaced laterally around the building naturally increased with H. The cavity length then increased with building height. Evans' (1957) original report should be studied for information on the effects of roof overhang, building orientation, and more elaborate building configurations.

Empirical expressions for the length of the recirculation zones behind flat-roof block buildings normal to the wind have been fitted to Evan's (1957) data. It was reasoned that the cavity length x_r must depend on the three basic building dimensions, the incident wind speed and its vertical variation, the turbulence intensity and scale and bulk stability of the incident flow, the aerodynamic characteristics of the upwind surface, and the fluid viscosity. For neutrally-stable, uniform, low-turbulence flow over smooth flat ground upwind of a simple sharp-edged body, however, x_r should be primarily a function of the building dimensions and the flow Reynolds number. If the Reynolds number is quite large, then the flow field no longer depends on it; forming nondimensional groups from the remaining variables, we expect that $x_r/H = fn(L/H, W/H)$. The extent of the cavity should be measured from the separation point. Hence two different expressions, for "short" ($L/H \lesssim 2$, say) and "long" ($L/H \gtrsim 3$, say) buildings, will be required, since for short buildings the recirculation length is reckoned from the upwind face of the building, while for long buildings, where the flow has reattached to the roof, the cavity length is measured from the lee face. Several limiting cases suggest themselves: as the obstacle length and width approach zero, the cavity should disappear. For very wide bodies (large W/H), the results should become independent of W/H (the two-dimensional limit). In particular, for $W/H \to \infty$ and $L/H \to 0$, the short building expression should reduce to a result suitable for a two-dimensional fence. For $W/H \to \infty$ and $L/H \to \infty$, the long building expression should approach values observed behind two-dimensional rear-facing steps.

The following equation, developed to fit Evans' (1957) data for short ($L/H \leq 2$) block buildings, meets most of the pertinent requirements:

$$\frac{x_r}{H} = \frac{L}{H} + \frac{A \cdot (W/H)}{1.0 + B \cdot (W/H)} \quad , \tag{1a}$$

where A and B are weak functions of L/H:

$$A = -2.0 + 3.7(L/H)^{-1/3} \tag{1b}$$

and

$$B = -0.15 + 0.305(L/H)^{-1/3} \quad .$$

Equation (1) is indicated in Figures 3a, b, c together with Evans' (1957) data; the agreement is generally within $\pm$ 15% or better. For $W/H \to 0$, $x_r/H \to L/H$; i.e., the cavity, which is measured from the upwind building face, disappears. For $W/H \to \infty$ and $L/H \to 0$, $x_r/H \to 12.1$; thus Eqn. (1) underpredicts two-dimensional fence data (Arie and Rouse, 1956; Good and Joubert, 1968; Frost, 1973) by roughly 10 to 20%. Independent data from several authors (Castro and Robins, 1977; Lemberg, 1973; Leutheusser and Baines, 1967; Vincent, 1977 and 1978) are also plotted in Figures 3a, b, c. The agreement with Eqn. (1) is typically within 20% or better, with a slight tendency toward underprediction of the data. The figures suggest several ranges where more data would be useful for additional validation and/or adjustment of the equation.

For obstacles where $L/H > 2$, Evans (1957) observed reattachment of the initial separation streamline on to the building roof; final separation then occurred at the trailing edge of the (flat) roof, with the streamlines leaving nearly parallel to the roof. The flow is then independent of L/H and is rather reminiscent of flow behind a rear-facing step as the body width becomes large. If the cavity extent is measured from the final separation point (i.e., from the lee side of the building), then the expression

$$\frac{x_r}{H} = \frac{1.75(W/H)}{1.0 + 0.25(W/H)} \tag{2}$$

fits Evans' (1957) data fairly well, typically within $\pm$ 15%, as indicated in Figure 4. As $W/H \to \infty$, $x_r/H \to 7.0$, which agrees reasonably well with the results behind two-dimensional steps cited by Tani (1957), Bearman (1965), and Bradshaw and Wong (1972) and also plotted in Figure 4. One point from Leutheusser and Baines (1967) is also included there for comparison. Equation (2) should suffice for predicting x_r/H within $\approx$ 25% in uniform flows where the flow reattaches to the building roof.

3. CAVITY SIZE IN BOUNDARY LAYER FLOWS

The flow around a bluff body immersed in a turbulent boundary layer is considerably more complex than in the preceding case. In particular, the wake cavity flow should depend on the relative curvature of the mean velocity profile and on the intensity and scale of the incident turbulence, as well as on building geometry, Reynolds number, etc.

Ranga Raju et al. (1976) have suggested, however, that only the part of the velocity profile which is close to the ground significantly affects the separation upstream of a fence, the velocity of the separating streamline at the top of the fence (and hence the cavity pressure distribution), and the drag. The major effect in their study

seemed to be due to H/z_o, the height of the fence relative to the aerodynamic roughness of the upwind surface. This ratio has long been known to be of importance in laboratory modeling from the studies of Jensen (1958). Van Eimern et al. (1964) cite Tani's work on shelterbelts, indicating that the length of the protected zone Lp, say, depends rather weakly on H/z_o: $Lp/H \simeq \ln (H/z_o)$. The above discussion suggests that at least the crude features of a cavity flow (such as its size) may not be enormously sensitive to the details of the approach flow. Hence Eqns. (1) and (2) were compared to laboratory and field wake data taken in turbulent boundary layers.

Agreement of Eqn. (1) with the data is seen to be fair in Figures 5a, b, c; the scatter is a great deal larger than in the uniform flow case, probably because of the effects of the many different incident boundary layers. The worst magnitude of disagreement between Eqn. (1) and the data arises from the field work of Frost and Shahabi (1977), which is underpredicted by almost 5 building heights (≃ 40%). The reason for this sizeable difference is not known. Figures 5a, b, c suggest a wide range of W/H values for which additional data would be welcome.

Figure 5c, for $L/H \simeq 2$, must be regarded as tentative in these turbulent boundary layer flows, since the flow may actually be reattached to the roof and sides of the structures; if this is true, then Eqn. (1) does not apply. Vincent (1977) has examined the effect of turbulence on uniform flow near cubes (L/H = 1). He finds reattachment of the separated boundary layer on to the roof and sides when the parameter $\Lambda \equiv q\ell/UH > 2.5 \times 10^{-3}$, where q and ℓ are the characteristic turbulence velocity and scale, respectively. In an atmospheric boundary layer we expect ℓ to scale with height, and the largest eddies near the building will be of order H. Under neutral conditions, $q/U \sim [\ell n(H/z_o)]^{-1}$ (Lumley and Panofsky, 1964), which will almost always be greater than 0.1. That is, if Vincent's (1977) criterion carries over to the boundary layer, then flow about even relatively short bodies may be reattached to the sides and roof, so that Eqn. (1) is not appropriate.

For such cases, Eqn. (2) applies, at least in near-uniform flows. Data obtained in boundary layers for $L/H \geq 2$ and/or for cases where the investigator explicitly stated that the flow had reattached were added to Figure 4 (those labeled "BL"). The agreement is as good as for Evan's (1957) uniform flow data from which the equation was derived. Evidently the exact nature of the incident flow is not too critical for cases where the boundary layers reattach to the body surface.

4. COMMENTS AND CONCLUSIONS

An empirically-derived equation (1) has been demonstrated to predict to a reasonable degree of accuracy the along-wind extent of the cavity zone behind sharp-edged simple structures in nearly uniform flow, if the flow does not reattach to the top and sides. If the incident flow is a deep turbulent boundary layer and reattachment to the top and sides still does not occur, then the predictions are not as good, but are generally within 50% or so of the observed values. When the boundary layers on the structure do reattach to its surface, a second empirical equation (2) predicts the available data quite well, regardless of the nature of the incident flow field.

In order that future work toward understanding the scatter in the boundary layer data be facilitated, it is recommended that experimentalists specify whenever possible the values of H/z_o and boundary layer depth which apply. Additional information on the turbulence characteristics and the locations of separation and reattachment would be most useful. Field observations of cavity behavior seem to be rather rare, and should be encouraged, to permit comparisons with laboratory work.

ACKNOWLEDGEMENT

This work has been carried out under agreements among the National Oceanic and Atmospheric Administration, the U.S. Department of Energy, and the U.S. Nuclear Regulatory Commission.

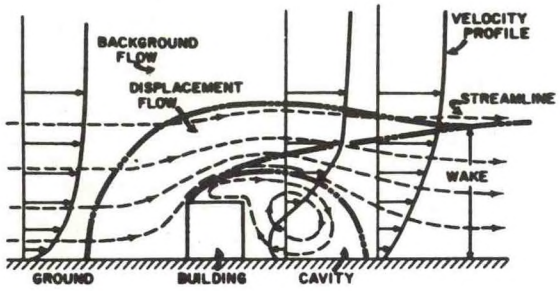

Figure 1. Simple model of flow near a sharp-edged building (ASME, 1973).

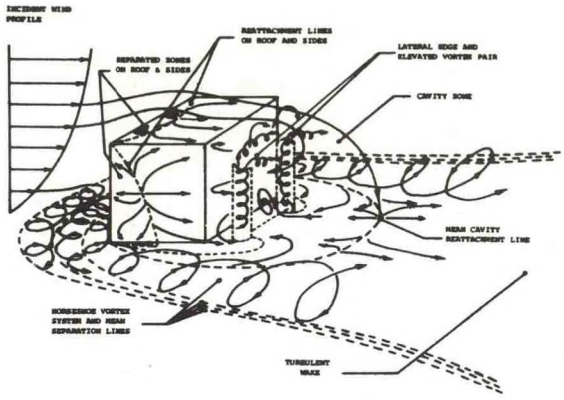

Figure 2. Recent model of flow near a sharp-edged building (based on Woo et al., 1977, and Hunt et al., 1978).

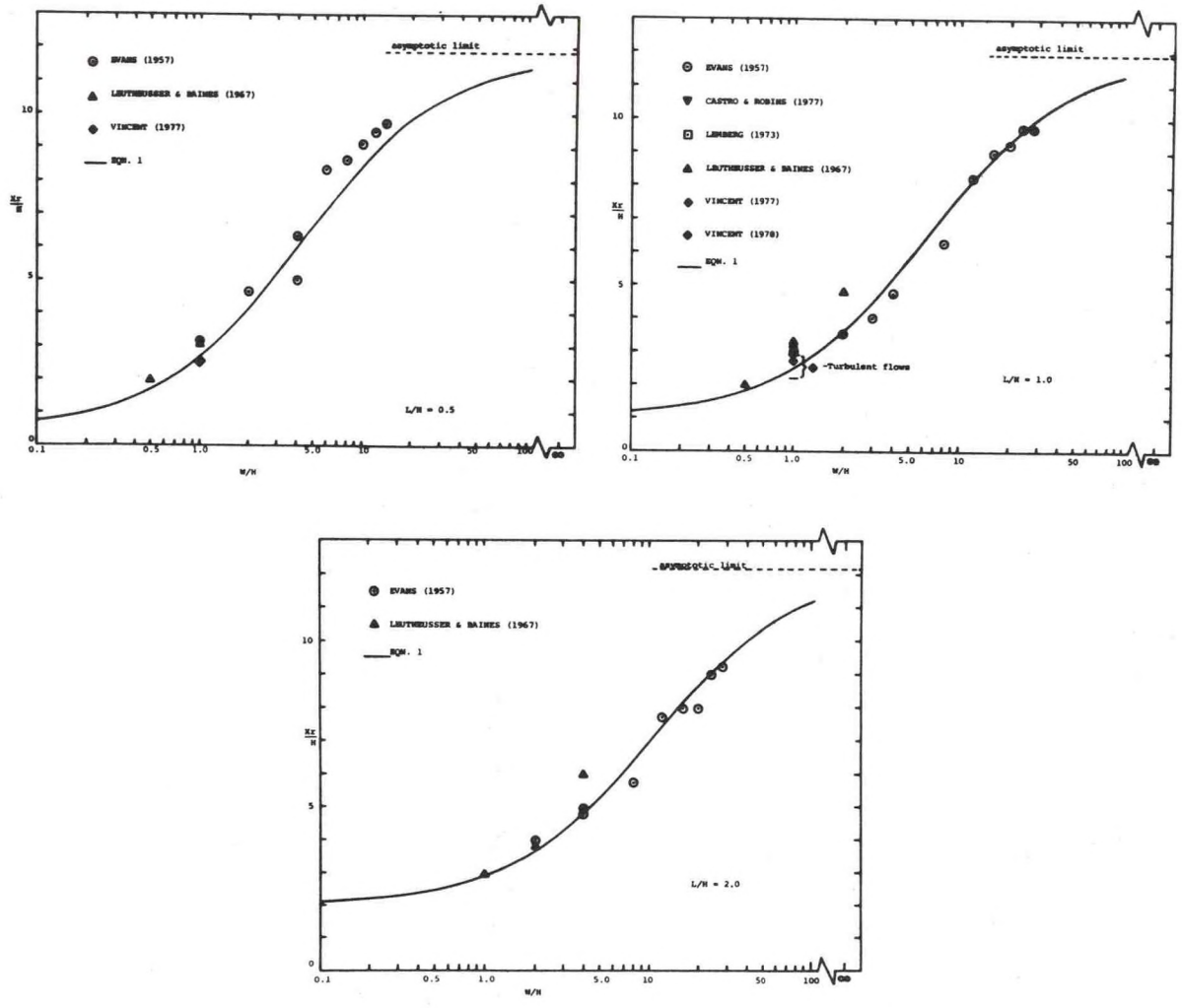

Figure 3. Comparisons of data with estimates (Eqn. (1)) of wake cavity length x_r for "short" sharp-edged buildings in nearly uniform flow. The building height is H, the along-wind length is L, and the crosswind width is W. Cavity length is measured from the upwind face where the flow separation occurs. Three L/H ratios are shown: (a) L/H = 0.5, (b) L/H = 1.0, (c) L/H = 2.0.

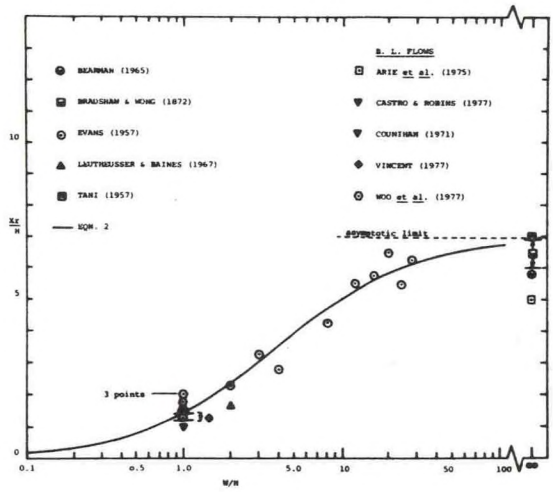

Figure 4. Comparisons of data with estimate (Eqn. (2)) of wake cavity length x_r for "long" sharp-edged buildings. The cavity length is measured from the lee face. The flow has reattached to the top and sides in this case. Both nearly-uniform and boundary-layer data are shown.

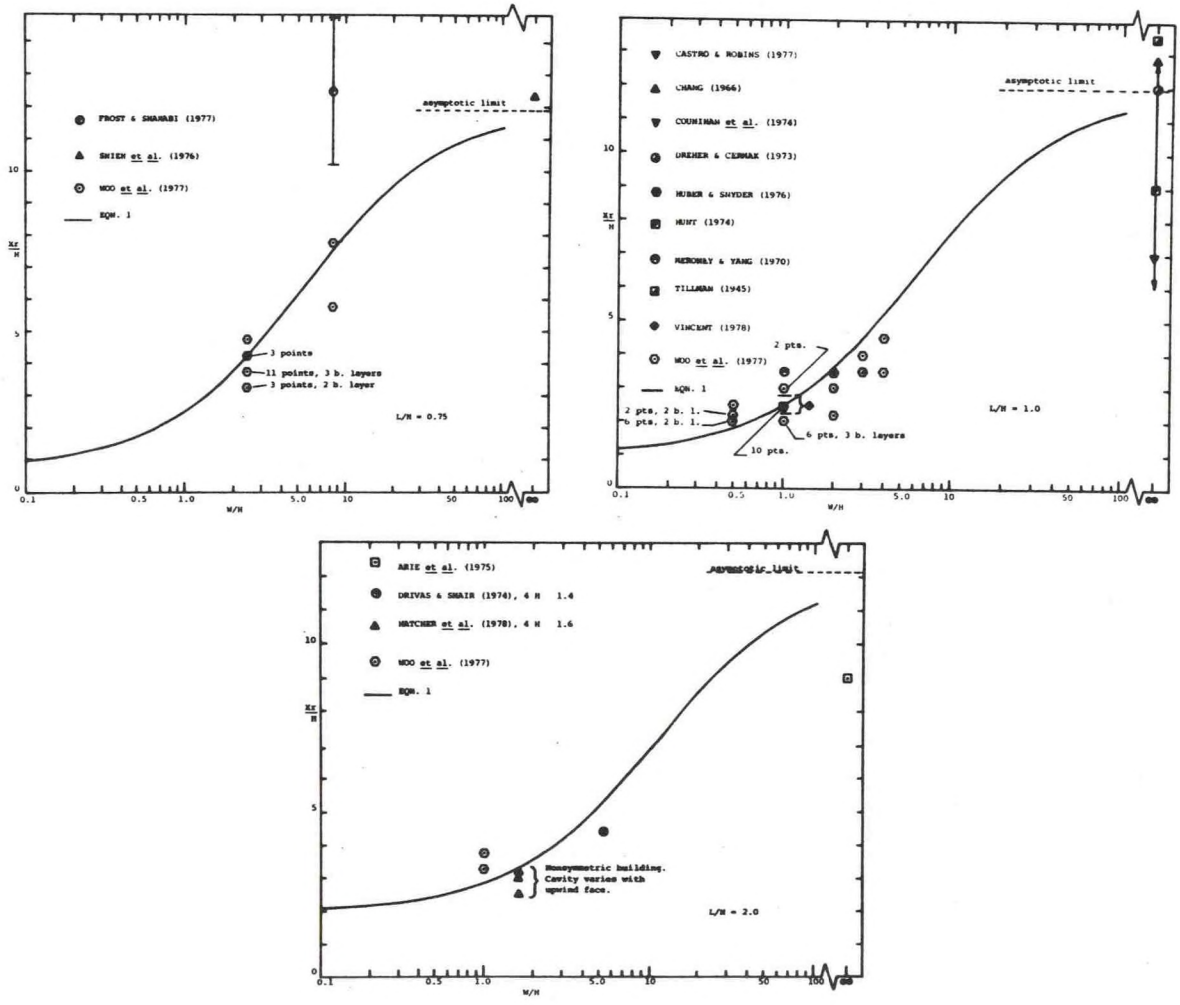

Figure 5. Comparisons of data with estimates (Eqn. (1)) of wake cavity length x_r for "short" sharp-edged buildings in deep boundary-layer flows. Building dimensions are the same as in Figure 3. Cavity length is measured from the upwind face. Three L/H ratios are shown: (a) L/H = 0.75, (b) L/H = 1.0, (c) L/H = 2.0.

REFERENCES

Arie, M., M. Kiya, H. Tamura, M. Kosugi, and K. Takoaka, 1975: Flow over rectangular cylinders immersed in a turbulent boundary layer (Part 2, flow patterns and pressure distributions). Bulletin of the JSME 18, no. 125, 1269-1276.

Arie, M., and H. Rouse, 1956: Experiments on two-dimensional flow over a normal wall. J. Fluid Mech. 1, part 2, 129-141.

A.S.M. E., 1973: Recommended Guide for the Prediction of the Dispersion of Airborne Effluents, second edition (ASME, New York), 85 pp.

Bearman, P.W., 1965: Investigation of the flow behind a two-dimensional model with a blunt trailing edge and fitted with splitter plates. J. Fluid Mech. 21, part 2, 241-255.

Bearman, P. W., 1972: Some recent measurements of the flow around bluff bodies in smooth and turbulent streams. In Proc. of Symposium on External Flows, Univ. of Bristol, July 4-6 (Univ. of Bristol, U.K., 1972), B.1 - B.15.

Bitte, J., and W. Frost, 1976: Atmospheric Flow Over Two-Dimensional Bluff Surface Obstructions. NASA contracts report CR-2750 (Avail. NTIS, Springfield, VA), 224 pp.

Bradshaw, P., and F.Y.F. Wong, 1972: The reattachment and relaxation of a turbulent shear layer. J. Fluid Mech. 52, part 1, 113-135.

Britter, R. E., J. C. R. Hunt, and J. S. Puttock, 1976: Predicting pollution concentrations near buildings and hills. Presented at Conference on Systems and Models in Air and Water Pollution, Instit. of Measurement and Control, London, Sept. 22-24, paper no. 7.

Castro, I. P., and A. G. Robins, 1977: The flow around a surface-mounted cube in uniform and turbulent streams. J. Fluid Mech. 79, part 2, 307-335.

Chang, S.-C., 1966: Velocity Field in Separated Flow Behind a Model Hill. M. S. thesis, Colorado State Univ., Ft. Collins, CO, 101 pp.

Counihan, J., 1971: An Experimental Investigation of the Wake Behind a Two-Dimensional Block and Behind a Cube in a Simulated Boundary Layer Flow. Central Electricity Research Laboratories laboratory note no. RD/L/N 115/71 (CERL, Leatherhead, Surrey, U.K.), 45 pp.

Counihan, J., J. C. R. Hunt, and P. S. Jackson, 1974: Wakes behind two-dimensional surface obstacles in turbulent boundary layers. J. Fluid Mech. 64, part 3, 529-563.

Dreher, K. J., and J. E. Cermak, 1973: Wind Loads on a House Roof. Colordo State Univ. Tech. Report CER 72-73 KJD-JEC 22 (March), 100 pp.

Drivas, P. J., and F. H. Shair, 1974: Probing the air flow within the wake downwind of a building by means of a tracer technique. Atmos. Environment 8, 1165-1175.

Evans, B. H., 1957: Natural Air Flow Around Buildings. Texas Engineering Experiment Station research report no. 59 (Texas A & M Univ., College Station, TX), 13 pp.

Frost, W., 1973: Review of data and prediction techniques for wind profiles around manmade surface obstructions. AGARD Report CP-140 presented at NATO meeting, May, Woburn Abbey, U.K.), section 4.

Frost, W., and A. M. Shahabi, 1977: A Field Study of wind Over a Simulated Block Building. NASA contractor report CR-2804, March (avail. NTIS, Springfield, VA), 131 pp.

Good, M. C., and P. N. Joubert, 1968: The form drag of two-dimensional bluff plates immersed in turbulent boundary layers. J. Fluid Mech. 31, part 3, 547-582.

Hatcher, R. V., R.N. Meroney, J. A. Peterka, and K. Kothari, 1978: Dispersion in the Wake of a Model Industrial Complex. U.S. Nucl. Reg. Comm. NUREG-0373 (avail. NTIS, Springfield, VA), 231 pp.

Huber, A. H., and W. H. Snyder, 1976: Building wake effects on short stack effluents. In Preprints of Third Symp. on Atmos. Turb., Diff. and Air Quality. Raleigh, NC, Oct. 19-22 (AMS, Boston, MA), 235-242.

Hunt, J. C. R., 1974: Wakes behind buildings. Presented at the Aeronautical Research Council's Atmospheric Environment Committee Meeting, Oct. 23 (ARC report 35601, Atmos., 22).

Hunt, J. C. R., C. J. Abell, J. A. Peterka, and H. Woo, 1978: Kinematical studies of the flows around free or surface - mounted obstacles; applying topology to flow visualization. J. Fluid Mech. 86, part 1, 179-200.

Jensen, M., 1958: The model-law for phenomena in natural wind. Ingenioren (Internat. Edition) 2, no. 1, 121-128.

Kiya, M., and M. Arie, 1972: A free-streamline theory for bluff bodies attached to a plane wall. J. Fluid Mech. 56, part 2, 201-219.

Lemberg, R., 1973: On the Wakes Behind Bluff Bodies in a Turbulent Boundary Layer. Ph.D thesis and Boundary Layer Wind Tunnel report no. BLWT-3-73 (Univ. Western Ontario, London, Ontario, Canada), 159 pp.

Leutheusser, H. J., and W. D. Baines, 1967: Similitude problems in building aerodynamics. J. of Hydraulics Div., Proc. of ASCE 93, HY 3, 35-49.

Lumley, J. L., and H. A. Panofsky, 1964: The Structive of Atmospheric Turbulence (John Wiley - Interscience, New York), 239 pp.

Meroney, R. N., and B. T. Yang, 1970: Gaseous plume diffusion about isolated structures of simple geometry. Presented at Second Internat. Clean Air Congress of the Internat. Union of Air Pollution Prevention Associations, Washington DC, Dec. 6-11, 32 pp.

Morkovin, M. V., 1972: An approach to flow engineering via functional flow modules. Beitr. z. Strömungsmechanik, A. Walz 65th Anniversary Volume, Deutche Luft und Raumfahrt Forschungsvericht, paper no. 72-27.

Ranga Raju, K. G., J. Loeser, and E. J. Plate, 1976: Velocity profiles and fence drag for a turbulent boundary layer along smooth and rough flat plates. J. Fluid Mech. 76, part 2, 383-399.

Shieh, C. F., W. Frost, and J. Bitte, 1977: Neutrally Stable Atmospheric Flow Over a Two-Dimensional Rectangular Block. NASA contractor report CR-2926 (avail. NTIS, Springfield, VA), 107 pp.

Tani, I., 1957: Experimental investigation of flow separation over a step. In Görtler, H., editor, Proc. of Boundary Layer Research Symposium at Freiburg, Aug 26-29. (Springer-Verlag, Berlin, 1958), 377-386.

Tillman, W., 1945: Volkenrode translation MAP-VG 34-45T (British Ministry of Aircraft Production, London).

Van Eimern, J., R. Karschon, L. A. Razumova, and G. W. Robertson, 1964: Windbreaks and Shelterbelts. WMO Technical Note no. 59 (WMO Secretariat, Geneva, No. 147.TP.70), 188 pp.

Vincent, J. H., 1977: Model experiments on the nature of air pollution transport near buildings. Atmos. Environment 11, no. 8, 765-774.

Vincent, J. H., 1978: Scalar transport in the near aerodynamic wakes of surface-mounted cubes. Atmos. Environment 12, no. 6/7, 1319-1322.

Woo, H. G. C., J. A. Peterka, and J. E. Cermak, 1977: Wind-Tunnel Measurements in the Wakes of Structures. NASA contractor report CR-2806 (avail. NTIS, Springfield, VA), 243 pp.

Reprinted from Preprint Volume: Fourth Symposium on Turbulence, Diffusion, and Air Pollution, Jan. 15-18, 1979, Reno, NV. Published by the American Meteorological Society, Boston, Mass.

1.4

A STATISTICAL DIFFUSION MODEL FOR USE WITH VARIABLE WIND FIELDS

Steven R. Hanna

Air Resources
Atmospheric Turbulence and Diffusion Laboratory
National Oceanic and Atmospheric Administration
Oak Ridge, Tennessee 37830

1. INTRODUCTION

Atmospheric diffusion is caused by atmospheric turbulence. Most diffusion models in use today, such as the Gaussian plume model, first (K) and second order closure models, and the boundary layer similarity models (Pasquill, 1974) are based on parameterizations of turbulence. Taylor's (1921) statistical theory of diffusion relates diffusion directly to turbulent velocity fluctuations. However, Taylor's theory has not found widespread application because it involves an integration of the Lagrangian autocorrelation function, which is not well known.

The statistical model described in this paper calculates diffusion using measurements of the mean wind field, the Lagrangian autocorrelation function $R(\tau)$, and the turbulent energy $\sigma_{u'}^2$. Because the procedure is somewhat lengthy, requiring the calculation of air parcel trajectories, it is best suited to situations in which the simpler models do not apply, such as complex terrain or time-varying turbulence. The model will be described first, and then applications to diffusion in a uniform mean wind field and a sinusoidal mean wind field will be described.

2. MODEL DESCRIPTION

The diffusion of thousands of very small air parcels released from a given source is estimated by following the trajectory of each parcel, and then computing the statistics of the ensemble of parcels for given travel times. It is assumed that the velocity $\vec{u}$ of an air parcel at time t and location (x,y,z) is the sum of a mean and a turbulent component:

$$\vec{u}(t,x,y,z) = \vec{U}(t,x,y,z) + \vec{u}'(t,x,y,z) \qquad (1)$$

The mean velocity $\vec{U}$ is given by a mesoscale observation network or by the output of a mesoscale wind model. The averaging time for the mean velocity $\vec{U}$ is typically about one hour, which determines the fraction of the energy spectrum accounted for by the turbulent velocity $\vec{u}'$.

It is further assumed, following a suggestion by Smith (1968), that the turbulent fluctuation at time $t + \tau$ is linearly related to the turbulent fluctuation at time t:

$$u'(t + \tau) = u'(t)\, R(\tau) + u'' \qquad (2)$$

where $R(\tau)$ is the autocorrelation coefficient for time lag τ and u" is a random turbulent component with variance:

$$\sigma_{u''}^2 = \sigma_{u'}^2 (1 - R^2(\tau)) \qquad (3)$$

In the applications described here, it is assumed that these formulas are valid for each of the three velocity components u,v, and w, and that they are all independent. Modifications are underway that will permit correlations among the velocity components, so that diffusion in shear flows can be more satisfactorily treated.

The validity of the linearity assumption given by equation (2) was tested by Hanna (1978) using Eulerian wind data from the Minnesota boundary layer experiment (Readings et al., 1974) and Lagrangian wind data from Idaho Falls and Las Vegas tetroon experiments (Angell et al., 1968 and 1971). Since the Lagrangian data are more appropriate to diffusion calculations, wind data from the two tetroon experiments are plotted in Figures 1 and 2. In preparing these figures, each data set was searched for values of w'(t) in a certain narrow range. The values of $w'(t + \tau)$ at a time τ later were then found and averaged to give $\overline{w'(t + \tau)}$. Thus each point on the figure represents many actual occurrences of w'(t) in the indicated range. It would be impractical to plot the hundreds or thousands of actual data pairs $(w'(t + \tau)\ ,\ w'(t))$ on a single figure. The figures show that a linear relationship does indeed exist between the turbulent fluctuations at times separated by the time lag τ, and that the proportionality factor equals the correlation coefficient $R(\tau)$. A slight departure from linearity occurs in Figure 2 for fluctuations at the tails of the distribution, but the data sample is very slim at those points.

ATDL Contribution File No. 78/14

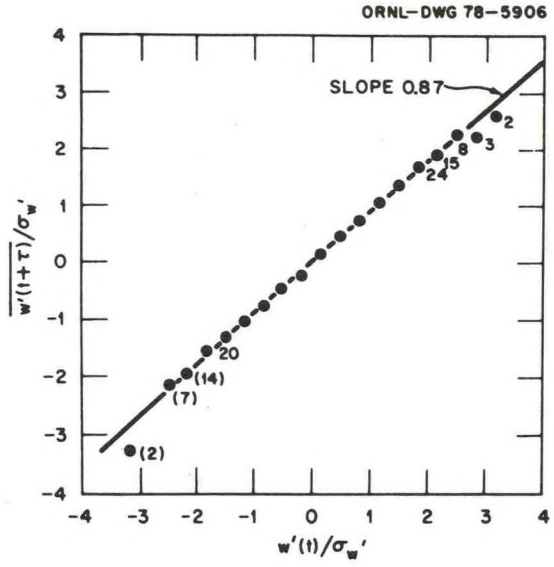

Figure 1: Normalized average $w'(t+\tau)/\sigma_{w'}$, at any time $t+\tau$ plotted versus the normalized initial fluctuation $w'(t)/\sigma_{w'}$, at time t. 25 Lagrangian tetroon runs from Idaho Falls with $R(\tau) > 0.8$ are used. Where numbers appear beneath the point, they indicate the number of runs represented (if less than 25). The straight line has a slope equal to the average correlation $R(\tau)$.

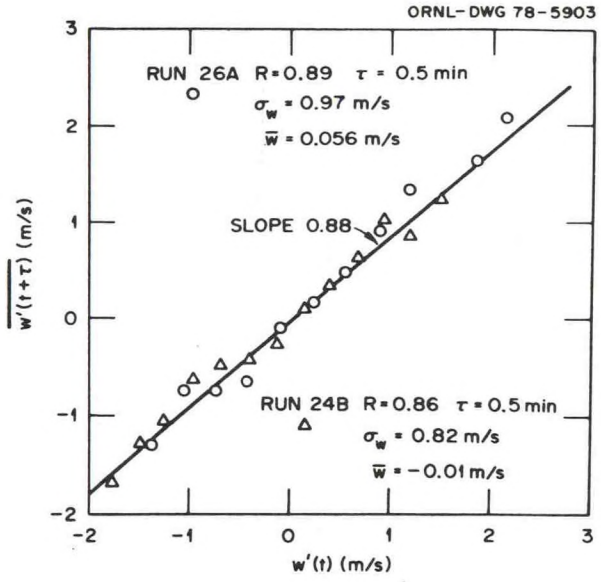

Figure 2: Average vertical velocity fluctuation $\overline{w'(t+\tau)}$ at any time $t+\tau$ plotted versus the fluctuation $w'(t)$ at time t, for two unstable Las Vegas runs. Lagrangian tetroon data.

In applying the diffusion model, it is necessary to impose a random initial distribution of turbulent speeds so that the diffusion is not conditioned by the initial speed selection. In this model, initial turbulent speeds are selected randomly from a Gaussian distribution with zero mean and variance $\sigma_{u'}^2$.

3. APPLICATION TO DIFFUSION IN UNIFORM MEAN FLOW

To test the diffusion calculation technique, the model was applied to the simplest possible mean wind field, a uniform mean flow. A time step of five minutes, turbulent variance $\sigma_{u'}^2$ of $2 m^2/s^2$, and correlation R(5 minutes) equal to 0.9 were used. At each time step, the standard deviation σ of the particle distribution was calculated, yielding the variation of σ with travel time t plotted in Figure 3. It is seen that there is a smooth transition from the power law $\sigma \propto t$ at small times ($t \ll 100$ min) to the power law $\sigma \propto t^{1/2}$ at large times ($t \gg 100$ m). This curve coincides almost exactly with the theoretical solution to Taylor's diffusion equation for an exponential correlogram ($R(t) = \exp(-t/T)$):

$$\sigma^2 = 2\sigma_v^2 T^2 (t/T - 1 + \exp(-t/T)), \qquad (4)$$

where the time scale T equals 50 minutes. With this time scale, R(5 min) = 0.9, as assumed above. As Pasquill (1974) suggests, a similar solution is obtained for other simple forms for R, such as a square wave or a ramp function, as long as the time scale T remains the same.

4. APPLICATION TO DIFFUSION IN SPATIALLY VARYING MEAN FLOW.

The following analytical expressions were chosen as an example of a steady state, non-divergent, spatially-varying mean flow:

$$U = 5\cos(\pi x/X)\sin(\pi y/Y) \quad (m/s) \qquad (5)$$

$$V = 5\sin(\pi x/X)\sin(\pi y/Y - \pi/2) (m/s) \qquad (6)$$

Mean wind vectors representing the solution to equations (5) and (6) over the domain ($0 < x < 5000$ m, $0 < y < 10000$m), for X and Y equal to 10000m, are given in Figure 4.

In the diffusion calculations, 1000 parcels were started from the point (x = 0, y = 5000m), where U = 5 m/s and V = 0. The x and y components of turbulence were assumed to be independent with $\sigma_{u'}^2 = \sigma_{v'}^2 = 1 m^2/s^2$. A time step of 10s was used, and it was assumed that $R_{u'}(10s) = R_{v'}(10s) = 0.7$. Calculations were carried out for 1000s at which time the centroid of the parcels was located at x = 3700m,

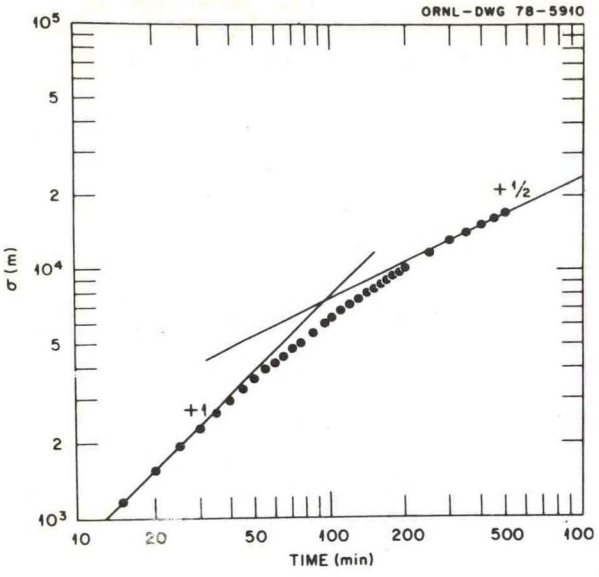

Figure 3: Dotted line is the calculated standard deviation σ of the spread of 1000 parcels from a fixed axis as a function of time after release in a uniform mean wind. Time step is 5 minutes, R(τ) is 0.9, and σ_u^2 is $2m^2/s^2$. The curve is asymptotic to lines representing power laws with slopes 1 and 1/2.

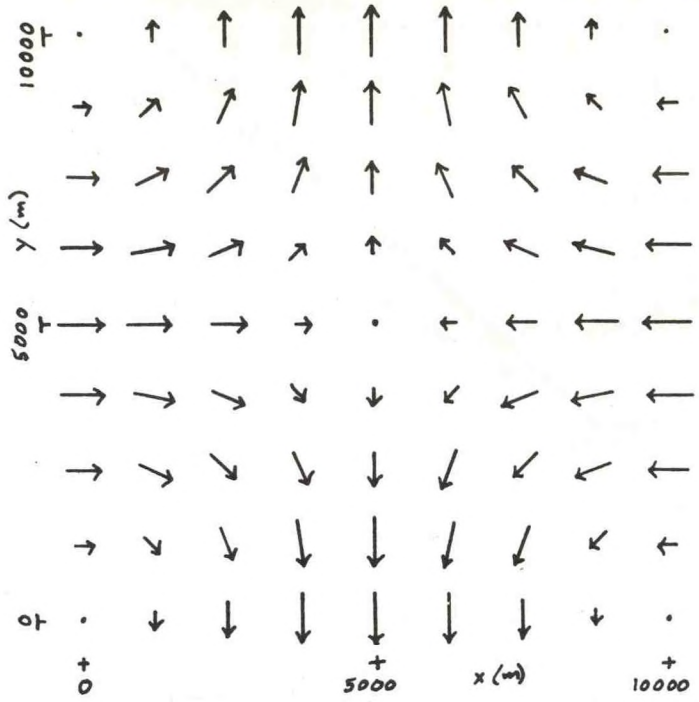

Figure 4: Pattern of wind vectors for the mean flow field defined by eqs. (5) and (6), for X = Y = 10000m.

y = 5000m; in other words the parcels travelled about 37% of the way across Figure 4. The resulting variation of σ_x and σ_y with time are given in Figure 5. Also shown are the total $\sigma = (\sigma_x^2 + \sigma_y^2)^{1/2}$ and the σ_x obtained for a uniform wind field with all other conditions the same.

For the first 3000s, σ_y equals σ_x, because ∂U/∂x and ∂V/∂y are very small. However, as the parcels approach the point (x = 5000m, y = 5000m), the mean wind gradient ∂U/∂x becomes progressively more negative, ∂V/∂y becomes progressively larger and the calculated σ_y consequently becomes greater than σ_x. In fact, σ_x remains constant at t > 5000 sec due to the balance between turbulent diffusion and convergence in the x direction. At t = 10000 sec, σ_y is about three times larger than σ_x. Also note that the slope of the σ versus t curve is increasing with time at t > 3000 sec because of the effect of mean wind shears.

These calculations illustrate the applicability of this model to any given spatial or time varying mean wind field. The turbulence parameters σ_u^2 and R(τ) can also vary with space and time. In the future this model will be applied to sets of field observations of diffusion in varying wind fields.

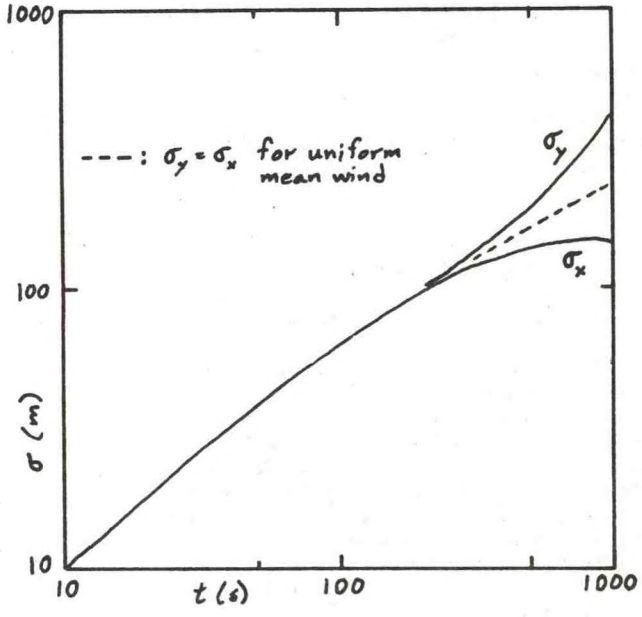

Figure 5: Standard deviation of distributions of parcel positions as a function of travel time t, for parcels originating at point (x = 0, y = 5000m) in Figure 4. $\sigma_u^2 = \sigma_v^2 = 1m^2/s^2$, $R_u(10s) = R_v(10s) = 0.7$. Eqs. (1) and (2) are used to calculate parcel trajectories.

ACKNOWLEDGEMENT

This work was performed under an agreement between the National Oceanic and Atmospheric Administration and the Department of Energy.

REFERENCES

Angell, J. K., D. H. Pack, and C. R. Dickson, 1968: A Lagrangian study of helecal circulations in the planetary boundary layer. J. Atmos. Science, 25, 707-717.

_____, and N. Delver, 1971: Lagrangian-Eulerian time-scale ratios estimated from constant volume balloon flights past a tall tower. Q. J. Roy. Meteorol. Soc., 97, 87-92.

Hanna, S. R., 1978: Some statistics of Lagrangian and Eulerian wind fluctuations. Submitted to J. Appl. Meteorol., available as report 78/6 from ATDL, P.O. Box E, Oak Ridge, TN 37830, 27 pp.

Pasquill, F., 1974: Atmospheric Diffusion, 2nd ed. Halsted Press, Ellis Horwood, NY, 429 pp.

Readings, C. J., D. A. Haugen, and J. C. Kaimal, 1974: The 1973 Minnesota atmospheric boundary layer experiment. Weather, 29, 309-312.

Smith, F. B., 1968: Conditioned particle motion in a homogeneous turbulent field. Atmos. Environ., 2, 491-508.

Reprinted from Preprint Volume: Fourth Symposium on Turbulence, Diffusion, and Air Pollution. Jan. 15-18, 1979, Reno, Nevada. Published by the American Meteorological Society, Boston, Mass.

RELATIVE AND SINGLE PARTICLE DIFFUSION ESTIMATES DETERMINED FROM SMOKE PLUME PHOTOGRAPHS

Carmen J. Nappo Jr.

Atmospheric Turbulence and Diffusion Laboratory
National Oceanic and Atmospheric Administration
Oak Ridge, Tennessee 37830

1. INTRODUCTION

Beginning with the earliest studies of the subject, see e.g. Richardson (1920), (1926), Taylor (1921), and Roberts (1923), smoke plumes and puffs have been used as measures of atmospheric turbulence and diffusion. Gifford (1957) demonstrated that space-varying values of particle dispersion parameters can be obtained from smoke puff photographs using Robert's (1923) opacity model. This treatment was later extended (Gifford 1959) to the continuous plume case. Assuming that the visible edge of a puff or plume represents a constant, line-of-sight visual threshold of integrated concentration, and that the cross-wind material destribution is Gaussian, the formula for the plume-width parameter, σ_Y, is

$$\sigma_Y^2(X) = Y_E/\ln(eYm^2/\sigma_Y^2) \qquad (1)$$

where Y_E is the half-width of the plume at a distance X from the source, Ym the maximum half-width of the plume, and e the base of natural logarithms.

When applied to an instantaneous realization of a plume, e.g. a photograph, Gifford's formula results in estimates of relative or "two-particle" diffusion; however, by superimposing several images with respect to a fixed coordinate system, or by using time-exposure photography a "time-averaged" plume can be formed and (1) then provides estimates of "single particle" or Taylor diffusion. A related technique was used by Byzova et al. (1970), who performed a comprehensive analysis of the Lagrangian time scale of turbulence using estimates of relative diffusion obtained from smoke plume motion pictures.

In this paper, eq. (1) is applied to high-altitude U-2 photographs of a long smoke plume generated during the morning hours of 17 June, 1977 at the Idaho National Engineering Laboratory near Idaho Falls.

2. THE DATA

The smoke plume was photographed four times at approximately 15 minute intervals between 0735 and 0838 (MDT). A sample photograph is shown in Fig. 1. The circles centered on the smoke source have radii of 100, 200, 400, 800 and 1,000 m. These distances were used to scale plume dimensions. During the experiment, data was also collected from a 60 m tower located near the smoke source. These data include wind speed and direction sampled about every two seconds at the 6.1, 12.2, 21.6, 30.5, 45.7 and 59.4 m levels.

Figure 1: Sample smoke plume photograph

3. RESULTS

Estimates of diffusion for the instantaneous and time-averaged plumes are shown in Fig. 2. The instantaneous plume estimates are seen to agree with Batchelor's similarity theory for the initial and intermediate diffusion times of a cluster of particles, i.e. $\sigma_Y^2 \propto t^2$ for $t < t^*$ and $\sigma_Y^2 \propto t^3$ for $t > t^*$ where t^* is a function of the initial width of the plume and the eddy dissipation rate. The time-averaged plume results agree with Taylor's theory of single-particle diffusion, i.e. $\sigma_Y^2 \propto t^2$ for $t < \tau_L$ where τ_L is the Lagrangian integral time scale.

One way of checking these results is to compare the turbulence time scale derived from the smoke plume photographs with that derived from the met. tower data. Byzova et al. (1970) show that the Lagrangian integral time scale,

ATDL Contribution File No. 78/15

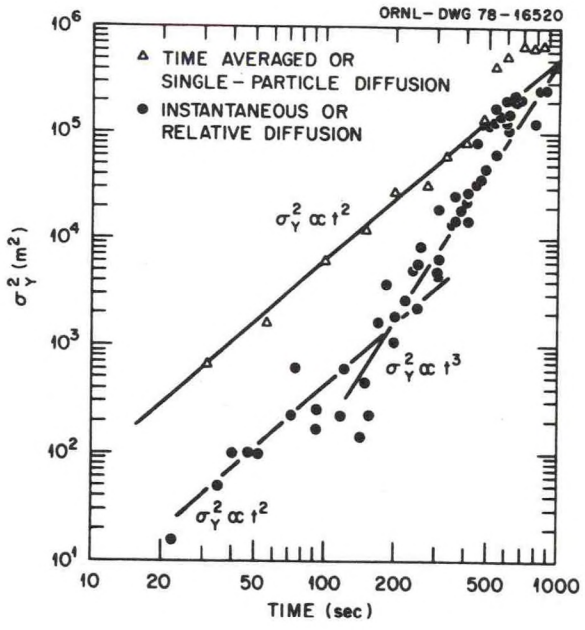

Figure 2: σ_Y^2 versus time for the instantaneous and time-averaged plumes.

τ_L, can be obtained from

$$\tau_L = \tau_B/2.32 \qquad (2)$$

where τ_B is defined by the condition

$$\sigma_1^2(\tau_B) = 0.8\,\sigma_2^2(\tau_B) \qquad (3)$$

where σ_2^2 refers to single particle diffusion and σ_1^2 refers to two particle diffusion. From Fig. 2, it is determined that $\tau_B \simeq 400$ sec. so that from (2) $\tau_L \simeq 170$ sec. Using the wind speed data from the 59.4 m level of the met tower, the Eulerian integral time scale, τ_E, was found to be about 30 sec. Gifford (1967) showed that the ratio of the Lagrangian to Eulerian time scale, β, varies with stability being equal to 1-3 during daytime, unstable conditions and 6-12 during nighttime, stable conditions. If we choose for β a value of 6, reflecting the early morning stable to neutral condition, then $\tau_L = \beta\tau_E \simeq 180$ sec. This value agrees reasonably well with that derived from the plume photograph analysis.

4. CONCLUSION

The application of eq. (1) to individual and composite photographs of a single long smoke plume generates estimates of diffusion which are in agreement with single-and two-particle diffusion theory. These results indicate that the use of eq. (1) in conjunction with high-altitude (e.g aircraft of satelite) smoke plume photographs is an economical way to obtain atmospheric diffusion estimates over long distances and/or over very complex terrain.

5. ACKNOWLEDGMENTS

This study could not have been made without the help of the U.S. Air Force. Special thanks goes to Col. William Lawson and Lt. Col. Ibbotson of Beale Air Force Base for their arrangement of U2 flights over the test area.

This work was performed under an agreement between the National Oceanic and Atmospheric Administration and the Department of Energy.

References

Richardson, L. F., 1920: Some measurements of atmospheric turbulence. (Phil. Trans. A 582. pp. 1 - 28.

_____, 1926: Atmospheric diffusion shown on a distance neighbor graph. Proc. Roy. Soc. A110, pp. 709-737.

Taylor, G. I., 1921: Diffusion by continuous movements. Proc. Lond. Math. Soc. 20, pp. 196-212.

Roberts, O.F.T., 1923: The theoretical scattering of smoke in a turbulent atmosphere. Proc. Roy. Soc. A 104 pp. 640-654.

Gifford, F. A., 1957: Relative atmospheric diffusion of smoke puffs. J. Met. 14, pp. 410-414.

_____, 1959: Smoke plumes as quantitative air pollution indices, Int. J. of Air Poll., 2 pp 42-50.

_____ 1967: Variation of the Lagrangian - Eulerian time scale relationship with stability. Proc. USAEC Meteorological Information Meeting, Sept 11-14, Chalk River Nuclear Laboratories, Atomic Energy of Canada Limited, Chalk River, Ontario.

Byzova, N. L., Ye.K Garger and V. N. Ivanov, 1970: Experimental estimation of the Lagrangian time scale of turbulence. Izv. Atmos. Oceanic Phys., 6 pp. 315-320.

CLIMATOLOGICAL MONITORING PROGRAM BY ATDL AT FOREST METEOROLOGY SITE ON WALKER BRANCH WATERSHED

Detlef R. Matt

Air Resources
Atmospheric Turbulence and Diffusion Laboratory
National Oceanic and Atmospheric Administration
Oak Ridge, Tennessee 37830

I. Introduction

The Atmospheric Turbulence and Diffusion Laboratory (ATDL), National Oceanic and Atmospheric Administration (NOAA), has monitored climatological parameters at the forest meteorology research site adjacent to the Walker Branch Watershed (WBW) since November, 1977. The purpose of this monitoring program is to provide needed baseline data for several research programs at ATDL and Oak Ridge National Laboratory (ORNL), in particular the terrestrial and aquatic ecology sections of the Environmental Sciences Division (ESD).

Historically, the ATDL has furnished meteorological data for the Oak Ridge area since the 1940's periodically publishing extensive reports summarizing its findings (Ref. 1,2,3,4). Additionally, these climatological records for Oak Ridge are archived and available from NWS, Federal Office Building, Ashville, NC. The new monitoring program on WBW is not intended to replace the historical program but to provide complimentary data not currently available. The climatological variables monitored are primarily concerned with radiation balance and air flow characteristics above a forested landscape.

ATDL Contribution File No. 78/16

Although the data recorded would suffice to estimate dose and predict potential radiological hazards in event of an accidental release, the nature of the data logging system and data retrieval routines are such that minimum turnaround would be several hours. Thus it is felt that the data collected at WBW cannot take the place of a meteorological monitoring program at ORNL.

II. Site Description

The forest meteorology research site is located on a ridgetop immediately west of WBW and its location is shown relative to historical monitoring sites in Fig. 1. The ridgetop vegetative cover consists of a mixed deciduous forest composed primarily of various species of oaks and hickory with the dominant trees being 24 m tall. The instruments are mounted on a 44 m aluminum walkup tower which allows meteorological measurements to be made to twice the height of the dominant trees. Additionally, the tower affords unobstructed views of the Bull Run power plant stack (14 km) to east and the Kingston power plant stacks (22 km) to west which together with the Y-12 power plant (4 km to northeast) have been studied as major sources of pollutant inputs to the WBW (5,6). A more complete description and other components of the forest meteorology research program is given elsewhere (7).

III. Measurement Program

The forest meteorology measurement program is segregated into two distinct data collection schemes which are labeled continuous and intermittent. The continuous program is intended to provide baseline data of climatological parameters that are of interest to various DOE research

programs in Oak Ridge (8). Intermittent data collection is intended to coincide with specific experiments performed at the forest meteorology site or to coincide with experiments by ORNL on WBW (or elsewhere) for which the data are useful.

The continuous measurements consist primarily of electromagnetic radiation measured in the earth-sun wavebands. A list of instruments and variables monitored is given in Table 1. A schematic representation of waveband components measured by different instruments is shown in figure 2 on a logarithmic scale. The electromagnetic spectrum measured is broken into wavebands characterized by ultraviolet, visible (photosynthetically active), near infra-red and far infra-red. The direct

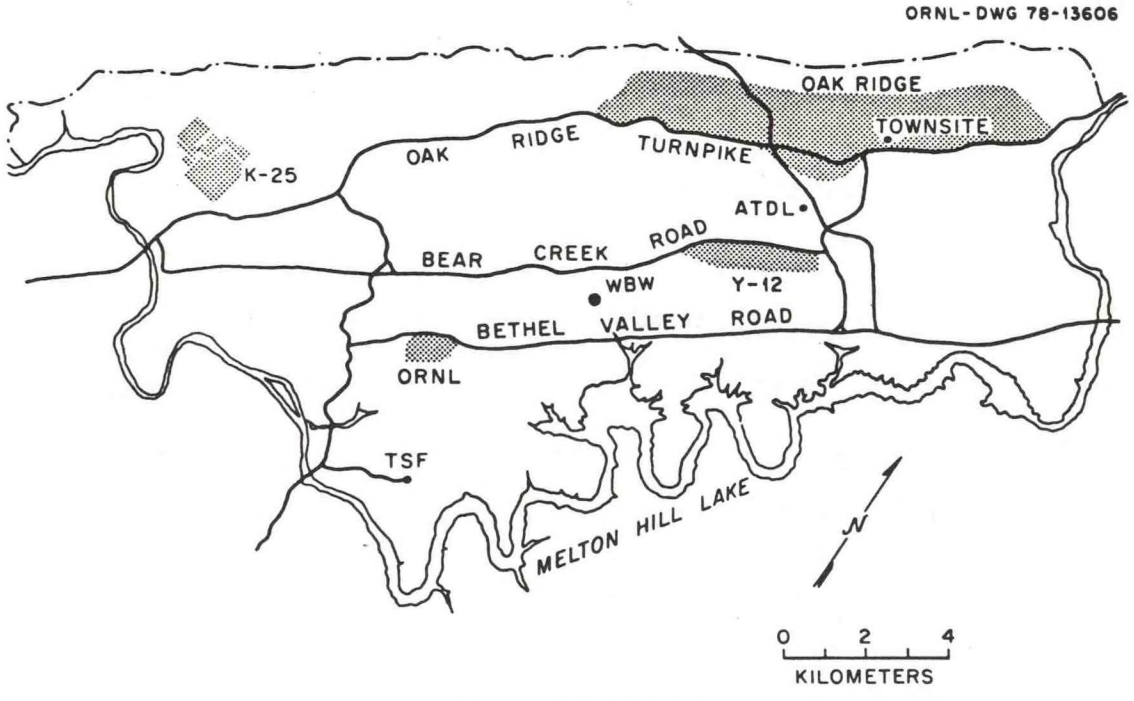

Figure 1: Location of Forest Meteorology Research site adjacent to Walker Branch Watershed (WBW), relative to historical monitoring sites. A 44 m. walkup tower and two 33.5 m triangular towers are available for instrument platforms.

TABLE 1 SOLAR RADIATION MONITORING STATION INSTRUMENTATION

Item	Measurement	Instrument	Wave band	Manufacturer & Model	Comments
1	global	pyranometer	.285 - 2.8 μ	Eppley Model II PSP	Cosine response ± 1%, linearity ± 0.5%, temperature compensated, double domed WG7 glass
2	diffuse	pyranometer	.285 - 2.8μ	Eppley Model II	same as #1
3	net all wave	net pyradiometer	.3 - 60 μ	Swissteco Model S-1	Cosine response - 4% single polyethylene dome inflated & desiccated with N_2 gas.
4	incident all wave	net pyradiometer with black body cav.	.3 - 60 μ	Solar Radiation Instruments	Same as #3 above with black body cavity on lower hemisphere, T monitered with YSI thermisters
5	near infra-red	pyranometer with RG-8 filter	.7 - 2.8 μ	Eppley Model II PSP	Same as #1 above except outer dome is made of RG-8 filter with .7μ cutoff
6	photosyn thetically active radia-tion (PAR)	pyranometer	.4 - .7 μ	Lambda Instru. Model LI-190S	Silicon cell quantum detector with interference filters.
7	reflected PAR	pyranometer	.4 - .7 μ	Lambda Instr. Model LI-190S	Same as #6 above except mounted with sensor surface facing down.
8	ultraviolet	ultraviolet radiometer	.295 - .385 μ	Eppley TUVR	Selenium quantum detector with quartz coating 2.5% cosine response
9	normal incident	normal incident pyrheliometer	.25 - 4. μ	Eppley N.I.P.	Pyrheliometer is mounted on solar tracker and has wheel for mounting OG-1, RG-2, RG-8 filters
10	shortwave albedo	pyranometer	.3 - 2.5 μ	Kipp & Zonen pyranometers	Two K & Z. pyranometers one upright, one inverted, cosine response + 5%

TABLE 1 SOLAR RADIATION MONITORING STATION INSTRUMENTATION (continued)

Item	Measurement	Instrument	Wave band	Manufacturer & Model	Comments
11	temperature	thermisters		Yellow Springs YSI-44032	± 0.1°C interchangeability mounted in aspirated shelters at 44 & 29.5 m, and on tra system
12	wind	cup anem. & dir. vane	0-44 m/s 0-540°	Weathermeasure Model W-1034	1% accuracy at 44 & 29.5 m hts.
13	pressure	electronic barometer	26-32 in Hg	Sensotec, Inc. TJE	
14	short wave inclined	pyranometer at 45°	.3-2.5 μ	Kipp & Zonen	same instrument as #10

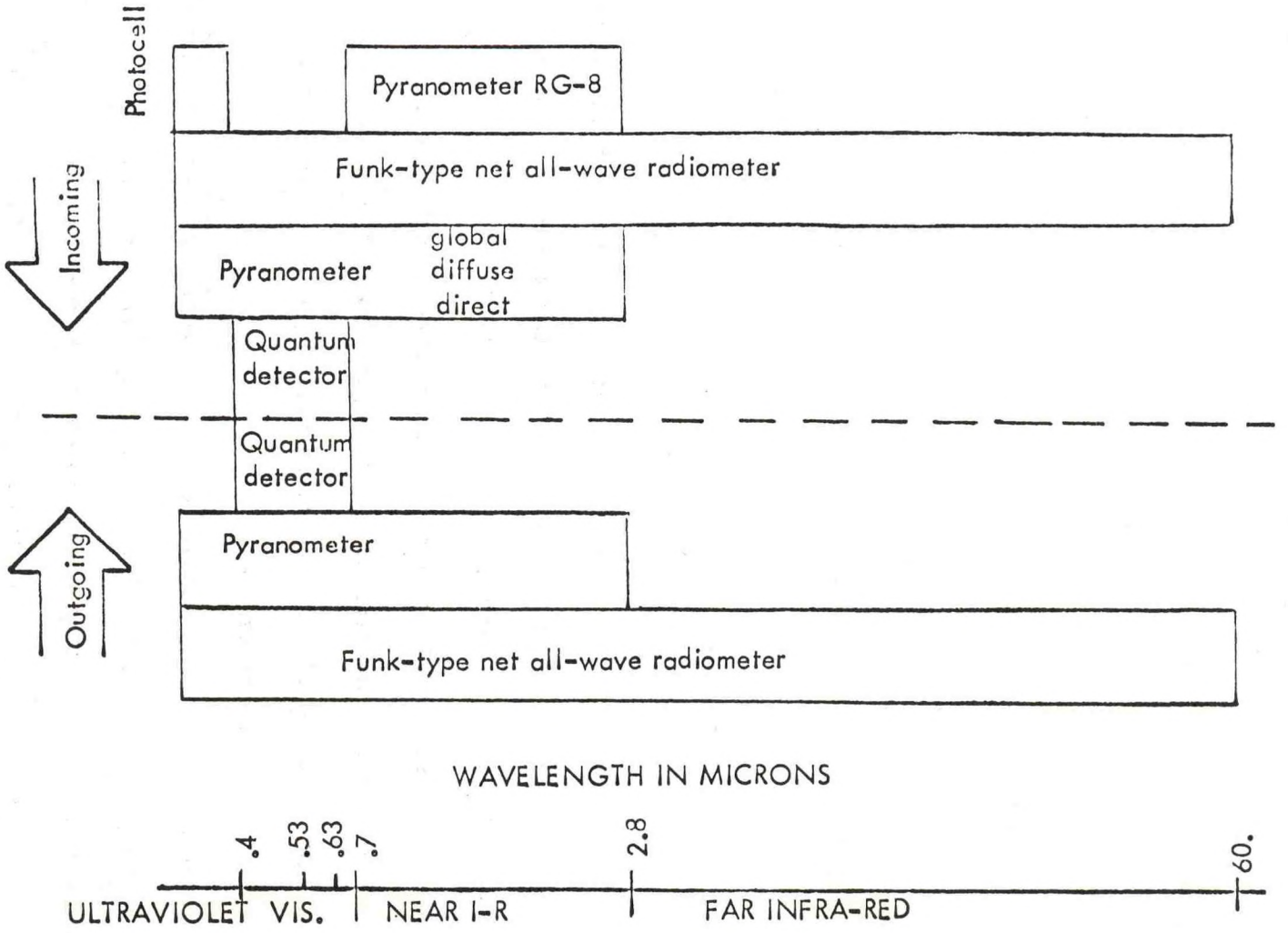

Figure 2 ELECTROMAGNETIC RADIATION WAVEBANDS MEASURED BY SOLAR MONITORING STATION

component measured by a normal incident pyrheliometer can be further divided by cutoff filters at the .53μ, .63μ, and .7μ wavelengths. Instruments measuring the incident radiation are mounted on platforms atop a 44 m walkup tower. These include items 1,2,5,8,9,11, and 12 listed in Table 1. The radiation balance components are measured by instruments mounted on a tram riding on cables 33.5 m above the ground surface and 9 m above the forest canopy (items 3,4,6,7,10, and 11 in table 1). Thus the radiation balances measured in various wavebands above the forest yield the values from a natural surface. The tram is shown in Fig. 3, as seen from the top of the walkup tower. For routine data collection the tram is located 10 m from the walkup tower.

The incident global radiation can be divided into diffuse and direct components since one pyranometer is provided with a shade ring. Accurate correction factors for sky occluded by shade ring is determined from normal incident pyranometer measurements of direct beam radiation. These measurements are particularly useful for scientists and engineers in the field of solar heating and cooling. (ref. 8)

In addition to the radiation measurements, the horizontal component of the wind speed and direction and temperature are measured continuously at 44 m and 29.5 m. Precipitation is measured at 44 m and 0 m with tipping bucket raingauges.

During experiments the number of variables monitored are normally increased significantly. The investigator can choose the number, location and type of instruments to be monitored. Table 2 gives a partial list of convenient measurements that can be made at the forest meteorology research site. Normally an experiment would not incorporate all measurements simultainously since interpretation of results would

Figure 3:

Instrumented tram used to measure radiation fluxes to forested landscape in visible, short wave and all-wave wave bands.

Table 2

Item	Measurement	Comments
1.	temperature	bead thermisters are located in aspirated shelters at 1,3,9,18,20.5,26,27, 32m.
2.	humidity	six Vaisala relative humidity probes are available to be mounted in any of the aspirated shelters or on an instrument tram.
3.	radiation fluxes	tram cable ways are located at 1,6,10.5,14,17,21,26,33.5 m heights in and above the forest. Seven complete instrument packages are available to measure radiant fluxes as discussed in text above. These trams are moveable and capable automatically transversing the center 30 m between towers.
4.	wind speed	The heated film anemometers are available to measure horizontal components of wind vector.
5.	turbulent fluxes above canopy	two gill uvw anemometers are available for momentum flux measurements above the canopy.
6.	vector wind	a propeller bivane anemometer and item 5 can give wind vector above canopy.
7.	eddy correlation	heat, mass, and momentum fluxes can be determined within the canopy using eddy correlation techniques. Instruments are fast response platinum wire resistance thermometers, ion flow anemometers, and Lyman alpha humidiometers.

tax several investigators for a long time.

IV. Quality Control and Availability

An Esterline-Angus PD2064 data acquisition system is used for monitoring the instruments in continuous measurement scheme. This data logger is microprocesser controlled and has the capability of scanning up to 25 channels/sec. with resolution of 40,000:1 in ranges of $\pm$ 4V, $\pm$ 400mV and $\pm$ 40 mV. The current configuration allows sampling up to 64 channels, numerically averaging over a specified number of scans and writing average results on 9 track IBM compatible magnetic tape.

In the normal operating mode, instruments are scanned every 10-15 sec and one minute averages are recorded on magnetic tape. Battery powered 0-10 mV strip charts are used as backup for global and diffuse radiation. Instruments are checked for alignment and level and the domes are cleaned daily.

Engineering units are converted to scientific units on IBM 360/91 at ORNL. Comparison of instruments to shelf standard is done quarterly. The shelf standard is compared once a year to the NOAA reference standard at the Solar Radiation Calibration Facility, Air Resources Laboratory, Boulder, Colorado and thus pyranometer measurements are given on the Absolute Pyrheliometric Scale.

During experiments additional data logging capabilities are required. A computer controlled (PDP 8e) data acquisition system capable of scanning 200 channels under six separate scan sequences is available. Thus a total of 264 channels can be monitored automatically at any time. The data loggers, instrument translators and power supplies are all protected by surge suppressors. All

instrument signals are transmitted by shielded pairs of #20 wire, all encased in aluminum conduit. Fuses and surge suppressers across signal lines afford additional protection to data acquisition systems.

After conversion into scientific units, data sets are stored on magnetic tapes and direct access disks on the ORNL computer system. Local users can directly access hourly values through the Ecosystem Analysis Data Center, ORNL. The current contact is Ms. J. Watts, ESD, Bldg. 1505, room 354 tel. 3-0493.

The climatological records are archived as a cooperating station to the NOAA-DOE Solar Network and summary tapes are available from the National Climatic Center, Federal Building, Asheville, NC. Because of the large amount of data accumulated, only hourly totals are normally available, however limited record lengths of one minute values are available on magnetic tape through D. R. Matt, ATDL-NOAA, P.O. Box E, Oak Ridge, TN. (Telephone FTS 850-4081).

References

1. USAEC ORO-99, A Meteorological Survey of the Oak Ridge area (1953).

2. USAEC ORO-199. Supplementary Meteorological Data for Oak Ridge (1963).

3. U.S. Dept. of Commerce, NOAA, ERL, ATDL. Daily, Monthly, and Annual Climatological Data for Oak Ridge, Tennessee, Townsite and Area stations January 1951 through December 1971 (1972). ATDL Contribution file No. 61.

4. Culkowski, W. M., Average Daily Solar Radiation for Oak Ridge, Tennessee, 1956-1975. U.S. Dept. of Commerce, NOAA, ATDL contribution file No. 77/2.

5. Andren, A. W., S. E. Lindberg, and L. C. Bate, "Atmospheric Input and Geochemical Cycling of Selected Trace Elements in Walker Branch Watershed", ORNL-NSF-EATC-13 (1975).

6. Lindberg, S. E., A. W. Andren, R. T. Raridon and W. Fulkerson, "Mass Balance of Trace Elements in Walker Branch Watershed: Relation to Coal-Fired Steam Plants", Envir. Health Persp. Vol. 17, pp 9-18, (1975).

7. Hutchison, B. A., Atmospheric Turbulence and Diffusion Laboratory Deciduous Forest Meteorology Research Program: An Overview, ATDL Contr. File No. 77/1.

8. Kronenberger, E. J., J. S. Newman, C. V. Dentriou and R. D. Orlandi, "Comparison of Flat Plate and Cylindrical Parabolic Focusing Solar Energy Collectors for Oak Ridge", ORNL-MIT-192, (1974).

METEOROLOGICAL EFFECTS OF HEAT AND MOISTURE RELEASES FROM HYPOTHETICAL POWER PARKS

K. S. Rao and R. P. Hosker
Atmospheric Turbulence and Diffusion Laboratory
National Oceanic and Atmospheric Administration
Oak Ridge, Tennessee

ATDL Contribution File No. 78/17

WITHDRAWN

[Reprinted from BULLETIN OF THE AMERICAN METEOROLOGICAL SOCIETY, Vol. 60, No. 4, April 1979]
Printed in U. S. A.

Forest Meteorology, Research Needs for an Energy and Resource Limited Future, 28–30 August 1978, Ottawa, Ontario, Canada

Boyd A. Hutchison [1]

A workshop entitled *Forest Meteorology, Research Needs for an Energy and Resource Limited Future,* was convened 28–30 August 1978 at the University of Ottawa in Ottawa, Ontario. This workshop was held in conjunction with the World Meteorological Organization's International Symposium on Forest Meteorology and was sponsored by the Division of Biomedical and Environmental Research, U.S. Department of Energy.

Forty-two scientists representing Canada and the United States as well as Spain, Sweden, and the United Kingdom participated in the workshop. Current research efforts were discussed and research needs critical to the development of unifying theories in forest meteorology were identified.

The lack of knowledge most seriously limiting the development of unifying theories at this time involves the mechanics of turbulent exchanges. Studies are needed of the mechanisms by which turbulence is created, transported, and destroyed in forest canopies, of the structural characteristics and aeroelastic properties of forests which control the generation and dissipation of turbulence, and of the turbulence structure of the boundary layer above forests.

Less critical but of considerable importance in view of societal problems of energy and resource limitations is the problem of radiation exchanges in and above forests and of how they relate to forest productivity. Simple techniques must be developed for the determination of the structural features of forests that control radiation exchanges and these structural data must then be used to validate existing radiation exchange models which have largely been developed and tested in agricultural crop canopies. With a better understanding of how forest structure controls radiation penetration and consequently, photosynthetic production, possibilities for genetically engineering highly productive forests for energy, fiber, or saw logs could be better assessed.

It was further noted that the historical absence of responsibility for forest meteorology in either the forestry or weather service bureaucracies of Canada and the U.S. has seriously hampered advancement of scientific knowledge in this field. Most forest meteorology research conducted in the past was made in support of other research efforts; as a result, there has been little continuity in our research efforts. The workshop recommended that serious consideration be given to the establishment of federal agency responsibility for forest meteorology and suggested that an organization along the lines of the Pinchot Institute or the Eisenhower Consortium of the U.S. Forest Service may serve to administer such responsibility.

Finally, the workshop created a task force on forest meteorology that was charged to continue efforts on behalf of this field of science in terms of specific workshop recommendations. Task force members include Lloyd W. Gay, University of Arizona, Tucson; James Harrington, Forest Fire Research Institute, Ottawa, Ontario; Willy Z. Sadeh, Colorado State University, Fort Collins; Roger H. Shaw, Purdue University, West Lafayette, Indiana; Stan Tajchman, West Virginia University, Morgantown; and chairman, Boyd A. Hutchison, Atmospheric Turbulence and Diffusion Laboratory, National Oceanic and Atmospheric Administration, Oak Ridge, Tenn.

Proceedings of this workshop will be published early in 1979. Copies will be available from B. A. Hutchison, ATDL, NOAA, P.O. Box E, Oak Ridge, Tenn. 37830. •

[1] Atmospheric Turbulence and Diffusion Laboratory, NOAA, Oak Ridge, Tenn. 37830.

0003-0007/79/040331-01$04.50

ATDL Contribution File No. 78/18

Environmental Research Laboratories

Air Resources
Atmospheric Turbulence and Diffusion Laboratory

Oak Ridge, Tennessee

1977 ANNUAL REPORT

MEASURED σ_y AND σ_θ IN COMPLEX TERRAIN
NEAR THE TVA WIDOWS CREEK, AL, STEAM PLANT

by
Steven R. Hanna

Air Resources
Atmospheric Turbulence and Diffusion Laboratory
National Oceanic and Atmospheric Administration
Oak Ridge, TN 37830
September 1979

Accepted for publication in Atmospheric Environment.

ATDL Contribution File No. 78/20

MEASURED σ_y AND σ_θ IN COMPLEX TERRAIN NEAR THE TVA WIDOWS CREEK, AL, STEAM PLANT

By
Steven R. Hanna

Air Resources
Atmospheric Turbulence and Diffusion Laboratory
National Oceanic and Atmospheric Administration
Oak Ridge, TN 37830

ABSTRACT

The Widows Creek Steam Plant, operated by the Tennessee Valley Authority (TVA), is located on the banks of the Tennessee River, with a 250m terrain step two kilometers to the southeast and an irregular 300m plateau ten kilometers to the northwest. Two years of hourly meteorological and ground level SO_2 concentration data from the valley and plateau adjacent to the step were studied. Strong channeling of flow in the valley was found. Horizontal wind fluctuations measured at a height of 61m on the valley meteorological tower were enhanced by about 60% during cross valley flows, due to large horizontal eddies set up by the terrain irregularities.

Thirty cases of northwest flow persisting for at least six hours towards the step were analyzed in detail. Observed one hour and ten

hour averages of σ_y on an SO_2 sampling arc on the plateau at a distance of 3.2 km from the steam plant were 500m and 670m, respectively. Predictions of σ_y were made by the formula $\sigma_y(x) = (\sigma_{yo}^2 + (\sigma_\theta \times f(x))^2)^{1/2}$ where σ_{yo} is an initial value (200m) due to the finite size of the source, σ_θ is the standard deviation of wind direction fluctuations measured at a height of 61m on the meteorological tower in the valley, and f(x) is a dimensionless function given by Pasquill (1976). The predicted σ_y's are 28 to 39% less than observed values. The discrepancy may be caused by increased diffusion as the air flows up the terrain step.

1. Introduction

There is much current interest in diffusion in complex terrain, but very little quantitative information is available (Egan, 1975). The 2600 Mw Widows Creek, AL, Steam Plant of the Tennessee Valley Authority provides an excellent location for the study of the effects of complex terrain on air flow and diffusion. As shown in Figure 1, the coal-fired steam plant is located in a flat valley about 1.6 km northwest of the base of a fairly steep (15° slope) nearly two dimensional step, which rises 250m in a horizontal distance of 1000m to a plateau called Sand Mountain. Diffusion from the plant is also influenced by an irregular 300m plateau which begins from five to ten kilometers northwest of the plant, as seen in Figure 2. The six 82m stacks and two 152m stacks are marked on Figure 1, as well as the two 61m meteorological towers and six SO_2 stations used in this study.

The Tennessee Valley Authority collects and stores continuous high-quality hourly data from Widows Creek, but has not used these data for research purposes. We obtained data tapes from TVA for the two year period January 1976 through December 1977. During the last six months of this period, effluents from the short 82m stacks were gradually switched over to a new 305m stack. Data studied from the mountain and valley meteorological towers included wind speed and direction, temperature, and σ_E and σ_θ (vertical and horizontal cross wind standard deviations of wind direction fluctuations,) at heights of 10m and 61m. To supplement these meteorological observations, vertical profiles of wind speed and temperature through the full depth of the planetary boundary layer are obtained at least once each day by means of aircraft flights, radiosonde releases, and pibal tracking. There are usually about ten to twenty SO_2 monitors in operation at any given time, but the six in the southeast sector were the only ones used in this report. Because TVA had a problem with high ground level concentrations on the plateau, an arc of five SO_2 stations was set up at a distance of about three to four kilometers from the plant. Estimates of σ_y were made from SO_2 observations on this arc.

2. Wind Velocity Variations on the Meteorological Towers.

The 61m meteorological towers on the plateau and in the valley provide an opportunity to compare wind velocities. Figure 3 contains the wind roses for the plateau and valley sites, showing the nearly uniform wind direction frequency distribution on the plateau

and the strong channeling of winds at the valley site. At the valley station, up or down valley winds occur about five times more often than cross-valley winds.

Joint frequency distributions of wind direction at the 61m levels on the valley and plateau towers were also tabulated. For SW or NE wind directions at the plateau station, which probably more accurately represents the synoptic wind direction, the valley wind directions are also strongly SW or NE. But, for example, when the plateau wind direction is from 0 to 160°, the valley wind direction is most likely from 20 to 40° (down valley). Similarly, when the plateau wind direction is from 180° to 280°, the valley wind direction is most likely from 200 to 220° (up valley). However, for NW winds, the plateau and valley wind directions are similar, probably due to the tendency for NW winds to be associated with high wind speeds following cold front passage, when the winds are too strong to be deflected.

3. σ_θ Variations on the Meteorological Towers.

Panofsky et al. (1978) showed that the standard deviation of wind direction fluctuations, σ_θ, was sensitive to mesoscale terrain properties. Their observations 500m to the lee of a low mountain suggested that σ_θ was 2.5 times as strong in that location as over horizontal terrain. They also concluded that σ_θ was enhanced by 40% in slightly rolling terrain. The reason for the increase is the presence of persistent low frequency horizontal eddies set up by the hills.

The Widows Creek σ_θ data were studied to see if σ_θ was enhanced during flow from the mountains to the SE or NW of the plant. In the surface layer over horizontal terrain in neutral conditions, σ_θ is theoretically a function of roughness length, z_o:

$$\sigma_\theta = \sigma_v/U = 0.8/\ln(z/z_o) \qquad (1)$$

Therefore the data were first analyzed to determine the variation of roughness length, z_o, as a function of wind direction at each tower. The usual assumption of a logarithmic wind profile was made. To insure neutral conditions, only those data were used for which two conditions were satisfied:

u(61m) > 2 m/s, and a bulk stability parameter,

$$B = (T(61m) - T(10m) + .51)/U_{61}^2 \qquad (2)$$

was between -.005 and +.005. The numerator in this expression is the potential temperature difference between the two levels. A total of about 50 hours of data was used to determine the roughness for each wind direction. These roughnesses are probably representative of the local terrain out to a distance of about 600m ten times the tower height from the towers, and do agree qualitatively with patterns of agricultural fields and woodlands surrounding the two towers.

The important feature of the "roughness roses" in Figure 4 is that the local roughness at the valley tower is least (.2m to .6m) for SE and NW wind directions, and greatest (.7 to 1.6m) for SW and NE wind directions. In other words, wind trajectories from the mountains are characterized by relatively low local roughnesses, and on the basis of

equation (1) alone, the ratio σ_θ (NW or SE)/σ_θ (NE or SW) at the valley tower would be predicted to be about 0.8.

Measured variation of σ_θ with wind direction on the valley tower has the opposite behavior (see Figure 5), with the observed ratio σ_θ (NW or SE)/σ_θ(NE or SW) equal to about 1.3. The data given in the figure are restricted to nearly neutral conditions ($0 < B < .005$) in order to minimize the influence of stability on the results. Thus, taking into account the factor 0.8 introduced by roughness differences, the total enhancement of σ_θ at the valley tower due to upstream complex terrain is a factor of about $1.3/0.8 = 1.6$. This factor is less than that found by Panofsky et al. (1978), but the difference can be explained by the fact that the mountains at Widows Creek are two to ten kilometers from the tower, whereas the mountain in the experiment by Panofsky et al. (1978) was only 0.5 km from their tower.

Graphs of σ_θ versus wind direction on the valley tower were drawn for other stability (B) classes. It was found that the σ_θ enhancement factor was about the same (1.6) for unstable conditions and slightly greater (about two) for stable conditions. It is expected that the enhancement would be greater during stable conditions, when the high frequency component of σ_θ is reduced but the low frequency, terrain induced component persists.

Vertical fluctuations σ_E were also studied at each tower to try to verify the conclusion by Panofsky et al. (1978) that σ_E is not

influenced by complex terrain. Presumably vertical eddies set up by the complex terrain rapidly die out due to the inhibiting effects of the ground surface and stability. But there was definitely a variation of σ_E with wind direction at the valley tower. During neutral conditions the enhancement of σ_E was about 30%, or one half that of σ_θ. However, in stable conditions σ_E shows no enhancement at the valley site, probably due to the rapid decay of terrain induced fluctuations.

No significant variation of σ_E or σ_θ with wind direction at the mountain tower was found.

4. Analysis of Hourly SO_2 data during NW Winds

The data tapes for 1976 - 1977 were searched for periods during which NW wind directions (295° - 335°) persisted at both the valley and mountain stations for six hours or more. These wind directions would assure a fairly steady plume direction toward the terrain step located 1.6 km SE of the plant. During the two year period these conditions were satisfied on thirty occasions with average duration of ten hours mostly during the winter season. All occasions were associated with cold air advection following frontal passage with wind speeds at 61m on the plateau tower ranging from 4.4 to 8.4 m/s. On the average, the hourly valley and plateau wind directions agree within three degrees. Inspection of radiosonde, pibal, and aircraft profiles suggests a well mixed layer extends to a height averaging one kilometer or four times the step height.

To understand the ground level SO_2 concentration patterns, it is necessary to know the source characteristics. The six

82m stacks and two 152m stacks are located on the map in Figure 1 and a photograph of these stacks is given in Figure 6. Stacks 1 to 6 have exit diameters of 4.3m, are spaced 16m apart, and are on a 37m high by 79m long building. Stacks 7 and 8 have exit diameters of 6.8m, are spaced 50m apart, and are on a 47m high by 41m long building. Emissions of SO_2 from the two groups of units (1-6 and 7-8) are approximately equal, averaging 2500 g/sec.

Because of ground level SO_2 problems due to the short stacks on units 1 to 6, TVA constructed a 305m stack to replace them, and the old units were tied into the new stack on days 357, 214, 121, 178, 261, and 328 of 1977, respectively. Five of our NW wind days occur during this transition period and two occur after all six units were tied into the 305m stacks, giving the opportunity to see how ground level SO_2 concentrations changed as stack height increased.

Table 1 contains the average meteorological and SO_2 data for the thirty NW wind days during the 1976 - 1977 period. It is possible to see the plume axis swing from the south side (station 6) to the north side (station 9) as wind directions swing from NNW to WNW. Also apparent is that there is no dependence of ground level concentrations on wind speed for these data. This is probably due to the fact that all these cases represent similar meteorological conditions with less than a factor of two variation in wind speed. The primary 3 hr federal SO_2 air quality standard (1700 $\mu g/m^3$) is not reached in this data set.

At the end of Table 1 the data are summarized for the cases of zero, four, five, and six units tied into the tall stack. SO_2 observations at other stations upwind of the plant suggest that the background SO_2 concentration is essentially zero. It can be concluded that for the similar meteorological conditions represented by these data, the maximum ground level concentration on the plateau has been reduced by a factor of about four by the construction of the tall stack.

Ground level concentrations on the plume axis at the bottom (station 13 or 24) and top (station 3) of the terrain step are nearly the same for the days when the short stacks are in operation. After the tall stacks were put into operation, the concentration at the bottom was reduced to one third of that at the top, and about one tenth of that prior to tall stack operation. H. Leckenby, the TVA meteorologist at the site, notes that downwash commonly occurred for the six short stacks with strong NW winds, as expected for stacks whose height is less than 2.5 times the building height. In addition to the building wake, there is a wake behind the stacks, which are so close together that they provide a 20% obstruction to the flow. However, stations 13 or 24 are 1.6 km from the source, and it is expected that the strongly buoyant stack plumes would lift off the ground to some extent by this distance.

5. Estimating σ_y on the Plateau

Dispersion on the NW wind days in Table 1 is associated with well-mixed neutral conditions, since wind speed is relatively high and clouds are usually present. A workshop conducted by the American Meteorological Society (Hanna et al., 1977) suggests that it is best to use a direct measurement of turbulence such as σ_θ to estimate σ_y. For these thirty runs, there is little difference between hourly σ_θ values on the plateau and in the valley at a height of 61m on the towers, and also there is less than 50% day to day or hour to hour variability. As mentioned before, the meteorological conditions for these runs are very similar. The mean hourly average σ_θ at 61m is about 12° or 0.21 radians. Using the formula

$$\sigma_y = \sigma_\theta \times f(x) \qquad (3)$$

with f(x) equal to .55 and .45 at x equal to 1.6 km and 3.2 km (Pasquill, 1976), it is possible to predict that the average hourly σ_y, due to diffusion alone, equals 180m and 300m at x equal to 1.6 km and 3.2 km, respectively. If it is arbitrarily assumed that there is an initial σ_{yo} equal to 200m or one half of the separation of the 8 units, and that σ_y^2 at downwind distance x equals σ_y^2 from equation (3) plus the initial σ_{yo}^2, then the following formula gives our best estimate for average hourly σ_y at x equal to 3.2 km:

$$\sigma_y(1\text{ hr}) = (\sigma_{yo}^2 + (\sigma_\theta\ (1\text{ hr}) \times f(x))^2)^{1/2} = 360\text{m}. \qquad (4)$$

Hourly SO_2 concentrations at stations 3, 6, and 9 in Table 1 were used to estimate observed hourly σ_y values at x equal to 3.2 km. Stations 10 and 11 on Figure 1 were generally not used in this analysis because their SO_2 concentrations were usually zero. The cross-plume distances from stations 6 to 3 and 9 to 3 were measured to be 1000m and 800m, respectively. A Gaussian distribution in the plume was assumed. The ratios of concentrations at the stations are then:

$$\chi_6/\chi_3 = \exp\ (-10^6 m^2 + 2000\ y)/2\sigma_y^{\ 2} \qquad (5)$$

$$\chi_9/\chi_3 = \exp\ (-6.4x10^5 m^2 - 1600\ y)/2\sigma_y^{\ 2} \qquad (6)$$

where y is the distance the plume centerline is SW of station 3. If the logarithm of equations (5) and (6) is taken, they can easily be solved for $\sigma_y^{\ 2}$:

$$\sigma_y^{\ 2} = -7.2x10^5 m^2/(.8\ell n\ \chi_6/\chi_3 + \ell n\ \chi_9/\chi_3). \qquad (7)$$

If χ_3 is much less than χ_6 or χ_9, or if the concentration is zero at one of the stations, σ_y is indeterminate. For the NW wind runs in Table 1, the median observed hourly average σ_y at a downwind distance of 3.2 km is about 500m. Thus the average predicted σ_y(1 hr) is less than the observed value by 140m or about 28%.

To calculate σ_y averaged over a several hour run, it is necessary to know the variation in wind direction from hour to

hour. The additional σ_θ contributed by these long period oscillations is listed in Table 1, showing that the additional σ_θ averages 8.2° or .14 radians. The total average σ_θ for a run of about ten hours duration then equals $(.21^2 + .14^2)^{1/2} = .25$ radians, and the average σ_y over a run of several hours duration can be calculated using equation (3) to equal 220m and 360m at downwind distances of 1.6 and 3.2 km, respectively. Accounting for σ_{yo} gives a final prediction for σ_y of 300m and 410m, respectively. Average observed σ_y on the 3.2 km arc for runs averaging 10 hours duration is about 670m. Thus the predicted σ_y is 39% less than the observed value.

In both the one and ten hour cases, the theory underpredicts the observed σ_y. The error is probably not due to an error in estimating σ_{yo}, because our assumed value of 200m is, if anything, an overestimate. Similarly, the underprediction cannot be due to using σ_θ measured at 61m rather than at plume height for σ_θ is known to decrease with height. The relatively large σ_y may be caused by increased horizontal dispersion as the air flows up the terrain step, or inaccuracies in Pasquill's f(x) function when applied to this problem. If f(x) were to equal unity, the predicted σ_y would be very close to the observed σ_y.

6. Future Plans

Whenever the wind direction is right, it is planned to use a double theodolite network at Widows Creek to track neutral density

pilot balloons during strong NW flow conditions. From these measurements the amount of deflection of streamlines by the terrain step can be determined.

An idealized step similar to that at Widows Creek has been modeled by W. Snyder in the $9m^2$ EPA wind tunnel at Research Triangle Park, NC. Several step angles were tried, and detailed three dimensional measurements of flow and pollutant concentrations were made for the 15° angle. The ratio of the boundary layer height to step height was four, in agreement with the situation at Widows Creek. Stack heights of ground level, one half step, and full step were used. These data are currently being analyzed and will be reported at a later date.

ACKNOWLEDGEMENTS

T. Crawford, J. Coleman and H. Leckenby of the Tennessee Valley Authority have been very cooperative in supplying us with data from Widows Creek. D. Elliott, H. Snodgrass, and S. Rao of ATDL contributed to the computer analysis of the Widows Creek data tapes. J. Waite (University of Colorado) and T. Hughes (Beloit College) performed much of the data analysis during their work as student trainees at ATDL under an Oak Ridge Associated Universities program.

This research was performed under an agreement between the Department of Energy and the National Oceanic and Atmospheric Administration.

REFERENCES

Egan, B. A., 1975: Turbulent Diffusion in Complex Terrain, in Lectures on Air Poll. and Envir. Impact Analysis, S. Hagen, ed., Am. Met. Soc., 45 Beacon St., Boston, Mass., 02108, 112-135.

Hanna, S. R., G. A. Briggs, J. Deardorff, B. A. Egan, F. A. Gifford, and F. Pasquill, 1977: AMS Workshop on Stability Classification Schemes and Sigma Curves - Summary of Recommendations. Bull. Am. Meteorol. Soc., 58, 1305-1309.

Panofsky, H. A., C. A. Egolf, and R. Lipschutz, 1978: On characteristics of Wind Direction Fluctuations in The Surface Layer. Bound.-Layer Meteorol., 15, 439-446.

Pasquill, F., 1976: Atmospheric Dispersion Parameters in Gaussian Plume Modeling, Part 2, Possible Requirements for Change in the Turner Workbook Values. EPA-600/4-76-0306, Washington, DC.

Table 1

Daily Meteorology (61m level) and SO_2 Concentrations For NW Winds During 1976 and 1977. σ_y is obtained from the SO_2 concentrations using Equation (7).

Day	Short Stacks Operating	Hours of Run	Wind Speed (m/s)		Wind Direction		Average Hourly σ_θ		σ_θ Due to Hourly Variation		SO_2 Conc. ($\mu g/m^3$)				σ_y (m)
			Vall.	Plat.	Vall.	Plat.	Vall.	Plat.	Vall.	Plat.	13	3	6	9	
1976/3	6	13	4.6	6.3	321	313	10.9	10.1	6.0	6.3	350	530	360	100	600
8	6	7	5.5	-	321	323	11.1	-	9.2	-	290	340	210	200	880
21	6	7	4.8	5.8	319	315	8.7	11.4	12.2	11.0	180	190	160	110	1060
26	6	6	3.5	-	322	321	12.5	9.5	8.2	4.2	140	370	480	40	-
32	6	15	5.9	-	319	315	13.4	12.4	11.2	8.2	480	420	280	270	850
37	6	10	4.7	-	318	315	10.0	9.6	10.0	5.6	170	400	30	90	490
53	6	11	5.1	-	320	316	12.3	11.5	8.1	6.9	530	750	170	210	540
73	6	6	5.4	-	305	301	10.0	9.8	5.1	4.0	53	10	10	190	-
76	6	7	5.0	-	326	320	11.1	11.6	6.7	5.8	460	870	200	200	320
95	6	6	6.0	6.7	318	318	12.8	13.7	13.1	13.0	260	140	280	130	-
139	6	9	4.3	6.0	318	313	-	10.7	10.8	6.5	340	480	140	150	580
195	6	8	4.6	4.8	320	319	10.7	12.9	6.8	9.8	410	190	140	90	350
294	6	18	9.0	5.9	318	312	11.8	10.8	12.0	9.0	240	310	120	260	880
326	6	7	5.4	5.9	312	307	9.0	12.6	9.8	4.1	200*	140	10	5	360
342	6	6	3.5	4.4	310	310	12.8	10.2	9.9	7.3	110	240	50	25	450
355	6	21	6.0	8.4	324	306	12.6	11.2	7.5	4.5	200	260	60	90	570
1977/16	6	8	6.7	7.6	326	320	14.0	15.2	3.5	9.1	320	350	240	180	860
18	6	6	4.9	6.3	326	325	14.0	15.0	8.7	7.7	300	350	270	120	750
20	6	9	4.4	6.3	315	316	8.8	12.8	10.8	7.3	150	420	130	160	610
47	6	8	4.8	5.0	316	319	13.8	15.0	10.8	9.4	360	330	103	130	630
50	6	12	5.3	6.9	315	312	10.8	10.8	7.7	6.6	190	220	30	110	580
58	6	13	4.4	5.7	321	318	10.3	10.7	11.7	8.8	-	-	-	-	-
115	6	9	5.4	5.9	315	321	15.2	15.3	11.6	7.9	530	220	270	150	-
275	2	10	5.2	6.3	321	323	-	11.7	6.0	4.4	220	170	320	0	-
289	2	15	5.5	6.8	316	325	-	14.0	7.8	6.2	410	540	330	110	600
316	2	8	5.0	5.4	320	317	-	15.5	6.2	9.9	150	130	180	100	-
329	1	12	6.1	7.4	316	311	-	12.4	6.1	7.2	60	260	80	40	500
340	1	11	6.1	7.2	316	310	-	-	11.3	11.1	10	140	80	60	750
343	0	17	6.0	7.0	320	315	-	11.4	11.0	9.2	30	120	100	20	610
361	0	6	4.6	5.5	315	318	-	-	8.4	9.0	20	50	0	20	-
Average for 6 short stacks			5.0	6.1	319	316	11.7	11.9	9.2	7.4	280	340	170	140	670
Average for 2 short stacks			5.2	6.2	319	322	-	13.7	6.7	6.8	270	280	270	70	600
Average for 1 short stack			6.1	7.3	316	311	-	12.4	5.7	9.2	30	200	80	50	670
Average for 0 short stacks			5.3	6.3	318	317	-	11.4	10.2	9.1	30	90	50	20	610
Overall Average			5.1	6.2	319	316	11.7	12.1	9.0	7.6					660

*As of this date, station 13 was removed and station 24 set up a short distance away.

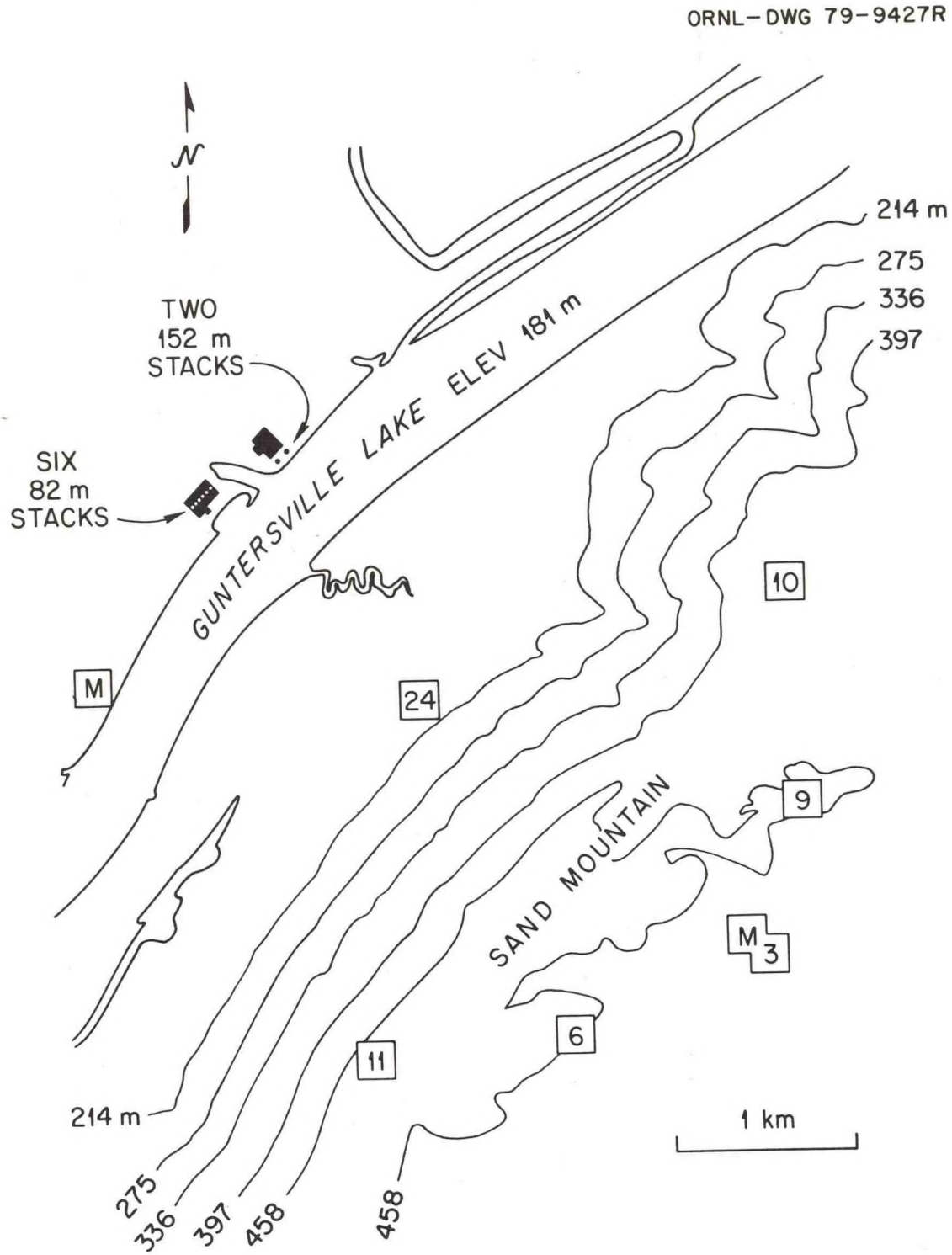

Figure 1: Map of area within 4 km of Widows Creek Steam Plant. The two meteorological stations (M) and six of the SO_2 stations are shown. Elevations are given in meters.

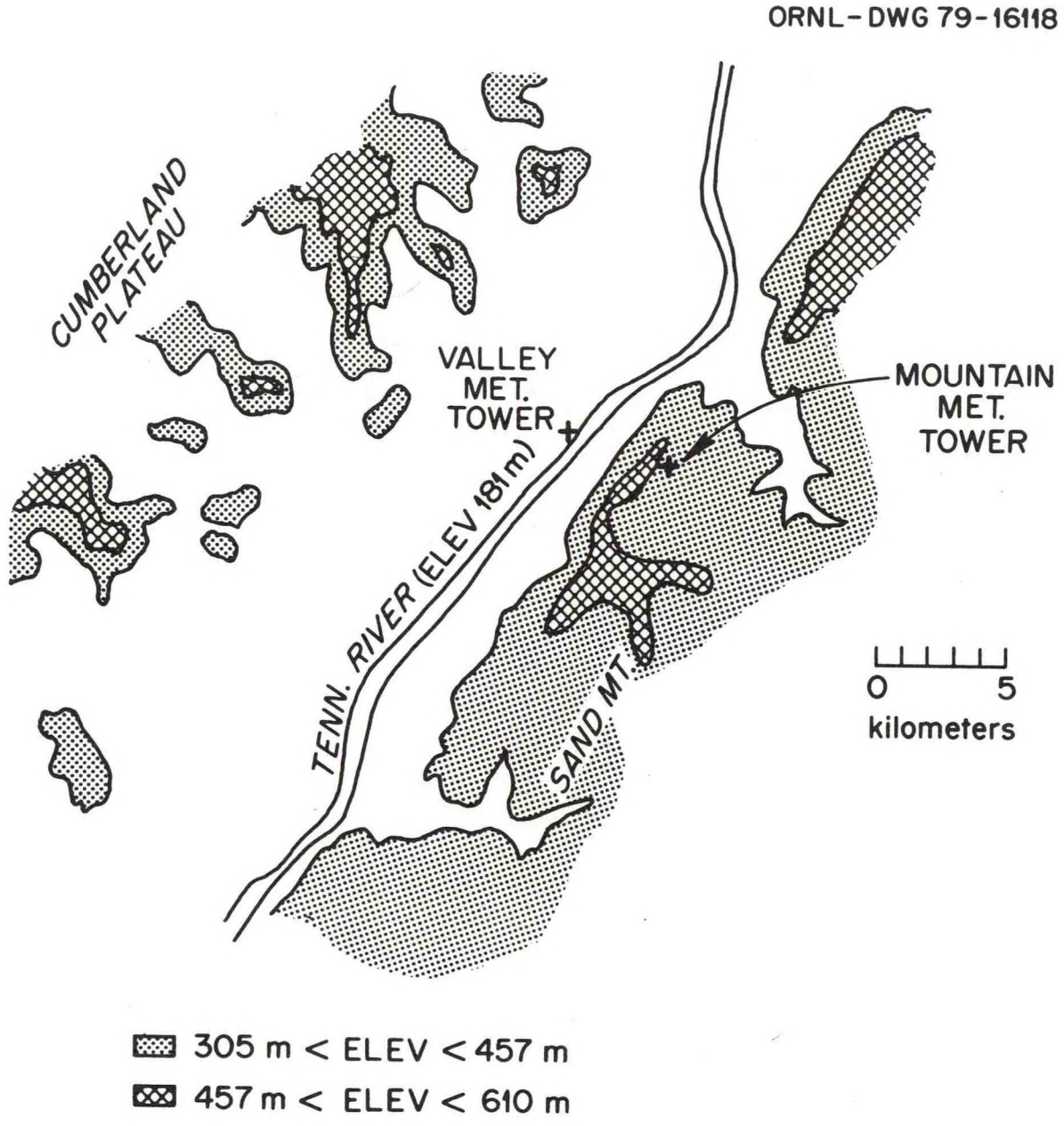

Figure 2: Map of area within 10 km of Widows Creek Steam Plant. Meteorological station locations are given.

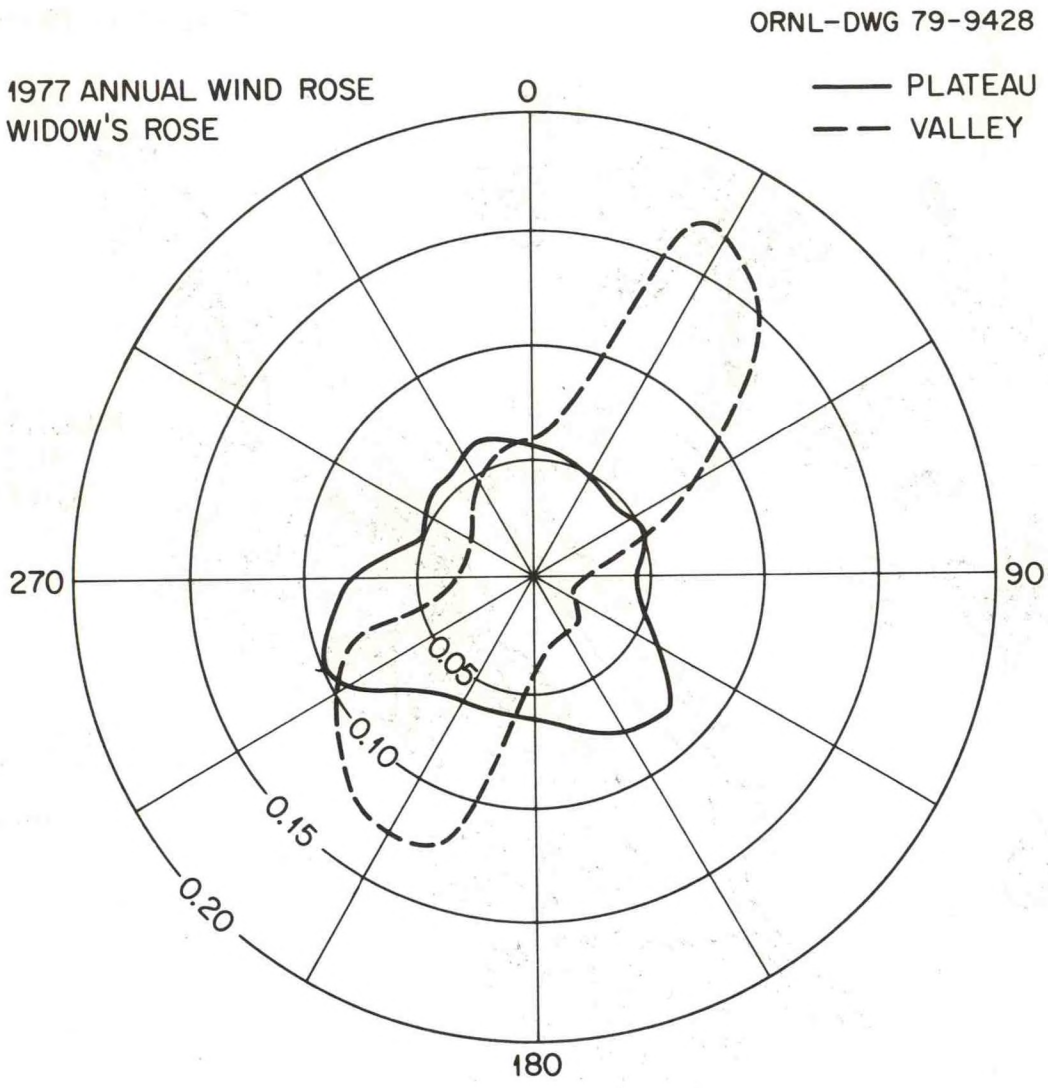

Figure 3: 1977 annual wind rose for valley and plateau meteorological stations (61m level) at Widows Creek. Numbers are frequency per $22\frac{1}{2}^{o}$ sector.

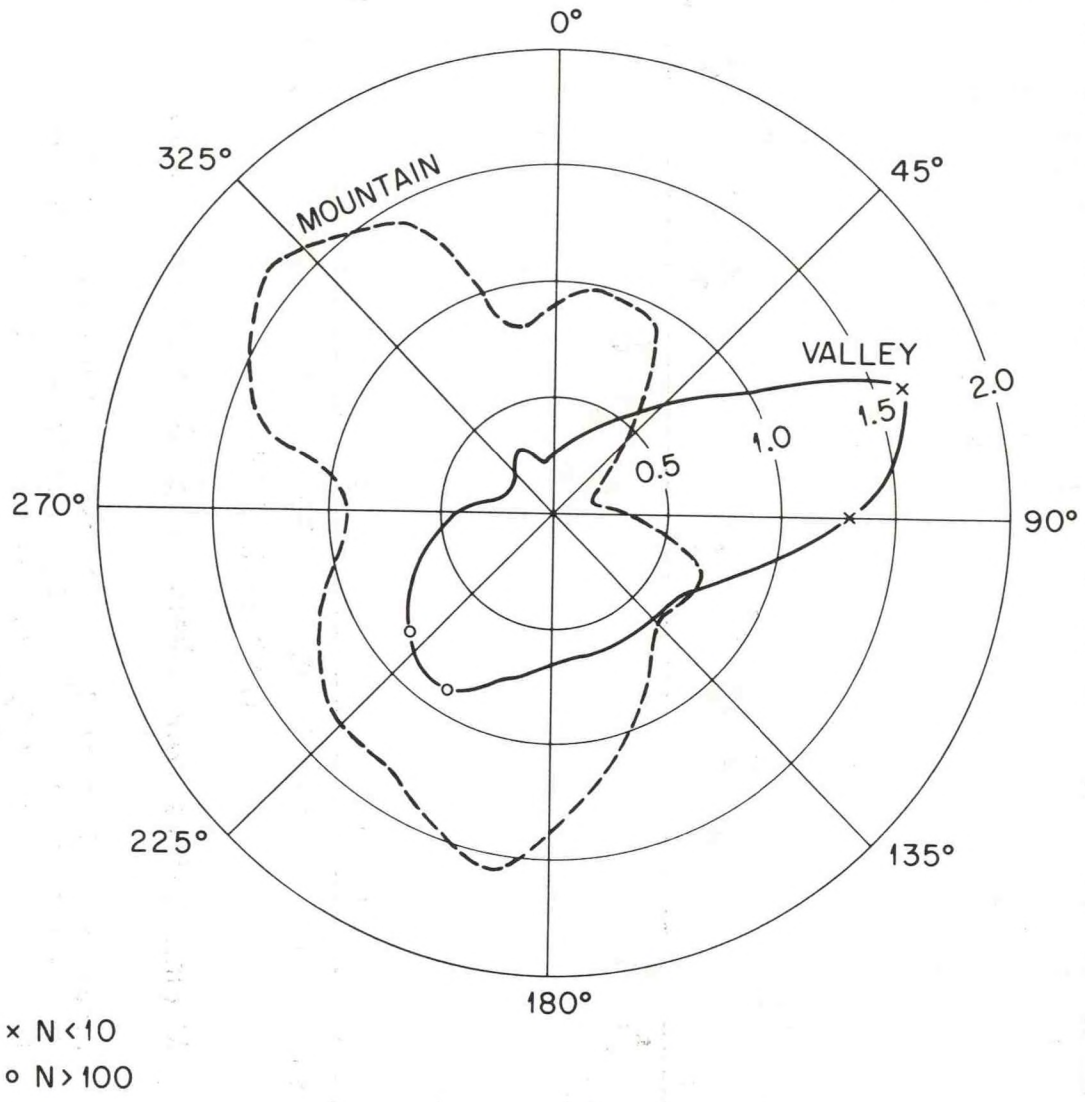

Figure 4: Calculated roughness roses for the Valley and Mountain meteorological towers.

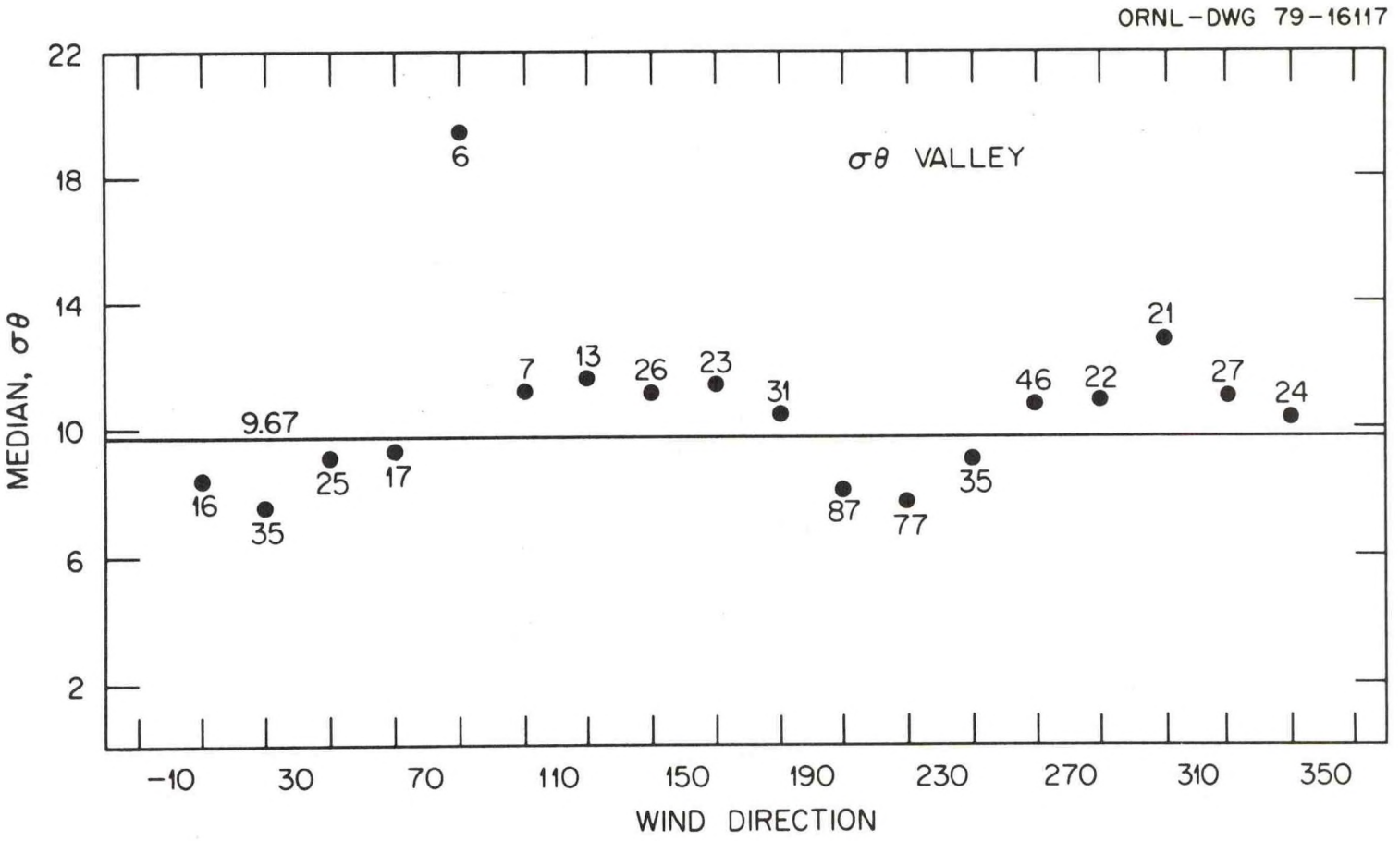

Median $\sigma\theta$ vs Wind Direction for β = 0.0 to 0.005

Figure 5: Observed σ_θ at the valley tower as a function of wind direction, for $0 < B < 0.005$ (nearly neutral conditions). Two years of hourly σ_θ data were analyzed. The number of hours used for each wind direction class is given near each point.

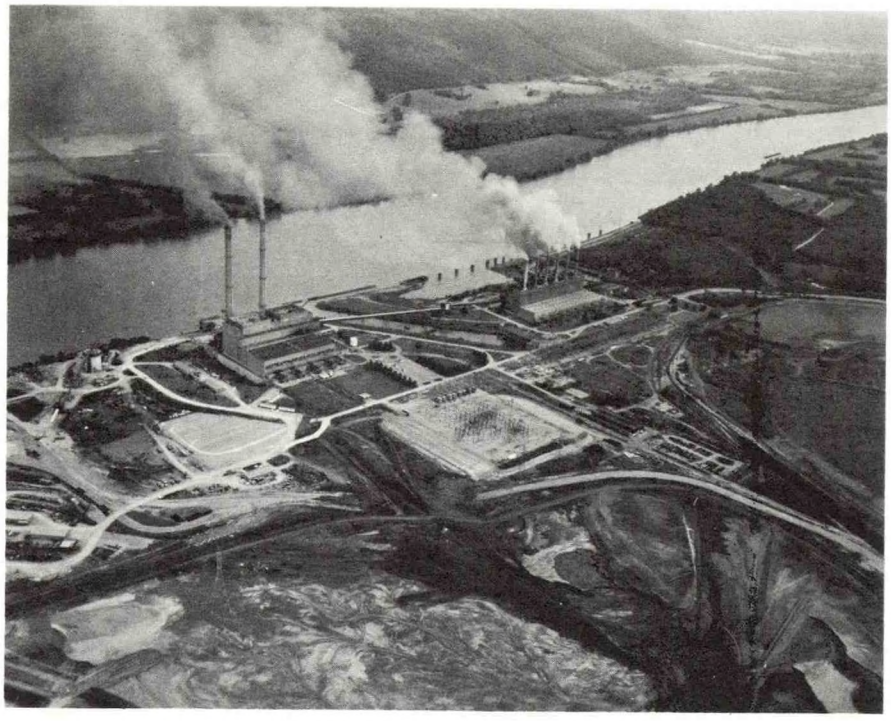

Figure 6: Widows Creek Steam Plant (1975). Photograph courtesy of T. Crawford, Tennessee Valley Authority.

U. S. DEPARTMENT OF COMMERCE
NATIONAL OCEANIC AND ATMOSPHERIC ADMINISTRATION

POSTAGE AND FEES PAID
U.S. DEPARTMENT OF COMMERCE
COM-210

U.S.MAIL

ATMOSPHERIC TURBULENCE & DIFFUSION LABORATORY
P. O. BOX E
OAK RIDGE, TENNESSEE 37830

OFFICIAL BUSINESS
PENALTY FOR PRIVATE USE, $300

NOAA FORM 61-32A
(9-73)